CRANFIELD INSTITUTE OF TECHNOLOGY

COLLEGE OF AERONAUTICS

AEROSPACE VEHICLE DESIGN

PhD Thesis

1985 - 87

V. C. SERGHIDES

DESIGN SYNTHESIS FOR CANARD-DELTA COMBAT AIRCRAFT

Supervisor: Dr. J.P. Fielding

December 1987

Volume I

SUMMARY

This thesis presents the development of a computerized Design Synthesis for canard-delta combat aircraft. This is complementary to and follows the philosophy of an existing RAE system for conventional combat aircraft with swept wings (Ref.1).

The background to the work and the Research Programme objectives and limitations are initially examined. The design of a baseline canard-delta combat aircraft is then described together with all the assumptions and decisions which led to its final configuration.

The philosophy behind the progressive evolution of the aircraft geometry and packaging modules from the baseline configuration, is explained in detail. The development of detailed modules for the estimation of the aircraft aerodynamics and performance is then presented. A full description of the investigations into the effects of canard-delta interference on the aircraft aerodynamics, is also included. The mathematical content of the aircraft geometry, packaging, aerodynamics and performance modules is presented separately in the appendices, in greater detail.

The development and architecture of the Design Synthesis and graphics programs are finally presented and the program operation is described with the aid of flow-charts. A comprehensive user's manual and a design example are also provided.

ACKNOWLEDGEMENTS

Acknowledgements are gratefully made to the Ministry of Defence/ Royal Aircraft Establishment (Farnborough) for providing full financial support for this Research Programme.

I am deeply grateful to my supervisor Dr. J.P. Fielding for his continued support, invaluable advice, suggestions and information.

I also wish to express my sincere appreciation and gratitude to Professor D. Howe for his participation in the Programme and for offering me the opportunity to undertake this work in the College of Aeronautics.

I am particularly indebted to Mr. D. Lovell, Mr. J. Smith and Dr. R. Bartlett from the Aerodynamics Department, RAE Farnborough, who closely monitored this Research Programme on behalf of the RAE and provided invaluable assistance and information. Thanks are also due to all the RAE staff who were involved in this Programme over the last two years.

Special thanks to Miss L. Cummins whose typing skill and patience made the presentation of this work possible.

CONTENTS

		PAGE
CHAPTER 1	INTRODUCTION	1
	1.1 Aircraft Design Synthesis	2
	1.2 Optimization	2
	1.3 Background	2
	1.4 Advantages of the canard-delta layout	4
	1.5 Research programme objectives	4
	1.6 Baseline limitations	6
CHAPTER 2	BASELINE AIRCRAFT DESIGN	7
	2.1 Introduction	8
	2.2 General description of the baseline aircraft	8
	2.3 Design assumptions and decisions	9
CHAPTER 3	AIRCRAFT GEOMETRY	24
	3.1 Introduction	25
	3.2 Sizing of the fixed items	26
	3.3 Fairing curve development	29
	3.4 Fuselage geometry	30
	3.5 Flying surface geometry	34
CHAPTER 4	AIRCRAFT PACKAGING	37
	4.1 Introduction	38
	4.2 Aircraft mass prediction	38
	4.3 Volume accounting	41
	4.4 Longitudinal moment arms	42
	4.5 Aircraft longitudinal centre of gravity	43

		PAGE
CHAPTER 5	AIRCRAFT AERODYNAMICS	45
	5.1 Introduction	46
	5.2 Lift-curve-slope	46
	5.3 Lift increment due to flaps	54
	5.4 Lift coefficient	54
	5.5 Aerodynamic centre	55
	5.6 Longitudinal static stability	55
	5.7 Aerodynamic drag	56
CHAPTER 6	AIRCRAFT PERFORMANCE	62
	6.1 Introduction	63
	6.2 Engine performance	63
	6.3 Sortie performance	64
	6.4 Take-off and landing performance	66
	6.5 Point performance	67
CHAPTER 7	COMPUTER PROGRAM ARCHITECTURE	70
	7.1 Introduction	71
	7.2 The computer programs	71
	7.3 Computer program development	73
	7.4 Computer program architecture	76
	7.5 Program operation	85
CHAPTER 8	DISCUSSION	102
	8.1 Research Programme review	103
	8.2 Baseline aircraft design	105
	8.3 Aircraft geometry	106
	8.4 Aircraft packaging	108
	8.5 Aircraft aerodynamics	109
	8.6 Aircraft performance	111
	8.7 Computer programs	112

		PAGE
CHAPTER 9	CONCLUSIONS	114
	9.1 Design Synthesis system	115
	9.2 Canard-delta layout	116
CHAPTER 10	RECOMMENDATIONS	118
	10.1 Recommendations for future work	119
APPENDIX A	VARIABLE NAMING CONVENTION	130
APPENDIX B	SIZING OF THE FIXED ITEMS	137
	B.1 Introduction	138
	B.2 Cockpit	138
	B.3 Undercarriage	140
	B.4 Undercarriage bays	145
	B.5 Gross wing	149
	B.6 Engine sizing	150
	B.7 Engine bay clearances	154
	B.8 Intake diffuser inlets	155
	B.9 Fuselage length	157
	B.10 Boundary layer diverter sizing	166
	B.11 Atmospheric properties	167
APPENDIX C	FAIRING CURVE DEVELOPMENT	176
	C.1 Introduction	177
	C.2 Fairing curve coefficients	177
	C.3 Fairing curve equations	181
APPENDIX D	FUSELAGE GEOMETRY	184
	D.1 Introduction	185
	D.2 Fuselage station R	186
	D.3 Fuselage station A	186
	D.4 Radome section	188
	D.5 Fuselage section R-A	190
	D.6 Intake diffusers	190

		PAGE
	D.7 Fuselage station D	194
	D.8 Fuselage station B	197
	D.9 Fuselage section A-B	200
	D.10 Fuselage station C	203
	D.11 Fuselage section B-C	205
	D.12 Boundary layer diverter	208
	D.13 Fuselage section C-D	209
	D.14 Fuselage-mounted weapons	216
	D.15 Fuselage station E	219
	D.16 Fuselage section D-E	221
	D.17 Fuselage section E-F	223
	D.18 Fuselage station F	225
	D.19 Fuselage section F-G	227
	D.20 Fuselage station G	229
	D.21 Engine bays	230
	D.22 Fuselage section G-H	232
	D.23 Fuselage station H	236
	D.24 Fuselage section H-J	238
	D.25 Fuselage station J	241
	D.26 Fuselage section J-K	243
	D.27 Fuselage station K	247
	D.28 Fuselage volume and surface area	251
	D.29 Miscellaneous geometry calculations	252
APPENDIX E	FLYING SURFACE GEOMETRY	272
	E.1 Introduction	273
	E.2 Net wing	273
	E.3 Net foreplane	280
	E.4 Gross foreplane	282
	E.5 Fin(S)	283

		PAGE
APPENDIX F	PACKAGING	288
	F.1 Introduction	289
	F.2 Aircraft mass prediction	289
	F.3 Volume accounting	310
	F.4 Longitudinal moment arms	312
	F.5 Wing-store stations	322
	F.6 Aircraft longitudinal centre of gravity	323
APPENDIX G	AERODYNAMIC LIFT	328
	G.1 Introduction	329
	G.2 Lift-curve-slope	329
	G.3 Lift increment due to flaps	342
	G.4 Aerodynamic centre	343
APPENDIX H	AERODYNAMIC DRAG	361
	H.1 Introduction	362
	H.2 Basic zero lift drag	362
	H.3 Wave drag	369
	H.4 Spillage drag	381
	H.5 Store drag	382
	H.6 Canard-delta interference effects on lift-dependent drag	384
	H.7 Lift-dependent drag	385
	H.8 Total aircraft drag	390
APPENDIX I	AIRCRAFT PERFORMANCE ESTIMATION	400
	I.1 Introduction	401
	I.2 Engine performance	401
	I.3 Sortie performance	406
	I.4 Take-off and landing performance	414
	I.5 Point performance	418

		PAGE
APPENDIX J	COMPUTER PROGRAM USER'S MANUAL	425
	J.1 Introducion	426
	J.2 User-created data files	426
	J.3 Computer program compilation and execution	440
	J.4 Computer program implementation procedure	441
	J.5 Computer program statistics	444
APPENDIX K	DESIGN EXAMPLE	461

FIGURES

2.1 Baseline configuration drawings

7.1 User/program interrelation-Simplified flow chart

7.2 User/program interrelation - Expanded flow chart

7.3 Program CANARD - Expanded flow chart

7.4 Computer generated images (Example)

B.1 Cockpit geometry

B.2 Main undercarriage and bay geometry

B.3 Nose undercarriage and bay geometry

B.4 Gross-wing geometry

B.5 Engine and bay geometry

C.1 Fairing curve

D.1 Fuselage geometry - Station R

D.2 Fuselage geometry - Station A

D.3 Fuselage geometry - Radome

D.4 Intake diffuser geometry

D.5 Fuselage geometry - Station D

D.6 Fuselage geometry - Station B

D.7 Fuselage geometry - Section A-B

D.8 Fuselage geometry - Station C

D.9 Fuselage geometry - Section B-C

D.10 Fuselage geometry - Section C-D

D.11 Fuselage geometry - Station E

D.12 Fuselage geometry - Section D-E

D.13 Fuselage geometry - Section E-F

D.14 Fuselage geometry - Station F

D.15 Fuselage geometry - Section F-G

D.16 Fuselage geometry - Station G

D.17 Fuselage geometry - Section G-H

D.18 Fuselage geometry - Station H

D.19 Fuselage geometry - Section H-J

D.20 Fuselage geometry - Station J

D.21 Fuselage geometry - Section J-K

D.22 Fuselage geometry - Station K

D.23 List of geometric constraints

E.1 Net wing geometry

E.2 Foreplane geometry

E.3 Fin geometry

G.1 Transonic force-break Mach number for zero sweep

G.2 Transonic sweep correction for force-break Mach number

G.3 Correction to wing l-c-s at force-break Mach number

G.4 Wing transonic l-c-s at MA

G.5 Wing transonic l-c-s at MB

G.6 Wing supersonic l-c-s

G.7 Wing supersonic l-c-s correction factor for sonic leading-edge region

G.8 Supersonic l-c-s for body

G.9 Wing-body interference factors KWB and KBW

G.10 Lift on body in presence of wing

G.11 Canard-delta interference effects (lift-curve-slope)

G.12 Wing aerodynamic centre position

H.1 Canard-delta interference effects (lift-dependent drag)

J.1 Computer program implementation procedure - Flow chart

J.2 Arrangement of input variables in file CANARD.DAT

J.3 List of input variables

J.4 File LDD2.DAT (Example)

J.5 File STDRAG.DAT (Example)

NOTATION

2-D	Two-dimensional
3-D	Three-dimensional
a.c	Aerodynamic centre
b.l.d.	Boundary layer diverter
c.g.	Centre of gravity
CPU	Central processing unit
fig.	Figure
l-c-s	Lift-curve-slope
LPV	Lower plan view
MVO	Multivariate optimization
no.	Num ber
RAE(F)	Royal Aircraft Establishment (Farnborough)
ref.	Reference
stn.	Station
SV	Side view
u/c	Undercarriage
UPV	Upper plan view
$\sum$	Sum

********** LIST OF VARIABLES **********
******* DESIGN SYNTHESIS FOR CANARD-DELTA COMBAT AIRCRAFT *******
********** BY V.C.SERGHIDES **********

Note: EV = External Variable
---- IV = Independent Variable
DV = Dependent Variable
The variables in this list which are not marked as either EV's or IV's are defined as DV's.

Symbol	Definition	Type
AC	Gross foreplane aspect ratio.	
ACN	Net foreplane aspect ratio.	EV
AEFN	Net fin aspect ratio.	EV
AH	Speed of sound at a given altitude.	
AII	Aspect ratio of an intake diffuser at the intake plane.	EV
AL	Aircraft incidence.	
ALH	Maximum sustained aircraft incidence at maximum thrust.	
ALM	Maximum sustained aircraft incidence for a engine throttle setting.	
AMMX	Maximum design Mach number for the structure.	EV
ATE	Total aircraft pitching moment about nose with empty fuel tanks,no external stores, no ammunition.	
ATEW	Total aircraft pitching moment about nose with empty internal or external fuel tanks, plus external stores and ammunition.	
ATR	Attained turn rate.	
ATT	Total aircraft pitching moment about nose with full fuel tanks,no external stores, no ammunition.	
ATTW	Total aircraft pitching moment about nose with full internal or external fuel tanks, plus external stores and ammunition.	
AW	Gross wing aspect ratio.	IV
AWA	Aspect ratio of each aileron.	EV
AWB	Aspect ratio of gross wing-box.	
AWN	Net wing aspect ratio.	
AWN1	Net aspect ratio of wing or foreplane.	
AWR	Reference wing aspect ratio for wing-box mass calculation.	
BC	Gross foreplane span.	
BCN	Net foreplane span.	
BEFN	Net fin span.	
BETA1	Square-root of (1-M**2)	
BETA2	Square-root of (M**2-1)	
BFA	Fuselage width at stn A.	
BFB	Fuselage width at stn B.	
BFBCL	Width of a lower corner of fuselage stn B.	
BFBCLX	Width of a lower corner of fuselage section A-B at any stn X.	
BFBCU	Width of an upper corner of fuselage stn B.	
BFBCUX	Width of an upper corner of fuselage section	

	A-B at any stn X.
BFBS	Minimum fuselage width at stn B.
BFC	Fuselage width at stn C.
BFCCL	Width of a lower corner of the fuselage stn C.
BFCCLX	Width of a lower corner of the fuselage section B-C at any stn X.
BFCCU	Width of an upper corner of fuselage stn C.
BFCCUX	Width of an upper corner of the fuselage section B-C at any stn X.
BFCS	Minimum fuselage width at stn C.
BFD	Fuselage width at stn D.
BFDCLX	Width of a lower corner of the fuselage section C-D at any stn X.
BFDCU	Width of an upper corner at fuselage stn D.
BFDCUX	Width of an upper corner of the fuselage section C-D at any stn X.
BFDS	Minimum allowable BFD.
BFE	Fuselage width at stn E.
BFECU	Width of an upper corner at fuselage stn E.
BFECUX	Width of an upper corner of the fuselage section D-E at any stn X.
BFES	Minimum fuselage width at stn E.
BFF	Fuselage width at stn F.
BFFCU	Width of an upper corner at fuselage stn F.
BFFS	Minimum fuselage width at stn F.
BFG	Fuselage width at stn G.
BFGCU	Width of an upper corner at fuselage stn G.
BFGCUX	Width of an upper corner of the fuselage section F-G at any stn X.
BFGS	Minimum fuselage width at stn G.
BFH	Fuselage width at stn H.
BFHCU	Width of an upper corner at fuselage stn H.
BFHCUX	Width of an upper corner of the fuselage section G-H at any stn X.
BFHS	Minimum fuselage width at stn H.
BFJ	Fuselage width at stn J.
BFJCL	Width of a lower corner at fuselage stn J.
BFJCLX	Width of a lower corner of the fuselage section H-J at any stn X.
BFJCU	Width of an upper corner at fuselage stn J.
BFJCUX	Width of an upper corner of the fuselage section H-J at any stn X.
BFJS	Minimum fuselage width at stn J.
BFK	Fuselage width at stn K.
BFKCL	Width of a lower corner at fuselage stn K.
BFKCLX	Width of a lower corner of the fuselage section J-K at any stn X.
BFKCU	Width of an upper corner at fuselage stn K.
BFKCUX	Width of an upper corner of the fuselage section J-K at any stn X.
BFKS	Minimum fuselage width at stn K.
BFPR3K	Inner width of upper fuselage recess at stn K.
BFPR3X	Inner width of upper fuselage recess at a stn X
BFPRL	Outer width of the underfuselage recess.
BFPRUH	Inner width of the underfuselage recess at stn H.
BFPRUJ	Inner width of the underfuselage recess at stn J.
BFPRUK	Inner width of the underfuselage recess at stn K.

BFPRUX	Inner width of the underfuselage recess at any stn X.	
BGFA	Average width of the gun fairing.	EV
BGFX	Width of the gun fairing at any stn X.	
BIDD	Width of an intake diffuser at stn D.	
BIDX	Width of an intake diffuser at any stn X.	
BII	Width of an intake diffuser at the intake plane	
BIIH	Maximum allowable width of an intake diffuser at the intake plane.	
BIX	Half-width of the intake fairing at any stn X.	
BMS	Wing bending moment.	
BRA	Radar antenna width.	EV
BUMB	Width of a main u/c bay.	
BUMWG	Grown width of a main u/c tyre.	
BUMWH	Maximum width of a main u/c tyre.	
BUMWN	Nominal width of a main u/c tyre.	
BUMWS	Minimum width of a main u/c tyre.	
BUNB	Width of the nose u/c bay.	
BUNWG	Grown width of the nose wheel tyre.	
BUNWH	Maximum width of the nose u/c tyre.	
BUNWN	Nominal width of the nose u/c tyre.	
BUNWS	Minimum width of the nose u/c tyre.	
BUWG	Grown tyre width.	
BUWH	Maximum tyre width.	
BUWN	Nominal tyre width.	
BUWS	Minimum tyre width.	
BVI	Width of the b.l.diverter stream-tube at the intake plane.	
BVIX	Width of the b.l.diverter stream-tube at a stn X.	
BVIX1	Width of the b.l.diverter splitter at a stn X.	
BW	Gross wing span.	
BW1	Gross span of wing or foreplane.	
BWA	Gross span of the ailerons.	
BWBB	Span of the center section of the wing-box.	
BWF	Gross span of trailing edge flaps.	
BWN	Net wing span.	
BWNF	Span of fuel tank in wing-box external to the fuselage.	
CCB	Net foreplane root chord.	
CCCC	Centerline chord of the gross foreplane .	
CCCT	Foreplane tip chord.	
CCMA	Gross foreplane mean aerodynamic chord.	
CCMAN	Net foreplane mean aerodynamic chord.	
CCMG	Gross foreplane mean geometric chord.	
CCMGN	Net foreplane mean geometric chord.	
CD	Drag coefficient.	
CDO8	Total aircraft basic zero lift drag coefficient at M=0.8.	
CDOC	Zero lift drag coefficient of the canopy.	
CDOEC	Zero lift drag coefficient of the foreplane.	
CDOEF	Zero lift drag coefficient of the fin.	
CDOF	Zero lift drag coefficient of the fuselage.	
CDOFG	Zero lift drag coefficient of the gross fuselage.	
CDOV	Basic aircraft zero lift drag coefficient,up to M=0.8.	
CDOW	Zero lift drag coefficient of the wing.	
CDB	Subsonic drag coefficient of the fuselage afterbody.	

CDB1	Drag coefficient of wing-store no.1.
CDB2	Drag coefficient of wing-store no.2.
CDB3	Drag coefficient of wing-store no.3.
CDB4	Drag coefficient of wing-store no.4.
CDCCW1	Wave drag coefficient of the complete canopy for M=1.
CDCCW2	Wave drag coefficient of the complete canopy for M=1.3.
CDCTW1	Wave drag coefficient of the rear part of the canopy for M=1.
CDCTW2	Wave drag coefficient of the rear part of the canopy for M=1.3.
CDCW1	Wave drag coefficient of the foreplane for M=1.
CDCW2	Wave drag coefficient of the foreplane for M=1.3.
CDCWW1	Wave drag coefficient of the front part of the canopy for M=1.
CDCWW2	Wave drag coefficient of the front part of the canopy for M=1.3.
CDEFW1	Wave drag coefficient of the fin for M=1.
CDEFW2	Wave drag coefficient of the fin for M=1.3.
CDFMW1	Wave drag coefficient of the fuselage section from the intake plane to the maximum cross-sectional area of the fuselage for M=1.
CDFMW2	Wave drag coefficient of the above fuselage section for M=1.3.
CDFSW1	Wave drag coefficient of the fuselage forebody for M=1.
CDFSW2	Wave drag coefficient of the fuselage forebody for M=1.3.
CDFTD1	Wave drag coefficient of the equivalent afterbody for M=1.
CDFTD2	Wave drag coefficient of the equivalent afterbody for M=1.3.
CDFTW1	Wave drag coefficient of the afterbody for M=1.
CDFTW2	Wave drag coefficient of the afterbody for M=1.3.
CDGC	Drag coefficient of the gun port.
CDH	Maximum drag coefficient corresponding to ALH in sortie performance.
CDIV	Subsonic drag coefficient of the b.l.diverter.
CDMUF1	Drag coefficient of fuselage-mounted missile no.1.
CDMUF2	Drag coefficient of fuselage-mounted missile no.2.
CDMUF3	Drag coefficient of fuselage-mounted missile no.3.
CDMUF4	Drag coefficient of fuselage-mounted missile no.4.
CDPRE	Intake pre-entry drag coefficient.
CDS	Intake spillage drag coefficient.
CDSTOR	Total installed store drag coefficient.
CDTOT	Total aircraft drag coefficient.
CDTW	Total aircraft wave drag coefficient for a given Mach number.
CDTW1	Total aircraft wave drag coefficient for M=1.
CDTW2	Total aircraft wave drag coefficient for M=1.3
CDUT	Drag coefficient of the extended u/c.
CDV	Lift dependent drag coefficient.
CDWW1	Wave drag coefficient of the wing for M=1.

CDWW2	Wave drag coefficient of the wing for M=1.3.	
CDXP1	Drag coefficient of the external wing-pylon no.1.	
CDXP2	Drag coefficient of the external wing-pylon no.2.	
CDXP3	Drag coefficient of the external wing-pylon no.3.	
CDXP4	Drag coefficient of the external wing-pylon no.4.	
CEFB	Fin root chord.	
CEFCT	Fin tip chord.	
CEFMA	Fin mean aerodynamic chord.	
CEFMG	Fin mean geometric chord.	
CFR	Skin friction coefficient.	
CL	Lift coefficient.	
CL1	Initial estimate of maximum sustained lift coefficient used in sortie performance calcs.	EV
CL2	Actual maximum sustained lift coefficient in sortie performance calculations.	
CL3	Initial estimate of maximum sustained lift coefficient for a selected throttle setting, used in STR calculations.	EV
CL4	Actual maximum sustained lift coefficient for a selected throttle setting,in STR calculations	
CLC	Critical lift coefficient.	EV
CLCSIF	Wing-on-foreplane lift-curve-slope interference factor.	
CLDES	Manoeuvring design lift coefficient.	EV
CLMAX	Maximum lift coefficient (trimmed) at a given Mach number.	EV
CLMAXL	Maximum lift coefficient in the landing config.	
CLT	Maximum lift coefficient in the take-off config	
CWA	Aileron mean chord.	
CWBB	Wing-box chord at the body side.	
CWBT	Wing-box tip chord.	
CWCA2	Wing chord at mid-span of each aileron.	
CWCB	Net wing root chord.	
CWCB1	Net wing or foreplane root chord.	
CWCC	Centerline chord of the gross wing.	
CWCCT	Wing chord at outboard end of T.E. flaps.	
CWCT	Wing-tip chord.	
CWFM	Mean chord of T.E. flaps.	
CWMA	Wing mean aerodynamic chord.	
CWMN	Mean chord of the net wing.	
CWMG	Wing mean geometric chord.	
DBUMW1	Initial estimate of,(DUMWN**0.5)*(BUMWN**0.75).	
DBUNW1	Initial estimate of,(DUNWN**0.5)*(BUNWN**0.75).	
DBUW	=(DUNWN**0.5)*(BUNWN**0.75) for the selected standard tyre.	
DCB1	Drag code for wing-store no.1.	EV
DCB2	Drag code for wing-store no.2.	EV
DCB3	Drag code for wing-store no.3.	EV
DCB4	Drag code for wing-store no.4.	EV
DCDF	Drag coefficient increment due to T.E. flap deflection.	
DCLF	Lift coefficient increment due to T.E. flaps.	
DCLFH	Increment in the maximum lift coefficient due to T.E. flaps.	
DCMUF1	Drag code for fuselage-mounted missile no.1.	EV
DCMUF2	Drag code for fuselage-mounted missile no.2.	EV

DCMUF3	Drag code for fuselage-mounted missile no.3.	EV
DCMUF4	Drag code for fuselage-mounted missile no.4.	EV
DCXP1	Drag code for external wing-pylon no.1.	EV
DCXP2	Drag code for external wing-pylon no.2.	EV
DCXP3	Drag code for external wing-pylon no.3.	EV
DCXP4	Drag code for external wing-pylon no.4.	EV
DE1	Depth of the wing-box at the body side.	
DE6	Depth of the wing-box at the tip.	
DF	Flap thickness function used in the estimation of flap mass.	
DF21	Gradient of net propulsive force with aircraft speed.	
DFH	Average fuselage width at the wing-body junction.	
DFH1	DFH or DFHC.	
DFHC	Average fuselage width at the foreplane-body junction.	
DHUML	Stroke of a main u/c leg.	
DHUMW	Deflection of a main u/c tyre.	
DHUNL	Stroke of the nose u/c leg.	
DHUP	Height difference between the nose and main u/c pintles.	EV
DK2	Increment on K1 to define lift dependent drag parameter K2.	EV
DM	Mach number increment.	EV
DMUF1	Diameter of fuselage-mounted missile no.1.	EV
DMUF1X	Diameter of fuselage-mounted missile no.1, at any stn X.	
DMUF2	Diameter of fuselage-mounted missile no.2.	EV
DMUF2X	Diameter of fuselage-mounted missile no.2, at any stn X.	
DMUF3	Diameter of fuselage-mounted missile no.3.	EV
DMUF3X	Diameter of fuselage-mounted missile no.3, at any stn X.	
DMUF4	Diameter of fuselage-mounted missile no.4.	EV
DMUF4X	Diameter of fuselage-mounted missile no.4, at any stn X.	
DP1	Engine compressor inlet diameter.	
DP1R	Compressor inlet diameter of datum engine.	EV
DP12X	Engine diameter at any stn X between engine stns 1 and 2.	
DP2	Turbine section exit diameter.	
DP2R	Turbine section exit diameter of datum engine.	EV
DP23X	Engine diameter at any stn X between engine stns 2 and 3.	
DP3	Afterburner section exit diameter.	
DP3R	Afterburner section exit diameter of datum eng.	EV
DP34X	Engine diameter at any stn X between engine stns 3 and 4.	
DP4	Nozzle exit diameter.	
DP4R	Nozzle exit diameter of datum engine.	EV
DT	Acceleration time.	
DTE	Average depth of the rear spar.	
DUMWG	Grown diameter of a main u/c tyre.	
DUMWH	Maximum diameter of a main u/c tyre.	
DUMWN	Nominal diameter of a main u/c tyre.	
DUMWS	Minimum diameter of a main u/c tyre.	
DUML	Diameter of a main u/c leg.	
DUNL	Diameter of the nose u/c leg.	
DUNWG	Grown diameter of the nose u/c tyre.	

DUNWH	Maximum diameter of the nose u/c tyre.	
DUNWN	Nominal diameter of the nose u/c tyre.	
DUNWS	Minimum diameter of the nose u/c tyre.	
DUWG	Grown tyre diameter.	
DUWH	Maximum tyre diameter.	
DUWN	Nominal tyre diameter.	
DUWS	Minimum tyre diameter.	
DXAC	Total shift of the aerodynamic center due to the fuselage.	
DXAC1	Aerodynamic center shift due to the front and rear fuselage.	
DXAC2	Aerodynamic center shift due to the fuselage carry-over lift.	
DXF	Axial distance between two successive fuselage stns.	
DXFAB	Axial spacing between two successive stns of fuselage section A-B.	
DXFBC	Axial spacing between two successive stns of fuselage section B-C.	
DXFCD	Axial spacing between two successive stns of fuselage section C-D.	
DXFDE	Axial spacing between two successive stns of fuselage section D-E.	
DXFEF	Axial spacing between two successive stns of fuselage section E-F.	
DXFFG	Axial spacing between two successive stns of fuselage section F-G.	
DXFGH	Axial spacing between two successive stns of fuselage section G-H.	
DXFHJ	Axial spacing between two successive stns of fuselage section H-J.	
DXFJK	Axial spacing between two successive stns of fuselage section J-K.	
DXFR	Axial spacing between two successive radome stns.	
DXFRA	Axial spacing between two successive stns of fuselage section R-A.	
EBFD	Total width clearance between diffusers and fuselage at stn D.	EV
EBP1	Engine bay width clearance at the compressor inlet.	
EBP12X	Engine bay width clearance at any stn X between eng. stns 1,2.	
EBP1H	Maximum value of clearance EBP1.	EV
EBP1S	Minimum value of clearance EBP1.	EV
EBP2	Engine bay width clearance at the turbine section exit.	
EBP23X	Engine bay width clearance at any stn X between eng. stns 2,3.	
EBP2H	Maximum value of clearance EBP2.	EV
EBP2S	Minimum value of clearance EBP2.	EV
EBP3	Engine bay width clearance at the afterburner section exit.	
EBP34X	Engine bay width clearance at any stn X between eng. stns 3,4.	
EBP3H	Maximum value of clearance EBP3.	EV
EBP3S	Minimum value of clearance EBP3.	EV
EBP4	Engine bay width clearance at the nozzle exit plane.	
EBP4H	Maximum value of clearance EBP4.	EV

EBP4S	Minimum value of clearance EBP4.	EV
EBRA	Radar antenna width clearance.	EV
EBUMW	Lateral clearance for a main u/c tyre.(Due to centrifugal forces)	
EBUNW	Lateral clearance for the nose u/c tyre.(Due to centrifugal forces)	
ECCDIV	Intake b.l.diverter drag increment due to compressibility.	
ECDFT	Afterbody wave drag increment due to interference effects of the front fuselage.	
EDUMW	Radial clearance for a main u/c tyre.(Due to centrifugal forces)	
EDUNW	Radial clearance for the nose u/c tyre.(Due to centrifugal forces)	
EFW	Term used for the moment arm estimation of fuselage structure.	
EFX	Term used for the moment arm estimation of fuselage skin.	
EHC5	Perpendicular distance between the seat-back and rear cockpit bulkhead.	EV
EHP1	Engine bay height clearance at the compressor inlet.	
EHP12X	Engine bay height clearance at any stn X between eng. stns 1,2.	
EHP1H	Maximum value of clearance EHP1.	EV
EHP1S	Minimum value of clearance EHP1.	EV
EHP2	Engine bay height clearance at the turbine section exit.	
EHP23X	Engine bay height clearance at any stn X between eng. stns 2,3.	
EHP2H	Maximum value of clearance EHP2.	EV
EHP2S	Minimum value of clearance EHP2.	EV
EHP3	Engine bay height clearance at the afterburner section exit.	
EHP34X	Engine bay height clearance at any stn X between eng. stns 3,4.	
EHP3H	Maximum value of clearance EHP3.	EV
EHP3S	Minimum value of clearance EHP3.	EV
EHP4	Engine bay height clearance at the nozzle exit plane.	
EHP4H	Maximum value of clearance EHP4.	EV
EHP4S	Minimum value of clearance EHP4.	EV
EHRA	Radar antenna height clearance.	EV
EHUMBL	Lower height clearance for a main u/c bay.	EV
EHUNBL	Lower height clearance for the nose u/c bay.	EV
ELFT	Rear fuselage length increment to form a complete afterbody.	
ELMUFA	Longitudinal separation between the rear ends of fuselage mounted missiles no.3 and no.4.	EV
ELUMBA	Aft length clearance for a main u/c bay.	EV
ELUMBF	Forward length clearance for a main u/c bay.	EV
ELUNBA	Aft length clearance for the nose u/c bay.	EV
ELUNBF	Forward length clearance for the nose u/c bay.	EV
EMFG	Mass of miscellaneous items (e.g. gear for naval aircraft).	
EQWF	T.E. flap deflection.	EV
EQWFH	Maximum T.E. flap deflection.	EV
EQWFL	T.E. flap deflection in the landing configur.	EV
EQWFT	T.E. flap deflection in the take-off configur.	EV
ERR	Specified error for equality constraints.	EV

EUML	Main u/c leg efficiency.	EV
EUMW	Main u/c tyre efficiency.	EV
EXUNBF	Clearance between the intake lips and the forward end of the nose u/c bay.	EV
EYFC	Lateral clearance at stn C which accounts for the width of the fuselage structure on each side of the cockpit.	EV
EYPCH	Lateral clearance between the engines for protection purposes.	EV
EYFEF	Lateral clearance between the intake diffuser duct and fuselage wall in section E-F.	EV
EYFFG	Lateral clearance between the intake diffuser duct and fuselage wall in section F-G.	
F1	First estimate of the net propulsive force.	
F2	Second estimate of the net propulsive force.	
F3	Third estimate of the net propulsive force.	
FBP1K	Constant factor for engine bay width clearance, EBP1.	EV
FBP2K	Constant factor for engine bay width clearance, EBP2.	EV
FBP3K	Constant factor for engine bay width clearance, EBP3.	EV
FBP4K	Constant factor for engine bay width clearance, EBP4.	EV
FBWA	Total fractional span of all ailerons.	EV
FBWCF	Fractional span of the wing-box containing fuel tanks.	
FBWF	Fractional gross span of the T.E. flaps.	IV
FBWNF	Fractional span of the net wing-box containing fuel tanks.	IV
FCDTKC	Coefficient in cubic for the estimation of the total wave drag of the basic aircraft between MD and M=1. the total wave drag of the basic aircraft between MD and M=1.	
FCDVK	Advanced aerodynamic technology factor used for the estimation of the constant subsonic value of K1.	
FCDVK0	Coefficient in cubic transition region of lift dependent drag vs CL function.	
FCDVK1	Coefficient in cubic transition region of lift dependent drag vs CL function.	
FCDVK2	Coefficient in cubic transition region of lift dependent drag vs CL function.	
FCDVK3	Coefficient in cubic transition region of lift dependent drag vs CL function.	
FCLL	Fraction of CLMAX available for landing.	EV
FCLT	Fraction of CLMAX available for take-off.	EV
FCWD	Front spar position as a fraction of the local wing chord.	IV
FCWLFT	Chord of fixed L.E. forward of front spar as a fraction of local wing chord.	EV
FCWLHT	Distance of the T.E. of the L.E. high lift device, forward of the front spar as a fraction of the local wing chord.	EV
FCWR	Rear spar position as a fraction of the local wing chord.	IV
FCWTFT	Distance of the T.E. of the fixed section of the wing T.E. aft of the rear spar as fraction of the local wing chord.	EV

FCWTHL	Distance of the L.E. of the T.E. flaps aft of the rear spar as a fraction of the local wing chord.	EV
FDUNL	Fraction of DUNL related to the thickness of the lower end of the nose u/c leg.	EV
FHP1K	Constant factor for engine bay height clearance, EHP1.	EV
FHP2K	Constant factor for engine bay height clearance, EHP2.	EV
FHP3K	Constant factor for engine bay height clearance, EHP3.	EV
FHP4K	Constant factor for engine bay height clearance, EHP4.	EV
FK	Bending moment factor in mass estimation of the wing-box.	
FK1D0	Subsonic datum value for K1.	
FK1D1	Supersonic datum value for K1.	
FK1HK1	First factor in the expression for FK1H.	
FK1HK2	Second factor in the expression for FK1H.	
FK1HK3	Third factor in the expression for FK1H.	
FK1H	Value of K1 at supersonic speeds.	
FK1H1	Value of K1 for M=1.4.	
FK1H2	Value of K1 for M=2.0.	
FK1K0	Coefficient in cubic for the estimation of K1 for Mach numbers between 0.3 and 1.2.	
FK1K1	Coefficient in cubic for the estimation of K1 for Mach numbers between 0.8 and 1.2.	
FK1K2	Coefficient in cubic for the estimation of K1 for Mach numbers between 0.8 and 1.2.	
FK1K3	Coefficient in cubic for the estimation of K1 for Mach numbers between 0.8 and 1.2.	
FK1SK1	First factor for the estimation of FK1SK4.	
FK1SK2	Second factor for the estimation of FK1SK4.	
FK1SK3	Third factor for the estimation of FK1SK4.	
FK1SK4	Factor for the estimation of FK1D0.	
FLMUF1	Nose length fraction of fuselage-mounted missile no.1.	EV
FLMUF2	Nose length fraction of fuselage-mounted missile no.2.	EV
FLMUF3	Nose length fraction of fuselage-mounted missile no.3.	EV
FLMUF4	Nose length fraction of fuselage-mounted missile no.4.	EV
FLP1K	Exponent in correlation for length of engine gas generator.	EV
FLP2K	Exponent in correlation for length of engine reheat fuelling section.	EV
FLP3K	Exponent in correlation for length of engine nozzle.	EV
FLVK	Constant factor related to LVG.	EV
FMC	Foreplane materials mass factor.	EV
FMCB1	Multiple carriage factor for wing-store stn no.1.	EV
FMCB2	Multiple carriage factor for wing-store stn no.2.	EV
FMCB3	Multiple carriage factor for wing-store stn no.3.	EV
FMCB4	Multiple carriage factor for wing-store stn no.4.	EV
FMD1	First constant factor for the estimation of MD.	EV

FMD2	Second constant factor for the estimation of MD, which allows for improvements in aerodynamic technology.	EV
FMEF	Fin materials mass factor.	EV
FMEF2	Twin-fin mass factor.	
FMF1	Materials mass factor for fuselage miscellania.	EV
FMF2	Materials mass factor for fuselage.	EV
FMFIR	State-of-the-art mass factor for the intake ramps.	EV
FMPBK	Factor in estimation of the mass of engine gas gas generator.	EV
FMPIK	Factor in estimation of the engine installation mass.	EV
FMPRK	Exponent in estimation of mass of the engine reheat system.	EV
FMSC	State-of-the-art mass factor for the flying controls.	EV
FMSCK	Constant factor for the prediction of the flying control mass.	EV
FMSA	Mass fraction of air systems parts other than ducts.	EV
FMSAK	Constant factor for the prediction of the air systems mass.	EV
FMSEK	Constant factor for the prediction of the electrics mass.	EV
FMSFK	Constant factor for the prediction of fuel system mass.	EV
FMTSW	Wing mass-loading at take-off.	
FMUHK	Constant factor for the prediction of the u/c hydraulics mass.	EV
FMUM	State-of-the-art mass factor for the main u/c.	EV
FMUN	State-of-the-art mass factor for the nose u/c.	EV
FMUMK	Constant factor for the prediction of the main u/c mass.	EV
FMUNK	Constant factor for the prediction of the nose u/c mass.	EV
FMWB	Materials mass factor for the wing-box.	EV
FMWBH	Factor which corrects the MWB estimates for thin wings of moderate to high aspect ratio.	
FMWL	Materials mass factor for the wing L.E.	EV
FMWT	Materials mass factor for the wing T.E.	EV
FOT6N	Increment in cross-sectional area at the nozzle exit above datum value (OII+OVI).	IV
FPS	Engine throttle setting.	
FPUNLV	Constant factor which allows for the additional load on the nose u/c leg due to steady braking.	EV
FQWF	Factor for the estimation of the lift increment due to T.E. flaps.	
FRK	Ground rolling friction coefficient.	EV
FTPGC	Fraction defining the maximum available reverse thrust in terms of TPGC.	EV
FVCKPT	Cockpit volume factor.	EV
FVSTAP	Factor defining the approach speed in terms of the stall speed.	EV
FVSTTO	Factor defining the take-off speed in terms of the stall speed.	EV
FXWPCG	Fraction of the local wing-chord between the front and rear spars defining the position of the imaginary wing-store c.g. line.	EV
FYB1	Net wing span fraction defining the lateral	EV

	c.g.posn of wing-store stn 1.	
FYB2	Net wing span fraction defining the lateral c.g.posn of wing-store stn 2.	EV
FYB3	Net wing span fraction defining the lateral c.g.posn of wing-store stn 3.	EV
FYB4	Net wing span fraction defining the lateral c.g.posn of wing-store stn 4.	EV
FYFRAK	Constant power of the Y-coordinate of the radome.	
FZCAN1	Power of the Z-coordinate of the front canopy section.	EV
FZCAN2	Power of the Z-coordinate of the rear canopy section.	EV
FZFRAK	Constant power of the Z-coordinate of the radome.	
G	Gravitational acceleration.	
GCDTW1	Gradient of the wave drag coefficient with Mach number at M=1.	
GCL	Total aircraft lift curve slope.	
GCLA	Lift-curve-slope of the wing at M=MFB+0.07.	
GCLB	Lift-curve-slope of the wing at M=MFB+0.14.	
GCLBL	Lower interpolation value of GCLB.	
GCLBSP	Supersonic lift-curve-slope of the body.	
GCLBTR	Transonic lift-curve-slope of the body.	
GCLBU	Upper interpolation value of GCLB.	
GCLC	Lift-curve-slope of the foreplane.	
GCLCB	Lift-curve-slope of the isolated foreplane-body combination.	
GCLFB	Actual value of the lift-curve-slope of the wing at M=MFB.	
GCLFBL	Lower interpolation value of GCLFB.	
GCLFBU	Upper interpolation value of GCLFB.	
GCLW	Lift-curve-slope of the wing.	
GCLW06	Lift-curve-slope of the wing at M=0.6.	
GCLW10	Theoretical value of the lift-curve-slope of the wing at M=MFB.	
GCLW14	Lift-curve-slope of the wing at M=1.4.	
GCLWB	Lift-curve-slope of the wing-body combination.	
GCLWB1	Lift-curve-slope of the wing-body combination at M=0.6.	
GCLWB2	Lift-curve-slope of the wing-body combination at M=1.4.	
GCLWBR	Lift-curve-slope of the isolated wing-body or foreplane-body combination.	
GCLWK	Constant used in the estimation of GCLWSB.	
GCLWR	Lift-curve-slope of the wing or foreplane.	
GCLWS	Theoretical incompressible lift-curve-slope of the aerofoil section.	
GCLWSB	Subsonic lift-curve-slope of the wing (3-D).	
GCLWSP	Supersonic lift-curve-slope of the wing.	
GK1D1	Gradient of supersonic wave drag with Mach number.	
GLW	Product of GCLWSP and the tangent of leading edge sweep angle.	
GLWL1	First interpolation value of GLWL12.	
GLWL12	Lower interpolation value of GLW.	
GLWL2	Second interpolation value of GLWL12.	
GLWL1L	Left interpolation value of GLWL1.	
GLWL2L	Left interpolation value of GLWL2.	
GLWL1R	Right interpolation value of GLWL1.	

GLWL2R	Right interpolation value of GLWL2.	
GLWU1	First interpolation value of GLWU12.	
GLWU2	Second interpolation value of GLWU12.	
GLWU12	Upper interpolation value of GLW.	
GLWU1L	Left interpolation value of GLWU1.	
GLWU2L	Left interpolation value of GLWU2.	
GLWU1R	Right interpolation value of GLWU1.	
GLWU2R	Right interpolation value of GLWU2.	
GN	Load factor.	EV
GNA	Maximum attained load factor.	
GNH	Maximum sustained load factor.	
GNS	Sustained load factor.	
GNSH	Maximum permissible value of the sustained load factor.	
GOF1	Gradient of cross-sectional area of fuselage at stn R.	
GTCPH	Maximum human G-tolerance limit.	EV
HC1	Distance between thigh point and eye point.	EV
HC2	Distance between thigh point and heel point.	EV
HC3	Distance between thigh point and NSRP.	EV
HC4	Vertical gap between eye-point and canopy.	EV
HC5	Height of the fwd cockpit bulkhead above the cockpit floor.	
HC6	Height of the raised heel-line above the cockpit floor.	
HCEYE	Height of the eye-point above the cockpit floor	
HCSEAT	Height of the NSRP above the cockpit floor measured along the seat-back line.	EV
HFA	Height of fuselage at stn A.	
HFA1	Cockpit underfloor height at stn A.	EV
HFABX	Height of fuselage section A-B at any stn X.	
HFB	Height of fuselage at stn B.	
HFB1	Cockpit underfloor height at stn B.	
HFBCL	Height of a lower corner of fuselage stn B.	
HFBCLX	Height of a lower corner of fuselage section A-B at any stn X.	
HFBCU	Height of an upper corner of fuselage stn B.	
HFBCUX	Height of an upper corner of fuselage section A-B at any stn X.	
HFBCX	Height of fuselage section B-C at any stn X.	
HFC	Height of fuselage at stn C.	
HFC1	Cockpit underfloor height at stn C.	
HFC2	Height of the canopy centerline axis above the fuselage at stn C.	
HFC2X	Height of the canopy centerline axis above fuselage section B-C at any stn X.	
HFCCL	Height of a lower corner of fuselage stn C.	
HFCCLX	Height of a lower corner of fuselage section B-C at any stn X.	
HFCCU	Height of an upper corner of fuselage stn C.	
HFCCUX	Height of an upper corner of fuselage section B-C at any stn X.	
HFCDX	Height of fuselage section C-D at any stn X.	
HFD	Height of fuselage at stn D.	
HFD2	Height of the canopy centerline axis above fuselage section C-D at stn D.	
HFD2X	Height of the canopy centerline axis above fuselage section C-D at any stn X.	
HFDCLX	Height of a lower corner of fuselage section C-D at any stn X.	

HFDCU	Height of an upper corner of fuselage stn D.	EV
HFDCUX	Height of an upper corner of fuselage section C-D at any stn X.	
HFDEX	Height of fuselage section D-E at any stn X.	
HFDH	Maximum fuselage height at stn D.	
HFE	Height of fuselage at stn E.	
HFE2	Height of the fuselage spine at stn E.	
HFE2X	Height of the fuselage spine at any stn X of section D-E.	
HFECU	Height of an upper corner of fuselage stn E.	
HFECUX	Height of an upper corner of fuselage section D-E at any stn X.	
HFEFX	Height of fuselage section E-F at any stn X.	
HFF	Height of fuselage at stn F.	
HFF2	Height of the aircraft spine at stn F.	
HFFCU	Height of an upper corner of fuselage stn F.	
HFFGX	Height of fuselage section F-G at any stn X.	
HFG	Height of fuselage at stn G.	
HFGCU	Height of an upper corner of fuselage stn G.	
HFGCUX	Height of an upper corner of fuselage section F-G at any stn X.	
HFGHX	Height of fuselage section G-H at any stn X.	
HFG2X	Height of the aircraft spine at any stn X of section F-G.	
HFH	Height of fuselage at stn H.	
HFHCU	Height of an upper corner of fuselage stn H.	
HFHCUX	Height of an upper corner of fuselage section G-H at any stn X.	
HFHJX	Height of fuselage section H-J at any stn X.	
HFJ	Height of fuselage at stn J.	
HFJCL	Height of a lower corner of fuselage stn J.	
HFJCLX	Height of a lower corner of fuselage section H-J at any stn X.	
HFJCU	Height of an upper corner of fuselage stn J.	
HFJCUX	Height of an upper corner of fuselage section H-J at any stn X.	
HFJKX	Height of fuselage section J-K at any stn X.	
HFK	Height of fuselage at stn K.	
HFKCL	Height of a lower corner of fuselage stn K.	
HFKCLX	Height of a lower corner of fuselage section J-K at any stn X.	
HFKCU	Height of an upper corner of fuselage stn K.	
HFKCUX	Height of an upper corner of fuselage section J-K at any stn X.	
HFPR1H	Depth of the underfuselage recess at stn H.	
HFPR1X	Depth of the underfuselage recess at any stn X of section G-H.	
HFPR2J	Depth of the underfuselage recess at stn J.	
HFPR2K	Depth of the underfuselage recess at stn K.	
HFPR2X	Depth of the underfuselage recess at any stn X of section H-K.	
HFPR3K	Depth of the upper fuselage recess at stn K.	
HFPR3X	Depth of the upper fuselage recess at any stn X of section J-K.	
HIDD	Height of an intake diffuser at stn D.	
HIDX	Height of an intake diffuser at any stn X.	
HII	Height of an intake diffuser at the intake plane.	
HRA	Height of radar antenna.	EV
HT	Flight altitude.	EV

HTF	Airfield altitude.	EV
HTG	Geopotential height.	
HTH	Altitude at which MHH is reached.	EV
HTR	Equivalent surface roughness height.	EV
HVI	Height of the b.l.diverter at the intake plane.	
HUMB	Height of a main u/c bay.	
HUNBA	Height of the aft end of the nose u/c bay.	
HUNBD	Height of the nose u/c bay at stn D.	
HUNBF	Height of the fwd end of the nose u/c bay.	
HUNBX	Height of the nose u/c bay at any stn X.	
HWBB	Height of the center-section of the wing-box.	
K1	Lift dependent drag parameter for CL lower than CLC.	
K2	Lift dependent drag parameter for CL higher than CLC.	
KBW	Wing-on-body interference factor related to GCLWB.	
KBWF	Product of KBW.	
KBWFL	Lower interpolation value of KBWF.	
KBWFU	Upper interpolation value of KBWF.	
KN	Nose interference factor related to GCLWB.	
KWB	Body-on-wing interference factor related to GCLWB.	
LAR	Length of the radar avionics bay.	EV
LAX	Length of the extra avionics bay ,aft of the radar bay in section R-A.	EV
LBCF	Length of the forebody excluding the nose as defined in wing-body lift-curve-slope calcs.	
LBCF1	LBCF or LBCFC.	
LBCFC	Length of the forebody excluding the nose as defined in foreplane-body lift-curve-slope calculations.	
LBN	Nose length as defined in wing-body lift-curve-slope calculations.	
LBN1	LBN or LBNC.	
LBNC	Nose length as defined in foreplane-body lift-curve-slope calculations.	
LCCAN	Total length of canopy and windscreen.	EV
LCCQM	Foreplane moment arm measured between the mean 0.25-chord points of the wing and foreplane.	
LCEYE	Horizontal distance between fwd cockpit bulkhead and eye-point.	
LCFL	Length of the cockpit floor.	
LCFOOT	Horizontal distance between fwd cockpit bulkhead and heel-point.	EV
LCNSPR	Distance between the NSRP and the fwd bulkhead of the cockpit.	EV
LD	Landing distance (From 15m screen height to full stop).	
LDDK1F	Canard-delta interference factor for K1.	
LDDK2F	Canard-delta interference factor for K2.	
LEFCQM	Fin moment arm measured between the mean 0.25-chord points of the wing and fin.	
LFAB	Length of fuselage section A-B.	
LFBC	Length of fuselage section B-C.	
LFCD	Length of fuselage section C-D.	
LFGH	Length of fuselage section G-H.	
LFHJ	Length of fuselage section H-J.	
LFJK	Length of fuselage section J-K.	

LGC	Gun length.	EV
LMUF1	Length of fuselage-mounted missile no.1.	EV
LMUF2	Length of fuselage-mounted missile no.2.	EV
LMUF3	Length of fuselage-mounted missile no.3.	EV
LMUF4	Length of fuselage-mounted missile no.4.	EV
LNMUF1	Nose length of fuselage-mounted missile no.1.	
LNMUF2	Nose length of fuselage-mounted missile no.2.	
LNMUF3	Nose length of fuselage-mounted missile no.3.	
LNMUF4	Nose length of fuselage-mounted missile no.4.	
LP12	Length of the gas generator of engine.	
LP12R	Length of the gas generator of datum engine.	EV
LP22A	Length of the reheat fuelling section of engine	
LP22AR	Reference length of the reheat fuelling section of datum engine.	EV
LP23	Length of the reheat section of engine.	
LP2A4	Length of the reheat burning section of engine.	
LP2A4R	Length of the reheat burning section of datum engine.	EV
LP34	Engine nozzle length.	
LP34R	Nozzle length of datum engine.	EV
LPG	Total engine length.	
LUMB	Length of a main u/c bay.	
LUML	Length of a main u/c leg.	
LUNB	Length of the nose u/c bay.	
LUNL	Length of the nose u/c leg.	
LUNLB	Length of the front section of the nose u/c bay	
LUNWB	Length of the rear section of the nose u/c bay.	
LVG	Length of the b.l.diverter exit.	
LWBEF	Moment arm of the center of volume of the wing fuel tanks relative to L.E. of wing-box at wing root.	
LWFK	Length of flap tracks as a fraction of the wing chord.	EV
M	Mach number.	EV
M1	First Mach number value.	
M2	Second Mach number value.	
MA	MA=MFB+0.07,in wing lift-curve-slope estimation.	
MAPU	Mass of APU.	EV
MAR	Mass of radar avionics.	EV
MASS	Mass of the aircraft at the start of a leg.	
MAX	Mass of general avionics.	EV
MB	MB=MFB+0.14,in wing lift-curve-slope estimation.	
MB1	Mass of stores mounted at wing-pylon no.1.	EV
MB2	Mass of stores mounted at wing-pylon no.2.	EV
MB3	Mass of stores mounted at wing-pylon no.3.	EV
MB4	Mass of stores mounted at wing-pylon no.4.	EV
MC	Mass of the foreplane structure.	
MC1K	First constant for foreplane mass prediction.	EV
MC2K	Second constant for foreplane mass prediction.	EV
MC3K	Third constant for foreplane mass prediction.	EV
MCARM	Mass of cockpit armour protection.	
MCC	Mass of canopy.	
MCFI	Mass of cockpit flight instrumentation.	EV
MCFURN	Mass of cockpit furnishings.	
MCMI	Mass of cockpit miscellaneous instrumentation.	EV
MCMISC	Mass of miscellaneous cockpit equipment.	
MCPI	Mass of cockpit powerplant instrumentation.	EV
MCG	Total foreplane mass.	

MCI	Total mass of cockpit equipment.	
MCP	Mass of crew, including personal equipment.	EV
MCR	Critical Mach number.	
MCSEAT	Mass of ejection seat.	EV
MCW	Mass of the windscreen.	
MCXP	Mass of foreplane paint.	
MD	Drag rise Mach number.	
MDD	Drag rise Mach number at zero lift.	
MEF	Total mass of fin structure.	
MEF1K	First constant for the estimation of MEF.	EV
MEF2K	Second constant for the estimation of MEF.	EV
MEF3K	Third constant for the estimation of MEF.	EV
MEF4K	Fourth constant for the estimation of MEF.	EV
MEFC	Total mass of fin(s).	
MEFXP	Total mass of fin paint.	
MFAIB	Mass of the airbrake.	
MFB	Force-break Mach number corrected for leading edge sweep effects.	
MFBL	Lower interpolation value of MFB.	
MFBU	Upper interpolation value of MFB.	
MFBO	Force-break Mach number for zero leading edge sweep.	
MFBOL	Lower interpolation value of MFBO.	
MFBOU	Upper interpolation value of MFBO.	
MFG	Total mass of fuselage structure.	
MFGF	Total fuel mass stored inside the fuselage.	
MFIF	Fuel mass stored inside the fuselage, excluding any fuel stored in the central wing-box.	
MFIFDE	Mass of fuel stored inside fuselage section D-E, excluding any fuel stored in the central wing-box.	
MFIFEF	Mass of fuel stored inside fuselage section E-F, excluding any fuel stored in the central wing-box.	
MFIFFG	Mass of fuel stored inside fuselage section F-G, excluding any fuel stored in the central wing-box.	
MFIR	Mass of the intake ramps.	
MFX	Mass of fuselage shell.	
MFXP	Mass of fuselage paint.	
MFW	Mass of internal fuselage structure.	
MGA	Mass of ammunition.	EV
MGC	Mass of gun.	EV
MGCL	General Mach number for lift-curve-slope calcs.	
MHH	Maximum design Mach number for b.l.diverter sizing.	EV
MI	Initial Mach number.	
MLMUF	Total mass of missile launchers.	EV
MMAX	Maximum Mach number in level flight at a given throttle setting.	
MMUF1	Mass of fuselage-mounted missile no.1.	EV
MMUF2	Mass of fuselage-mounted missile no.2.	EV
MMUF3	Mass of fuselage-mounted missile no.3.	EV
MMUF4	Mass of fuselage-mounted missile no.4.	EV
MODE	Engine performance analysis mode (1-5).	
MPA	Air mass flow for the engine.	
MPAC	Air mass flow at maximum gross thrust.	
MPAD	Air mass flow rate at sea-level static conds.	
MPAD1	Value of MPAD for the datum engine.	EV
MPB	Gas generator mass.	

MPBR	Gas generator reference mass.	EV
MPF	Fuel mass flow rate of the engine.	
MPFB1	Initial estimate for MPFB2.	EV
MPFB2	Actual mass of fuel consumed along a sortie leg	
MPFB2T	Total fuel mass consumed during a sortie, up to the end of the leg under consideration.	
MPFC	Fuel mass flow at GNH.	
MPFD1	Value of MPFD for the datum engine.	EV
MPFD	Fuel mass flow rate at maximum gross thrust at sea-level.	
MPFS1	Minimum fuel mass flow rate at sea-level static conditions.	
MPG	Total propulsion system mass.	
MPI	Engine installation mass.	
MPR	Reheat system mass.	
MPRR	Reference reheat system mass.	EV
MPT	Thrust reverser mass.	
MPTR	Thrust reverser reference mass.	EV
MSA	Mass of air services (airconditioning and avionics cooling systems).	
MSAK	Constant related to MSA.	EV
MSC	Mass of flying controls.	
MSCK	Constant related to the flying controls mass.	EV
MSD	Mass of air systems ducts.	
MSE	Electrical system (generation & distribution) mass.	
MSEK	Constant related to MSE.	EV
MSF	Fuel system mass.	
MSTART	Initial Mach number value used in acceleration calculations.	EV
MTCR	Stressing mass for the wing.	
MTFI	Internal fuel mass.	
MTGFI	Total internal fuel mass.	
MTL	Aircraft landing mass.	
MTLF	Fuel mass required for landing.	EV
MTLR	Reference landing mass.	
MTOUF	Mass of oil and unused fuel.	
MTP	Total aircraft payload (fuel excluded).	
MTPR	Reference load for the definition of MTCR.	EV
MTR	Mass of fixed role equipment.	
MTS	Total mass of stores carried on the aircraft.	
MTT	Total aircraft take-off mass.	
MTTF	Fuel mass required for take-off.	EV
MTTR	Take-off reference mass.	EV
MU	Atmospheric air viscocity.	
MUH	Mass of u/c associated hydraulics.	
MUHK	Constant used in the calculation of MUH.	EV
MUM	Main u/c mass.	
MUMG	Main u/c mass plus mass of the associated hydraulics.	
MUMK	Constant used in the calculation of MUM.	EV
MUN	Nose u/c mass.	
MUNG	Nose u/c mass plus mass of the associated hydraulics.	
MUNK	Constant used in the calculation of MUN.	EV
MUSL	Sea-level atmospheric air viscocity.	
MWA	Total mass of ailerons.	
MWB	Total mass of the wing-box.	
MWBCF	Mass of fuel stored in the central wing-box.	
MWBEF	Mass of fuel stored in the wingbox outside	

	the fuselage.	
MWC	Total mass of the wing.	
MWCX	Mass of miscellaneous attachments.	
MWF	Total mass of the T.E. flaps.	
MWFK	Mass of flap tracks.	
MWL	Total mass of the wing L.E.	
MWS	Total spoiler mass.	
MWT	Total mass of the fixed section of the T.E.	
	of the wing.	
MWXF	Mass of miscellaneous fairings.	
MWXP	Wing paint mass.	
MXP1	Mass of external wing-pylon no.1.	EV
MXP2	Mass of external wing-pylon no.2.	EV
MXP3	Mass of external wing-pylon no.3.	EV
MXP4	Mass of external wing-pylon no.4.	EV
MXT	Total mass of external tanks.	
MXT1	Mass of external tank no.1.	
MXT2	Mass of external tank no.2.	
MXTF	Total mass of externally carried fuel.	
MXTF1	Mass of fuel in external tank no.1.	EV
MXTF2	Mass of fuel in external tank no.2.	EV
NB1	Number of stores mounted at wing-pylon no.1.	EV
NB2	Number of stores mounted at wing-pylon no.2.	EV
NB3	Number of stores mounted at wing-pylon no.3.	EV
NB4	Number of stores mounted at wing-pylon no.4.	EV
NCP	Number of crew.(=1,for this synthesis)	EV
NENG	Number of engines.(=2,for this synthesis)	EV
NFIN	Number of fins.	EV
NPP1	Number of points for STR estimates.	EV
NPP2	Number of points for ATR estimates.	EV
NPP3	Number of points for SEP estimates.	EV
NPP4	Number of points for MMAX estimates.	EV
NPP5	Number of points for SDT estimates.	EV
NPP6	Number of points for RQF estimates.	EV
NSF	Fuselage stn number.	
NSFAB	Number of fuselage stns of section A-B.(=3)	EV
NSFBC	Number of fuselage stns of section B-C.(=3)	EV
NSFCD	Number of fuselage stns of section C-D.(=3)	EV
NSFDE	Number of fuselage stns of section D-E.(=3)	EV
NSFEF	Number of fuselage stns of section E-F.(=3)	EV
NSFFG	Number of fuselage stns of section F-G.(=3)	EV
NSFGH	Number of fuselage stns of section G-H.(=3)	EV
NSFHJ	Number of fuselage stns of section H-J.(=3)	EV
NSFJK	Number of fuselage stns of section J-K.(=3)	EV
NSFR	Number of radome stns.(=3)	EV
NSFRA	Number of fuselage stns of section R-A.(=3)	EV
NSTAG	Number of sortie legs.	EV
NU	Kinematic viscocity of atmospheric air.	
NWFK	Number of flap tracks.	EV
NWP	Number of wing pylons.(=4)	EV
OFA	Fuselage cross-sectional area at stn A.	
OFABX	Cross-sectional area of the fuselage section	
	A-B at any stn X.	
OFB	Fuselage cross-sectional area at stn B.	
OFBCX	Cross-sectional area of the fuselage section	
	B-C at any stn X.	
OFC	Fuselage cross-sectional area at stn C.	
OFCDI1	Fuselage cross-sectional area just before the	
	intake plane.	
OFCDI2	Fuselage cross-sectional area at the intake	

	plane.	
OFCDX	Cross-sectional area of the fuselage section C-D at any stn X.	
OFCDXU	Cross-sectional area of the upper fuselage section C-D at any stn X.	
OFD	Fuselage cross-sectional area at stn D.	
OFDEX	Cross-sectional area of the fuselage section D-E at any stn X.	
OFE	Fuselage cross-sectional area at stn E.	
OFEFX	Cross-sectional area of the fuselage section E-F at any stn X.	
OFF	Fuselage cross-sectional area at stn F.	
OFFGX	Cross-sectional area of the fuselage section F-G at any stn X.	
OFG	Fuselage cross-sectional area at stn G.	
OFGHX	Cross-sectional area of the fuselage section G-H at any stn X.	
OFH	Fuselage cross-sectional area at stn H.	
OFHJX	Cross-sectional area of the fuselage section H-J at any stn X.	
OFHPRH	Cross-sectional area of the underfuselage recess at stn H.	
OFHPRX	Cross-sectional area of the underfuselage recess at any stn X of section G-H.	
OFJ	Fuselage cross-sectional area at stn J.	
OFJK	Cross-sectional area of the fuselage at the middle of section J-K.	
OFJKX	Cross-sectional area of the fuselage section J-K at any stn X.	
OFK	Fuselage cross-sectional area at stn K.	
OFKPR	Cross-sectional area of the underfuselage recess at stn K.	
OFKPRX	Cross-sectional area of the underfuselage recess at any stn X of section J-K.	
OFPR3K	Cross-sectional area of the upper fuselage recess at stn K.	
OFPR3X	Cross-sectional area of the upper fuselage recess at any stn X of section J-K.	
OFJPRJ	Cross-sectional area of the underfuselage recess at stn J.	
OFJPRX	Cross-sectional area of the underfuselage recess at any stn X of section H-J.	
OFR	Fuselage cross-sectional area at stn R.	
OFRAX	Cross-sectional area of the fuselage section R-A at any stn X.	
OFRX	Cross-sectional area of the radome at any stn X	
OFXH	Maximum cross-sectional area of the fuselage.	
OFXHS	Maximum net cross-sectional area of the fuselage.	
OFXTH	Maximum cross-sectional area of the afterbody.	
OGFA	Average cross-sectional area of the gun fairing.	EV
OGFX	Cross sectional area of the gun fairing at any stn X.	
OIDD	Cross-sectional area of an intake diffuser at stn D.	
OIDX	Cross-sectional area of an intake diffuser at any stn X.	
OIE	Total exit area of the intake diffusers.	
OII	Total inlet area of the intake diffusers.	

OIX	Cross-sectional area of the intake fairing at any stn X.	
OIXL1	Cross-sectional area of the fairing under the intake ducts and fwd of the nose u/c bay at any stn X.	
OIXL2	Cross-sectional area of the nose u/c bay fairing at any stn X.	
OMUF1X	Cross-sectional area of fuselage-mounted missile no.1 at any stn X.	
OMUF2X	Cross-sectional area of fuselage-mounted missile no.2 at any stn X.	
OMUF3X	Cross-sectional area of fuselage-mounted missile no.3 at any stn X.	
OMUF4X	Cross-sectional area of fuselage-mounted missile no.4 at any stn X.	
OP1	Cross-sectional area of the engine at stn 1.	
OP12BX	Cross-sectional area of the engine bay at any stn X between engine stns 1 and 2.	
OP12X	Cross-sectional area of each engine at any stn X between engine stns 1 and 2.	
OP2	Cross-sectional area of the engine at stn 2.	
OP23BX	Cross-sectional area of the engine bay at any stn X between engine stns 2 and 3.	
OP23X	Cross-sectional area of each engine at any stn X between engine stns 2 and 3.	
OP3	Cross-sectional area of the engine at stn 3.	
OP34BX	Cross-sectional area of the engine bay at any stn X between engine stns 3 and 4.	
OP34X	Cross-sectional area of each engine at any stn X between engine stns 3 and 4.	
OP4	Cross-sectional area of the engine at stn 4.	
OPJ	Jet exit area at general Mach no. and altitude.	
OPJD	Jet exit area at sea-level static conditions.	
OPJD1	Value of OPJD for the datum engine.	EV
OPN	Total nozzle exit area.	
OTA1K	Coefficient in cubic for cross-sectional area of aft fairing.	
OTA2K	Coefficient in cubic for cross-sectional area of aft fairing.	
OTA3K	Coefficient in cubic for cross-sectional area of aft fairing.	
OTA4K	Coefficient in cubic for cross-sectional area of aft fairing.	
OTF1K	Coefficient in cubic for cross-sectional area of front fairing.	
OTF2K	Coefficient in cubic for cross-sectional area of front fairing.	
OTF3K	Coefficient in cubic for cross-sectional area of front fairing.	
OTF4K	Coefficient in cubic for cross-sectional area of front fairing.	
OTF4K1	First coefficient for determining OTF4K.	
OTF4K2	Second coefficient for determining OTF4K.	
OTF4K3	Third coefficient for determining OTF4K.	
OTM	Maximum cross-sectional area of the fairing curve.	
OTXN	Cross-sectional area of the fairing curve at any stn X.	
OUMB	Cross-sectional area of main u/c bay.	
OUNLBS	Minimum cross-sectional area of the front	

	section of the nose u/c bay.
OUNLBH	Maximum cross-sectional area of the front section of the nose u/c bay.
OUNLBX	Cross-sectional area of the front section of nose u/c bay at any stn X.
OUNWB	Cross-sectional area of the rear section of the nose u/c bay.
OVI	Cross-sectional area of the b.l.diverter stream-tube at intake plane.
OVIX	Cross-sectional area of the b.l.diverter stream-tube at any stn X.
OVIX1	Cross-sectional area of the b.l.diverter splitter at any stn X.
OUMB	Cross-sectional area of a main u/c bay.
OWBB	Cross-sectional area of the center-section of the wing-box.
P	Atmospheric air pressure.
P1	General parameter used in lift-curve-slope estimation.
P2	General parameter used in lift-curve-slope estimation.
P3	General parameter used in lift-curve-slope estimation.
PFA	Fuselage perimeter at stn A.
PFABX	Perimeter of the fuselage section A-B at any stn X.
PFB	Fuselage perimeter at stn B.
PFBCX	Perimeter of the fuselage section B-C at any stn X.
PFC	Fuselage perimeter at stn C.
PFCDI2	Fuselage perimeter at the intake plane.
PFCDX	Perimeter of the fuselage section C-D at any stn X.
PFCDXL	Perimeter of the lower fuselage section C-D at any stn X.
PFCDXU	Perimeter of the upper fuselage section C-D at any stn X.
PFD	Fuselage perimeter at stn D.
PFDEX	Perimeter of the fuselage section D-E at any stn X.
PFE	Fuselage perimeter at stn E.
PFEFX	Perimeter of the fuselage section E-F at any stn X.
PFF	Fuselage perimeter at stn F.
PFFGX	Perimeter of the fuselage section F-G at any stn X.
PFG	Fuselage perimeter at stn G.
PFGHX	Perimeter of the fuselage section G-H at any stn X.
PFHJX	Perimeter of the fuselage section H-J at any stn X.
PFJ	Fuselage perimeter at stn J.
PFJKX	Perimeter of the fuselage section J-K at any stn X.
PFK	Fuselage perimeter at stn K.
PFR	Fuselage perimeter at stn R.
PFRAX	Perimeter of the fuselage section R-A at any stn X.
PFRX	Radome perimeter at any stn X.
PFTABX	Perimeter of windscreen at any stn X between

	stns A and B.	
PFTBCX	Perimeter of canopy at any stn X between stns B and C.	
PFTCDX	Perimeter of canopy at any stn X between stns C and D.	
PGFA	Average perimeter of gun fairing.	EV
PGFX	Perimeter of gun fairing at any stn X.	
PI	3.14	EV
PMUF1X	Perimeter of fuselage-mounted missile no.1 at any stn X.	
PMUF2X	Perimeter of fuselage-mounted missile no.2 at any stn X.	
PMUF3X	Perimeter of fuselage-mounted missile no.3 at any stn X.	
PMUF4X	Perimeter of fuselage-mounted missile no.4 at any stn X.	
PULV	Allowable tyre static load.	
PUMLV	Allowable static load of a main u/c tyre.	
PUMLV1	Estimated maximum static load on each main u/c leg.	
PUMW	Normal pressure of a main u/c tyre.	
PUMW1	Specified maximum pressure for a main u/c tyre.	EV
PUNLV	Allowable static load of the nose u/c tyre.	
PUNLV1	Estimated static load on the nose u/c leg.	
PUNW	Normal pressure of the nose u/c tyre.	
PUNW1	Specified maximum pressure for a nose u/c tyre.	EV
PUW	Normal tyre pressure.	
PWCTR	Reference take-off wing loading.	
Q	Dynamic pressure.	
Q1	Dynamic pressure for V1.	
Q2	Dynamic pressure for V2.	
Q3	Dynamic pressure for V3.	
QC2	Foreplane mid-chord sweep.	
QC4	Foreplane 0.25-chord sweep.	
QCCAN	Canopy centerline inclination above the horizontal.	EV
QCEYE	Pilot's forward and downward view angle measured from the eye-point.	EV
QCFOOT	Angle between the line joining the thigh-heel points and the horizontal.	
QCL	Foreplane L.E. sweep.	EV
QCSEAT	Seat-back angle.	EV
QCST	Total T.E. angle of the foreplane aerofoil.	EV
QCT	Foreplane T.E. sweep.	
QCWSC	Windscreen inclination to the horizontal.	EV
QEF2	Fin mid-chord sweep.	
QEF4	Fin 0.25-chord sweep.	
QEFL	Fin L.E. sweep.	EV
QEFT	Fin T.E. sweep.	
QFPR	Angle between the inner line of the underfuselage recess and the horizontal.	EV
QFPRH	Maximum allowable value of QFPR.	
QFPRU	Angle between the inner line of the upper fuselage recess and the horizontal.	EV
QFPRUH	Maximum allowable value of QFPRU.	
QFRA	Aircraft nose droop angle.	
QW2	Mid-chord sweep of the wing.	
QW21	Mid-chord sweep of the wing or foreplane.	
QW4	Quarter-chord sweep of the wing.	IV
QWA	Aileron L.E. sweep.	

QWB	Wing-box centerline sweep.	
QWL	Wing leading edge sweep.	
QWL1	Leading edge sweep of the wing or foreplane.	
QWPCG	Sweep angle of the imaginary wing-store c.g. line.	
QWST	Total trailing edge angle of the wing aerofoil.	EV
QWST1	Total trailing edge angle of the wing or foreplane aerofoil.	
QWT	Wing trailing edge sweep.	
R1	Engine throttle setting or gross thrust.	
R21	Function used in engine performance estimation.	
R22	Function used in engine performance estimation.	
R41	Function used in engine performance estimation.	
R42	Function used in engine performance estimation.	
RAC	Fraction used in the estimation of the transonic lift-curve-slope of the wing at M=MA.	
RACL	Lower interpolation value of RAC.	
RACU	Upper interpolation value of RAC.	
RAPU	APU density.	EV
RAR	Radar avionics density.	EV
RAX	General avionics density.	EV
RBC	Fraction used in the estimation of the transonic lift-curve-slope of the wing at M=MB.	
RBFN	Ratio ,BETA2/RFBN,used in the estimation of the supersonic lift-curve-slope of the body.	
RCDC	Form factor used in the estimation of the zero lift drag coefficient of the canopy.	
RCDEC	Form factor used in the estimation of the zero lift drag coefficient of the foreplane.	
RCDEF	Form factor used in the estimation of the zero lift drag coefficient of the fin.	
RCDF	Form factor used in the estimation of the zero lift drag coefficient of the fuselage.	
RCDFT	Factor for truncation of pointed afterbody in wave drag calculations.	
RCDK	Sharpness parameter for intake lips in spillage drag estimation.	EV
RCDVK	Factor on K1 to allow for the effects of advanced technology.	EV
RCDW	Form factor used in the estimation of the zero lift drag coefficient of the wing.	
RCECD	Weighting for foreplane mean chord for spanwise variation of Re.	
RCEFD	Weighting for fin mean chord for spanwise variation of Re.	
RCSW	Foreplane volume coefficient.	EV
RCWCD	Weighting for wing mean chord for spanwise variation of Re.	
RD	Relative density of atmospheric air.	
RDFL	Equivalent fineness ratio for the fuselage used in RCDF calculations.	
REFFC	Fin volume coefficient.	EV
RFAIB	Air-brake density.	EV
RFBC	Fineness ratio of the forebody excluding the nose.	
RFBCN	Ratio of RFBC to RFBN.	
RFBN	Fineness ratio of the nose of the body.	
RFIR	Intake ramp density.	EV
RFUL	Fuel density.	EV
RFW	Fuselage structure density.	EV

RGA	Ammunition density.	EV
RGC	Gun density.	EV
RGCL	Empirical thickness correction parameter.	
RGCLL	Lower interpolation value of RGCL.	
RGCLU	Upper interpolation value of RGCL.	
RH	Atmospheric air density at HTH.	
RIDL	Length to inlet depth ratio of the intake diffuser.	EV
RIDLS	Minimum allowable value for RIDL.	EV
RIDX	Corner radius of an intake diffuser at any stnX	
RIDX1	Initial corner radius of an intake diffuser.	EV
RNI	Reynold's number at the intake plane.	
RLDFI	Fineness ratio of the fuselage section from the intake plane to the stn at which OFXH occurs.	
RLDFS	Fineness ratio of the fuselage section from the nose to the intake plane.	
RLDFT	Fineness ratio of the equivalent afterbody.	
RLFD	Weighting for fuselage length to account for Re variation.	
RLMUF	Density of the fuselage-mounted missile launchers.	EV
RLTAFN	Ratio of the axial distance from the end of the center-section to the point at which the decrease in cross-sectional area is half the maximum increment to the length of the aft fairing.	IV
RLTCFN	Ratio of the length of the center-section to length of the fuselage aft of the fwd fairing.	IV
RLTFFN	Ratio of the axial distance from the end of the radome to the point at which the increase in cross-sectional area is half of the maximum increment to the length of the fwd fairing.	IV
RLTMFN	Ratio of the length of the fwd fairing to the overall fuselage length minus the length of the radome.	IV
RLUPCW	U/c c.g. position aft of mean 0.25-chord point as fraction MAC.	EV
RLWBC2	C.g. of central wing-box fuel tank from wing root L.E. / box chord.	
RLWCC	Wing c.g. position aft of mean 0.25-chord point as fraction MAC.	
RMPA1H	Non-dimensional maximum air mass flow rate for the engine.	
RMPF1	Non-dimensional fuel mass flow at combat dry thrust rating, at altitude.	
RMPF2	Non-dimensional fuel mass flow at combat reheat thrust rating.	
RMPF1H	Non-dimensional fuel mass flow at combat dry thrust rating, at 11000 m altitude.	
RMTLFI	Mass proportion of internal fuel remaining in tanks on landing.	EV
RND1	Reynold's number per unit meter.	
RNI	Reynold's number at the intake plane.	
RO	Atmospheric air density at a given altitude.	
ROFNMA	Area ratio, OFK/OFXTH, used in estimation of afterbody drag.	
ROIEI	Fixed area ratio for the intake diffusers.	EV
ROIID	Ratio of the intake capture area to the area of intake stream tube at infinity.	

ROPJ1	Non-dimensional jet exit area at the combat dry thrust rating.	
ROPJ2	Non-dimensional jet exit area at the combat reheat thrust rating.	
ROSL	Atmospheric air density at sea-level.	
RP	Relative pressure of the atmospheric air.	
RPUMLV	Main u/c leg load factor.	EV
RQF	Aircraft ride quality factor.	
RRIID	Ratio of the air density at the inlet to the freestream density.	
RRT	Square-root of RT.	
RRTP	Square-root of RTP.	
RRTPG	Ratio of gross thrusts of the engine (=RTPG/RTPG1).	
RSA	Air systems density.	EV
RSC	Flying control system density.	EV
RSCNW	Ratio of the net foreplane area to gross wing area.	
RSE	Electrics density.	EV
RSF	Fuel system density.	EV
RSLE1	Leading edge sharpness parameter of the wing or foreplane.	
RSLEW	Wing leading edge sharpness parameter.	EV
RSLEC	Foreplane leading edge sharpness parameter.	EV
RT	Relative temperature of atmospheric air.	
RT1	Time required to fly a sortie leg.	
RTC	Thickness to chord ratio of the foreplane.	EV
RTCD	Function of the foreplane thickness to chord ratio used in wave drag estimation.	
RTEF	Thickness to chord ratio of the fin.	EV
RTEFD	Function of the fin thickness to chord ratio used in wave drag estimation.	
RTP	Engine scale factor.	IV
RTPG	Non-dimensional gross thrust of engine at general M and HT.	
RTPG1	Non-dimensional combat dry thrust.	
RTPG1H	Maximum value of RTPG1 at any altitude.	
RTPG2	Non-dimensional combat reheat thrust.	
RTPGW	Aircraft thrust to weight ratio at take-off.	
RTQWT	Ratio, TAN(QWT)/TAN(QWL) ,used in estimation of K1.	
RTW	Thickness to chord ratio of the wing.	IV
RTW1	Thickness to chord ratio of the wing or foreplane.	
RTWD	Function of the wing thickness to chord ratio used in wave drag estimation.	
RXAC	Ratio of the axial distance between the wing-apex and its aerodynamic center to the centerline chord.	
RXACL	Lower interpolation value of RXAC.	
RXACLL	Left lower interpolation value of RXAC.	
RXACLR	Right lower interpolation value of RXAC.	
RXACU	Upper interpolation value of RXAC.	
RXACUL	Left upper interpolation value of RXAC.	
RXACUR	Right upper interpolation value of RXAC.	
RXB	Fraction of LCEYE defining the distance of stn B from the a/c nose.	EV
RXCCQM	Fraction of the fuselage length defining the distance of the mean 0.25-chord point of the foreplane from the aircraft nose.	IV

RXE	Fraction of (XH-XD) defining the distance of stn E from the a/c nose.	EV
RXFCG	Length fraction defining the distance of the c.g. of fuel inside the fuselage, excluding the fuel in the central wing-box.	
RXFR	Fraction of LAR defining the distance of stn R from the a/c nose.	EV
RXGF	Fraction of (XH-XD) defining the distance of the gun from the a/c nose.	EV
RXMUF1	Fraction of (XH-XD) defining the distance of fuselage-mounted missile no.1 from the a/c nose	EV
RXMUF2	Fraction of (XH-XD) defining the distance of fuselage-mounted missile no.2 from the a/c nose	EV
RXMUF3	Fraction of (XH-XD) defining the distance of fuselage-mounted missile no.3 from the a/c nose	EV
RXMUF4	Fraction of (XH-XD) defining the distance of fuselage-mounted missile no.4 from the a/c nose	EV
RXWCQM	Fraction of fuselage length defining the distance of the mean 0.25-chord point of the wing from the a/c nose.	IV
RZCC	Ratio of the foreplane height above the wing-chord plane to the mean geometric chord of the wing.	IV
SC	Gross foreplane area.	
SCN	Net foreplane area.	
SDT	Total time to accelerate over a Mach number increment.	
SEFN	Net area of each fin.	
SEP	Specific excess power.	
SFAIB	Total planform area of airbrakes.	EV
SLEG	Length of a sortie leg in km.	EV
SMSUB	Maximum longitudinal static stability margin, with the aerodynamic center in its most forward position.(Subsonic flight).	
SMSUBA	Longitudinal static stability margin, with the aerodynamic center in its most forward position and the center of gravity in its most aft position.	
SMSUBF	Longitudinal static stability margin, with the aerodynamic center and center of gravity in their most forward positions.	
SMSUP	Maximum longitudinal static stability margin, with the aerodynamic center in its most aft position.(Supersonic flight).	
SMSUPA	Longitudinal static stability margin, with the aerodynamic center and center of gravity in their most aft positions.	
SMSUPF	Longitudinal static stability margin, with the aerodynamic center in its most aft position and the center of gravity in its most forward position.	
SRB1	Release status for stores mounted at wing-pylon no.1.	EV
SRB2	Release status for stores mounted at wing-pylon no.2.	EV
SRB3	Release status for stores mounted at wing-pylon no.3.	EV
SRB4	Release status for stores mounted at wing-pylon no.4.	EV
SRMASS	Total mass of weapons released along the	

	previous sortie-leg.	
SRMUF1	Release status for fuselage-mounted missile no.1.	EV
SRMUF2	Release status for fuselage-mounted missile no.2.	EV
SRMUF3	Release status for fuselage mounted missile no.3.	EV
SRMUF4	Release status for fuselage-mounted missile no.4.	EV
SSPD	Speed of sound.	
STR	Sustained turn rate.	
SUC	Retractable u/c status.	EV
SW	Gross wing area.	IV
SW1	Gross wing or foreplane area.	
SWA	Planform area of the ailerons.	
SWB	Planform area of the wing-box.	
SWBF	Total planform area of the wing-box containing fuel tanks.	
SWF	Planform area of the T.E. flaps.	
SWL	Total planform area of the wing L.E.(fixed & movable).	
SWLF	Planform area of the fixed section of the L.E.	
SWLH	Planform area of the L.E. device (retracted).	
SWN	Net wing area.	
SWN1	Net wing or foreplane area.	
SWTF	Planform area of the fixed section of the wing T.E. aft of the rear spar.	
SWTG	Gross area of the wing T.E. aft of rear spar (including T.E. devices).	
T	Temperature.	
TA	Ambient temperature.	
TERM1B	First term for the estimation of the wing-box mass.	
TERM1F	First term for the estimation of the T.E. flaps mass.	
TERM1L	First term for the estimation of the wing L.E. mass.	
TERM1T	First term for the mass estimation of the fixed T.E. section of the wing.	
TERM2B	Second term for the estimation of the wing-box mass.	
TERM2F	Second term for the estimation of the T.E. flaps mass.	
TERM2L	Second term for the estimation of the wing L.E. mass.	
TERM2T	Second term for the mass estimation of the fixed T.E.section of the wing.	
TERM3B	Third term for the estimation of the wing-box mass.	
TERM3L	Third term for the estimation of the wing L.E. mass.	
TERM3T	Third term for the mass estimation of the fixed T.E. section of the wing.	
TERM4B	Fourth term for the estimation of the wing-box mass.	
TERM4L	Fourth term for the estimation of the wing L.E. mass.	
TERM5B	Fifth term for the estimation of the wing-box mass.	
TERM6B	Sixth term for the estimation of the wing-box	

	mass.	
TERM7B	Seventh term for the estimation of the wing-box mass.	
TERM8B	Eighth term for the estimation of the wing-box mass.	
TH	Temperature above 15 degrees C.	
TOA	Airborne take-off distance to clear a 15 m screen height.	
TOD	Total take-off distance (Ground + airborne).	
TOG	Take-off ground roll distance.	
TPG	Engine gross thrust.	
TPG1	Guess value of the gross thrust required along a sortie leg.	EV
TPG2	Actual value of the gross thrust required along a sortie leg.	
TPGC	Maximum gross thrust of engine.	
TPGD	Maximum sea-level static thrust of the engine with reheat.	
TPGD1	Datum value of TPGD.(Dry)	EV
TPGD2	Datum value of TPGD.(Reheat)	EV
TPGREV	Maximum reverse gross thrust of engine.	
TRATE	Fraction of TPGC available for take-off.	EV
TSL	Ambient temperature at sea-level.	
UC	Gross foreplane taper ratio.	
UCN	Net foreplane taper ratio.	EV
UEFN	Net fin taper ratio.	EV
UFIFDE	Volume utilization factor for the fuel stored inside section D-E.	IV
UFIFEF	Volume utilization factor for the fuel stored inside section E-F.	IV
UFIFFG	Volume utilization factor for the fuel stored inside section F-G.	IV
ULTN	Ultimate load factor for structural design (1.5 x proof factor).	EV
UW	Gross wing taper ratio.	IV
UWB	Taper ratio of the wing-box.	
UWBCF	Volume utilization factor of the center-section of the wing-box for fuel storage.	IV
UWBEF	Exposed wing-box volume utilization factor for fuel storage.	EV
UWCN	Net wing taper ratio.	
UWCN1	Net wing or foreplane aspect ratio.	
UWCNF	Taper ratio of the wing-box fuel tank external to the fuselage.	
V	Aircraft speed.	
V1	First estimate of maximum speed.	
V2	Second estimate of maximum speed.	
V3	Maximum speed.	
VAPR	Approach speed.	
VAPU	APU volume.	
VAR	Radar avionics volume.	
VAX	General avionics volume.	
VCC	Foreplane volume.	
VCKPT	Cockpit volume.	
VD	Maximum design diving speed.	EV
VEFC	Volume of each fin.	
VFAB	Total volume of fuselage section A-B.	
VFABX	Volume of fuselage section A-B up to a stn X.	
VFAIB	Airbrakes volume.	
VFBC	Total volume of fuselage section B-C.	

VFBCX	Volume of fuselage section B-C up to a stn X.	
VFCD	Total volume of fuselage section C-D.	
VFCDX	Volume of fuselage section C-D up to a stn X.	
VFCR	Required fuselage volume.	
VFDE	Total volume of fuselage section D-E.	
VFEF	Total volume of fuselage section E-F.	
VFFG	Total volume of fuselage section F-G.	
VFG	Estimated actual fuselage volume.	
VFGF	Total volume of fuel stored inside the fuselage	
VFGH	Total volume of fuselage section G-H.	
VFHJ	Total volume of fuselage section H-J.	
VFIF	Volume of fuel stored inside the fuselage, excluding any fuel stored in the central wing-box.	
VFIF1	Volume of fuselage section D-E, excluding the corresponding intake diffuser volume.	
VFIF2	Volume of fuselage section E-F, excluding the corresponding intake diffuser volume.	
VFIF3	Volume of fuselage section F-G, excluding the corresponding intake diffuser volume.	
VFIFDE	Volume of fuel stored inside fuselage section D-E, excluding any fuel stored in the center-section of the wing-box.	
VFIFEF	Volume of fuel stored inside fuselage section E-F, excluding any fuel stored in the center-section of the wing-box.	
VFIFFG	Volume of fuel stored inside fuselage section F-G, excluding any fuel stored in the center-section of the wing-box.	
VFIR	Volume of intake ramps.	
VFJK	Total volume of fuselage section J-K.	
VFR	Radome volume (total).	
VFRA	Total volume of fuselage section R-A.	
VFRAX	Volume of fuselage section R-A up to a stn X.	
VFRX	Radome volume up to a stn X.	
VFW	Volume of internal fuselage structure.	
VGA	Ammunition volume.	
VGC	Gun volume.	
VIDC	Total volume of one intake diffuser.	
VIDX	Volume of an intake diffuser up to a stn X.	
VLMUF	Total volume of the fuselage-mounted missile launchers.	
VPBC	Total volume of a single engine bay.	
VSA	Air systems volume.	
VSC	Flying controls volume.	
VSE	Electrics volume.	
VSF	Fuel system volume.	
VSTAPP	Aircraft stall speed in the landing configur.	
VSTTO	Aircraft stall speed in the take-off configur.	
VTGFI	Total internal fuel volume.	
VTLV	Maximum vertical landing velocity.	EV
VTO	Take-off speed.	
VUMB	Volume of a main u/c bay.	
VUNB	Total volume of the nose u/c bay.	
VUNLB	Volume of the front section of the nose u/c bay	
VUNLBX	Volume of the front section of the nose u/c bay at any stn X	
VUNWB	Volume of the rear section of the nose u/c bay.	
VWBB	Volume of the center-section of the wing-box.	
VWBCF	Fuel volume in center-section of the wing-box.	

VWBEF	Fuel volume in wing-box external to the fuselage.	
VWC	Wing volume.	
VXT	Total volume of external tanks.	
VXT1	Volume of external tank no.1.	
VXT2	Volume of external tank no.2.	
WB1	First parameter for the estimation of the supersonic values of KWB and KBW.	
WB2	Second parameter for the estimation of the supersonic values of KWB and KBW.	
WB3	Third parameter for the estimation of the supersonic values of KWB and KBW.	
WB4	Fourth parameter for the estimation of the supersonic values of KWB and KBW.	
WCCAN	Surface area of the canopy.	
WCWSC	Surface area of the windscreen.	
WFAB	Total surface area of fuselage section A-B.	
WFABX	Surface area of fuselage section A-B up to a stn X.	
WFBC	Total surface area of fuselage section B-C.	
WFBCX	Surface area of fuselage section B-C up to a stn X.	
WFCD	Total surface area of fuselage section C-D.	
WFCDX	Surface area of fuselage section C-D up to a stn X.	
WFDE	Total surface area of fuselage section D-E.	
WFEF	Total surface area of fuselage section E-F.	
WFFG	Total surface area of fuselage section F-G.	
WFG	Total surface area of fuselage.	
WFG3	Total footprint area of flying surafaces.	
WFGH	Total surface area of fuselage section G-H.	
WFHJ	Total surface area of fuselage section H-J.	
WFJK	Total surface area of fuselage section J-K.	
WFN	Net total surface area of fuselage.	
WFR	Total surface area of radome.	
WFRA	Total surface area of fuselage section R-A.	
WFRAX	Surface area of fuselage section R-A up to a stn X.	
WFRX	Radome surface area up to a stn X.	
WLCSIF	Foreplane-on-wing lift-curve-slope interference factor.	
WT	Aircraft weight as used in performance estimation methods.	EV
X	Axial distance from the aircraft nose.	
X1	Axial distance of fairing curve stn no.1 from the a/c nose.	
X2	Axial distance of fairing curve stn no.2 from the a/c nose.	
X3	Axial distance of fairing curve stn no.3 from the a/c nose.	
X4	Axial distance of fairing curve stn no.4 from the a/c nose.	
X5	Axial distance of fairing curve stn no.5 from the a/c nose.	
X6	Axial distance of fairing curve stn no.6 from the a/c nose.	
XA	Axial distance of fuselage stn A from the a/c nose.	
XAC06	Axial distance of the aerodynamic center of the aircaft,from the nose at M=0.6.	

XAC14	Axial distance of the aerodynamic center of the aircaft,from the nose at M=1.4.	
XAH	Maximum allowable value for XA.	
XAPUCG	Longitudinal moment arm of the APU.	
XARCG	Longitudinal moment arm of the radar avionics.	
XAXCG	Longitudinal moment arm of the general avionics	
XB	Axial distance of fuselage stn B from the a/c nose.	
XB1CG	Longitudinal moment arm of wing-store no.1.	
XB2CG	Longitudinal moment arm of wing-store no.2.	
XB3CG	Longitudinal moment arm of wing-store no.3.	
XB4CG	Longitudinal moment arm of wing-store no.4.	
XC	Axial distance of fuselage stn C from the a/c nose.	
XCAPEX	Axial distance of the foreplane apex from the a/c nose.	
XCCG	Longitudinal moment arm of the foreplane.	
XCCQM	Axial distance of the mean 0.25-chord point of the foreplane from a/c nose.	
XCCQMH	Maximum allowable value for XCCQM.	
XCCQMS	Minimum allowable value for XCCQM.	
XCICG	Longitudinal moment arm of cockpit equipment.	
XCLB	Distance of the L.E. of the foreplane root from the a/c nose.	
XCPCG	Longitudinal moment arm of the crew.	
XD	Axial distance of fuselage stn D from the a/c nose.	
XE	Axial distance of fuselage stn E from the a/c nose.	
XEFCG	Longitudinal moment arm of the fin(s).	
XF	Axial distance of fuselage stn F from the a/c nose.	
XFCG	Longitudinal moment arm of the fuselage structure and skin.	
XFH	Maximum allowable value for XF.	
XFIFCG	Longitudinal moment arm of fuel stored inside the fuselage.	
XFIFDE	Longitudinal moment arm of fuel stored inside fuselage section D-E.	
XFIFEF	Longitudinal moment arm of fuel stored inside fuselage section E-F.	
XFIFFG	Longitudinal moment arm of fuel stored inside fuselage section F-G.	
XFN	Axial distance of the nozzle exit from the a/c nose.	IV
XFNS	Minimum allowable value for XFN.	
XFOH	Axial distance of the stn at which OFXH occurs from the a/c nose.	
XFOHS	Axial distance of the stn at which OFXHS occurs from the a/c nose	
XFOTH	Axial distance of the stn at which OFXTH occurs from the a/c nose	
XFR	Axial distance of the rear end of the radome from the a/c nose.	
XFS	Minimum allowable value for XF.	
XFSTN	Distance of a fuselage stn from the a/c nose.	
XFWM	Distance of the center of the fuselage volume from the a/c nose.	
XFWM1	First term for the estimation of XFWM.	
XFWM2	Second term for the estimation of XFWM.	

XFXM	Distance of the center of the fuselage area from the a/c nose.
XFXM1	First term for the estimation of XFXM.
XFXM2	Second term for the estimation of XFXM.
XG	Axial distance of fuselage stn G from the a/c nose.
XGACG	Longitudinal moment arm of the ammunition.
XGCG	Longitudinal moment arm of the gun.
XGF	Axial distance of the gun fairing from the a/c nose.
XGFH	Maximum allowable XGF.
XGFS	Minimum allowable XGF.
XH	Axial distance of fuselage stn H from the a/c nose.
XII	Axial distance of the air intake plane from the a/c nose.
XJ	Axial distance of fuselage stn J from the a/c nose.
XK	Axial distance of fuselage stn K from the a/c nose.
XLMCG	Longitudinal moment arm of fuselage-mounted missile launchers.
XM1CG	Longitudinal moment arm of fuselage-mounted missile no.1.
XM2CG	Longitudinal moment arm of fuselage-mounted missile no.2.
XM3CG	Longitudinal moment arm of fuselage-mounted missile no.3.
XM4CG	Longitudinal moment arm of fuselage-mounted missile no.4.
XMUF1	Axial distance of fuselage-mounted missile no.1 from a/c nose.
XMUF1H	Maximum allowable XMUF1.
XMUF1S	Minimum allowable XMUF1.
XMUF2	Axial distance of fuselage-mounted missile no.2 from a/c nose.
XMUF2H	Maximum allowable XMUF2.
XMUF2S	Minimum allowable XMUF2.
XMUF3	Axial distance of fuselage-mounted missile no.3 from a/c nose.
XMUF3H	Maximum allowable XMUF3.
XMUF3S	Minimum allowable XMUF3.
XMUF4	Axial distance of fuselage-mounted missile no.4 from a/c nose.
XMUF4H	Maximum allowable XMUF4.
XMUF4S	Minimum allowable XMUF4.
XP1	Axial distance of the engine compressor face from the a/c nose.
XP2	Axial distance of the engine turbine exit from the a/c nose.
XP3	Axial distance of the engine afterburner exit from the a/c nose.
XP4	Axial distance of the engine nozzle exit plane from the a/c nose.
XPBCG	Longitudinal moment arm of the engine gas generator.
XPICG	Longitudinal moment arm of the engine installation.
XPRCG	Longitudinal moment arm of the engine reheat section.

XPTCG	Longitudinal moment arm of the engine thrust reverser.	
XSACG	Longitudinal moment arm of the air systems.	
XSCCG	Longitudinal moment arm of the flying controls.	
XSECG	Longitudinal moment arm of the electrics.	
XSFCG	Longitudinal moment arm of the fuel system.	
XTACG	Aft longitudinal c.g. position of the aircraft.	
XTECG	Aircraft longitudinal c.g. position with empty internal fuel tanks,no external stores, no ammunition.	
XTEWCG	Aircraft longitudinal c.g. position with empty internal or external fuel tanks,with external stores plus ammunition.	
XTFCG	Fwd longitudinal c.g. position of the aircraft.	
XTTCG	Aircraft longitudinal c.g. position with full internal fuel tanks,no external stores, no ammunition.	
XTTWCG	Aircraft longitudinal c.g. position with full internal or external fuel tanks,external stores plus ammunition.	
XUMCG	Longitudinal moment arm of the main u/c.	
XUNBF	Axial distance of the fwd end of the nose u/c bay from a/c nose.	
XUNCG	Longitudinal moment arm of the nose u/c.	
XV	Engine throttle setting,or,gross thrust.	EV
XVE	Axial distance of the b.l.diverter exit from the a/c nose.	
XWAPEX	Axial distance of the gross wing apex from the a/c nose.	
XWBCCG	Longitudinal moment arm of the fuel in the central wing-box.	
XWBECG	Longitudinal moment arm of the fuel in the wing-box external to the fuselage.	
XWCG	Longitudinal moment arm of the wing.	
XWCQM	Axial distance of the wing mean 0.25-chord point from a/c nose.	
XWLB	Distance of the L.E. of the wing root from the a/c nose.	
YB1	Lateral c.g. position of wing-store no.1.	
YB2	Lateral c.g. position of wing-store no.2.	
YB3	Lateral c.g. position of wing-store no.3.	
YB4	Lateral c.g. position of wing-store no.4.	
YCCANC	Y-coordinate of the canopy at stn C.	EV
YCCAND	Y-coordinate of the canopy at stn D.	
YCCANX	Y-coordinate of the canopy at any stn X.	
YCPG	Spanwise position of the center of pressure of the gross wing.	
YCPX	Spanwise position of the center of pressure of the net wing.	
YCWSCB	Y-coordinate of the windscreen at stn B.	
YCWSCX	Y-coordinate of the windscreen at any stn X.	
YFABX	Y-coordinate of the fuselage section A-B at stn X.	
YFABXS	Minimum allowable YFABX.	
YFBCX	Y-coordinate of the fuselage section B-C at stn X.	
YFBCXS	Minimum allowable YFBCX.	
YFCDX	Y-coordinate of the fuselage section C-D at stn X.	
YFCDXS	Minimum allowable YFCDX.	

YFDEX	Y-coordinate of the fuselage section D-E at stn X.
YFDEXS	Minimum allowable YFDEX.
YFE2	Y-coordinate of the fuselage spine at stn E.
YFE2X	Y-coordinate of the fuselage spine at any stn X of section D-E.
YFEFX	Y-coordinate of the fuselage section E-F at stn X.
YFEFXS	Minimum allowable YFEFX.
YFF2	Y-coordinate of the fuselage spine at stn F.
YFFGX	Y-coordinate of the fuselage section F-G at stn X.
YFFGXS	Minimum allowable YFFGX.
YFG2X	Y-coordinate of the fuselage spine at any stn X of section F-G.
YFGHX	Y-coordinate of the fuselage section G-H at stn X.
YFGHXS	Minimum allowable YFGHX.
YFHJX	Y-coordinate of the fuselage section H-J at stn X.
YFHJXS	Minimum allowable YFHJX.
YFJKX	Y-coordinate of the fuselage section J-K at stn X.
YFJKXS	Minimum allowable YFJKX.
YFR	Y-coordinate of the fuselage at stn R.
YFRAX	Y-coordinate of the fuselage section R-A, from its axis at any stn X.
YFRX	Y-coordinate of the radome, from its axis at a stn X.
YIDCX	Y-coordinate of the intake diffuser center-line at any stn X.
YIDIX	Y-coordinate of the inner line of the intake diffuser at any stn X.
YIDOX	Y-coordinate of the outer line of the intake diffuser at any stn X.
YPCH	Distance between the engine centerlines.
ZCCANX	Z-coordinate of the canopy at any stn X.
ZCCANC	Z-coordinate of the canopy at stn C.
ZCWSCB	Z-coordinate of the windscreen at stn B.
ZCWSCX	Z-coordinate of the windscreen at any stn X.
ZFR	Z-coordinate of the fuselage at stn R.
ZFRAX	Z-coordinate of the fuselage section R-A at any stn X.
ZFRX	Z-coordinate of the radome, at any stn X.
ZIDCX	Z-coordinate of the centerline of the intake diffuser at any stn X.
ZIDLX	Z-coordinate of the lower line of the intake diffuser at any stn X.
ZIDUX	Z-coordinate of the upper line of the intake diffuser at any stn X.
ZPC	Height of the engine centerline above the flat bottom surface of the fuselage.

CHAPTER 1

INTRODUCTION

1.1 AIRCRAFT DESIGN SYNTHESIS

Aircraft Design Synthesis is the process which interfaces all the preliminary design methods, constraints and decisions which lead to the definition and analysis of a new aircraft configuration and its characteristics. This is therefore a long and complex process which involves a large number of analytical and empirical calculations for the sizing and geometry of the aircraft and its major components, the prediction of its mass and volume and the estimation of its aerodynamics, stability and performance.

1.2 OPTIMIZATION

The Design Synthesis process is normally subjected to a Multivariate Optimization (MVO) in oder to produce an optimum configuration to meet a given requirement. For this purpose , a set of variables in the mathematical model of the aircraft are initially chosen to be at the disposal of the optimization algorithm. These are known as Independent Variables. They are assigned with initial values and then the Design Synthesis process is carried out and the selected objective functions and constraints are evaluated. The results are compared by the optimizer against their corresponding predefined optimum values to assess the progress of optimization. If any discrepancies exist, the initial values of the Independent Variables are appropriately revised and the Design Synthesis is repeated until a satisfactory optimum configuration is produced. Several such iterations are normally required.

1.3 BACKGROUND

This need for correct and accurate repetition of this long and complex process, in a short time with minimum effort, led some aircraft manufacturers and research

institutions to the development of computerised Design Synthesis and optimization systems. Some examples of such systems are described in refs. 17 - 23. Systems are often based on the design methods and experience of each organization, the available computational facilities and the state-of-the-art at the time of its development. Therefore every system incorporates a different degree of complexity and level of sophistication and it is usually applicable to a specific class of aircraft, limited by a number of constraints.

The Royal Aircraft Establishment (Farnborough) has been studying MVO since 1970. The initial work concentrated on transport aircraft design synthesis the latest version of which is described in ref. 19. Work on the application of MVO to combat aircraft design began in 1976. As part of these studies, a Design Synthesis was produced in 1980, for conventional high-wing, aft-tail, single-engine, combat aircraft with side air intakes and trapezoidal, aft-swept, fixed geometry wings (ref.1). A twin-engine version was also produced a year later (ref.18). This initial system was designed with a number of constraints to limit its complexity. Some of the methods used, were therefore simplified and this reduced the system's sensitivity to configurational changes. The need for a more sophisticated and flexible Design Synthesis, complementary to the existing system was then anticipated in the concluding remarks of ref.17. The rapidly changing design requirements and the increasing interest in canard-delta layout with the forthcoming European Fighter Aircraft (EFA), finally led to a proposal for the development of a new Design Synthesis and analysis system, suitable for use with canard-delta configuration combat aircraft. This is the subject of this Research Programme.

1.4 ADVANTAGES OF THE CANARD-DELTA LAYOUT

The ever increasing emphasis on supermanoeuvrability and performance recently led to the widespread application of the close-coupled canard-delta layout in advanced combat aircraft design. This layout, which has become practically feasible today due to major advances in fly-by-wire technology coupled with artificial stability, offers superior aerodynamic and performance advantages over its conventional aft-tail counterparts (refs. 24 - 29).

The close proximity of the foreplane produces favourable interference which enhances the lift on the delta wing at high angles of attack and delays the onset of the stall. The total maximum lift of the combined surfaces is typically 20 - 30% higher than the sum of the isolated lift values. This favourable effect confers high attained manoeuvrability for air-to-air combat. In subsonic flight, this layout produces a lightly-loaded foreplane and lift/drag ratios similar to those of an efficient aft-tail configuration. In supersonic flight, the positive lift yields a higher lift/drag ratio than a conventional aircraft with a down-loaded tailplane. This results in better cruise performance and sustained manoeuvrability. With the wing flaps lowered, the foreplane trim-load adds to the total lift allowing lower take-off and landing speeds and hence shorter distances. The absence of the tailplane produces a clean afterbody and therefore reduces drag. The configuration is inherently more suitable for active ride control due to the positive foreplane lift.

1.5 RESEARCH PROGRAMME OBJECTIVES

This two-year Research Programme funded by the Ministry of Defence/Royal Aircraft Establishment (Farnborough), started in October 1985 with the main

objective being the development of a computerised Design Synthesis and analysis system suitable for use with canard-delta configuration combat aircraft.

According to the RAE requirements, the proposed system would not be concerned with optimization but it would concentrate on the Design Synthesis process. Any proposed modules, however, would be compatible with the general requirements for use with RAE numerical optimization algorithms. The system would also use, wherever possible, modules of the existing RAE system (ref.1). All data supplied by the RAE should be effectively unclassified. As the main use of the proposed system is concerned with performance, consideration of stability and control aspects would be limited to those that significantly affect the aircraft layout. The Design Synthesis would be automatically implemented by a modular computer program written in standard FORTRAN 77 which would also contain simple 2-D graphics suitable for producing simple general arrangement drawings of the synthesized aircraft. The use of GINO-F would be investigated for this purpose. The Design Synthesis would specifically apply to advanced close-coupled, cropped delta-canard configurations and would therefore provide suitable solutions to special preliminary design problems associated with the new canard-delta layout and the introduction of new technology in combat aircraft design. The Research Programme would therefore also include a detailed investigation into the canard-delta interference effects on the aircraft aerodynamics. At a subsequent stage, the effects of single or twin fins and various air intake locations would be investigated. The proposed system would be accurate, efficient, flexible and sensitive to configurational changes.

1.6 BASELINE LIMITATIONS

The RAE(F) also set a number of limitations on the baseline aircraft.

The proposed system would use a baseline aircraft having a low-wing, twin engines, and chin air intakes. The aircraft would use conventional take-off and landing techniques. The aim would be to be able to scale this baseline in terms of engine scale factor over the range 0.5 - 2.0. Further detailed limitations were agreed with RAE(F) at a later meeting which led to a full definition of the baseline aircraft, described in chapter 2.

CHAPTER 2

BASELINE AIRCRAFT DESIGN

2.1 INTRODUCTION

The Research Programme started with a preliminary investigation into the aerodynamics, performance, packaging and weapon requirements for advanced combat aircraft, which led to the initial design of a baseline canard-delta configuration. The baseline design went through several transformations before it was frozen, during which fundamental design decisions and compromises were made. The final configuration which formed the basis for the development of the Synthesis was designed to offer maximum geometric flexibility with minimum constraints.

The baseline aircraft and all the assumptions and decisions made in its design are presented in detail in the following sections of this chapter.

2.2 GENERAL DESCRIPTION OF THE BASELINE AIRCRAFT

The baseline aircraft has a low cropped delta wing with an all-moving, closely coupled foreplane located above the wing-chord plane and behind the cockpit. A single fin is located on the flat upper surface of the fuselage afterbody. A twin fin option is also provided. The fuselage is aerodynamically shaped for minimum supersonic drag. Chin air intakes with limited variable geometry supply a continuous and undistorted flow of air to the engines through two smooth 'S' - shaped diffusers. Propulsion is provided by two low-bypass ratio, reheated turbofans, fitted with thrust reversers. An advanced high - 'g' cockpit is used with an inclined ejection seat, raised heel platform and bubble canopy. The undercarriage is designed for operation from semi-prepared runways. Four semi-submerged medium range missiles and a single-barrel gun are fitted under the fuselage. A combination of stores may

be carried on four wing-pylons. The aircraft is equipped with the latest state-of-the-art systems, including fly-by-wire or fly-by-light, auxiliary power unit, radar, sophisticated avionics and cockpit displays. Both composite and metal structural materials are used. The aircraft has good STOL performance, is highly manoeuvrable and capable of speeds in excess of Mach 2.0.

Five different views of the baseline configuration are presented in fig.2.1.

2.3 DESIGN ASSUMPTIONS AND DECISIONS

2.3.1 Fuselage

The fuselage is designed to have an optimum longitudinal cross-sectional area distribution for minimum wave drag. Eleven principal fuselage stations are defined as shown in fig. 2.1 (Stations: R, A, B, C, D, E, F, G, H, J, K). The letter I is deliberately ommitted in the notation for the principal stations because it is used to denote the intake plane location. The position of each principal station usually coincides with a significant point of the aircraft anatomy. Station R coincides with the position of the radar antenna while station A is located at the forward cockpit bulkhead. Station B is at the lower rear end of the windscreen and C at the pilot's eye position. Station D coincides with the rear end of the canopy. Station E is aft of the foreplane root-chord and F is aft of the front underfuselage missiles and gun. Station G is located upstream of the engine compressor inlet at a distance equal to its diameter. Station H coincides with the turbine exit, J with the afterburner exit and K with the nozzle exit.

The above principal stations divide the fuselage into eleven sections. These are the radome, R-A, A-B, B-C, C-D,

D-B, B-F, F-G, G-H, H-J, and J-K, as shown in fig. 2.1. The fuselage geometry varies uniformly along each section and successive sections blend uniformly together.

The cross-sectional shape of the fuselage at the eleven principal stations is shown in fig. 2.1. The shape is fully elliptical at stations R and A while at all the other stations it is described by a series of straight lines and elliptically-shaped corners. The ellipses and elliptical corners were incorporated in the fuselage cross-sectional shape because of their high geometric flexibility. A wide variety of cross-sectional shapes may be produced during the Design Synthesis by adjusting the axes of the elliptic corners in conjunction with the defined straight lines. The combination of lines and corners at each principal station was carefully determined during the development of the baseline configuration, so that the transition from curved to flat fuselage surfaces or vice-versa, is always uniform.

The size of the fuselage cross-section at station R is defined by the size and working clearances of the radar antenna. The coordinates of the radome and section R-A are assumed to vary in the form of a power series cylinder function, for minimum wave drag. The common axis of these two sections is drooped to provide a clear visual path from the pilot's eye point.

It is assumed that the upper elliptical fuselage corners begin to form at station A (See side view in fig. 2.1). The corner height decreases linearly between stations A and D, remains constant along section D-E and increases linearly again, between stations E and G. From station G to station K, the upper corners are assumed to start at the height of the engine centreline. The lower elliptical corners of the forward fuselage begin at station

A and their height reduces linearly to zero at the boundary layer diverter exit. Lower fuselage corners begin again to form at G and their height increases linearly until they blend with the upper corners at station K.

The underfuselage surface between stations D and H, is flat and serves as a weapon carriage platform. From H to K, the underfuselage surface converges towards the engine nozzles. An underfuselage recess begins to form at station G and extends up to station K, increasing linearly in both width and depth.

The fuselage height relative to the flat aircraft belly is asumed to remain constant along the sections A-B, B-C and C-D. From D to K, it decreases linearly down to the height of the engine bay at the afterburner exit. Hence, a low engine position, increases the slenderness of the afterbody.

A flat surface begins to form on the upper fuselage, along the aircraft centreline, which increases linearly in width along section G-H. Its width becomes and remains equal to the distance between the engine centrelines along section H-J. This flat surface minimizes the drag at the fin root. The fuselage spine begins at station B, and its height relative to the upper fuselage surface increases linearly to a maximum at station D and then decreases again until it blends with the flat upper fuselage surface at station G. The width of the spine is also assumed to decrease linearly from a maximum at B to zero at G (See plan view fig. 2.1). Fuselage section J-K has an upper recess which begins to form at station J and increases linearly in both depth and width along J-K.

The fuselage width is assumed to vary linearly along section D-E in order to allow free rotation of the all

moving foreplane. The extent of flatness of the sides of section D-E depends on the height of the upper elliptical corners.

All the above assumptions formed the basis for the development of the mathematical models describing the fuselage geometry.

2.3.2 Wing

The baseline aircraft uses a fixed geometry, low, cropped delta wing which has low taper, aspect and thickness to chord ratios. It is assumed that the wing has zero twist, zero dihedral and zero wing-body angle. It uses no leading-edge devices but only plain trailing-edge flaps and ailerons. The thickness to chord ratio is assumed to remain constant along the wing-span. The wing has a straight supersonic leading-edge and a slightly forward-swept trailing-edge. An investigation into delta wing planforms showed that an equivalent wing with the same area, aspect ratio, taper ratio and span but with a subsonic leading-edge results in an aft swept trailing-edge. This reduces the effectiveness of the trailing-edge devices. Similarly, a wing with a subsonic leading-edge but with a lower taper ratio and hence an approximately unswept trailing-edge results in a long net wing root chord which imposes unwanted limitations on the minimum length of the fuselage. A delta wing with a supersonic leading-edge, however, does not present such problems and it is therefore more favourable.

2.3.3 Foreplane

It is assumed that the axis of rotation of the all moving foreplane passes perpendicularly through its net mean quarter-chord point. The foreplane surfaces are driven by separate but symmetrically operated actuators. The axis of

rotation of the foreplane is assumed to be always within section D-E. The foreplane is located in close proximity to the wing and above the wing-chord plane in order to induce the desired close-coupled canard-delta interference. It is located aft of the cockpit in order to maintain an excellent all-round visibility from the pilot's eye point. A more forward position for the foreplane on this baseline aircraft would not only degrade the all-round visibility but would also lead to a long-coupled canard-delta configuration which is outside the scope of this Design Synthesis. This is due to the adopted low wing concept and chin intakes which physically limit the foremost position of the wing leading-edge at the fuselage side, around station D. A forward foreplane position would only be possible with a mid-wing concept and the use of leading-edge extensions, both of which were clearly excluded from the RAE requirements for this Synthesis.

As for the wing, the foreplane is assumed to have zero twist, zero dihedral and a constant thickness to chord ratio along its span. It also has low taper, aspect and thickness to chord ratios.

2.3.4 Fin(s)

The baseline aircraft uses a large single fin with low taper and thickness to chord ratios. Twin fins may be also used alternatively. The trailing-edge of the fin(s) is always assumed to intersect the fuselage at station J.

A single tall fin may easily maintain the directional stability of the aircraft at high angles of attack.Twin fins are low and rigid compared to an equivalent single fin which is tall and flexible. Their reduced height results in less torque on the fuselage and less susceptibility to flutter. It also allows the use of low hangars which is particularly

desirable on aircraft carriers. A further advantage is that the availability of a second fin increases the aircraft's combat survivability. From the aerodynamics point of view, there is always a vertical surface in relatively clean flow to provide directional stability, regardless of the angle of attack/sideslip combination.

It is assumed that whenever twin fins are used, extra structure is added to the fuselage, to support them. The lateral separation between the two fins should be enough to overcome the mutual aerodynamic interference.

2.3.5 Intake

A twin rectangular chin air intake is used with limited variable geometry at the lower intake lips. This type of intake is ideal for highly manoeuvrable combat aircraft because it provides a high pressure recovery and low distortion at high angles of attack due to the aerodynamic shielding provided by the forward fuselage. For this reason the total inlet width of the intake plane is constrained not to exceed the local fuselage width and the maximum forward position of the intake plane is limited up to station C.

A smoothly curved F-16 type intake was also investigated during the design of the baseline aircraft but it was finally rejected due to its unsuitability for limited variable geometry at the lower lips.

2.3.6 Boundary layer diverter

The height of the b.l. diverter is assumed to remain constant from entry to exit and the width of the splitter plate is assumed to vary in a sinusoidal form along its

length. These assumptions are based on several combat aircraft observations and they are in agreement with ref.1.

2.3.7 Intake diffusers

Two smooth S-shaped diffusers are used which at the intake plane have rectangular cross-sections with small corner radii. The rectangular cross-sectional shape of each diffuser gradually changes along its length until it becomes fully circular at station G, with a diameter equal to that of the compressor inlet. The length to depth ratio of each diffuser is maintained within specified minimum and maximum values to prevent any losses due to internal airflow separation. As the depth of the diffusers at the intake plane increases however, the overall aircraft height increases too, because the chin air intake must be maintained above a certain minimum height from the ground in order to prevent any ingestion of foreign matter, that may lead to engine damage. It is assumed that the diffuser height gradually increases between the intake plane and station G. The diffuser width is assumed to remain constant between the intake plane and station E. Between these stations and station G the shape of the diffuser lines is assumed to vary smoothly both laterally and vertically, in the form of a sinusoidal function.

2.3.8 Engines

Propulsion is provided by two low by-pass ratio, reheated military turbofans, fitted with thrust reversers and conventional variable geometry exhaust nozzles. The engine centreline height above the underfuselage surface is kept to a minimum in order to improve the slenderness of the fuselage afterbody. This minimum is defined by the height of the main undercarriage bay, the engine diameter at the compressor inlet and the corresponding engine bay height

clearance. The engines are latterally separated and a firewall is assumed to exist between them.

Four principal engine stations are defined for use in the Synthesis. Station no.1 coincides with the compressor inlet, no.2 with the turbine exit, no. 3 with the afterburner exit and no. 4 with the nozzle exit.

2.3.9 Engine bays

Each engine bay is assumed to have an elliptical cross-sectional shape defined by a set of height and width clearances at each principal engine station. Its cross-sectional dimensions between successive engine stations are assumed to vary linearly along its length. The engine bay clearances depend on maintainability criteria and on the specified engine envelope which includes the accessories around the engine.

2.3.10 Cockpit

The baseline aircraft has an advanced, single-seat, high-'g' cockpit. It is equipped with an inclined ejection seat at an angle greater than 30 degrees and a raised heel platform, which increase the pilot's 'g'-tolerance. The pilot is seated at the highest point of the aircraft, for good all-round visibility. For this purpose the aircraft is equipped with a bubble canopy which also allows good rearward and downward visibility. The cross-sectional shape of the canopy is assumed to be semi-elliptical and its longitudinal curvature is described by a power series cylinder function. The windscreen has also semi-elliptical cross-sectional shape and a slope of about 30 degrees for clear and undistorted over the nose visibility.

2.3.11 Undercarriage

The main and nose undercarriage legs are fitted with single wheels and oleo-pneumatic shock absorbers. An optimum static load distribution is assumed between the nose and main undercarriage. The nose undercarriage is located aft of the intake plane in order to prevent the ingestion of any foreign matter into the intakes. This however, limits the maximum wheelbase and also requires extra space under the intake diffusers for a nose undercarriage bay. These problems are partially alleviated by the adopted nose undercarriage retraction concept. The nose undercarriage pintle is located near the forward end of the bay in order to utilize the maximum possible wheelbase and the undercarriage retracts backwards while simultaneously rotates the nose wheel 90 degrees in order to minimize the depth of the nose undercarriage bay. In order to improve the intake fairing aerodynamics, the depth of the front section of the bay which accommodates the leg, increases gradually as shown on the side view of the baseline aircraft in fig. 2.1. The intake lips are joined with the forward end of the nose undercarriage bay by a separate fairing.

The main undercarriage pintles are located near the rear walls of the main undercarriage bays. The legs retract forward and the wheels are rotated 90 degrees in order to reduce the depth of the rectangular bays.

It is assumed that the associated hydraulics are also installed inside the undercarriage bays.

2.3.12 Underfuselage weapons

The baseline aircraft carries up to four medium range air to air missiles, semi-submerged into the flat underfuselage surface between stations D and H. It is also

equipped with a single barrel gun. (See lower plan view, fig. 2.1). the depicted arrangement of the four AMRAAM's was dictated by the presence of the undercarriage bays and by the need for adequate space for the installation of the missile launchers. The longitudinal overlap between the rear missiles allows them to be installed closer to each other in order to allow adequate space for the main undercarriage bays. The front missiles and gun are assumed to be located between stations D and F and the rear missiles between F and H.

The underfuselage missiles are numbered (1 - 4) from port to starboard.

Three possible gun locations were investigated during the design of the baseline aircraft. The first was over the aircraft nose. This was rejected mainly because of the adverse effects of the gun-blast on the radar avionics and the need for a long nose. The second location considered, was in the upper port corner of fuselage section D-E, but that had several disadvantages; a clear gun firing line could not be easily established because of the local fuselage shape; rearming was poor because of the high location of the gun; the presence of the foreplane just underneath the gun could prove hazardous; an extra electronic flight control device was required to automatically counteract any aircraft attitude changes due to gun recoil and blast loads. The third and finally selected gun location was under the intake diffusers and aft of the nose undercarriage bay. The single barrel is protruding under the flat fuselage surface and is covered by a smooth fairing for minimum drag. The gun is on the aircraft centre-line and it is directly accessible from the ground. The ammunition drum and bin, are located inside the fuselage.

2.3.13 Wing-stores

A combination of different types of stores may be carried on four wing-pylons, numbered 1 - 4 from port to starboard. Stores of the same type may be mounted in pairs on a single pylon, in tandem or in parallel. External fuel tanks may be mounted on pylons no. 2 and 3.

2.3.14 Internal fuel tanks

It is assumed that fuel is stored in the centre section of the wing-box and in the wing-box external to the fuselage. Fuel tanks are also located in fuselage sections D-E. E-F and F-G.

SIDE VIEW

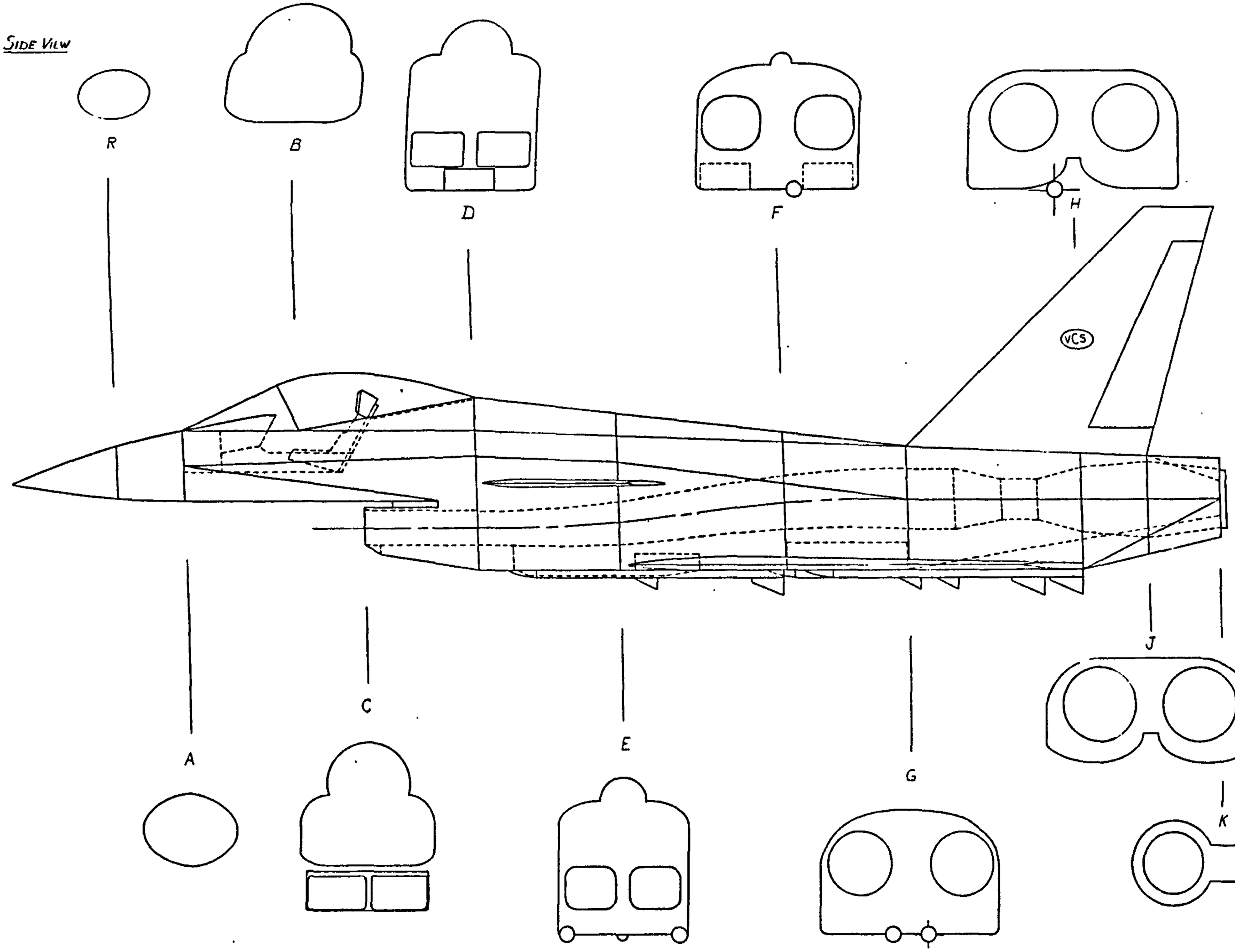

FIG.2.1 BASELINE CONFIGURATION DRAWINGS

DRAWN	CHK'D	APP'D	SCALE	TITLE:- CANARD/DELTA COMBAT AIRCRAFT (BASELINE CONFIGURATION)
SERGHIDES V.			1:25	

COLLEGE OF AERONAUTICS
CRANFIELD INSTITUTE OF TECHNOLOGY
CRANFIELD.

DRAWING No.

SHT / OF 4 SHEETS

PLAN VIEW

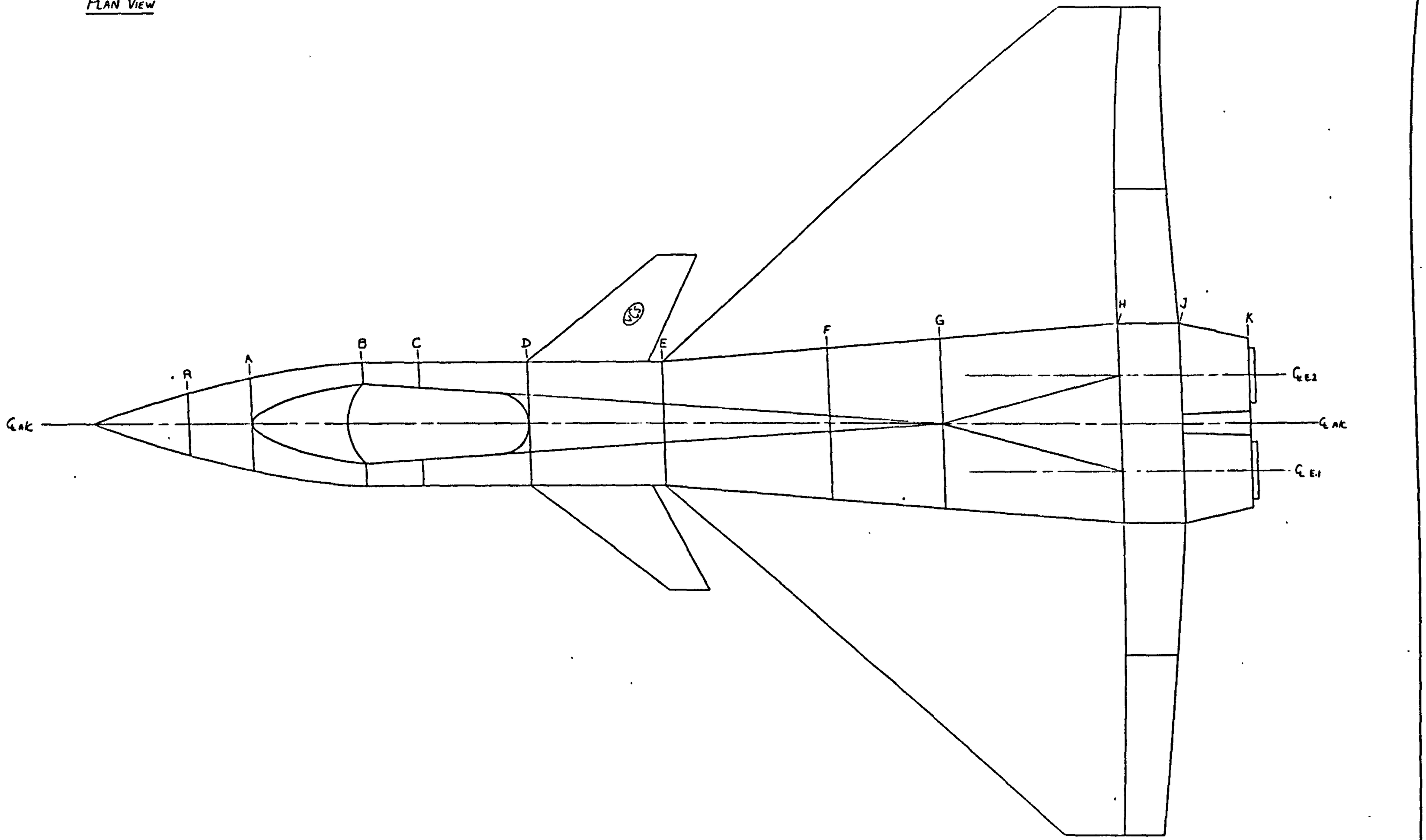

FIG.2.1 (Continued ...)

DRAWN	CHK'D	APP'D	SCALE	TITLE:-CANARD/DELTA COMBAT AIRCRAFT (BASELINE CONFIGURATION)
SEAGHDES'd			1:25	
COLLEGE OF AERONAUTICS CRANFIELD INSTITUTE OF TECHNOLOGY CRANFIELD.				DRAWING No
				SHT 2 OF 4 SHEETS

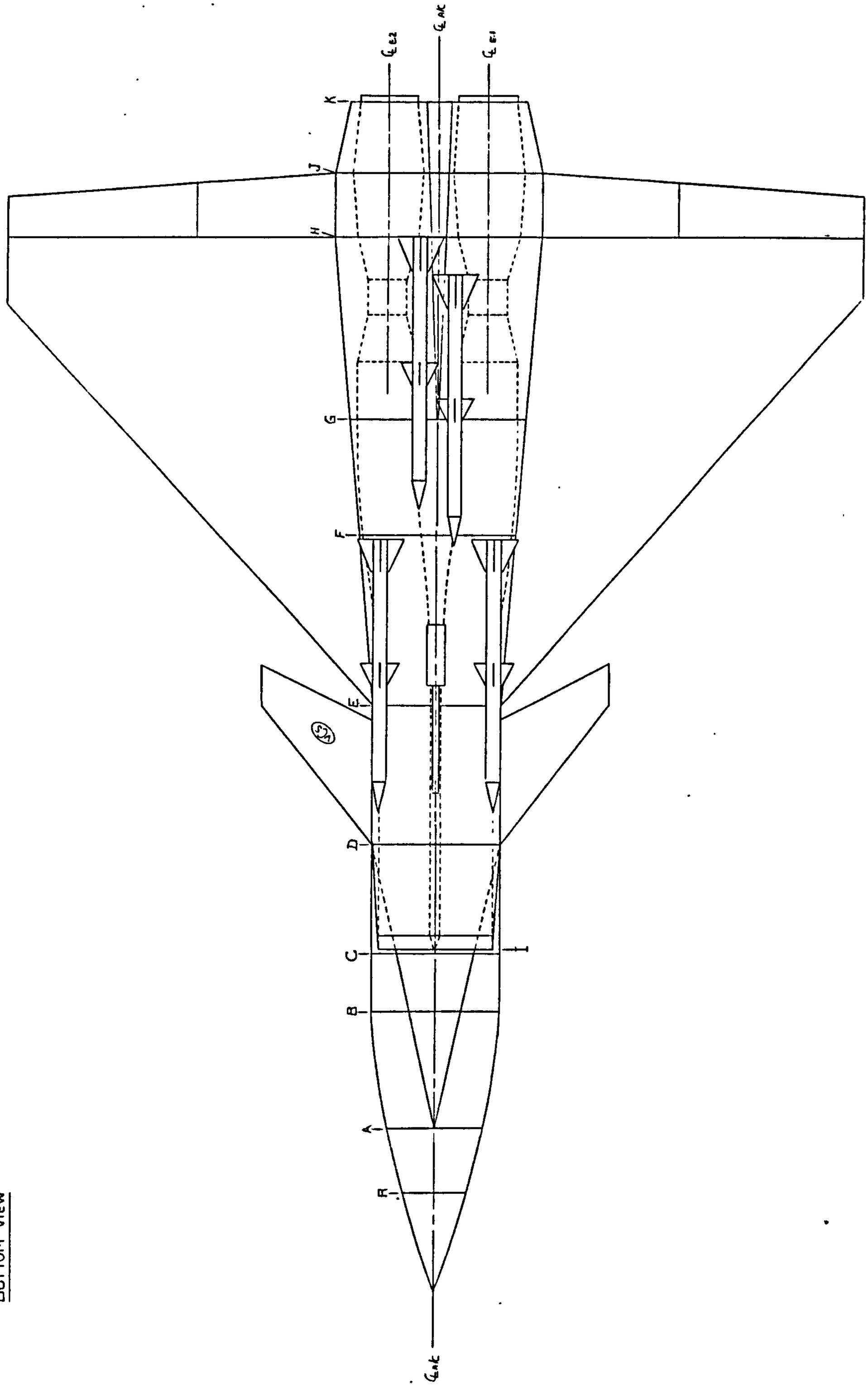

BOTTOM VIEW

FIG.2.1 (Continued ...)

DRAWN	CHK'D	APP'D	SCALE	TITLE:-CANARD/DELTA COMBAT AIRCRAFT (BASELINE CONFIGURATION)	DRAWING No.	SHT 3 OF 4 SHEETS
SEMSHOF'S			1:25			

COLLEGE OF AERONAUTICS
CRANFIELD INSTITUTE OF TECHNOLOGY
CRANFIELD.

FRONT VIEW

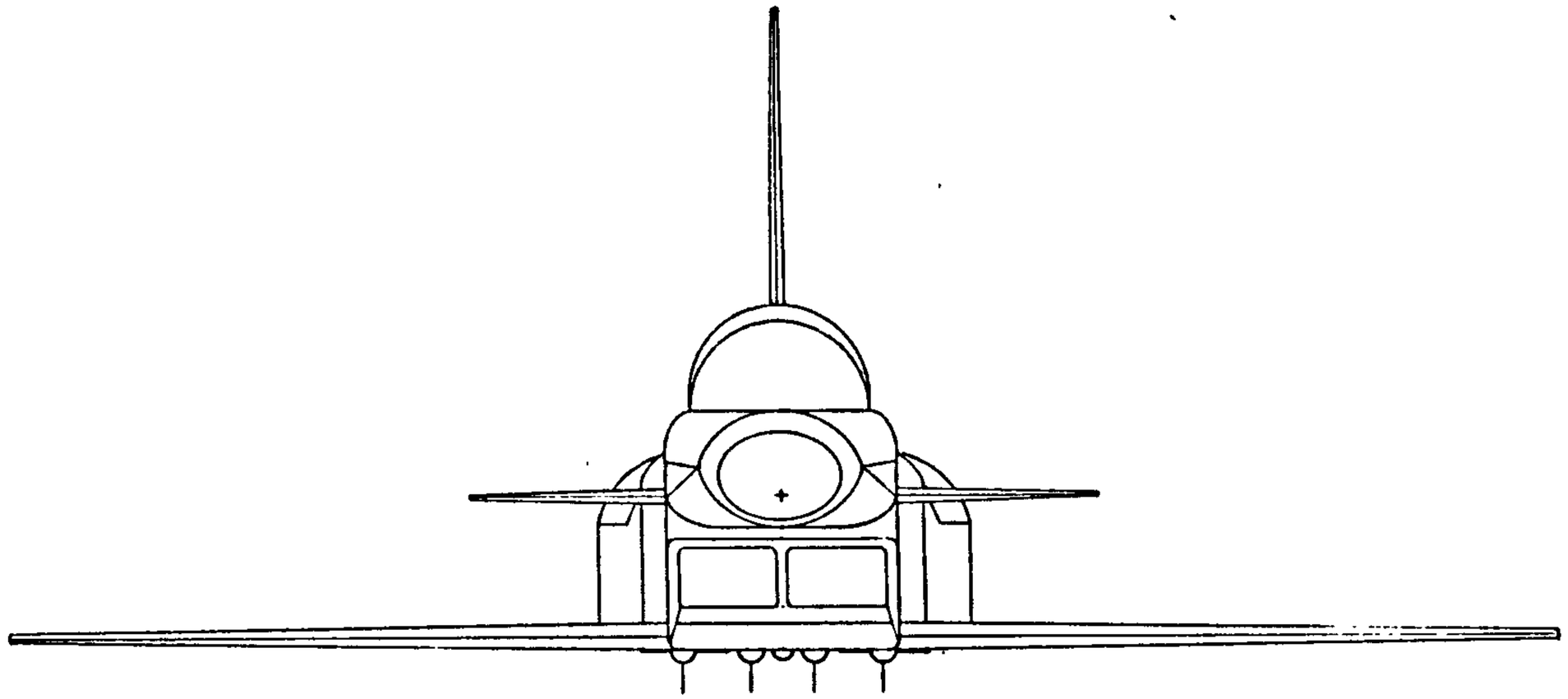

VCS

REAR VIEW

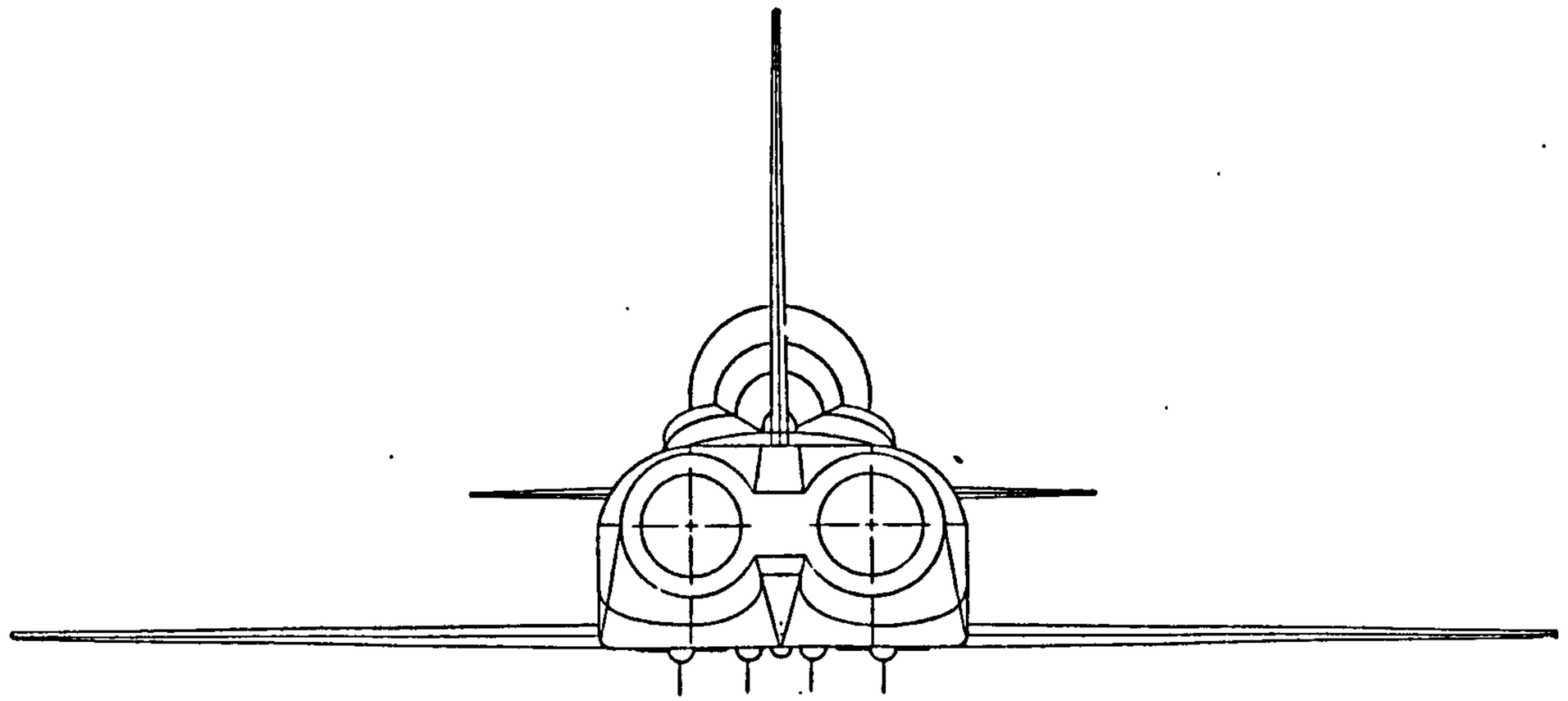

DRAWN	CHK'D	APP'D	SCALE	TITLE:-CANARD/DELTA COMBAT AIRCRAFT (BASELINE CONFIGURATION)
A.ERGHIDES V.			1:25	
COLLEGE OF AERONAUTICS CRANFIELD INSTITUTE OF TECHNOLOGY CRANFIELD.				DRAWING No.
				SHT 4 OF 4 SHEETS

FIG.2.1 (Continued)

CHAPTER 3

AIRCRAFT GEOMETRY

3.1 INTRODUCTION

The aircraft geometry is a major and fundamental section of the overall Design Synthesis process. It defines the shape of the aircraft and determines its detailed dimensions and any other geometric characteristics which are essential for the subsequent packaging, aerodynamics and performance calculations. These calculations are in reality very sensitive to configurational changes. An important objective in this Research Programme was therefore to develop suitable methods with which small adjustments in the aircraft geometry could be translated as performance changes at the end of the Design Synthesis loop. This sensitivity to configurational changes could be further enhanced by high geometric flexibility which would allow the shape and size of the aircraft to be altered within certain reasonable limits, in order to study the resulting effect on the overall design.

The above goals were successfully achieved by the development of a long series of computerised aircraft geometry modules which are based on the detailed baseline aircraft assumptions given in chapter 2. These modules define in detail the shape and size of the synthesized configuration.

The philosophy behind the development of the aircraft geometry modules is explained in this chapter in four separate sections. These cover the sizing of fixed items, the development of a fairing curve, and the geometry of the fuselage and flying surfaces. The associated mathematical models are presented and explained in detail in appendices B, C, D and E.

3.2 SIZING OF THE FIXED ITEMS

The fixed items of the aircraft are the basic items incorporated in the fuselage. Their shape and size, however, are independent from those of the fuselage. These are the cockpit, undercarriage and bays, engines and bays, gross wing, boundary layer diverter and inlet. The aircraft geometry modules within this group, estimate the physical dimensions of the above items from a number of mathematical expressions and design data. The sizing calculations are carried out in accordance with the baseline aircraft assumptions. The calculated dimensions of the fixed items are used to define the geometric constraints which are incorporated in the mathematical models for the fuselage.

3.2.1 Cockpit

The geometry of a basic single-seat cockpit for combat aircraft is defined in ref. 67. This was combined with information from refs. 68,69, 70 to define the geometry of an advanced high-'g' cockpit for this Synthesis. Special mathematical models were then developed which calculate all the vital cockpit dimensions for various different seat-back angles, anthropometric variations, ejection seat and visibility data.

3.2.2 Undercarriage

The undercarriage sizing calculations are divided into two parts. The first deals with the tyre selection process and the second with the preliminary sizing of the undercarriage legs. An automated tyre selection process was developed for this computerized Design Synthesis. The most appropriate standard-size tyre for each undercarriage leg, is automatically selected from a data-bank of tyre characteristics, which was compiled from manufacturer's

specifications published in ref.79. This method allows the use of realistic tyre data for the sizing of the undercarriage legs and bays and thus minimizes significantly any errors that could be caused by any other approximations. The basic selection criteria are the required maximum tyre pressure and the static load. The latter is determined for each leg by assuming an optimum distribution of the reference maximum take-off mass between the nose and main undercarriage legs. Both criteria are therefore fixed design data and consequently cannot produce any non-linearities during an optimization process. The automated tyre selection process is explained in more detail in appendix B.3.2.1.

The preliminary sizing of the undercarriage legs is carried out using well-established empirical methods from refs. 77 and 78. These determine the basic leg dimensions and stroke.

3.2.3 Undercarriage bays

The minimum sizes of the main and nose undercarriage bays are determined by considering the leg and grown tyre dimensions together with a set of recommended working clearances, for retraction, leg deformation, and centrifugal tyre expansion from ref. 79.

3.2.4 Gross wing

The geometric characteristics of the gross wing are determined from given values of wing area, aspect ratio, taper ratio and quarter-chord sweep angle. The leading-edge, mid-chord and trailing-edge sweep angles are estimated by using expressions which were derived by considering the assumed wing planform.

3.2.5 Engine sizing

The engine sizing module was developed by RAE(F). It scales the principal engine dimensions from a set of datum dimensions for a military turbofan engine using a scale factor based on the maximum sea-level, static thrust. It also estimates the reference engine performance at sea-level static conditions.

3.2.6 Engine bay clearances

The engine bays are defined by a set of height and width clearances at the principal engine stations. These clearances are fractions of the corresponding principal engine diameters and they are constrained within specified minimum and maximum limits, which are defined by the specified engine envelope and maintainability criteria.

3.2.7 Inlets

The total cross-sectional area of the intake diffuser inlets is obtained from a specified fixed area ratio and the total cross-sectional area of the engines at the compressor inlets. The inlet width and height may be then calculated by considering a given inlet aspect ratio. The width of each inlet however, is constrained not to exceed the local fuselage half-width, in order to remain always shielded under the fuselage.

3.2.8 Boundary layer diverter

The height of the boundary layer diverter at the intake plane is estimated by an empirical equation from ref. 4, which considers the local Reynold's number.

3.2.9 Fuselage length

The dimensions of the fixed items together with specified design data and a number of geometric constraints derived from the baseline aircraft assumptions are used to define the minimum allowable fuselage length and the axial distances of significant stations from the aircraft nose. The imposed length constraints are listed in mathematical form in fig. 3.1 (nos. 31-40) and explained in detail in appendix B.9.

3.3 FAIRING CURVE DEVELOPMENT

A fairing curve is an optimum longitudinal distribution of fuselage cross-sectional area for minimum supersonic drag. It comprises forward and aft fairings which are defined by cubics, joined by a cylindrical centre section (fig. C.1). This is effectively the shape of the cross-sectional area distribution given by the application of the sonic area rule but with the foreplane, fin(s) and wing contributions removed. The fairing curve is therefore used in the Design Synthesis for the numerical application of the sonic area rule to the fuselage. The fairing curve was first defined in ref.1, but in this Synthesis its application to the fuselage is based on a new philosophy.

Initially, some investigations were carried out to confirm that the assumed shape for the fairing curve applies to canard-delta combat aircraft. For this purpose the area distributions of the Northrop HATOL (ref.11) and SAAB Viggen aircraft were plotted and examined. It was concluded that the cross-sectional area distribution of the foreplane is small compared to the wing and that the two distributions blend uniformly on the plot due to the proximity between the foreplane and wing in a close-coupled canard-delta configuration. Therefore when the flying surface

contributions were subtracted, the shape of the fuselage distribution was similar to that assumed for the fairing curve, especially in the case of the Viggen which is well known for its area ruling.

The fairing curve equations were then derived as shown in appendix C. Mathematical expressions were also developed for the evaluation of the coefficients of the forward and aft cubics, by assuming a set of boundary conditions. The fairing curve equations may be solved at any station of the fuselage, to give the corresponding optimum cross-sectional area.

The fairing curve is divided into six sections the lengths of which may be adjusted by a set of Independent Variables in order to match them with various sections of the fuselage. This facility allows adjustment of the cross-sectional area distribution along the fuselage, for best aerodynamic results. The value of these Independent Variables are constrained within certain limits (fig. D.23, nos. 8-11) in order to maintain the validity of the assumed boundary conditions for the fairing curve.

3.4 FUSELAGE GEOMETRY

3.4.1 Fuselage geometry modules

The complete fuselage shape is defined in detail in 3-D, by a large number of specially derived mathematical models. These determine the detailed cross-sectional dimensions, area and perimeter of the fuselage at the eleven principal stations and also at any station of the eleven intermediate sections. The mathematical models for each principal station or intermediate section are grouped in separate modules, hence, a total of 22 main fuselage geometry modules are used. These are used in conjunction

with another four auxiliary modules which determine separately, the geometry of the boundary layer diverter, intake diffusers, underfuselage weapons and engine bays at any fuselage station. All these modules are presented and explained in detail in appendix D.

3.4.2 Estimation of cross-sectional dimensions

The cross-sectional dimensions of the fuselage at any station along its length are estimated by the appropriate geometry modules in such a way as to simultaneously satisfy the following three criteria:

1) Packaging constraints
2) Optimum cross-sectional area (Fairing curve)
3) Uniform blending of successive fuselage surfaces

The first criterion defines the minimum allowable fuselage dimensions at each station according to the calculated sizes and assumed locations of the fixed items. These impose geometric constraints on the fuselage dimensions which must not be violated. The lateral coordinates of the intake diffusers and engine bays together with a set of specified clearances, impose a continuous series of fuselage width constraints from the intake plane to the nozzle exit plane. The mathematical models of the intake diffusers and engine bays, however, are designed to produce smooth contour lines for these items, and therefore if the constraints imposed by them become active, the local fuselage lines will simply follow the smooth shape of their contour lines and hence any chance of undesirable non-uniformities appearing on the fuselage surface due to packaging, is eliminated.

The vertical fuselage coordinates are assumed to vary linearly along each fuselage section between stations A and

K and their size is controlled by packaging requirements at some specific principal stations. The height of the afterbody for example, relative to the flat underfuselage surface, is controlled by the maximum engine bay height which occurs at the afterburner exit where the engine diameter is largest. In order to minimize this height and hence increase the slenderness of the afterbody the engine centreline is located at the lowest position permitted by the main undercarriage bay and the engine bay height at the compressor inlet.

Both the lateral and vertical coordinates of the radome and section R-A vary uniformly in the form of a power series cylinder function. The degree of curvature of their lines is automatically adjusted by the corresponding mathematical models so that the smoothness of the two sections is always maintained. The coordinates at station R are defined by the dimensions and working clearances of the radar antenna.

According to the second criterion, the net cross-sectional area of the fuselage should be adjusted to match that of the fairing curve. This is achieved at any station by adjusting the local fuselage width. The decision to adjust the width for this purpose was taken after an investigation into the fuselage shape variations of modern twin-engine combat aircraft which indicated that in the majority of cases the fuselage width varies according to area ruling while the height varies linearly along the fuselage length. Such variations were also assumed in the baseline aircraft design.

The mathematical models for the fuselage width at each station are of varying complexity depending on the assumed geometric detail. They were basically derived by equating the net cross-sectional area of the fuselage to the local

fairing curve area and then solving for the local fuselage width. The net cross-sectional area of the fuselage does not include the local b.l. diverter, intake diffuser or engine contributions.

According to the third criterion, successive fuselage surfaces should blend uniformly together. This criterion was considered during the development of the shape of the baseline fuselage and it was therefore included in the derivation of the mathematical models which consequently determine the cross-sectional dimensions of the fuselage so that successive surfaces always blend uniformly together.

3.4.3 Estimation of cross-sectional areas and perimeters

The cross-sectional area and perimeter of the fuselage at any station along its length are calculated by considering the assumed local cross-sectional shape and the previously estimated dimensions.

3.4.4. Estimation of fuslelage volume and surface area

The fuselage volume and surface area of each fuselage section are estimated by numerically integrating its cross-sectional areas and perimeters respectively, at three equally spaced stations. The use of a significantly greater number of stations for integration purposes was fully investigated but produced no apparent improvement in accuracy. Therefore the number of stations was finally fixed to a minimum of three for maximum computational efficiency. The numerical integration methods used are based on Simpson's rule which proved sufficiently accurate for the purpose of this Synthesis due to the linearity and uniformity of the fuselage sections. The total fuselage volume and surface area are simply obtained by summation of the individual section results. The windscreen and canopy

surface areas are similarly estimated by numerical integration.

3.4.5 Miscellaneous geometry calculations

A number of miscellaneous calculations are also performed as part of the fuselage geometry, for later use in the packaging and aerodynamics methods. These are based on the detailed results of the fuselage geometry modules. The calculations are concerned with the estimation of the maximum gross and net cross-sectional areas of the fuselage, the maximum cross-sectional area of the afterbody and the fuselage positions at which these areas occur, the volume of the intake diffusers and engine bays, the fuselage volume available for internal fuel tanks, the centre of the fuselage surface area and the centre of the fuselage structure. The methods used for these calculations are explained in appendix D.29.

3.5 FLYING SURFACE GEOMETRY

The geometry of the flying surfaces of the aircraft is determined after the estimation of the fuselage dimensions. The geometric characteristics of the net wing, net and gross foreplane and fin(s) are calculated in four separate modules, which are described in detail in appendix E.

3.5.1 Net wing

The net wing geometry is determined by considering the previously estimated geometric characteristics of the gross wing and the fuselage dimensions. The net wing module also includes the mathematical models for the wing-box, ailerons, trailing-edge flaps, leading and trailing-edge sections and internal fuel tanks.

3.5.2 Net foreplane

The geometric characteristics of the net foreplane are determined in a similar way to the wing but the net foreplane area is calculated from a given volume coefficient by considering the longitudinal position of the mean quarter-chord point of the foreplane which is specified as a fraction of the fuselage length. Therefore for a fixed foreplane volume coefficient, the net foreplane area is automatically adjusted whenever the foreplane position relative to the wing, changes. According to the baseline aircraft assumptions however, the longitudinal position of the mean quarter-chord point of the foreplane, through which its axis of rotation passes perpendicularly, is constrained within the fuselage section D-E, the sides of which are flat to allow free foreplane rotation.

The height of the foreplane above the wing-chord plane is specified as a fraction of the mean geometric chord of the wing.

3.5.3 Gross foreplane

The geometry of the gross foreplane is simply determined by considering the net foreplane results and the local fuselage width.

3.5.4 Fin(s)

According to the baseline aircraft assumptions, single or twin fins may be used. The fin geometry is determined from given values of leading-edge sweep, aspect, taper and thickness to chord ratios and fin volume coefficient. The fin moment arm is initially unknown but it is assumed that the fin trailing-edge always intersects the fuselage at station J. This assumption led to the derivation of an

equation of which both sides are expressed in terms of the unknown fin area which is then estimated by solving this equation iteratively using the rapidly converging Newton-Raphson's method. The above equation and that for the fin moment arm incorporate an adjustment for single or twin fins.

CHAPTER 4

AIRCRAFT PACKAGING

4.1 INTRODUCTION

This chapter on aircraft packaging encompasses all the methods used in the Design Synthesis for the detailed prediction of the aircraft mass, the accounting of the volume of all items and fuel inside the fuselage, the estimation of the longitudinal moment arms of all main aircraft systems, components and fuel and the subsequent calculation of the forward and aft centre of gravity positions of the aircraft.

These methods are described in the following sections of this chapter, while their mathematical content is presented and explained in detail in appendix F.

4.2 AIRCRAFT MASS PREDICTION

The aircraft mass prediction is based on well-established empirical methods, extracted from refs. 1, 2, 4. These methods predict separately at first, the individual mass of each main aircraft part or system, from its physical characteristics, the mass of its constituent components and a number of empirical constants. All the results, including the fuel mass, are then added together to give the total aircraft mass.

Information on physical characteristics is provided from the aircraft geometry calculations. The volumes of the fuel tanks inside the wing-box and fuselage are also obtained from the same source and a specified set of volume utilization factors.

The total mass of the internally stored fuel is simply estimated by considering the volume of each tank and the specified fuel density.

A reference maximum take-off mass is specified for use in several prediction equations. This is also used to define a reference landing mass.

The undercarriage mass is predicted by considering the reference landing mass. The gross undercarriage mass also includes the mass of the associated hydraulics.

The propulsion system mass receives contributions from the gas generator, reheat system, thrust reverser and installation structure. These contributions are scaled from a mass breakdown of a reference engine, provided by RAE(F).

The mass of the air systems, electrics and flight controls are empirically related to the maximum take-off reference mass.

The equations for the undercarriage, air systems, flight controls and intake ramps, were modified to include suitable state-of-the-art factors, to account for any mass changes due to advances in the system related technology.

The fuel mass is directly proportional to the total internal fuel quantity.

The methods for the estimation of the mass of the fuselage and wing are long and detailed. These were both developed by British Aerospace. The total fuselage mass includes contributions from the fuselage shell and internal structure, the windscreen and canopy, air-brakes, intakes, external paint and other miscellaneous structural items. Similarly, the total mass of the wing is the sum of contributions from the wing-box, leading-edge, trailing-edge, flaps, flap-tracks, ailerons, miscellaneous fairings and attachments and paint.

Due to the existing similarity between an all moving foreplane and an all moving tailplane, the mass of the foreplane structure is predicted using an empirical equation for a tailplane.

The mass of a single fin is obtained from an empirical equation similar to that for the foreplane. The single fin equation was modified for use in the twin-fin case by the addition of a twin-fin mass factor which accounts for the mass of the extra fuselage structure needed to support the two fins.

The above methods for the prediction of the mass of the fuselage, wing, foreplane and fin(s), include factors which may be adjusted to reflect any mass savings due to the use of composite or other structural materials.

The mass of the exteral fuel tanks if fitted, is estimated from their specified content. The mass of the unused fuel and oil is expressed as a fraction of the reference maximum take-off mass.

The cockpit mass is the sum of the contributions from flight, engine and miscellaneous instruments and displays, furnishings, ejection seat, armour protection and miscellaneous equipment.

The masses of certain aircraft equipment are specified from information supplied by their manufacturers or other sources, accordingly. These are, the complete gun and its ammunition, wing-stores, pylons, underfuselage missiles and launchers, external fuel, pilot and his personal equipment, ejection seat, radar, avionics, cockpit instruments and displays and auxiliary power unit.

Finally the payload, fixed role-equipment and total aircraft take-off masses are calculated by adding up the appropriate mass estimates from the above methods.

The above mass prediction methods were validated against published mass statements in refs. 11, 12, for VSTOL canard-delta combat aircraft. Most of the predicted masses were within six per cent of their corresponding published figures.

4.3 VOLUME ACCOUNTING

The object of the volume accounting methodology is to determine the required volume to adequately acommodate all the systems, components and fuel tanks installed inside the fuselage. The required volume may be then compared to the actual fuselage volume estimated previously in the fuselage geometry calculations. The actual volume should always be greater than the required. The actual fuselage volume is controlled by appropriate adjustments of the independent variables of the fairing curve.

The volumes of the intake diffusers,engine bays, main and nose undercarriage bays, radome and internal fuel tanks are known from the aircraft geometry calculations. The volume occupied by the cockpit is estimated from its geometry. The volumes of the remaining items are determined from their predicted masses and specified density figures. These items are the radar and general avionics, flight controls, electrics, air systems, fuel system, complete gun, ammunition, missile launchers, auxiliary power unit, intake ramps, air-brakes and internal fuselage structure.

The density figures used in this method are installed densities which include allowances for maintainability, cooling etc. Typical installed system densities for

supersonic combat aircraft are given in ref. 66 and for avionics in ref. 71. Useful information on avionics, fly-by-wire and fly-by-light systems which may be used with good engineering judgement to determine installed density and mass figures, can be found in refs. 72 - 76.

4.4 LONGITUDINAL MOMENT ARMS

The longitudinal moment arms of all the aircraft systems, major components and fuel are determined separately for later use in the estimation of the overall aircraft centre of gravity positions. All moment arms are measured from the aircraft nose.

Many of the mathematical expressions used for this purpose were derived according to the guidelines set up in ref.2, where it is assumed that fixed mass proportions of each system group are installed at specific points of the aircraft anatomy. These guidelines were the result of averaging actual balance data for a broad spectrum of types of conventional aircraft. The expressions for a few items for which no information was available, were derived according to logical estimates based on engineering judgement. All the assumptions in the derivation of each of the longitudinal moment arm equations are stated clearly in appendix F.4.

The longitudinal moment arms of the flying surfaces, fuselage, powerplant and undercarriage are calculated according to ref.1. The centre of gravity of the fuselage structure for example, is assumed to act midway between its surface area and volume centres, which are estimated during the fuselage geometry calculations.

The longitudinal moment arms of the wing-stores and pylons are determined separately by assuming that the c.g.'s

of all the stores and pylons located on the same side of the aircraft centreline, lie on a common imaginary aft-swept line, the position of which is defined as a fraction of the local wing-chord between the forward and rear spars. The longitudinal c.g. position of the stores at each wing-pylon is therefore calculated from its lateral position which is specified as a fraction of the net wing span. The above assumption was made after an analysis of several combat aircraft drawings. The mathematical expressions derived according to this assumption are explained in detail in appendix F.5.

4.5 AIRCRAFT LONGITUDINAL CENTRE OF GRAVITY

The results of the mass prediction and longitudinal moment arm calculations are used in the estimation of the forward and aft longitudinal c.g. limits of the aircraft. These limits may be compared to the aerodynamic centre limits which are estimated later in the aerodynamics calculations, in order to determine the static stability of the aircraft.

The aircraft c.g. limits are estimated in this Design Synthesis by considering the following four extreme loading cases:

a) Empty internal fuel tanks, no external stores, no ammunition.
b) Full internal fuel tanks, no external stores, no ammunition.
c) Empty internal or external fuel tanks, plus external stores, plus ammunition.
d) Full internal or external fuel tanks, plus external stores, plus ammunition.

The minimum and maximum longitudinal c.g. positions with respect to the aircraft nose, for any two out of the four above cases, correspond to the forward and aft c.g. limits of the aircraft, respectively.

CHAPTER 5

AIRCRAFT AERODYNAMICS

5.1 INTRODUCTION

Detailed methodologies are employed in the Design Synthesis for the accurate estimation of the aircraft aerodynamics because these translate the aircraft geometry into flight performance characteristics. The sensitivity of the final performance estimates to small changes in the aircraft geometry, therefore depends directly on the accuracy of the aerodynamic calculations. The preliminary aerodynamic design of a combat aircraft is a complex process and in the case of close-coupled canard-delta configurations presents special problems which are mainly associated with the interference effects between the foreplane and the delta wing. A major objective of the Research Programme was therefore the study of these interference effects and the development of suitable preliminary design methods for the solution of these problems. These methods are discussed in the following paragraphs of this chapter together with the estimation of the lift-curve-slope, lift increment due to flaps, lift coefficient, aerodynamic centre, longitudinal static stability and drag. The calculations involved in these methods are presented in detail in appendices G and H.

5.2 LIFT-CURVE-SLOPE (l-c-s)

The aircraft l-c-s is a very important lift characteristic. It represents the tangent to the lift curve and describes its linear range. It is used extensively in the performance methods of this Design Synthesis, for the estimation of the aircraft lift coefficient at a given aircraft incidence within the linear range. The l-c-s varies with Mach number and reaches its maximum at the force-break Mach number.

A complete and detailed l-c-s estimation process was developed for this Design Synthesis. The process is

applicable to close-coupled canard-delta aircraft, flying at speeds up to a maximum of Mach 2.85. A selection of methods from ref. 15 are used initially to predict the isolated wing-body and foreplane-body l-c-s values. These are then individually corrected for the effects of canard-delta interference which were quantified by the author and they are finally added together to give an accurate estimate of the total aircraft l-c-s. These methods are described in the following sub-sections and explained in full detail in appendix G.2.

5.2.1 Isolated wing-body combination

The wing and body are considered separately at first. Different methods are used in each case for the subsonic, transonic and supersonic speed regimes.

In the subsonic regime, the theoretical incompressible l-c-s of the aerofoil section is firstly estimated by an equation based on the Kutta - Joukowski hypothesis of finite velocity at the trailing-edge. This low-speed value of the section is then corrected for compressibility effects by applying the Prandtl - Glauert compressibility correction. The result is used in another equation which was derived from a modified lifting line theory. The equation calculates the 3-D subsonic l-c-s of the wing. This is a function of the wing thickness to chord ratio, total trailing-edge angle, aspect-ratio, mid-chord sweep and Mach number.

The transonic method for the wing is based largely on experimental data obtained from wind-tunnel tests. The force-break Mach number for zero wing sweep is first obtained for given aspect and thickness to chord ratios. A sweep correction is applied by considering the mid-chord sweep angle. The theoretical l-c-s at the force-break Mach

number is then computed using the equations for the subsonic case. The actual l-c-s at the force-break Mach number is found from the theoretical value, the aspect and thickness to chord ratios. The l-c-s at Mach numbers 0.07 and 0.14 above the force-break are directly proportional to the actual force-break l-c-s value. For any other Mach number within the transonic regime the wing l-c-s is found by interpolating between any two of the above known points.

In the supersonic regime, theoretical wing l-c-s values are obtained from a series of charts (ref.15), for the given leading-edge sweep, aspect ratio and Mach number. For wings approaching the sonic leading-edge condition, the theoretical values are multiplied by an empirical thickness correction factor which is a function of the leading-edge parameter, thickness to chord ratio, leading-edge sweep and Mach number.

The body contributions to the l-c-s in the subsonic regime is estimated using slender body theory. In the supersonic regime, the forebody effects become very significant. These are dependent on the forebody fineness ratio and Mach number. The transonic gap is faired out between the boundary subsonic and supersonic values. Body l-c-s values in that regime are obtained by interpolation.

The l-c-s of the isolated wing-body combination is calculated for the three regimes by considering the nose interference, the interference on the wing in the presence of the body and on the body in the presence of the wing. The nose interference factor is proportional to the body/wing l-c-s and reference area ratios. The body-on-wing interference factor is a function of the local fuselage width to gross-wing span ratio, while the wing-on-body factor in the transonic and supersonic regimes, is dependent

on the wing characteristics and in particular. its aspect and taper ratios, leading-edge sweep and Mach number.

5.2.2 Isolated foreplane-body combination

The isolated foreplane-body l-c-s estimation procedure is basically the same as that for the wing-body combination described above, but all the wing parameters are simply replaced by the corresponding foreplane parameters.

5.2.3 Canard-delta interference

The aerodynamic interference between the foreplane and wing in a close-coupled canard-delta configuration, has significant effects on the aircraft lift and drag. Accurate prediction of these interference effects is consequently a fundamental step in the aerodynamic design process. However, no method is known to exist, capable of predicting these effects for preliminary aircraft design purposes. Considerable time was therefore devoted during this Research Programme, for a detailed investigation into the canard-delta interference effects and the development of suitable preliminary design methods for use in the Synthesis.

5.2.3.1 Preliminary inestigation

The preliminary investigation concentrated on the availability of coherent aerodynamic information, specifically applicable to close-coupled canard-delta configurations. After a careful study of several aerodynamics reports discovered during the initial literature search (refs. 24-50), only four related NASA reports (refs. 31-34) were found to contain suitable information for use in the development of the new canard-delta interference prediction methods. These reports contain a large number of wind-tunnel data, obtained over a

long series of tests based on the same wind-tunnel models. The data are presented as plots of lift coefficient versus angle of attack, for the isolated foreplane-body, wing-body combinations and also for each combination in the presence of the other, for a set of different geometric parameters and Mach numbers within the subsonic, transonic and supersonic speed regimes. Preliminary examinations of these plots revealed significant variations of the l-c-s of the non-isolated combinations with the following parameters; the ratio of the height at which the foreplane is located above the wing-chord plane to the mean geometric chord of the wing (RZCC), the ratio of the net foreplane area to the gross-wing area (RSCNW), the leading-edge sweep angle of the wing (QWL) and the Mach number. The observed l-c-s variations were due to canard-delta interference effects. The foreplane sweep and dihedral angles were also studied, but the available data were insufficient for any practical results and their effects on interference was little. It was therefore finally decided to analyse and process in detail the wind-tunnel data from refs. 31 - 34 in order to quantify these interference effects, in the form of factors depending on RZCC, RSCNW, QWL and M. These factors can be used to individually correct the estimated isolated wing-body and foreplane-body l-c-s values and thus obtain an accurate estimate of the aircraft l-c-s.

5.2.3.2 Wind-tunnel models

The same wind-tunnel models were used in all the tests presented in refs. 31 - 34. Each model had a cropped delta wing, a closely-coupled foreplane and a body with a rectangular cross-sectional shape and elliptically shaped corners. Two separate wings of the same area, taper and thickness-to-chord ratios but with different leading-edge and hence trailing-edge sweep angles, were tested. The first had a QWL of 44 degrees and a forward swept trailing-

edge and the second a QWL of 60 degrees and an aft swept trailing-edge. Both wings had zero twist, zero dihedral and zero wing-body angles. The average thickness-to-chord ratio of each wing was 5 per cent.

Two different foreplanes were tested. Both foreplanes had a leading-edge sweep angle of 51.5 degrees, an aft swept trailing-edge, an average thickness-to-chord ratio of 5 per cent, zero twist, zero dihedral and zero foreplane-body angles, but different net planform areas, so that the ratio RSCNW was equal to 0.16 with the one foreplane and 0.28 with the other. During all the tests the foreplane trailing-edge at the body side was positioned just ahead of the leading-edge of the wing. Each foreplane was tested at two vertical positions, at which the ratio RZCC was equal to 0.0 and 0.185.

5.2.3.3 Wind-tunnel data analysis

The analysis of the wind-tunnel data was long and laborious. The lift curves shown in the reports were initially divided into groups, according to the corresponding test values of RZCC, RSCNW and QWL. These were then further divided into groups of curves for the isolated and non-isolated, foreplane-body and wing-body combinations. All the curves were then examined and the limit of linearity was identified in each case. Straight lines were then plotted through each set of data points within the linear range of each curve and hence the corresponding lift-curve-slope values were estimated in each case for different test Mach number values between 0.3 and 2.85. The analysis was carried out in three stages, i.e. subsonic, transonic and supersonic l-c-s estimation. The l-c-s results for the non-isolated combinations were divided by the corresponding l-c-s results for the isolated combinations to form the canard-delta interference factors

for the l-c-s which were plotted versus Mach number for different values of RSCNW, QWL and RZCC as shown in fig. G.11. A few of these factors were obtained by interpolation because some of the wind-tunnel data were incomplete.

5.2.3.4 Interference factors

An examination of the graphs in fig. G.11, reveals that all the curves for the foreplane-on-wing l-c-s interference factors show a distinct similarity in shape. The same observation also applies for all the curves for the wing-on-foreplane interference factors. It is emphasized that these interférence factors also include the body effects.

The graphs show a favourable wing-on-foreplane interference up to Mach 0.9, which increases the lifting capability of the foreplane. This is due to the upwash induced by the wing, which increases the effective angle-of-attack of the foreplane and hence its lift. This favourable subsonic interference increases as the foreplane size increases relative to the wing, because the upwash is acting over a larger net foreplane area and hence the foreplane lift increases. The foreplane height above the wing chord plane and the leading-edge sweep angle of the wing have no significant effect on the wing-on-foreplane interference. The favourable interference effects of the wing on the foreplane diminish as the Mach number increases. Supersonically there is no interference from the wing on the foreplane. The unfavourable supersonic interference shown in fig. G.11, however, is solely due to the body. This may be partly related to the use of foreplane-body fairings in some of the wind-tunel tests from which the data were obtained. According to refs. 31-34, some of the data were obtained with fairings 'on' and others with fairings 'off'. These changes in body shape produced some changes in body

lift contribution which became significant supersonically. These body effects, according to refs. 31-34 were probably not treated properly during the wind-tunnel tests and this may account for some differences between theory and experiment.

The graphs in fig. G.11 also show that an unfavourable foreplane-on-wing interference exists at all speeds. This is due to the foreplane downwash which reduces the lift on the wing. The downwash is proportional to the foreplane lift and hence to its l-c-s. Therefore the foreplane-on-wing interference becomes more unfavourable as the speed increases from low subsonic to Mach 1.0 and becomes most unfavourable near Mach 1.0 where the foreplane l-c-s is maximum. The interference then gradually becomes less unfavourable in the higher transonic and lower supersonic speed regimes where the foreplane l-c-s gradually decreases.

The foreplane-on-wing interference becomes more unfavourable as the wing leading-edge sweep angle increases because the distance between the foreplane trailing-edge and the wing leading-edge increases and hence the downwash on the wing increases reducing its lift.

A comparison of the curves for the foreplane-on-wing interference with the foreplane in the low and high positions (RZCC = 0.0 and RZCC = 0.185) shows that the high foreplane location is superior to the low one. This is because the foreplane in the high location is farther from the wing flow field and hence its downwash effects on the wing are reduced.

Limited data from the same wind-tunnel tests, show that when the foreplane is located below the wing-chord plane, the

interference effects become substantially unfavourable, making this location practically unacceptable.

It should be pointed out, however, that although the foreplane has an unfavourable effect on the wing lift within the linear range of angles-of-attack, the total aircraft lift is higher than that of the isolated wing-body combination and at high angles-of-attack the foreplane delays the stall and also raises the limit of linearity of the lift curve of the aircraft.

5.2.4 Total aircraft l-c-s

The previously estimated l-c-s values for the isolated wing-body and foreplane-body combinations, at a given Mach number, are corrected by the corresponding foreplane-on-wing and wing-on-foreplane interference factors, respectively. These are determined from the graphs in fig. G.11 by multiple linear interpolation, for the given values of RZCC, RSCNW, QWL and Mach number. The total aircraft l-c-s is finally estimated by appropriately adding together the corrected l-c-s values of the wing-body and foreplane-body combinations.

5.3 LIFT INCREMENT DUE TO FLAPS

Accord_ng to the baseline assumptions, the aircraft uses only plain trailing-edge flaps as high-lift devices. The lift coefficient increment due to a given flap deflection is estimated by using an expression from ref. 57. The results of this expression are accurate in the subsonic speed regime. At higher speeds, however, a correction becomes necessary, due to the variations in flap lift effectiveness with Mach number. It was therefore decided to incorporate in this expression a set of correction factors which become active in the transonic and supersonic speed regimes, where the use of combat flaps may be assumed. These correction factors are expressed in mathematical form and were derived after an analysis of lift curves in ref.11 corresponding to various deflection angles of plain trailing-edge flaps at different Mach numbers. The corrected lift increment given by the above expression applies within the linear range of angles-of-attack. The maximum lift increment which occurs in the non-linear range is assumed to be equal to half of the corresponding increment given by the equation. This is in agreement with ref. 57 and it was also verified by the lift curves in ref. 11.

5.4 LIFT COEFFICIENT

The aircraft lift coefficient at a given incidence is estimated in the performance calculations of the Design Synthesis, from the aircraft l-c-s. The maximum lift coefficient (trimmed) and also the critical lift coefficient, depend on the technology used in the design of the wing and high lift system and they are therefore not estimated but supplied in tabular form versus Mach number, as data applicable only to each specific case. The lift-increment due to flaps which was estimated previously, is

added to the aircraft lift coefficient to give the total aircraft lift coefficient value.

5.5 AERODYNAMIC CENTRE

The longitudinal position of the aerodynamic centre of the wing is initially estimated at Mach 0.6 and Mach 1.4, using a DATCOM method. The aerodynamic centre of the wing-body combination is then estimated by considering in each of the above cases, the contributions of the front and rear fuselage and the effects of the fuselage carry-over lift, which are calculated by two expressions from ref. 3. The above two cases are sufficient for the purpose of this Design Synthesis because they represent the forward and aft positions of the aerodynamic centre due to the transonic shift, which may be compared to the maximum forward and aft centre of gravity positions of the aircraft in order to determine its longitudinal static stability.

5.6 LONGITUDINAL STATIC STABILITY

The stability calculations in this Design Synthesis are confined to the estimation of the maximum longitudinal static stability margins in subsonic and supersonic flight, which for the final synthesized aicraft should be within acceptable limits. These stability margins are expressed as fractions of the mean aerodynamic chord of the gross wing and they are estimated by comparing the forward and aft longitudinal positions of the aerodynamic centre to the forward and aft centre of gravity positions of the aircraft. The aircraft may be designed to be stable or unstable in the subsonic and supersonic regimes.

5.7 AERODYNAMIC DRAG

The overall aircraft drag is estimated in detail in the Design Synthesis by considering the separate contributions of the basic zero lift drag, wave drag, spillage drag, store drag and lift-dependent drag components. The latter also includes the effects of the canard-delta interference which were quantified by the author after a detailed analysis of relevant wind-tunnel data. The first three components are basically estimated using methods from ref. 1, but several modifications were made to the geometric parameters used in the equations, in order to make them compatible with the baseline configuration.

5.7.1 Trim drag

The trim drag component is not considered in the estimation of the aircraft drag because of the absence of detailed stability and control calculations in this Design Synthesis and also because of lack of any wind-tunnel data on the trim drag of close-coupled canard-delta configurations. Some analytical information on this subject, however, was found in ref. 28 but its application to this Design Synthesis was not possible again because of its dependence on stability and control aspects. These, were clearly excluded from the RAE requirements for this Research Programme(see paragraph 1.5), therefore in the performance calculations of this Design Synthesis, it is assumed that the aircraft is always neutrally stable with zero pitching moment and hence the trim drag is zero. A parallel investigation into the stability and control aspects and trim drag of canard delta combat aircraft, was conducted by British Aerospace Warton on behalf of RAE.

5.7.2 Basic zero lift drag

The basic zero lift drag in the subsonic regime is determined by estimating and adding up the contributions of the wing, foreplane, fin(s), fuselage, canopy, gun port and boundary layer diverter. Allowance is also made for the interference effects between components, small excrescences, control gaps and surface irregularities. The basic zero lift drag at Mach 0.8 is scaled to provide the drag estimates at transonic and supersonic speeds. The scaling factor is a function of the Mach number. An increment is also added to account for the compressibility effects on intake diverter drag.

5.7.3 Wave drag

The drag rise Mach number is calculated initially, and then the wave drag of the wing, foreplane, fin(s), fuselage and canopy at Mach 1.0 and Mach 1.3. The sum of the above components is used in conjunction with empirical factors, to define the aircraft wave drag variation with Mach number in the range between the drag rise Mach number and Mach 1.3. It is assumed that above Mach 1.3 the aircraft wave drag coefficient remains constant.

5.7.4 Spillage drag

The ratio of the intake capture area to the area of the intake stream tube at infinity is first calculated to examine if spillage of the intake airflow occurs for the given flight conditions. Intake airflow spillage is associated with spillage drag. This, in the subsonic and transonic speed regimes up to Mach 1.1, is directly proportional to the pre-entry drag. The latter is a function of the ratio of the air density at the inlet of the

intake to the free-stream air density, which is determined by an iteration process.

5.7.5 Store drag

The store drag module was developed specifically for this Design Synthesis and offers maximum flexibility for the selection of the number, types and combinations of underfuselage-and wing mounted stores. Installed drag coefficients for various types of stores including semisubmerged or pylon-mounted missiles, bombs, external fuel tanks, pylons etc., may be tabulated versus Mach number in a data file from which they can be read automatically by means of special drag codes. Installed drag coefficient data for some typical stores are given in ref.12. Data for other types of stores may be obtained from store manufacturers or from research establishments. The drag coefficients of pairs of stores mounted on the same pylon are automatically corrected by multiple carriage factors. The total store drag coefficient is the sum of the contributions of all the stores installed on the aircraft. This is automatically revised to reflect the drag changes due to any store releases during a hypothetical sortie in the performance estimation.

5.7.6 Canard-delta interference

As mentioned earlier in paragraph 5.2.3, the aerodynamic interference between the foreplane and wing in a close-coupled canard-delta configuration, has also significant effects on the aircraft drag. Another long and detailed investigation was therefore carried out during this Research Programme, in order to study the effects of canard-delta interference on drag and hence develop a preliminary design method compatible with that for the l-c-s.

5.7.6.1 Preliminary investigation

The information used in this investigation was again contained in refs. 31 - 34, in the form of drag polars which were produced after a series of wind-tunnel tests using the same models described in paragraph 5.2.3.2, for the same values of RZCC, RSCNW and QWL used for the lift-curve data and for Mach numbers within the subsonic, transonic and supersonic speed regimes, up to a maximum of Mach 2.0. An initial examination of these drag polars, indicated that the addition of a close-coupled foreplane to a delta wing-body combination, significantly reduces the values of the lift-dependent drag parameters K1 and K2, which define the lower and upper regions of a drag polar. It was therefore decided to analyse in detail the available data in order to determine suitable canard-delta interference factors which can individually adjust the estimated values of K1 and K2 for the wing-body combination in order to produce accurate estimates of these parameters for the complete aircraft.

5.7.6.2 Wind-tunnel data analysis

The drag polars presented in refs. 31 - 34 were initially divided into two main groups. Included in the first group were the drag polars for the wing-body combination and in the second, those for the wing-body-foreplane combination. The second group was further subdivided according to the corresponding test values of RZCC, RSCNW and QWL. The drag coefficient data of every drag polar in each group were then replotted versus the corresponding squared lift coefficient data for each test Mach number, using computerised Benson plotting routines, in order to speed up the process and simultaneously eliminate any plotting errors. The points on each plot were next joined manually by two successive straight lines with different slopes, which clearly defined the lower and upper

regions and also the critical lift coefficient of each drag polar. The lines were drawn with great accuracy and in the majority of cases, they were passing exactly over the corresponding data points. The slopes of these lines and hence the values of parameters K1 and K2 for each drag polar were then determined. The canard-delta interference factors for K1 and K2, for a given Mach number and for given values of RZCC, RSCNW and QWL, were determined by dividing the values of parameters K1 and K2 for the wing-body-foreplane combination with the corresponding values for the wing-body alone.

The variations of these factors with Mach number, for different values of RZCC, RSCNW and QWL are presented in graphical form in fig. H.1. The values of factors for speeds higher than Mach 2.0 are obtained by extrapolation.

5.7.6.3 Interference factors

The graphs in fig. H.1 clearly show that the addition of a close-coupled foreplane to a delta wing-body combination, significantly reduces the values of the lift-dependent drag parameters K1 and K2. This is associated with the reduction of the wing-body lift and also with the improvement of the elliptic lift distribution produced by the interaction of the foreplane vortices with the flow field of the wing.

The magnitude of both factors varies with Mach number and reaches its minimum and maximum values near Mach 1.0. The magnitude variations are more significant for the factors of K2. The supersonic values of both interference factors are generally higher than their subsonic values for a given combination of RZCC, RSCNW and QWL because as explained in paragraph 5.2.3.4 the reduction in wing-body lift due to the addition of a foreplane is less

supersonically than it is subsonically. The observed interference factor magnitude variations with Mach number, for a given combination of QWL and RZCC, are generally very similar in shape.

The graphs in fig. H.1 also show that an increase in foreplane size always results in a reduction of the values of both K1 and K2, at any Mach number, because the increased foreplane lift causes a further reduction of the wing-body lift (see paragraph 5.2.3.4).

It is also observed that the values of K1 and K2 reduce as the wing leading edge sweep decreases (QWL = 44°) or as the foreplane height above the wing-chord plane increases (RZCC = 0.185), because the foreplane vortices interact with the flow field of the wing in a manner more favourable for the improvement of the elliptic lift distribution and hence the increase of the wing planform efficiency.

The high foreplane location is therefore superior to the low one with regard to both lift-dependent drag and l-c-s.

5.7.7 Lift-dependent drag

The values of the lift-dependent drag parameters K1 and K2 are initially estimated for the wing-body combination alone, using methods from ref. 1. The canard-delta interference factors for K1 and K2 are then determined from the graphs in fig. H.1, by multiple linear interpolation, for the given values of RZCC, RSCNW, QWL and Mach number. These factors are multiplied by the previously estimated values of K1 and K2 to determine the corresponding parameters for the complete aircraft and hence estimate its lift-dependent drag coefficient.

5.7.8 Total aircraft drag

The total aircraft drag coefficient is finally estimated by adding up the estimated coefficients for the basic zero lift drag, wave drag, spillage drag, store drag and lift-dependent drag and also the separately considered low-speed afterbody, extended undercarriage and flap contributions

CHAPTER 6

AIRCRAFT PERFORMANCE

6.1. INTRODUCTION

The aircraft performance estimation is the last but vital step in the Design Synthesis process. It is the step at which the capabilities of the synthesized aircraft are assessed to see if it fullfils the specified requirements for its combat role.

The aircraft performance methods used in the Design Synthesis are divided into four groups:

a) Engine Performance
b) Sortie Performance
c) Take-off and Landing Performance
d) Point Performance

These methods are discussed in the following sections of this chapter. The mathematical processes involved in each method are explained in detail in appendix I.

6.2 ENGINE PERFORMANCE

The engine performance is estimated by a set of empirical relationships which are based on a modern military turbofan engine. These relationships are all grouped in a single module developed and supplied by RAE(F), together with a separate module which evaluates the atmospheric properties at a specified altitude. The results of the reference engine performance at sea-level static conditions, estimated earlier by the engine sizing module are used as a basis for the calculations in the engine performance module. This operates in five different modes. In the first mode, for example, given the total gross thrust at a specified flight altitude and Mach number, it calculates the air mass flow rate, the fuel mass flow rate, the jet exit area and the engine throttle setting. In the third mode however,

given the throttle setting and flight conditions, it calculates the mass flow rates and exit area as above and also the corresponding total gross thrust.

This module is used in all the other performance methods, in the appropriate mode, for defining the variation of the engine performance characteristics with different flight conditions.

6.3 SORTIE PERFORMANCE

The main object of the sortie performance estimation is to calculate the fuel and time required for the synthesized aircraft to fly a hypothetical sortie, comprising a number of legs of specified length. In order to increase the computational efficiency, it is assumed that each sortie leg is flown at a constant altitude, Mach number and load factor. The performance calculations for those sortie legs involving climbing, descending or longitudinal acceleration flight, are therefore approximated by appropriately modifying the leg length or the corresponding load factor. According to ref. 1, any errors incurred by this simplified approach are minor in comparison with the results from more comprehensive mission analysis programs. It is also assumed that the first sortie leg starts immediately after the end of the take-off phase while the last leg finishes just before the start of the landing phase of the flight, hence the fuel required for take-off and landing is not calculated but simply specified at the beginning of the sortie performance calculations.

The sortie performance module operates in conjunction with other modules which provide the necessary information on atmospheric properties, engine performance characteristics, lift-curve-slope, lift increment due to flaps and aircraft drag, for each set of calculations. This

also increases the flexibility of the sortie performance module which can therefore calculate the effects of configurational changes along any of the sortie-legs, such as the release of any combination of stores, flap deflection or undercarriage retraction. A further facility is incorporated in the module which allows automatic jettissoning of any empty external fuel tanks. The aircraft mass used in the sortie calculations is automatically revised at the beginning of each leg by subtracting the mass of the stores released and fuel burnt along the previous leg.

The maximum possible sustained aircraft incidence and lift coefficient for each sortie-leg are estimated by an iteration process assuming a full engine throttle setting.

The results of the first iteration process are used in a further set of iterations for the estimation of the maximum sustained load factor halfway along the sortie leg under consideration. This is constrained not to exceed the maximum human 'g'-tolerance limit.

A third and final iteration process is used for the estimation of the consumed fuel mass gross-thrust, aircraft incidence and lift coefficient, for the actual flight conditions specified for the leg.

The aircraft landing mass is calculated by subtracting the specified fuel mass for the landing phase from the estimated aircraft mass at the end of the last leg.

The above iteration processes were developed according to the guidelines given in ref. 1, while the equations involved were derived from first principles.

6.4 TAKE-OFF AND LANDING PERFORMANCE

The total take-off distance is calculated using two empirical equations from ref. 60. The first estimates the ground roll distance and the second the airborne distance travelled to clear a 15.2 m screen height. Both equations are expressed in terms of the wing mass loading and thrust to weight ratio at take-off. The maximum static gross thrust available for take-off at a specified airfield altitude, is estimated by the engine performance module. The above equations allow the use of a specified fraction of this maximum thrust, during take-off. The lift coefficient in the take-off configuration is equal to a specified fraction of the maximum available lift coefficient plus an increment due to flaps which is estimated by the corresponding module. The stall speed in the take-off configuration is calculated by considering the predicted take-off mass of the aircraft and hence the take-off speed.

The landing distance from an approach height of 15.2 m to a full stop is estimated by an empirical equation from ref. 2. This considers the retardation effects of the thrust reversers. It is assumed that reverse thrust is applied at 70% of the approach speed. The maximum reverse thrust at the assumed speed is equal to a specified fraction of the maximum available forward thrust estimated by the engine performance module. The retardation effects of the airbrakes may be also considered in this equation, by an appropriate adjustment of the ground rolling friction coefficient. The maximum lift coefficient in the landing configuration is determined in a way similar to that for the take-off configuration. The corresponding stall speed and hence, approach speed are also similarly determined. The aircraft mass used in these calculations is equal to the landing mass calculated at the end of the hypothetical sortie.

6.5 POINT PERFORMANCE

During the point performance estimation, six parameters are calculated. Each parameter may be calculated several times for different specified flight conditions. These parameters are:

a) Sustained turn rate
b) Attained turn rate
c) Specific excess power
d) Maximum Mach number
e) Acceleration time
f) Ride quality factor

Each parameter is calculated by a separate module.

6.5.1 Sustained turn rate

Sustained turn rate is the most important measure of air combat potential. It is the ability of the aircraft to turn at a constant rate, continuously. The ability of the aircraft to do this is dependent upon having enough thrust to balance the drag in the turn while maintaining speed. The sustained turn rate is therefore thrust dependent.

The sustained turn rate for a specified flight Mach number, altitude, aircraft weight, engine throttle setting and flap deflection angle is a function of the sustained load factor which is estimated first, iteratively. This is constrained, however, not to exceed the maximum human 'g'-tolerance limit or the proof load factor of the aircraft structure.

6.5.2 Attained turn rate

Attained turn rate is another turn characteristic of importance and is the maximum turn rate which can be

attained. It is governed by the amount of lift available, or by the structural limitation on the airframe. It is not a steady-state condition and is associated with loss of speed or height or both.

The attained turn rate for a specified flight Mach number, altitude, aircraft weight, engine throttle setting and flap deflection angle is a function of the maximum attained load factor, which is calculated first, by considering the maximum (trimmed) lift coefficient. This is constrained not to exceed the proof load factor of the aircraft structure.

6.5.3 Specific excess power

Specific excess power is the measure of power available, under a given flight condition, for changing the state of the aircraft. It is a measure of the excess power available after the drag of the aircraft has been overcome by thrust.

This module calculates the specific excess power in 1 - g flight, for a specified Mach number, altitude, engine throttle setting and aircraft weight.

6.5.4 Maximum Mach number

The maximum Mach number which the synthesized aircraft can reach in 1 - g flight at a specified altitude and for a specified engine throttle setting and aircraft weight, is estimated using an iteration process during which the net propulsive force is evaluated repeatedly until it converges to a minimum. The corresponding Mach number is the estimated maximum.

6.5.5 Acceleration time

The time to accelerate from a given Mach number, through a fixed increment in Mach number, at a specified altitude, aircraft weight and engine throttle setting, in 1 - g flight, is estimated iteratively. The net propulsive force per unit mass is evaluated in each iteration, with gradually increasing Mach numbers and the time to accelerate through each small Mach number interval is calculated by considering the corresponding gradual changes in net propulsive force. The iterations stop when the desired Mach number is reached. The total time to accelerate through the initially specified Mach number increment is the sum of the results of all iterations.

6.5.6 Ride quality factor

The ride quality or gust response of the aircraft during a low altitude high-speed penetration depends on a factor which is directly proportional to the aircraft lift-curve-slope, gross wing area and speed and inversely proportional to the aircraft weight.

CHAPTER 7

COMPUTER PROGRAM ARCHITECTURE

7.1 INTRODUCTION

The main objective of this Research Programme was the development of a large modular computer program for the implementation of the Design Synthesis. This program would be compatible with existing RAE Multivariate Optimization algorithms. A further objective was also the development of a Graphics program, capable of producing enhanced 2-D computer generated images of the aircraft designed by the Design Synthesis program.

The development and architecture of these two computer programs are described in this chapter. A detailed User's manual is provided in appendix J. A design example, showing the application of these programs is presented in appendix K.

7.2 THE COMPUTER PROGRAMS

The above objectives were fully achieved by the successful development of programs CANARD and VIEW.

7.2.1 Program CANARD

Program CANARD implements the Design Synthesis. It is written in standard FORTRAN 77, has a total length of about 8500 lines and consists of 77 modules and 15 auxiliary data files. The program uses a total of about 1500 variables, 23 of which are classified as Independent (IV's), 323 as External (EV's) and the rest as Dependent Variables (DV's). These variable types are defined in appendix A. All the variables used in the program are listed, explained and identified in alphabetical order at the beginning of this thesis. Program CANARD performs the entire Design Synthesis calculations quickly and efficiently, starting from a specified set of input data (IV's and EV's) which define

some essential geometric characteristics and design data for the proposed aircraft (see appendix J). After a successful execution the proram produces a detailed numerical output containing the results of the Synthesis calculations. It also automatically creates, an input data file for the Graphics program.

7.2.2 Program VIEW

Program VIEW is the Computer Graphics program. It is also written in FORTRAN 77 using GINO-F library subroutines. It has a total length of about 1600 lines and consists of three modules which generate three clear and detailed images of the synthesized configuration, from the input data file produced by program CANARD. The execution of program VIEW, however, is controlled by the User.

7.2.3 User/Program Interrelation

The interrelation between the User and programs CANARD and VIEW is diagramatically presented in fig.7.1. At the start of a manual optimization process, the User creates or revises the necessary input data files and then runs the Design Synthesis program. The numerical output is then critically examined with regard to the desired optimum. If the images of the aircraft are needed to facilitate and speed-up this initial assessment, then the User runs the Graphics program and examines the graphical output produced. It is a normal procedure, however, to check both the numerical and graphical output during the first loop (see appendix J). The same process is repeated by the User for several times and during each loop, the values of some IV's are revised accordingly until the desired optimum results are reached. During an automated optimization process the optimizer (MVO program) will automatically repeat the above process and vary the values of the IV's within a User-

specified range until an optimum aircraft design is produced.

The User-controlled execution of program VIEW, offers two distinct advantages; it permits the use of program CANARD alone, on computer systems which cannot accept GINO-F software or where this industry standard graphics package is not available; it prevents unnecessary waste of CPU in generating images of intermediate configurations during optimization. The initial and final configurations are normally of interest to the User.

7.3 COMPUTER PROGRAM DEVELOPMENT

7.3.1 Program CANARD

The development of program CANARD was an enormous and complex task. The program was developed on the DEC VAX-11/750 mainframe computer system of the College of Aeronautics. It was anticipated right from the start that the program would have an enormous size, because of the large number of calculations and processes involved in the Design Synthesis for Canard-Delta combat aircraft. Therefore, it was decided to adopt a modular programming approach in the design of this program. This is a style of programming in which the complete program is broken down into a set of components, called modules. Each module is of manageable size, has a well-defined purpose and has a well-defined boundary. Each module involves a set of related design calculations and decisions. This programming style allows independent development, testing and debugging for each module.

The use of standard FORTRAN 77 as a language is ideal for aircraft design calculations and allows implementation

of the program on mainframes and a large number of expensive personal computers.

The development of program CANARD was a parallel activity with the development of the Design Synthesis methods, from the start to the finish of the Research Programme. The Synthesis calculations were divided into eight main groups:

a) Sizing of fixed items
b) Fairing curve development
c) Fuselage geometry
d) Flying surface geometry
e) Packaging
f) Aerodynamic lift
g) Aerodynamic drag
h) Aircraft performance

Each of the above groups was subdivided into a number of modules with each module dealing with a particular set of design calculations. The derivation of equations for the Synthesis started and continued in the order in which these are used in the design loop. Therefore, the corresponding modules were developed in the same order, as soon as each set of equations was finalized. Every module was programmed carefully for maximum computing efficiency and then compiled, debugged and tested separately from the others. Each finalized module was then added to the previous ones and all together were tested to ensure that they were still producing correct results. This laborious but reliable process continued up to the finish of each of the above eight main groups of calculations. Upon successful completion, each group was added to the previous ones in the loop and tested in a similar way as the modules. This methodical and systematic programming strategy led to the

gradual built-up and successful completion of program CANARD.

7.3.2 Program VIEW

Program VIEW was also developed on the College of Aeronautics VAX following a programming procedure similar to that for program CANARD. This program, however, is inherently different from the first, due to its graphics nature and the use of GINO-F library subroutines. It consists of three large and independent modules which produce computer generated images of the side view, lower plan view and upper plan view, of the synthesized configuration. Each module produces one of the above views by using a large number of GINO-F statements which join by straight lines, several groups of points that define the aircraft geometry. The coordinates of every one of these points relative to a selected system of axes, are expressed in each module by mathematical equations which were specially derived for this purpose by considering the detailed dimensions of the aircraft configuration, calculated by program CANARD. A very large number of points is needed for each view and the required number of coordinate equations is consequently twice as large. The derivation of all the coordinate equations used in program VIEW was therefore a long and delicate process but the results proved to be very worthwhile. The computer generated images of an aircraft designed by program CANARD are shown in fig. 7.4. The fuselage contour line is plotted only around points at the eleven principal fuselage stations, in order to save CPU. The fuselage contour shown in the images therefore has a slightly less uniform shape than what is actually produced by program CANARD, at 22 stations.

Program VIEW was fully tested during its development, for flexibility, clarity and accuracy over a variety of canard-delta configurations and the results were always impressive.

7.4 COMPUTER PROGRAM ARCHITECTURE

7.4.1 Program CANARD

The program comprises a main segment and 77 modules. It uses 15 auxiliary data files during its operation, two of which are User-created, plus a main input data file. It produces two output files, one of which contains the main results of the Design Synthesis and the other the input data for program VIEW. These architectural elements of the program are described in more detail in the following sub-sections.

7.4.1.1 Main segment

The main segment of this program controls the order of execution of all the modules of program CANARD and allows communication between the modules via common blocks. It reads data from the main input file and relays them to the appropriate modules. It also writes the results of the appropriate Synthesis modules, in the input data file for the graphics program. The main segment of program CANARD also includes all the Synthesis processes involving numerical integration. These are, the volume estimation for the fuselage, intake diffusers, engine bays and fuselage fuel tanks, the surface area estimation for the fuselage and canopy, the footprint area calculation for the flying surfaces and the estimation of the moment arms of the fuselage structure and skin.

A listing of all the arrays, variables and common blocks used in program CANARD, is included at the beginning of the main segment.

7.4.1.2 Modules

Each module is a program of its own but it is designed to communicate with the main segment and other modules of the Synthesis via common blocks. Every module was given a name which is an abbreviation of its function in the design loop, for easy identification. All the variables related to the calculations in a given module were grouped in a single, common block with the same name as the corresponding module. The variables involved in those design calculations which are included in the main segment, however, were grouped in extra common blocks, with appropriate names. This naming similarity between modules and commons proved to be very beneficial during program development. Common blocks were selected for module communication instead of arguments, because of the large number of variables involved in the calculations of each module.

Several modules incorporate WRITE statements for their results. The engine performance, lift-curve-slope and drag modules which are used in relatively long iterations, do not have their own WRITE statements, but their final results are listed together with the corresponding performance estimates. This improves the efficiency of the program.

All the Design Synthesis modules are listed below in eight main groups and the function of each module is briefly explained.

a) Sizing of fixed items.

COCKPG:	Determines the geometry of the cockpit
MUNDCG:	Sizes the main undercarriage
NUNDCG:	Sizes the nose undercarriage
MUNDCBG:	Determines the geometry of the main undercarriage bays
NUNDCBG:	Determines the geometry of the nose undercarriage bay
GWINGG:	Determines the gross wing geometry
ENGSIZ:	Sizes the engines
ENGBCLR:	Calculates the engine bay clearances
INLET:	Sizes the intake diffuser inlets
LENGTH:	Determines the actual length of the fuselage and the positions of various significant stations
BLDIVG1:	Sizes the boundary layer diverter at the intake plane
ATMOS:	Determines the atmospheric properties

b) Fairing curve development

FAIRCUR1:	Calculates the fairing curve coefficients
FAIRCUR2:	Determines the fairing curve area at any station X.

c) Fuselage geometry

The modules FUSSTNR, FUSSTNA, FUSSTNB, FUSSTNC, FUSSTND, FUSSTNE, FUSSTNF, FUSSTNG, FUSSTNH, FUSSTNJ and FUSSTNK, determine the fuselage geometry at stations R, A, B, C, D, E, F, G, H, J and K, respectively.

The modules RADOME, FSECTRA, FSECTAB, FSECTBC, FSECTCD, FSECTDE, FSECTEF, FSECTFG, FSECTGH, FSECTHJ and FSECTJK, determine the fuselage geometry at any station X, of the radome and sections R-A, A-B, B-C, C-D, D-E, E-F, F-G, G-H, H-J and J-K, respectively.

The modules INTDIFG, BLDIVG2, WEAPONG and ENGBAYG, determine the geometry of the intake diffusers, boundary layer diverter, fuselage-mounted weapons and engine bays, at any station X, respectively.

d) Flying surface geometry

NWINGG:	Determines the geometry of the net wing
NFOREPG:	Determines the geometry of the net foreplane
GFOREPG:	Determines the geometry of the gross foreplane
FING:	Determines the geometry of the fin(s)

e) Packaging

MASSPR:	Predicts the aircraft mass
VOLACC:	Performs a volume accounting for everything inside the fuselage
MOMARM:	Determines the longitudinal moment arms
STORSTN:	Estimates the c.g. positions for the wing-stores
CG:	Calculates the aircraft longitudinal c.g. positions

f) Aerodynamic lift

WLSUB:	Estimates the subsonic l-c-s for the wing or foreplane
WLTRAN:	Estimates the transonic l-c-s for the wing or foreplane

WLSUP:	Estimates the supersonic l-c-s for the wing or foreplane
TCOR:	Determines an empirical thickness correction
BLSUP:	Estimates the supersonic l-c-s for the body
WBLCS:	Estimates the l-c-s for the isolated wing-body or foreplane-body combination
LCSINT:	Determines the canard-delta interference effects on l-c-s
LIFTSL:	Calculates the total aircraft l-c-s
DLFLAP:	Estimates the lift increment due to flaps
AEROC:	Estimates the longitudinal positions of the aerodynamic centre of the wing-body combination.

g) Aerodynamic drag

ZLDRAG:	Estimates the basic zero lift drag
WDRAG:	Estimates the wave drag
SPDRAG:	Estimates the intake spillage drag
STDRAG:	Estimates the total store drag
LDDINT:	Determines the canard-delta interference effects on the lift-dependent drag
LDDRAG:	Estimates the lift-dependent drag
DRAG:	Calculates the total aircraft drag

h) Aircraft performance

ENGPER:	Estimates the engine performance
SORTIE:	Estimates the Sortie performance of the aircraft
TOLPERF:	Estimates the take-off and landing performance
PPSTR:	Estimates the sustained turn rate
PPATR:	Estimates the attained turn rate
PPSEP:	Calculates the specific excess power
PPMMAX:	Estimates the maximum Mach number

PPDT: Calculates the acceleration time

PPRQF: Determines the ride quality factor

7.4.1.3 Data files

A total of 18 data files are associated with program CANARD. Three of these are main files and the rest are auxiliary files. These are listed below and their roles, size and contents are briefly explained.

a) Main files

CANARD.DAT: This is the main input data file of program CANARD. It is a User-created file and contains the data values of 23 IV's and 304 EV's. Details about this file are given in appendix J.

CANARD.RES: This is the main output file of program CANARD. It contains the numerical results of the Design Synthesis in the right order and in a clear format (See example in appendix K).

VIEW.DAT: This is the input file of program VIEW, and an output file of program CANARD. It contains the data values of the input variables of program VIEW.

b) Auxiliary files

TYREM.DAT: This file stores the specified characteristics of a wide range of standard-size aircraft tyres. It is used during the automated tyre selection process (See section B.3.2.1). The data are arranged in 46 rows and 10 columns.

GINTEGR.DAT: This is a scratch file which is created temporarily by program CANARD, to store some aircraft geometry results for numerical integration purposes. The data are arranged in 33 rows and 5 columns. The file is automatically deleted after serving its purpose.

LCS1.DAT: This file stores data from fig. G.1, for determining the force-break Mach number for zero leading-edge sweep. The data are arranged in 28 rows and 6 columns.

LCS2.DAT: This file stores data from fig. G.2, for determining the force-break Mach number value corrected for leading-edge sweep effects. The data are arranged in 40 rows and 3 columns.

LCS3.DAT and LCS4.DAT: Both files store data from the charts in fig. G.6, for estimating the supersonic l-c-s of the wing or foreplane. The data in each file are arranged in 176 rows and 12 columns.

LCS5.DAT: This file stores data from fig. G.8 for estimating the supersonic l-c-s of the body The data are arranged in 30 rows and 4 columns.

LCS6.DAT: This file stores data from fig, G.9 for determining the factor for body-on-wing interference in the estimation of the l-c-s of the wing - or foreplane-body combination. The data are arranged in 11 rows and 3 columns.

LCS7.DAT: This file stores data from fig. G.10 for determining a product of the factor for wing-on-body interference in the estimation of the l-c-s of the wing - or foreplane-body combination. The data are arranged in 90 rows and 3 columns.

LCS8.DAT: This file stores data from fig.G.7 for determining the value of the empirical thickness correction parameter used in the estimation of the supersonic l-c-s of the wing or foreplane. The data are arranged in 88 rows and 4 columns.

LCS9.DAT: This file stores data from fig. G.11, for determining the canard-delta l-c-s interference factors. The data are arranged in 116 rows and 9 columns.

LDD1.DAT: This file stores data from fig. H.1 for determining the canard-delta interference factors for the lift-dependent drag parameters K1 and K2. The data are arranged in 82 rows and 9 columns.

LDD2.DAT: This is a User-created file which contains the data values of CLC, DK2 and CLMAX with Mach numbers. These are arranged in 25 rows and 4 columns. Details about this file are given in appendix J.

STDRAG.DAT: This is a User-created file containing the installed drag coefficient values with Mach number for different types of aircraft stores. These are arranged in 25 rows and 9 columns. Details about this file are given in appendix J.

AEROC.DAT: This file stores data from fig. G.12 for the estimation of the aerodynamic centre of the wing. The data are arranged in 36 rows and 11 columns.

7.4.2 Program VIEW

The architecture of program VIEW is relatively simple. It comprises a main segment, three modules and a graphics output file. The necessary input data are read from file VIEW.DAT.

7.4.2.1 Main segment

This section of the program reads the input data, defines the plotting paper size and image scale and controls the order of execution of the graphics modules. The input data are relayed to these modules via two common blocks.

7.4.2.2 Graphics modules

These are three separate subroutines consisting of a large number of GINO-F statements which generate all the graphical details shown on each image of the synthesized configuration (fig. 7.4). The module names and functions are:

SVIEW:	Generates the side view
BVIEW:	Generates the lower plan view
PVIEW:	Generates the upper plan view

7.4.2.3 Graphics output file

File FOR007.DAT is produced by program VIEW and contains the three computer generated images (fig.7.4), which can be displayed on a graphics terminal or plotter as explained in appendix J. The images are displayed in sequence.

7.5 PROGRAM OPERATION

The operation of programs CANARD and VIEW is presented diagrammatically by the flow charts in figs. 7.2 and 7.3. Fig. 7.2 is an expanded version of the flow-chart in fig. 7.1 and shows the main operations involved in each program and the interrelation between programs and User. A more detailed flow-chart for program CANARD is presented in fig. 7.3. The program operation is briefly described below with the aid of these diagrams.

Program CANARD starts by reading the input data in file CANARD.DAT. The first part of the Design synthesis calculations is the sizing of the fixed items. The cockpit geometry is determined at first and then the dimensions of the main and nose undercarriage legs and bays. Suitable standard-size tyres are automatically selected from file TYREM.DAT. The engine size is then estimated and hence the engine bay clearances and the intake diffuser inlet dimensions. The gross wing size and geometric characteristics are then defined. The dimensions of the above fixed items in conjunction with the input data are used to define the actual aircraft length and the longitudinal positions of various significant fuselage stations. The sizing calculations finish with the estimation of the b.l diverter dimensions, at the intake plane.

The fuselage geometry calculations start by firstly considering station R. Its cross-sectional area is then used in the calculation of the fairing curve coefficients. The fuselage geometry at stations A to K and also at any station X of the sections defined by the above stations, is determined by considering the corresponding fairing curve area and geometry of the intake diffusers, b.l. diverter, underfuselage weapons and engine bays. Some of the fuselage

geometry results at predefined stations, are temporarily stored in file GINTEGR.DAT.

Following the definition of the fuselage shape, the sizes and geometric characteristics of the net wing, foreplane and fin are then determined. The gross foreplane geometry is determined by considering the net foreplane results.

The data in file GINTEGR.DAT are numerically integrated to estimate the volume of the fuselage intake diffusers and engine bays, the gross surface area of the fuselage, the surface area of the canopy and the moment arms of the fuselage structure and skin. The net surface area of the fuselage is obtained by calculating and subtracting the total footprint area of the flying surfaces, from the gross surface area of the fuselage. The volume of the fuel tanks inside the fuselage sections D-E, E-F and F-G is estimated by considering the available volume and specified utilization factors.

The packaging calculations start with the aircraft mass prediction. A volume accounting is then performed for everything installed inside the fuselage, to ensure that there is adequate space. The moment arms, including those of the external stores are then determined and used to calculate the forward and aft longitudinal c.g. positions of the aircraft.

The isolated wing-body and foreplane-body l-c-s are estimated following the procedure presented in appendix G. Data from the auxiliary files LCS1-8.DAT are also used at various stages of this process. The total aircraft l-c-s is finally estimated by considering the corresponding canard-delta l-c-s interference factors in file LCS9.DAT. The

l-c-s results are then used to estimate the position of the aerodynamic centre and the transonic shift. Data related to the aerodynamic centre of the wing are supplied from file AEROC.DAT. The lift increment due to flaps and the total lift coefficient at a given aircraft incidence are also estimated using the l-c-s results. The corresponding maximum trimmed lift coefficient is obtained from file LDD2.DAT.

The engine performance is estimated for the specified flight conditions and then the corresponding aerodynamic drag of the aircraft which receives contributions from the basic zero lift drag, wave drag, store drag,spillage drag and lift-dependent drag components. Information on installed drag coefficients for the types of stores used is obtained from file STDRAG.DAT. The values of the critical lift coefficient and increment DK2, used in the estimation of the lift-dependent drag are obtained from file LDD2.DAT. The lift-dependent drag estimate is corrected for the effects of canard-delta interference with factors from file LDD1.DAT.

The aircraft performance estimation is the last part of the Design Synthesis calculations, during which the above described program operations for the estimation of the lift, drag and engine performance are repeated for every specified flight condition. The sortie performance is estimated for a hypothetical sortie and the take-off and landing performance is determined by considering the aircraft mass at the start and finish of the sortie. Six point performance parameters are finally calculated. These are the sustained and attained turn rates, specific excess power, maximum Mach number, acceleration time and aircraft ride quality factor. Each parameter may be estimated for any specified number of times and for different flight conditions.

The Design Synthesis results are all stored in file CANARD.RES.

The program VIEW may be then run by the user, to generate images of the side, lower plan and upper plan views of the synthesized configuration. These views are all stored in file FOR007.DAT.

An optimization process may then follow, as described in section 7.2.3.

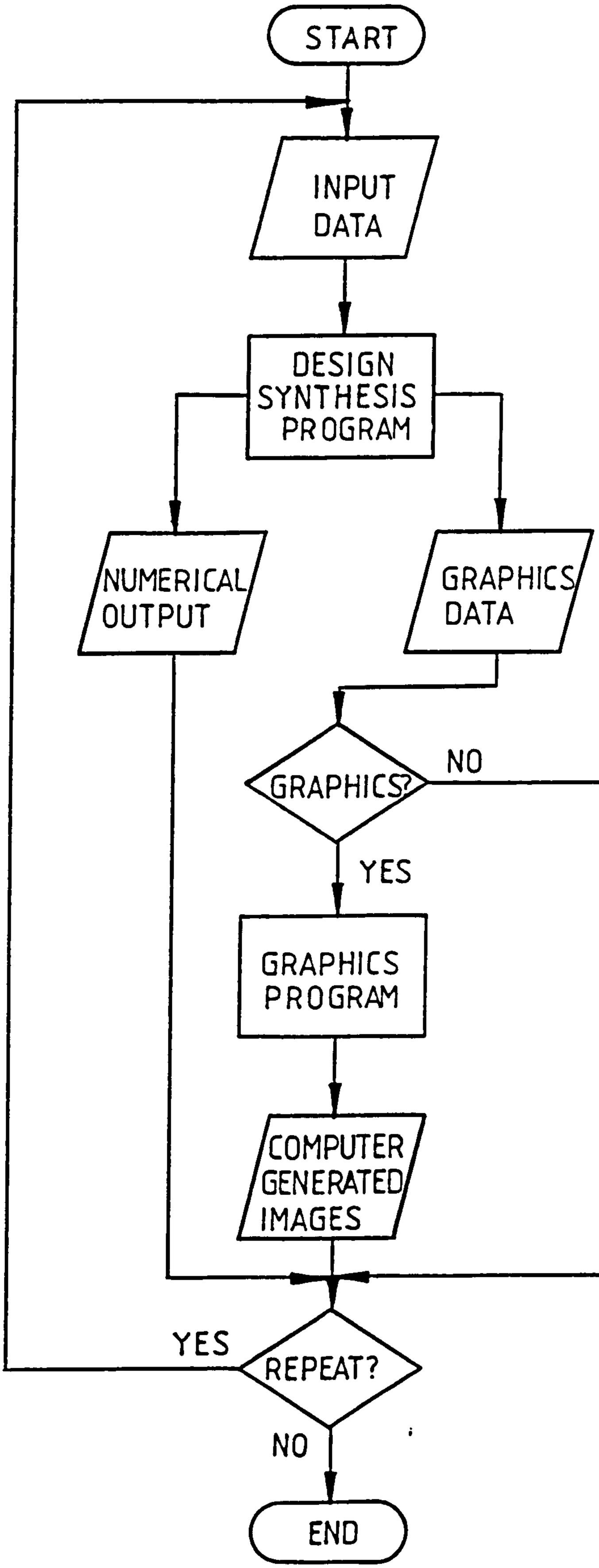

FIG.7.1 USER/PROGRAM INTERRELATION - SIMPLIFIED FLOW CHART

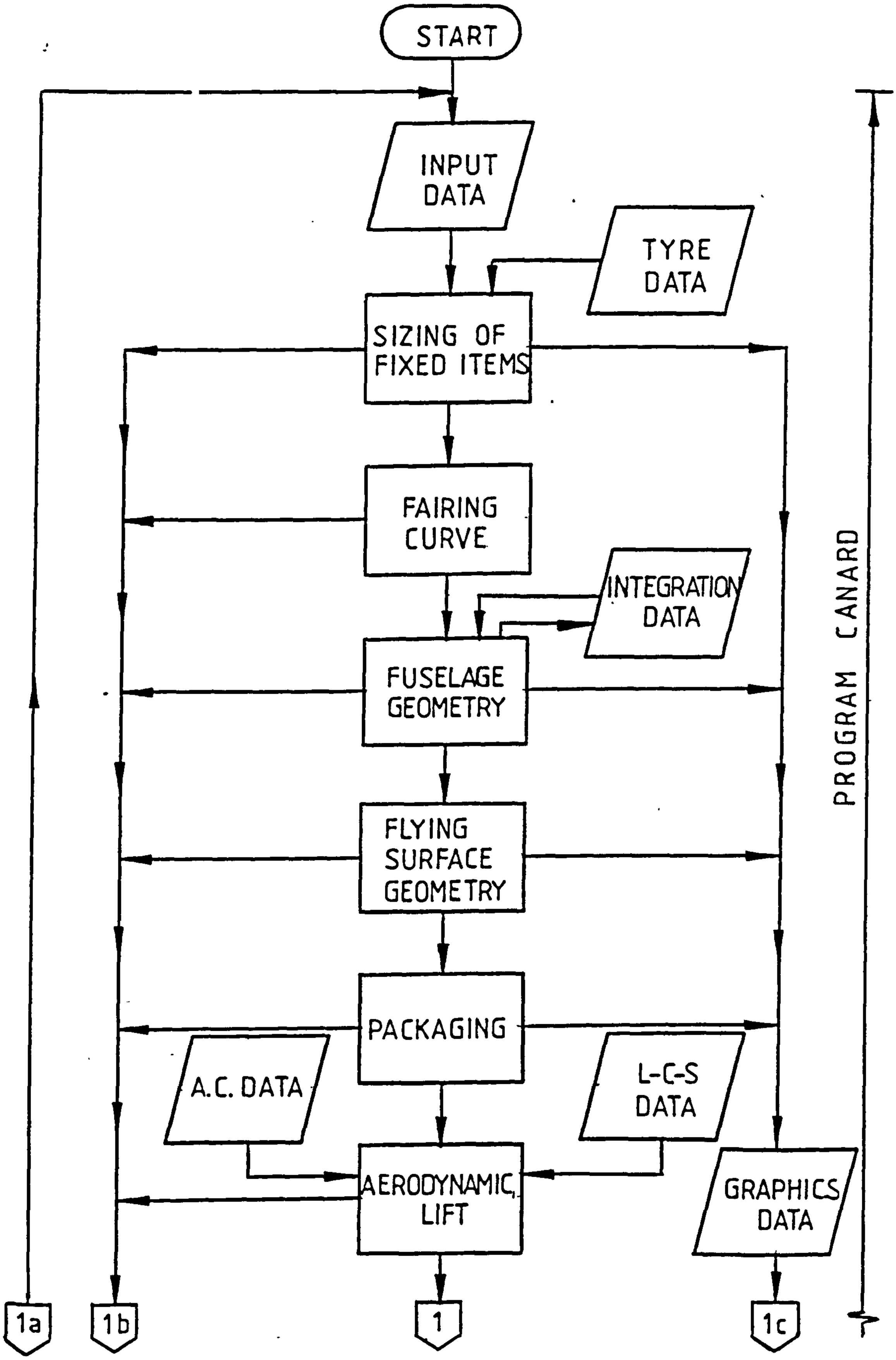

FIG.7.2 USER/PROGRAM INTERRELATION - EXPANDED FLOW CHART

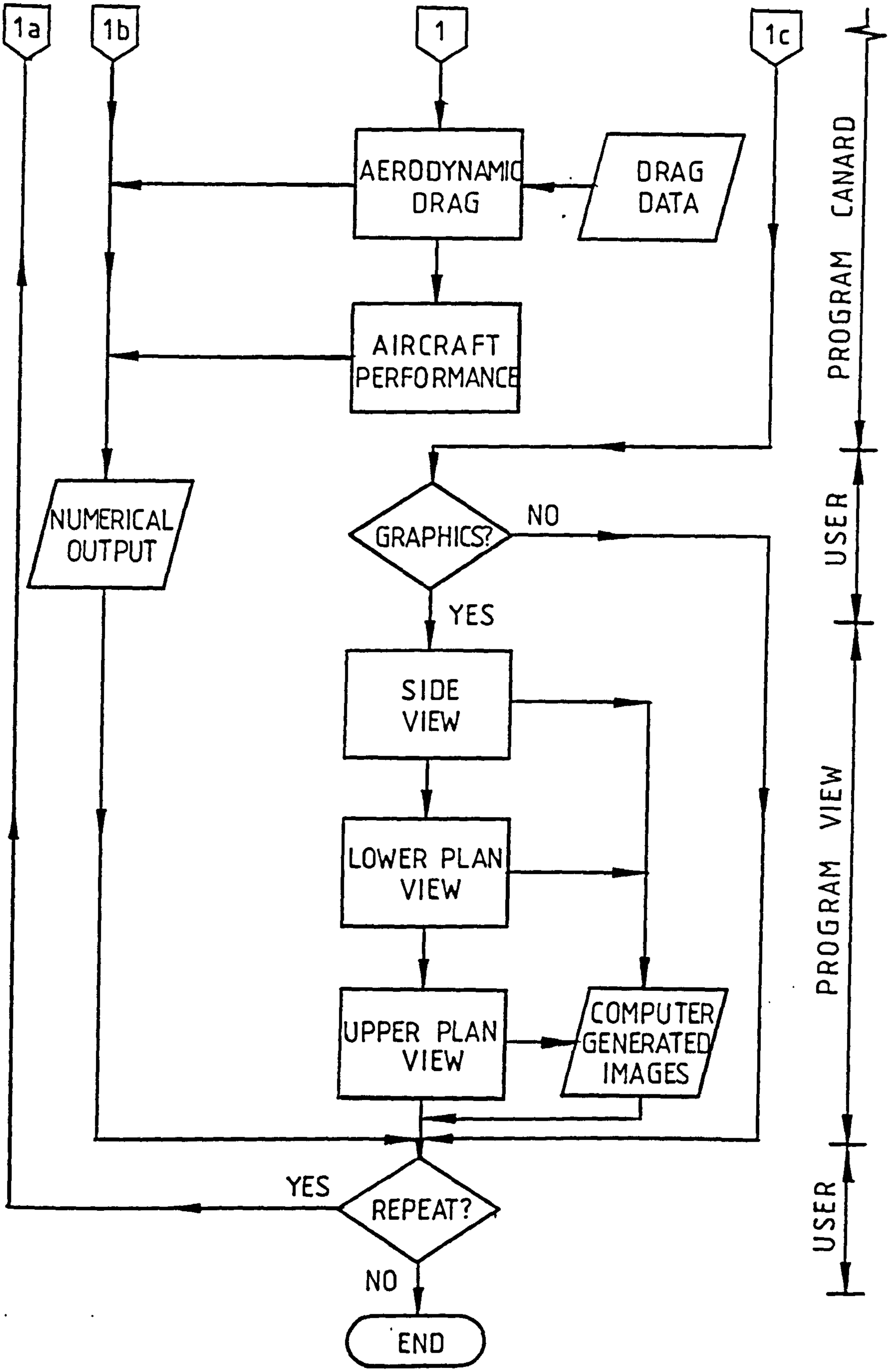
1a
1b
1
1c
AERODYNAMIC DRAG
DRAG DATA
AIRCRAFT PERFORMANCE
NUMERICAL OUTPUT
GRAPHICS?
NO
YES
SIDE VIEW
LOWER PLAN VIEW
UPPER PLAN VIEW
COMPUTER GENERATED IMAGES
REPEAT?
YES
NO
END
CANARD
PROGRAM
USER
PROGRAM VIEW
USER

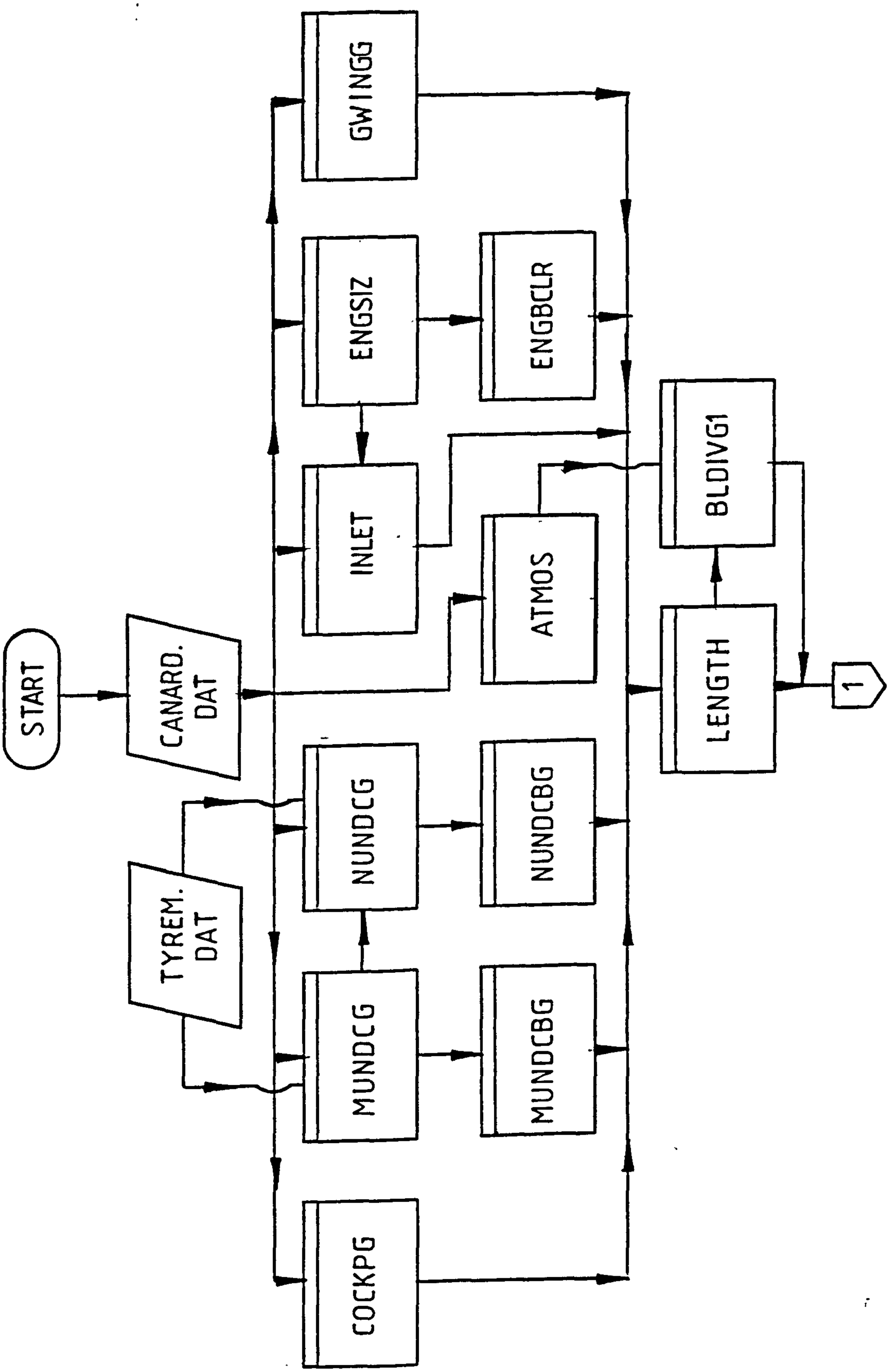

FIG. 7.3 PROGRAM CANARD - EXPANDED FLOW CHART

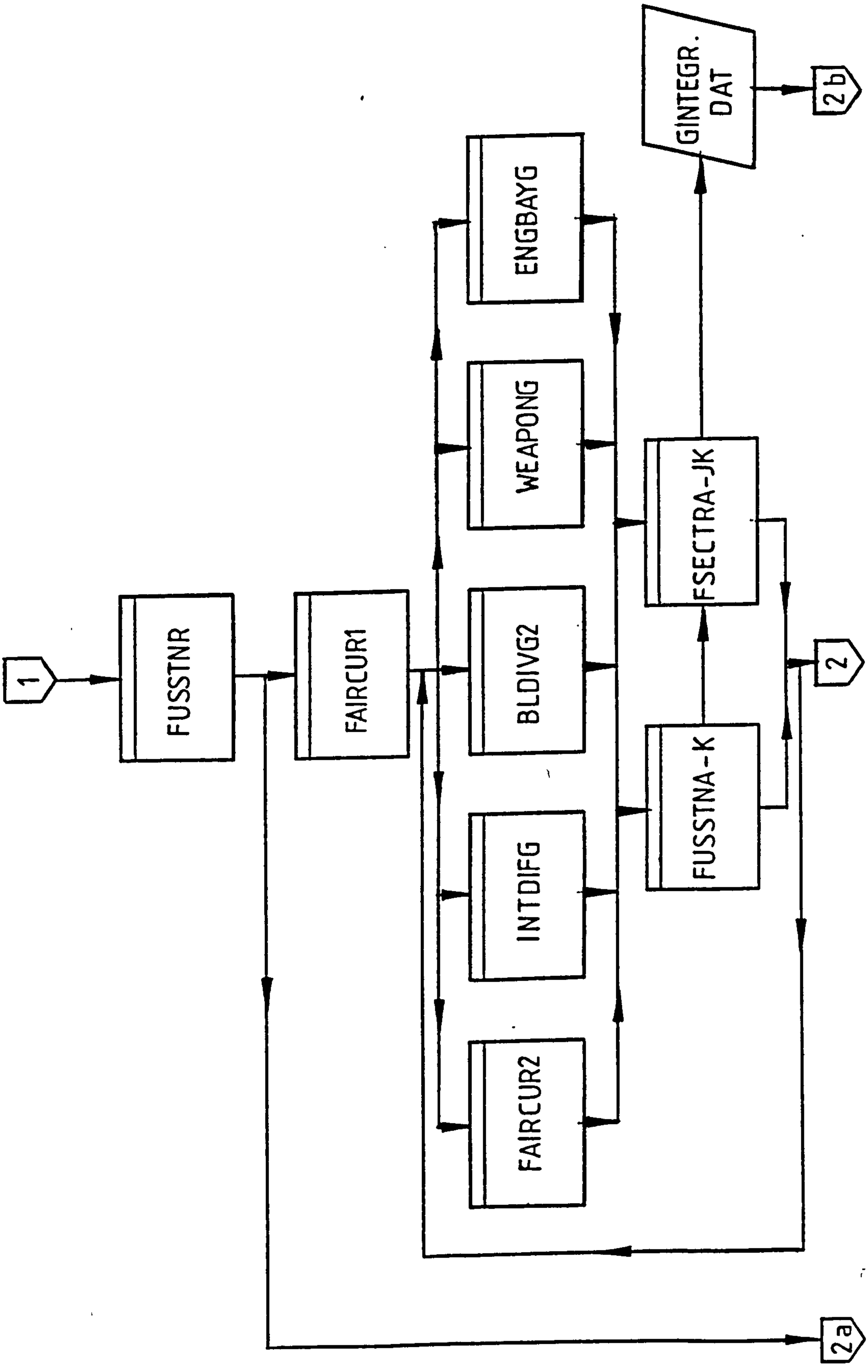
1
FUSSTNR
FAIRCUR1
BLDIVG2
INTDIFG
FAIRCUR2
ENGBAYG
WEAPONG
GINTEGR.
DAT
2b
FSECTRA-JK
FUSSTNA-K
2
2a

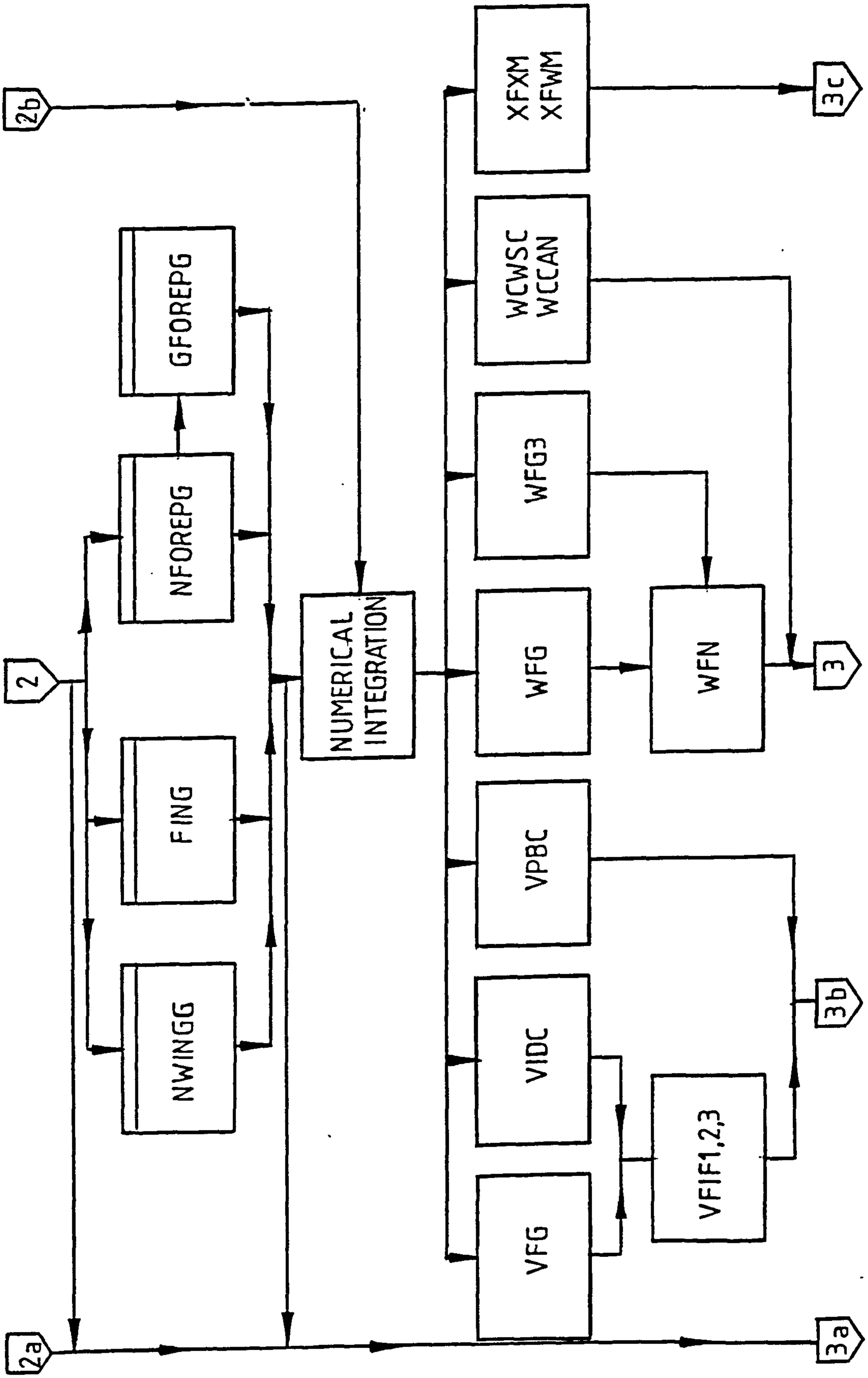
2b
GFOREPG
NFOREPG
2
FING
NWINGG
NUMERICAL INTEGRATION
XFXM XFWM
3c
WCWSC WCCAN
WFG3
WFG
WFN
3
VPBC
VIDC
VFG
VFIF1,2,3
3b
2a
3a

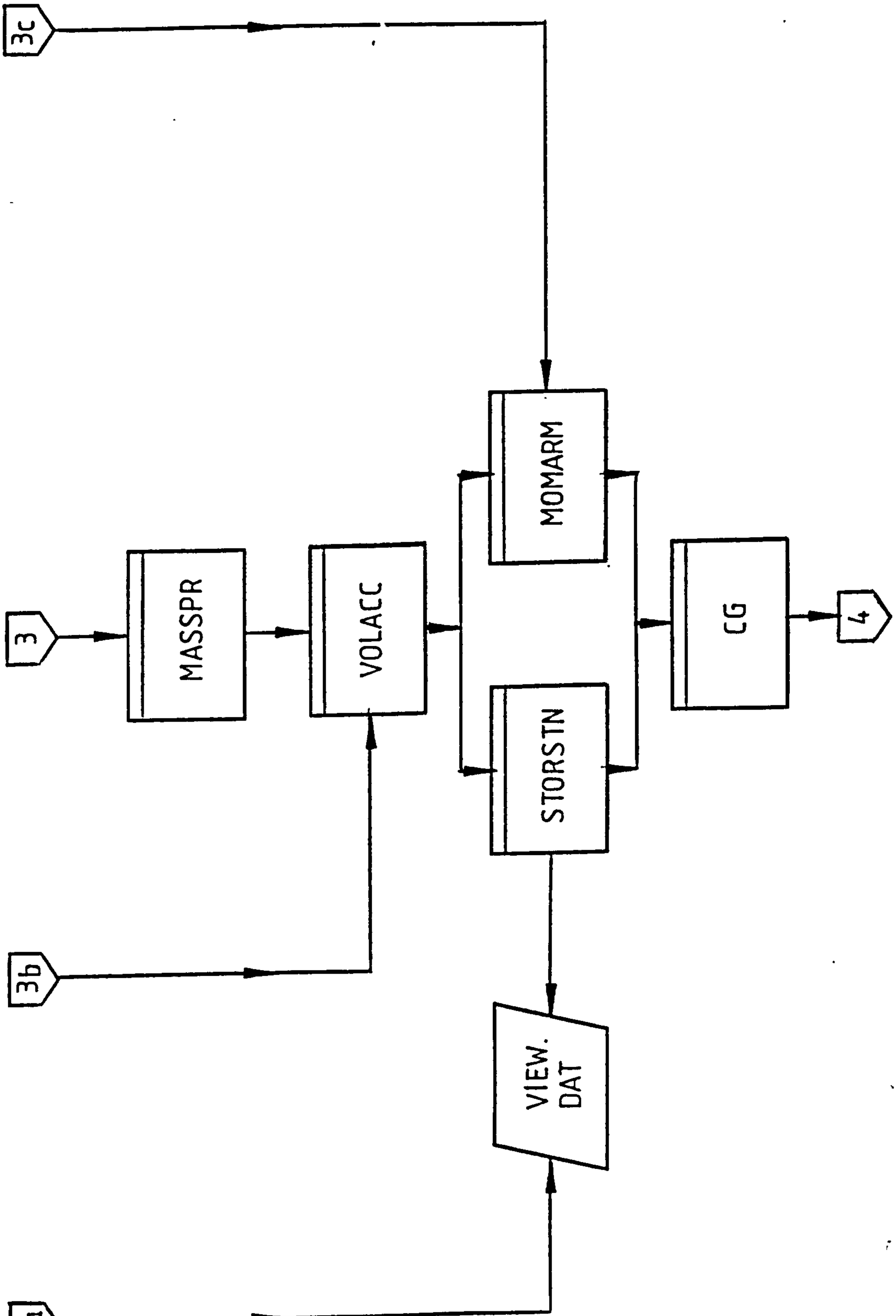
3c
3
MASSPR
VOLACC
MOMARM
CG
4
STORSTN
3b
VIEW.
DAT
3a

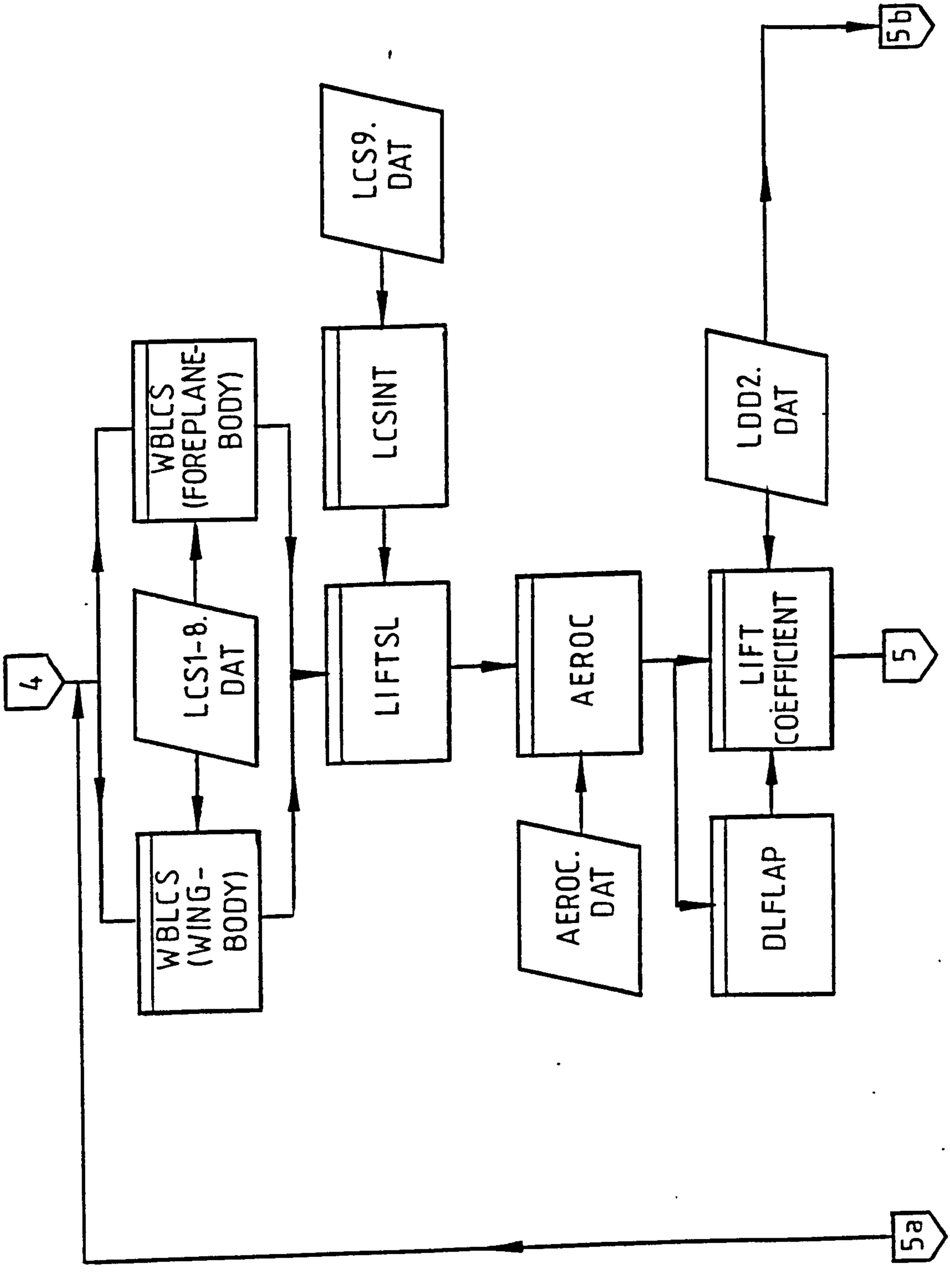
5b
LCS9.
DAT
LCSINT
WBLCS
(FOREPLANE-
BODY)
LCS1-8.
DAT
LIFTSL
AEROC
LOD2.
DAT
LIFT
COEFFICIENT
4
5
WBLCS
(WING-
BODY)
AEROC.
DAT
DLFLAP
5a

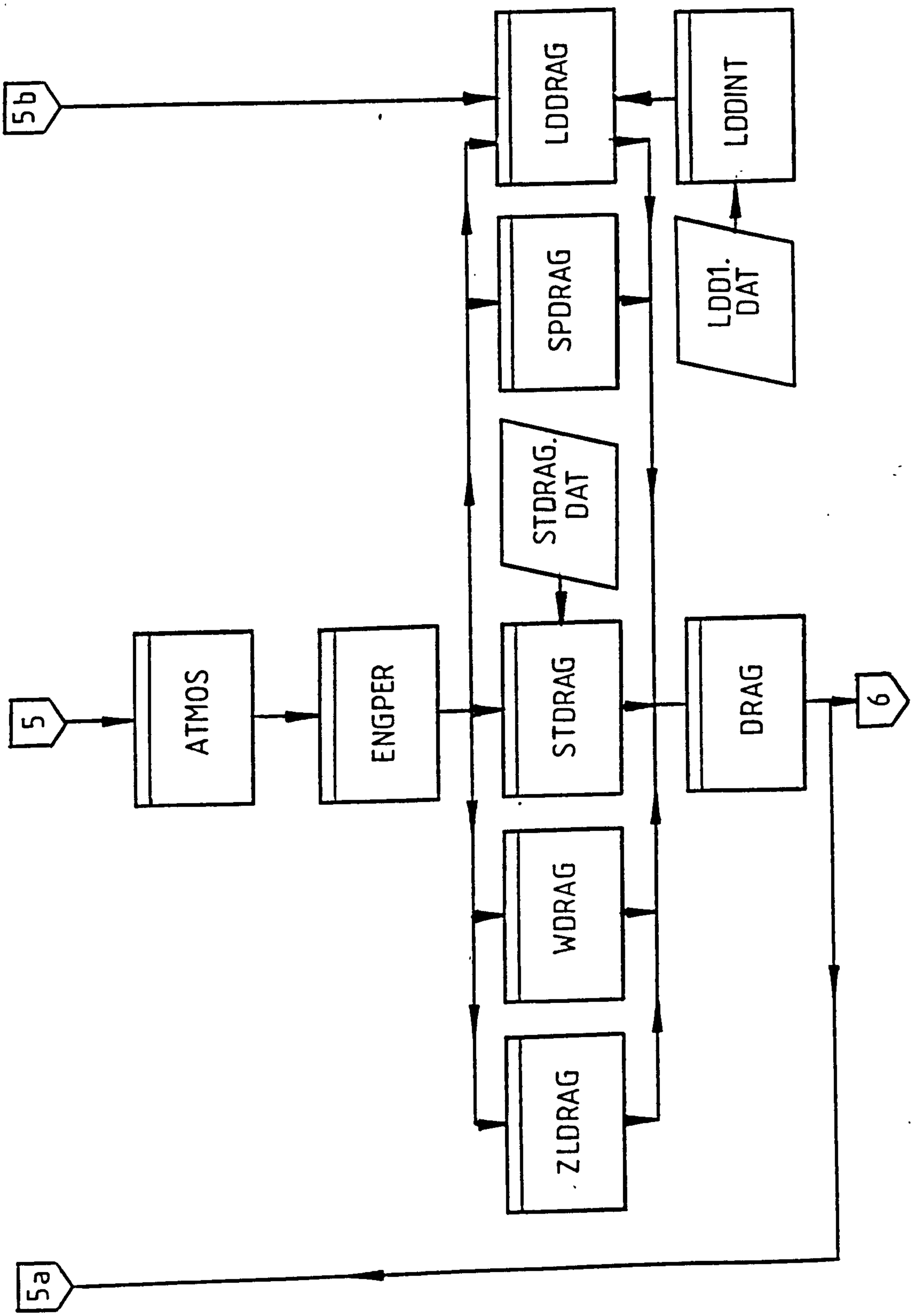
5b
LDDRAG
LDDINT
SPDRAG
LDD1.
DAT
STDRAG.
DAT
5
ATMOS
ENGPER
STDRAG
DRAG
6
WDRAG
ZLDRAG
5a

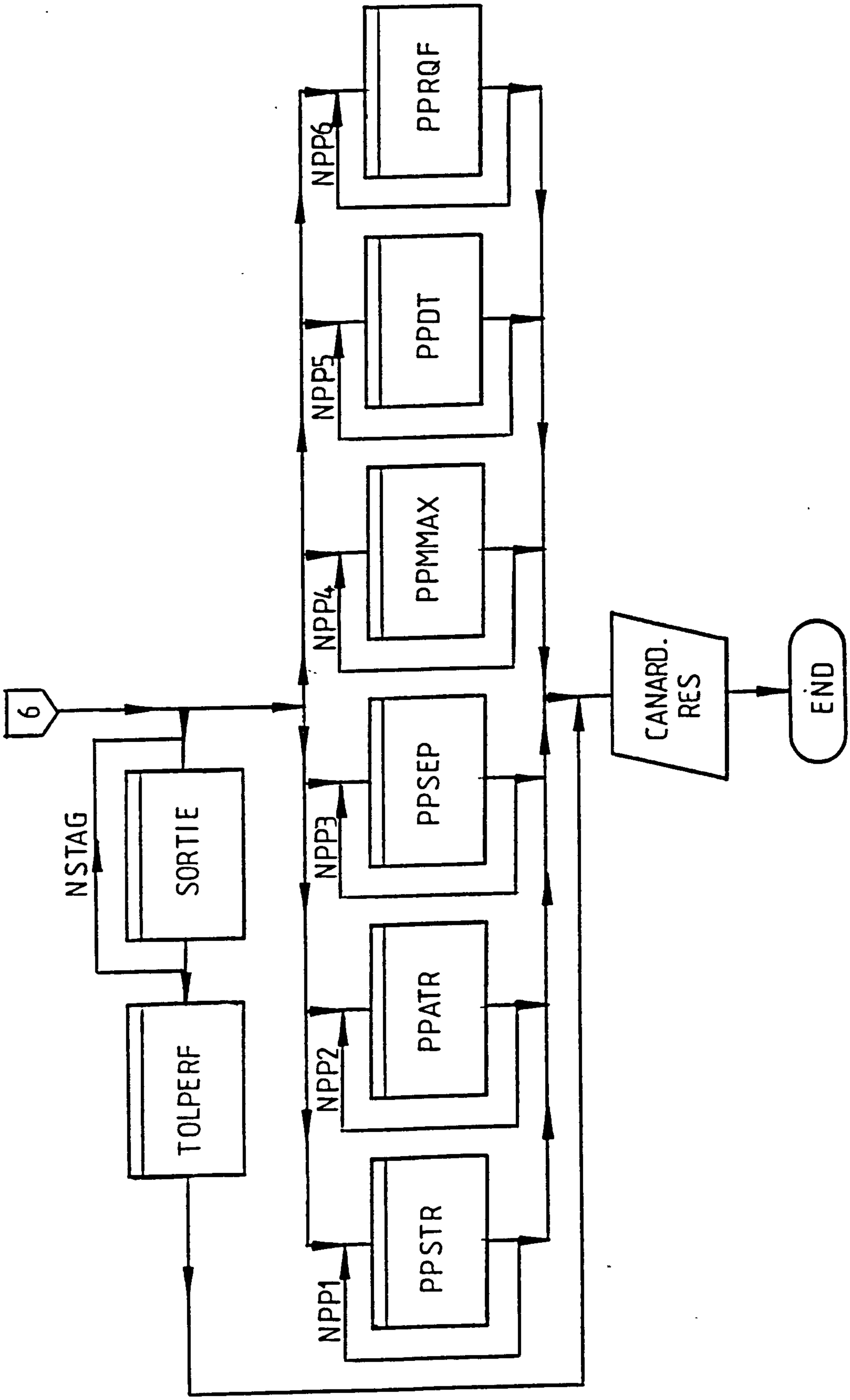
6
NSTAG
SORTIE
TOLPERF
NPP6
PPRQF
NPP5
PPDT
NPP4
PPMMAX
NPP3
PPSEP
NPP2
PPATR
NPP1
PPSTR
CANARD.
RES
END

COMPUTER GENERATED IMAGE OF THE SYNTHESIZED CONFIGURATION

(SIDE VIEW)

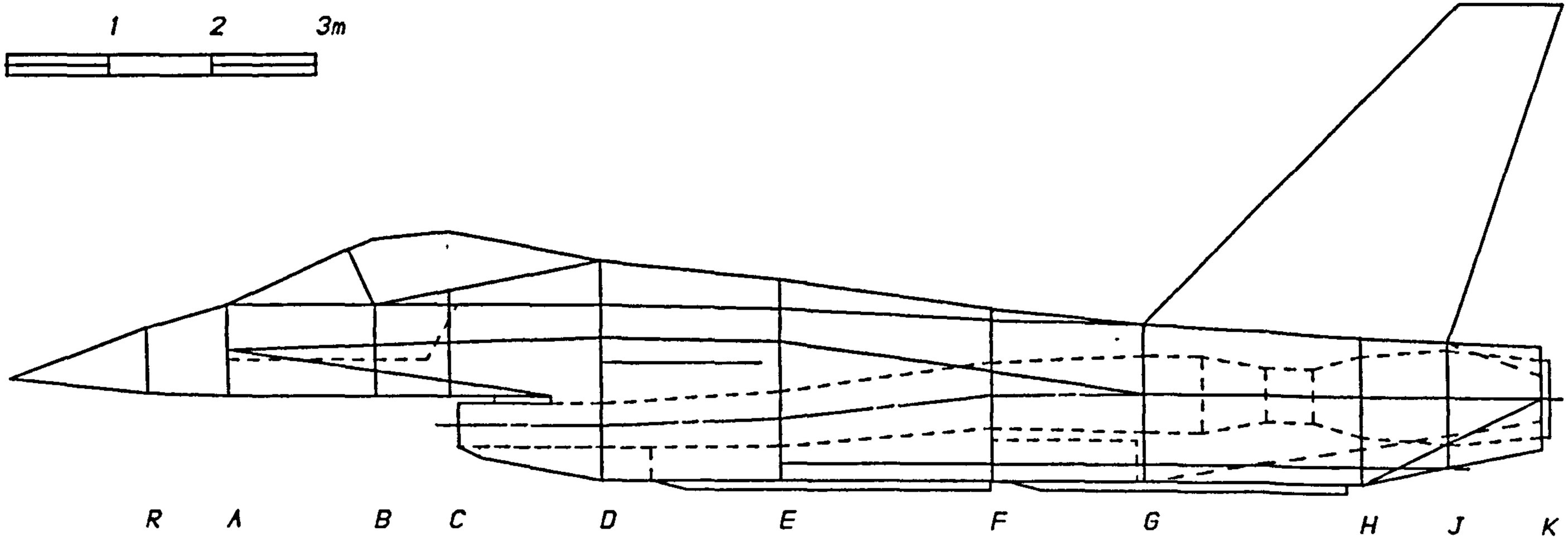

DESIGN SYNTHESIS
FOR
CANARD-DELTA COMBAT AIRCRAFT
BY, V.C.SERGHIDES
1985/87
COLLEGE OF AERONAUTICS
CRANFIELD INSTITUTE OF TECHNOLOGY

FIG. 7.4 COMPUTER GENERATED IMAGES (EXAMPLE)

COMPUTER GENERATED IMAGE OF THE SYNTHESIZED CONFIGURATION

(UPPER PLAN VIEW)

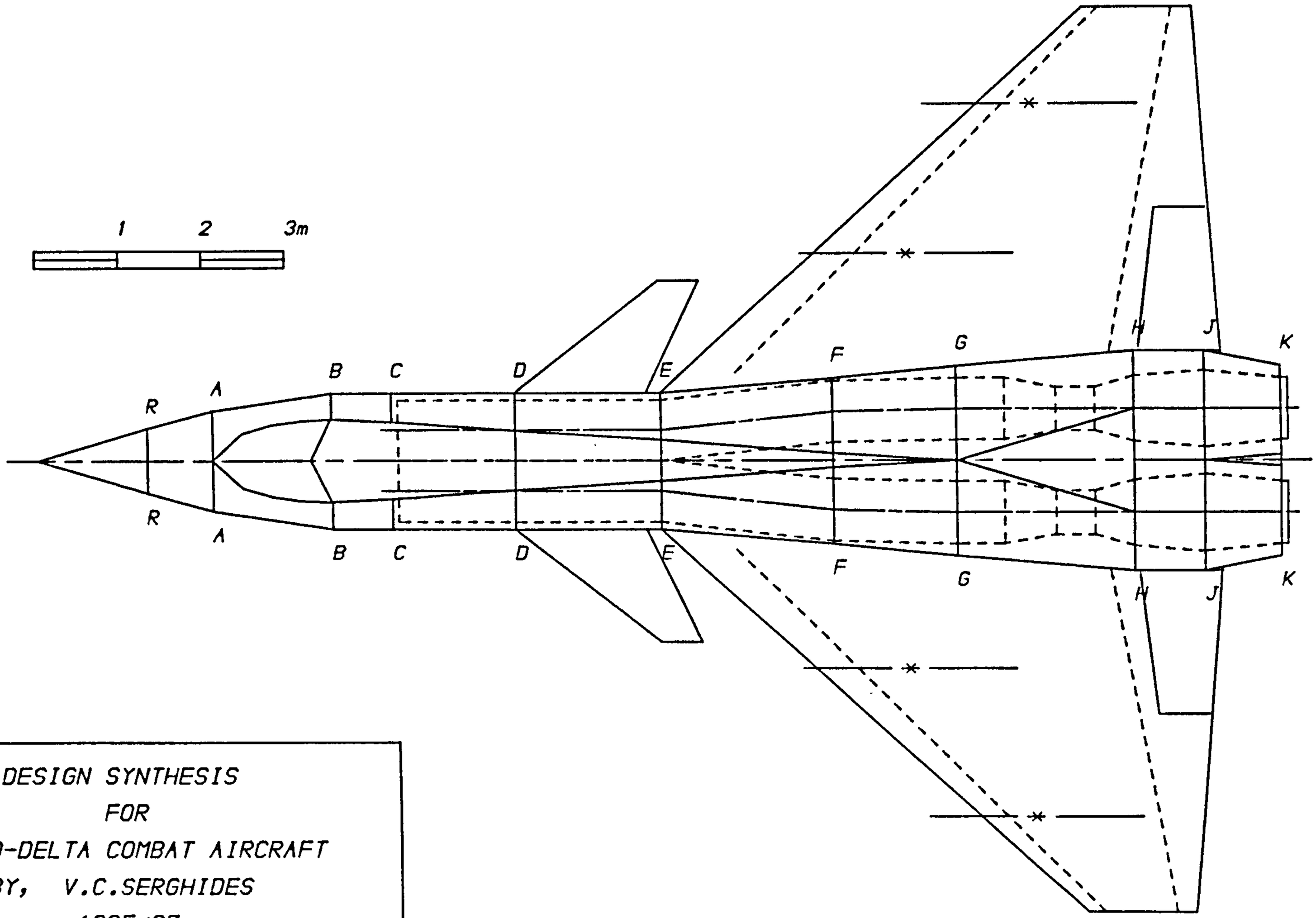

DESIGN SYNTHESIS
FOR
CANARD-DELTA COMBAT AIRCRAFT
BY, V.C.SERGHIDES
1985/87
COLLEGE OF AERONAUTICS
CRANFIELD INSTITUTE OF TECHNOLOGY

FIG. 7.4 (Continued ...)

COMPUTER GENERATED IMAGE OF THE SYNTHESIZED CONFIGURATION
(LOWER PLAN VIEW)

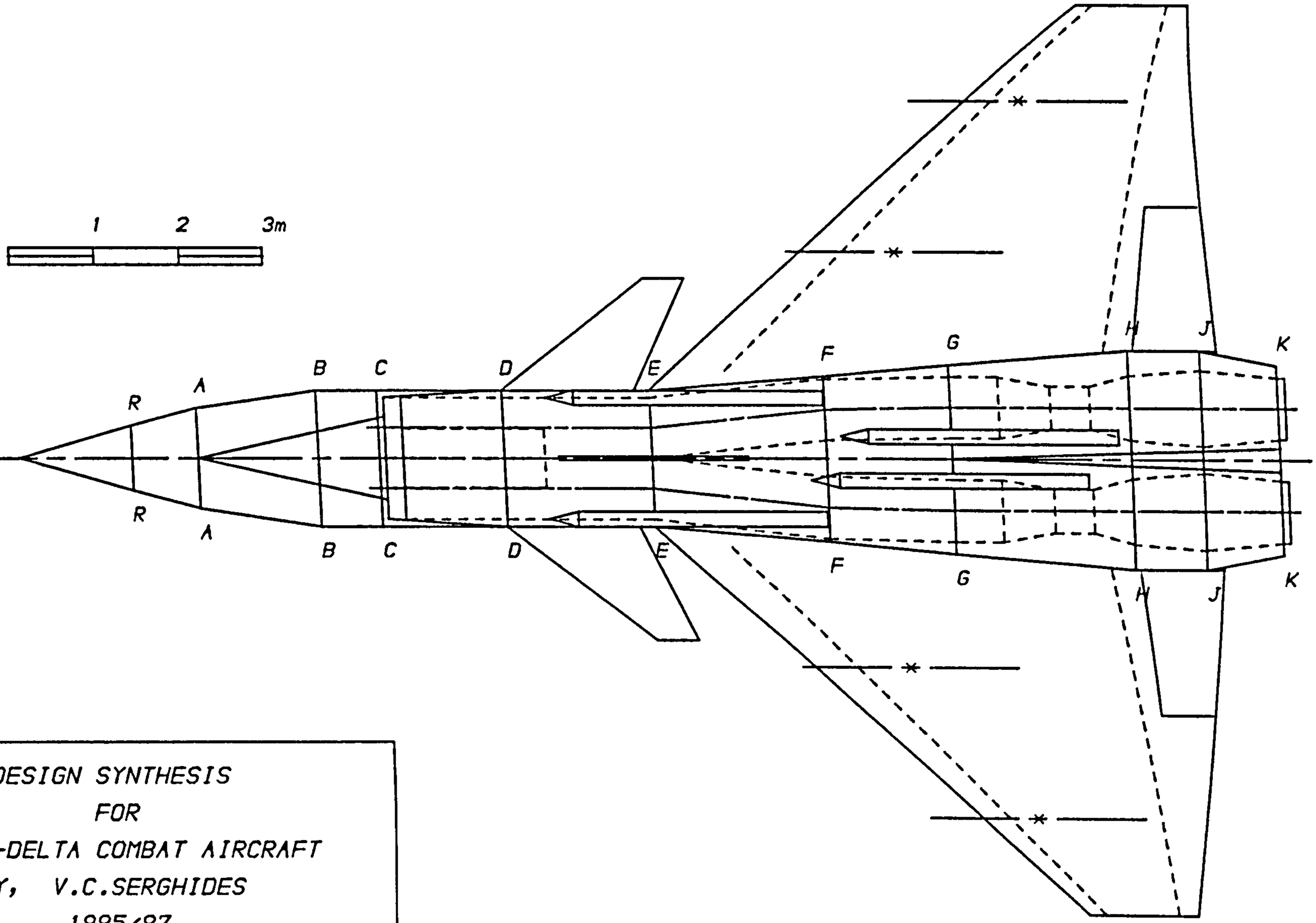

DESIGN SYNTHESIS
FOR
CANARD-DELTA COMBAT AIRCRAFT
BY, V.C.SERGHIDES
1985/87
COLLEGE OF AERONAUTICS
CRANFIELD INSTITUTE OF TECHNOLOGY

FIG. 7.4 (Continued)

CHAPTER 8

DISCUSSION

8.1 RESEARCH PROGRAMME REVIEW

The development of the Design Synthesis for canard-delta combat aircraft was a full-time Research Programme, undertaken in two consecutive phases, each of one year duration.

8.1.1 Phase I

This started in October 1985 with detailed automated and manual literature searches which were mainly directed towards reports and technical papers in the fields of combat aircraft design, computerized synthesis, advanced configurations, packaging, aerodynamics and performance. Special emphasis was placed on items specific to canard-delta configurations. These initial searches were carried back to 1970 and yielded several useful references. The literature search continued however, as a subsidiary activity, until the end of the programme in order to make use of the latest available information. All the initial references were examined carefully. A draft copy of ref.1 was also supplied by RAE(F). This was studied in depth in order to familiarize with the existing RAE system and a list of variables was produced. At the end of the first quarter a detailed plan was proposed for the development of the Design Synthesis.

During the second quarter, a baseline canard-delta configuration was developed. A study was also conducted, of typical weapon requirements in order to assess their effects on the overall aircraft geometry. The whole baseline configuration was mathematically modelled in 3-D detail and several modules were developed for the sizing of the fixed items, the fairing curve, and the geometry of the fuselage and flying surfaces.

A major part of the work during the third quarter was devoted to the coding and testing of the modules developed during the previous quarter. Any arising limitations were identified and eliminated and all geometry modules were further refined. Extra modules were also developed and coded, including that for the prediction of the aircraft mass.

New modules for the aircraft packaging and performance were developed during the fourth quarter and finally at the end of the first year, a skeleton Design Synthesis program was produced and run successfully by temporarily using dummy aerodynamic variables.

8.1.2 Phase II

The research during the first quarter of the second year concentated on the aerodynamics of the Synthesis and in particular on methods for the estimation of lift-curve-slope, canard-delta interference. lift due to flaps, aerodynamic centre, longitudinal static stability and drag. Many methods were investigated in order to establish their accuracy and applicability and the most suitable were finally selected for the Synthesis. The most significant findings of that quarter, however, concerned the close-coupled canard-delta interference effects on the lift-curve-slope, which were analysed in detail and quantified. Several new modules based on the above methods, were developed and coded and then added to the main program.

The canard-delta interference effects on the lift-dependent drag of the aircraft were investigated in detail during the second quarter and a method was hence determined for use in the Synthesis. The method was coded and tested initially with all the other drag modules, and then added to the main program. The performance modules were slightly

modified and the dummy aerodynamic variables were eliminated. Various other modules were also further developed to enhance the flexibility of the Synthesis program. The complete program was tested to a great extent for flexibility, sensitivity and accuracy and produced very sensible results.

A separate computer graphics program capable of producing three clear and detailed 2-D views of the synthesized configuration, was developed and successfully tested during the third quarter. The use of twin fins was also investigated and incorporated in the Design Synthesis as an option, for further configuration flexibility. The initial requirement for an investigation into the use of various air intake locations was finally excluded from the Research Programme with the approval of RAE, due to its low priority and lack of time.The two computer programs were successfully tested together for a wide range of independent variable values and the bounds of these variables were hence established.

The final quarter of the second year was mainly devoted to the preparation of the appendices of this thesis. All the methods and equations used were also concurrently checked for correctness, for a last time and a Final Version of the Design Synthesis computer program was produced.

8.2 BASELINE AIRCRAFT DESIGN

The baseline configuration, formed the basis for the development of the Design Synthesis. It was therefore developed according to the RAE requirements and agreed limitations. The final configuration was reached after several transformations and it was the result of a long series of logical design assumptions, decisions and compromises. It is realistic and incorporates a level of

Variable Print Quality

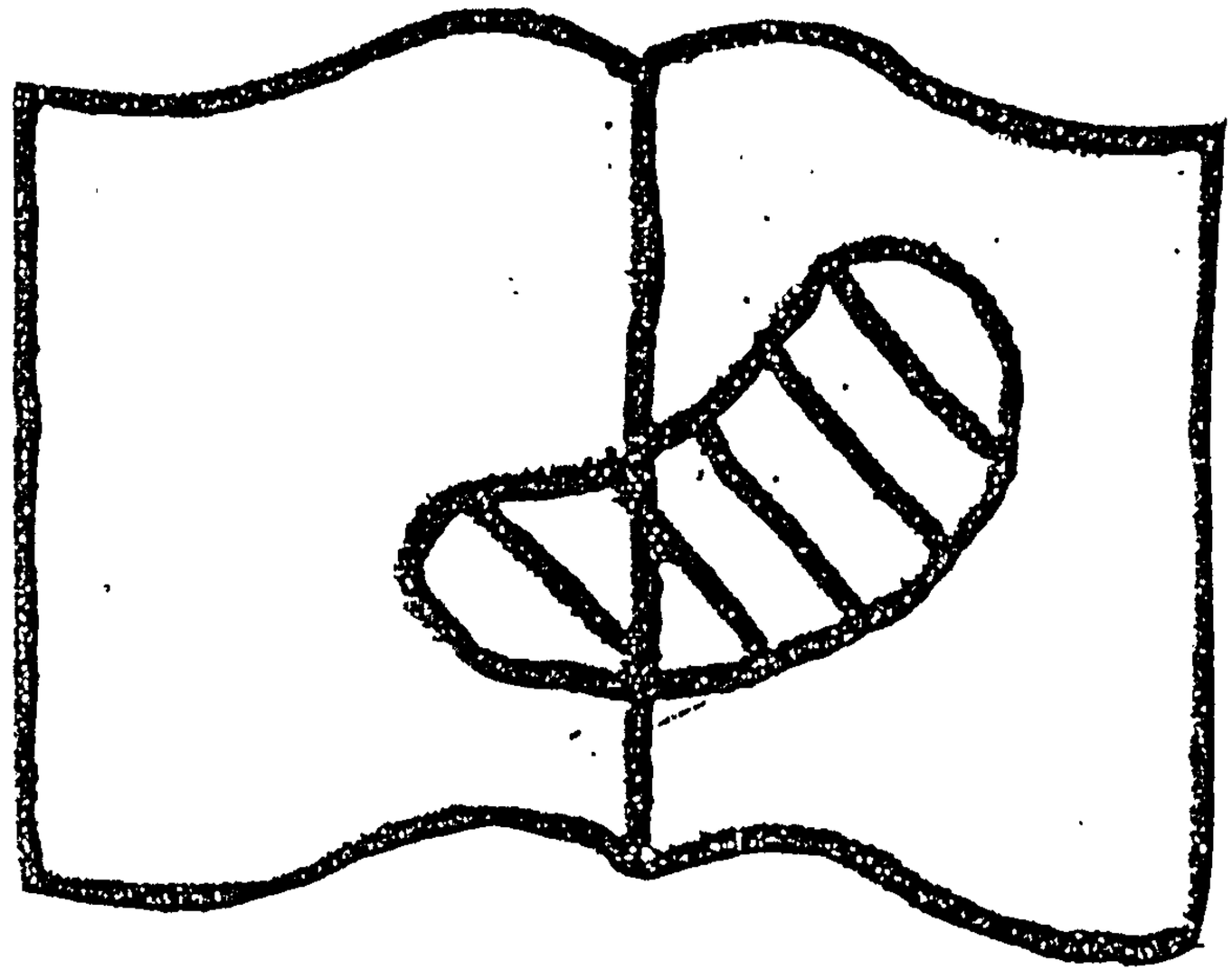

complexity equal to that expected in the preliminary design of a modern combat aircraft. All the items and lines shown on the baseline drawings (fig.2.1) are purely functional and they are included in the mathematical model of the aircraft. The surfaces of successive fuselage sections blend together uniformly. The fuselage shape was designed from the outset to offer maximum geometric flexibility with minimum constraints. The constraints are mainly imposed by the assumed packaging requirements. The baseline design assumptions in effect define the applicability of the Design Synthesis and reflect its sophistication.

8.3 AIRCRAFT GEOMETRY

The fuselage, flying surfaces and fixed items of the baseline configuration, were mathematically modelled in 3-D detail, by a large number of expressions which together define the shape and detailed dimensions of the aircraft, subject to the imposed constraints. The dimensions and geometric characteristics of the aircraft are essential for the subsequent packaging, aerodynamics and performance calculations. The mathematical models describe accurately every detail of the baseline aircraft. This detailed geometric representation of the aircraft is very significant in the Design Synthesis, because it allows the study of the effects of even minor configurational changes on the overall design. The Design Synthesis modules are interlinked in several complex combinations. A configurational change signalled by any of the geometry modules is therefore transmitted through the appropriate channels to all the related modules and it is hence translated as changes in the packaging, aerodynamics, or performance results. This increases considerably the sensitivity of the Design Synthesis.

The dimensions of the fixed items of the aircraft are estimated using empirical equations, mathematical models and design data. The estimated dimensions are used to define the packaging constraints which are also mathematically expressed. The empirical equations used for the sizing of the undercarriage are accurate and well-established. The automated standard-size tyre selection process was specially developed for this Design Synthesis. It allows the use of realistic tyre data for the sizing of the undercarriage legs and bays and thus minimises significantly any errors that could be caused by any tyre sizing approximations. The engine sizing module was supplied by RAE. All the other fixed items were mathematically modelled and their dimensions are estimated by substituting a set of design data. The correctness of those mathematical models was fully verified by applying them to the baseline aircraft.

The fairing curve defines the optimum longitudinal distribution of fuselage cross-sectional area for minimum supersonic drag. This proved to be a very good alternative method for the numerical application of the sonic area rule to the fuselage. Its validity was verified in comparison with the area distributions of the Saab Viggen and Northrop Hatol.

The mathematical models for the fuselage are the most complex. They can accurately determine the detailed cross-sectional dimensions, area and perimeter of the fuselage at any station along its length. The dimensions are determined in such a way so that the local packaging constraints are not violated, the fuselage surface blends uniformly with the adjacent surfaces and the net cross-sectional area of the fuselage is equal to that of the fairing curve. The fuselage shape may change substantially by adjusting the values of the appropriate fuselage variables in the above mathematical models. The correctness of the fuselage

geometry modules was verified by applying them to the baseline aircraft.

A minimum number of stations is considered in the numerical integrations for the estimation of the fuselage volume and surface area. This improved considerably the computational efficiency of the Design Synthesis program. The use of a significantly greater number of stations for this purpose, was fully investigated but produced no apparent improvement in accuracy, because of the assumed linearity and uniformity of the fuselage sections.

The mathematical models for the flying surfaces are also detailed and allow high geometric flexibility. The geometric characteristics of the flying surfaces, however,should always remain within the bounds of the Design Synthesis applicability. The fin geometry module also provides an option for twin-fins.

8.4 AIRCRAFT PACKAGING

The aircraft mass prediction module is based on well-established empirical methods which predict the mass of each main aircraft part or system, from its physical characteristics, the mass of its constituent components and a number of empirical constants. Some of these methods were modified to include suitable state-of-the-art factors, to account for any mass changes due to advances in the system-related technology. The methods for the estimation of the mass of the fuselage and flying surfaces, include allowances for the use of composites or other structural materials. A twin-fin mass factor was added to the single-fin equation, to account for the extra fuselage structure needed to support the two fins. The mass prediction methods were validated against published mass statements in refs. 11, 12

for VSTOL canard-delta combat aircraft and yielded results within six per cent of the corresponding published figures.

The volume accounting module was developed for this Design Synthesis, to provide an estimate of the required minimum fuselage volume, for comparison with the calculated actual fuselage volume. The accuracy of this module simply depends on the accuracy of the installed density figures and predicted masses, which are used for this purpose. Published information on aircraft system densities however, is scarce, but reasonable estimates were made.

The forward and aft c.g. limits of the aircraft are estimated by considering four extreme loading cases with regard to fuel state external stores and ammunition. The c.g. and longitudinal moment arm equations were consistently checked for correctness.

8.5 AIRCRAFT AERODYNAMICS

The sensitivity of the performance estimates to minor configurational changes, depends directly on the accuracy of the aerodynamic calculations. The aircraft aerodynamics translate the aircraft geometric characteristics to flight performance characteristics. Therefore, every effort was made during the development of the Design Synthesis, for the accurate and detailed estimation of the aircraft lift and drag.

The aircraft l-c-s is used in the performance modules of the Design Synthesis, to calculate the lift coefficient at a given aircraft incidence, within the linear range. L-c-s information is also used in the estimation of the lift increment due to flaps and the aerodynamic centre. A very detailed methodology was therefore developed for the estimation of the l-c-s. A selection of DATCOM methods are

used for the isolated wing-body and foreplane-body l-c-s values. The results are then individually corrected for the effects of canard-delta interference and added together to give an accurate estimate of the total aircraft l-c-s.

The long investigation into the effects of canard-delta interference on l-c-s, proved their significance and led to the development of a preliminary design method for their prediction. The investigation revealed that the magnitude of these effects varies with Mach number and depends on the height at which the foreplane is located above the wing-chord plane, the ratio of the net foreplane area to the gross-wing area and on the leading-edge sweep angle of the wing. Within the linear range of angles of attack, the wing-on-foreplane interference effects on l-c-s are favourable subsonically. These generally become more favourable as the foreplane size or height increase relative to the wing. The foreplane-on-wing interference effects however, are unfavourable at all speeds. These become more unfavourable as the wing leading-edge sweep or the foreplane size increases and less unfavourable as the foreplane height increases. The same investigation also showed that the total aircraft lift coefficient is higher than that of the isolated wing-body combination and that at high angles of attack the foreplane delays the stall and also raises the limit of linearity of the lift curve of the aircraft.

The detailed investigation into the effects of canard-delta interference on lift-dependent drag, indicated that the addition of a close-coupled foreplane to a delta wing-body combination, significantly reduces the values of the lift-dependent drag parameters K1 and K2 which define the lower and upper regions of a drag polar. Another preliminary design method was therefore developed for the prediction of these interference effects. The magnitude of

these effects varies with Mach number and depends again on the same parameters as those for the interference effects on l-c-s. The investigation showed that the values of K1 and K2 always reduce as the foreplane size or height relative to the wing increases. These also reduce as the wing leading-edge sweep decreases.

Both investigations were carried out scholastically and accurately and were based on coherent data, therefore the confidence in their results is very high. The data availabe for analysis, however, were rather limited and consequently this confidence is confined within the bounds of the data values used in the analysis. The interference factors were fully checked for correctness against the wind-tunnel data used in the analysis but no other independent data were available for a complete validation.

The store drag module was developed specifically for this computerized Synthesis and allows maximum flexibility, combined with accuracy. The estimation of all the other drag components is based on detailed methods from ref. 1. The trim drag component was excluded from the drag calculations because of the absence of detailed stability and control calculations in this Synthesis. (See paragraph 5.7.1)

Some of the lift and drag results for the Design Example, at Mach 0.4, 1.0 and 1.8, were plotted in various forms as shown at the end of appendix K. The first set of plots shows the variation of the total aircraft lift with incidence within the linear range for each of the above three Mach number values, while the second shows clearly the individual contributions of the non-isolated foreplane-body and wing-body combinations, to the above total aircraft lift. These results were obtained from equation G.41, assuming neutral stability with zero pitching moment. The

third and fourth sets of plots show the total aircraft untrimmed drag polars and lift/drag ratios assuming that the aircraft is 'clean', i.e. without external stores. The plots for Mach 1.0 and 1.8 include a small spillage drag contribution. The values of the lift and drag data shown in the above four sets of plots and also their observed variations with incidence and Mach number are all very sensible and compare favourably with similar plots in refs. 11 and 12.

Only the forward and aft longitudinal positions of the wing-body aerodynamic centre are estimated, because these are needed to determine the maximum longitudinal static stability margins in subsonic and supersonic flight.

8.6 AIRCRAFT PERFORMANCE

The Design Synthesis calculations finish with the estimation of the sortie, point, take-off and landing performance of the synthesized aircraft. These modules operate in conjunction with several other modules of the Synthesis which continuously provide them with the necessary data on aircraft lift, drag, engine performance and atmospheric properties. The modules for the engine performance and atmospheric properties were supplied by RAE(F). The sortie performance module in effect simulates a specified hypothetical sortie, to mainly estimate the fuel and time required by the synthesized aircraft to fly it. It is very flexible and accurate. It is based on iteration procedures which were developed according to guidelines given in ref. 1 and on equations derived from first principles. The take-off and landing performance module is based on proven empirical equations. The take-off equations were validated by estimating the take-off distances for the Tornado, Jaguar and Hawk. The results were all within 5% of the actual distances. The point performance parameters are

mainly estimated iteratively using equations derived from first principles, therefore their accuracy is high.

8.7 COMPUTER PROGRAMS

The objectives of this Research Programme were fully achieved with the successful development of two advanced computer programs for the automated implementation of the Design synthesis and Graphics. Both programs were developed following a methodical and systematic programming strategy. They are fully modular, easy to use and also fast and efficient, considering the enormous size and complexity of the processes they perform.

The Design Synthesis program was designed from the start for maximum efficiency, flexibility and accuracy. There was a constant battle during its development to maintain a correct balance between computational efficiency and Design Synthesis complexity, because of the need to run the program several times during optimization. The balance was successfully maintained with good programming and persistent testing. Out of the 77 modules of this program, only 3 were supplied by RAE(F). These are the modules for engine sizing, engine performance and atmospheric properties. All the other modules were developed from scratch but compatibility with the general requirements for use with the RAE system, was maintained throughout. The program was tested to a great extent and the bounds of its Independent Variables were established. The program fulfils all the RAE requirements.

The Graphics program produces three detailed and clear computer generated images of the synthesized configuration. The detail of these images is equal to that incorporated in the baseline configuration drawings. All the geometric results produced by the Design Synthesis program are clearly

and accurately presented in these images. These are extremely useful because they allow easy and quick assessment of the Design Synthesis results. The graphics program execution is controlled by the user in order to prevent unnecessary waste of CPU during the Design Synthesis optimization. The program was fully tested for flexibility, clarity and accuracy, with impressive results.

only 3 were supplied by RAE(F). These are the modules for engine sizing, engine performance and atmospheric properties. All the other modules were developed from scratch but compatibility with the general requirements for use with the RAE system, was maintained throughout. The program was tested to a great extent and the bounds of its Independent Variables were established. The program fulfils all the RAE requirements.

The Graphics program produces three detailed and clear computer generated images of the synthesized configuration. The detail of these images is equal to that incorporated in the baseline configuration drawings. All the geometric results produced by the Design Synthesis program are clearly and accurately presented in these images. These are extremely useful because they allow easy and quick assessment of the Design Synthesis results. The graphics program execution is controlled by the user in order to prevent unnecessary waste of CPU during the Design Synthesis optimization. The program was fully tested for flexibility, clarity and accuracy, with impressive results.

CHAPTER 9

CONCLUSIONS

9.1 DESIGN SYNTHESIS SYSTEM

A computerized Design Synthesis and analysis system has been developed, suitable for use with canard-delta configuration combat aircraft.

It is applicable to aircraft having a low cropped delta wing with a close-coupled foreplane, twin engines, chin air intakes and single or twin fins.

It is compatible with the general requirements for use with existing RAE multivariate optimization algorithms.

It provides suitable solutions to special preliminary design problems associated with the canard-delta layout and advances in aerospace technology.

It includes computer graphics which generate enhanced 2-D images of the synthesized configuration. These allow easy and quick assessment of the aircraft geometry results.

It produces a clear and detailed numerical output file with all the results of the aircraft geometry, packaging, aerodynamics and performance calculations.

It is fully modular and it may be therefore easily extended or modified.

It incorporates a level of complexity equal to that expected in the preliminary design of advanced combat aircraft.

It is based on sound methods and it is detailed, accurate, flexible, sensitive to minor configurational changes, computationally efficient and fast.

It must not be treated as a 'black box'. The user must be familiar with the system and needs to have aircraft design and computing experience.

It may be used for preliminary design and manual optimization, for assessing project studies or existing designs, for specifying operational requirements, for selecting configurations for more detailed consideration, for exploring the likely effects of research advances and for studying the effects of changing variables on the overall design.

9.2 CANARD-DELTA LAYOUT

The canard-delta layout offers superior aerodynamics and performance advantages over its conventional aft-tail counterparts.

The aerodynamic interference between a delta wing and a close-coupled foreplane, has significant effects on the aircraft lift-curve-slope and lift-dependent drag.

Preliminary design methods have been developed for the prediction of the canard-delta interference effects.

The magnitude of these effects varies with Mach number and depends on the ratio of the height at which the foreplane is located above the wing-chord plane to the mean geometric chord of the wing, the ratio of the net foreplane area to the gross wing area and the leading-edge sweep angle of the wing.

Within the linear range of angles of attack, the wing-on-foreplane interference effects on l-c-s are favourable subsonically. The foreplane-on-wing interference effects are unfavourable at

all speeds. The total aircraft coefficient, however, is higher than that of the isolated wing-body combination.

At high angles-of-attack the foreplane delays the stall and raises the limit of linearity of the lift curve of the aircraft.

The addition of a close-coupled foreplane to a delta wing-body combination significantly reduces the values of the lift-dependent drag parameters K1 and K2 which define the lower and upper regions of a drag polar.

CHAPTER 10

RECOMMENDATIONS

10.1 RECOMMENDATIONS FOR FUTURE WORK

A complete Design Synthesis Optimization program is to be the subject of further work this year. It will incorporate the present system described in this thesis together with existing RAE multivariate optimization algorithms.

It is recommended however, that work on the present system continues in the future beyond the optimization.

The flexibiliy and applicability of the system may be further increased with additional modules which will allow the use of a single engine, alternative intake locations and tandem seats.

The system may be enhanced with the development of stability and control modules which will also make possible the estimation of the trim drag.

The applicability of the canard-delta interference prediction methods may be extended beyond the present confidence limits, provided sufficient wind-tunnel data become available in the future.

The performance modules may be also extended to include the estimation of more parameters.

The graphics program may be upgraded to a 3-D version.

The present system may be also used as a basis for the future development of similar systems for other classes of aerospace vehicles.

REFERENCES

REFERENCES

1. LOVELL, D.A. — The application of Multivariate Optimization to Combat Aircraft Design, Unpublished Report, Aerodynamics Department, RAE(F)

2. HOWE, D. and FIELDING, J.P. — Aerospace Vehicle Design, MSc course notes, CoA, Cranfield Institute of Technology. 1985

3. TORENBEEK, E. — Synthesis of subsonic airplane design, Delft University Press, 1981

4. NICOLAI, L.M. — Fundamentals of Aircraft Design METS, Inc., 1975

5. CORNING, G. — Supersonic and Subsonic CTOL & VTOL Airplane Design, 4th edition, 1976

6. ANONYMOUS — Fighter aircraft design, AGARD-CP-241, 1977

7. ANONYMOUS — Preliminary aircraft design, AGARD-LSP-65, 1974

8. FLETCHER and BURNS, B.R.A — Supersonic combat aircraft design Aeronautical Journal, December 1979

9. BURNS, B.R.A. — Advanced aerodynamic design for future combat aircraft, ICAS Paper 1.1.2, 1982

10. MANGOLD, P. — Some aerodynamic aspects of the design of future combat aircraft, ICAS Paper 1.1.3, 1982

11. BROWN, S.H. — Study of aerodynamic technology for VSTOL fighter/attack aircraft, horizontal attitude concept. Final report, Northrop Corp., NASA CR-152130, 1978

12. ANONYMOUS
Study of aerodynamic technology for VSTOL fighter/attack aircraft, phase 1, Final report, Vought Corp., NASA CR-152132, 1978

13. PATEL, T.S. and DIXIT, C.S.
Optimum selection of main parameters for the reverse design of a supersonic military aircraft, Canadian Aero & Space Journal, Vol 26, No.3, 3rd Quarter 1980

14. KUETHE, A.M. and CHOW, C.Y.
Foundations of Aerodynamics: Bases of aerodynamic design, 3rd edition, Wiley, 1976

15. ANONYMOUS
USAF Stability and Control DATCOM, Flight Control Division, Air Force Flight Dynamics Laboratory, 1975

16. ANONYMOUS
AVP970, MoD

17. LOVELL, D.A.
Some experiences with numerical optimization in aircraft specification and preliminary design studies, RAE Tech. Memo AERO 1850, May 1980

18. MOTHERSILL, R.J.
A twin-engine version of the combat aircraft multivariate optimization program, RAE Tech. Memo AERO 1902, Nov. 1981

19. COLLINGBOURNE, J.
Multivariate optimization applied to the initial design of transport aircraft, RAE Tech. Report 84044, 1984

20. LEE, V.A.
Computerized aircraft synthesis, Journal of Aircraft, Vol.4, No.5, 1967

21. HITCH, H.P.Y.
Computer aided aircraft project design, Aeronautical Journal, February 1977

22. HABERLAND, C. THORBECK, J. and FENSKE, W.
A computer augmented procedure for commercial aircraft preliminary design and optimization, ICAS Paper 4.8.1, 1984

23. COEN, P.G. and FOSS, W.E.
Computer sizing of fighter aircraft, Journal of Aircraft, Vol.23, No. 5, 1986

24. McGEER, and KROO, I.
A fundamental comparison of canard and conventional configurations, Journal of Aircraft, Vol.20, No.11, November 1983.

25. NICHOLAS, W.U. and HUFFMAN, J.K.
An evaluation of the relative merits of wing-canard, wing-tail and tailess arrangements for advanced fighter applications, ICAS Paper 2.7.3, 1984

26. WEDEKIND, G.
Tail vs Canard configurations, an aerodynamic comparison with regard to the suitability for future tactical combat aircraft, ICAS Paper 1.2.2, 1982

27. FELLERS, W.E
Tail configurations for highly manoeuvrable combat aircraft, AGARD CP-319, October 1981

28. GOLDSTEIN, S.E. and COMBS, C.P.
Trimmed drag and maximum flight efficiency of aft-tail and canard configurations, AIAA Paper No. 74-69, 1974

29. LANDFIELD, J.P. and RAY, D.
Canard/Tail comparison for an advanced variable sweep wing fighter, AIAA Paper No. 84-2401, 1984

30. BEBRBOBM, H.
Basic low speed aerodynamics of the short-coupled canard configuration of small aspect ratio, SAAB TN-60, 1966

31. DOLLYHIGH, M.S. — Static longitudinal aerodynamic characteristics of close-coupled wing-canard configurations at Mach numbers from 1.6 to 2.86, NASA TN D-6597

32. GLOSS, B.B. — Effect of canard location and size on canard-wing interference and aerodynamic-center shift related to manoeuvering aircraft at transonic speeds, NASA TN D-7505, June 1974

33. GLOSS, B.B. — The effect of canard leading-edge sweep and dihedral angle on the longitudinal and lateral aerodynamic characteristics of a close-coupled canard-wing configuration, NASA TN D-7814, December 1974

34. GLOSS, B.B. — Effect of wing planform and canard location and geometry on the longitudinal aerodynamic characteristics of a close-coupled canard-wing model at subsonic speeds, NASA TN D-7910, June 1975

35. GLOSS, B.B. and McKINNEY, L.W. — Canard-wing lift interference related to manoeuvering aircraft at subsonic speeds, NASA TM X-2897

36. LACEY, D. and CHORNEY, W. — Subsonic aerodynamic characteristics of close-coupled canards, David W Taylor Naval Ship Research and Development Center, March 1971

37. KROUSE, J.R. — Effects of canard planform on the subsonic aerodynamic characteristics of a 25-degree and 50-degree swept wing, David W Taylor Naval Ship Research and Development Center, May 1972

38. LACEY, D.W. — Aerodynamic characteristics of the close-coupled canard as applied to low-to-moderate swept wings; Vols 1,2 & 3, David W Taylor Naval Ship Research and Development Center, 1979

39. PAULSON, J.W. and THOMAS, J.L. — Transition aerodynamics for close-coupled wing-canard configurations, AIAA Paper No. 79-0336, 1979

40. STOLL, F. and MINTER, E. — Large scale wind-tunnel tests of a sting-supported V/STOL fighter model at high angles of attack, AIAA Paper No. 81-2621, 1981

41. STOLL, F. and KOENIG, D.G. — Large scale wind-tunnel investigation of a close coupled canard-delta-wing fighter model through high angles of attack. AIAA Paper No.83-2554,1983

42. DE SILVA, B.M.E. and CARMICHAEL, R.L. — Canard-wing shape optimization with aerodynamic requirements, Journal of Aircraft, Nov. 1978

43. FEISTEL, T.W. — Wind-tunnel measurements of wing-canard interference and comparison with various theories, SAE Tech.Paper 810575, April 1981

44. KRAUS, W. — Delta-canard configurations at high angle of attack, Zeitschrift fur flugwissenschaften und Weltraumforschung, vol. 7, Jan-Feb. 1983

45. KRAUS, W. — Wing design for delta-canard configurations, ICAS Paper 2.7.4, 1984

46. HOERNER, S.F. — Fluid dynamic drag, Published by the author, 1958

47. NELSON, R.L. and WELSH, C.J. — Some examples of the application of the transonic and supersonic area rules to the prediction of wave drag. NASA TN-D-446, September 1960

48. KROO, I.M. and McGEER, T.M. — Optimization of canard configurations - an integrated approach and practical drag estimation method, ICAS Paper 6.8.1, 1982

49. BUTLER, G.F. — Effect of downwash on the induced drag of canard-wing combinations, Journal of Aircraft, Vol.19, No. 5

50. BUTLER, G.F. — An analytical study of the induced drag of canard-wing-tail aircraft configurations with various levels of static stability, Aeronautical Journal, October 1983

51. FRAENKEL, L.E. — The external drag of some pitot-type intakes at supersonic speeds, part II, RAE Farnborough, Report No. AERO 2422, June 1951

52. SEDDON, J. — Note on the spillage drag of pitot-type air intakes at transonic speeds. RAE Farnborough Tech. Note No. AERO 2315, August 1954

53. WINTER, K.G. and GAUDET, L. — Some recent work on compressible turbulent boundary layers and excrescence drag, RAE Tech. Memo. AERO 1115, December 1968

54. MOUNT, J.S. — Additive drag on inlet cowls and its effect on aircraft performance, Paper in AGARDOGRAPH 103, 1965

55. SEDDON, J. and GOLDSTEIN — Intake Aerodynamics. Collins, 1985

56. NEUMANN, H.E. — An analytical and experimental study of a short S-shaped subsonic diffuser of a supersonic inlet, AIAA Paper No. 80-0386, 1980

57. HUNTER, C.J. — Mini Cas aircraft aerodynamics, CoA - CIT, 1980

58. PERKINS, C.D. and HAGE, R.E. — Airplane performance, stability and control, Wiley, 1949

59. WILLIAMS, J. — Aircraft Performance AGARD-LS-56, March 1973

60. DAVIES, L. — An analysis of conventional and partly jet-borne take-off, RAE Tech.Report 76112, 1976

61. FOSS, W.E. — A computer technique for detailed analysis of mission radius and manoeuvrability characteristics of fighter aircraft, NASA TP 1837, 1981

62. MANGOLD, P. — Possibilities for the valuation of different combat aircraft configurations with respect to flight mechanics, ICAS Paper 2.2, 1980

63. FISHER, V.A. — Engine controls for the 1980 and 1990, ICAS Paper 4.6.3, 1982

64. HERRMANN, O. — Effect of engine technology on advanced fighter design and cost, ICAS Paper 5.1.1, 1984

65. BOWERS, D.L. — Application of advanced exhaust nozzles for tactical aircraft, ICAS Paper 4.1.1, 1982

66. SMITH, H.W. and BURNHAM, R. — The outside has to be bigger than the inside, Journal of Aircraft, June 1981

67. ANONYMOUS — Aircrew station geometry for Military aircraft, U.S. MIL-STD-1333, DoD, 1970

68. ROE, G.
The design of future cockpits for high performance fighter aircraft,
Aeronautical Journal,
April 1978

69. LYONS, J.W.
A theoretical and practical design investigation of the future Military cockpit,
ICAS Paper 8.3, 1980

70. SERGHIDES, V.C.
Advanced Technology Ejection Seats,
BSc Project, Honours School of Aeronautical Engineering,
University of Manchester, 1984

71. HIRST, M.
Avionics-Functional Design
Lecture notes, section K,
CoA - CIT, 1985

72. ANONYMOUS
Jane's Avionics
Jane's Publishing Co. Ltd. 1987

73. KUCHTA, B.J.
Use of fly-by-wire to obtain performance improvements in a delta-canard design,
AIAA Paper No. 75-1061, 1975

74. FOLKESSON, K.
Design and experience with a low-cost digital fly-by-wire system in the SAAB JA37 Viggen aircraft,
ICAS Paper 3.2.2, 1982

75. KAUL, H.J.
SELLA, F. and
WALKER, M.J.
The flight control system for the Experimental Aircraft Programme (EAP) Demonstrator aircraft,
Paper in AGARD CP-384, 1985

76. COTTA, R.
Fly-by-Light,
Aviation (Magazine), June 1979

77. CONWAY, H.G.
Landing gear design,
Chapman and Hall, 1958

78. CURREY, N.S.
Undercarriage design hand-book,
Lockheed-Georgia, 1982

79. ANONYMOUS
Aircraft tyre specifications,
Dunlop

80. TAYLOR, J.W.R. — Jane's all the world's aircraft, Jane's Publishing Co.Ltd.,1987

81. ANONYMOUS — Air superiority fighter, Dornier Post, March 1972

82. BAVITZ, P.C. — Future strike fighter options, SAE Paper 811099, 1981

83. Flight International (Magazine)

84. Aviation Week and Space Technology (Magazine)

85. Interavia (Magazine)

APPENDIX A

VARIABLE NAMING CONVENTION

A.1 VARIABLE NAMING CONVENTION

The extremely large number of variables involved in the Design Synthesis calculations, imposed the need for a variable naming convention, to allocate unique and easily identifiable code names conforming with standard FORTRAN 77. The convention used in ref.] was therefore adopted, which is also compatible with existing RAE systems.

According to the convention, the maximum number of characters in each variable name is restricted to six. The length of each name, however, is kept as short as possible. The use of letters I to N inclusive, at the beginning of Fortan real variables, is minimized. The use of 0 and O in names is also minimized in order to avoid ambiguity and coding errors.

The characters in the variable names are allocated as follows:

Optional Prefix	Primary Function	Primary Component	Qualifier for Primary Component	Optional extra Qualifier for Component	Qualifier for Primary Function

Typical Primary Function Characters

A: Aspect ratio or moment

B: Span or breadth

C: Chord or aerodynamic coefficient

D: Diameter or drag

H: Height

L: Length or lift

M: Mass

O: Cross-sectional area

P: Perimeter or pressure

Q: Angle

R: Radius or density
S: Planform area
T: Thickness or thrust or temperature
U: Utilization factor or taper ratio
V: Volume or velocity
W: Wetted area
X: Longitudinal coordinate from fuselage nose
Y: Lateral coordinate from fuselage centre line
Z: Vertical coordinate

Typical Primary Component Characters

A: Avionics
B: Stores
C: Cockpit
E: Empennage
F: Fuselage
G: Gun
I: Intake
K: Fuel
P: Powerplant
S: Systems
T: Total aircraft
U: Undercarriage
V: b.l. diverter
W: Wing
X: External pylons or tanks

Typical Qualifiers for each of the Primary Component Characters

A	R:	Radar		
	X:	Extra		
B	1:	Store 1	3:	Store 3
	2:	Store 2	4:	Store 4

C

- C: Canopy
- E: Pilot's eye
- F: Floor
- H: Pilot's heel
- I: Instruments
- P: Pilot
- S. Seat
- V: View
- W: Windscreen

E

- F: Fin(s)
- C: Foreplane

F

- A, B, C, D, E, F, G, H, J,K: Fuselage stations
- AB: Airbrake
- I: Intake
- N: Nozzle
- R: Radome
- W: Internal structure
- X: Skin structure

G

- A: Ammunition
- C: Complete gun

I

- I: Inlet
- E: Exit
- D: Diffuser

P

- 1, 2, 3, 4: Engine stations
- B: Basic
- F: Fuel flow
- I: Installation
- J: Jet
- N: Nozzle
- A: Air flow
- R: Reheat
- S: Throttle setting
- T: Thrust reverser

S

- A: Air
- C: Flying controls
- E: Electrical
- F: Fuel

T	A:	Aft	F:	Forward	P: Payload
	B:	Burnt	L:	Landing	R: Role equipment
	C:	Combat	M:	Maximum section	T: Take-off
	E:	Empty	N:	Nose	
U	H:	Hydraulics	N:	Nose	
	L:	Legs	T:	Total	
	M:	Main	W:	Wheels	
V	I:	Inlet			
	E:	Exit			
W	A:	Aileron	F:	Flap	S: Spoiler
	B:	Box	H:	Fixed trailing-egde	T: Trailing-edge
	C:	Complete	L:	Leading-edge	
	D:	Front spar	R:	Rear spar	
X	P:	Pylons			
	T:	Tanks			

Typical Qualifiers for Primary Function

A: Aft or trailing-edge
B: Body side or root section
C: Centre or centre of gravity
D: Datum or design
F: Fuel
G: Gross
H: Highest or maximum
I: Internal or initial condition
K: Constant
L: Leading-edge

M: Mean

N: Net

Q: Quarter chord

R: Reference conditions

T: Tip

S: Smallest or minimum

U: Unused or empty

X: External

Typical characters that may be used as a prefix to the Primary Function.

D: Elemental increase

E: Clearance

F: Factor or fraction

G: Gradient

R: Ratio

A total of about 1500 variables are used in this Design Synthesis. The names of the majority of these variables comply with the above convention, apart from some exceptions. All the variables used, however, are listed and fully explained at the beginning of this report. They are also explained in the subsequent appendices when used for the first time.

For optimization purposes these variables are also divided into three main groups, i.e. Independent (IV), Dependent (DV) and External (EV) variables. These are clearly identified in the list of variables.

An Independent Variable is a quantity in the mathematical model of an aircraft, that is chosen to be at the disposal of the optimization algorithm.

A Dependent Variable is that whose value is dependent on the set of values of the IV's and EV's.

An External Variable is a quantity variable externally to the optimization process, i.e. part of the design data.

The variables used as input to the Design Synthesis are defined as either IV's or EV's, accordingly. All the others are DV's and form the biggest group of variables.

APPENDIX B

SIZING OF THE FIXED ITEMS

B.1 INTRODUCTION

The design synthesis calculations start with the sizing of the fixed items of the aircraft. This involves the estimation of the physical dimensions of the cockpit, u/c bays, gross-wing, engine bays, boundary layer diverter and inlet. The above dimensions are used to determine the values of fundamental geometric constraints which are subsequently incorporated in the mathematical models of the aircraft.

The mathematical expressions used in these sizing calculations are presented in this appendix and explained in the order in which they are evaluated in the corresponding computer program modules.

B.2 COCKPIT (Module COCKPG)

An advanced 'high-g' cockpit is considered, with a seat back angle in excess of thirty degrees and a raised heel-line.

The following expressions were derived with reference to fig. B.1.

The angle (QCFOOT), between the line joining the thigh-heel points and the horizontal is given by,

$$QCFOOT = \cos^{-1}\left[\frac{LCNSPR - LCFOOT - HC3 * \cos(QCSEAT)}{HC2}\right] \quad \text{(rads)} \qquad \text{(B.1)}$$

where,

LCNSPR = Horizontal distance between the Neutral Seat Reference Point (NSRP) and the forward bulkhead of the cockpit (m).

LCFOOT = Horizontal distance between the forward bulkhead of the cockpit and the heel point. (m)

QCSEAT = Seat-back angle (rads)

HC2 = Distance between the thigh and heel points. (m)

HC3 = Distance between the thigh point and NSRP. (m)

The heel-line is raised to a height (HC6) above the cockpit floor.

$$HC6 = HC3 * \sin(QCSEAT) + HCSEAT * \cos(QCSEAT) - HC2 * \sin(QCFOOT) \quad (m) \qquad (B.2)$$

where, HCSEAT = Height of (NSRP) above the cockpit floor, measured along the seat-back line. (m)

The height (HCEYE) of the pilot's design eye-point above the cockpit floor is,

$$HCEYE = HC1 * \cos(QCSEAT) + HC3 * \sin(QCSEAT) + HCSEAT * \cos(QCSEAT) \quad (m) \qquad (B.3)$$

where, HC1 = Distance between the thigh point and eye point. (m)

The horizontal distance (LCEYE) between the forward bulkhead of the cockpit and the eye-point is,

$$LCEYE = HC1 * \sin(QCSEAT) + HC2 * \cos(QCFOOT) + LCFOOT \quad (m) \qquad (B.4)$$

The length of the cockpit floor (LCFL) is given by,

$$LCFL = HC2 * \cos(QCFOOT) + LCFOOT + HC3 * \cos(QCSEAT) - HCSEAT * \sin(QCSEAT) + \left[\frac{EHC5}{\cos(QCSEAT)}\right] \quad (m) \qquad (B.5)$$

where, EHC5 = Distance between the seat-back and the rear bulkhead of the cockpit. (m)

The height (HC5) of the front bulkhead of the cockpit above the floor is,

$$HC5 = HCEYE - LCEYE * \tan(QCEYE) \quad \text{(m)} \quad \text{(B.6)}$$

where, QCEYE = Pilot's forward and downward view angle measured from the eye point. (rads)

HC1, HC2, HC3, HC4, HCSEAT, EHC5, LCNSPR, LCFOOT, QCSEAT and QCEYE, are the required input data for which suitable values may be obtained from the appropriate MIL-STD.

B.3 UNDERCARRIAGE (u/c)

B.3.1 General

Both the nose and main undercarriage sizing modules, consist of two main parts. The first, is an automated process for the selection of standard-size tyres and the other contains preliminary sizing calculations for the corresponding undercarriage leg.

The following assumptions were made during the development of the undercarriage modules:

a) Each leg is fitted with a single wheel and an oleo-pneumatic shock absorber.
b) An optimum distribution of aircraft static load exists between the nose and main u/c legs (8% of the load is carried by the nose u/c and 46% by each main u/c).

The static load at this stage of the synthesis is expressed in terms of the reference take-off mass (MTTR), which is specified in the input data and represents the maximum design static load for the synthesized aircraft.

B.3.2 Main Undercarriage (Module MUNDCG)

B.3.2.1 Tyre Selection Process

An automated process was developed by the author, which selects the smallest available standard-size tyre, that is suitable for use on each u/c leg. The available tyres and their characteristics are tabulated in metric units in file 'TYREM DAT'. These were obtained from ref. Each row of data corresponds to one standard-size tyre. The first row corresponds to the smallest diameter tyre and the last to the largest. The tyre characteristics are tabulated in ten columns. These are from left to right: DUMWN, BUMWN, DUMWH, DUMWS, BUMWH, BUMWS, DUMWG, BUMWG, PUMW, PUMLV,

where,

DUMWN	= Nominal diameter of a main u/c tyre	(m)
BUMWN	= Nominal width	(m)
DUMWH	= Maximum diameter	(m)
DUMWS	= Minimum diameter	(m)
BUMWH	= Maximum width	(m)
BUMWS	= Minimum width	(m)
DUMWG	= Grown diameter	(m)
BUMWG	= Grown width	(m)
PUMW	= Normal pressure	(Pa)
PUMLV	= Allowable static load	(kg)

The basis of the selection process is an empirical expression which relates the nominal tyre diameter and width to the allowable load and normal pressure. The expression was initially obtained from ref. 2 , but it was later revised by the author after a correlation analysis of standard tyre characteristics. The expression in its final form, is given below:

$$DUMWN^{0.5} * BUMWN^{1.5} = \frac{PUMLV1}{0.0611 \times PUMW1} \qquad (B.7)$$

where, PUMLV1 = Estimated maximum static load on each main u/c leg.

This is,

$$PUMLV1 = 0.46 \times MTTR \quad (kg) \qquad (B.8)$$

also,

PUMWI = Specified maximum pressure for a main u/c tyre (Pa)

The selected value for PUMW1, should be compatible with the runway surface from which the aircraft is designed to operate. It is specified in the input data and expressed in Pa.

During the automated selection process each row of data in file 'TYREM.DAT' is read in succession, starting from the top. The data are checked if they satisfy all the selection criteria listed below:

$$\begin{aligned} DUMWN^{0.5} * BUMWN^{1.5} &> DBUMW1 \\ PUMW &< PUMW1 \\ PUMLV &> PUMLV1 \end{aligned} \qquad (B.9)$$

where, DBUMW1 = Right-hand side of empirical equation

$$= \frac{PUMLV1}{0.0611 * PUMW1} \qquad (B.10)$$

The process stops immediately after finding the first set of data to satisfy all the above criteria. The corresponding standard-size tyre is hence selected for use.

B.3.2.2 Preliminary Sizing of a Main u/c Leg

The basic dimensions of each main u/c leg are determined, using well proven empirical relationships which were obtained from refs. 3, 77, 78.

First, the tyre deflection (DHUMW) is estimated using the previously determined tyre characteristics.

$$DHUMW = \frac{0.5 * RPUMLV * PUMLV}{PUMW * (DUMWN * BUMWN)^{0.5}} \quad (m) \quad (B.11)$$

where, RPUMLV = Main u/c leg load factor.

The leg stroke (DHUML) is given by:

$$DHUML = \left(\frac{1.0}{EUML}\right) * \left[\frac{VTLV^2}{1.84 * 9.81 * RPUMLV} - (EUMW * DHUMW)\right] + 0.0254 (m) \quad (B.12)$$

where, EUML = Main u/c leg efficiency
EUMW = Main u/c tyre efficiency
VTLV = Maximum vertical landing velocity (m/s)

The leg diameter (DUML) is given by the following empirical equation:

$$DUML = \frac{1.3 + 0.11 * (PUMLV1)^{0.5}}{100.0} \quad (m) \quad (B.13)$$

and its length (LUML) is,

$$LUML = 2.5 * DHUML \quad (m) \quad (B.14)$$

B.3.3 Nose Undercarriage (Module NUNDCG)

B.3.3.1 Tyre Selection Process

The selection process for the nose-wheel tyre is identical to that for the main u/c, which is described in section B.3.2.1. The corresponding tyre characteristics are, DUNWN, BUNWN, DUNWH, DUNWS, BUNWH, BUNWS, DUNWG, BUNWG, PUNW, PUNLV.

The nose u/c static load (PUNLV1) however is,

$$PUNLV1 = 0.08 * MTTR * FPUNLV \quad (kg) \quad (B.15)$$

where, FPUNLV = Constant factor which allows for the additional load on the nose u/c leg due to steady braking.

B.3.3.2 Preliminary Sizing of the Nose u/c Leg

The length of the nose u/c leg (LUNL) is estimated by assuming that the total length of the fully extended nose u/c leg and wheel assembly measured from the lower fuselage surface, is equal to the corresponding length of the main u/c assembly, hence,

$$LUNL = LUML + 0.5 * DUMWH - 0.5 * DUNWH + DHUP \quad (m) \quad (B.16)$$

where, DHUP = Height difference between the nose and main u/c pintles.

DHUP is negative if the nose u/c pintle is located at a lower height relative to that of the main u/c.

The stroke of the nose u/c leg (DHUNL) is given by,

$$DHUNL = \frac{LUNL - 0.5 * DUNWH}{3.0} \quad (m) \qquad (B.17)$$

The leg diameter is,

$$DUNL = \frac{1.3 + 0.11 * (PUNLV1)^{0.5}}{100.0} \quad (m) \qquad (B.18)$$

B.4 UNDERCARRIAGE BAYS

B.4.1 General

The dimensions, cross-sectional area and volume of the main and nose u/c bays are determined by considering the previously estimated leg and tyre sizes in conjunction with a set of recommended working clearances. The expressions used in the following modules are mainly derived with the aid of simplified views of the bays and retracted u/c.

B.4.2 Main Undercarriage Bays (Module MUNDCBG)

The assumed main u/c bay geometry and retraction concept are shown in fig.B.2. Each bay is assumed to have a rectangular cross-section which allows adequate extra space for the installation of u/c associated hydraulics and other parts.

Aircraft tyre manufacturers recommend the provision of adequate radial and lateral clearances for each tyre size, which allow for an increase in tyre dimensions due to the effect of centrifugal forces at high ground rolling speeds.

According to graphs in ref.79, for speeds up to 200 mph, the recommended radial clearance is expressed as,

$$EDUMW = 9.906 * 10^{-3} + 0.047 * BUMWG \quad (m) \quad (B.19)$$

and the corresponding lateral clearance , as,

$$EBUMW = 5.842 * 10^{-3} + 0.019 * BUMWG \quad (m) \quad (B.20)$$

The use of BUMWG in the above expressions, automatically allows for tyre growth effects.

Further minimum clearances (ELUMBF, ELUMBA, EHUMBL) are specified in the input data, which allow free u/c retraction.

The length of a main u/c bay (LUMB), is therefore,

$$LUMB = LUML + 0.5 * DUMWG + EDUMW + ELUMBF + ELUMBA \quad (m) \quad (B.21)$$

where, ELUMBF = Forward length clearance for a main u/c bay (m)

ELUMBA = Aft length clearance for a main u/c bay (m)

The height (HUMB) is,

$$HUMB = BUMWG + DUML + 2.0 * EBUMW + EHUMBL \quad (m) \quad (B.22)$$

where,

EHUMBL = Lower height clearance for a main u/c bay. (m)

The width (BUMB) is,

$$BUMB = DUMWG + 2.0 * EDUMW \quad (m) \quad (B.23)$$

The longitudinal cross-sectional area of a main u/c bay (OUMB) is,

$$OUMB = BUMB * HUMB \qquad (m^2) \qquad (B.24)$$

and its volume (VUMB) is,

$$VUMB = BUMB * HUMB * LUMB \qquad (m^3) \qquad (B.25)$$

B.4.3 Nose Undercarriage Bay (Module NUNDCBG)

An approach similar to that for the sizing of a main u/c bay is also used for the nose u/c bay. The nose u/c bay geometry and retraction concept are shown in fig. B.3.

The recommended radial clearance for the nose wheel tyre is,

$$EDUNW = 9.906 * 10^{-3} + 0.047 * BUNWG \qquad (m) \qquad (B.26)$$

and the corresponding lateral clearance is,

$$EBUNW = 5.842 * 10^{-3} + 0.019 * BUNWG \qquad (m) \qquad (B.27)$$

The following expressions are derived with reference to fig.B.3.

The length of the nose u/c bay (LUNB) is,

$$LUNB = LUNL + 0.5 * DUNWG + ELUNBF + EDUNW + ELUNBA \qquad (m) \qquad (B.28)$$

where, ELUNBF = Forward length clearance for the nose u/c bay (m)

ELUNBA = Aft length clearance for the nose u/c bay (m)

The height of the aft end of the bay (HUNBA) is,

$$HUNBA = BUNWG + 2.0 * EBUNW + DUNL * FDUNL + EHUNBL \quad (m) \quad (B.29)$$

where, EHUNBL = Lower height clearance for the nose u/c bay (m)

FDUNL = Fraction of DUNL related to the thickness of the lower end of the nose u/c leg.

The height of the forward end of the bay (HUNBF) is,

$$HUNBF = 0.5 * (DUNL + BUNWG) + EBUNW \quad (m) \quad (B.30)$$

The width of the bay (BUNB) is,

$$BUNB = DUNWG + 2.0 * EDUNW \quad (m) \quad (B.31)$$

The length of the rear section of the nose u/c bay (LUNWB) is,

$$LUNWB = DUNL * FDUNL + DUNWG + 2.0 * EDUNW + ELUNBA \quad (m) \quad (B.32)$$

The length of the front section of the bay (LUNLB) is,

$$LUNLB = LUNB - LUNWB \quad (m) \quad (B.33)$$

The minimum cross-sectional area of the front section of the bay (OUNLBS) is,

$$OUNLBS = BUNB * HUNBF \quad (m^2) \quad (B.34)$$

and the maximum (OUNLBH) is,

$$OUNLBH = BUNB * HUNBA \quad (m^2) \quad (B.35)$$

The cross-sectional area of the rear section of the bay (OUNWB) is,

$$OUNWB = BUNB * HUNBA \quad (m^2) \quad (B.36)$$

The volume of the rear section of the bay (VUNWB) is,

$$VUNWB = LUNWB * HUNBA * BUNB \quad (m^3) \quad (B.37)$$

The volume of the front section of the bay (VUNLB) is,

$$VUNLB = 0.5 * LUNLB * (HUNBA + HUNBF) * BUNB \quad (m^3) \quad (B.38)$$

The total volume of the nose u/c bay (VUNB) is,

$$VUNB = VUNWB + VUNLB \quad (m^3) \quad (B.39)$$

B.5 GROSS WING (Module GWINGG)

The geometric characteristics of the gross wing are determined from given values of wing area (SW), aspect ratio (AW), taper ratio (UW) and quarter-chord sweep angle (QW4). (Refer to fig.B.4)

The following general equations apply:

Gross wing span : $BW = (AW * SW)^{0.5}$ (B.40)

Centre line chord : $$CWCC = \frac{2.0 * SW}{BW * (1.0 + UW)} \quad (m) \quad (B.41)$$

Wing-tip chord : $CWCT = UW * CWCC$ (m) (B.42)

Mean geometric chord : $CWMG = 0.5 * CWCC * (1.0 + UW)$ (m)

Mean aerodynamic chord : $$CWMA = \left(\frac{2.0}{3.0}\right) * CWCC * \left[UW + \frac{1.0}{1.0 + UW}\right]^{(m)} \quad (B.44)$$

The equations for the various sweep angles of the wing are derived from the wing geometry (fig.B.4).

The leading-edge sweep angle of the wing (QWL) is,

$$QWL = \tan^{-1}\left[\tan(QW4) + \frac{CWCC * (1.0 - UW)}{2.0 * BW}\right] \quad \text{(rads)} \quad (B.45)$$

The mid-chord sweep angle of the wing (QW2) is,

$$QW2 = \tan^{-1}\left[\tan(QW4) - \frac{CWCC * (1.0 - UW)}{2.0 * BW}\right] \quad \text{(rads)} \quad (B.46)$$

The trailing-edge sweep angle of the wing (QWT) is,

$$QWT = -\tan^{-1}\left[\frac{2.0 * [CWCC - CWCT - 0.5 * BW * \tan(QWL)]}{BW}\right] \text{(rads)} \quad (B.47)$$

B.6 ENGINE SIZING (Module ENGSIZ)

The engine sizing module was developed by RAE(F). It scales the principal engine dimensions from a set of datum dimensions for a military turbofan engine using a scale factor RTP, based on the maximum sea-level, static thrust.

The relevant engine dimensions which are determined by the empirical equations incorporated in the module, are shown in fig.B.5. The engine is divided into three main sections which are clearly defined by four engine stations.

Stations 1 and 2 define the gas generator, 2 and 3 the reheat section and 3 and 4 the nozzle.

The length of the gas generator (LP12) is,

$$LP12 = LP12R * RTP * FLP1K \quad (m) \quad (B.48)$$

where, LP12R = Length of the gas generator of datum engine (m)
FLP1K = Constant exponent

The length of the reheat fuelling section of the engine (LP22A) is,

$$LP22A = LP22AR * (RTP)^{FLP2K} \quad (m) \quad (B.49)$$

where, LP22AR = Length of the reheat fuelling section of datum engine (m)
FLP2K = Constant exponent

The length of the reheat burning section of the engine (LP2A4) is,

$$LP2A4 = LP2A4R \quad (m) \quad (B.50)$$

where, LP2A4R = Length of reheat burning section of datum engine. (m)

The nozzle length (LP34) is,

$$LP34 = LP34R * (RTP)^{FLP3K} \quad (m) \quad (B.51)$$

where, LP34R = Length of nozzle of datum engine (m)
FLP3K = Constant exponent

The length of the reheat section of the engine (LP23) is,

$$LP23 = LP22A + LP2A4 - LP34 \quad (m) \quad (B.52)$$

The total engine length (LPG) is the sum of the individual lengths of the three main sections.

$$LPG = LP12 + LP23 + LP34 \quad (m) \quad (B.53)$$

The principal engine diameters are directly proportional to (RRTP), where,

$$RRTP = RTP^{0.5} \quad (B.54)$$

Hence,

$$DP1 = RRTP * DP1R \quad (m) \quad (B.55)$$
$$DP2 = RRTP * DP2R \quad (m) \quad (B.56)$$
$$DP3 = RRTP * DP3R \quad (m) \quad (B.57)$$
$$DP4 = RRTP * DP4R \quad (m) \quad (B.58)$$

where,

DP1 = Compressor inlet diameter
DP2 = Turbine section exit diameter
DP3 = Afterburner section exit diameter
DP4 = Nozzle exit diameter

and DP1R, DP2R, DP3R, DP4R are the corresponding datum engine diameters.

The nozzle exit area (OPN) is,

$$OPN = NENG * 0.25 * PI * RTP * DP4R^{2.0} \quad (m^2) \quad (B.59)$$

where, NENG = Number of engines (=2, for this synthesis)

The reference engine performance at sea-level static conditions, is estimated with the following equations:

The maximum sea-level static thrust, with reheat (TPGD) is,

$$TPGD = NENG * RTP * TPGD2 \quad (N) \quad (B.60)$$

where, TPGD2 = Value of TPGD for the datum engine (N)

The fuel mass flow rate at maximum gross thrust at sea-level (MPFD) is,

$$MPFD = NENG * RTP * MPFD1 \quad (kg/s) \quad (B.61)$$

where, MPFD1 = Value of MPFD for the datum engine (kg/s)

The air mass flow rate at sea-level static conditions (MPAD) is,

$$MPAD = NENG * RTP * MPAD1 \quad (kg/s) \quad (B.62)$$

where, MPAD1 = Value of MPAD for the datum engine (kg/s)

Finally the jet exit area at sea-level static conditions (OPJD) is,

$$OPJD = NENG * RTP * OPJD1 \quad (m^2) \quad (B.63)$$

where, OPJD1 = Value of OPJD for the datum engine.

B.7 ENGINE BAY CLEARANCES (Module ENGBCLR)

A set of height and width clearances are determined for the engine bay. These are specified initially in the input data as fractions of the principal engine diameters (Engine stations 1-4, fig.B.5)

Hence, the required height and width clearances are determined using the following expressions:

At the compressor inlet,

$$EHP1 = FHP1K * DP1 \qquad EBP1 = \frac{FBP1K * DP1}{NENG} \quad (m) \quad (B.64)$$

At the turbine section exit,

$$EHP2 = FHP2K * DP2 \qquad EBP2 = \frac{FBP2K * DP2}{NENG} \quad (m) \quad (B.65)$$

At the afterburner section exit,

$$EHP3 = FHP3K * DP3 \qquad EBP3 = \frac{FBP3K * DP3}{NENG} \quad (m) \quad (B.66)$$

At the nozzle exit plane,

$$EHP4 = FHP4K * DP4 \qquad EBP4 = \frac{FBP4K * DP4}{NENG} \quad (m) \quad (B.67)$$

In the above expressions, FHP1K, FHP2K, FHP3K, FHP4K, FBP1K, FBP2K, FBP3K, FBP4K are specified constant fractions of the local engine diameter.

The size of the estimated clearances however, is automatically limited within specified minimum and maximum values as shown below:

$$EHP1S < EHP1 < EHP1H$$
$$EBP1S < EBP1 < EBP1H \qquad \text{(B.68)}$$

$$EHP2S < EHP2 < EHP2H$$
$$EBP2S < EBP2 < EBP2H \qquad \text{(B.69)}$$

$$EHP3S < EHP3 < EHP3H$$
$$EBP3S < EBP3 < EBP3H \qquad \text{(B.70)}$$

$$EHP4S < EHP4 < EHP4H$$
$$EBP4S < EBP4 < EBP4H \qquad \text{(B.71)}$$

where, EHP1S, EHP2S, EHP3S, EHP4S, EBP1S, EBP2S, EBP3S, EBP4S are the corresponding minimum allowable clearances.

and, EHP1H, EHP2H, EHP3H, EHP4H, EBP1H, EBP2H, EBP3H, EBP4H are the corresponding maximum allowable clearances.

B.8 INTAKE DIFFUSER INLETS (Module INLET)

The intake diffuser inlets are assumed to be rectangular in cross-section with corner radii RIDX1.

The required total cross-sectional area of the intake diffuser inlets (OII) is obtained from a specified fixed area ratio (ROIEI), where,

$$ROIEI = \frac{OIE}{OII} \qquad \text{(B.72)}$$

OIE = Total cross-sectional area of the intake diffuser exits. This is given by,

$$OIE = 0.25 * NENG * PI * DP1^{2.0} \quad (m^2)\ (B.73)$$

Therefore,

$$OII = \frac{OIE}{ROIEI} \quad (m^2)\ (B.74)$$

It is further assumed that the inner side of each intake diffuser lies on the aircraft's centre-line and that the forward fuselage always provides shielding for the intake. Therefore, the width of each intake difuser (BII), is geometrically constrained not to exceed the local fuselage half-width.

Hence the maximum allowable value for BII is,

$$BIIH = YCCANC + EYFC \quad (m)\ (B.75)$$

where YCCANC = Half-width of the canopy at the pilot's eye-point position. (m)

EYFC = Clearance, allowing for the local width of the fuselage structure. (m)

For a specified aspect ratio (AII), the corresponding value of BII is given by the following expression:

$$BII = \left[\frac{OII - 2.0 * RIDX1^{2.0} * (PI - 4.0)}{2.0 * AII}\right]^{0.5} \quad (m)\ (B.76)$$

and the height (HII) is,

$$HII = AII * BII \quad (m)\ (B.77)$$

If the above estimated value of BII is greater than BIIH, then,

$$BII = BIIH \qquad \text{(m)} \quad \text{(B.78)}$$

and

$$HII = \frac{OII - 2.0 * (PI - 4.0) * RIDX1^{2.0}}{2.0 * BII} \qquad \text{(m)} \quad \text{(B.79)}$$

B.9 FUSELAGE LENGTH (Module LENGTH)

The axial distances of principal fuselage stations from the aircraft nose are determined in this module, by considering a number of fundamental geometric constraints which are derived from the intital assumptions made for the baseline aircraft.

Station R is located at an axial distance (XFR) from the aircraft nose.

$$XFR = RXFR * LAR \qquad \text{(m)} \quad \text{(B.80)}$$

where, LAR = Length of the radar avionics bay (m)
RXFR = Fraction of LAR

Both LAR and RXFR are specified in the input data.

An extra avionics bay is assumed to be located just behind that for the radar avionics. This has a specified length, LAX. Its rear end is assumed to coincide with fuselage station A. Therefore the axial distance of station A from the aircraft nose, is,

$$XA = XFR + LAR + LAX \qquad \text{(m)} \quad \text{(B.81)}$$

The maximum aft position of station A, (XAH), however is limited by pilot's vision considerations, over the aircraft nose and in particular by the minimum allowable

value for QCEYE. The maximum aft position is defined by the following expression, which was derived by assuming that the aircraft nose is long enough so that the minimum QCEYE requirement is just met.

$$XAH = XFR + \frac{HC5 + HFA1 - HRA - 2.0 * EHRA}{2.0 * \tan(0.5 * QCEYE)} \quad (m) \quad (B.82)$$

where, HFA1 = Cockpit under-floor height at station A. (m)
HRA = Height of radar antenna (m)
EHRA = Height clearance for radar antenna. (m)

Whenever the above constraint becomes active, the values of XA and LAX are automatically revised. Therefore,

if XA > XAH and XAH ≥ XFR + LAR, then,

$$XA = XAH \text{ and } LAX = XA - XFR - LAR \quad (m) \quad (B.83)$$

Otherwise, if XA > XAH and XAH < XFR + LAR, then,

$$XA = XFR + LAR \text{ and } LAX = 0.0 \quad (m) \quad (B.84)$$

The distance of station B, (XB) is given by the following expression:

$$XB = XA + RXB * LCEYE \quad (m) \quad (B.85)$$

where, RXB = Fraction of LCEYE

Fuselage station C is assumed to coincide with the pilot's eye point, therefore,

$$XC = XA + LCEYE \quad (m) \quad (B.86)$$

The position of station D, (XD) is limited by the length of the canopy and the position of the b.l.diverter exit. The length of the b.l. diverter exit (LVG) is,

$$LVG = 2.0 * FLVK * BII \quad \text{(m)} \quad \text{(B.87)}$$

where, FLVK = Constant factor

The first estimate of XD is,

$$XD = XA + LCCAN \quad \text{(m)} \quad \text{(B.88)}$$

where, LCCAN = Total length of canopy and windscreen. (m)

If however, XD < XC + 1.25 * LVG then, XD and LCCAN automatically become,

$$XD = XC + 1.25 * LVG \quad \text{(m)} \quad \text{(B.89)}$$
$$LCCAN = XD - XA \quad \text{(m)} \quad \text{(B.90)}$$

The axial distance of the nozzle exit plane from the aircraft nose (XFN) is an independent variable which is initially specified in the input data. This distance is equal to the fuselage length. The size of the latter however, is naturally constrained by the items installed inside the fuselage, not to be less than a certain minimum (XFNS). Therefore a set of minimum constraints are defined below.

The fuselage-mounted semi-submerged missiles no.1 and no.2 are assumed to be installed between stations D and F, while no.3 and no.4, are installed between F and H. The engine reheat section is always located between H and J and the nozzle between J and K. It is also assumed that there is an axial separation (ELMUFA) between the rear ends of

missiles no.3 and no.4. Considering the above assumptions, the following constraints are derived:

If LMUF1 ≥ LMUF2 and LMUF3 ≥ LMUF4 + ELMUFA

then, XFNS = XD + LMUF1 + LMUF3 + LP23 + LP34 (m) (B.91)

where, LMUF1, LMUF2, LMUF3 and LMUF4 are the corresponding lengths of missiles no.1, 2, 3 and 4.

If LMUF1 < LMUF2 and LMUF3 ≥ LMUF4 + ELMUFA

then, XFNS = XD + LMUF2 + LMUF3 + LP23 + LP34 (m) (B.92)

If LMUF1 ≥ LMUF2 and LMUF3 < LMUF4 + ELMUFA

then, XFNS = XD + LMUF1 + LMUF4 + ELMUFA + LP23 + LP34(m) (B.93)

Otherwise, if LMUF1 < LMUF2 and LMUF3 < LMUF4 + ELMUFA

then, XFNS = XD + LMUF2 + LMUF4 + ELMUFA + LP23 + LP34 (m) (B.94)

It is also assumed that the gun is located between stations D and F, behind the nose u/c bay. This leads to two more constraint values for XFNS.

If LMUF3 ≥ LMUF4 + ELMUFA

then, XFNS = XC + EXUNBF + LUNB + LGC + LMUF3 + LP23 + LP34 (m)(B.95)

Else if LMUF3 < LMUF4 + ELMUFA

then, XFNS = XC + EXUNBF + LUNB + LGC + LMUF4 + ELMUFA + LP23 + LP34 (m)(B.96)

where, EXUNBF = Clearance between the intake lips and the forward end of the nose u/c bay. (m)

LGC = Gun length (m)

Both EXUNBF and LGC are specified in the input data.

Experimental results quoted in reference suggest a range of intake diffuser length to depth ratios (RIDL) which minimize internal airflow separation. An initial value for RIDL is initially specified in the input data together with the allowable minimum (RIDLS). The latter imposes a further constraint for XFNS, as shown below:

$$XFNS = XC + RIDLS * HII + LPG \quad (m) \quad (B.97)$$

If the above constraint becomes active then,

$$RIDL = RIDLS \quad (B.98)$$

From all the above estimated values for XFNS only the largest is finally considered. Therefore if the initially specified value for XFN is lower than XFNS, then,

$$XFN = XFNS \quad (m) \quad (B.99)$$

The axial distance of the intake plane from the aircrat nose (XII) is then calculated by,

$$XII = XFN - LPG - (RIDL * HII) \quad (m) \quad (B.100)$$

The value of XII is constrained according to the baseline aircraft assumptions, so that,

$$XC + 0.01 < XII < XD - 1.25 * LVG$$

When, XII + 1.25 * LVG > XD the values of XII and RIDL are automatically adjusted, so that,

$$XII = XD - 1.25 * LVG \quad \text{(m)} \quad \text{(B.101)}$$

and $$RIDL = \frac{XEN - LPG - XII}{HII} \quad \text{(B.102)}$$

Similarly when, XII < XC + 0.01 then,

XII = XC + 0.01 and RIDL is revised as previously (B.103)

The axial distance of the forward end of the nose u/c bay from the aircraft nose (XUNBF) is,

$$XUNBF = XII + EXUNBF \quad \text{(m)} \quad \text{(B.104)}$$

It is assumed that the rear section of the nose u/c bay is located only between stations D and E. Therefore if XUNBF + LUNLB < XD then, the initial values of EXUNBF and XUNBF are revised automatically as shown below:

$$EXUNBF = XD - LUNLB - XII \quad \text{(m)} \quad \text{(B.105)}$$

and $$XUNBF = XII + EXUNBF \quad \text{(m)} \quad \text{(B.106)}$$

Stations G, H, J and K are always assumed to coincide with principal engine stations. The nozzle exit plane is fixed at the rear end of the fuselage.

Station G is at a distance equal to DP1 forward of the compressor inlet. Hence,

$$XG = XFN - LPG - DP1 \quad \text{(m)} \quad \text{(B.107)}$$

Station H coincides with engine station no.2, therefore,

$$XH = XFN - LP34 - LP23 \quad \text{(m)} \quad \text{(B.108)}$$

Station J coincides with engine station no.3, therefore,

$$XJ = XFN - LP34 \qquad \text{(m)} \quad \text{(B.109)}$$

Finally station K,

$$XK = XFN \qquad \text{(m)} \quad \text{(B.110)}$$

The axial distance of station E from the aircraft nose (XE) is given by,

$$XE = XD + RXE * (XH - XD) \qquad \text{(m)} \quad \text{(B.111)}$$

where, RXE = Length fraction
RXE is specified in the input data.

The axial distance of station F from the aircraft nose (XF) is constrained between a set of minimum (XFS) and maximum (XFH) values, which are defined by the assumed configuration of the fuselage-mounted weapons.
These values are:

$$XFS = \left.\begin{matrix} XD + LMUF1 \\ XD + LMUF2 \\ XUNBF + LUNB + LGC \\ XE \end{matrix}\right] \text{(the largest)} \qquad \text{(m)} \quad \text{(B.112)}$$

$$XFH = \left.\begin{matrix} XH - LMUF3 \\ XH - LMUF4 - ELMUFA \\ XG \end{matrix}\right] \text{(the smallest)} \qquad \text{(m)} \quad \text{(B.113)}$$

The distance of the nose of fuselage-mounted missile no.1 from the aircraft nose (XMUF1) is,

$$XMUF1 = XD + RXMUF1 * (XH - XD) \qquad \text{(m)} \quad \text{(B.114)}$$

where, RXMUF1 = Length fraction

RXMUF1 is specified in the input data and provides a means for varying the missile position. XMUF1 however is constrained between a minimum (XMUF1S) and a maximum (XMUF1H) which are estimated according to the initial assumptions. Hence,

$$XD \leq XMUF1 \leq XFH - LMUF1 \qquad (m)$$

Similarly, for missile no.2,

$$XMUF2 = XD + RXMUF2 * (XH - XD)$$

and
$$XD \leq XMUF2 \leq XFH - LMUF2 \qquad (m) \quad (B.115)$$

Similarly for the gun,

$$XGF = XD + RXGF * (XH - XD) \qquad (m) \quad (B.116)$$

and
$$XUNBF + LUNB \leq XGF \leq XFH - LGC$$

The next step, is to determine XF.

$$XF = \left[\begin{array}{l} XMUF1 + LMUF1 \\ XMUF2 + LMUF2 \\ XGF + LGC \\ XFS \end{array}\right] \quad \text{(the largest)} \qquad (m) \quad (B.117)$$

The axial distances of missiles no. 3 and 4 from the aircraft nose are determined in the same way as for missiles no.1 and 2. Thus,

$$XMUF3 = XD + RXMUF3 * (XH - XD) \qquad (m) \quad (B.118)$$

and
$$XF \leq XMUF3 \leq XH - LMUF3$$

$$XMUF4 = XD + RXMUF4 * (XH - XD) \qquad (m) \quad (B.119)$$

$$XF \leq XMUF4 \leq XH - LMUF4 - ELMUFA$$

The distances of the principal engine stations 1 - 4 are XP1, XP2, XP3 and XP4 respectively, where,

$$XP1 = XFN - LPG \quad \text{(m)} \quad \text{(B.120)}$$

$$XP2 = XP1 + LP12 = XH \quad \text{(m)} \quad \text{(B.121)}$$

$$XP3 = XP2 + LP23 = XJ \quad \text{(m)} \quad \text{(B.122)}$$

$$XP4 = XP3 + LP34 = XFN \quad \text{(m)} \quad \text{(B.123)}$$

The distance of the mean 0.25- chord point of the wing from the aircraft nose (XWCQM) is,

$$XWCQM = RXWCQM * XFN \quad \text{(m)} \quad \text{(B.124)}$$

where, RXWCQM = Length fraction

RXWCQM is an independent variable which is initially specified in the input data.

The gross-wing apex is located at a distance (XWAPEX) from the aircraft nose:

$$XWAPEX = XWCQM - 0.25 * CWMA - 0.5 * BW * \left(\frac{CWCC - CWMA}{CWCC - CWCT}\right) * \tan(QWL) \quad \text{(m)} \quad \text{(B.125)}$$

Similarly, the distance of the mean 0.25- chord point of the foreplane from the aircraft nose (XCCQM) is:

$$XCCQM = RXCCQM * XFN \quad \text{(m)} \quad \text{(B.126)}$$

where, RXCCQM = Length fraction

RXCCQM is also an independent variable which is initially defined in the input data.

According to the initial assumptions made for the baseline aircraft, the mean 0.25-chord point of the all moving foreplane always lies within fuselage section DE. This constraints XCCQM between a minimum (XCCQMS) and a

maximum (XCCQMH) which correspond with XD and XE respectively, Hence,

$$XD \leq XCCQM \leq XE$$

B.10 BOUNDARY LAYER DIVERTER SIZING (Module BLDIVG1)

The basic boundary layer diverter (b.l.d.) design data are determined in this module, for later use in BLDIVG2 during the mathematical modelling of the fuselage.

The height of the b.l.d. at the intake plane (HVI) is estimated using an empirical equation from ref. 4. . This is related to the local thickness of the boundary layer on the fuselage. Hence,

$$HVI = \frac{0.67 * XII}{RNI^{0.2}} \quad (m) \quad (B.127)$$

where, RNI = Reynold's number at the intake plane.

$$RNI = \frac{RH * MHH * SSPD * XII}{MU} \quad (B.128)$$

where,
- RH = Atmospheric air density at HTH (kg/m³)
- SSPD = Speed of sound (m/s)
- MU = Atmospheric air viscocity (kg/ms)
- MHH = Maximum design Mach number for b.l.d sizing purposes
- HTH = Altitude at which MHH is reached (m)

The required values for MHH and HTH are specified in the input data, while the atmospheric properties RH, SSPD and MU at HTH are automatically evaluated by a previous call

to module ATMOS, which is presented in the next section of this appendix.

The axial distance of the b.l.d exit from the aircraft nose (XVE) is,

$$XVE = XII + LVG \quad (m) \quad (B.129)$$

The width of the b.l.d streamtube at the intake plane (BVI) is,

$$BVI = 2.0 * BII \quad (m) \quad (B.130)$$

while its cross-sectional area (OVI) is,

$$OVI = BVI * HVI \quad (m^2) \quad (B.131)$$

B.11 ATMOSPHERIC PROPERTIES (Module ATMOS)

This module was supplied by RAE(F). It evaluates the atmospheric properties at a given geometric height (HT) and temperature above 15 degrees C (TH). The module is mainly used during the aircraft performance estimation .

The geopotential height (HTG) is initially calculated using the following expression:

$$HTG = HT * (1.0 - 1.57 * 10^{-7} * HT) \quad (m) \quad (B.132)$$

When, HTG $\leq$ 11000.0, the ambient temperature (TA) and relative pressure (RP), are:

$$TA = 288.15 - 0.0065 * HTG \qquad (K)\ (B.133)$$

$$RP = \left(\frac{TA}{288.15}\right)^{5.25588} \qquad (B.134)$$

When, 11000.0 < HTG ≤ 20000.0, then,

$$TA = 216.65 \qquad (K)\ (B.135)$$

$$RP = \frac{0.223361}{\exp\left[1.57688 * 10^{-4} * (HTG - 11000.0)\right]} \qquad (B.136)$$

Otherwise, if HTG > 20000.0, then

$$TA = 216.65 + 0.001 * (HTG - 20000.0) \qquad (K)\ (B.137)$$

$$RP = 0.0540328 * \left(\frac{216.65}{TA}\right)^{34.1632} \qquad (B.138)$$

The temperature (T) is,

$$T = TA + TH \qquad (K)\ (B.139)$$

and the sea-level temperature (TSL) is,

$$TSL = 288.15 + TH \qquad (K)\ (B.140)$$

The relative temperature (RT) is,

$$RT = \frac{T}{TSL} \qquad (B.141)$$

and the relative density (RD) is,

$$RD = \frac{RT}{RT} \qquad \text{(B.142)}$$

The sea-level air density (ROSL) is,

$$ROSL = \frac{1.225 * 288.15}{TSL} \qquad (kg/m^3)\ \text{(B.143)}$$

The air density at a given HT, (RO) is,

$$RO = ROSL * RD \qquad (kg/m^3)\ \text{(B.144)}$$

The pressure (P) is,

$$P = 101325.0 * RP \qquad (Pa)\ \text{(B.145)}$$

The speed of sound (SSPD) is,

$$SSPD = 20.0468 * (T)^{0.5} \qquad (m/s)\ \text{(B.146)}$$

The sea-level air viscocity (MUSL) is,

$$MUSL = \left(\frac{7.1316537 * 10^{-3}}{TSL + 110.4}\right) * \left(\frac{TSL}{288.15}\right)^{1.5} \qquad (kg/m.s)\ \text{(B.147)}$$

The air viscocity at a given HT, (MU) is,

$$MU = \frac{MUSL * (TSL + 110.4) * RT^{1.5}}{T + 110.4} \qquad (kg/m.s)\ \text{(B.148)}$$

The kinematic viscocity (NU) is,

$$NU = \frac{MU}{RO} \qquad (m^2/s) \qquad (B.149)$$

The grantational acceleration at a given HT, (G) is,

$$G = 9.80665 * (1.0 - 3.14 * 10^{-7} * HT) \qquad (m/s^2) \qquad (B.150)$$

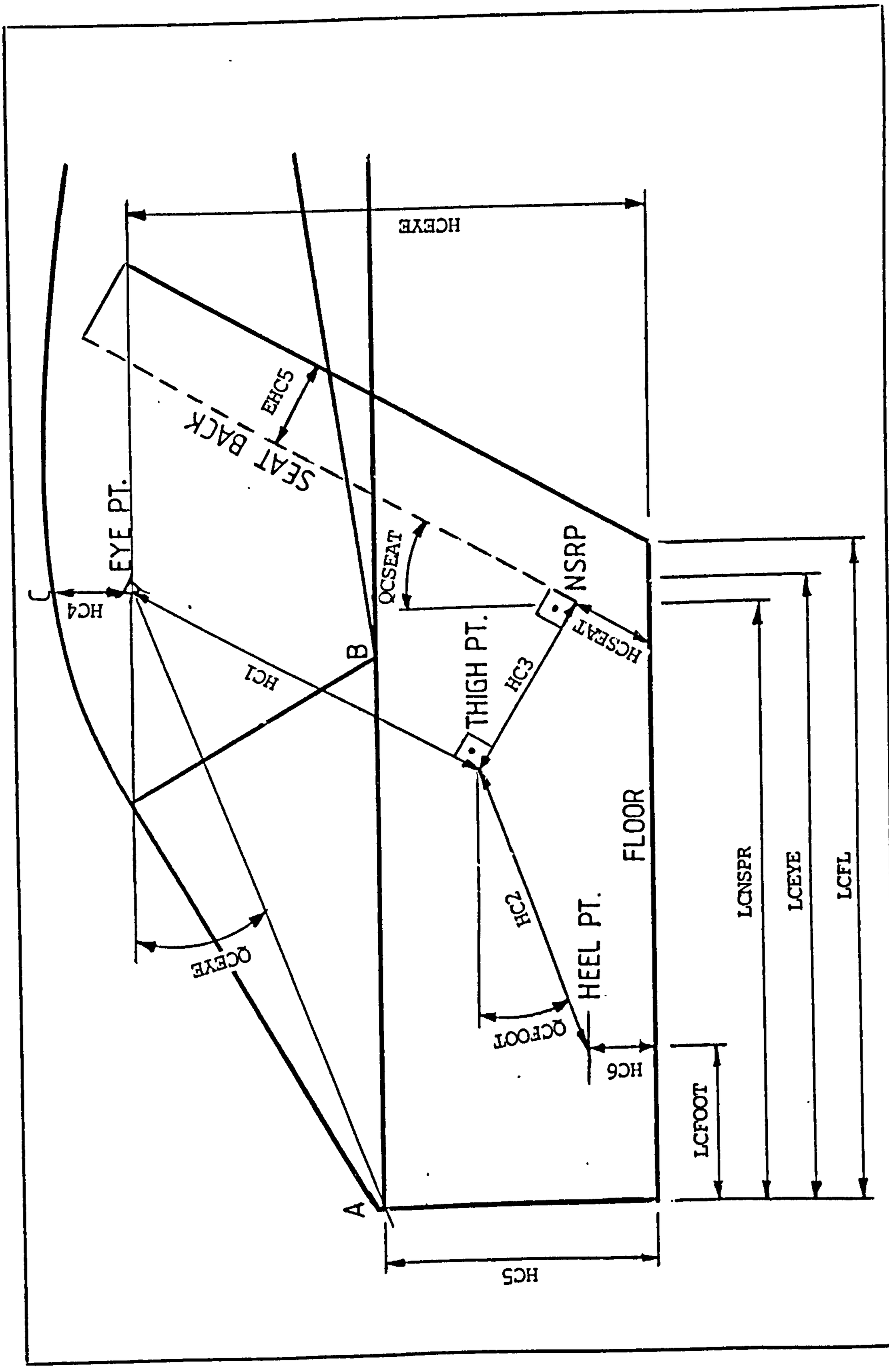

FIG. B.1 COCKPIT GEOMETRY

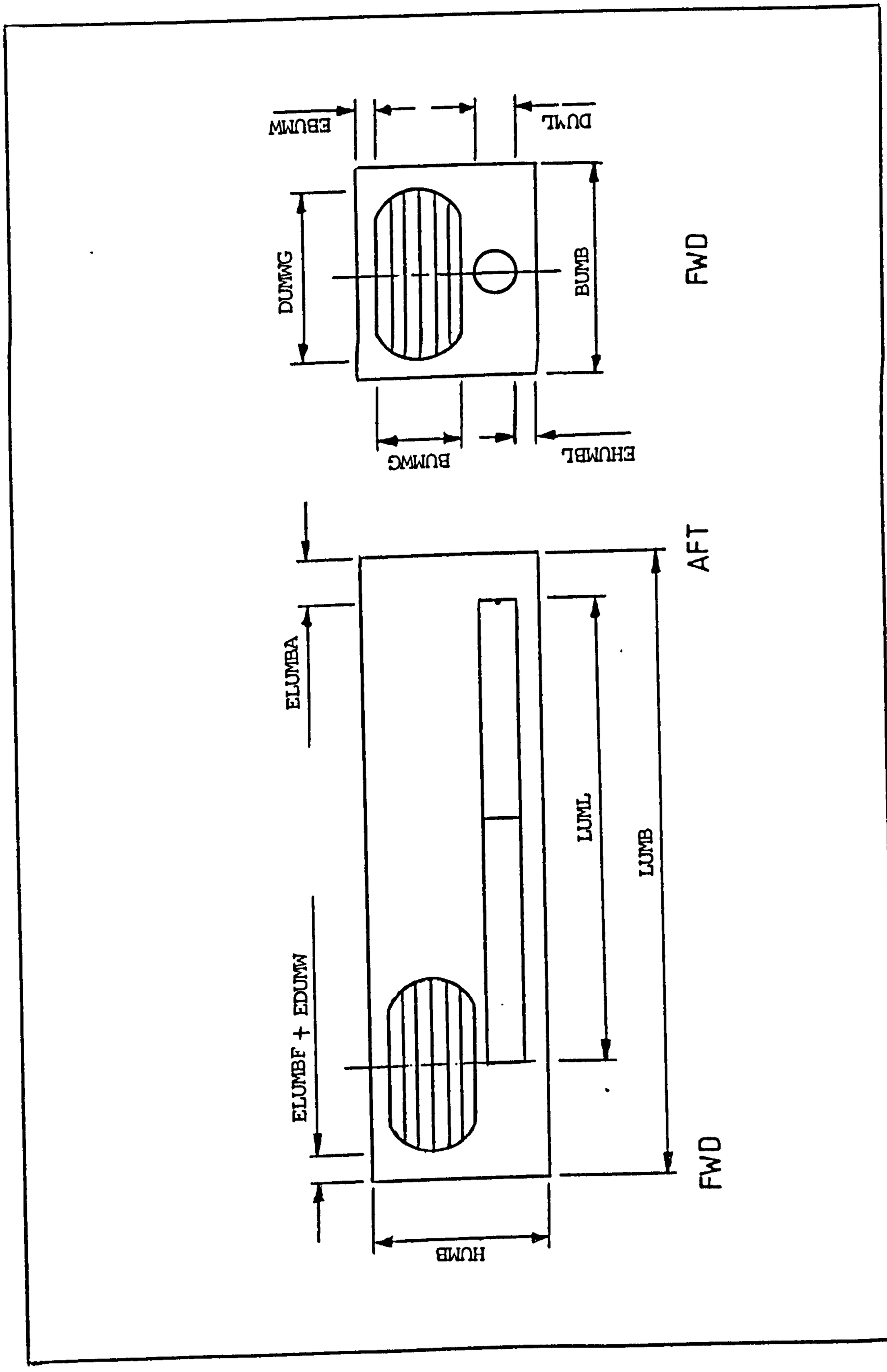

FIG. B.2 MAIN UNDERCARRIAGE AND BAY G

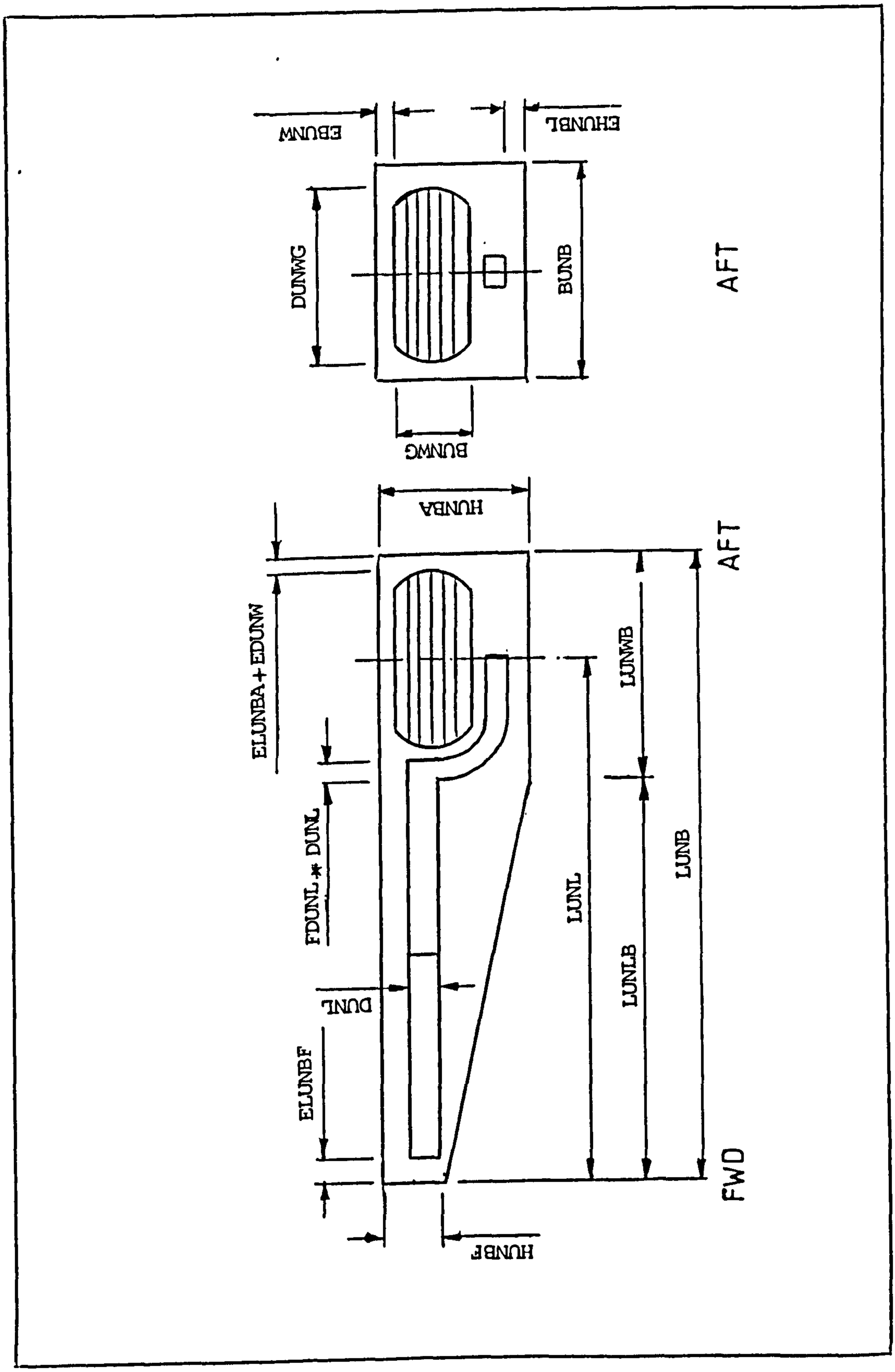

FIG.B.3 NOSE UNDERCARRIAGE AND BAY GEOMETRY

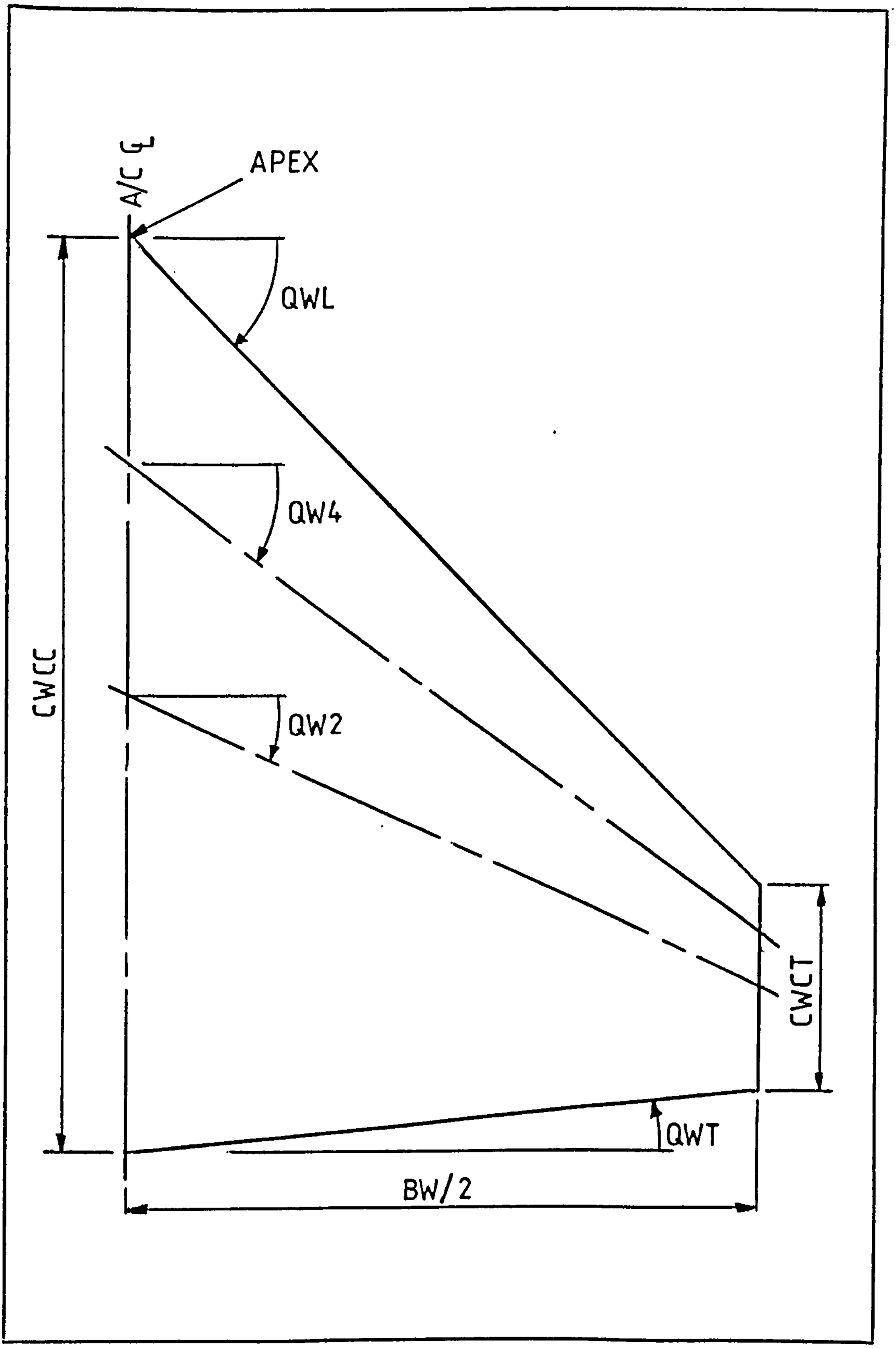

FIG. B.4 GROSS WING GEOMETRY

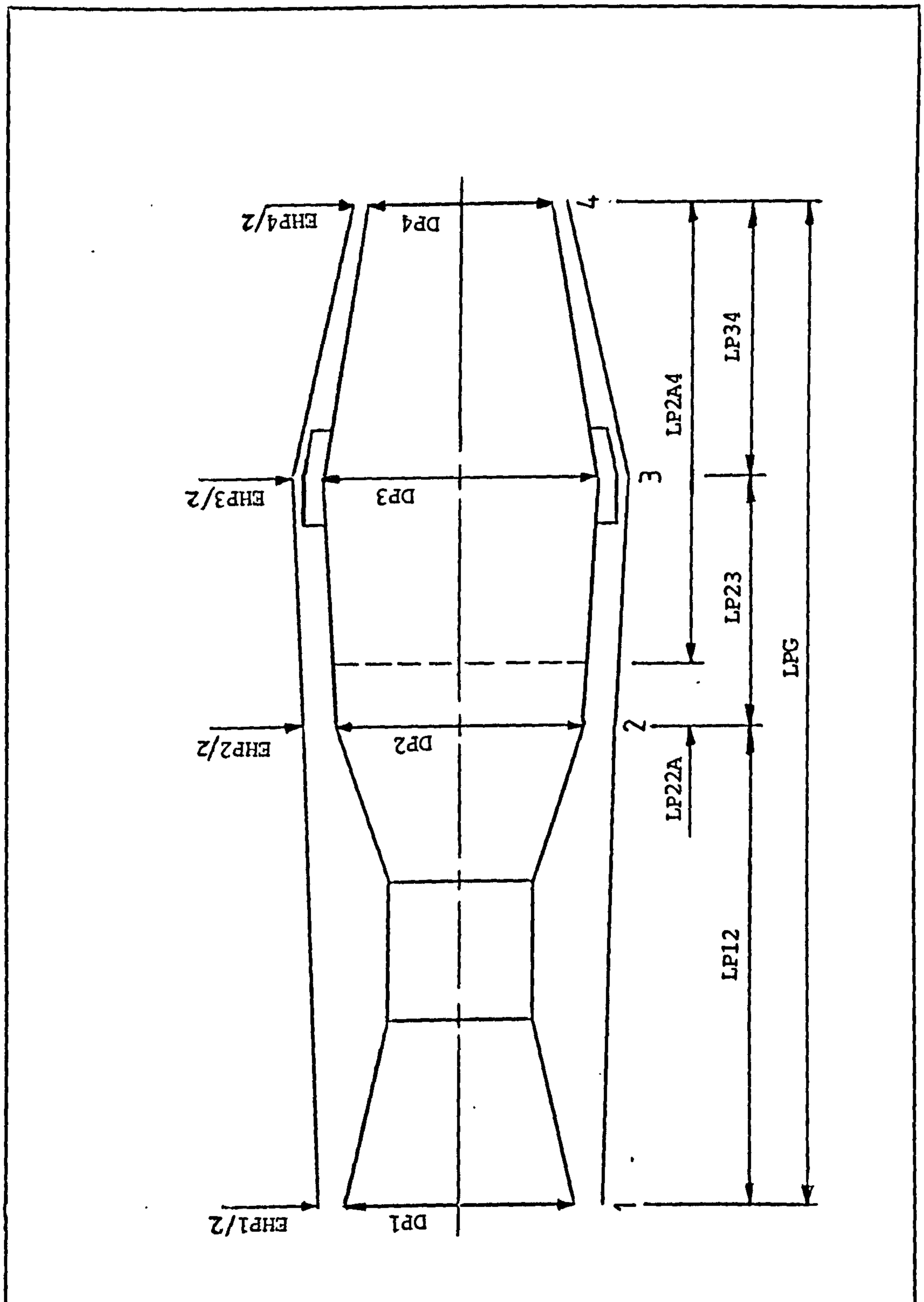

FIG. B.5 ENGINE AND BAY GEOMETRY

APPENDIX C

FAIRING CURVE DEVELOPMENT

C.1 INTRODUCTION

The development of a fairing curve for the definition of the fuselage shape, is presented and explained in this appendix. A fairing curve is basically a given fuselage cross-sectional area distribution (see fig.C.1) which comprises forward and aft fairings which are defined by cubics, joined by a cylindrical centre section. It is effectively a practical method for the application of the sonic area rule in a computerised design synthesis. The fairing curve method is obtained from ref. 1.

The following sections of this appendix describe the mathematical development of the fairing curve expressions used in the synthesis modules FAIRCUR1 and FAIRCUR2.

C2 FAIRING CURVE COEFFICIENTS (Module FAIRCUR1)

The fairing curve is divided into six sections by six stations (1 to 6). The distances of these stations from the aircraft nose are defined by six independent variables, XFN, RLTMFN, RLTFFN, RLTCFN, RLTAFN and FOT6N,

where, RLTMFN = Ratio of the length of the forward fairing to the overall fuselage length minus the length of the radome.

RLTFFN = Ratio of the axial distance from the end of the radome to the point at which the increase in cross-sectional area is half of the maximum increment, to the length of the forward fairing.

RLTCFN = Ratio of the length of the centre section to the length of the fuselage aft of the forward fairing

RLTAFN = Ratio of the axial distance from the end of the centre section to the point at which the decrease in cross-sectional area is half the maximum increment, to the length of the aft fairing.

FOT6N = Increment in cross-sectional area, at the nozzle exit, above the datum value

The axial distances of the six stations from the aircraft nose are given by the following expressions:

$$X1 = XFR \tag{C.1}$$

$$X2 = XFR + RLTFFN * RLTMFN * (XFN - XFR) \tag{C.2}$$

$$X3 = XFR + RLTMFN * (XFN - XFR) \tag{C.3}$$

$$X4 = X3 + RLTCFN * (XFN - X3) \tag{C.4}$$

$$X5 = X4 + RLTAFN * (XFN - X4) \tag{C.5}$$

$$X6 = XFN \tag{C.6}$$

Since a cubic variation of the net cross-sectional area (OTXN) with axial distance is assumed for the forward fairing, then,

$$OTXN = OTF1K + OTF2K * (X3 - X) + OTF3K * (X3 - X)^2 + OTF4K * (X3 - X)^3 \tag{C.7}$$

where, X = Axial distance from the aircraft nose.

Expressions for the coefficients OTF1K, OTF2K, OTF3K and OTF4K in the above cubic are derived by first considering a set of boundary conditions which are determined with the aid of fig.C.1.

b.c.1: At X = X3 $\frac{d(OTXN)}{dx} = 0$

b.c.2: At X = X2 OTXN = 0.5 * OTM

where, OTM = Maximum net cross-sectional area of the fairing curve.

b.c.3: At X = X1 OTXN = OFR

where, OFR = Cross-sectional area of the fuselage at station R.

b.c.4: At X = X1 $\frac{d(OTXN)}{dx} = GOF1 = \frac{OFR}{XFR}$

where, GOF1 = Gradient of fuselage cross-sectional area at station R.

From b.c.1, OTF2K = 0.0 (C.8)

From b.c.4, $OTF3K = \frac{-GOF1 - 3.0 * OTF4K * (X3 - X1)^{2.0}}{2.0 * (X3 - X1)}$ (C.9)

At X = X3, OTXN = OTM, therefore, OTM = OTF1K (C.10)

From b.c.3, $OFR - OTM = OTF3K * (X3 - X1)^{2.0} + OTF4K * (X3 - X1)^{3.0}$ (C.11)

From b.c.2, $OTM = -2.0 * OTF3K * (X3-X2)^{2.0} - 2.0 * OTF4K * (X3-X2)^{3.0}$ (C.12)

Combining the above two expressions,

$OFR = OTF3K * (X3-X1)^{2.0} - 2.0 * (X3-X2)^{2.0} + OTF4K * (X3-X1)^{3.0} - 2.0 * (X3-X2)^{3.0}$ (C.13)

Substituting the previously derived expressions for OTF3K, in the above equation and then solving for OTF4K,

$$OTF4K = \frac{OTF4K1}{OTF4K2 * OTF4K3} \qquad (C.14)$$

where,

$$OTF4K1 = -\{2.0 * OFR * (X3 - X1) + GOF1 * [(X3 - X1)^{2.0} - 2.0 * (X3 - X2)^{2.0}]\} \qquad (C.15)$$

$$OTF4K2 = (X3 - X1) * [(X3 - X1) - 2.0 * (X3 - X2)] \qquad (C.16)$$

and

$$OTF4K = \{(X3 - X2) * [(X3 - X1) - 2.0 * (X3 - X2)] + (X3 - X1) * [(X3 - X1) + (X3 - X2)]\} \qquad (C.17)$$

From b.c.2,

$$OTF1K = -2.0 * (X3-X2)^{2.0} * [OTF3K + OTF4K * (X3-X2)] \qquad (C.18)$$

A cubic variation of OTXN with axial distance is also assumed for the aft fairing, hence,

$$OTXN = OTA1K + OTA2K * (X - X4) + OTA3K * (X - X4)^{2.0} + OTA4K * (X - X4)^{3.0} \qquad (C.19)$$

The following boundary conditions are considered in order to derive expressions for the coefficients OTA1K, OTA2K, OTA3K and OTA4K.

b.c.5: At X = X4 OTXN = OTM

b.c.6: At X = X4 $\frac{d(OTXN)}{dx} = 0$

b.c.7: At X = X5 OTXN = 0.5 * OTM

b.c.8: At X = X6 OTXN = FOT6N

From b.c.5, OTA1K = OTM (C.20)

From b.c.6, OTA2K = 0.0 (C.21)

From b.c.7, $OTA3K = - \frac{0.5 * OTM}{(X5-X4)^{2.0}} - OTA4K * (X5-X4)$ (C.22)

From b.c.8, $OTA4K = \left(\frac{1.0}{X6-X5} \right) * \left[\frac{FOT6N-OTM}{(X6-X4)^{2.0}} + \frac{0.5 * OTM}{(X5-X4)^{2.0}} \right]$ (C.23)

C.3 FAIRING CURVE EQUATIONS (Module FAIRCUR2)

The cross-sectional area of the fairing curve at any fuselage station X is given by the following equations:

If 0.0 ≤ X ≤ X1 then

$$OTXN = GOF1 * X \quad (C.24)$$

If X1 < X < X3 then,

$$OTXN = OTF1K + OTF2K * (X3 - X) + OTF3K * (X3 - X)^{2.0} + OTF4K * (X3 - X)^{3.0} \quad (C.25)$$

If X3 ≤ X ≤ X4 then,

$$OTXN = OTM \tag{C.26}$$

If X4 < X ≤ X6 then,

$$OTXN = OTA1K + OTA2K * (X-X4) + OTA3K * (X-X4)^{2.0} + OTA4K * (X-X4)^{3.0} \tag{C.27}$$

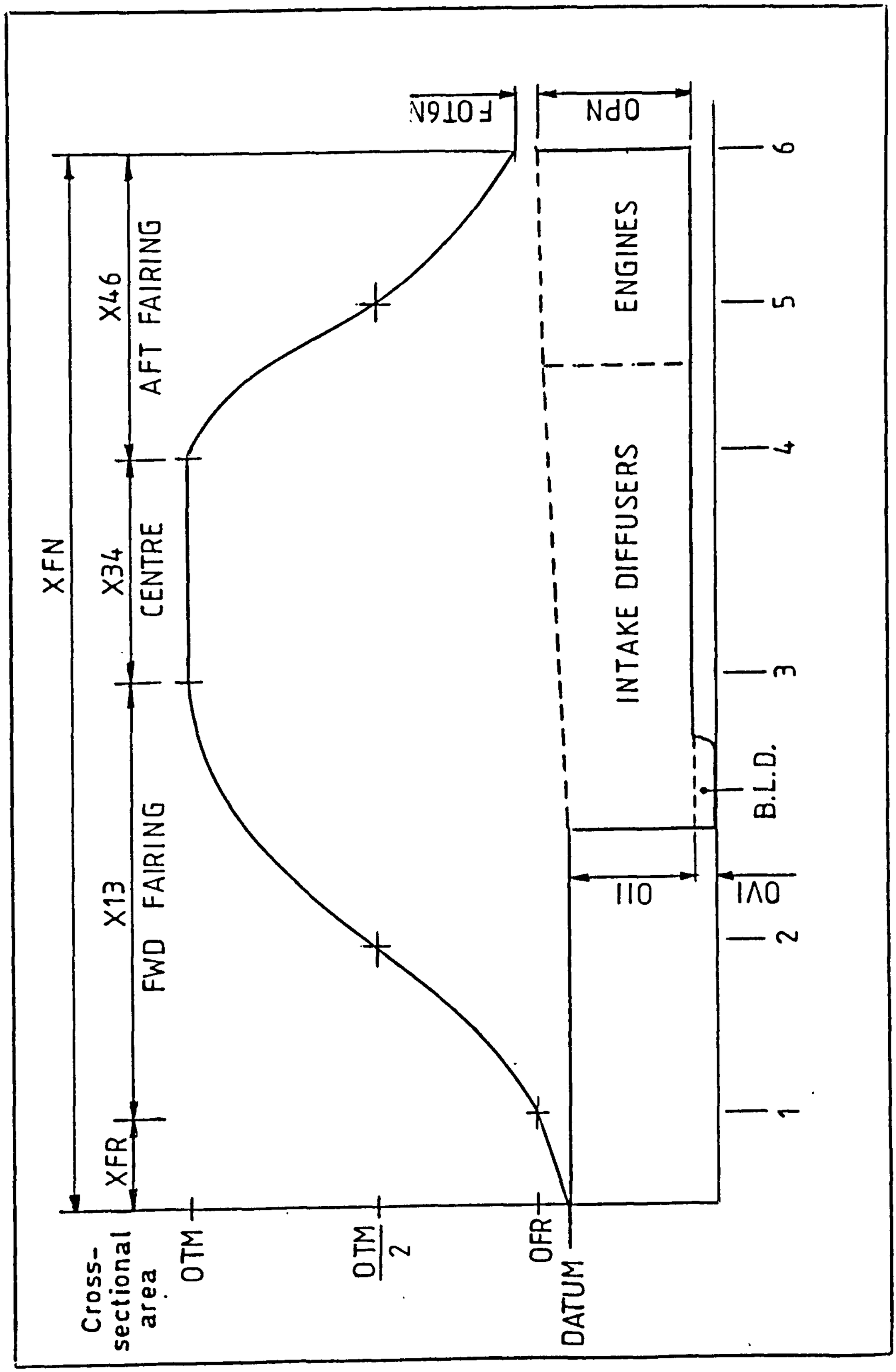

FIG. C.1 FAIRING CURVE

APPENDIX D

FUSELAGE GEOMETRY

D.1 INTRODUCTION

The fuselage is mathematically modelled in 3-D, from the nose to the nozzle exit by a large number of equations which were derived according to the baseline aircraft assumptions, by considering the previously generated fairing curve and the geometric constraints imposed by the sizes of the fixed items of the aircraft. These equations are designed to provide uniform geometric blending between successive fuselage sections. A total of eleven fuselage sections are considered in this appendix, which are defined by the positions of the principal fuselage stations, R, A, B, C, D, E,F, G, H, J and K. The detailed dimensions cross-sectional area and perimeter of the fuselage at the above stations and also at any station X along its length, are determined by twenty-two separate modules in conjunction with four extra modules for the estimation of the 3-D geometry of the intake diffusers, boundary-layer diverter, fuselage-mounted weapons and engine bays, at any station X. The calculated longitudinal cross-sectional area and perimeter distributions, of the fuselage are numerically integrated to produce an accurate estimate of its volume and surface area.

The above fuselage geometry modules are presented in this appendix in the order in which they are executed in the design synthesis. In the following calculations, the X-coordinates are measured axially from the aircraft nose, the Y-coordinates from the aircraft centreline and the Z-coordinates from appropriately defined origins.

D.2 FUSELAGE STATION R (Module FUSSTNR)

The Y- and Z- coordinates of the fuselage at station R are determined by considering the width (BRA) and height (HRA) of the radar antenna together with the corresponding clearances (EBRA) and (EHRA). The local fuselage cross-section and the radar antenna are both assumed to be elliptical in shape as shown in figure D.1.

The Z- and Y- coordinates are therefore,

$$ZFR = 0.5 * HRA + EHRA \qquad (D.1)$$

$$YFR = 0.5 * BRA + EBRA \qquad (D.2)$$

and hence the fuselage cross-sectional area (OFR) and perimeter (PFR) are,

$$OFR = PI * ZFR * YFR \qquad (D.3)$$

and

$$PFR = 2.0 * PI * [0.5 * (ZFR^{2.0} + YFR^{2.0})]^{0.5} \qquad (D.4)$$

BRA, HRA, EBRA and EHRA are external variables specified in the input data.

D.3 FUSELAGE STATION A (Module FUSSTNA)

The fuselage cross-section at station A is assumed to be elliptical as shown in figure D.2.

The local fuselage height (HFA) is,

$$HFA = HC5 + HFA1 \qquad (D.5)$$

The local width (BFA) is automatically adjusted by the following expression in oder to match the local fuselage cross-sectional area (OFA) to the corresponding value (OTXN) given by the fairing curve, therefore,

$$BFA = \frac{4.0 * OTXN}{PI * HFA} \qquad (D.6)$$

The actual fuselage cross-sectional area and perimeter (PFA) are,

$$OFA = 0.25 * PI * HFA * BFA \qquad (D.7)$$

and

$$PFA = 2.0 * PI * [0.125 * (HFA^{2.0} + BFA^{2.0})]^{0.5} \qquad (D.8)$$

The fuselage section between the aircraft nose and station A is drooped in order to provide a clear and unobstructed visual path from the pilot's eye point. The droop angle (QFRA) is defined as the angle between the line through the geometric centres of stations R and A, and the horizontal. It is observed from fig.D.3 that in order to achieve the specified angle QCEYE (Section B.2), the optimum QFRA must be,

$$QFRA = 0.5 * QCEYE \quad \text{(rads)} \qquad (D.9)$$

D.4 RADOME SECTION (Module RADOME)

This is the fuselage section between the aircraft nose and station R.

The Y- and Z- coordinates of the radome are assumed to vary from zero to YFR and ZFR respectively, in the form of a power series cylinder function, for minimum ware drag. The radome cross-section at any station X is assumed to be elliptical in shape. In order to achieve uniform blending of the radome with fuselage section R-A, it is further

assumed that the shape variation of the radome continues up to station A.

The Y- and Z- coordinates of the radome at any station X, are therefore,

$$YFRX = 0.5 * BFA * \left(\frac{X}{XA}\right)^{FYFRAK} \qquad (D.10)$$

And

$$ZFRX = 0.5 * HFA * \left(\frac{X}{XA}\right)^{FZFRAK} \qquad (D.11)$$

The correct values of powers FYFRAK and FZFRAK are determined by considering a set of boundary conditions which are derived from the above assumptions.

b.c.1: At X = XFR ZFRX = ZFR = 0.5 * HRA + EHRA

b.c.2: At X = XA ZFRX = 0.5 * HFA

b.c.3: At X = XFR YFRX = YFR = 0.5 * BRA + EBRA

b.c.4: At X = XA YFRX = 0.5 * BFA

Therefore from, b.c.1 and b.c.2,

$$FZFRAK = \frac{\ln\left(\frac{HRA + 2.0 * EHRA}{HFA}\right)}{\ln\left(\frac{XFR}{XA}\right)} \qquad (D.12)$$

and from b.c.3 and b.c.4,

$$FYFRAK = \frac{\ln\left(\frac{BRA + 2.0 * EBRA}{BFA}\right)}{\ln\left(\frac{XFR}{XA}\right)} \qquad (D.13)$$

The radome cross-sectional area (OFRX) and perimeter (PFRX) at any station X are,

$$OFRX = PI * ZFRX * YFRX \qquad (D.14)$$

and

$$PFRX = 2.0 * PI * [0.5 * (ZFRX^{2.0} + YFRX^{2.0})]^{0.5} \qquad (D.15)$$

D.5 FUSELAGE SECTION R-A (Module FSECTRA)

According to the assumptions made in the previous section the expressions for the geometry of fuselage section R-A are similar to those for the radome.

The values of FZFRAK and FYFRAK are equal to those for the radome. The Y- and Z- coordinates of section R-A, YFRAX and ZFRAX respectively, are,

$$YFRAX = 0.5 * BFA * \left(\frac{X}{XA}\right)^{FYFRAK} \qquad (D.16)$$

and

$$ZFRAX = 0.5 * HFA * \left(\frac{X}{XA}\right)^{FZFRAK} \qquad (D.17)$$

The cross-sectional area of section R-A (OFRAX) and perimeter (PFRAX) at any station X, are,

$$OFRAX = PI * ZFRAX * YFRAX \qquad (D.18)$$

and

$$PFRAX = 2.0 * PI * [0.5(ZFRAX^{2.0} + YFRAX^{2.0})]^{0.5} \qquad (D.19)$$

D.6 INTAKE DIFFUSERS (Module INTDIFG)

This module comprises detailed mathematical models for the estimation of the Y-, Z- coordinates, height, width, corner radii and cross-sectional area of each intake diffuser at any fuselage station X.

The mathematical models were developed with reference to the side and plan views of an intake diffuser shown in fig.D.4. It is assumed that each intake diffuser starts at the intake plane (X = XII) and finishes at the inlet of the engine compressor (X = XP1). Its cross-section starts with a rectangular shape which gradually becomes circular at a distance equal to DP1 upstream of the engine. At the intake plane, each diffuser corner has a specified radius RIDX1, which gradually increases to 0.5 * DP1 at the point where the diffuser cross-section becomes circular (X = XP1-DP1). The height gradually increases from HII at XII, to DP1 at XP1 - DP1. Similarly the width is assumed to remain constant between XII and XE and also between XP1 - DP1 and XP1. The width gradually increases from BII at XE, to DP1 at XP1 - DP1. The diffusers have a smooth S-shape in both the X - Y and X - Z planes between the above stated boundaries. This shape is mathematically modelled by a sinusoidal variation of the diffuser's Z- and Y- coordinates with X.

The Z-coordinates of the lower, centre and upper diffuser lines ZIDLX, ZIDCX and ZIDUX respectively, at any station X are determined with respect to the flat bottom surface of the fuselage: Hence,

If XII $\leq X <$ XD then,

ZIDLX = Equation D.23 (D.20)

ZIDCX = Equation D.24 (D.21)

ZIDUX = Equation D.25 (D.22)

If XD $\leq$ X $\leq$ XP1 - DP1 then,

$$ZIDLX = \left\{1.0 - \sin^{2.0}\left[0.5 * P1 * \left(\frac{XP1-DP1-X}{XP1-DP1-XII}\right)\right]\right\} * (ZPC - HUNBA - 0.5 * DP1) \quad (D.23)$$

$$ZIDCX = \left\{1.0 - \sin^{2.0}\left[0.5 * P1 * \left(\frac{XP1-DP1-X}{XP1-DP1-XII}\right)\right]\right\} * (ZPC - HUNBA - 0.5 * HII) + 0.5 * HII \quad (D.24)$$

$$ZIDUX = \left\{1.0 - \sin^{2.0}\left[0.5 * P1 * \left(\frac{XP1-DP1-X}{XP1-DP1-XII}\right)\right]\right\} * (ZPC - HUNBA - HII + 0.5 * DP1) + HII \quad (D.25)$$

Otherwise if, $XP1 - DP1 < X \leq XP1$ then,

$$ZIDLX = ZPC - 0.5 * DP1 \quad (D.26)$$

$$ZIDCX = ZPC \quad (D.27)$$

$$ZIDUX = ZPC + 0.5 * DP1 \quad (D.28)$$

where ZPC = Height of the engine centreline above the flat bottom surface of the fuselage

$$ZPC = HUMB + 0.5 * (DP1 + EHP1) \quad (D.29)$$

Similarly, the Y- coordinates of the inner, centre and outer diffuser lines YIDIX, YIDCX and YIDOX respectively, at any station X are determined with respect to the aircraft centreline. Hence,

If $X11 \leq X < XE$ then,

$$YIDIX = 0.0 \quad (D.30)$$

$$YIDCX = 0.5 * BII \quad (D.31)$$

$$YIDOX = BII \quad (D.32)$$

If however, $XE \leq X \leq XP1 - DP1$ then,

$$YIDIX = \left\{1.0 - \sin^{2.0}\left[0.5 * PI * \left(\frac{XP1-DP1-X}{XP1-DP1-XE}\right)\right]\right\} * [0.5 * (YPCH - DP1)] \quad (D.33)$$

$$YIDCX = \left\{1.0 - \sin^{2.0}\left[0.5 * PI * \left(\frac{XP1-DP1-X}{XP1-DP1-XE}\right)\right]\right\} * [0.5 * (YPCH - BII)] + 0.5 * BII \quad (D.34)$$

$$YIDOX = \left\{1.0 - \sin^{2.0}\left[0.5 * PI * \left(\frac{XP1-DP1-X}{XP1-DP1-XE}\right)\right]\right\} * [0.5 * (YPCH + DP1) - BII] + BII \quad (D.35)$$

Otherwise if, XP1 - DP1 < X ≤ XP1 then,

$$YIDIX = 0.5 * (YPCH - DP1) \quad (D.36)$$

$$YIDCX = 0.5 * YPCH \quad (D.37)$$

$$YIDOX = 0.5 * (YPCH + DP1) \quad (D.38)$$

where, YPCH = Distance between the engine centrelines,

$$YPCH = 0.5 * EBP3 + DP3 + EYPCH \quad (D.39)$$

where, EYPCH = Lateral clearance between the engines for protection against common cause failures.

The height (HIDX) and width (BIDX) of each intake diffuser at any station X, are therefore given by the following expressions:

$$HIDX = ZIDUX - ZIDLX \quad (D.40)$$

$$BIDX = YIDOX - YIDIX \quad (D.41)$$

The size of the diffuser corner radii (RIDX) at any station X, is as follows:

If $XII \leq X < XD$ then $RIDX = RIDX1$

If however, $XD \leq X \leq XP1 - DP1$ then,

$$RIDX = RIDX1 + \left(\frac{X-XD}{XP1-DP1-XD}\right) * (0.5 * DP1 - RIDX1) \qquad (D.42)$$

If $XP1 - DP1 < X \leq XP1$ then

$$RIDX = 0.5 * DP1 \qquad (D.43)$$

Finally, having determined HIDX, BIDX and RIDX, the cross-sectional area of each intake diffuser (OIDX) at any station X, is estimated using the following expression:

$$OIDX = (HIDX - 2.0 * RIDX) * (BIDX - 2.0 * RIDX) + 2.0 * RIDX * (BIDX - 2.0 * RIDX) + 2.0 * RIDX * (HIDX - 2.0 * RIDX) + PI * RIDX^{2.0} \qquad (D.44)$$

D.7 FUSELAGE STATION D (Module FUSSTND)

The dimensions, cross-sectional area and perimeter of the fuselage at station D are determined in this module using expressions which were derived according to the initial baseline aircraft geometry assumptions. These expressions are listed and explained below.

A view of the fuselage cross-section at station D is shown in fig.D.5. This is made up from rectangular and elliptical sections, which are considered separately.

The following expression for the Y- coordinate of the canopy at station D (YCCAND) was derived with reference to the plan view of the baseline aircraft.

$$YCCAND = YCCANC - \left(\frac{YCWSCB - YCCANC}{XC - XB}\right) * (XD - XC) \qquad (D.45)$$

where, YCCANC = Y-coordinate of the canopy at station C.
YCWSCB = Y-coordinate of the windscreen at station B.

YCCANC is specified in the input data and represents the canopy half-width at the pilot's shoulders.

YCWSCB is obtained from the following expression:

$$YCWSCB = YCCANC + \left(\frac{YCCANC}{XFN-LPG-DP1-XC}\right) * (XC - XD) \qquad (D.46)$$

In the derivation of the above expression it was assumed that the canopy side lines extend up to X = XFN - LPG - DP1 where they cross. These extended lines form the fuselage spine.

The height of the nose u/c bay (HUNBD) at station D is,

$$HUNBD = HUNBF + \left(\frac{HUNBA - HUNBE}{LUNLB}\right) * (XD - XUNBF) \qquad (D.47)$$

The fuselage height (HFD) is,

$$HFD = HFA + HVI + HIDX + HUNBD \qquad (D.48)$$

HIDX is evaluated at X = XD, by a previous call to module INTDIFG.

When fuselage station D passes through the aft section of the nose u/c bay, then HFD reaches its maximum value (HFDH) where,

$$HFDH = HFA + HVI + HIDX + HUNBA \qquad (D.49)$$

The canopy is assumed to have a semi-elliptical cross-sectional shape. Its longitudinal centreline is inclined at an angle (QCCAN) to the horizontal (see fig.D.9). Therefore the height of this centreline above the upper corner line of fuselage section C - D, (HFD2) is,

$$HFD2 = (XD - XB) * \tan (QCCAN) \qquad (D.50)$$

QCCAN is specified in the input data and it is expressed in rads.

The expression for the fuselage width (BFD), was derived by assuming that the net fuselage cross-sectional area at station D is equal to its corresponding fairing curve value, OTXN.

$$BFD = \frac{OTXN + 2.0 * OIDX - YCCAND * [(2.0 - 0.5 * PI) * HFDCU + (0.5 * PI * HFD2)]}{(0.25 * PI - 1.0) * HFDCU + HFD} \qquad (D.51)$$

where, HFDCU = Height of upper fuselage corner at station D
HFDCU is specified in the input data.
OIDX is evaluated at X = XD by a previous call to INTDIFG.

The above determined value of BFD is constrained not to be less than BFDS, which is the minimum allowable width at

/

station D, in order to accommodate the intake diffusers, hence,

$$BFDS = 2.0 * BIDX + EBFD \qquad (D.52)$$

where, EBFD = Total width clearance between diffusers and fuselage at station D.

The width of an upper fuselage corner (BFDCU) at station D is,

$$BFDCU = 0.5 * (BFD - 2.0 * YCCAND) \qquad (D.53)$$

Having determined all the dimensions of the fuselage section, its cross-sectional area (OFD) and perimeter (PFD) are then obtained using the following expressions:

$$OFD = 0.5 * PI * [(YCCAND * HFD2) + (HFDCU * BFDCU)] + (HFD - HFDCU) * BFD + (BFD - 2.0 * BFDCU) * HFDCU \qquad (D.54)$$

and

$$PFD = PI * [0.5 * (YCCAND^{2.0} + HFD2^{2.0})]^{0.5} + PI * [0.5 * (HFDCU^{2.0} + BFDCU^{2.0})]^{0.5} + 2.0 * (HFD - HFDCU) + BFD \qquad (D.55)$$

D.8 FUSELAGE STATION B (Module FUSSTNB)

An approach similar to that used for fuselage station D is also used to determine the geometry of the fuselage at station B. The mathematical models included in this module were derived with reference to the cross-sectional view in fig.D.6 and according to the initial baseline aircraft geometry assumptions.

A semi-elliptical cross-sectional shape is assumed for the windscreen which is defined by Z- and Y- coordinates. ZCWSCB and YCWSCB respectively. YCWSCB was determined in module FUSSTND, while ZCWSCB is given by,

$$ZCWSCB = (XB - XA) * \tan(QCWSC) \qquad (D.56)$$

where, QCWSC = Windscreen inclination to the horizontal. QCWSC is an external variable, specified in the input data in rads.

The height of fuselage (HFB) at station B is assumed equal to HFA, hence,

$$HFB = HFA \qquad (D.57)$$

The fuselage section has four elliptically shaped corners. From the side-view of the baseline aircraft, the height of the upper corners is,

$$HFBCU = 0.5 * HFA - \left(\frac{0.5 * HFA - HFDCU}{XD - XA}\right) * (XB - XA) \qquad (D.58)$$

and the height of the lower corners (HFBCL) is,

$$HFBCL = 0.5 * HFA - \left(\frac{0.5 * HFA}{XVE + 0.25 * LVG - XA}\right) * (XB - XA) \qquad (D.59)$$

The fuselage width (BFB) is automatically adjusted by the following expression to match the net fuselage cross-sectional area at station B, to the corresponding fairing-curve area. Hence,

$$BFB = \frac{OTXN - \{(0.5 * PI * YCWSCB * ZCWSCB) - (0.5 * PI - 2.0) * [YCWSCB * HFBCU + \left(\frac{0.5 * BFD}{XD-XA}\right) * (XB - XA) * HFBCL]\}}{0.5 * [(0.5 * PI - 2.0) * (HFBCL + HFBCU) + 2.0 * HFB]} \quad (D.60)$$

The above estimated value of BFB is constrained however, not to be less than the minimum allowable width (BFBS), where,

$$BFBS = 2.0 * YCWSCB \quad (D.61)$$

After determining BFB, it is possible to estimate the width of the fuselage corners. The width of each of the upper corners (BFBCU) is,

$$BFBCU = 0.5 * BFB - YCWSCB \quad (D.62)$$

and the width of each of the lower corners (BFBCL) is,

$$BFBCL = 0.5 * BFB - \left(\frac{0.5 * BFD}{XD - XA}\right) * (XB - XA) \quad (D.63)$$

The above two expressions were derived with reference to the upper and lower plan views of the baseline aircraft, respectively.

The cross-sectional area of the fuselage (OFB) at station B. is,

$$OFB = 0.5 * PI * [YCWSCB * ZCWSCB + BFBCU * HFBCU + BFBCL * HFBCL] + BFB * (HFB - HFBCU - HFBCL) + 2.0 * [(0.5 * BFB - BFBCU) * HFBCU + (0.5 * BFB - BFBCL) * HFBCL] \quad (D.64)$$

and the fuselage perimeter (PFB) is,

$$PFB = PI * \{[0.5 * (YCWSCB^{2.0} + ZCWSCB^{2.0})]^{0.5} + [0.5 * (BFBCU^{2.0} + HFBCU^{2.0}]^{0.5} + [0.5 * (BFBCL^{2.0} + HFBCL^{2.0})]^{0.5}) + 2.0 * [(HFB - HFBCU - HFBCL) + (0.5 * BFB - BFBCL)]$$

(D.65)

D.9 FUSELAGE SECTION A - B (Module FSECTAB)

This module determines the geometry of fuselage section A - B. Fig.D.7 presents different views of this section.

The Z- coordinate of the windscreen (ZCWSCX) is assumed to increase linearly with X from 0.0 at station A to ZCWSCB at station B. Since QCWSC is a specified external variable,

$$ZCWSCX = (X - XA) * \tan(QCWSC) \qquad (D.66)$$

The plan view of the windscreen is represented by a semi-ellipse. Therefore its Y- coordinate (YCWSCX) at any station X, which increases from 0.0 at station A to YCWSCB at station B, is,

$$YCWSCX = \left\{\left[1.0 - \frac{(XB - X)^{2.0}}{(XB - XA)^{2.0}}\right] * YCWSCB^{2.0}\right\}^{0.5} \qquad (D.67)$$

The perimeter of the windscreen (PFTABX) at any station X of fuselage section A - B is,

$$PFTABX = PI * [0.5 * (YCWSCX^{2.0} + ZCWSCX^{2.0})]^{0.5} \qquad (D.68)$$

The fuselage height (HFABX) remains constant along section A - B, therefore,

$$HFABX = HFA \tag{D.69}$$

The height of the upper (HFBCUX) and lower (HFBCLX) elliptically shaped fuselage corners at any station X of section A - B, is,

$$HFBCUX = 0.5 * HFA - \left(\frac{0.5 * HFA - HFDCU}{XD - XA}\right) * (X - XA) \tag{D.70}$$

and

$$HFBCLX = 0.5 * HFA - \left(\frac{0.5 * HFA}{XVE + 0.25 * LVG - XA}\right) * (X - XA) \tag{D.71}$$

The Y- coordinate of section A - B (YFABX) at any station X is estimated by considering the corresponding fairing curve area, hence,

$$YFABX = \frac{OTXN - \{(0.5 * PI * YCWSCX * ZCWSCX) - (0.5 * PI - 2.0) * [YCWSCX * HFBCUX + \left(\frac{0.5 * BFD}{XD - XA}\right) * (X - XA) * HFBCLX]\}}{[(0.5 * PI - 2.0) * (HFBCLX + HFBCUX) + 2.0 * HFABX]} \tag{D.72}$$

The above estimated value of YFABX is constrained not to be less than a minimum (YFABXS), where,

$$YFABXS = \begin{matrix} YCWSCX \\ 0.5 * BFA + \left(\frac{YCWSCB - 0.5 * BFA}{XB - XA} \right) * (X - XA) \end{matrix} \Bigg\rceil \begin{matrix} \text{the} \\ \text{largest} \end{matrix} \qquad (D.73)$$

The width of each of the upper and lower corners at any station X of fuselage section A - B, (BFBCUX) and (BFBCLX) respectively, is estimated by the following expressions:

$$BFBCUX = YFABX - YCWSCX \qquad (D.74)$$

$$BFBCLX = YFABX - \left(\frac{0.5 * BFD}{XD - XA} \right) * (X - XA) \qquad (D.75)$$

The cross-sectional area (OFABX) and perimeter (PFABX) at any station X of section A - B are given by the following expressions:

$$\begin{aligned} OFABX = {} & 0.5 * PI * [YCWSCX * ZCWSCX + BFBCUX * HFBCUX + \\ & BFBCLX * HFBCLX] + 2.0 * [(HFABX - HFBCUX - HFBCLX) * \\ & YFABX + (YFABX - BFBCUX) * HFBCUX + (YFABX - BFBCLX) \\ & * HFBCLX] \end{aligned} \qquad (D.76)$$

and

$$\begin{aligned} PFABX = {} & PI * \{[0.5 * (YCWSCX^{2.0} + ZCWSCX^{2.0})]^{0.5} + [0.5 * \\ & (BFBCUX^{2.0} + HFBCUX^{2.0})]^{0.5} + [0.5 * (BFBCLX^{2.0} + \\ & HFBCLX^{2.0})]^{0.5}) + 2.0 * [(HFABX - HFBCUX - HFBCLX) + \\ & (YFABX - BFBCLX)]. \end{aligned} \qquad (D.77)$$

D.10 FUSELAGE STATION C (Module FUSSTNC)

A view of the fuselage cross-section at station C is presented in fig.D.8. Its dimensions, cross-sectional area and perimeter are again estimated in a similar way to that for the previous stations.

The fuselage height (HFC) is assumed to be equal to HFB , hence,

$$HFC = HFB \tag{D.78}$$

Similarly the cockpit under-floor height (HFC1) at station C is equal to HFA1, hence,

$$HFC1 = HFA1 \tag{D.79}$$

The height of the canopy's centreline (HFC2) above the upper fuselage corners at station C is,

$$HFC2 = (XC - XB) * \tan (QCCAN) \tag{D.80}$$

Since station C coincides with the pilot's eye-point position, the local Z- coordinate of the canopy (ZCCANC) is,

$$ZCCANC = HC4 + HCEYE + HFC1 - HFC - HFC2 \tag{D.81}$$

The height of the upper and lower corners, (HFCCU) and (HFCCL) respectively, is,

$$HFCCU = 0.5 * HFA - \left(\frac{0.5 * HFA - HFDCU}{XD - XA} \right) * (XC - XA) \tag{D.82}$$

and

$$HFCCL = 0.5 * HFA - \left(\frac{0.5 * HFA}{XVE + 0.25 * LVG - XA}\right) * (XC - XA) \quad (D.83)$$

The local fuselage width (BFC) is obtained by considering the corresponding fairing curve area, therefore,

$$BFC = \frac{\{OTXN + YCCANC * [(0.5 * PI - 2.0) * HFCCU - 0.5 * PI * (ZCCANC + HFC2)] + (0.5 * PI - 2.0) * \left(\frac{0.5 * BFD}{XD - XA}\right) * (XC - XA) * HFCCL\}}{(0.25 * PI - 1.0) * (HFCCL + HFCCU) + HFC} \quad (D.84)$$

The minimum allowable fuselage width (BFCS) at station C, is

$$BFCS = 2.0 * BII \quad (D.85)$$

The above constraint ensures that the chin air intakes always remain shielded under the forward fuselage,

The width of each of the upper and lower elliptically shaped fuselage corners, (BFCCU) and (BFCCL) respectively is,

$$BFCCU = 0.5 * BFC - YCCANC \quad (D.86)$$

and

$$BFCCL = 0.5 * BFC - \left(\frac{0.5 * BFD}{XD - XA}\right) * (XC - XA) \quad (D.87)$$

The following expressions give the cross-sectional area (OFC) and perimeter (PFC) of the fuselage at station C.

$$OFC = 0.5 * PI * [YCCANC * (ZCCANC + HFC2) + BFCCL * HFCCL + BFCCU * HFCCU] + (BFC - 2.0 * BFCCU) * HFCCU + (BFC - 2.0 * BFCCL) * HFCCL + (HFC - HFCCU - HFCCL) * BFC \quad (D.88)$$

and

$$PFC = PI * \{[0.5 * (YCCANC^{2.0} + (ZCCANC + HFC2)^{2.0})]^{0.5} + [0.5 * (HFCCU^{2.0} + BFCCU^{2.0})]^{0.5} + [0.5 * (HFCCL^{2.0} + BFCCL^{2.0})]^{0.5} + 2.0 * (HFC - HFCCL - HFCCU) + (BFC - 2.0 * BFCCL)\} \quad (D.89)$$

D.11 FUSELAGE SECTION B-C (Module FSECTBC)

The expressions presented in this section are included in module FSECTBC and determine in detail the geometry of fuselage section B-C. Different views of the latter are shown in fig.D.9.

The height of section B-C (HFBCX), is assumed to remain constant at any station X. Therefore,

$$HFBCX = HFB \quad (D.90)$$

The height of the canopy centreline above the upper fuselage corners (HFC2X), at any station X, is,

$$HFC2X = (X - XB) * \tan (QCCAN) \quad (D.91)$$

The Y- coordinate of the canopy (YCCANX) at any station X is,

$$YCCANX = YCWSCB - \left(\frac{YCWSCB - YCCANC}{XC - XB}\right) * (X - XB) \qquad (D.92)$$

and the corresponding Z- coordinate (ZCCANX) is,

$$ZCCANX = ZCWSCB - HFC2 + (ZCCANC + HFC2 - ZCWSCB) * \left(\frac{X - XB}{XC - XB}\right)^{FZCAN1} \qquad (D.93)$$

The above expression was derived on the assumption that ZCCANX varies in the form of a power series cylinder function. The longitudinal curvature of the canopy within section B-C, is controlled by the value of power FZCAN1 which is an external variable specified in the input data.

The perimeter of the canopy (PFTBCX) at any station X of fuselage section B-C, is,

$$PFTBCX = PI * [0.5 * (YCCANX^{2.0} + ZCCANX^{2.0})]^{0.5} \qquad (D.94)$$

The height of the upper (HFCCUX) and lower (HFCCLX) fuselage corners is,

$$HFCCUX = 0.5 * HFA - \left(\frac{0.5 * HFA - HFDCU}{XD - XA}\right) * (X - XA) \qquad (D.95)$$

and

$$HFCCLX = 0.5 * HFA - \left(\frac{0.5 * HFA}{XVE + 0.25 * LVG - XA}\right) * (X - XA) \qquad (D.96)$$

The Y- coordinate of fuselage section B-C (YFBCX) at any station X, is adjusted according to the corresponding fairing curve area, by the following expression:

$$YFBCX = \frac{\{OTXN + YCCANX * [(0.5 * PI - 2.0) * HFCCUX - 0.5 * PI * (ZCCANX + HFC2X)] + (0.5 * PI - 2.0) * \left(\frac{0.5 * BFD}{XD - XA}\right) * (X - XA) * HFCCLX\}}{2.0 * [(0.25 * PI - 1.0) * (HFCCLX + HFCCUX) + HFBCX]} \quad (D.97)$$

Since BFCS = 2.0 * BII, the minimum allowable value (YFBCXS) for YFBCX at any station X of section B-C is,

$$YFBCXS = 0.5 * BFB + \left(\frac{BII - 0.5 * BFB}{XC - XB}\right) * (X - XB) \quad (D.98)$$

The width of each of the upper (BFCCUX) and lower (BFCCLX) elliptically shaped fuselage corners is,

$$BFCCUX = YFBCX - YCCANX \quad (D.99)$$

and

$$BFCCLX = YFBCX - \left(\frac{0.5 * BFD}{XD - XA}\right) * (X - XA) \quad (D.100)$$

The cross-sectional area (OFBCX) of fuselage section B-C at any station X is,

$$OFBCX = 0.5 * PI * [(ZCCANX + HFC2X) * YCCANX + (HFCCUX * BFCCUX) + (HFCCLX * BFCCLX)] + 2.0 * [(YFBCX - BFCCLX) * HFCCLX + (HFBCX - HFCCUX - HFCCLX) * YFBCX + (YFBCX - BFCCUX) * HFCCUX] \quad (D.101)$$

and the corresponding perimeter (PFBCX) is,

$$PFBCX = PI * \{[0.5 * ((ZCCANX + HFC2X)^{2.0} + YCCANX^{2.0})]^{0.5} + [0.5 * (HFCCUX^{2.0} + BFCCUX^{2.0})]^{0.5} + [0.5 * (HFCCLX^{2.0} + BFCCLX^{2.0})]^{0.5}) + 2.0 * [(HFBCX - HFCCLX - HFCCUX) + (YFBCX - BFCCLX)]$$

(D.102)

D.12 BOUNDARY LAYER DIVERTER (Module BLDIVG2)

The results of module BLDIVG1 are used in module BLDIVG2 to estimate the width and cross-sectional areas of the b.l. diverter splitter and streamtube at any station X.

The halfwidth of the b.l. diverter (BIX) is defined by the width of the intake fairing at any station X. Hence,

If $XII \leq X \leq XD$ then,

$$BIX = BII + \left(\frac{0.5 * BFD - BII}{XD - XII}\right) * (X - XII) \qquad (D.103)$$

For values of X outside the above range, BIX = 0.0.

The cross-sectional area (OVIX1) of the b.l. diverter splitter plate at any station X is assumed to vary as follows:

If $XVE - 0.25 * LVG \leq X \leq XVE + 0.25 * LVG$ then,

$$OVIX1 = BIX * HVI * \left\{1.0 + \sin\left[0.5 * PI * \left(\frac{X - XVE}{0.25 * LVG}\right)\right]\right\} \qquad (D.104)$$

If $XVE + 0.25 * LVG < X \leq XD$ then,

$$OVIX1 = 2.0 * BIX * HVI \qquad (D.105)$$

For any other values of X, OVIX1 = 0.0. (D.106)

The width of the b.l. diverter splitter (BVIX1) at any station X is,

$$BVIX1 = \frac{OVIX1}{HVI} \qquad (D.107)$$

The width of the b.l. diverter streamtube at any station X is,

$$BVIX = 2.0 * BIX - BVIX1 \qquad (D.108)$$

while its cross-sectional area (OVIX) is as follows:

If $XII \leq X < XVE - 0.25 * LVG$ then,

$$OVIX = BVIX * HVI \qquad (D.109)$$

If $XVE - 0.25 * LVG \leq X \leq XVE + 0.25 * LVG$

$$OVIX = 2.0 * BIX * HVI - BIX * HVI * \left\{1.0 + \sin\left[0.5 * PI * \left(\frac{X - XVE}{0.25 * LVG}\right)\right]\right\} \qquad (D.110)$$

For any other values of X, OVIX = 0.0 (D.111)

D.13 FUSELAGE SECTION C-D (Module FSECTCD)

The geometry of fuselage section C-D, is determined by dividing it into two separate sections. The first,

comprises the intake fairing, b.l. diverter and nose u/c bay and is known as the lower section. The second comprises all the remaining parts of C-D and is known as the upper section. Different views of the complete section C-D are shown in fig.D.10.

The cross-sectional area of the intake fairing (OIX) is as follows:

If XII ≤ X ≤ XD then,

$$OIX = 2.0 * BIX * HII \qquad (D.112)$$

Outside the above range of values of X, OIX = 0.0. (D.113)

The cross-sectional area of the fairing under the intake ducts and forward of the nose u/c bay (OIXL1) at any station X is as follows:

If XII ≤ X ≤ XUNBF then ,

$$OIXL1 = 2.0 * \left(\frac{HUNBF}{XUNBF - XII}\right) * (X - XII) * BIX \qquad (D.114)$$

Outside the above range of values of X, OIXL1 = 0.0 (D.115)

The cross-sectional area of the nose u/c bay fairing (OIXL2) at any station X of fuselage section C-D is as follows:

If XUNBF ≤ X ≤ XD then,

$$OIXL2 = 2.0 * [HUNBF + \left(\frac{HUNBA - HUNBF}{LUNLB}\right) * (X - XUNBF)] * BIX \qquad (D.116)$$

Outside the above range of values of X, OIXL2 = 0.0. (D.117)

The length of fuselage section C-D (LFCD) is,

$$LFCD = XD - XC \tag{D.118}$$

The height of the canopy centreline above the upper fuselage corners (HFD2X) at any station X is,

$$HFD2X = HFC2 + (X - XC) * \tan(QCCAN) \tag{D.119}$$

The Z- coordinate of the canopy (ZCCANX) at any station X is,

$$ZCCANX = ZCCANC + HFC2 - HFD2X - (ZCCANC + HFC2 - HFD2) * \left(\frac{X - XC}{XD - XC}\right)^{FZCAN2} \tag{D.120}$$

The above expression was derived, on the same assumption as for section B-C, i.e., ZCCANX varies in the form of a power series cylinder function. The longitudinal curvature of the canopy within section C-D however, is controlled by the value of power FZCAN2 which is also an external variable, specified in the input data.

The Y- coordinate of the canopy (YCCANX) at any station X is,

$$YCCANX = YCCANC - \left(\frac{YCWSCB - YCCANC}{XC - XB}\right) * (X - XC) \tag{D.121}$$

The perimeter of the canopy (PFTCDX) at any station X of fuselage section C-D is,

$$PFTCDX = PI * [0.5 * (YCCANX^{2.0} + ZCCANX^{2.0})]^{0.5} \tag{D.122}$$

The height of the upper fuselage corners (HFDCUX) at any station X of section C-D is,

$$HFDCUX = 0.5 * HFA - \left(\frac{0.5 * HFA - HFDCU}{XD - XA}\right) * (X - XA) \qquad (D.123)$$

According to the baseline aircraft geometry assumptions the height (HFDCLX) of the elliptically shaped lower fuselage corners becomes zero at X = XVE + 0.25 * LVG, therefore,

If XC ≤ X ≤ XVE + 0.25 * LVG then,

$$HFDCLX = 0.5 * HFA - \left(\frac{0.5 * HFA}{XVE + 0.25 * LVG - XA}\right) * (X - XA) \qquad (D.124)$$

If X > XVE + 0.25 * LVG then HFDCLX = 0.0 (D.125)

The height of fuselage section C-D (HFCDX), varies with X as follows:

If XC ≤ X < XII then,

HFCDX = HFC (D.126)

If XII ≤ X ≤ XUNBF then,

$$HFCDX = HFC + HVI + HII + \left(\frac{HUNBF}{XUNBF - XII}\right) * (X - XII) \qquad (D.127)$$

If XUNBF < X ≤ XD then,

$$HFCDX = HFC + HVI + HII + HUNBF + \left(\frac{HUNBA - HUNBF}{LUNLB}\right) * (X - XUNBF) \qquad (D.128)$$

The width of the lower section C-D varies linearly with X, from X = XII to X = XD and depends only on the local packaging and fuselage section blending considerations. The width of the upper section however, varies with X according

to the corresponding fairing curve area. Therefore the Y-coordinate of the upper section C-D, (YFCDX) is,

$$YFCDX = \frac{\{OTXN - [(OIX - 2.0 * OIDX) + OIXL1 + OIXL2 + OVIX1] - 0.5 * PI * (ZCCANX + HFD2X) * YCCANX + (0.5 * PI - 2.0) * [HFDCUX * YCCANX + \left(\frac{0.5 * BFD}{XD - XA}\right) * (X - XA) * HFDCLX]\}}{(0.5 * PI - 2.0) * (HFDCUX + HFDCLX) + 2.0 * HFC} \quad (D.129)$$

Fuselage section blending considerations however, impose a minimum allowable value for YFCDX, which is,

$$YFCDXS = 0.5 * BFC + 0.5 * \left(\frac{BFD - BFC}{XD - XC}\right) * (X - XC) \quad (D.130)$$

The width of each of the upper (BFDCUX) and lower (BFDCLX) elliptically shaped fuselage corners, at any station X, is,

$$BFDCUX = YFCDX - YCCANX \quad (D.131)$$

If $XC \leq X < XVE + 0.25 * LVG$ then,

$$BFDCLX = YFCDX - \left(\frac{0.5 * BFD}{XD - XA}\right) * (X - XA) \quad (D.132)$$

If $X \geq XVE + 0.25 * LVG$ then, $BFDCLX = 0.0$ (D.133)

The cross-sectional area of the upper fuselage section C-D (OFCDXU) at any station X is,

$$OFCDXU = 0.5 * PI * [(ZCCANX + HFD2X) * YCCANX + HFDCUX * BFDCUX + HFDCLX * BFDCLX] + 2.0 * [(YFCDX - BFDCUX) * HFDCUX + (YFCDX - BFDCLX) * HFDCLX + (HFC - HFDCUX - HFDCLX) * YFCDX] \quad (D.134)$$

The cross-sectional area of the complete fuselage section C-D (OFCDX) at any station X, is,

$$OFCDX = OFCDXU + OIX + OIXL1 + OIXL2 + OVIX1 + OVIX \quad (D.135)$$

The perimeter of the upper fuselage section C-D (PFCDXU) at any station X, is as follows:

If $XC \leq X < XVE - 0.25 * LVG$ then,

$$PFCDXU = PI * \{[0.5 * ((ZCCANX + HFD2X)^{2.0} + YCCANX^{2.0})]^{0.5} + [0.5 * (HFDCUX^{2.0} + BFDCUX^{2.0})]^{0.5} + [0.5 * (HFDCLX^{2.0} + BFDCLX^{2.0})]^{0.5}\} + 2.0 * [(HFC - HFDCUX - HFDCLX) + (YFCDX - BFDCLX)] \quad (D.136)$$

If $XVE - 0.25 * LVG \leq X \leq XVE + 0.25 * LVG$

$$PFCDXU = PI * \{[0.5 * ((ZCCANX + HFD2X)^{2.0} + YCCANX^{2.0})]^{0.5} + [0.5 * (HFDCUX^{2.0} + BFDCUX^{2.0})]^{0.5}) + 2.0 * [(HFC - HFDCUX) + (YFCDX - 0.5 * BVIX1)] \quad (D.137)$$

Finally if, $XVE + 0.25 * LVG < X \leq XD$ then,

$$PFCDXU = PI * \{[0.5 * ((ZCCANX + HFD2X)^{2.0} + YCCANX^{2.0})]^{0.5} + [0.5 * (HFDCUX^{2.0} + BFDCUX^{2.0})]^{0.5}) + 2.0 * (HFC - HFDCUX) \quad (D.138)$$

The perimeter of the lower fuselage section C-D (PFCDXL), at any station X is as follows:

If XII ≤ X < XUNBF and BVIX1 > 0.0 then,

$$PFCDXL = 2.0 * [2.0 * BIX + HII + \left(\frac{HUNBF}{XUNBF - XII}\right) * (X - XII)] - BVIX1 + 2.0 * \left(\frac{QVIX1}{BVIX1}\right) \quad (D.139)$$

If XII ≤ X < XUNBF and BVIX1 ≤ 0.0 then,

$$PFCDXL = 2.0 * [2.0 * BIX + HII + \left(\frac{HUNBF}{XUNBF - XII}\right) * (X - XII)] \quad (D.140)$$

If XUNBF ≤ X ≤ XD and BVIX1 > 0.0 then,

$$PFCDXL = 2.0 * [2.0 * BIX + HII + HUNBF + \left(\frac{HUNBA - HUNBF}{LUNLB}\right) * (X - XUNBF)] - BVIX1 + 2.0 * \left(\frac{QVIX1}{BVIX1}\right) \quad (D.141)$$

Finally if XUNBF ≤ X ≤ XD and BVIX1 ≤ 0.0 then,

$$PFCDXL = 2.0 * [2.0 * BIX + HII + HUNBF + \left(\frac{HUNBA - HUNBF}{LUNLB}\right) * (X - XUNBF)] \quad (D.142)$$

The total perimeter of the complete fuselage section C-D (PFCDX), at any station X, is the sum of the perimeters of the upper and lower sections, hence,

$$PFCDX = PFCDXU + PFCDXL \quad (D.143)$$

D.14 FUSELAGE-MOUNTED WEAPONS (Module WEAPONG)

Module WEAPONG determines the dimensions, cross-sectional areas and perimeters of the fuselage-mounted missiles and gun fairing at any station X. It is assumed that the installed missiles (no.1 - 4) are semi-submerged into the flat fuselage belly. The gun is also submerged but its barrel protrudes beneath the fuselage belly in order to establish a clear firing line. A smooth fairing covers the protruding gun surface and reduces the drag.

The nose length of each missile is defined by one of the following expressions:

$$LNMUF1 = FLMUF1 * LMUF1 \quad (D.144)$$

$$LNMUF2 = FLMUF2 * LMUF2 \quad (D.145)$$

$$LNMUF3 = FLMUF3 * LMUF3 \quad (D.146)$$

$$LNMUF4 = FLMUF4 * LMUF4 \quad (D.147)$$

where, LNMUF1, LNMUF2, LNMUF3 and LNMUF4 are the nose lengths of missiles no.1, 2, 3 and 4 respectively.
LMUF1, LMUF2, LMUF3 and LMUF4, are the corresponding missile lengths.
FLMUF1, FLUMF2, FLUMF3 and FLUMF4 are the corresponding nose length fractions, which are external variables specified in the input data together with the individual missile lengths.

It is assumed that each missile consists of a nose section the diameter of which increases linearly with X and a cylindrical body section.

Therefore the diameter of missile no.1 (DMUF1X) at any station X is as follows:

If XMUF1 ≤ X ≤ XMUF1 + LNMUF1 then,

$$DMUF1X = \left(\frac{DMUF1}{LNMUF1}\right) * (X - XMUF1) \qquad (D.148)$$

If XMUF1 + LNMUF1 < X ≤ XMUF1 + LMUF1 then,

$$DMUF1X = DMUF1 \qquad (D.149)$$

The cross-sectional area of missile no. 1 (OMUF1X) and perimeter (PMUF1X), at any station X are,

$$OMUF1X = 0.25 * PI * DMUF1X^{2.0} \qquad (D.150)$$

and

$$PMUF1X = PI * DMUF1X \qquad (D.151)$$

Similarly for missile no.2,

If XMUF2 ≤ X ≤ XMUF2 + LNMUF2 + then,

$$DMUF2X = \left(\frac{DMUF2}{LNMUF2}\right) * (X - XMUF2) \qquad (D.152)$$

If XMUF2 + LNMUF2 < X ≤ XMUF2 + LMUF2 then,

$$DMUF2X = DMUF2 \qquad (D.153)$$

$$OMUF2X = 0.25 * PI * DMUF2X^{2.0} \qquad (D.154)$$

$$PMUF2X = PI * DMUF2X \qquad (D.155)$$

For missile no.3,

If XMUF3 ≤ X ≤ XMUF3 + LNMUF3 then,

$$DMUF3X = \left(\frac{DMUF3}{LNMUF3}\right) * (X - XMUF3) \qquad (D.156)$$

If XMUF3 + LNMUF3 < X ≤ XMUF3 + LMUF3 then,

$$DMUF3X = DMUF3 \tag{D.157}$$

$$OMUF3X = 0.25 * PI * DMUF3X^{2.0} \tag{D.158}$$

$$PMUF3X = PI * DMUF3X \tag{D.159}$$

Finally for missile no. 4,

If XMUF4 ≤ X ≤ XMUF4 + LNMUF4 then,

$$DMUF4X = \left(\frac{DMUF4}{LNMUF4}\right) * (X - XMUF4) \tag{D.160}$$

If XMUF4 + LNMUF4 < X ≤ XMUF4 + LMUF4 then,

$$DMUF4X = DMUF4 \tag{D.161}$$

$$OMUF4X = 0.25 * PI * DMUF4X^{2.0} \tag{D.162}$$

$$PMUF4X = PI * DMUF4X \tag{D.163}$$

DMUF1, DMUF2, DMUF3 and DMUF4 are the diameters of the cylindrical sections of missiles no.1, 2, 3 and 4 respectively. These are external variables, specified in the input data.

For simplicity, the average gun fairing width (BGFA), cross-sectional area (OGFA) and perimeter (PGFA) are also specified in the input data. So, at any station X between X = XGF and X = XGF + LGC,

$$BGFX = BGFA \tag{D.164}$$

$$OGFX = OGFA \tag{D.165}$$

$$PGFX = PGFA \tag{D.166}$$

D.15 FUSELAGE SECTION E (Module FUSSTNE)

A cross-sectional view of the fuselage at station E is shown in fig.D.11. The fuselage dimensions, cross-sectional area and perimeter at this station are determined by this module using the expressions presented in this section.

The height of the upper fuselage corners (HFECU) is,

$$HFECU = HFDCU \tag{D.167}$$

The height of the fuselage spine (HFE2) at station E, is,

$$HFE2 = HFD2 - \left(\frac{HFD2}{XFN - LPG - DP1 - XD}\right) * (XE - XD) \tag{D.168}$$

and its corresponding Y- coordinate is,

$$YFE2 = YCCAND - \left(\frac{YCCAND}{XFN - LPG - DP1 - XD}\right) * (XE - XD) \tag{D.169}$$

The above expressions were derived by assuming that HFE2 and YFE2 become equal to zero at X = XFN - LPG - DP1

The fuselage height (HFE) at station E. is,

$$HFE = HFDH - \left[\frac{HFDH - ZPC - 0.5 * (DP3 + EHP3)}{XFN - LP34 - XD}\right] * (XE - XD) \tag{D.170}$$

The expression for HFE was derived according to the baseline aircraft geometry assumption, that the fuselage height measured from the flat fuselage belly, reduces linearly with X, from HFDH at station D to ZPC + 0.5 * (DP3 + EHP3) at X = XFN - LP34

The width of the fuselage section (BFE) is adjusted according to the local fairing curve area. Therefore,

$$BFE = \frac{\{OTXN + 2.0 * OIDX + 0.5 * (OMUF1X + OMUF2X) - OGFX - YFE2 * [0.5 * PI * HFE2 - (0.5 * PI - 2.0) * HFECU]\}}{(0.25 * PI - 1.0) * HFECU + HFE} \quad (D.171)$$

The values of OTXN, OIDX, OMUFIX, OMUF2X and OGFX are obtained by a previous call to modules FAIRCUR2, INTDIFG and WEAPONG.

The minimum allowable fuselage width (BFES) at station E, is,

$$BFES = BFD \quad (D.172)$$

The width of each of the upper elliptically-shaped fuselage corners (BFECU) is,

$$BFECU = 0.5 * BFE - YFE2 \quad (D.173)$$

The cross-sectional area (OFE) and perimeter (PFE) of the fuselage at station E are,

$$OFE = 0.5 * PI [YFE2 * HFE2 + BFECU * HFECU] + 2.0 * HFECU * YFE2 + (HFE - HFECU) * BFE - 0.5 * (OMUF1X + OMUF2X) + OGFX \quad (D.174)$$

and

$$PFE = PI * \{[0.5 *(YFE2^{2.0} + HFE2^{2.0})]^{0.5} + [0.5 * (BFECU^{2.0} + HFECU^{2.0})]^{0.5}) + 2.0 * (HFE - HFECU) + BFE - DMUF2X + 0.5 * PMUF2X - DMUF1X + 0.5 * PMUF1X - BGFX + PGFX \quad (D.175)$$

D.16 FUSELAGE SECTION D-E (Module FSECTDE)

Module FSECTDE determines the geometry of fuselage section D-E, at any station X. Views of the section are shown in fig.D.12.

The height of section D-E (HFDEX) at any station X, depends on the axial position of the nose u/c bay. Therefore,

If $XD \leq X \leq XUNBF + LUNLB$ then,

$$HFDEX = HFDH - \left[\frac{HFDH - ZPC - 0.5 * (DP3 + EHP3)}{XFN - LP34 \_ XD}\right] * (X - XD) - HUNBA + HUNBX \quad (D.176)$$

where,

$$HUNBX = HUNBF + \left(\frac{HUNBA - HUNBF}{LUNLB}\right) * (X - XUNBF) \quad (D.177)$$

If $XUNBF + LUNLB < X \leq XE$ then,

$$HFDEX = HFDH - \left[\frac{HFDH - ZPC - 0.5 * (DP3 + EHP3)}{XFN - LP34 - XD}\right] * (X - XD) \quad (D.178)$$

The height of the fuselage spine (HFE2X) at any station X of section D-E is,

$$HFE2X = HFD2 - \left(\frac{HFD2}{XFN - LPG - DP1 - XD}\right) * (X - XD) \quad (D.179)$$

The corresponding Y- coordinate of the spine (YFE2X) is,

$$YFE2X = YCCAND - \left(\frac{YCCAND}{XFN - LPG - DP1 - XD}\right) * (X - XD) \qquad (D.180)$$

The height of the upper fuselage corners (HFECUX) is assumed to remain constant along section D-E, hence,

$$HFECUX = HFDCU \qquad (D.181)$$

According to the baseline aircraft assumptions, the axis of rotation of the all-moving foreplane is located across section D-E. In order to allow free rotation of the all moving foreplane, the sides of section D-E are assumed to be flat and its Y-coordinate (YFDEX) is consequently assumed to vary linearly from 0.5 * BFD at station D to 0.5 * BFE at station E. Hence,

$$YFDEX = 0.5 * BFD + 0.5 * \left(\frac{BFE - BFD}{XE - XD}\right) * (X - XD) \qquad (D.182)$$

In order to satisfy the local packaging requirements a minimum allowable value (YFDEXS) is imposed for the Y-coordinate of D-E. This is,

$$YFDEXS = 0.5 * BFD \qquad (D.183)$$

The width of each of the elliptically-shaped upper fuselage corners (BFECUX) at any station X is,

$$BFECUX = YFDEX - YFE2X \qquad (D.184)$$

The cross-sectional area (OFDEX) and perimeter (PFDEX) at any station X of this section are,

$$OFDEX = 0.5 * PI\ (YFE2X * HFE2X + HFECUX * BFECUX) + 2.0 * [YFE2X * HFECUX + YFDEX * (HFDEX - HFECUX)] + OGFX - 0.5 * (OMUF1X + OMUF2X) \quad (D.185)$$

and

$$PFDEX = PI * \{[0.5 * (YFE2X^{2.0} + HFE2X^{2.0})]^{0.5} + [0.5 * (HFECUX^{2.0} + BFECUX^{2.0}]^{0.5}) + 2.0 * [(HFDEX - HFECUX) + YFDEX] - DMUF1X + 0.5 * PMUF1X - DMUF2X + 0.5 * PMUF2X - BGFX + PGFX \quad (D.186)$$

D.17 FUSELAGE SECTION E-F (Module FSECTEF)

The dimensions, cross-sectional area and perimeter of fuselage section E-F are estimated in module FSECTEF using the expressions presented in this section. Fuselage section E-F is shown in fig.D.13.

The height of the fuselage spine (HFF2X) at any station X, of section E-F is,

$$HFF2X = HFD2 - \left(\frac{HFD2}{XFN - LPG - DP1 - XD}\right) * (X - XD) \quad (D.187)$$

and the corresponding Y-coordinate of the spine (YFF2X) is,

$$YFF2X = YCCAND - \left(\frac{YCCAND}{XFN - LPG - DP1 - XD}\right) * (X - XD) \quad (D.188)$$

The fuselage section height (HFEFX) at any station X of E-F is,

$$HFEFX = HFDH - \left[\frac{HFDH - ZPC - 0.5 * (DP3 + EHP3)}{XFN - LP34 - XD}\right] * (X - XD) \quad (D.189)$$

According to the baseline aircraft geometry assumptions the height of the upper corners of the fuselage, increases from HFECU at station E to HFG - ZPC at station G. HFG is the fuselage height at station G.

Therefore the height of the upper corners (HFFCUX) at any station X of E-F is,

$$HFFCUX = HFEFX - HFE + HFECU + \left(\frac{HFE - HFECU - ZPC}{XG - XE}\right) * (X - XE) \qquad (D.190)$$

The width of section E-F is dependent on the local fairing curve area. Therefore its Y-coordinate (YFEFX) at any station X is,

$$YFEFX = \frac{\begin{array}{l}(OTXN + 2.0 * OIDX + 0.5 * (OMUF1X + OMUF2X) - OGFX \\ + YFF2X * [(0.5 * PI - 2.0) * HFFCUX - 0.5 * PI * \\ HFF2X])\end{array}}{(0.5 * PI - 2.0) * HFFCUX + 2.0 * HFEFX} \qquad (D.191)$$

In order to satisfy local packaging requirements the Y- coordinate is constrained not to be less than a minimum allowable value (YFEFXS).

$$YFEFXS = YIDOX + EYFEF \qquad (D.192)$$

where, EYFEF = Lateral clearance between an intake diffuser duct and the wall of fuselage section E-F.

$$EYFEF = 0.5 * EBFD \qquad (D.193)$$

The width of each of the elliptically shaped upper corners of section E-F (BFFCUX) at any station X, is,

$$BFFCUX = YFEFX - YFF2X \qquad (D.194)$$

The cross-sectional area (OFEFX) and perimeter (PFEFX) of the fuselage, at any station X of section E-F, is,

$$OFEFX = 0.5 * PI * (HFF2X * YFF2X + BFFCUX * HFFCUX) + 2.0 * [YFF2X * HFFCUX + (HFEFX - HFFCUX) * YFEFX] - 0.5 * (OMUF1X + OMUF2X) + OGFX \qquad (D.195)$$

and

$$PFEFX = PI *([0.5 * (HFF2X^{2.0} + YFF2X^{2.0})]^{0.5} + [0.5 * (BFFCUX^{2.0} + HFFCUX^{2.0})]^{0.5}) + 2.0 * [(HFEFX - HFFCUX) + YFEFX] - DMUF1X + 0.5 * PMUF1X - DMUF2X + 0.5 * PMUF2X - BGFX + PGFX \qquad (D.196)$$

D.18 FUSELAGE STATION F (Module FUSSTNF)

Presented in this section are the mathematical expressions which define the geometry of the fuselage at station F. A view of the fuselage section at this station is shown in fig.D.14.

The height (HFF2) and Y- coordinate (YFF2) of the fuselage spine at station F is,

$$HFF2 = HFD2 - \left(\frac{HFD2}{XFN - LPG - DP1 - XD}\right) * (XF - XD) \qquad (D.197)$$

and

$$YFF2 = YCCAND - \left(\frac{YCCAND}{XFN - LPG - DP1 - XD}\right) * (XF - XD) \qquad (D.198)$$

The height of the fuselage section at F (HFF) is,

$$HFF = HFDH - \left[\frac{HFDH - ZPC - 0.5 * (DP3 + EHP3)}{XFN - LP34 - XD}\right] * (XF - XD) \qquad (D.199)$$

Similarly to section E-F, the height of the upper corners (HFFCU) at station F is,

$$HFFCU = HFF - HFE + HFECU + \left(\frac{HFE - HFECU - ZPC}{XG - XE}\right) * (XF - XE) \qquad (D.200)$$

The width of the fuselage section (BFF) is,

$$BFF = \frac{2.0 * (OTXN + 2.0 * OIDX + 0.5 * (OMUF1X + OMUF2X) - OGFX + YFF2 * [(0.5 * PI - 2.0) * HFFCU - 0.5 * PI * HFF2])}{(0.5 * PI - 2.0) * HFFCU + 2.0 * HFF} \qquad (D.201)$$

The minimum allowable fuselage section width (BFFS), however is,

$$BFFS = 2.0 * (YIDOX + EYFEF) \qquad (D.202)$$

The width of each of the upper corners (BFFCU) is,

$$BFFCU = 0.5 * BFF - YFF2 \qquad (D.203)$$

The local cross-sectional area (OFF) and perimeter (PFF) of the fuselage are,

$$OFF = 0.5 * PI * (HFF2 * YFF2 + HFFCU * BFFCU) + 2.0 * YFF2 * HFFCU + (HFF - HFFCU) * BFF - 0.5 * (OMUF1X + OMUF2X) + OGFX \qquad (D.204)$$

and

$$PFF = PI * \{[0.5 * (HFF2^{2.0} + YFF2^{2.0})]^{0.5} + [0.5 * (HFFCU^{2.0} + BFFCU^{2.0})]^{0.5}) + 2.0 * (HFF - HFFCU) + BFF - DMUF1X + 0.5 * PMUF1X - DMUF2X + 0.5 * PMUF2X - BGFX + PGFX \quad (D.205)$$

D.19 FUSELAGE SECTION F-G (Module FSECTFG)

Fuselage section F-G is basically a uniform extension of section E-F. Therefore the mathematical expressions which define the geometry of F-G are similar to those used for section E-F. Different views of fuselage section F-G are presented in fig.D.15

The height (HFG2X) and Y- coordinate (YFG2X) of the fuselage spine at any station X of this section, is,

$$HFG2X = HFD2 - \left(\frac{HFD2}{XFN - LPG - DP1 - XD}\right) * (X - XD) \quad (D.206)$$

and

$$YFG2X = YCCAND - \left(\frac{YCCAND}{XFN - LPG - DP1 - XD}\right) * (X - XD) \quad (D.207)$$

The fuselage section height (HFFGX) at any station X of section F-G is,

$$HFFGX = HFDH - \left[\frac{HFDH - ZPC - 0.5 * (DP3 + EHP3)}{XFN - LP34 - XD}\right] * (X - XD) \quad (D.208)$$

The height of the upper fuselage corners (HFGCUX) is,

$$HFGCUX = HFFGX - HFE + HFECU + \left(\frac{HFE - HFECU - ZPC}{XG - XE}\right) * (X - XE) \quad (D.209)$$

The Y- coordinate of the fuselage (YFFGX) at any station X of section F-G is,

$$YFFGX = \frac{\begin{aligned}&(OTXN + 2.0 * OIDX + 0.5 * (OMUF3X + OMUF4X) - \\ &OGFX + YFG2X * [(0.5 * PI - 2.0) * HFGCUX - \\ &0.5 * PI * HFG2X])\end{aligned}}{(0.5 * PI - 2.0) * HFGCUX + 2.0 * HFFGX} \qquad (D.210)$$

The minimum allowable value (YFFGXS) for the Y-coordinate of the fuselage is,

$$YFFGXS = YIDOX + EYFFG \qquad (D.211)$$

where, EYFFG = Lateral clearance between an intake diffuser duct and the wall of fuselage section F-G.

$$EYFFG = 0.5 * EBFD \qquad (D.212)$$

The width of each of the upper fuselage corners (BFGCUX) at any station X of section F-G are,

$$BFGCUX = YFFGX - YFG2X \qquad (D.213)$$

The cross-sectional area (OFFGX) and perimeter (PFFGX) of the fuselage at any station X of F-G are,

$$\begin{aligned}OFFGX = {} & 0.5 * PI * (HFG2X * YFG2X + HFGCUX * BFGCUX) + \\ & 2.0 * [YFG2X * HFGCUX + YFFGX * (HFFGX - HFGCUX)] - \\ & 0.5 * (OMUF3X + OMUF4X) + OGFX\end{aligned} \qquad (D.214)$$

and

$$PFFGX = PI * \{[0.5 *(HFG2X^{2.0} + YFG2X^{2.0})]^{0.5} + [0.5 *(HFGCUX^{2.0} + BFGCUX^{2.0})]^{0.5}) + 2.0 * [(HFFGX - HFGCUX) + YFFGX] - DMUF3X + 0.5 * PMUF3X - DMUF4X + 0.5 * PMUF4X - BGFX + PGFX \quad (D.215)$$

D.20 FUSELAGE STATION G (Module FUSSTNG)

Presented in this section are the equations defining the geometry of the fuselage at station G. The relevant cross-sectional view is shown in fig.D.16.

The fuselage height at G (HFG) is,

$$HFG = HFDH - \left[\frac{HFDH - ZPC - 0.5 * (DP3 + EHP3)}{XFN - LP34 - XD}\right] * (XG - XD) \quad (D.216)$$

The height of the upper fuselage corners (HFGCU) is,

$$HFGCU = HFG - ZPC \quad (D.217)$$

The local fuselage width (BFG) is adjusted according to the corresponding fairing curve area, hence,

$$BFG = \frac{2.0 * [OTXN + 2.0 * OIDX + 0.5 *(OMUF3X + OMUF4X)]}{(0.5 * PI - 2.0) * HFGCU + 2.0 * HFG} \quad (D.218)$$

The minimum allowable fuselage width (BFGS) is,

$$BFGS = 2.0 * (YIDOX + EYFFG) \quad (D.219)$$

According to the initial assumptions the fuselage spine ends at station G, therefore the local width of the upper elliptically shaped corners (BFGCU) is,

$$BFGCU = 0.5 * BFG \qquad (D.220)$$

The local fuselage cross-sectional area (OFG) and perimeter (PFG) are,

$$OFG = 0.5 * PI * HFGCU * BFGCU + (HFG - HFGCU) * BFG - 0.5 * (OMUF3X + OMUF4X) \qquad (D.221)$$

and

$$PFG = PI * [0.5 * (HFGCU^{2.0} + BFGCU^{2.0})]^{0.5} + 2.0 * (HFG - HFGCU) + BFG - DMUF3X + 0.5 * PMUF3X - DMUF4X + 0.5 * PMUF4X \qquad (D.222)$$

D.21 ENGINE BAYS (Module ENGBAYG)

This module estimates the diameter of each engine and the cross-sectional area of its bay, at any station X. The expressions presented in this section, were derived using the previously determined engine diameters and bay clearances at the four principal engine stations. A linear variation is assumed between successive engine stations for the cross-sectional dimensions of both the engine and its bay. (Refer to fig.B.5). The cross-sectional shape of the engine bay at any station X is assumed to be elliptical.

Therefore, at any station X, between engine stations 1 and 2,

If $XP1 \leq X \leq XP2$ then,
the engine diameter (DP12X) is,

$$DP12X = DP1 - \left(\frac{DP1 - DP2}{LP12}\right) * (X - XP1) \qquad (D.223)$$

the engine bay height clearance (EHP12X) is,

$$EHP12X = EHP1 - \left(\frac{EHP1 - EHP2}{LP12}\right) * (X - XP1) \qquad (D.224)$$

the engine bay clearance (EBP12X) is,

$$EBP12X = EBP1 - \left(\frac{EBP1 - EBP2}{LP12}\right) * (X - XP1) \qquad (D.225)$$

and the engine bay cross-sectional area (OP12BX) is,

$$OP12BX = 0.25 * PI * (DP12X + EHP12X) * (DP12X + 0.5 * EBP12X) \qquad (D.226)$$

Similarly between engine stations 2 and 3,

If XP2 ≤ X ≤ XP3 then,

$$DP23X = DP2 - \left(\frac{DP2 - DP3}{LP23}\right) * (X - XP2) \qquad (D.227)$$

$$EHP23X = EHP2 - \left(\frac{EHP2 - EHP3}{LP23}\right) * (X - XP2) \qquad (D.228)$$

$$EBP23X = EBP2 - \left(\frac{EBP2 - EBP3}{LP23}\right) * (X - XP2) \qquad (D.229)$$

$$OP23BX = 0.25 * PI * (DP23X + EHP23X) * (DP23X + 0.5 * EBP23X) \qquad (D.230)$$

Finally between engine stations 3 and 4,

If XP3 ≤ X ≤ XP4 then,

$$DP34X = DP3 - \left(\frac{DP3 - DP4}{LP34}\right) * (X - XP3) \qquad (D.231)$$

$$EHP34X = EHP3 - \left(\frac{EHP3 - EHP4}{LP34}\right) * (X - XP3) \qquad (D.232)$$

$$EBP34X = EBP3 - \left(\frac{EBP3 - EBP4}{LP34}\right) * (X - XP3) \qquad (D.233)$$

$$OP34BX = 0.25 * PI * (DP34X + EHP34X) * (DP34X + 0.5 * EBP34X) \qquad (D.234)$$

D.22 FUSELAGE SECTION G-H (Module FSECTGH)

Views of fuselage section G-H are shown in fig.D.17. Two special features are observed; an underfuselage recess which increases in both depth and width, linearly with X and a flat triangular top surface. These are incorporated in the mathematical expressions which define the geometry of fuselage section G-H.

According to the baseline aircraft geometry assumptions, the length of this fuselage section (LFGH) is,

$$LFGH = XH - XG = DP1 + LP12 \qquad (D.235)$$

The fuselage height (HFGHX) at any station X of section G-H is,

$$HFGHX = HFDH - \left[\frac{HFDH - ZPC - 0.5 * (DP3 + EHP3)}{XFN - LP34 - XD}\right] * (X - XD) \qquad (D.236)$$

The height of the upper fuselage corners (HFHCUX) at any station X of this section is,

$$HFHCUX = HFGHX - ZPC \qquad (D.237)$$

The underfuselage recess starts at station G. It is assumed to extend up to the jet exit plane where its maximum allowable depth relative to the flat fuselage belly, is assumed to be equal to ZPC. Therefore the maximum allowable angle between the inner line of the recess and the horizontal (QFPRH) is,

$$QFPRH = \tan^{-1}\left(\frac{ZPC}{LPG + DP1}\right) \quad \text{(rads)} \quad \text{(D.238)}$$

The required angle (QFPR) however, is an external variable, specified in the input data. This is constrained not to exceed QFPRH.

The depth of the underfuselage recess (HFPR1X) at any station X of section G-H consequently is,

$$HFPR1X = (X - XG) * \tan (QFPR) \quad \text{(D.239)}$$

In order to satisfy local packaging and fuselage section blending requirements, it is assumed that the outer width of the recess (BFPRL) is equal to the lateral distance between the engine centrelines, hence,

$$BFPRL = YPCH \quad \text{(D.240)}$$

The inner width of the recess (BFPRUX) at any station X is,

$$BFPRUX = \left(\frac{YPCH - DP3 - 0.5 * EBP3}{DP1 + LP12 + LP23}\right) * (X - XG) \quad \text{(D.241)}$$

The cross-sectional area of the underfuselage recess (OFHPRX) at any station X of section G-H is,

$$OFHPRX = HFPR1X * BFPRL - 0.25 * PI * (BFPRL - BFPRUX) * HFPR1X \quad (D.242)$$

The Y-coordinate of the fuselage (YFGHX) at any station X of section G-H 1 estimated as follows:

If $XG \leq X < XP1$ then,

$$YFGHX = \frac{[OTXN + 2.0 * OIDX + OFHPRX + 0.5 * (OMUF3X + OMUF4X) + (0.5 * PI - 2.0) * \left(\frac{0.5 * YPCH}{LFGH}\right) * (X - XG) * HFHCUX]}{(0.5 * PI - 2.0) * HFHCUX + 2.0 * HFGHX} \quad (D.243)$$

The minimum allowable value for the Y-coordinate in this region (YFGHXS) is defined according to local packaging and blending considerations, hence,

$$YFGHXS = YIDOX + 0.5 * \left[EBFD - \left(\frac{EBFD - 0.5 * EBP1}{DP1}\right) * (X - XG)\right] \quad (D.244)$$

If $XP1 \leq X \leq XH$ then,

$$YFGHX = \frac{[OTXN + 2.0 * OP12X + OFHPRX + 0.5 * (OMUF3X + OMUF4X) + (0.5 * PI - 2.0) * \left(\frac{0.5 * YPCH}{LFGH}\right) * (X - XG) * HFHCUX]}{(0.5 * PI - 2.0) * HFHCUX + 2.0 * HFGHX} \quad (D.245)$$

where, OP12X = Cross-sectional area of each engine at any station X, between 1 and 2.

$$OP12X = 0.25 * PI * DP12X^{2.0} \quad (D.246)$$

In this region however, YFGHXS is,

$$YFGHXS = 0.5 * (YPCH + DP12X) + 0.25 * EBP12X \qquad (D.247)$$

The width of each upper fuselage corners (BFHCUX) at any station X of section G-H is,

$$BFHCUX = YFGHX - \left(\frac{0.5 * YPCH}{LFGH}\right) * (X - XG) \qquad (D.248)$$

The cross-sectional area of the fuselage (OFGHX) and perimeter (PFGHX) at any station X of G-H are,

$$\begin{aligned} OFGHX = {} & 0.5 * PI * HFHCUX * BFHCUX + 2.0 * [(YFGHX - BFHCUX) * \\ & HFHCUX + (YFGHX - 0.5 * BFPRL) * (HFGHX - HFHCUX)] + \\ & BFPRL * (HFGHX - HFHCUX) - OFHPRX - 0.5 * \\ & (OMUF3X + OMUF4X) \end{aligned} \qquad (D.249)$$

and

$$\begin{aligned} PFGHX = {} & PI\,[0.5 * (HFHCUX^{2.0} + BFHCUX^{2.0})]^{0.5} + \\ & 2.0 * [(YFGHX - BFHCUX) + (HFGHX - HFHCUX) + \\ & (YFGHX - 0.5 * BFPRL)] + BFPRUX - DMUF3X + 0.5 * \\ & PMUF3X - DMUF4X + 0.5 * PMUF4X + PI * \left\{0.5 * \left[\left(\frac{BFPRL - BFPRUX}{2.0}\right)^{2.0} + HFPR1X^{2.0}\right]\right\}^{0.5} \end{aligned} \qquad (D.250)$$

D.23 FUSELAGE STATION H (Module FUSSTNH)

The mathematical expressions which define the geometry of the fuselage at station H are presented in this section while the relevant cross-sectional view is shown in fig.D.18.

The height of the fuselage (HFH) at this station is,

$$HFH = HFDH - \left[\frac{HFDH - ZPC - 0.5 * (DP3 + EHP3)}{XFN - LP34 - XD}\right] * (XH - XD) \quad (D.251)$$

The height of the upper fuselage corners (HFHCU) at the same station is,

$$HFHCU = HFH - ZPC \quad (D.252)$$

The depth of the underfuselage recess (HFPR1H) at station H is,

$$HFPR1H = (XH - XG) * \tan(QFPR) \quad (D.253)$$

The inner width of the recess (BFPRUH) is,

$$BFPRUH = \left(\frac{YPCH - DP3 - 0.5 * EBP3}{DP1 + LP12 + LP23}\right) * (XH - XG) \quad (D.254)$$

The local cross-sectional area of the underfuselage recess (OFHPRH) is,

$$OFHPRH = HFPR1H * BFPRL - 0.25 * PI * (BFPRL - BFPRUH) * HFPR1H \quad (D.255)$$

The cross-sectional area of each engine (OP2) at station 2 is,

$$OP2 = 0.25 * PI * DP2^{2.0} \qquad (D.256)$$

The local fuselage width (BFH) is,

$$BFH = \frac{\{2.0 * [OTXN + 2.0 * OP2 + OFHPRH + 0.5 * (OMUF3X + OMUF4X) + (0.5 * PI - 2.0) * 0.5 * YPCH * HFHCU]\}}{(0.5 * PI - 2.0) * HFHCU + 2.0 * HFH} \qquad (D.257)$$

The minimum allowable fuselage width (BFHS) at station H is,

$$BFHS = YPCH + DP2 + 0.5 * EBP2 \qquad (D.258)$$

The width of each of the upper fuselage corners (BFHCU) at this station is,

$$BFHCU = 0.5 * (BFH - YPCH) \qquad (D.259)$$

The cross-sectional area (OFH) and perimeter (PFH) of the fuselage at station H are,

$$OFH = 0.5 * PI\ HFHCU * BFHCU + (BFH - 2.0 * BFHCU) * HFHCU + (BFH - BFPRL) * (HFH - HFHCU) + BFPRL * (HFH - HFHCU) - OFHPRH - 0.5 * (OMUF3X + OMUF4X) \qquad (D.260)$$

and

$$PFH = PI * [0.5*(HFHCU^{2.0} + BFHCU^{2.0})]^{0.5} + BFH - 2.0 * BFHCU + 2.0 * (HFH - HFHCU) + BFH - BFPRL + BFPRUH - DMUF3X + 0.5 * PMUF3X - DMUF4X + 0.5 * PMUF4X + PI * \left\{0.5 * \left[\left(\frac{BFPRL - BFPRUH}{2.0}\right)^{2.0} + HFPR1H^{2.0}\right]\right\}^{0.5} \qquad (D.261)$$

D.24 FUSELAGE SECTION H-J (Module FSECTHJ)

According to the initial baseline aircraft geometry assumptions, the lower side of the fuselage begins at station H, to converge linearly towards the engine nozzles at the jet exit plane. This also leads to the gradual formation of two elliptically shaped lower fuselage corners which provide a uniform transformation of the cross-sectional shape of the fuselage between stations H and K. These features are mathematically incorporated in the expressions presented below, which define the geometry of section H-J. Views of the latter are shown in fig.D.19.

The fuselage height (HFHJX) at any station X of section H-J is,

$$HFHJX = HFDH - \left[\frac{HFDH - ZPC - 0.5 * (DP3 + EHP3)}{XFN - LP34 - XD}\right] * (X - XD) - \left[\frac{ZPC - 0.5 * (DP4 + EHP4)}{XFN - XH}\right] * (X - XH) \qquad (D.262)$$

The height of the upper fuselage corners (HFJCUX) is,

$$HFJCUX = HFDH - \left[\frac{HFDH - ZPC - 0.5 * (DP3 + EHP3)}{XFN - LP34 - XD}\right] * (X - XD) - ZPC \qquad (D.263)$$

According to the above stated assumptions, the height of the lower fuselage corners (HFJCLX) at any station X of H-J is,

$$HFJCLX = \left[\frac{0.5 * (DP4 + EHP4)}{XFN - XH}\right] * (X - XH) \qquad (D.264)$$

The depth of the underfuselage recess (HFPR2X) at any station X of section H-J is,

$$HFPR2X = (X - XG) * \tan(QFPR) - \left[\frac{ZPC - 0.5 * (DP4 + EHP4)}{XFN - XH}\right] * (X - XH) \quad (D.265)$$

The cross-sectional area of the underfuselage recess (OFJPRX) at any station X of section H-J is,

$$OFJPRX = HFPR2X * BFPRL - 0.25 * PI * (BFPRL - BFPRUX) * HFPR2X \quad (D.266)$$

The Y- coordinate of the fuselage (YFHJX) at any station X of this section is,

$$YFHJX = \frac{[OTXN + 2.0 * OP23X + OFJPRX - YPCH * (1.0 - 0.25 * PI) * (HFJCUX + HFJCLX)]}{(0.5 * PI - 2.0) * (HFJCUX + HFJCLX) + 2.0 * HFHJX} \quad (D.267)$$

where, OP23X = Cross-sectional area of each engine at any station X, between 2 and 3.

$$OP23X = 0.25 * PI * DP23X^{2.0} \quad (D.268)$$

Local packaging considerations impose a minimum allowable value (YFHJXS) for the Y- coordinate ofsection H-J at any station X. This is,

$$YFHJXS = 0.5 * (YPCH + DP23) + 0.25 * EBP23X \qquad (D.269)$$

The width of each of the upper fuselage corners (BFJCUX) of section H-J is,

$$BFJCUX = YFHJX - 0.5 * YPCH \qquad (D.270)$$

The width of each of the lower fuselage corners (BFJCLX) is equal to that of its corresponding upper corner, hence,

$$BFJCLX = BFJCUX \qquad (D.271)$$

The cross-sectional area (OFHJX) and perimeter (PFHJX) of the fuselage at any station X of section H-J are,

$$OFHJX = 2.0 * [HFJCUX * (YFHJX - BFJCUX) + (HFHJX - HFJCUX - HFJCLX) * YFHJX] + 0.5 * PI * (HFJCUX * BFJCUX + HFJCLX * BFJCLX) + HFJCLX * YPCH - OFJPRX \qquad (D.272)$$

and

$$PFHJX = PI * \left\{[0.5 * (HFJCUX^{2.0} + BFJCUX^{2.0})]^{0.5} + [0.5 * (HFJCLX^{2.0} + BFJCLX^{2.0})]^{0.5} + \left[0.5 * \left[\left(\frac{BFPRL - BFPRUX}{2.0}\right)^{2.0} + HFPR2X^{2.0}\right]\right]^{0.5}\right\} + 2.0 * (HFHJX - HFJCUX - HFJCLX) + YPCH + BFPRUX \qquad (D.273)$$

D.25 FUSELAGE STATION J (Module FUSSTNJ)

The cross-sectional view of the fuselage at station J is shown in fig.D.20. Its geometry is defined by the following expressions.

The fuselage height (HFJ) at station J is,

$$HFJ = HFDH - \left[\frac{HFDH - ZPC - 0.5 * (DP3 + EHP3)}{XFN - LP34 - XD}\right] * (XJ - XD) - \left[\frac{ZPC - 0.5 * (DP4 + EHP4)}{XFN - XH}\right] * (XJ - XH) \quad (D.274)$$

The height of the upper (HFJCU) and lower (HFJCL) fuselage corners at this station is,

$$HFJCU = HFDH - \left[\frac{HFDH - ZPC - 0.5 * (DP3 + EHP3)}{XFN - LP34 - XD}\right] * (XJ - XD) - ZPC \quad (D.275)$$

and

$$HFJCL = \left[\frac{0.5 * (DP4 + EHP4)}{XFN - XH}\right] * (XJ - XH) \quad (D.276)$$

The local depth (HFPR2J) and inner width (BFPRUJ) of the underfuselage recess, is,

$$HFPR2J = (XJ - XG) * \tan(QFPR) - \left[\frac{ZPC - 0.5 * (DP4 + EHP4)}{XFN - XH}\right] * (XJ - XH) \quad (D.277)$$

and

$$BFPRUJ = \left(\frac{YPCH - DP3 - 0.5 * EBP3}{DP1 + LP12 + LP23}\right) * (XJ - XG) \quad (D.278)$$

The corresponding cross-sectional area of the underfuselage recess (OFJPRJ) is,

$$OFJPRJ = HFPR2J * BFPRL - 0.25 * PI * (BFPRL - BFPRUJ) * HFPR2J \quad (D.279)$$

The fuselage width (BFJ) at station J is,

$$BFJ = \frac{2.0 * [OTXN + 2.0 * OP3 + OFJPRJ - YPCH * (1.0 - 0.25 * PI) * (HFJCU + HFJCL)]}{(0.5 * PI - 2.0) * (HFJCU + HFJCL) + 2.0 * HFJ} \quad (D.280)$$

where, OP3 = Cross-sectional area of each engine at station 3.

$$OP3 = 0.25 * PI * DP3^{2.0} \quad (D.281)$$

The minimum allowable fuselage width (BFJS) at this station is,

$$BFJS = YPCH + DP3 + 0.5 * EBP3 \quad (D.282)$$

The width of each of the upper (BFJCU) and lower (BFJCL) fuselage corners is,

$$BFJCU = 0.5 * (BFJ - YPCH) \quad (D.283)$$

and

$$BFJCL = BFJCU \quad (D.284)$$

The local cross-sectional area (OFJ) and perimeter (PFJ) of the fuselage is,

$$OFJ = HFJCU * (BFJ - 2.0 * BFJCU) + (HFJ - HFJCU - HFJCL) * BFJ + HFJCL * YPCH - OFJPRJ + 0.5 * PI * (HFJCU * BFJCU + HFJCL * BFJCL) \quad (D.285)$$

and

$$PFJ = PI * \left\{ [0.5 * (HFJCU^{2.0} + BFJCU^{2.0})]^{0.5} + [0.5 * (HFJCL^{2.0} + BFJCL^{2.0})]^{0.5} + \left[0.5 * \left[\left(\frac{BFPRL - BFPRUJ}{2.0} \right)^{2.0} + HFPR2J^{2.0} \right] \right]^{0.5} \right\} + YPCH + 2.0 * (HFJ - HFJCU - HFJCL) + BFPRUJ \quad (D.286)$$

D.26 FUSELAGE SECTION J-K (Module FSECTJK)

Views of fuselage section J-K are shown in fig.D.21. A special feature of this section is an upper fuselage recess, which starts at J and increases linearly with X in both depth and width. This is incorporated in the following expressions which define the geometry of section J-K.

The fuselage height (HFJKX) at any station X of section J-K is,

$$HFJKX = HFDH - \left[\frac{HFDH - ZPC - 0.5 * (DP3 + EHP3)}{XFN - LP34 - XD} \right] * (X - XD) - \left[\frac{ZPC - 0.5 * (DP4 + EHP4)}{XFN - XH} \right] * (X - XH) \quad (D.287)$$

The height of the upper (HFKCUX) and lower (HFKCLX) fuselage corners of section J-K is,

$$HFKCUX = HFDH - \left[\frac{HFDH - ZPC - 0.5 * (DP3 + EHP3)}{XFN - LP34 - XD}\right] * (X - XD) - ZPC \quad (D.288)$$

and

$$HFKCLX = \left[\frac{0.5 * (DP4 + EHP4)}{XFN - XH}\right] * (X - XH) \quad (D.289)$$

The depth (HFPR2X) and inner width (BFPRUX) of the underfuselage recess at any station X is,

$$HFPR2X = (X - XG) * \tan(QFPR) - \left[\frac{ZPC - 0.5 * (DP4 + EHP4)}{XFN - XH}\right] * (X - XH) \quad (D.290)$$

and

$$BFPRUX = \left(\frac{YPCH - DP3 - 0.5 * EBP3}{DP1 + LP12 + LP23}\right) * (X - XG) \quad (D.291)$$

The depth of the upper fuselage recess is defined by an angle QFPRU which is an external variable specified in the input data. This is the angle between the inner line of the upper fuselage recess and the horizontal. QFPRU is constrained not to exceed a maximum allowable value (QFPRUH) which is estimated by the following expression.

$$QFPRUH = \tan^{-1}\left(\frac{HEJCU}{LP34}\right) \quad (rads) (D.292)$$

The depth of the upper fuselage recess (HFPR3X) at any station X of section J-K is, therefore,

$$HFPR3X = \left[\tan(QFPRU) - \left(\frac{HFJCU - HFKCU}{LP34}\right)\right] * (X - XJ) \qquad (D.293)$$

where, HFKCU = Height of the upper fuselage corners at station K.

The maximum allowable inner width of the upper recess is equal to (YPCH - DP4 - 0.5 * EBP4) at station K. This limit is imposed by the local engine bay dimensions. Therefore, the inner width of the upper recess (BFPR3X) at any station X is,

$$BFPR3X = \left(\frac{YPCH - DP4 - 0.5 * EBP4}{LP34}\right) * (X - XJ) \qquad (D.294)$$

The corresponding cross-sectional area of the upper recess (OFPR3X) is,

$$OFPR3X = HFPR3X * YPCH - 0.25 * PI * (YPCH - BFPR3X) * HFPR3X \qquad (D.295)$$

Similarly the local cross-sectional area of the underfuselage recess (OFKPRX) is,

$$OFKPRX = HFPR2X * YPCH - 0.25 * PI * (YPCH - BFPRUX) * HFPR2X \qquad (D.296)$$

The Y- coordinate of the fuselage (YFJKX) at any station X of section J-K is,

$$YFJKX = \frac{[OTXN + 2.0 * OP34X + OFPR3X + OFKPRX - YPCH * (1.0 - 0.25 * PI) * (HFKCUX + HFKCLX)]}{(0.5 * PI - 2.0) * (HFKCUX + HFKCLX) + 2.0 * HFJKX} \quad (D.297)$$

where, OP34X = Cross-sectional area of each engine at any station X between 3 and 4.

$$OP34X = 0.25 * PI * DP34X^{2.0} \quad (D.298)$$

The above estimated Y- coordinate is constrained not to be less than a minimum allowable value (YFJKXS) which is defined by the local engine bay dimensions.

$$YFJKXS = 0.5 * BFJ - \left\{\frac{0.5 *[BFJ - (YPCH + DP4 + 0.5 * EBP4)]}{LP34}\right\} * (X - XJ) \quad (D.299)$$

The width of each of the upper (BFKCUX) and lower (BFKCLX) fuselage corners at any station X of section J-K is,

$$BFKCUX = YFJKX - 0.5 * YPCH \quad (D.300)$$

and

$$BFKCLX = BFKCUX \quad (D.301)$$

The corresponding cross-sectional area (OFJKX) and perimeter (PFJKX) of the fuselage are,

$$OFJKX = 0.5 * PI * (HFKCUX * BFKCUX + HFKCLX * BFKCLX) + 2.0 * YFJKX * (HFJKX - HFKCUX - HFKCLX) + YPCH * (HFKCUX + HFKCLX) - OFPR3X - OFKPRX \quad (D.302)$$

and

$$PFJKX = PI * \left\{ [0.5 * (HFKCUX^{2.0} + BFKCUX^{2.0})]^{0.5} + [0.5 * (HFKCLX^{2.0} + BFKCLX^{2.0})]^{0.5} + \left[0.5 * \left[\left(\frac{YPCH - BFPRUX}{2.0}\right)^{2.0} + HFPR2X^{2.0}\right]\right]^{0.5} + \left[0.5 * \left[\left(\frac{YPCH - BFPR3X}{2.0}\right)^{2.0} + HFPR3X^{2.0}\right]\right]^{0.5} \right\} + 2.0 * (HFJKX - HFKCUX - HFKCLX) + BFPRUX + BFPR3X \quad (D.303)$$

D.27 FUSELAGE STATION K (Module FUSSTNK)

Station K coincides with the rear end of the fuselage. A view of the latter is shown in fig.D.22. The expressions defining its geometry are presented in this section.

The fuselage height (HFK) at station K is,

$$HFK = HFDH - \left[\frac{HFDH - ZPC - 0.5 * (DP3 + EHP3)}{XFN - LP34 - XD}\right] * (XFN - XD) - ZPC + 0.5 * (DP4 + EHP4) \quad (D.304)$$

The height of the upper (HFKCU) and lower (HFKCL) fuselage corners is,

$$HFKCU = HFDH - \left[\frac{HFDH - ZPC - 0.5 * (DP3 + EHP3)}{XFN - LP34 - XD}\right] * (XFN - XD) - ZPC \quad (D.305)$$

and

$$HFKCL = 0.5 * (DP4 + EHP4) \quad (D.306)$$

The depth (HFPR2K) and inner width (BFPRUK) of the underfuselage recess at station K are,

$$HFPR2K = (XFN - XG) * \tan(QFPR) - ZPC + 0.5 * (DP4 + EHP4) \quad (D.307)$$

and

$$BFPRUK = \left(\frac{YPCH - DP3 - 0.5 * EBP3}{DP1 + LP12 + LP23}\right) * (XFN - XG) \quad (D.308)$$

The depth (HFPR3K) and inner width (BFPR3K) of the upper fuselage recess at the same station are,

$$HFPR3K = LP34 * \tan(QFPRU) - HFJCU + HFKCU \quad (D.309)$$

and

$$BFPR3K = YPCH - DP4 - 0.5 * EBP4 \quad (D.310)$$

The corresponding cross-sectional area of the upper fuselage recess (OFPR3K) is,

$$OFPR3K = HFPR3K * YPCH - 0.25 * PI * (YPCH - BFPR3K) * HFPR3K \quad (D.311)$$

The cross-sectional area of the underfuselage recess (OFKPR) is,

$$OFKPR = HFPR2K * YPCH - 0.25 * PI * (YPCH - BFPRUK) * HFPR2K \quad (D.312)$$

The local fuselage width (BFK) is,

$$BFK = \frac{\{2.0 * [OTXN + 2.0 * OP4 + OFPR3K + OFKPR - YPCH * (1.0 - 0.25 * PI) * (HFKCU + HFKCL)]\}}{(0.5 * PI - 2.0) * (HFKCU + HFKCL) + 2.0 * HFK} \quad (D.313)$$

where. OP4 = Cross-sectional area of each engine at station 4

The minimum allowable fuselage width (BFKS) at station K is,

$$BFKS = YPCH + DP4 + 0.5 * EBP4 \quad (D.314)$$

The width of each of the upper (BFKCU) and lower (BFKCL) fuselage corners is,

$$BFKCU = 0.5 * (BFK - YPCH) \quad (D.315)$$

and

$$BFKCL = BFKCU \quad (D.316)$$

Finally, the cross-sectional area (OFK) and perimeter (PFK) of the fuselage at station K are,

$$OFK = 0.5 * PI * (HFKCU * BFKCU + HFKCL * BFKCL) + BFK * (HFK - HFKCU - HFKCL) + YPCH * (HFKCU + HFKCL) - OFPR3K - OFKPR \quad (D.317)$$

and

$$PFK = PI * \left\{ [0.5 * (HFKCU^{2.0} + BFKCU^{2.0})]^{0.5} + [0.5 * (HFKCL^{2.0} + BFKCL^{2.0})]^{0.5} + \left[0.5 * \left[\left(\frac{YPCH - BFPRUK}{2.0} \right)^{2.0} + HFPR2K^{2.0} \right] \right]^{0.5} + \left[0.5 * \left[\left(\frac{YPCH - BFPR3K}{2.0} \right)^{2.0} + HFPR3K^{2.0} \right] \right]^{0.5} \right\} + 2.0 * (HFK - HFKCU - HFKCL) + BFPRUK + BFPR3K \quad (D.318)$$

D.28 FUSELAGE VOLUME AND SURFACE AREA

Fuselage volume and surface area calculations are included in the main segment of the Design Synthesis computer program. The total fuselage volume (VFG) and gross surface area (WFG) and also the surface areas of the windscreen (WCWSC) and canopy (WCCAN) are estimated by numerical integration methods. The net surface area of the fuselage (WFN) is also estimated in the same segment, following the calculation of the total footprint area of the flying surfaces (WFG3). These volume and surface area results are used later in the packaging and drag modules.

The numerical integration methods employed for these calculations are based on Simpson's Rule. This proved sufficiently accurate for the purpose of this Synthesis due to the built-in linearity and uniformity of the eleven principal fuselage sections. Each of these sections is initially considered separately and its volume and surface area are estimated by integrating its cross-sectional areas and perimeters, respectively, which are determined by execution of the previously presented fuselage geometry modules, at three equally spaced stations, in each case. A total of twenty-two different fuselage stations are therefore considered for the complete fuselage integrations.

VFG and WFG are obtained by summation of the individual fuselage section volume and surface area estimates, respectively. Hence,

$$VFG = VFR + VFRA + VFAB + VFBC + VFCD + VFDE + VFEF + VFFG + VFGH + VFHJ + VFJK \tag{D.319}$$

and

$$WFG = WFR + WFRA + WFAB + WFBC + WFCD + WFDE + WFEF + WFFG + WFGH + WFHJ + WFJK \quad (D.320)$$

The value of WCWSC is obtained by integrating the windscreen perimeters (PFTABX) which are evaluated by module FSECTAB at three equally spaced stations. Similarly, WCCAN is estimated by integrating the canopy perimeters (PFTBCX and PFTCDX) which are calculated by modules FSECTBC and FSECTCD.

The total footprint area of the flying surfaces, is given by the following expression from ref.1.

$$WFG3 = 0.69282 * [2.0 * RTW * CWCB^{2.0} + 2.0 * RTC * CCB^{2.0} + RTEF * CEFB^{2.0}] \quad (D.321)$$

RTW, RTC and RTEF, are the thickness to chord ratios for the wing, foreplane and fin, while CWCB, CCB and CEFB, are the corresponding root-chords. These are estimated by the flying surface geometry modules, presented in appendix E. Therefore, the net surface area of the fuselage is,

$$WFN = WFG - WFG3 \quad (D.322)$$

D.29 MISCELLANEOUS GEOMETRY CALCULATIONS

A number of miscellaneous geometry calculations are also included in the main segment of the computer program. These determine the values of some special parameters used in the packaging and aerodynamics modules. These parameters and the methods used for their estimation are described in this section.

The maximum cross-sectional area of the fuselage (OFXH) is determined by comparing the cross-sectional area results at fifteen fuselage stations, from C to K. The axial distance of the station at which OFXH occurs is XFOH.

The maximum net cross-sectional area of the fuselage (OFXHS) and corresponding distance (XFOHS) are also determined in a similar manner.

The maximum cross-sectional area of the afterbody (OFXTH) and its corresponding distance (XFOTH) are again obtained by comparing the cross-sectional areas of the fuselage at seven stations from G to K.

The cross-sectional area of the fuselage just before the intake plane (OFCDI1) and also the fuselage perimeter (PFCDI2) and cross-sectional area (OFCDI2) at the intake plane, are calculated by executing module FSECTCD for X = XII - 0.01 and X = XII.

The total volume of each intake diffuser (VIDC) and engine bay (VPBC), are estimated by numerically integrating their cross-sectional areas which are determined by execution of modules INTDIFG and ENGBAYG at several stations along their length.

The fuselage volumes VFIF1, VFIF2 and VFIF3 which are used later in the packaging modules for estimating the volume available for fuel tanks inside the fuselage, are determined by subtracting the intake diffuser volume contributions from the volumes of fuselage sections D-E, E-F and F-G, respectively.

The centre of the fuselage surface area (XFXM) and the centre of the fuselage structure (XFWM), used in the calculation of the moment arm of the fuselage structure and

skin, are estimated by considering the fuselage as a series of frustra of cones of height DXF(I), having radii derived from the local perimeter of the fuselage PFX(I) in the case of XFXM, or radii derived from the local cross-sectional area of the fuselage OFX(I) in the case of XFWM.

Hence,

$$XFXM1 = \sum_{I=1}^{22} 0.5 * [XFSTN(I) + XFSTN(I - 1)] * EFX(I) \qquad (D.323)$$

$$XFXM2 = \sum_{I=1}^{22} EFX(I) \qquad (D.324)$$

and

$$XFXM = \frac{XFXM1}{XFXM2} \qquad (D.325)$$

$$\text{where, } EFX(I) = 0.5 * [PFX(I) + PFX(I - 1)] * \left\{ \left(\frac{0.25}{PI^{2.0}} \right) * [PFX(I) - PFX(I - 1)]^{2.0} + [DXF(I)]^{2.0} \right\}^{0.5} \qquad (D.326)$$

XFSTN(I) = Distance of a given fuselage station from the aircraft nose.

and

$$XFWM1 = \sum_{I=1}^{22} 0.5 * [XFSTN(I) + XFSTN(I-1)] + EFW(I) \qquad (D.327)$$

$$XFWM2 = \sum_{I=1}^{22} EFW(I) \qquad (D.328)$$

and

$$XFWM = \frac{XFWM1}{XFWM2} \qquad (D.329)$$

$$\text{where, } EFW(I) = \left[\frac{DXF(I)}{3.0}\right] * \left\{OFX(I) + OFX(I-1) + [OFX(I) * OFX(I-1)]^{0.5}\right\} \qquad (D.330)$$

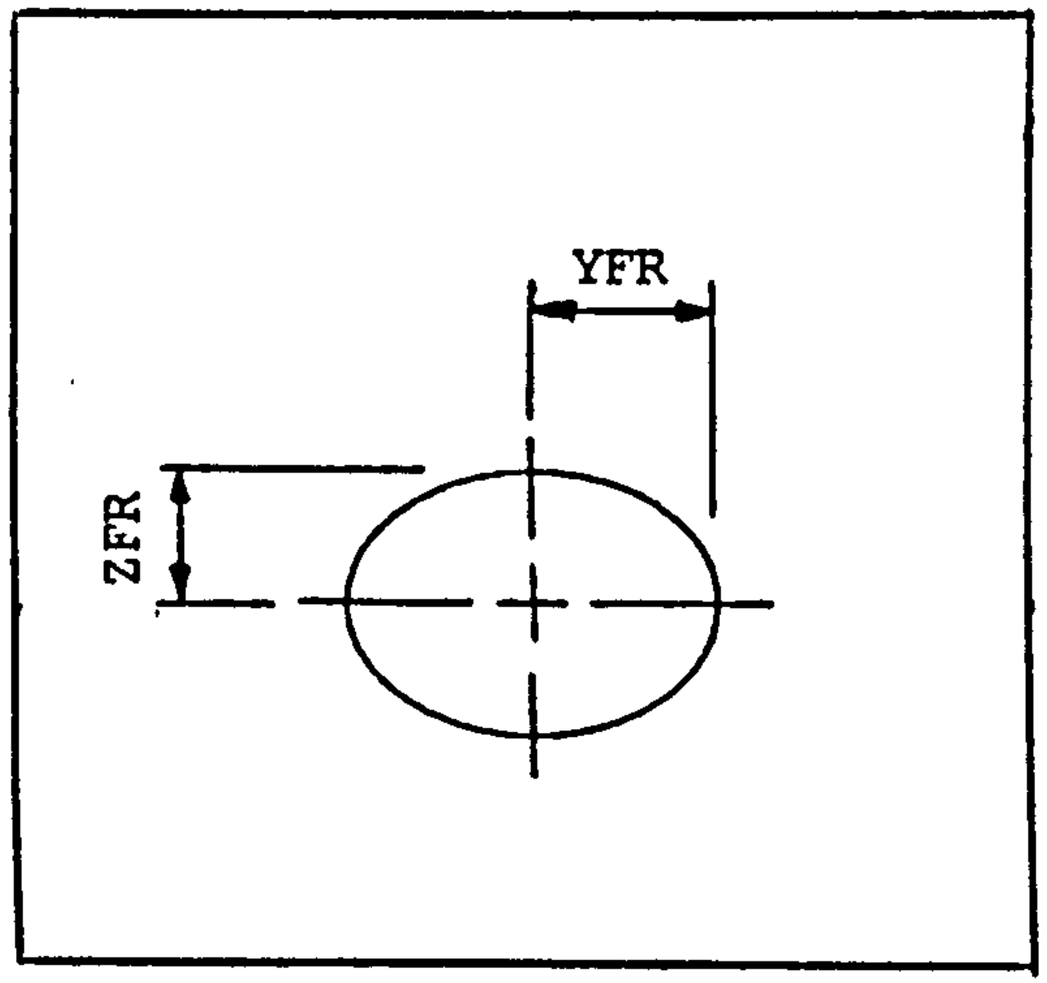

FIG. D.1 FUSELAGE GEOMETRY - STATION R

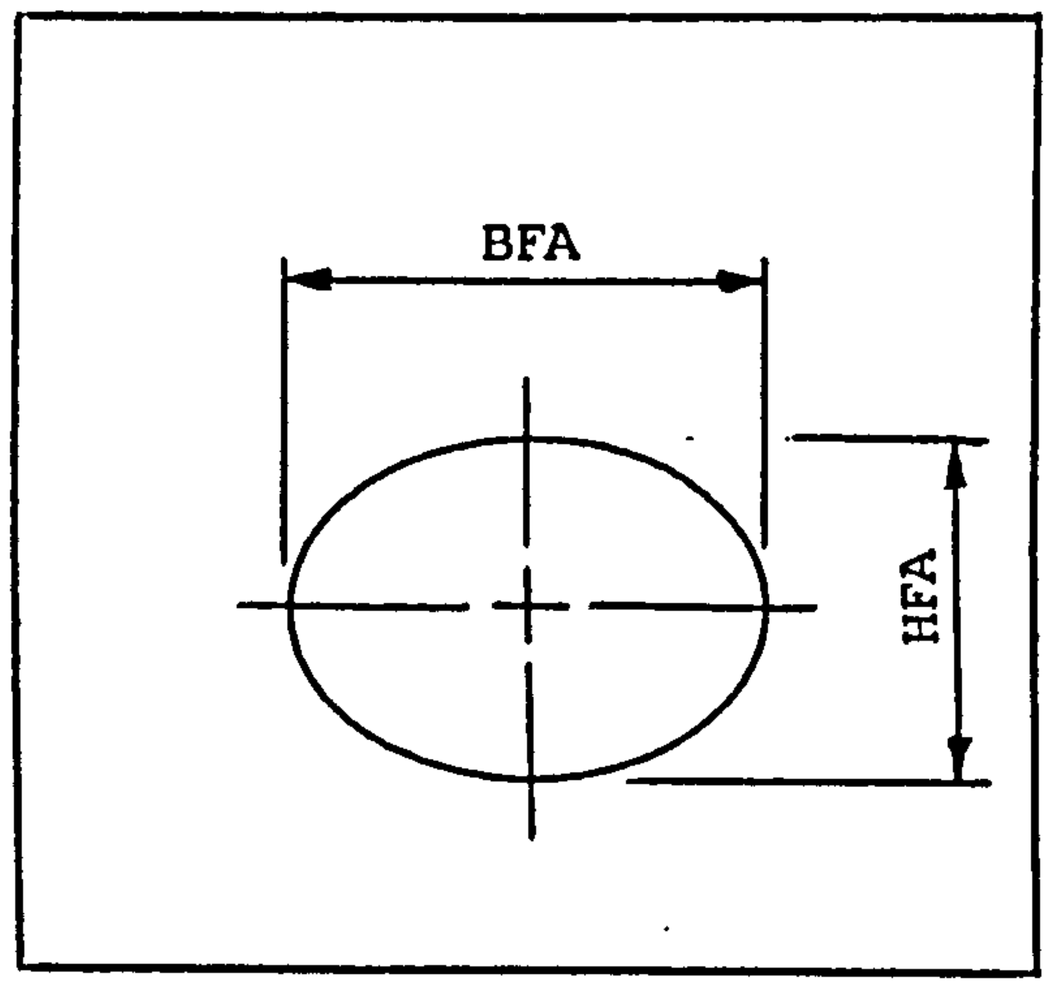

FIG. D.2 FUSELAGE GEOMETRY - STATION A

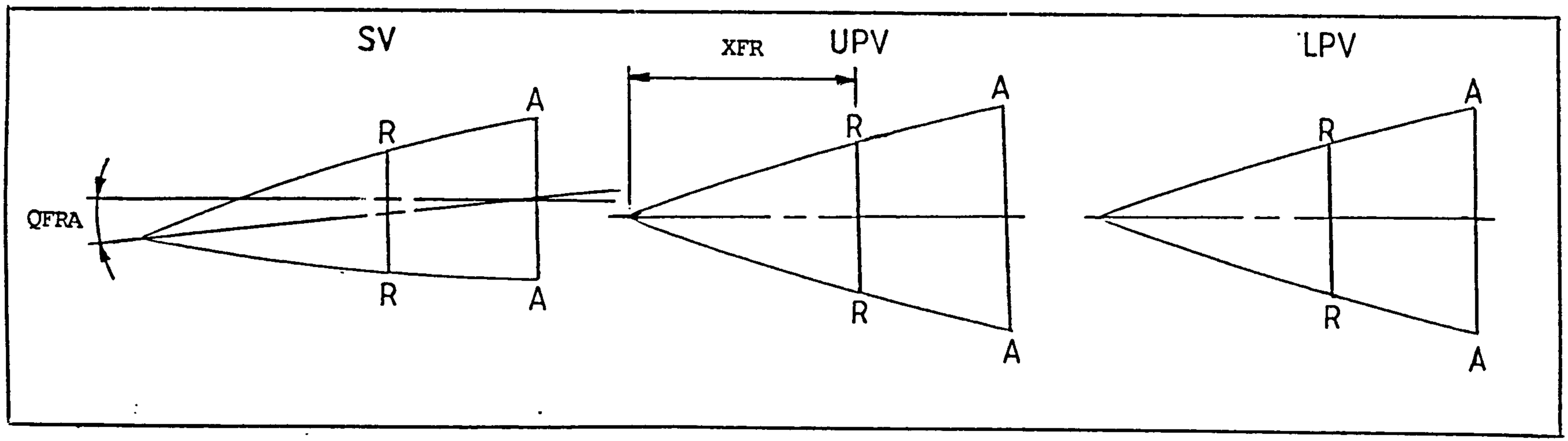

FIG. D.3 FUSELAGE GEOMETRY - RADOME AND SECTION R-A

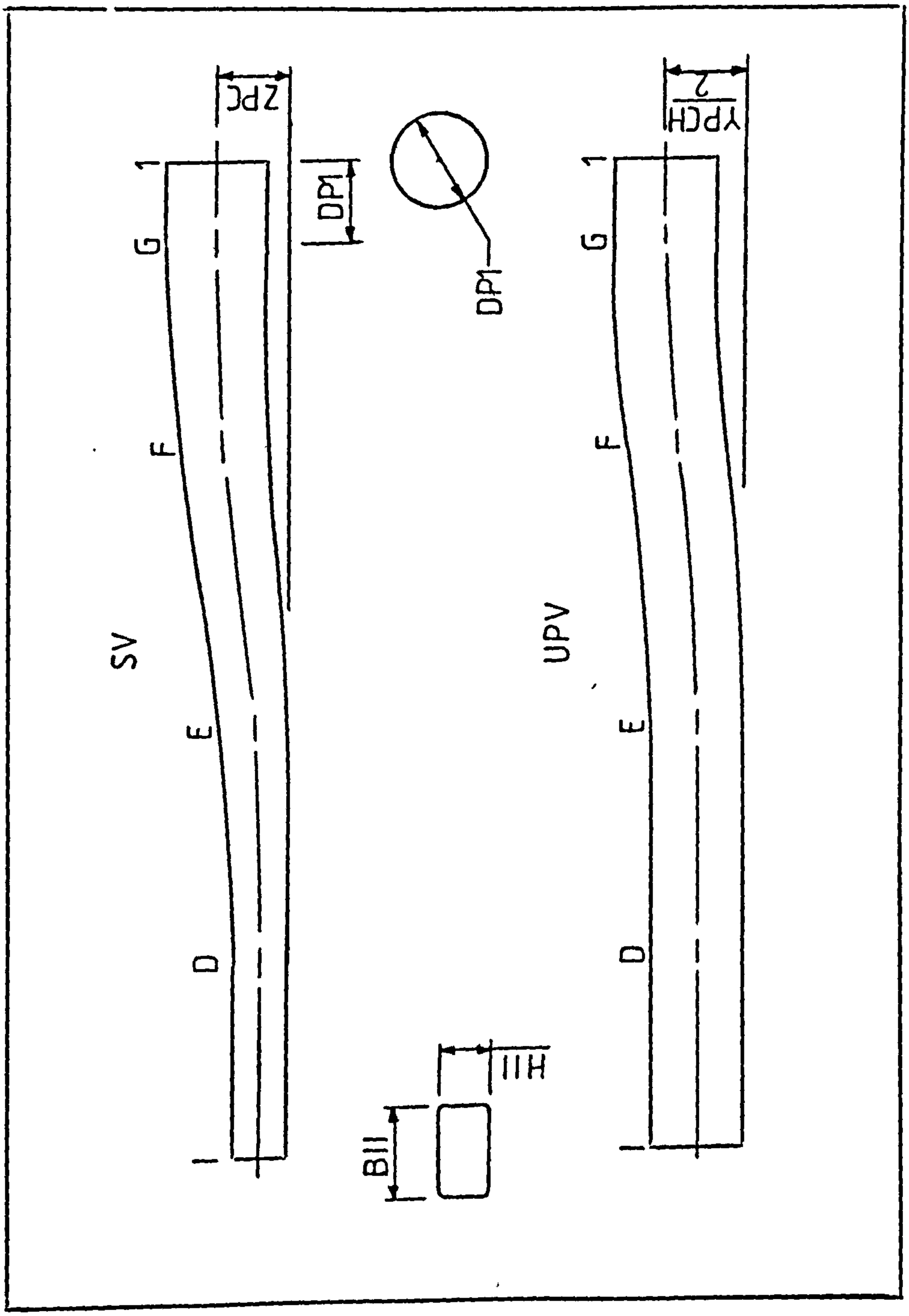
ZPC
DPM
G 1
F
SV
E
D
DPM
YPCH
2
G 1
F
UPV
E
D
IIH
BII

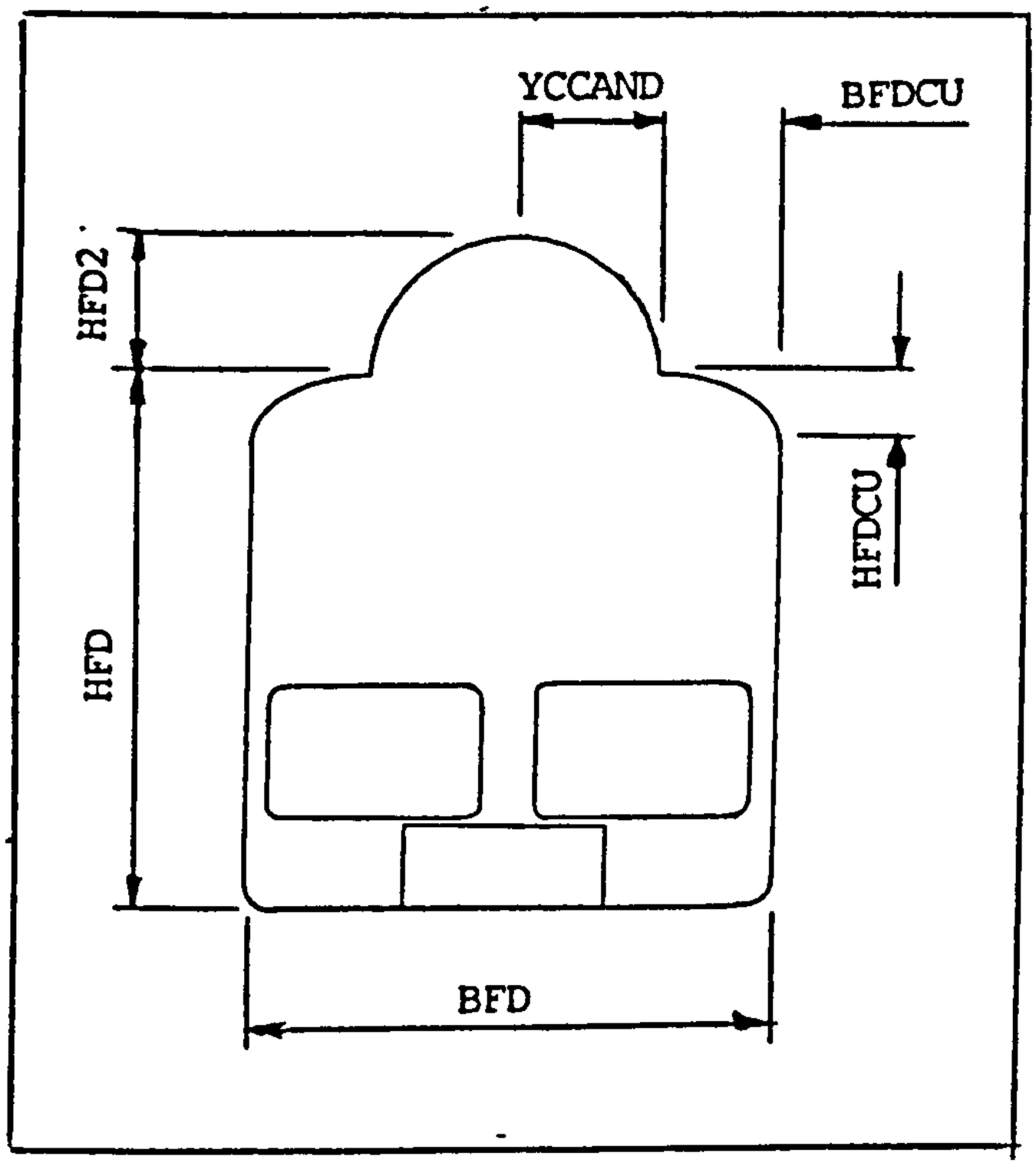

FIG. D.5 FUSELAGE GEOMETRY - STATION D

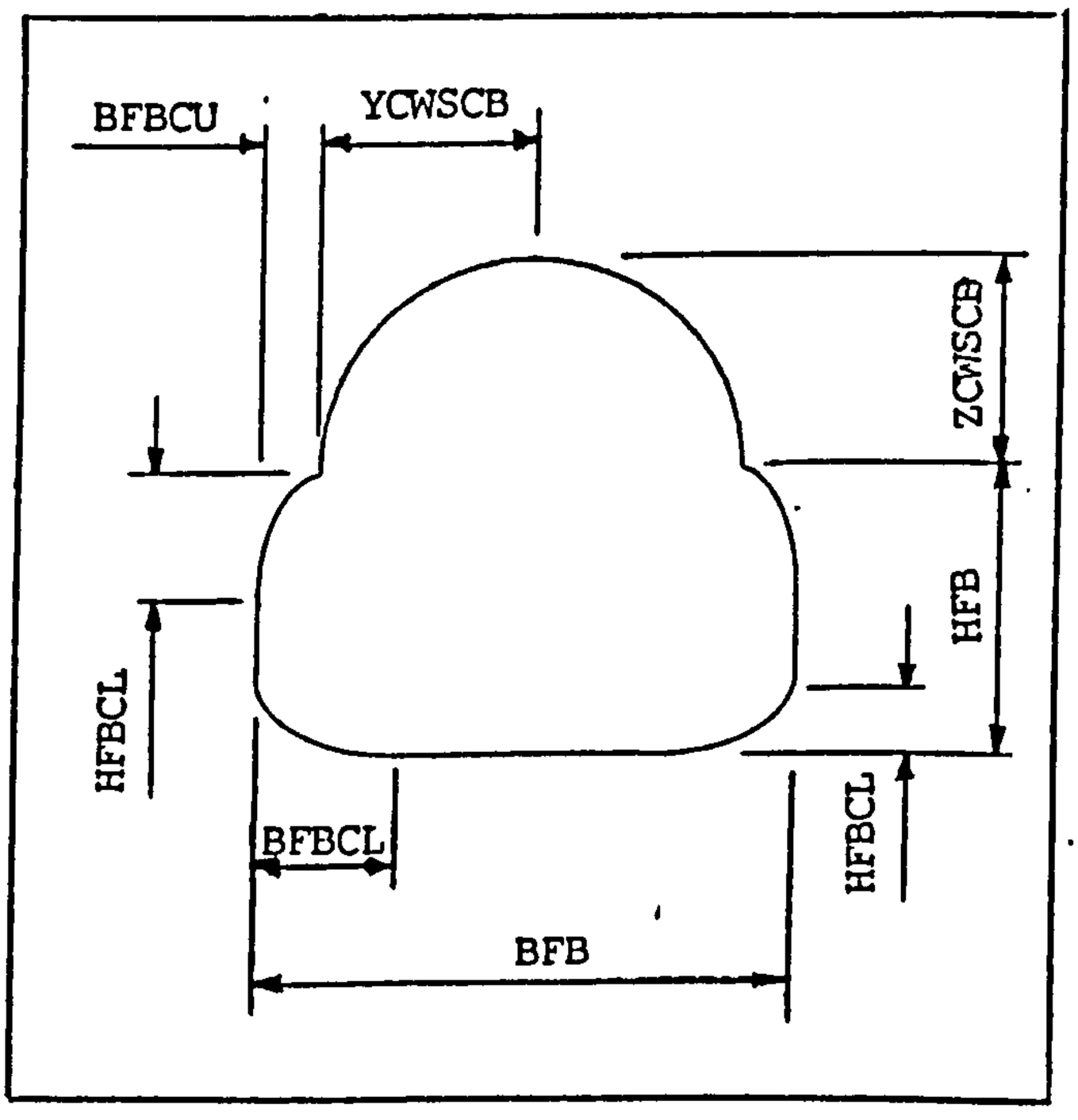

FIG. D.6 FUSELAGE GEOMETRY - STATION B

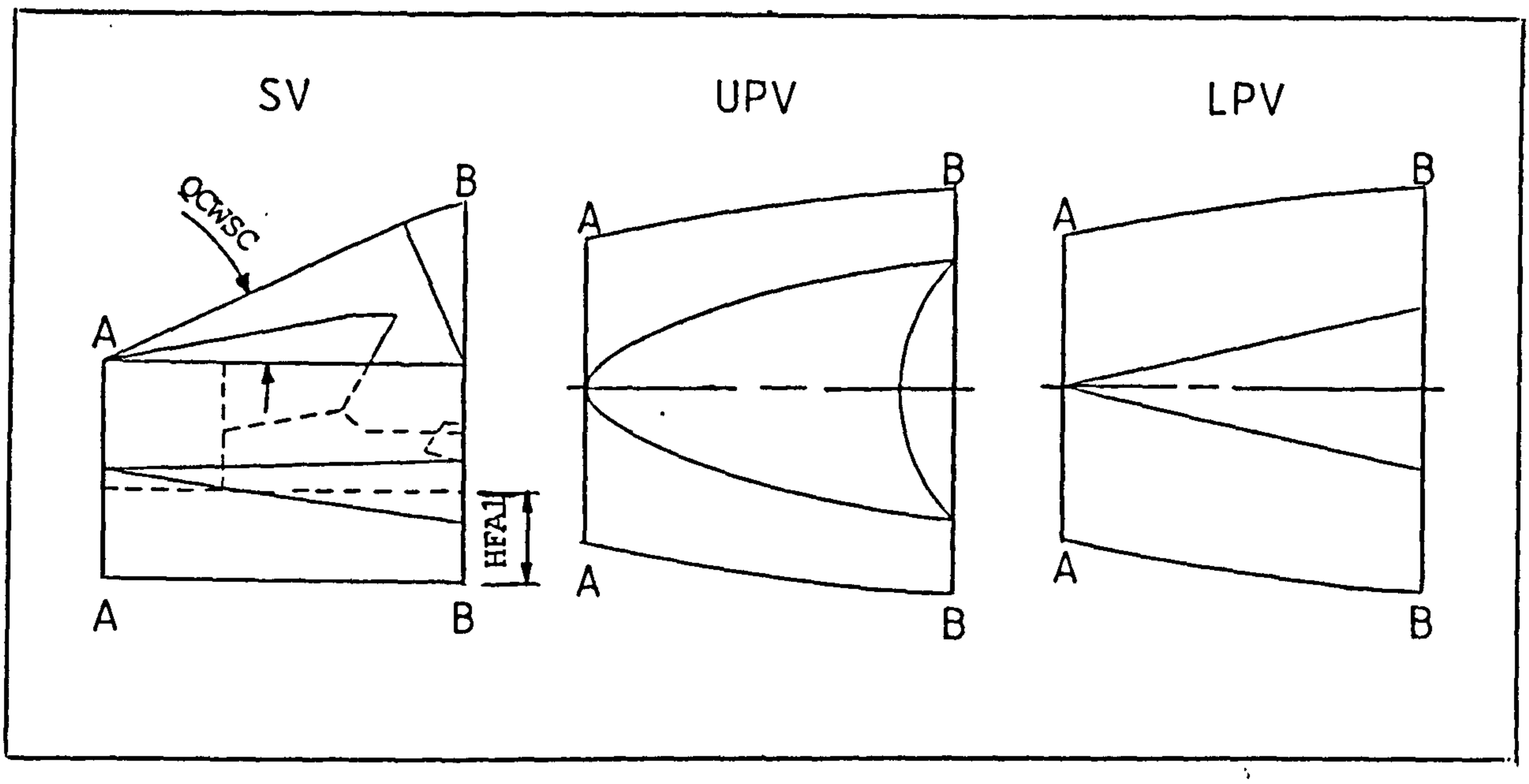

FIG. D.7 FUSELAGE GEOMETRY - SECTION A-B

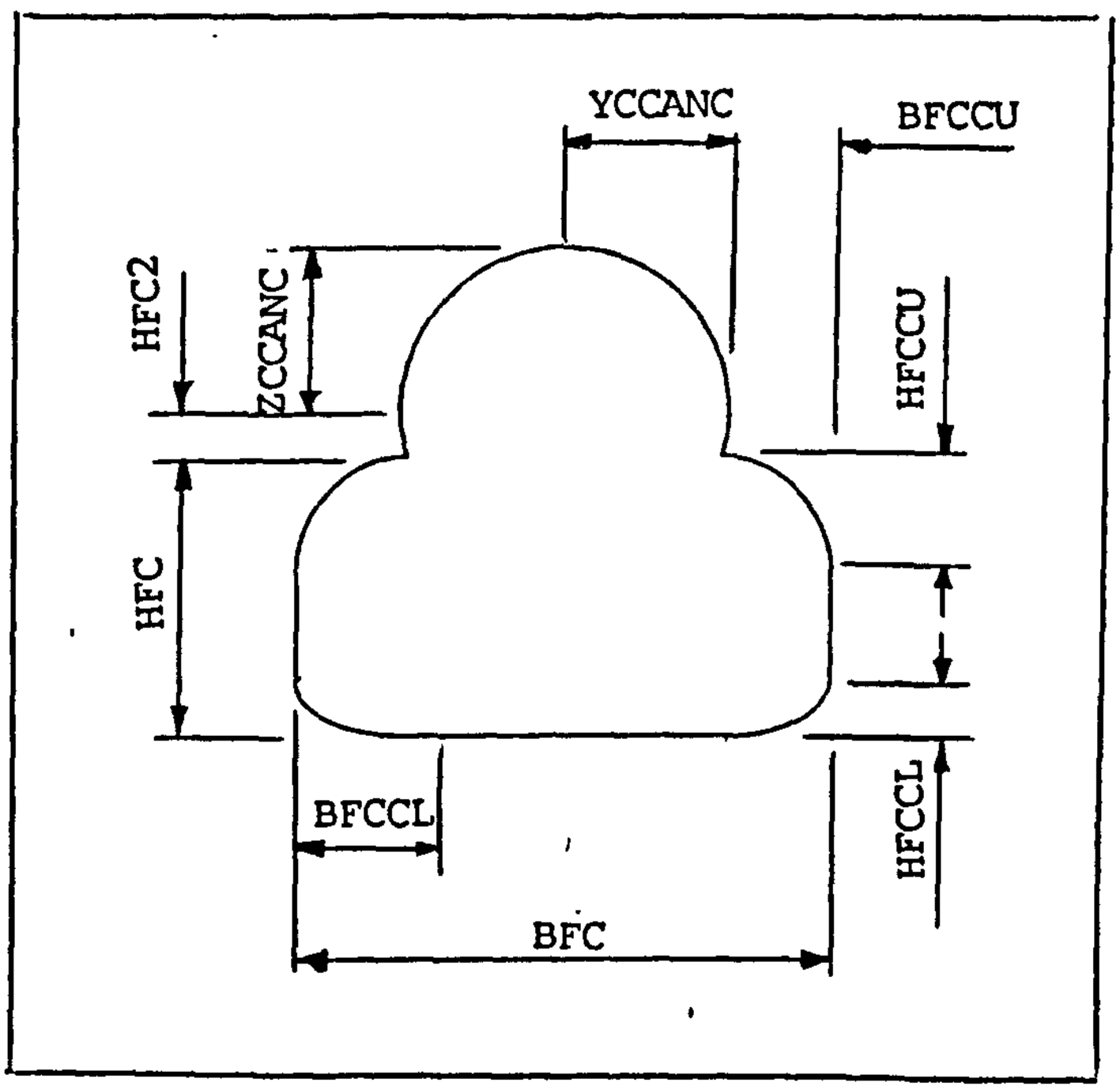

FIG. D.8 FUSELAGE GEOMETRY - STATION C

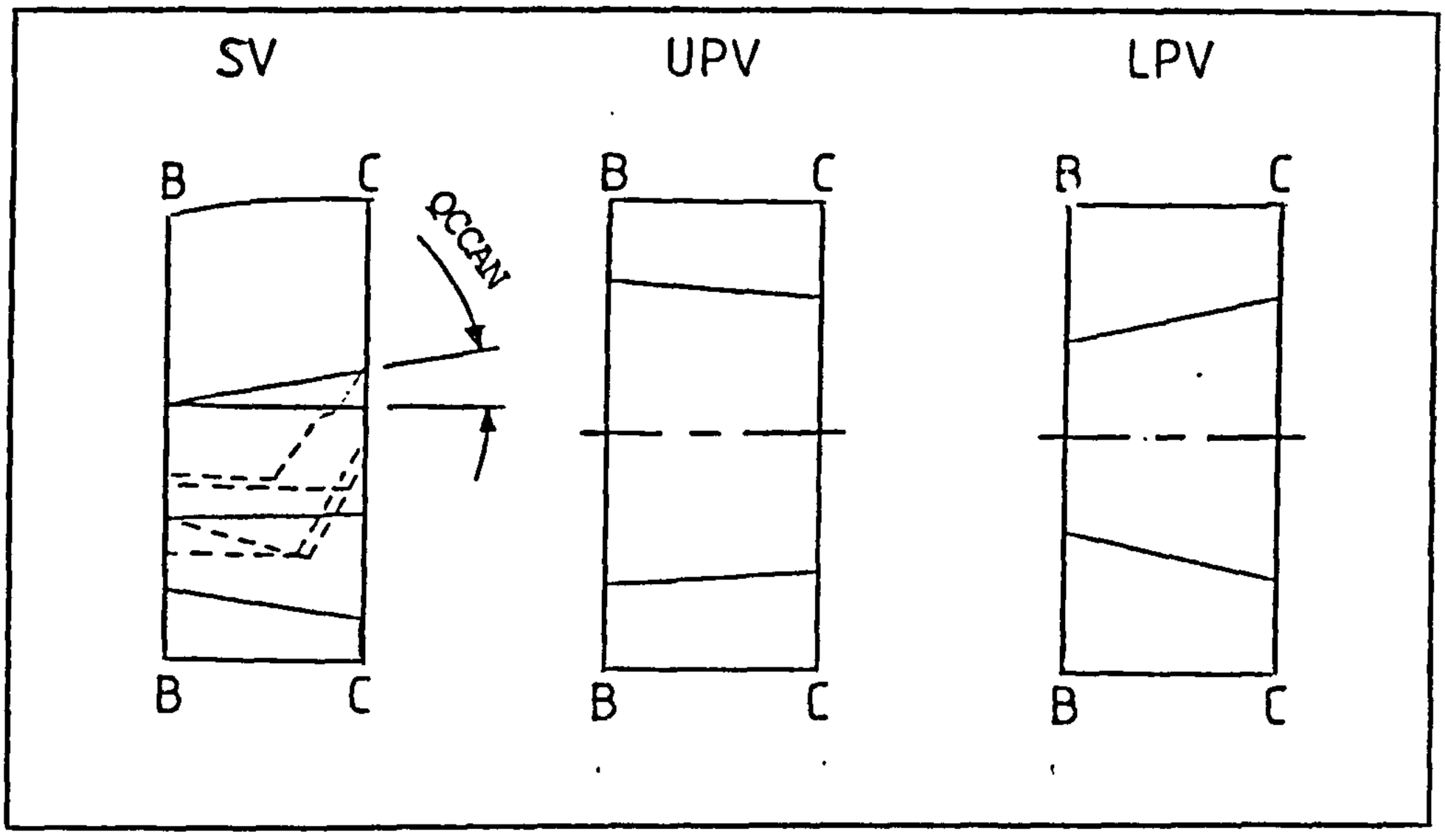

FIG. D.9 FUSELAGE GEOMETRY - SECTION B-C

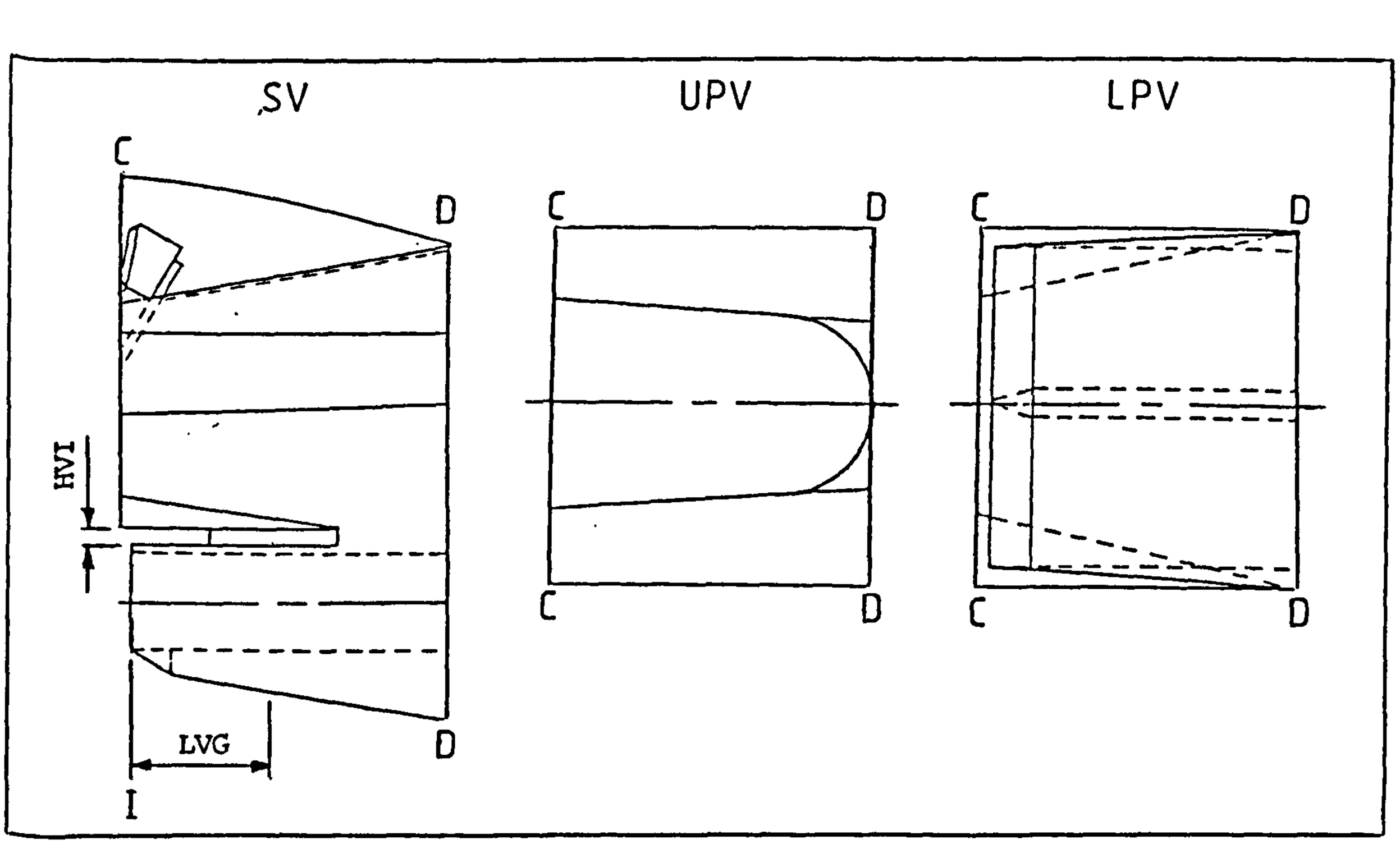

FIG. D.10 FUSELAGE GEOMETRY - SECTION C-D

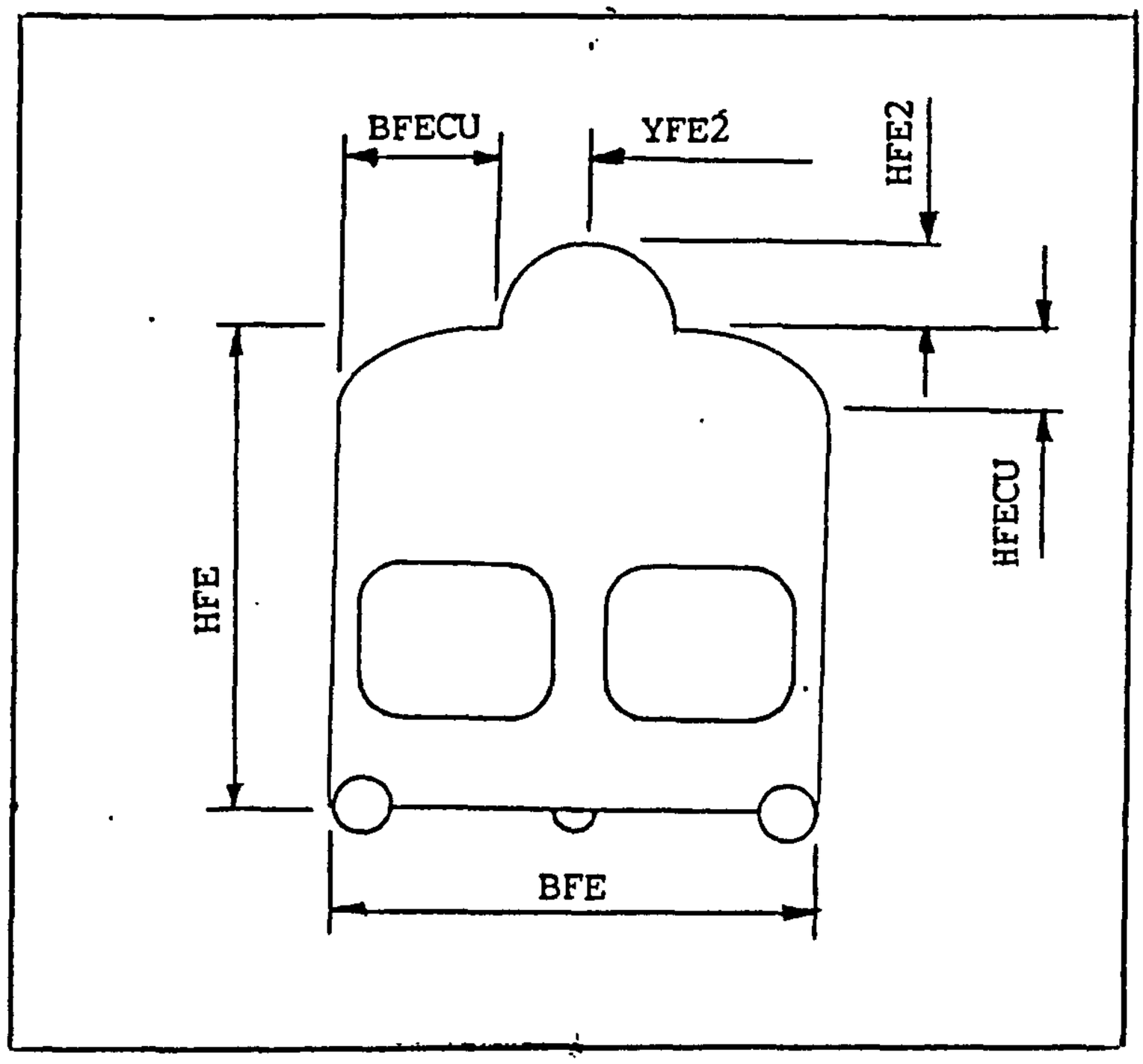

FIG. D.11 FUSELAGE GEOMETRY - STATION E

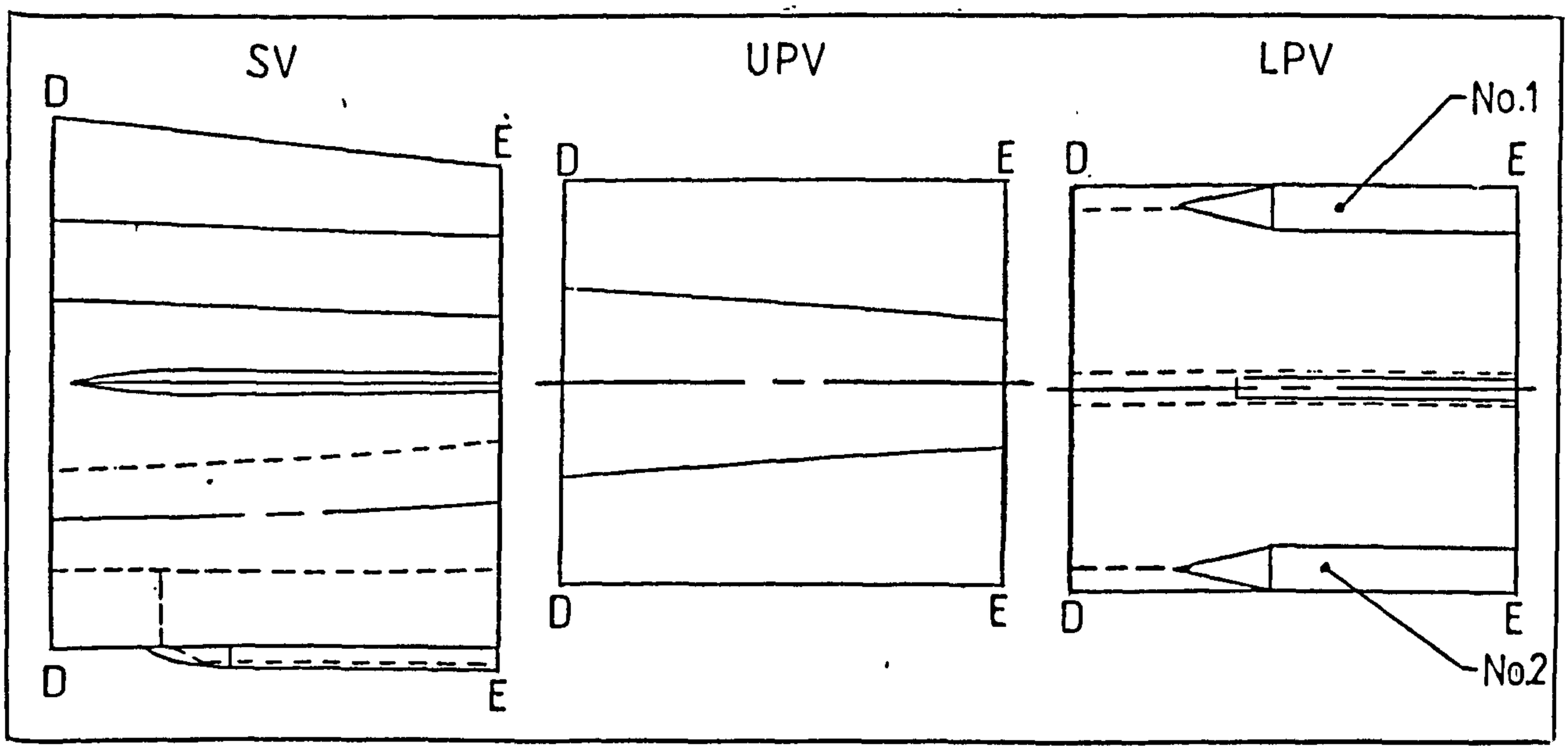

FIG. D.12 FUSELAGE GEOMETRY - SECTION D-E

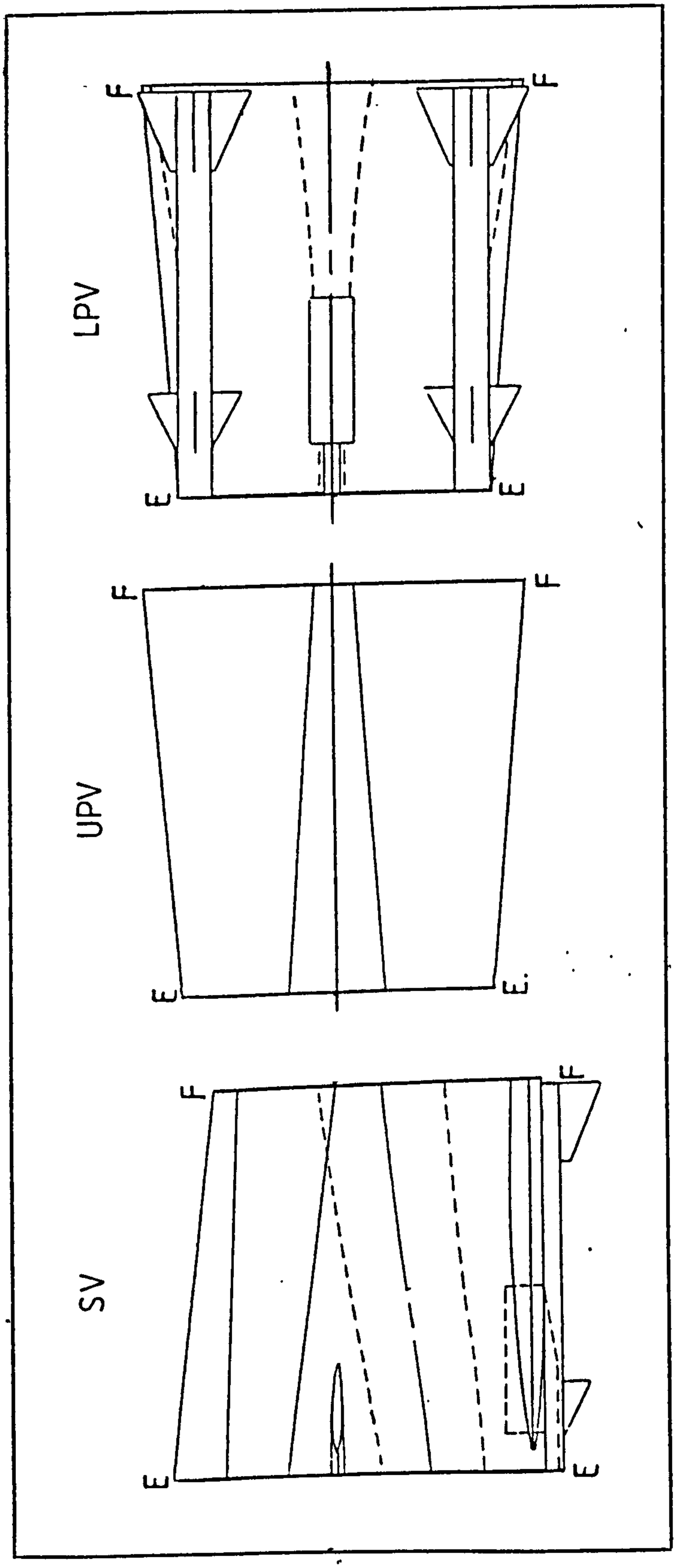

FIG. D.13 FUSELAGE GEOMETRY - SECTION E-F

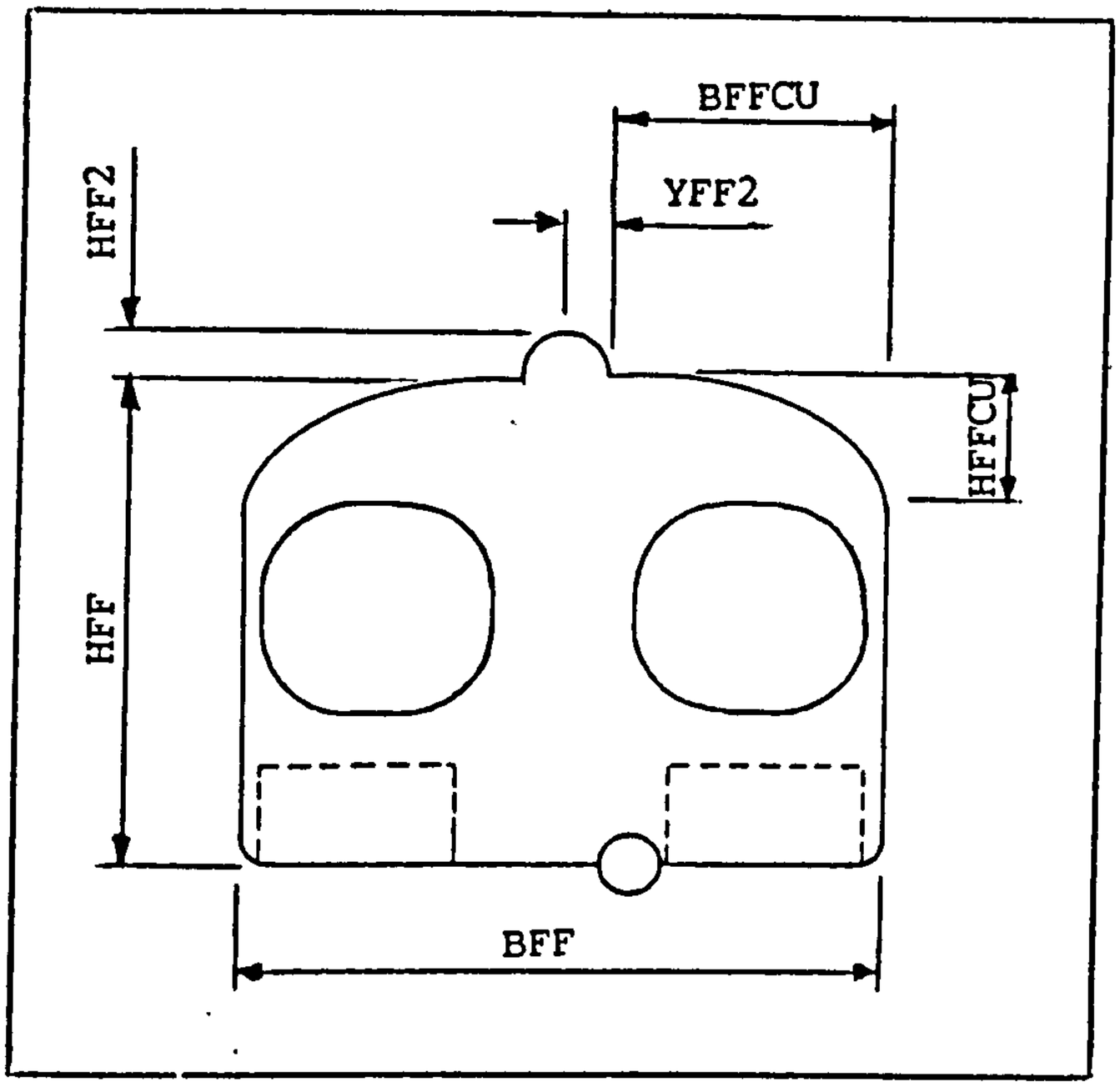

FIG. D.14 FUSELAGE GEOMETRY - STATION F

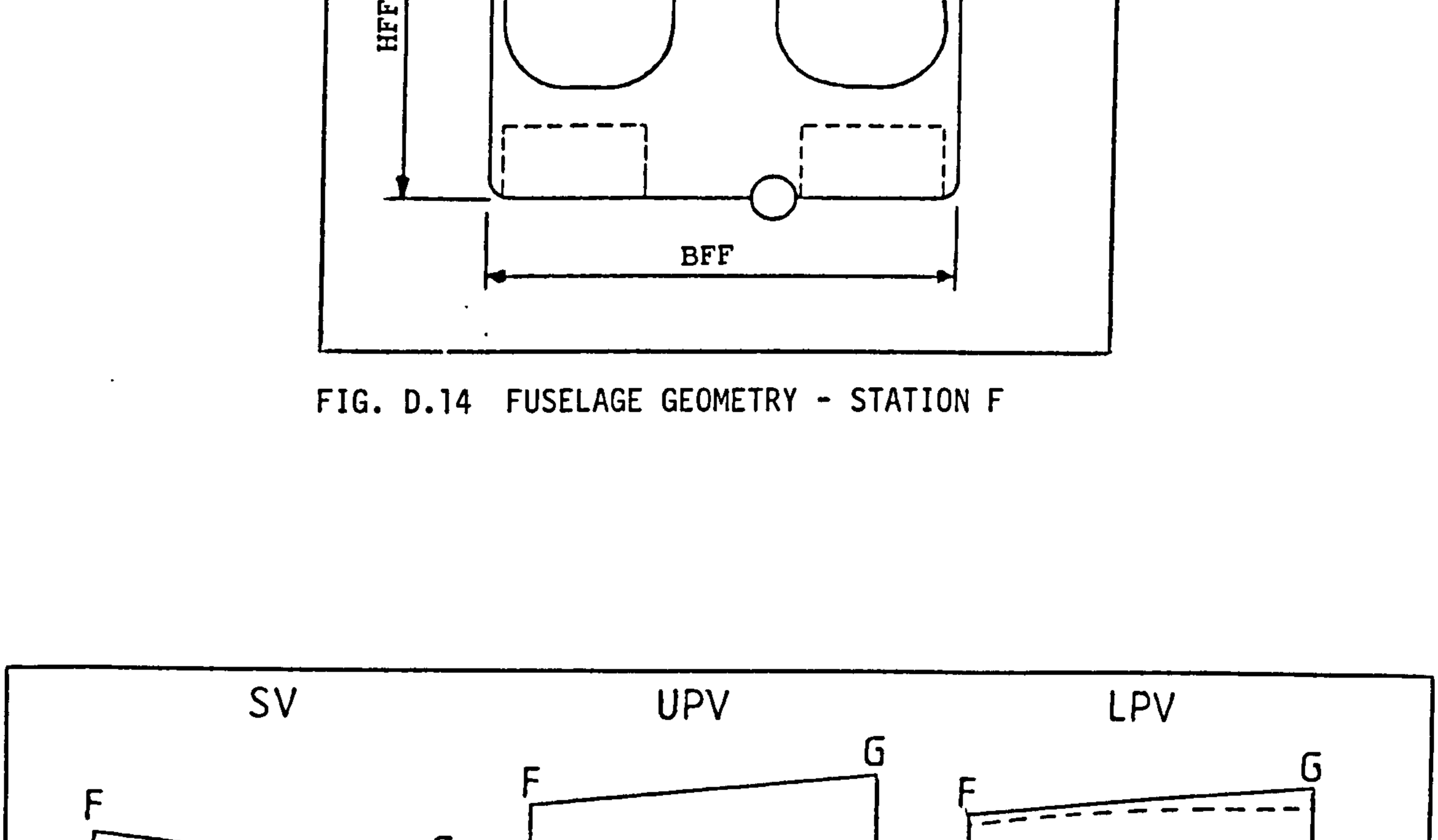

FIG. D.15 FUSELAGE GEOMETRY - SECTION F-G

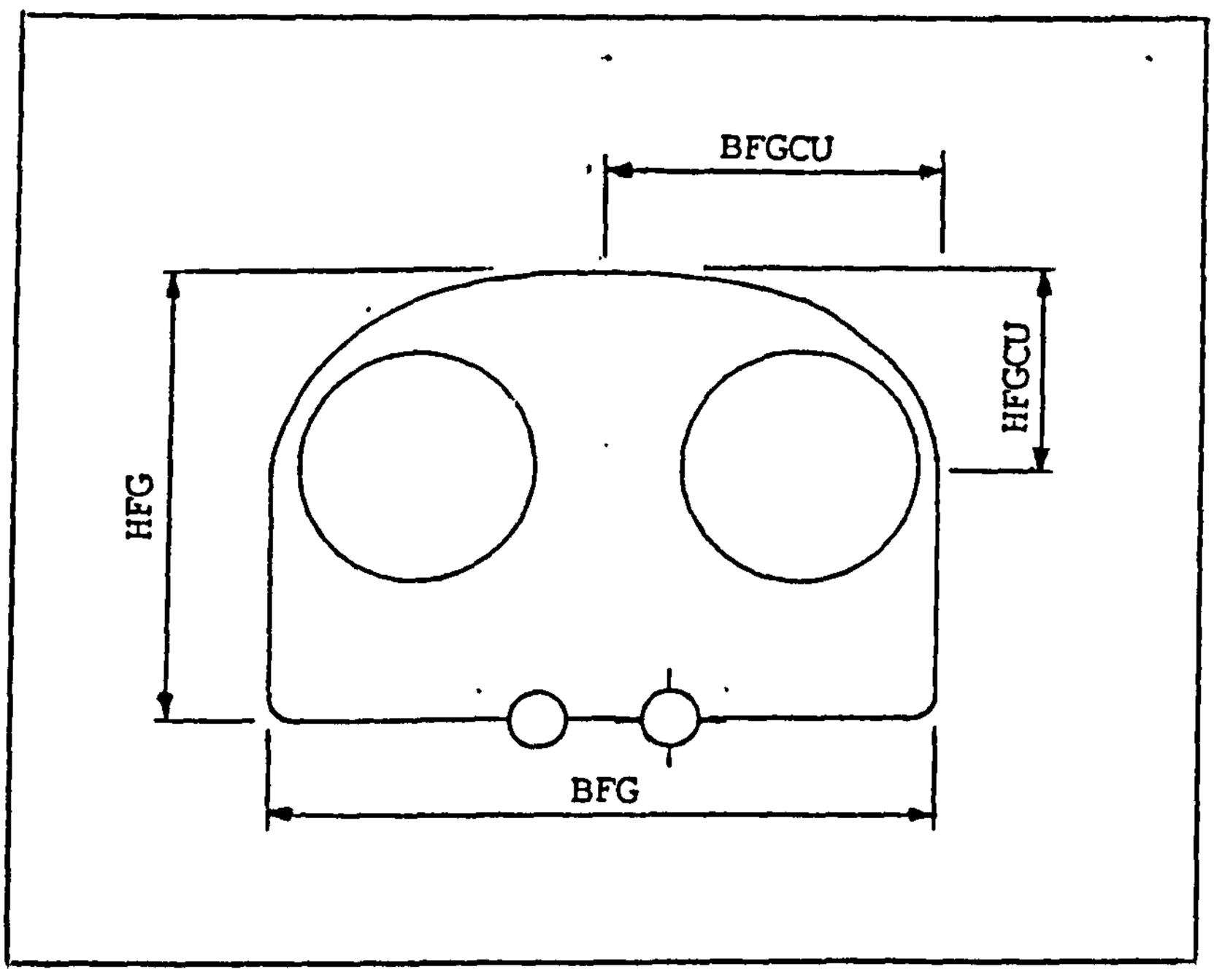

FIG. D.16 FUSELAGE GEOMETRY - STATION G

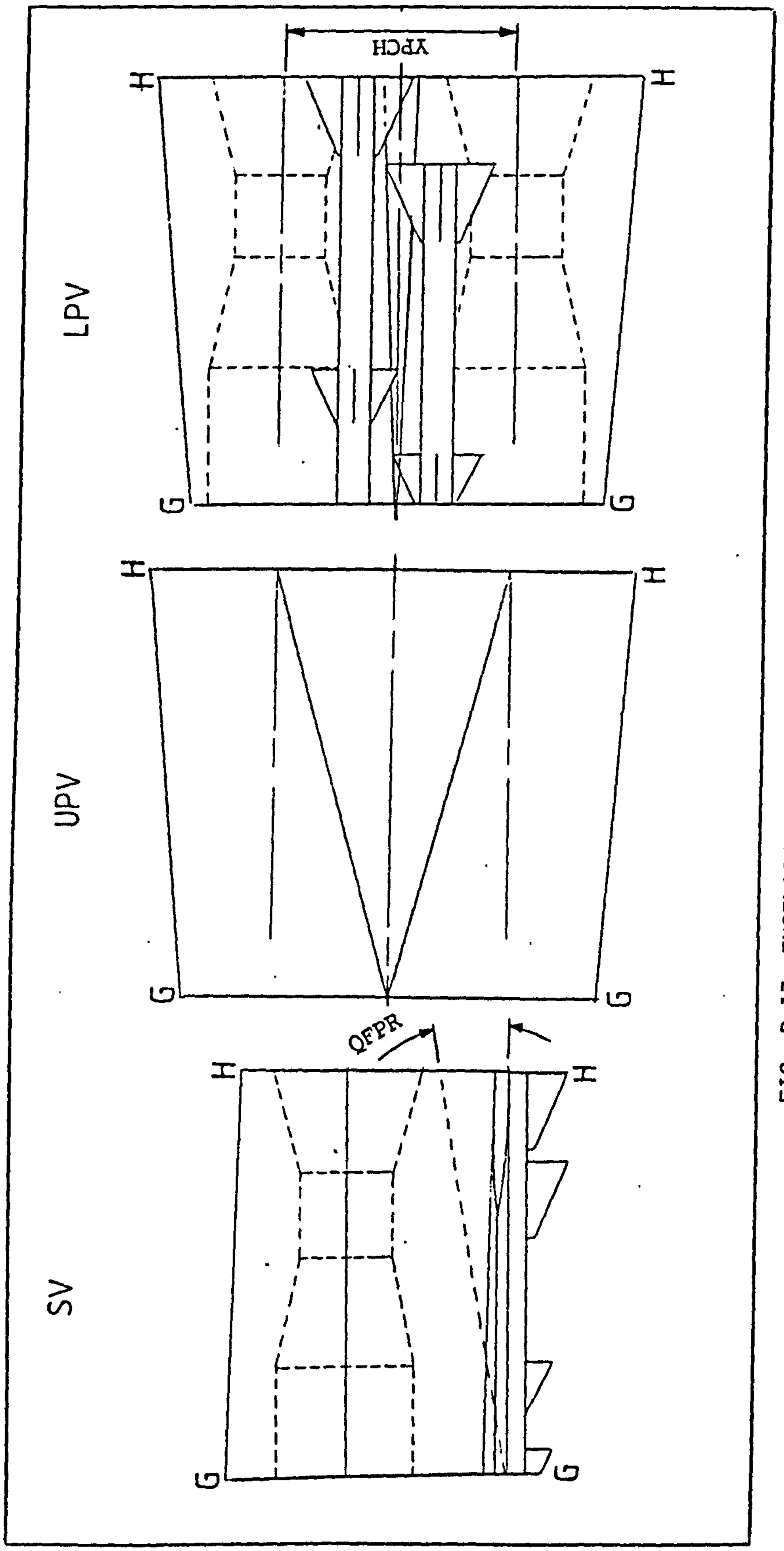

FIG. D.17 FUSELAGE GEOMETRY - SECTION G-H

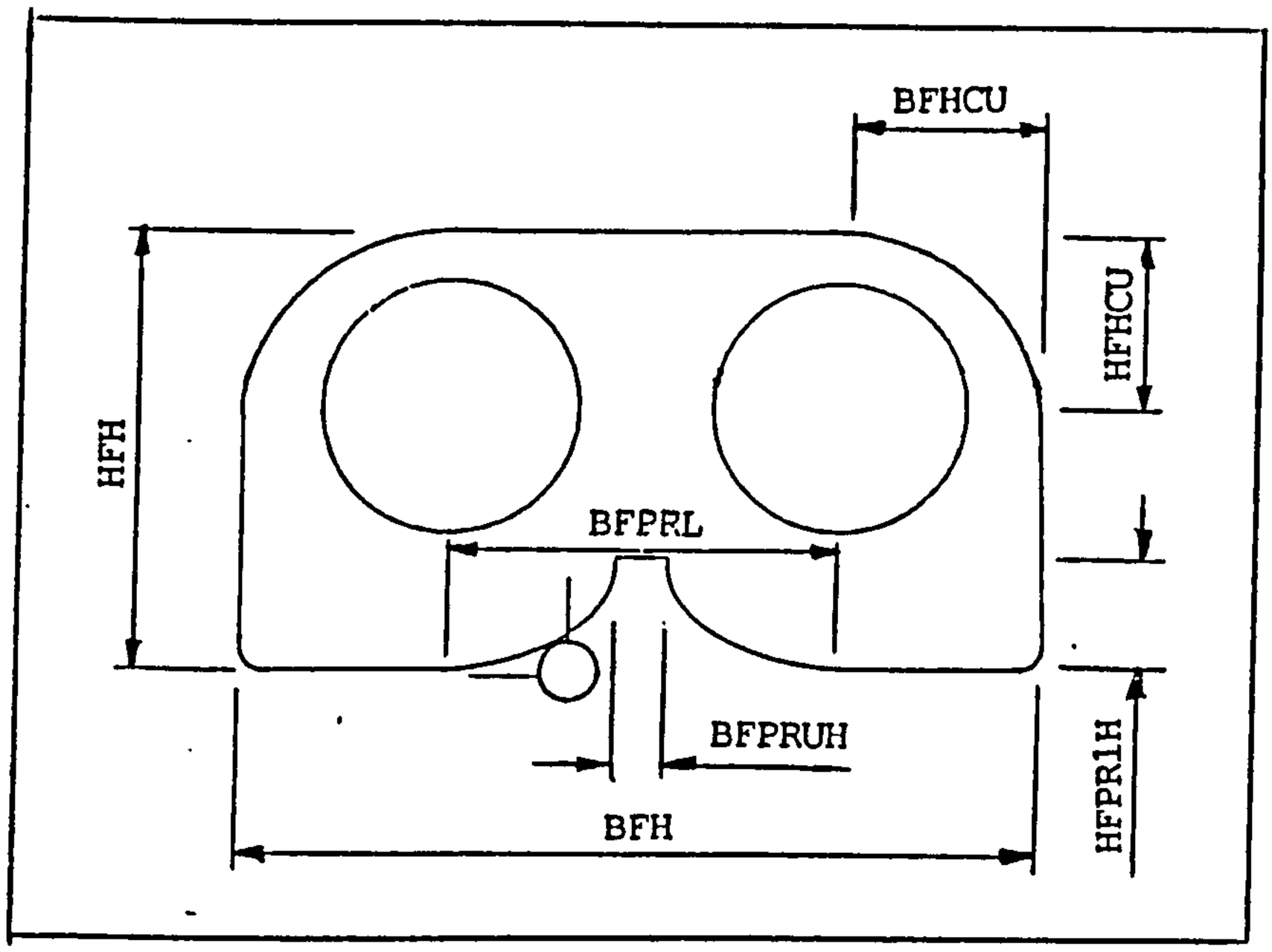

FIG. D.18 FUSELAGE GEOMETRY - STATION H

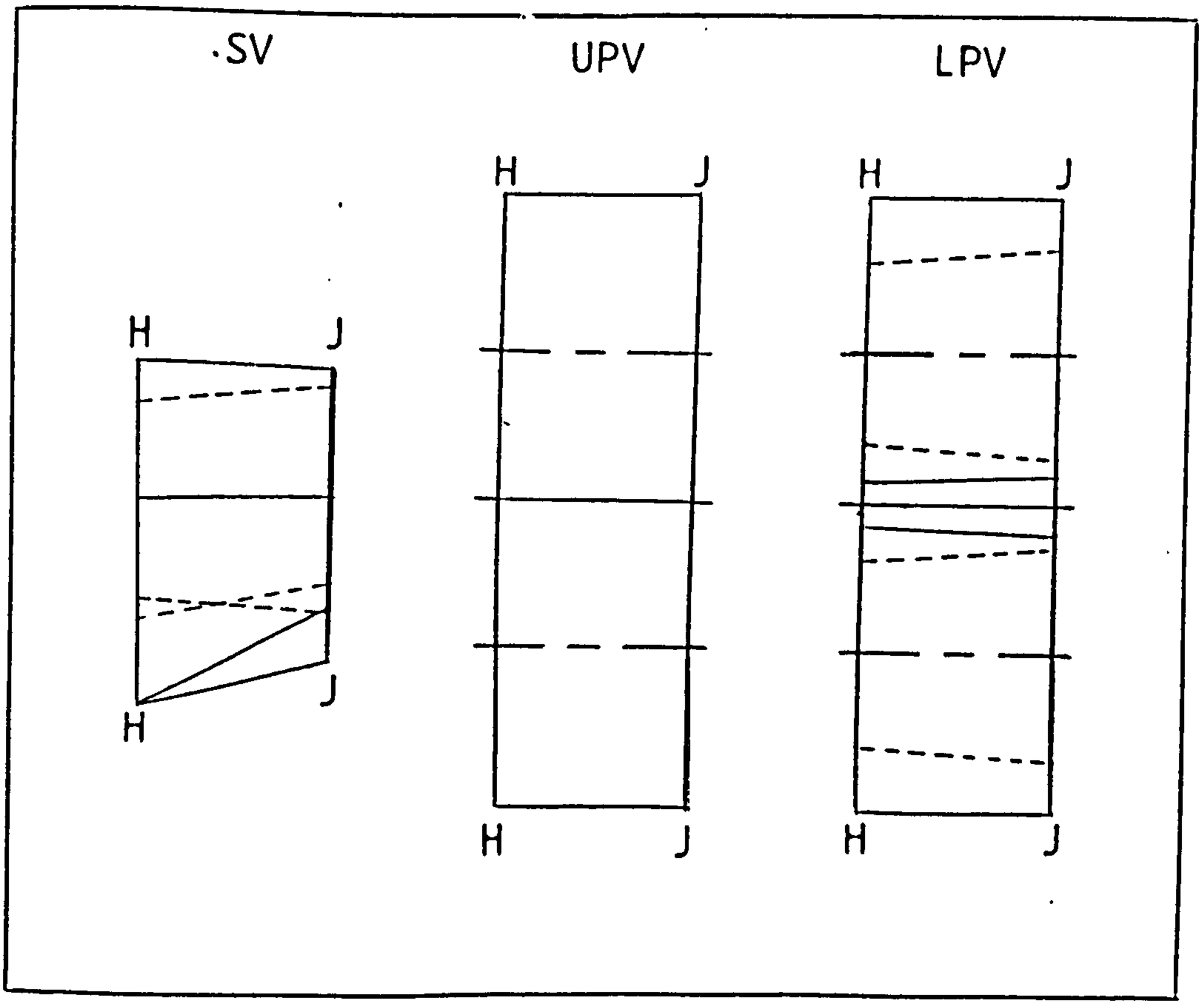

FIG. D.19 FUSELAGE GEOMETRY - SECTION H-J

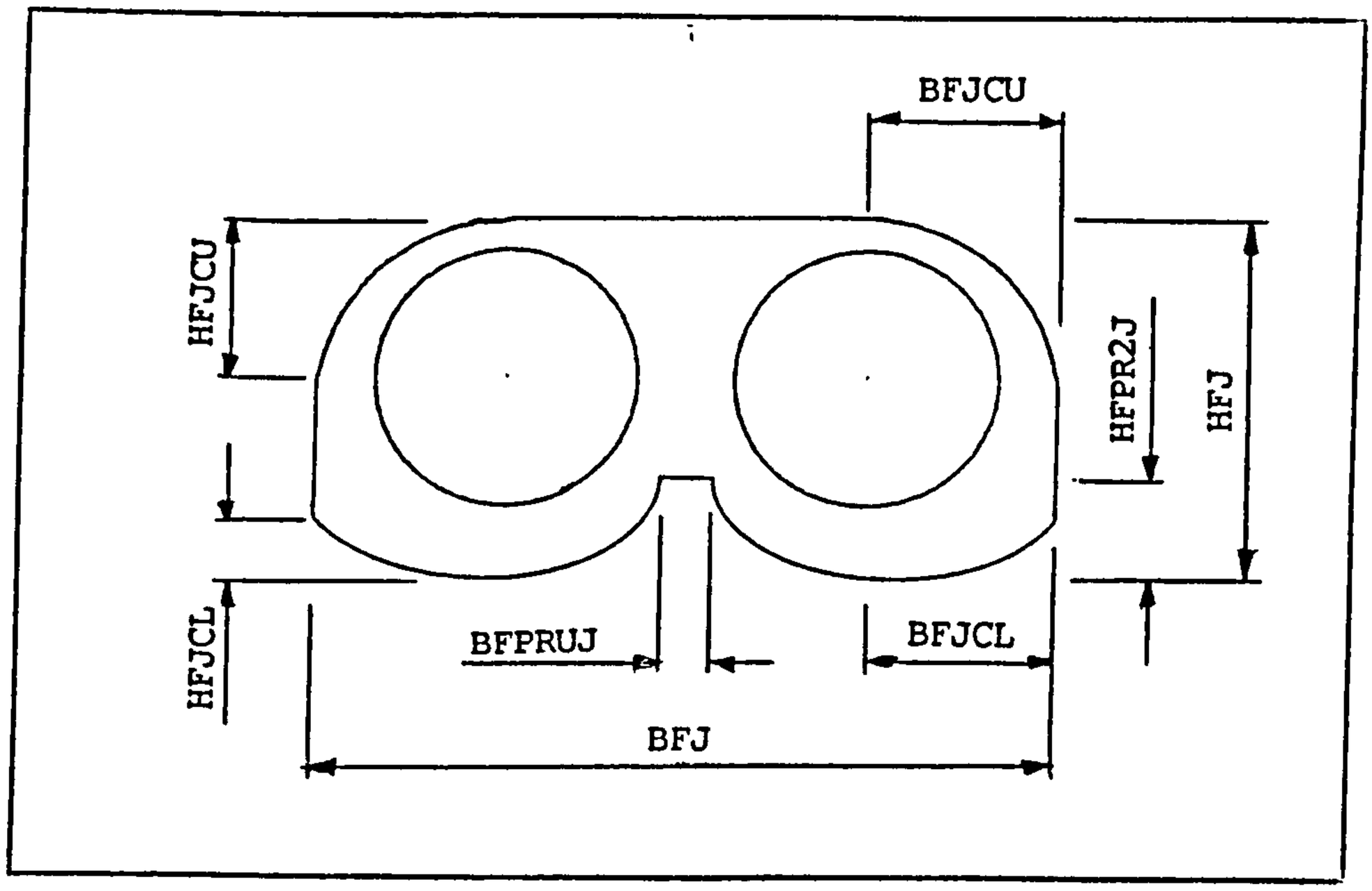

FIG. D.20 FUSELAGE GEOMETRY - STATION J

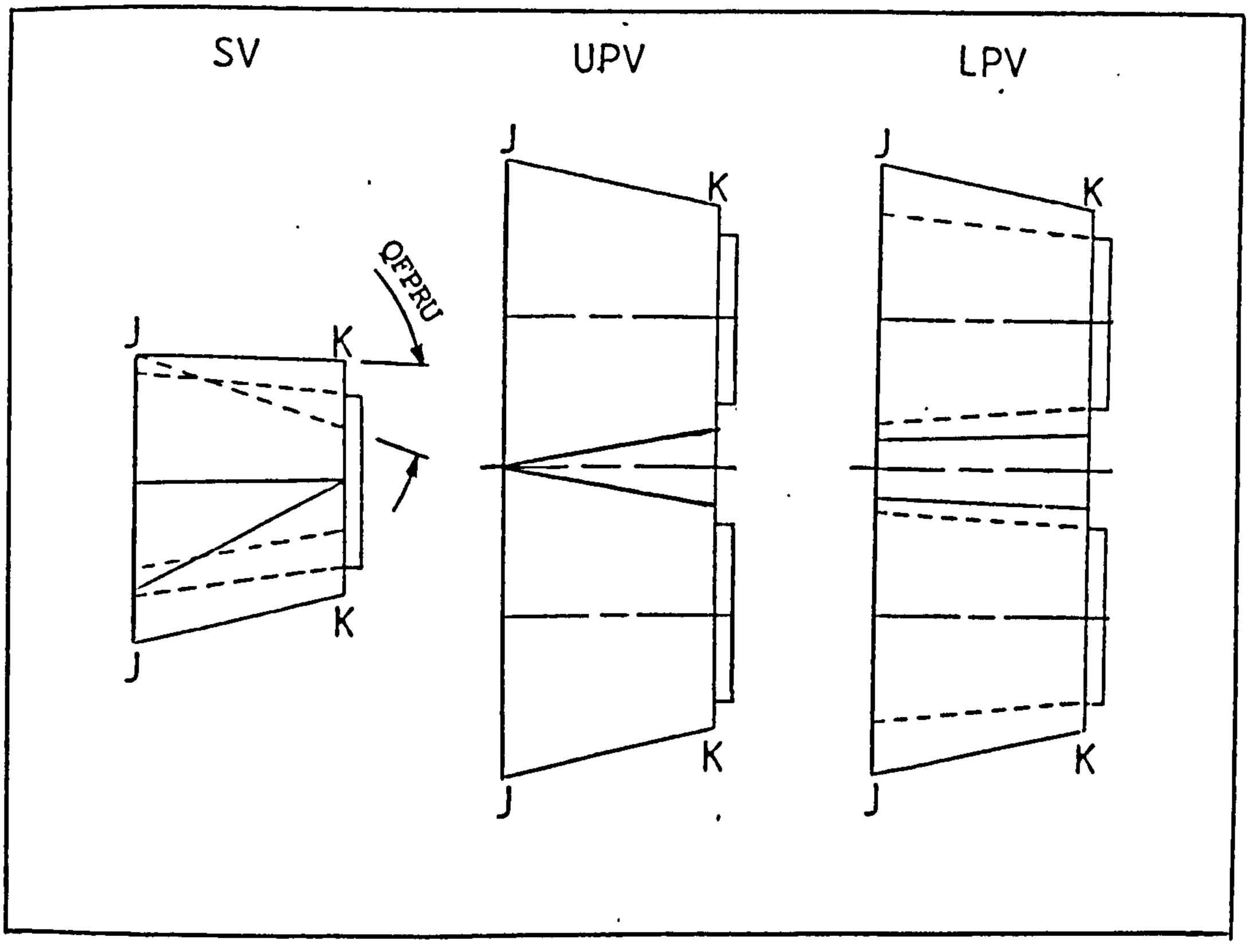

FIG. D.21 FUSELAGE GEOMETRY - SECTION J-K

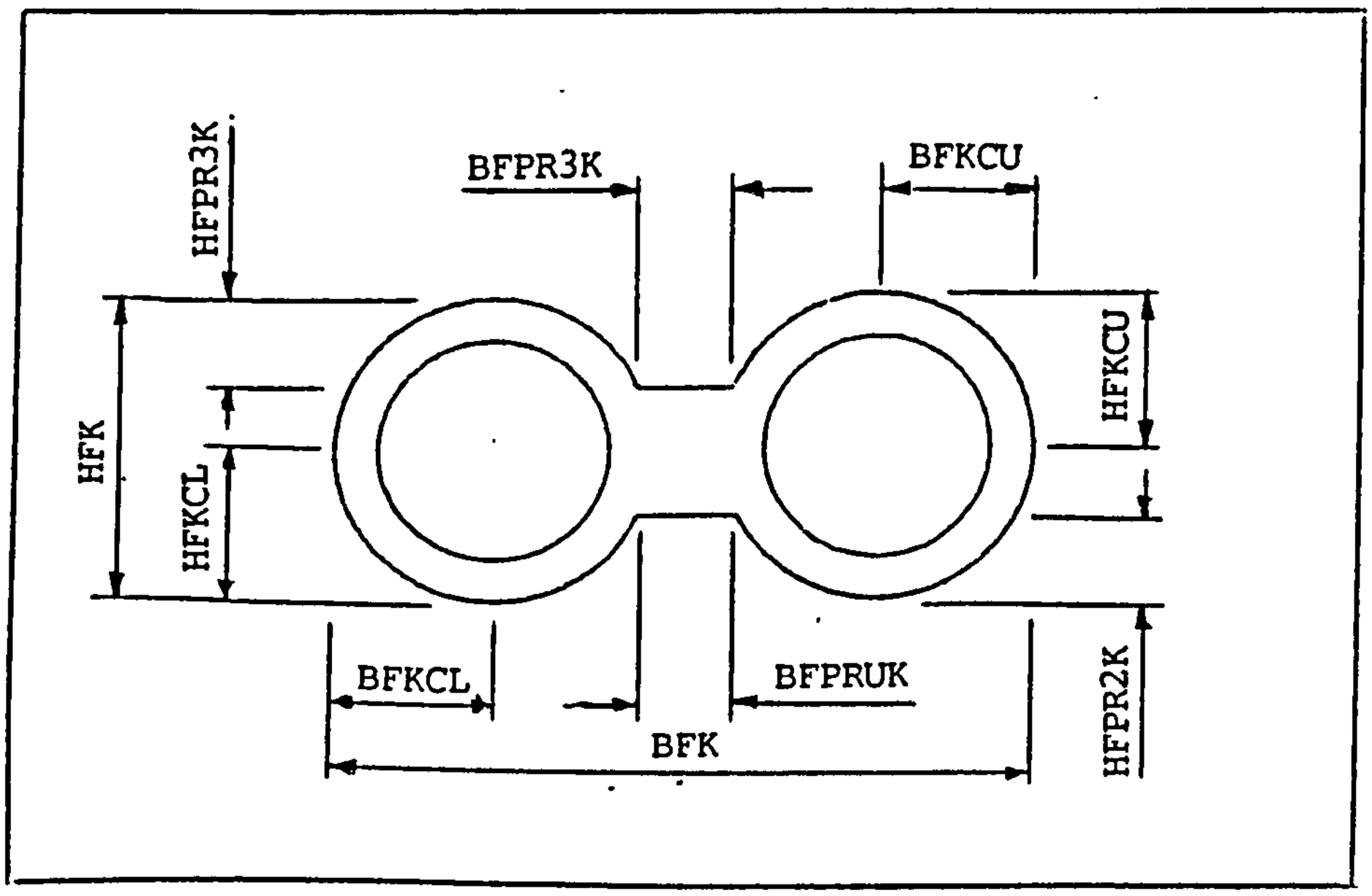

FIG. D.22 FUSELAGE GEOMETRY - STATION K

LIST OF GEOMETRIC CONSTRAINTS INCORPORATED IN THE SYNTHESIS

No.	Definition	Module
1	If BII > YCCANC+EYFC , BII = YCCANC+EYFC	INLET
2	ZPC = HUMB+0.5*(DP1+EHP1)	INTDIFG
3	YPCH=0.5*EBP3+DP3+EYPCH	INTDIFG
4	If XII < X < XD , HIDX=HII	INTDIFG
5	If XII < X < XE , BIDX=BII	INTDIFG
6	If (XP1-DP1) < X < XP1 , BIDX=DP1 , HIDX=DP1	INTDIFG
7	If XII < X < XD , RIDX=RIDX1	INTDIFG
8	0.0 < RLTMFN < 1.0	FAIRCUR1
9	0.0 < RLTFFN < 0.5	FAIRCUR1
10	0.0 < RLTCFN < 1.0	FAIRCUR1
11	0.5 < RLTAFN < 1.0	FAIRCUR1
12	BFDS = 2.0*BIDX+EBFD	FUSSTND
13	BFBS = 2.0*YCWSCB	FUSSTNB
14	YFABXS = YCWSCX (largest) $= 0.5*BFA + \left(\frac{YCWSCB-0.5*BFA}{XB-XA}\right) * (X-XA)$	FSECTAB
15	$YFBCXS = 0.5*BFB + \left(\frac{BII-0.5*BFB}{XC-XB}\right) * (X-XB)$	FSECTBC
16	BFCS = 2.0*BII	FUSSTNC
17	$YFCDXS = 0.5*BFC + \left(\frac{0.5*(BFD-BFC)}{XD-XC}\right) * (X-XC)$	FSECTCD
18	BFES = BFD	FUSSTNE
19	YFDEXS = 0.5*BFD	FSECTDE
20	BFFS = 2.0*(YIDOX+EYFEF)	FUSSTNF
21	YFFGXS = YIDOX+EYFFG	FSECTFG
22	YFEFXS = YIDOX+EYFEF	FSECTEF
23	BFGS = 2.0*(YIDOX+EYFFG)	FUSSTNG

```
24 | If XG < X < XP1 ,                                                          | FSECTGH
   |                                        EBFD-0.5*EBP1                       |
   | YFGHXS=YIDOX+0.5*[EBFD-(--------------)*(X-XG)]                            |
   |                                           DP1                              |
   |                                                                            |
   | If XP1 < X < XH ,                                                          |
   |                                                                            |
   | YFGHXS = 0.5*(YPCH+DP12X)+0.25*EBP12X                                      |
   |                                                                            |
   |                  -1    ZPC                                                 |
25 | QFPRH = tan    (-------)                                                   | FSECTGH
   |                  LPG+DP1                                                   |
   |                                                                            |
26 | BFHS = YPCH+DP2+0.5*EBP2                                                   | FUSSTNH
   |                                                                            |
27 | YFHJXS = 0.5*(YPCH+DP23X)+0.25*EBP23X                                      | FSECTHJ
   |                                                                            |
28 | BFJS = YPCH+DP3+0.5*EBP3                                                   | FUSSTNJ
   |                                                                            |
   |                          0.5*(BFJ-YPCH-DP4-0.5*EBP4)                       |
29 | YFJKXS=0.5*BFJ-(-------------------------------)*                          | FSECTJK
   |                                LFJK                                        |
   |          (X-XJ)                                                            |
   |                                                                            |
30 | BFKS = YPCH+DP4+0.5*EBP4                                                   | FUSSTNK
   |                                                                            |
   |                  HC5+HFA1-HRA-2.0*EHRA                                     |
31 | XAH = XFR+(-----------------------)                                        | LENGTH
   |                  2.0*tan(0.5*QCEYE)                                        |
   |                                                                            |
32 | If XD < XC+1.25*LVG , XD=XC+1.25*LVG                                       | LENGTH
   |                                                                            |
33 | XFNS = XD+LMUF1+LMUF3+LP23+LP34                                            | LENGTH
   |  l   = XD+LMUF2+LMUF3+LP23+LP34                                            |
   |  a   = XD+LMUF1+LMUF4+ELMUFA+LP23+LP34                                     |
   |  r   = XD+LMUF2+LMUF4+ELMUFA+LP23+LP34                                     |
   |  g   = XC+EXUNBF+LUNB+LGC+LMUF3+LP23+LP34                                  |
   |  e   = XC+EXUNBF+LUNB+LGC+LMUF4+ELMUFA+LP23                                |
   |  s     +LP34                                                               |
   |  t   = XC+RIDLS*HII+LPG                                                    |
   |                                                                            |
34 | If XII+1.25*LVG > XD , XII = XD-1.25*LVG                                   | LENGTH
   |                                                                            |
35 | If XII < XC , XII = XC+0.01                                                | LENGTH
   |                                                                            |
36 | If XUNBF+LUNLB < XD , EXUNBF = XD-LUNLB-XII                                | LENGTH
   |                                                                            |
37 | XFS = XD+LMUF1          |                                                  | LENGTH
   |     = XD+LMUF2          | (largest)                                        |
   |     = XUNBF+LUNB+LGC    |                                                  |
   |     = XE                -                                                  |
   |                                                                            |
   |                         -                                                  |
38 | XFH = XH-LMUF3          |                                                  | LENGTH
   |     = XH-LMUF4-ELMUFA   | (least)                                          |
   |     = XG                -                                                  |
   |                                                                            |
   |                                                                            |
39 | XMUF1S = XD , XMUF1H = XFH-LMUF1                                           | LENGTH
   | XMUF2S = XD , XMUF2H = XFH-LMUF2                                           |
   | XMUF3S = XF , XMUF3H = XH-LMUF3                                            |
   | XMUF4S = XF , XMUF4H = XH-LMUF4-ELMUFA                                     |
```

```
    | XGFS = XUNBF+LUNB , XGFH = XFH-LGC                              |
    |                                                                 |
 40 | XCCQMS = XD , XCCQMH = XE                                       | LENGTH
```

FIG. D.23 LIST OF GEOMETRIC CONSTRAINTS

CRANFIELD INSTITUTE OF TECHNOLOGY

COLLEGE OF AERONAUTICS

AEROSPACE VEHICLE DESIGN

PhD Thesis

1985 - 87

V. C. SERGHIDES

DESIGN SYNTHESIS
FOR
CANARD-DELTA COMBAT AIRCRAFT

Supervisor: Dr. J.P. Fielding

December 1987

Volume II

APPENDIX E

FLYING SURFACE GEOMETRY

E.1 INTRODUCTION

Presented in this appendix are the modules comprising the mathematical models which define in detail the geometry of the flying surfaces of the aircraft.

E.2 NET WING (Module NWINGG)

The net wing geometry is determined following the estimation of the dimensions of the gross-wing and fuselage. This module determines in detail the geometric characteristics of the net-wing, including the wing-box, ailerons, t.e.flaps, leading and trailing edge sections and fuel tanks. A diagram of the net wing is shown in fig.E.1.

The span of the net wing (BWN) is determined by considering an appropriate mean value for the span of the centre-section of the wing-box (BWBB).

$$BWBB = 0.5 * (BFE + BFH) \tag{E.1}$$

hence,

$$BWN = BW - BWBB \tag{E.2}$$

The root-chord of the net wing (CWCB) is,

$$CWCB = CWCC * \left(1.0 - \frac{BWBB}{BW}\right) * (1.0 - UW) \tag{E.3}$$

The taper ratio of the net wing (UWCN) is,

$$UWCN = \frac{CWCT}{CWCB} \tag{E.4}$$

and the mean chord (CWMN) is,

$$CWMN = 0.5 * (CWCB + CWCT) \qquad (E.5)$$

The net wing area (SWN) and aspect ratio (AWN) is,

$$SWN = CWMN * BWN \qquad (E.6)$$

and $$AWN = \frac{BWN}{CWMN} \qquad (E.7)$$

The chord of the wing-box at the wing root (CWBB) is,

$$CWBB = CWCB * (FCWR - FCWD) \qquad (E.8)$$

where, FCWR = Rear spar position, expressed as a fraction of the local wing-chord.

FCWD = Front spar position, expressed as a fraction of the local wing-chord.

Both FCWR and FCWD are independent variables. Similarly, the tip-chord of the wing-box (CWBT) is,

$$CWBT = CWCT * (FCWR - FCWD) \qquad (E.9)$$

The sweep angle of the wing-box centreline (QWB) is,

$$QWB = \tan^{-1}\left[\tan(QWL) - \left(\frac{CWCC}{BW}\right) * (FCWR - FCWD) * (1.0 - UW)\right] \text{ (rads)} \qquad (E.10)$$

The taper ratio of the wing-box (UWB) is,

$$UWB = \frac{CWBT}{CWBB} \qquad (E.11)$$

The total planform area of the wing-box (SWB) is

$$SWB = 0.5 * CWBB * (BW + BWBB + UWB * BWN) \qquad (E.12)$$

The aspect ratio of the gross wing-box (AWB) is,

$$AWB = \frac{BW^{2.0}}{SWB} \qquad (E.13)$$

The height of the centre section of the wing-box (HWBB) is,

$$HWBB = RTW * CWCB \qquad (E.14)$$

The total span of the ailerons (BWA) is,

$$BWA = FBWA * BW \qquad (E.15)$$

where, FBWA = Total fractional span of the ailerons.
FBWA is an external variable

The mean chord of each aileron (CWA) is,

$$CWA = \frac{0.5 * BWA}{AWA} \qquad (E.16)$$

where, AWA = Aspect ratio of each aileron
AWA is an external variable

The total planform area of the ailerons (SWA) is,

$$SWA = CWA * BWA \qquad (E.17)$$

The wing-chord at the midspan position of each aileron (CWCA2) is,

$$CWCA2 = CWCC * [UW + 0.5 * FBWA * (1.0 - UW)] \qquad (E.18)$$

The aileron leading-edge sweep angle (QWA) is,

$$QWA = \tan^{-1} [\tan (QWL) - 2.0 * \left(\frac{CWCC}{BW * CWCA2}\right) * (CWCA2 - CWA) * (1.0 - UW)] \quad \text{(rads)} \qquad (E.19)$$

The gross span of the trailing-edge flaps (BWF) is,

$$BWF = FBWF * BW \qquad (E.20)$$

where, FBWF = Fractional gross span of the t.e.flaps
FBWF is an independent variable.

The wing-chord at the outboard end of each t.e flap (CWCCT) is,

$$CWCCT = CWCC * [1.0 - FBWF * (1.0- UW)] \qquad (E.21)$$

The mean chord of each t.e. flap (CWFM) is,

$$CWFM = 0.5 * \{CWCC * [1.0 - \left(\frac{BFI}{BW}\right) * (1.0 - UW)] + CWCCT\} * (1.0 - FCWR - FCWTHL) \qquad (E.22)$$

where, FCWTHL = Distance of the leading edge of the t.e. flaps aft of the rear span, expressed as a fraction of the local wing-chord.

FCWTHL is an external variable

The total planform area of the t.e. flaps (SWF) is,

SWF = CWFM * (BWF - BFJ) (E.23)

The planform area of the fixed section of the leading-edge of the wing (SWLF) is,

SWLF = FCWLFT * SWN (E.24)

where, FCWLFT = Chord of the fixed leading-edge forward of front spar as a fraction of the local wing-chord

The planform area of any leading edge devices (retracted) (SWLH) is,

SWLH = (FCWD - FCWLHT) * SWN (E.25)

where, FCWLHT = Distance of the trailing-edge of the leading-edge device forward of the front spar expressed as a fraction of the local wing-chord.

FCWLHT is an external variable

The total planform area of the leading-edge of the wing (SWL) is,

SWL = FCWD * SWN (E.26)

The total planform area of the trailing edge of the wing (SWTG) is,

SWTG = (1.0 - FCWR) * SWN (E.27)

The planform area of the fixed section of the wing trailing-edge aft of the rear spar (SWTF) is,

$$SWTF = SWTG - SWA - SWF \qquad (E.28)$$

The longitudinal cross-sectional area of the centre section of the wing-box (OWBB) is,

$$OWBB = 0.34641 * HWBB * CWCB * [5.0 * (FCWR^{1.5} - FCWD^{1.5}) - 3.0 * (FCWR^{2.5} - FCWD^{2.5})] \qquad (E.29)$$

therefore its volume (VWBB) is,

$$VWBB = OWBB * BWBB \qquad (E.30)$$

The volume available for fuel storage in the centre section of the wing-box (VWBCF) is,

$$VWBCF = UWBCF * VWBB \qquad (E.31)$$

where, UWBCF = Volume utilization factor of the centre section of the wing-box for fuel storage

UWBCF is an independent variable

The span of wing-box fuel tanks external to the fuselage (BWNF) is,

$$BWNF = FBWNF * BWN \qquad (E.32)$$

where, FBWNF = Fractional span of the net wing-box containing fuel tanks

FBWNF is an independent variable

The taper ratio of the wing-box fuel tank external to the fuselage (UWCNF) is,

$$UWCNF = 1.0 - \left[\left(\frac{BWNF}{BWN}\right) * (1.0 - UWCN)\right] \qquad (E.33)$$

The fuel volume in wing-box external to the fuselage (VWBEF) is,

$$VWBEF = UWBEF * OWBB * \left(\frac{BWNF}{3.0}\right) * (1.0 + UWCNF + UWCNF^{2.0}) \qquad (E.34)$$

The fractional span of the wing-box containing fuel tanks (FBWCF) is,

$$FBWCF = \frac{BWNF + BWBB}{BW} \qquad (E.35)$$

The total planform area of the wing-box containing fuel tanks (SWBF) is,

$$SWBF = SWB - 0.5 * BW * CWCB * (1.0 - FBWCF) * (FCWR - FCWD) * \left[1.0 + UWCN - \left(\frac{BWNF}{BWN}\right) * (1.0 - UWCN)\right] \qquad (E.36)$$

The total volume of the net wing is estimated using the following expression from ref.

$$VWC = 0.23094 * RTW * CWCB^{2.0} * BWN * (1.0 + UWCN + UWCN^{2.0}) \qquad (E.37)$$

The distance of the leading-edge of the wing at the root from the aircraft nose (XWLB) is,

$$XWLB = XWAPEX + \left[\frac{(CWCC - CWCB) * BW}{2.0 * (CWCC - CWCT)}\right] * \tan(QWL) \qquad (E.38)$$

E.3 NET FOREPLANE (Module NFOREPG)

The net foreplane size is determined by this module together with all its geometric characteristics. A diagram of the foreplane is shown in fig.E.2.

The foreplane moment arm (LCCQM) is first estimated from the previously determined longitudinal positions of the mean 0.25 chord points of the wing and foreplane hence,

$$LCCQM = XWCQM - XCCQM \qquad (E.39)$$

The foreplane volume coefficient (RCSW) is an external variable, an appropriate value of which is specified in the input data. Therefore the net foreplane area (SCN) may be determined from the following expression:

$$SCN = \frac{RCSW * SW * CVMA}{LCCQM} \qquad (E.40)$$

The span of the net foreplane (BCN) is,

$$BCN = (SCN * ACN)^{0.5} \qquad (E.41)$$

where, ACN = Net foreplane aspect ratio
ACN is an external variable

The root-chord(CCB) is,

$$CCB = \frac{2.0 * BCN}{ACN * (1.0 + UCN)} \qquad (E.42)$$

The tip-chord (CCCT) is,

$$CCCT = UCN * CCB \qquad (E.43)$$

where, UCN = Net foreplane taper ratio
UCN is an external variable

The mean geometric chord of the net foreplane (CCMGN) is,

$$CCMGN = 0.5 * CCB * (1.0 + UCN) \qquad (E.44)$$

and the mean aerodynamic chord of the net foreplane (CCMAN) is,

$$CCMAN = \left(\frac{2.0}{3.0}\right) * CCB * \left[UCN + \left(\frac{1.0}{1.0 + UCN}\right)\right] \qquad (E.45)$$

The 0.25 - chord sweep angle of the foreplane (QC4) is,

$$QC4 = \tan^{-1}\left[\tan(QCL) - \left(\frac{0.5 * CCB}{BCN}\right) * (1.0 - UCN)\right] \quad \text{(rads)} \qquad (E.46)$$

The mid-chord sweep angle (QC2) is,

$$QC2 = \tan^{-1}\left[\tan(QC4) - \left(\frac{0.5 * CCB}{BCN}\right) * (1.0 - UCN)\right] \quad \text{(rads)} \qquad (E.47)$$

Finally, the trailing-edge sweep angle (QCT) is,

$$QCT = \tan^{-1}\left\{\frac{2.0 * [CCB - CCT - 0.5 * BCN * \tan(QCL)]}{BCN}\right\} \quad \text{(rads)} \qquad (E.48)$$

The total volume of the net foreplane (VCC) is,

$$VCC = 0.23094 * RTC * CCB^{2.0} * BCN * (1.0 + UCN + UCN^{2.0}) \qquad (E.49)$$

E.4 GROSS FOREPLANE (Module GFOREPG)

The geometric characteristics of the gross foreplane are determined as shown below using the results of module NFOREPG. Refer to the foreplane diagram in fig.E.2.

The span of the gross foreplane (BC) is first estimated by considering an approximate mean value for the local fuselage width, hence,

$$BC = BCN + 0.5 * (BFD + BFE) \qquad (E.50)$$

The centreline chord of the foreplane (CCCC) is,

$$CCCC = CCB + 0.5 * (BFD + BFE) * [\tan (QCL) - \tan (QCT)] \qquad (E.51)$$

The taper ratio of the gross foreplane (UC) is,

$$UC = \frac{CCCT}{CCCC} \qquad (E.52)$$

The gross foreplane area (SC) is,

$$SC = 0.5 * BC * (CCCC + CCCT) \qquad (E.53)$$

The aspect ratio of the gross foreplane (AC) is,

$$AC = \frac{BC^{2.0}}{SC} \qquad (E.54)$$

The mean geometric chord (CCMG) is,

$$CCMG = 0.5 * CCCC * (1.0 + UC) \qquad (E.55)$$

The mean aerodynamic chord (CCMA) is,

$$CCMA = \left(\frac{2.0}{3.0}\right) * CCCC * \left[UC + \frac{1.0}{1.0 + UC}\right] \qquad (E.56)$$

The distance of the gross foreplane apex from the aircraft nose (XCAPEX) is,

$$XCAPEX = XCCQM - 0.25 * CCMAN - \left[\frac{(CCB - CCMAN)*BCN}{2.0 *(CCB - CCCT)}\right] * \tan(QCL) - 0.5 * (BC - BCN) * \tan(QCL) \qquad (E.57)$$

The distance of the leading edge of the nett foreplane root from the aircraft nose (XCLB) is also estimated in this module by substituting the above determined value for XCAPEX, in the following expression:

$$XCLB = XCAPEX + \left[\frac{(CCCC - CCB) * BC}{2.0 * (CCCC - CCCT)}\right] * \tan(QCL) \qquad (E.58)$$

E.5 FIN(S) (Module FING)

According to the baseline configuration assumptions the aircraft may have either single or twin fins. An external variable (NFIN) is used to specify the number of fins (1 or 2) in the input data. This variable is incorporated in the appropriate mathematical expressions of module FING which sizes each fin and determines its geometric characteristics from the given values of five more external variables. These are the aspect ratio (AEFN), taper ratio (UEFN), leading-edge sweep (QEFL), thickness/chord ratio (RTEF) and volume coefficient (REFFC) of the fin(s).

A diagram of a fin is shown in fig.E.3.

The distance of the mean 0.25-chord point of the fin from its trailing-edge, measured at the fin root is,

$$\left[\frac{SEFN^{0.5} * AEFN^{0.5}}{3.0 *(1.0 + UEFN)}\right] * \left[\frac{(5.0 + 5.0 * UEFN - UEFN^{2.0})}{AEFN * (1.0 + UEFN)} - (1.0 + 2.0 * UEFN) * \tan(QEFL)\right] \quad (E.59)$$

It is assumed that the trailing-edge of the fin, always intersects the fuselage at X = XJ. Therefore the fin moment arm (LEFCQM) which is measured between the mean 0.25-chord points of the wing and fin, is,

$$LEFCQM = XJ - XWCQM - [\text{Above expression}] \quad (E.60)$$

Also, from the definition of the fin volume coefficient,

$$LEFCQM = \frac{REFFC * SW * BW}{NFIN * SEFN} \quad (E.61)$$

where, SEFN = Net area of each fin.

By combining the above two expressions, LEFCQM is eliminated and hence an equation is obtained in which the only unknown, is SEFN. The required SEFN value is then estimated iteratively using the Newton-Raphson method.

The net fin span (BEFN) is,

$$BEFN = (SEFN * AEFN)^{0.5} \quad (E.62)$$

The root-chord (CEFB) is,

$$CEFB = \frac{2.0 * BEFN}{AEFN * (1.0 + UEFN)} \quad (E.63)$$

The fin moment arm is,

$$LEFCQM = \frac{REFFC * SW * BW}{NFIN * SEFN} \qquad (E.64)$$

The fin tip-chord (CEFCT) is,

$$CEFCT = UEFN * CEFB \qquad (E.65)$$

The mean geometric chord (CEFMG) is,

$$CEFMG = 0.5 * CEFB * (1.0 + UEFN) \qquad (E.66)$$

The mean aerodynamic chord (CEFMA) is,

$$CEFMA = \left(\frac{2.0}{3.0}\right) * CEFB * \left[UEFN + \left(\frac{1.0}{1.0 + UEFN}\right)\right] \qquad (E.67)$$

The 0.25-chord sweep angle of the fin (QEF4) is,

$$QEF4 = \tan^{-1}\left[\tan (QEFL) - \left(\frac{0.25 * CEFB}{BEFN}\right) * (1.0 - UEFN)\right] \quad (rads) \qquad (E.68)$$

The mid-chord sweep angle (QEF2) is,

$$QEF2 = \tan^{-1}\left[\tan (QEF4) - \left(\frac{0.25 * CEFB}{BEFN}\right) * (1.0 - UEFN)\right] \quad (rads) \qquad (E.69)$$

The trailing-edge sweep angle of the fin (QEFT) is,

$$QEFT = -\tan^{-1}\left[\frac{CEFB - CEFCT - BEFN * \tan (QEFL)}{BEFN}\right] \quad (rads) \qquad (E.70)$$

Finally, the volume of each fin (VEFC) is,

$$VEFC = 0.23094 * RTEF * CEFB^{2.0} * BEFN * (1.0 + UEFN + UEFN^{2.0}) \qquad (E.71)$$

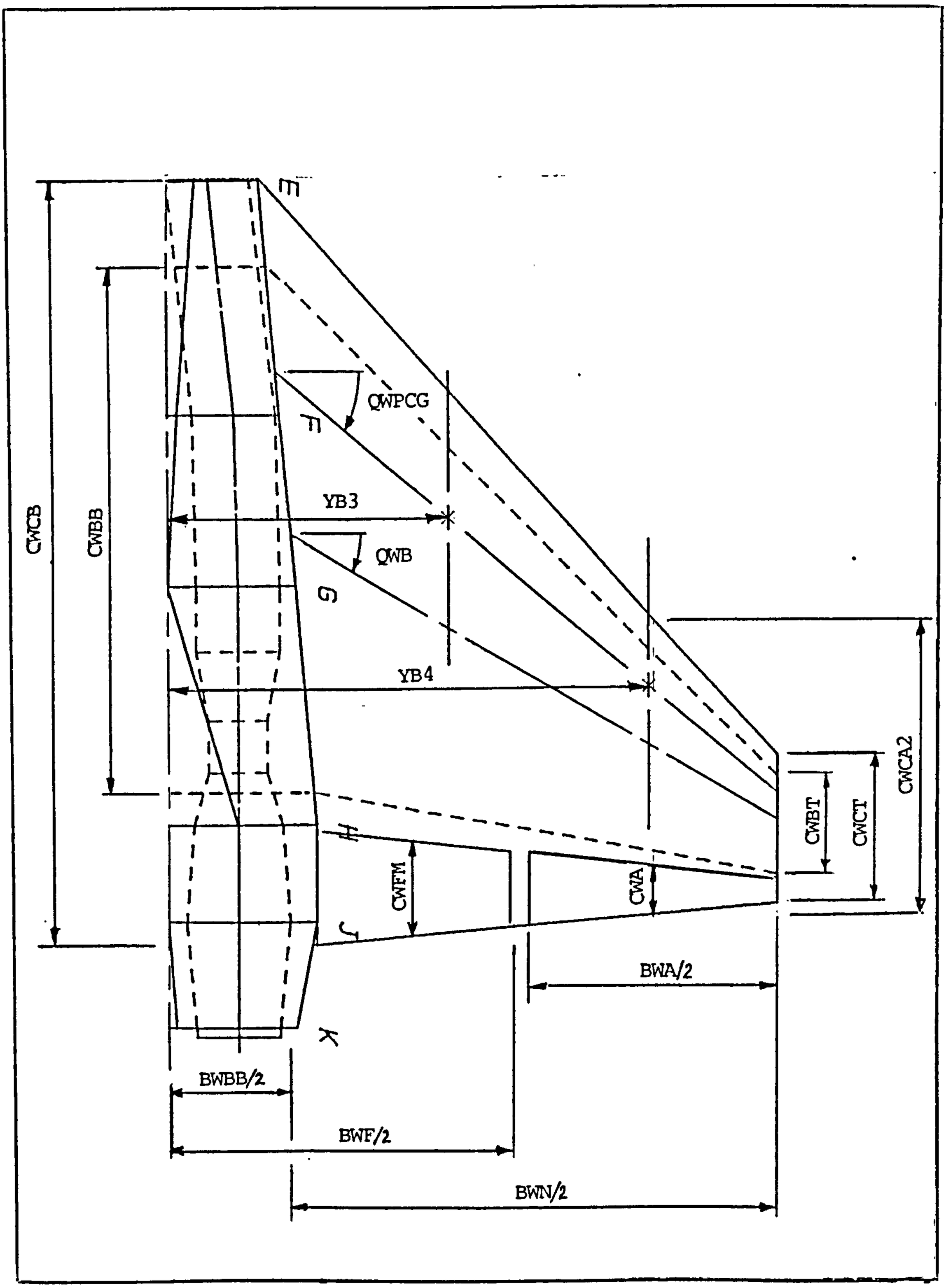

FIG. E.1 NET WING GEOMETRY

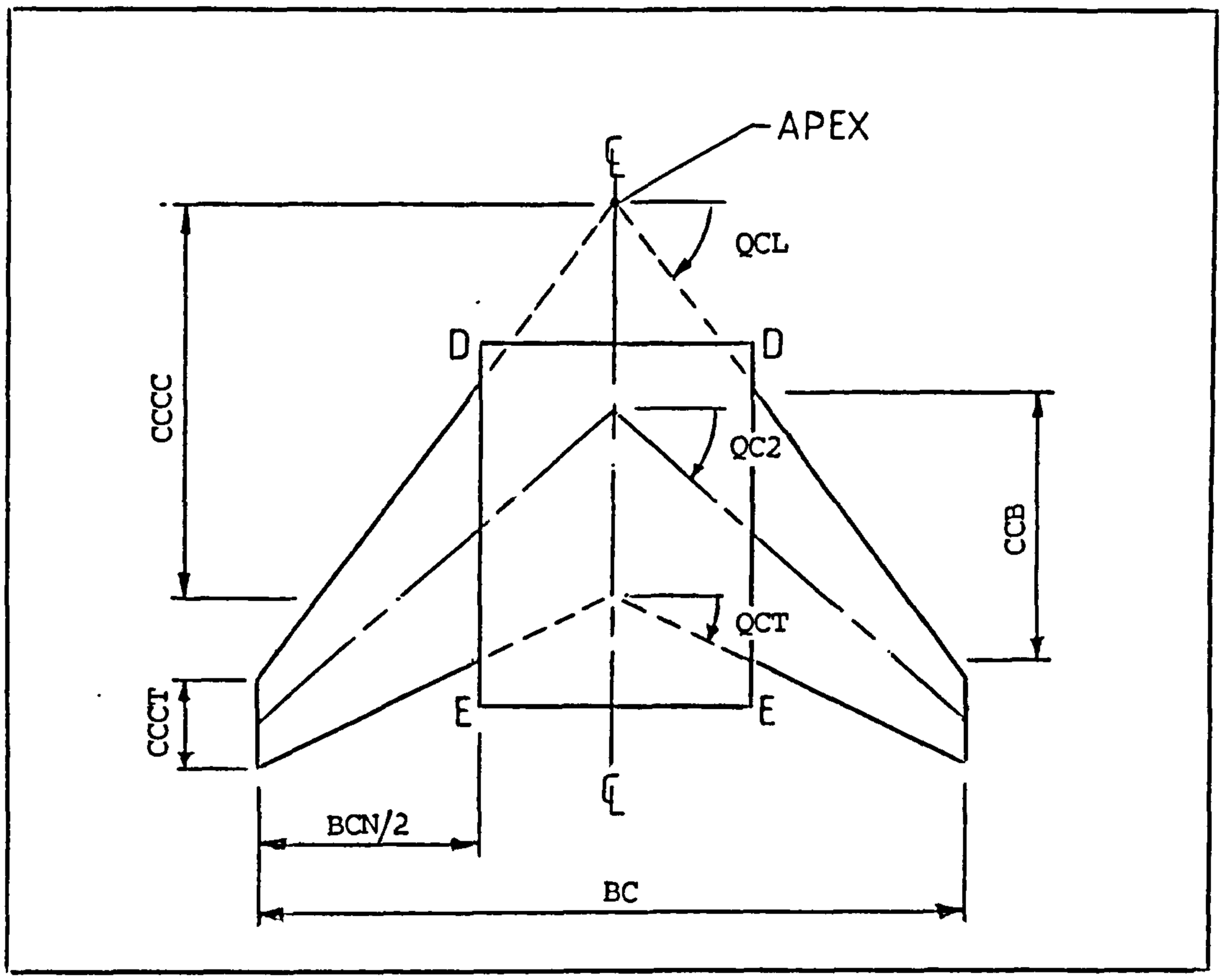

FIG. E.2 FOREPLANE GEOMETRY

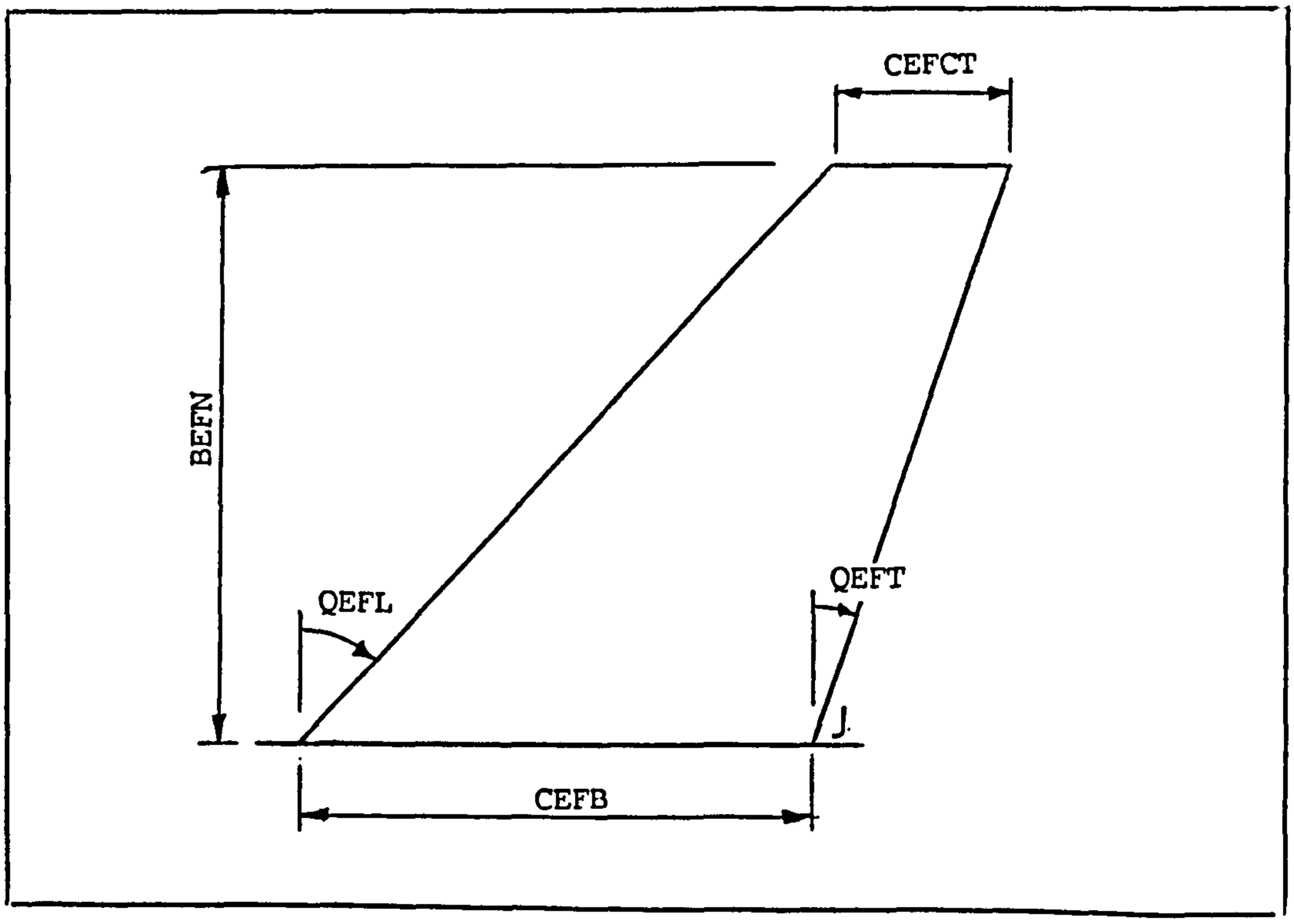

FIG. E.3 FIN GEOMETRY

APPENDIX F

PACKAGING

F.1 INTRODUCTION

Five separate modules are presented in this appendix. These include detailed methods for the prediction of the aircraft mass (module MASSPR), volume accounting (module VOLACC), the estimation of the longitudinal moment arms (modules MOMARM & STORSTN) and the forward and aft centre of gravity limits of the aircraft (module CG). In these packaging modules, the aircraft is divided into major systems and components which are initially considered individually. The separate results are then appropriately added together to produce the required aircraft estimates.

The modules and equations used, are explained in the following sections in the order in which they are executed during the Design Synthesis.

F.2 AIRCRAFT MASS PREDICTION (Module MASSPR)

F.2.1 General

The aircraft mass prediction module is based on a collection of empirical methods from refs. 1, 2, 4 . The module is divided into several groups of equations. Each group refers to a main aircraft system or part, the mass of which is predicted from its physical characteristics, the mass of its constituent components and a number of empirical constants.

The mass prediction methods for the airframe, are applicable to both metal and composite structures. Special factors were added by the author to some equations, to reflect any mass variations due to the introduction of state-of-the-art in the design of particular components.

The overall aircraft mass is the sum of the estimated contributions from each group.

The mass prediction equations for each group are presented and explained in detail, below.

F.2.2 Internal Fuel

It is assumed that fuel is stored internally in the wing-box and fuselage sections D-E, E-F, and F-G only. The wing-box fuel volume (VWBCF & VWBEF) is obtained from module NWINGG. The volume of fuel inside sections D-E, E-F and F-G, is specified by means of volume utilization factors (UFIFDE, UFIFEF and UFIFFG) which are used as independent variables in the following equations:

$$VFIFDE = VFIF1 * UFIFDE \quad (F.1)$$

$$VFIFEF = VFIF2 * UFIFEF \quad (F.2)$$

$$VFIFFG = VFIF3 * UFIFFG \quad (F.3)$$

where, VFIFDE, VFIFEF and VFIFFG denote the fuel volume inside sections D-E, E-F and F-G respectively, excluding the fuel stored in the centre-section of the wing-box.

VFIF1, VFIF2 and VFIF3 denote the volume available for fuel storage in sections D-E, E-F and F-G respectively, when the corresponding intake diffuser volume is subtracted. These are estimated earlier in the fuselage geometry appendix.

The total internal fuel volume (VTGFI) therefore is,

$$VTGFI = VFIFDE + VFIFEF + VFIFFG + VWBEF + VWBCF \quad (F.4)$$

The total volume of fuel stored inside the fuselage, excluding any fuel stored inside the centre-section of the wing-box (VFIF) is,

$$VFIF = VFIFDE + VFIFEF + VFIFFG \qquad (F.5)$$

The total volume of fuel stored inside the fuselage (VFGF) is,

$$VFGF = VTGFI - VWBEF \qquad (F.6)$$

Having determined the internal fuel volume in each aircraft section, it is now possible to predict the corresponding fuel mass components, by considering the fuel density (RFUL) which is an external variable hence,

$$MWBEF = RFUL * VWBEF \qquad (F.7)$$
$$MWBCF = RFUL * VWBCF \qquad (F.8)$$
$$MFIFDE = RFUL * VFIFDE \qquad (F.9)$$
$$MFIFEF = RFUL * VFIFEF \qquad (F.10)$$
$$MFIFFG = RFUL * VFIFFG \qquad (F.11)$$
$$MFIF = RFUL * VFIF \qquad (F.12)$$
$$MFGF = RFUL * VFGF \qquad (F.13)$$

The total internal fuel mass (MTGFI) is,

$$MTGFI = RFUL * VTGFI \qquad (F.14)$$

The mass of oil and unused fuel (MTOUF) is,

$$MTOUF = 0.005 * MTTR \qquad (F.15)$$

At this stage, the reference landing mass (MTLR) may be defined as,

$$MTLR = MTTR - (1.0 - RMTLFI) * MTGFI \qquad (F.16)$$

where, RMTLFI = Mass proportion of total internal fuel, remaining in tanks on landing.

F.2.3 Undercarriage

The total main u/c mass (MUM) is predicted with the following empirically derived equation:

$$MUM = (FMUMK * MTLR + MUMK) * FMUM \qquad (F.17)$$

Similarly, the nose u/c mass (MUN) is,

$$MUN = (FMUNK * MTLR + MUNK) * FMUN \qquad (F.18)$$

where, FMUMK, FMUNK = Empirical constant factors.
MUMK, MUNK = Empirical constants
FMUM, FMUN = State-of-the-art mass factors

All the above variables are external and specified in the input data.

The mass of u/c associated hydraulics (MUH) is,

$$MUH = FMUHK * MTLR + MUHK \qquad (F.19)$$

where, FMUHK = Empirical constant factor
MUHK = Empirical constant

These are also external variables.

The mass of the nose u/c and its associated hydraulics (MUNG) is,

$$MUNG = MUN * \left[1.0 + \left(\frac{MUH}{MUN + MUM}\right)\right] \qquad (F.20)$$

Therefore the total mass of the main u/c and its associated hydraulics (MUMG) is,

$$MUMG = MUM + MUN + MUH - MUNG \qquad (F.21)$$

F.2.4 Propulsion System

The total propulsion system mass (MPG) is made up of four components. These are, MPB, MPR, MPT and MPI and they are scaled from a mass breakdown of a reference engine.

Since the propulsion system of the aircraft consists of two engines (NENG = 2) the above mass components as determined by the following empirical equations, represent the total values for both engines.

The gas generator mass (MPB) is,

$$MPB = NENG * (FMPBK * RTP + 1.0 - FMPBK) * MPBR \qquad (F.22)$$

The reheat system mass (MPR) is,

$$MPR = NENG * MPRR * RTP^{FMPRK} \qquad (F.23)$$

The thrust reverser mass (MPT) is,

$$MPT = NENG * MPTR * RTP \qquad (F.24)$$

The engine installation mass (MPI) is,

$$MPI = FMPIK * (MPB + MPR + MPT) \qquad (F.25)$$

In the above equations, MPBR, MPRR and MPTR are the datum engine values of MPB, MPR and MPT respectively, while, FMPBK, FMPRK and FMPIK are empirical constant factors. These

are all external variables and their values are defined in the input data.

The total propulsion system mass is therefore,

MPG = MPB + MPR + MPT + MPI (F.26)

F.2.5 Air Systems

The mass of the air systems (MSA), i.e., air-conditioning and avionics cooling systems, is,

MSA = MSAK + FMSAK * MTTR (F.27)

where, MSAK = Empirical constant
FMSAK = Empirical constant factor

The mass of the air systems ducts (MSD) is,

MSD = MSA * (1.0 - FMSA) (F.28)

where, FMSA = Mass proportion of air systems parts, other than ducts.

FMSA, FMSAK and MSAK are external variables.

F.2.6 Electrical System

The mass of the electrical system (MSE), i.e., generation and distribution, is,

MSE = MSEK + FMSEK * MTTR (F.29)

where, MSEK = Empirical constant
FMSEK = Empirical constant factor

Both MSEK and FMSEK are external variables

F.2.7 Flying Controls

The mass of the flying controls (MSC) is,

$$MSC = (MSCK + FMSCK * MTTR) * FMSC \qquad (F.30)$$

where, MSCK = Empirical constant
FMSCK = Empirical constant factor
FMSC = State-of-the-art mass factor

FMSC is adjusted to reflect mass variations due to the adoption of Fly-by-Wire or Fly-by-Light technology.

MSCK, FMSCK and FMSC are also external variables.

F.2.8 Fuel System

The fuel system mass (MSF) is,

$$MSF = FMSFK * MTGFI \qquad (F.31)$$

where, FMSFK = Empirical constant factor
FMSFK is an external variable

F.2.9 Fuselage

The mass prediction method for the fuselage was developed by British Aerospace.

The method starts with the prediction of the mass of the fuselage shell (MFX).

$$MFX = FMF2 * (WFG - WCWSC - WCCAN) * \left[0.07232 * (VD - 180.0)^{0.5} + \left(\frac{0.0000002602 * XFN * ULTN * TPGD^{0.5}}{BFJ + HFDH}\right) + 3.7\right] \quad (F.32)$$

WFG, WCWSC, WCCAN, XFN, TPGD, BFJ and HFDH are all estimated in previous modules.
FMF2, VD and ULTN however are external variables.

where, FMF2 = Mass factor for the fuselage structural materials
VD = Maximum design diving speed (m/s)
ULTN = Ultimate load factor for structural design (= 1.5 * proof factor)

The mass of the internal fuselage structure (MFW) is,

$$MFW = FMF2 * VFG * \left[0.000005906 * (VD * AMMX)^{2.0} + 13.0 + \left(\frac{0.018575 * ULTN * XFN}{CWBB^{2.0}}\right) + \left(\frac{0.01002 * ULTN}{HFDH}\right) * (1000.0 * |VFGF|)^{0.5}\right] \quad (F.33)$$

VFG, VFGF and CWBB are estimated in previous modules.

AMMX = Maximum design Mach number for the structure.
AMMX is an external variable.

The mass of the windscreen (MCW) is,

$$MCW = WCWSC * [0.0011475 * VD^{2.0} * \sin^2(QCWSC) + 5.83] \quad (F.34)$$

and the mass of the canopy (MCC) is,

$$MCC = WCCAN * (0.00011818 * VD^{2.0} + 10.74) \qquad (F.35)$$

WCWSC and WCCAN are both estimated in previous modules

Assuming that the airbrake(s) total planform area is SFAIB, then the airbrake mass (MFAIB) is,

$$MFAIB = 27.82 * FMF2 * SFAIB \qquad (F.36)$$

SFAIB is an external variable.

The mass of the intake ramps (MFIR) is,

$$MFIR = FMFIR * [0.038 * (MFX + MFW)] \qquad (F.37)$$

where, FMFIR = State-of-the-art mass factor.

The fuselage paint mass (MFXP) is,

$$MFXP = 0.5 * (WFG - WFG3 - WCWSC - WCCAN) \qquad (F.38)$$

The mass of miscellaneous structural items on the fuselage (EMFG), e.g. arrester and catapult gear on naval aircraft is,

$$EMFG = (FMF1 - 1.0) * (MFX + MFW + MCW + MCC + MFAIB + MFIR) \qquad (F.39)$$

where, FMF1 = Materials mass factor for fuselage miscellania.

Finally, the total mass of the fuselage structure (MFG) is given by the sum of all the above componet masses.

$$MFG = EMFG + MFX + MFW + MCW + MCC + MFAIB + MFIR + MFXP \quad (F.40)$$

F.2.10 Wing

The wing mass prediction method was also developed by British Aerospace.

In this method it is assumed that the most extreme loading case occurs when the fuel in the fuselage is unused and no fuel remains in the wing. It is also assumed that no relief loads are present on the wing.

The first step is the prediction of the total mass of the wing-box (MWB). This demands prior estimation of the stressing mass for the wing (MTCR), the spanwise position of the centre of pressure of the net (YCPX) and gross (YCPG) wing and hence the wing bending moment (BMS). These are given by the following expressions:

$$MTCR = MTTR - MWBEF - MTPR \quad (F.41)$$

where, MTPR = Reference load for the definition of stressing mass.

MTPR is an external variable

$$YCPX = 0.42 + 0.001 * AWN * [(4.4 + 5.0 * UWCN) * \tan(QW4) + 10.4 * UWCN^{0.5} - 6.7] \quad (F.42)$$

$$YCPG = 0.42 + 0.001 * AW * [(4.4 + 5.0 * UW) * \tan(QW4) + 10.4 * UW^{0.5} - 6.7] \quad (F.43)$$

Substituting the above results in the following expression for the bending moment,

$$BMS = 0.25 * YCPX * BWN * MTCR * ULTN * \left\{1.0 - 0.5 * \left(\frac{BWBB}{BW}\right) * \right.$$

$$\left[1.28 - 6.35 * (YCPG - 0.425) + 1.28 * \right.$$

$$\left(1.0 - \frac{BWBB^{2.0}}{BW^{2.0}}\right)^{0.5} + \left[14.13 * \left(\frac{BWBB}{BW}\right) - 6.35\right] *$$

$$\left.\left.(YCPG - 0.425)\right]\right\} \qquad \text{(N.m)} \qquad \text{(F.44)}$$

The mass per unit area of the wing-box structure is divided into eight terms (TERM1B, TERM2B, TERM3B, TERM4B, TERM5B, TERM6B, TERM7B and TERM8B) which are defined below:

$$TERM1B = \frac{0.0000889 * BMS}{CWBB * DE1 * \cos^2(QWB)} \qquad \text{(kg/m}^2\text{)} \qquad \text{(F.45)}$$

where, DE1 = Depth of the wing-box at the body side

$$DE1 = \left[\frac{RTW * CWCB * [1.25 - 0.462 * (FCWD + FCWR)]}{RTW * CWCB}\right]\left(\begin{matrix}\text{the}\\ \text{lesser}\end{matrix}\right) \qquad \text{(F.46)}$$

$$TERM2B = 0.82 * \left[\frac{AWB}{AW * \cos(QWB)}\right]^{2.0} * FK^{0.25} \quad (Kg/m^2) \quad (F.47)$$

where, FK = Bending moment factor

$$FK = \left[\frac{1.0}{\frac{BMS}{59500.0 * CWBB * DE1 * \cos(QWB)}}\right]\begin{pmatrix}\text{the}\\\text{greater}\end{pmatrix} \quad (F.48)$$

$$TERM3B = \frac{6.82 * (1.0 - UWB)^{2.0}}{\cos^2(QWB) * FK^{0.25}} \quad (Kg/m^2) \quad (F.49)$$

$$TERM4B = 0.00007063 * \left(\frac{AWB}{AW}\right)^{0.5} * VD^{2.0} * \cos^2(QWB) \quad (kg/m^2) \quad (F.50)$$

$$TERM5B = 25.98 * [0.5 * (DE1 + DE6)]^{1.5} * \sec^2(QWB) \quad (kg/m^2) \quad (F.51)$$

where, DE6 = Maximum depth of the wing-box at the tip.

$$DE6 = \left[\frac{RTW * CWCT * [1.25 - 0.462 * (FCWD + FCWR)]}{RTW * CWCT}\right]\begin{pmatrix}\text{the}\\\text{lesser}\end{pmatrix} \quad (F.52)$$

$$TERM6B = 0.522 * AMMX^{2.0} \quad (kg/m^2) \quad (F.53)$$

$$TERM7B = \frac{8.2 * FBWCF * SWBF}{SWB * FK} \quad (kg/m^2) \quad (F.54)$$

$$TERM8B = 0.00002785 * VD^{2.0} * \left(\frac{NWP}{FK}\right)^{0.25} \quad (kg/m^2) \quad (F.55)$$

where, NWP = Number of wing pylons
NWP is an external variable

The total mass of the wing box, is,

$$MWB = FMWB * SWB * FMWBH * (TERM1B + TERM2B + TERM3B + TERM4B + TERM5B + TERM6B + TERM7B + TERM8B) \quad (F.56)$$

where, FMWB = Mass factor which allows for changes in the structural materials used for the wing-box.
FMWB is an external variable
FMWBH = Factor which corrects the estimates of MWB for thin wings of moderate to high aspect ratio

In order to determine the value of FMWBH a reference aspect ratio (AWR) is defined for the wing, according to its thickness/chord ratio as shown below.

If RTW $\geq$ 0.033 then,

$$AWR = 14.29 * (RTW - 0.033)^{0.5} + 2.0 \quad (F.57)$$

Otherwise, AWR = 2.0 (F.58)

If AW > AWR then,

$$FMWBH = 1.0 + 0.3 * \left(\frac{AW}{AWR} - 1.0\right)^{1.2} \quad (F.59)$$

Otherwise, FMWBH = 1.0 (F.60)

The next step is the prediction of the total mass of the wing leading-edge (MWL). This includes both fixed and moving parts. The value of MWL per unit area is divided

into four terms (TERM1L, TERM2L, TERM3L and TERM4L) which are defined below.

$$TERM1L = 0.522 * \left(\frac{ULTN}{SW}\right) * MTCR * \left(\frac{SWL * RTW}{BWN}\right)^{2.0} \quad (kg/m^2) \quad (F.61)$$

$$TERM2L = 0.00007285 * \left(\frac{ULTN * MTCR}{SW * RTW}\right) * \left(\frac{SWL}{BWN}\right)^{0.125} \quad (kg/m^2) \quad (F.62)$$

$$TERM3L = 0.000056 * VD^{2.0} \quad (Kg/m^2) \quad (F.63)$$

$$TERM4L = 1.536 * BWN^{0.75} \quad (kg/m^2) \quad (F.64)$$

Therefore the total mass of the wing leading edge is,

$$MWL = FMWL * (SWLF + SWLH) * (TERM1L + TERM2L + TERM3L + TERM4L) \quad (F.65)$$

where, FMWL = Mass factor which allows for changes in the structural materials used for the wing leading-edge.

FMWL is an external variable

The mass per unit area of the fixed section of the trailing edge of the wing is divided into three terms (TERM1T, TERM2T and TERM3T) which are defined below.

$$TERM1T = 1.482 * \left(\frac{ULTN * MTCR}{SW}\right)^{0.25} * \left(\frac{SWTG}{BWN}\right)^{0.5} \quad (kg/m^2) \quad (F.66)$$

$$TERM2T = \left(\frac{0.0030223 * ULTN * MTCR * SWTG}{SW * BWN * DTE^{0.5}}\right) * \left[\left(\frac{SWTG}{BWN}\right) - \left(\frac{SWA + SWF}{BWA + BWF - BWBB}\right)\right]^{2.0} \quad (kg/m^2) \quad (F.67)$$

where, DTE = Average depth of rear spar

$$DTE = 1.54 * \left(\frac{SWTG * RTW}{BWN}\right) \qquad (F.68)$$

$$TERM3T = 0.646 * \left(\frac{SWTG}{SWTF}\right)^{2.0} * DTE^{0.5} \qquad (kg/m^2) \quad (F.69)$$

Hence, the total mass of the fixed section of the trailing edge of the wing (MWT) is,

$$MWT = FMWT * SWTF * (TERM1T + TERM2T + TERM3T) \qquad (F.70)$$

where, FMWT = Mass factor which allows for changes in the structural materials used for the wing trailing-edge

FMWT is an external variable

The mass per unit area of the trailing edge flaps, is divided into two terms (TERM1F and TERM2F) which are defined below:

$$TERM1F = 0.151 * \left(\frac{MTCR}{SW}\right) * \sin^2(EQWFH) * DF^{0.5} * SWF^{0.125} \qquad (kg/m^2) \quad (F.71)$$

where, EQWFH = Maximum trailing-edge flap deflection, expressed in **radians.**

EQWFH is an external variable

DF = Flap thickness function

$$DF = 1.54 * RTW * CWFM \qquad (F.72)$$

$$TERM2F = 0.384 * CWFM * \left(\frac{SWF^{0.5}}{DF}\right) \quad (kg/m^{2}) \quad (F.73)$$

Therefore, the total mass of the trailing-edge flaps (MWT) is,

$$MWF = FMWT * SWF * (TERM1F + TERM2F) \quad (F.74)$$

The mass of the flap tracks (MWFK) is,

$$MWFK = NWFK * \left[0.000323 * ULTN * MTCR * \left(\frac{SWF}{SW}\right) * LWFK^{2.0} * CWFM^{2.0} + 0.91\right] \quad (F.75)$$

where, NWFK = Number of flap tracks
LWFK = Length of the flaps tracks as a fraction of the wing-chord
NWFK and LWFK are both external variables

The total mass of the ailerons (MWA) is,

$$MWA = FMWT * SWA * \left[\frac{0.00009795 * VD^{2.0}}{AWA^{0.125}} + \frac{14.14 * CWA * \cos^{2}(QWA)}{CWCA2^{0.5}}\right] \quad (F.76)$$

The total mass of the miscellaneous attachments (MWCX) is,

$$MWCX = 0.0235 * (MWB + MWL + MWT + MWF + MWA) + 18.14 \quad (F.77)$$

The paint mass (MWXP) is,

$$MWXP = 0.341 * SWN \quad (F.78)$$

The mass of miscellaneous fairings (MWXF) is,

$$MWXF = 0.488 * SWN \qquad (F.79)$$

Finally the total mass of the wing (MWC) is the sum of the estimated masses of all the above wing components, hence,

$$MWC = MWB + MWL + MWT + MWF + MWA + MWFK + MWXP + MWXF + MWCX \qquad (F.80)$$

F.2.11 Foreplane

The existing close structural similarity between a foreplane and a tailpane allows the following empirical equation for a tailplane, from ref.] , to be used for the prediction of the mass of the foreplane structure (MC).

$$MC = FMC * MC1K * SCN * \left(\frac{VD^{MC2K}}{LCCQM^{MC3K}}\right) \qquad (F.81)$$

where, FMC = Mass factor which allows for changes in the structural materials used for the foreplane
MC1K, MC2K and MC3K are empirical constants.
All the above variables are external.

The foreplane paint mass (MCXP) is,

$$MCXP = 0.341 * SCN \qquad (F.82)$$

The total foreplane mass (MCG) is therefore,

$$MCG = MC + MCXP \qquad (F.83)$$

F.2.12 Fin(s)

The mass of a single fin structure (MEF) is obtained by an empirical relationship from ref.1 . Hence, for NFIN = 1,

$$MEF = FMEF * \left[\frac{MEF1K * SEFN^{MEF2K} * VD^{MEF3K}}{\left(\frac{LEFCQM}{XFN}\right)^{MEF4K}} \right] \qquad (F.84)$$

where, FMEF = Mass factor which allows for changes in the structural materials used for the fin(s)
MEF1K, MEF2K and MEF3K are empirical constants
All the above variables are external

When twin fins are used, extra fuselage structure is needed in order to support the two separate fins. This leads to a mass increase which is not considered in the above equation. For this reason the author appropriately modified the original single-fin equation into a twin-fin version, shown below,

i.e. for NFIN = 2

$$MEF = 2.0 * FMEF2 * FMEF * \left[\frac{MEF1K * SEFN^{MEF2K} * VD^{MEF3K}}{\left(\frac{LEFCQM}{XFN}\right)^{MEF4K}} \right] \qquad (F.85)$$

where, MEF = Total mass of fin structure
FMEF2 = Twin-fin mass factor
FMEF2 is also an external variable

The total mass of fin paint (MEFXP) is,

$$MEFXP = 0.341 * SEFN * NFIN \qquad (F.86)$$

Hence, the total mass of the fin(s) (MEFC) is,

$$MEFC = MEF + MEFXP \qquad (F.87)$$

F.2.13 External Fuel

According to the baseline assumptions, the aircraft may carry a maximum of two external fuel tanks on the inboard wing pylons.

The fuel mass in tanks no. 1 and 2 is specified by the external variables MXTF1 and MXTF2 respectively. Consequently, the corresponding external tank volumes VXT1 and VXT2 are,

$$VXT1 = \frac{MXTF1}{RFUL} \quad \text{and} \quad VXT2 = \frac{MXTF2}{RFUL} \qquad (F.88)$$

According to ref. 2 , the empty mass of each of these external tanks, is

$$MXT1 = VXT1 * 100.0 \text{ and } MXT2 = VXT2 * 100.0 \qquad (F.89)$$

Hence, the total empty mass of the external tanks (MXT) is,

$$MXT = MXT1 + MXT2 \qquad (F.90)$$

and the total external fuel mass (MXTF) is,

$$MXTF = MXTF1 + MXTF2 \qquad (F.91)$$

F.2.14 Cockpit

The total mass of cockpit equipment (MCI) receives contributions from the flight (MCFI), powerplant (MCPI) and miscellaneous (MCMI) instruments, cockpit furnishings (MCFURN), ejection seat (MCSEAT), armour protection (MCARM) and miscellaneous equipment (MCMISC).

The masses, MCFURN, MCARM and MCMISC are predicted using the following empirical expressions:

$$MCFURN = 90.0 * NCP \qquad (F.92)$$

where, NCP = Number of crew (=1 for this synthesis)

$$MCARM = 0.005 * MTTR \qquad (F.93)$$

$$MCMISC = 0.456 * 106.61 * \left(\frac{NCP * MTTR}{45600.0}\right)^{0.585} \qquad (F.94)$$

MCFI, MCPI, MCMI, MCSEAT are external variables and specified in the input data.

Therefore,

$$MCI = MCFI + MCPI + MCMI + MCSEAT + MCFURN + MCARM + MCMISC \qquad (F.95)$$

F.2.15 Stores

The baseline aircraft is assumed to have a maximum of four wing pylons (nos. 1-4), on which four sets of stores are carried. Each set of stores has a specified mass. (MB1, MB2, MB3 and MB4 respectively). The aircraft may also carry a maximum of four semi-submerged fuselage mounted missiles

of specified masses (MMUF1, MMUF2, MMUF3 and MMUF4). These are all external variables which are specified in the input data.

The total mass of stores carried on the aircraft (MTS) is therefore,

$$MTS = MB1 + MB2 + MB3 + MB4 + MMUF1 + MMUF2 + MMUF3 + MMUF4 \quad (F.96)$$

F.2.16 Payload

The payload of the aircraft (MTP) includes all the stores (MTS) the ammunition (MGA) and the pilot together with its personal equipment (MCP). Hence,

$$MTP = MCP + MGA + MTS \quad (F.97)$$

F.2.17 Fixed Role Equipment

The fixed role equipment mass (MTR) is,

$$MTR = MCI + MGC + MAR + MAX + MXP1 + MXP2 + MXP3 + MXP4 + MTOUF + MLMUF \quad (F.98)$$

where, MGC = Mass of the gun
MLMUF = Total mass of the missile launchers
MAR = Mass of the radar avionics
MAX = Mass of general avionics

MXP1, MXP2, MXP3, MXP4 = Mass of external wing pylon no. 1, 2, 3, 4 respectively.

F.2.18 Total Take-Off Mass

Finally, the total take-off mass of the aircraft (MTT) is,

$$MTT = MXTF + MTP + MTR + MPG + MCG + MEFC + MWC + MSA + MSE + MSC + MUM + MUN + MUH + MTGFI + MSF + MFG + MAPU \quad (F.99)$$

where, MAPU = Mass of the auxiliary power unit

MCP, MGA, MGC, MLMUF, MAR, MAX, MXP1, MXP2, MXP3, MXP4 and MAPU are external variables.

F.3 VOLUME ACCOUNTING (Module VOLACC)

The individual volumes of the systems and major components that are installed inside the fuselage, are estimated in this module from their predicted masses and specified densities. The volumes of the intake diffusers, engine bays, main and nose u/c bays, radome and internal fuel are known from previous modules. This leads to the prediction of the required fuselage volume to fully accomodate all the above systems and components.

The cockpit occupies only a part of sections A-B and B-C. Other equipment may be installed in the underfloor compartment and behind the rear cockpit bulkhead. An approximate estimate of the volume occupied by the cockpit (VCKPT) alone is given by the following simplified expression.

$$VCKPT = \underset{FVCKPT}{\left[VFAB + VFBC - \left(\frac{BFA + BFB + BFC}{3.0} \right) * (XC - XA) * HFA1 \right]} * \quad (F.100)$$

Where, FVCKPT = Cockpit volume factor

FVCKPT is an external variable that may provide a slight adjustment for the predicted cockpit volume, if necessary.

The volumes of the other fuselage systems and components are defined below in terms of their masses and densities.

Radar Avionics: $$VAR = \frac{MAR}{RAR} \quad \text{(F.101)}$$

General Avionics: $$VAX = \frac{MAX}{RAX} \quad \text{(F.102)}$$

Flight Controls: $$VSC = \frac{MSC}{RSC} \quad \text{(F.103)}$$

Electrical Systems: $$VSE = \frac{MSE}{RSE} \quad \text{(F.104)}$$

Air Systems: $$VSA = \frac{MSA}{RSA} \quad \text{(F.105)}$$

Fuel System: $$VSF = \frac{MSE}{RSF} \quad \text{(F.106)}$$

Gun: $$VGC = \frac{MGC}{RGC} \quad \text{(F.107)}$$

Ammunition: $$VGA = \frac{MGA}{RGA} \quad \text{(F.108)}$$

Missile Launchers: $$VLMUF = \frac{MLMUF}{RLMUF} \quad \text{(F.109)}$$

Auxiliary Power Unit: $$VAPU = \frac{MAPU}{RAPU} \quad \text{(F.110)}$$

Intake Ramps:

$$VFIR = \frac{MFIR}{RFIR} \qquad (F.111)$$

Air Brakes:

$$VFAIB = \frac{MFAIB}{RFAIB} \qquad (F.112)$$

Internal Fuselage Structure:

$$VFW = \frac{MFW}{RFW} \qquad (F.113)$$

where, RAR, RAX, RSC, RSE, RSA, RSF, RGC, RGA, RLMUF, RAPU, RFIR, RFAIB and RFW are the corresponding densities, which are external variables, specified in the input data in kg/m^3.

The required fuselage volume (VFCR) is,

$$VFCR = VCKPT + 2.0 * VIDC + 2.0 * VPBC + 2.0 * VUMB + VUNB + VFGF + VFR + VAR + VAX + VSC + VSE + VSA + VSF + VGC + VGA + VLMUF + VAPU + VFIR + VFAIB + VFW \qquad (F.114)$$

F.4 LONGITUDINAL MOMENT ARMS (Module MOMARM)

The longitudinal moment arms of all the aircraft systems, major components and fuel are determined in this module. These are measured from the aircraft nose and defined by mathematical expressions. The expressions for the flying surfaces, fuselage, powerplant, undercarriage and the fuel stored in the wing-box were obtained from ref.] . The rest of the moment arm expressions in this module were derived by the author and they are based, either on engineering judgement or on the guidelines set up in ref.2 , where it is assumed that fixed mass proportions of each system group are installed at specific points of the aircraft anatomy. These guidelines are the result of

averaging actual balance data for a broad spectrum of types of conventional aircraft.

F.4.1 Wing

The mass of the wing structure is assumed to act at the centre of volume of the wing, which is located at a distance RLWCC * CWMA aft of the mean quarter-chord points, where,

$$RLWCC = \left(\frac{1.0}{56.0}\right) * \left\{ 13.0 - \frac{\begin{array}{l}[27.0 * UW^{2.0} + 1.75 * AW * \\ (1.0 - UW^{2.0}) * (1.0 + 4.0 * UW + \\ UW^{2.0}) * \tan(QWL)]\end{array}}{(1.0 + UW + UW^{2.0})} \right\} \quad \text{(F.115)}$$

Therefore the longitudinal moment arm of the wing (XWCG) is,

$$XWCG = XWCQM + RLWCC * CWMA \quad \text{(F.116)}$$

F.4.2 Foreplane

The longitudinal moment arm of the foreplane (XCCG) is,

$$XCCG = XWCQM - LCCQM + \frac{CCB * (1.0 + UCN + UCN^{2.0})}{15.0 * (1.0 + UCN)} \quad \text{(F.117)}$$

F.4.3 Fin(s)

Similarly, the longitudinal moment arm of the fin(s) (XBFCG) is,

$$XEFCG = XWCQM + LEFCQM + \left[\frac{CEFB * (1.0 + UEFN + UEFN^{2.0})}{15.0 * (1.0 + UEFN)}\right] \quad (F.118)$$

F.4.4 Fuselage

The mass of the fuselage structure is assumed to act midway between the position of the centre of surface area (XFXM) and the centre of volume (XFWM) of the fuselage, to reflect the contributions of the shell and the internal structure respectively to the total fuselage mass. The exact values of XFXM and XFWM were determined in previous modules. Hence the longitudinal moment arm of the fuselage structure (XFCG) is,

$$XFCG = 0.5 * (XFXM + XFWM) \quad (F.119)$$

F.4.5 Propulsion System

The moment arms of the main sections of the propulsion system are determined separately, by assuming that the mass of each section acts midway along its length.

Hence, the longitudinal moment arm of the gas generator (XPBCG) is,

$$XPBCG = XP1 + 0.5 * LP12 \quad (F.120)$$

The longitudinal moment arm of the reheat section (XPRCG) is,

$$XPRCG = XP2 + 0.5 * LP24 \quad (F.121)$$

The longitudinal moment arm of the thrust reverser (XPTCG) is,

$$XPTCG = XP3 + 0.5 * LP34 \qquad (F.122)$$

Finally, the longitudinal moment arm of the engine installation (XPICG) is,

$$XPICG = XP1 + 0.5 * LPG \qquad (F.123)$$

F.4.6 Flight Controls

The mass of the flight controls is assumed to act at 75% of the wing mean aerodynamic chord, hence the longituidinal moment arm of the flight controls (XSCCG) is,

$$XSCCG = XWCQM + 0.5 * CWMA \qquad (F.124)$$

F.4.7 Electrical System

It is assumed that 50% of the mass of the electrical system acts midway along the fuselage length, 37.5% at the remote drives location and 12.5% at the middle of the cockpit floor. Hence, the longitudinal moment arm of the electrical system (XSECG) is,

$$XSECG = 0.25 * XFN + 0.375 * XP1 + 0.125 * (0.5 * LCFL + XA) \qquad (F.125)$$

F.4.8 Cockpit Equipment

It is assumed that the cockpit equipment mass, acts at the middle of the cockpit floor. Therefore the longitudinal moment arm of the cockpit equipment (XCICG) is,

$$XCICG = XA + 0.5 * LCFL \qquad (F.126)$$

F.4.9 Air Systems

It is assumed that 50% of the mass of the air services acts at the middle of fuselage section D-E (air cycle pack location), 25% of the mass halfway between the aft end of the cockpit and the engines and 25% at the front end of the cockpit. Hence, the longitudinal moment arm of the air systems (XSACG) is,

$$XSACG = 0.25 * (XD + XE) + 0.125 * (XC + XP1) + 0.25 * XA \qquad (F.127)$$

F.4.10 Radar Avionics

The mass of the radar avionics is assumed to act at the middle of fuselage section R-A. Therefore, the longitudinal moment arm of the radar avionics (XARCG) is,

$$XARCG = 0.5 * (XFR + XA) \qquad (F.128)$$

F.4.11 General Avionics

The mass of the general avionics is assumed to act at the middle of fuselage section C-D. Therefore, the longitudinal moment arm of the general avionics (XAXCG) is,

$$XAXCG = 0.5 * (XC + XD) \qquad (F.129)$$

F.4.12 Nose Undercarriage

The mass of the nose u/c is assumed to act midway along the nose u/c bay. Hence the longitudinal moment arm of the nose u/c (XUNCG) is,

$$XUNCG = XUNBF + 0.5 * LUNB \qquad (F.130)$$

F.4.13 Main Undercarriage

The mass of the main u/c is assumed to act at a point located at a distance RLUPCW * CWMA aft of the mean quarter-chord point of the wing.

where, RLUPCW = Fraction of CWMA

RLUPCW is an external variable which adjusts the position of the main u/c relative to the overall aircraft c.g.

The longitudinal moment arm of the main u/c (XUMCG) is,

$$XUMCG = XWCQM + RLUPCW * CWMA \qquad (F.131)$$

F.4.14 Gun

The mass of the gun is assumed to act at a point 75% along the gun length, hence the longitudinal moment arm of the gun (XGCG) is

$$XGCG = XGF + 0.75 * LGC \quad \text{(F.132)}$$

F.4.15 Ammunition

The mass of the ammunition is assumed to act at a point 90% along the gun length, where the ammunition belt feeds the gun. Therefore the longitudinal moment arm of the ammunition (XGACG) is,

$$XGACG = XGF + 0.9 * LGC \quad \text{(F.133)}$$

F.4.16 Crew

The mass of the pilot and its personal equipment acts at the Neutral Seat Reference Point. Therefore, the longitudinal moment arm of the crew (XCPCG) is,

$$XCPCG = XA + LCNSPR \quad \text{(F.134)}$$

F.4.17 Auxiliary Power Unit (APU)

This is assumed to be located just forward of the engines. Hence, the longitudinal moment arm of the APU (XAPUCG) is,

$$XAPUCG = 0.5 * (XP1 + XG) \quad \text{(F.135)}$$

F.4.18 Fuselage-Mounted Missiles

It is assumed that the mass of each of the four fuselage-mounted missiles, acts midway along its length. Therefore, the longitudinal arm of each missile is,

$$XM1CG = XMUF1 + 0.5 * LMUF1 \quad (F.136)$$

$$XM2CG = XMUF2 + 0.5 * LMUF2 \quad (F.137)$$

$$XM3CG = XMUF3 + 0.5 * LMUF3 \quad (F.138)$$

$$XM4CG = XMUF4 + 0.5 * LMUF4 \quad (F.139)$$

F.4.19 Missile Launchers

Four equal-size missile launchers are submerged into the fuselage. The longitudinal c.g position of each launcher is assumed to coincide with the longitudinal c.g. position of its corresponding missile. Therefore the longitudinal moment arm of all the missile launchers together, (XLMCG) is,

$$XLMCG = 0.25 * (XMUF1 + XMUF2 + XMUF3 + XMUF4) + 0.125 * (LMUF1 + LMUF2 + LMUF3 + LMUF4) \quad (F.140)$$

F.4.20 Internal Fuel

The longitudinal moment arm of the fuel stored in the centre-section of the wing-box (XWBCCG) is equal to the distance of the centre of volume of this section from the aircraft nose, hence,

$$XWBCCG = XWLB + CWCB * RLWBC2 \quad (F.141)$$

where,

$$RLWBC2 = \left(\frac{3.0}{7.0}\right) * \left[\frac{7.0 * (FCWR^{2.5} - FCWD^{2.5}) - 5.0 * (FCWR^{3.5} - FCWD^{3.5})}{5.0 * (FCWR^{1.5} - FCWD^{1.5}) - 3.0 * (FCWR^{2.5} - FCWD^{2.5})}\right] \quad (F.142)$$

The longitudinal moment arm of the fuel stored in the wing box external to the fuselage (XWBECG) is equal to the distance of the centre of volume of this wing-box section from the aircraft nose, hence,

$$XWBECG = XWLB + LWBEF \quad (F.143)$$

where,

$$LWBEF = \frac{[3.0 * CWCB * RLWBC2 * (1.0 + UWCNF) * (1.0 + UWCNF^{2.0}) + 0.5 * BWNF * \tan(QWL) * (1.0 + 2.0 * UWCNF + 3.0 * UWCNF^{2.0})]}{4.0 * (1.0 + UWCNF + UWCNF^{2.0})} \quad (F.144)$$

The longitudinal moment arm of the fuel stored in fuselage sections, D-E, E-F and F-G are:

$$XFIFDE = 0.5 * (XD + XE) \quad (F.145)$$

$$XFIFEF = 0.5 * (XE + XF) \quad (F.146)$$

$$XFIFFG = 0.5 * (XF + XG) \quad (F.147)$$

F.4.21 Fuel System

The mass of the fuel system is assumed to act at the centre of the internal fuel, at maximum capacity. Hence the longitudinal moment arm of the fuel system (XSFCG) is,

$$XSFCG = \frac{\begin{array}{l}[MFIFDE * XFIFDE + MFIFEF * XFIFEF + MFIFFG * \\ XFIFFG + MWBCF * (XWLB + CWCB * RLWBC2) + \\ MWBEF * (XWLB + LWBEF)]\end{array}}{MFIF + MWBCF + MWBEF}$$

(F.148)

F.5 WING STORE STATIONS (Module STORSTN)

According to the baseline aircraft assumptions there are four wing store stations (nos.1-4). The lateral and longitudinal c.g. positions of the stores at each of these stations are determined in this module by assuming that the c.g.'s of all stores located on the same side of the aircraft centreline, lie on a common imaginary aft-swept line, the position of which is defined as a fraction of the local wing-chord between the forward and rear spars. The longitudinal c.g. position and hence the moment arm of the stores at each station is automatically determined by specifying its lateral c.g. location, as a fraction of the net wing-span.

The expressions used in this module are presented below. These were derived with reference to fig.E.1.

The sweep angle of the imaginary c.g. line (QWPCG) is,

$$QWPCG = \tan^{-1}\left\{\left(\frac{2.0}{BW}\right) * \left[0.5 * BW * \tan(QWL) + (CWCT - CWCC) * [FCWD + (FCWR - FCWD) * FXWPCG]\right]\right\} \text{ (rads)} \quad \text{(F.149)}$$

where, FXWPCG = Fraction of the local wing-chord between the front and rear spars, defining the position of the imaginary c.g. line.

FXWPCG is an external variable

The lateral c.g. positions of the stores at stations no. 1 - 4, relative to the aircraft centreline are,

$$YB1 = 0.5 * (FYB1 * BWN + BWBB) \quad (F.150)$$

$$YB2 = 0.5 * (FYB2 * BWN + BWBB) \quad (F.151)$$

$$YB3 = 0.5 * (FYB3 * BWN + BWBB) \quad (F.152)$$

$$YB4 = 0.5 * (FYB4 * BWN + BWBB) \quad (F.153)$$

FYB1, FYB2, FYB3 and FYB4, are fractions of the net wing span, defining the lateral c.g. positions of the stores at stations no. 1 - 4.

The longitudinal moment arms of the stores at stations no. 1 - 4, measured from the aircraft nose are,

$$XB1CG = YB1 * \tan(QWPCG) + CWCC * [FCWD + (FCWR - FCWD) * FXWPCG] + XWAPEX \quad (F.154)$$

$$XB2CG = YB2 * \tan(QWPCG) + CWCC * [FCWD + (FCWR - FCWD) * FXWPCG] + XWAPEX \quad (F.155)$$

$$XB3CG = YB3 * \tan(QWPCG) + CWCC * [FCWD + (FCWR - FCWD) * FXWPCG] + XWAPEX \quad (F.156)$$

$$XB4CG = YB4 * \tan(QWPCG) + CWCC * [FCWD + (FCWR - FCWD) * FXWPCG] + XWAPEX \quad (F.157)$$

F.6 AIRCRAFT LONGITUDINAL CENTRE OF GRAVITY (Module CG)

The overall aircraft longitudinal c.g. position is estimated in this module for four different loading cases, using mass and moment arm information from the previous modules. The loading cases considered here, define the most forward and aft limits of the aircraft's c.g.

Case 1: Empty internal fuel tanks, no external stores, no ammunition

The total aircraft pitching moment about the nose, in case 1 (ATE) is,

```
ATE = MCP * XCPCG + MCI * XCICG + MGC * XGCG + MAR * XARCG +
      MAX * XAXCG + MTOUF * XSFCG + MLMUF * XLMCG + MPB *
      XPBCG + MPR XPRCG + MPT * XPTCG + MPI * XPICG + MCG *
      XCCG + MEFC * XEFCG + MWC * XWCG + MSA * XSACG + MSE *
      XSECG + MSC * XSCCG + MUMG * XUMCG + MUNG *XUNCG +
      MSF * XSFCG + MFG * XFCG + MAPU * XAPUCG
                                                    (Kg.m)
                                                    (F.158)
```

The aircraft longitudinal c.g. position in case 1 (XTECG) is,

```
XTECG =ATE/(MCP + MCI + MGC + MAR + MAX + MTOUF + MLMUF +
           MPB + MPR + MPT + MPI + MCG + MEFC + MWC + MSA +
           MSE + MSC + MUMG + MUNG + MSF + MFG + MAPU)
                                                    (F.159)
```

Case 2: Full internal fuel tanks, no external stores, no ammunition

The total aircraft pitching moment about the nose, in case 2 (ATT) is,

```
ATT = ATE + MWBEF * XWBECG + MWBCF * XWBCCG + MFIFDE *
      XFIFDE + MFIFEF * XFIFEF + MFIFFG * XFIFFG
                                                    (Kg.m)
                                                    (F.160)
```

The aircraft longitudinal c.g.position in case 2 (XTTCG) is,

$$XTTCG = ATT/(MCP + MCI + MGC + MAR + MAX + MTOUF + MLMUF + MPB + MPR + MPT + MPI + MCG + MEFC + MWC + MSA + MSE + MSC + MUMG + MUNG + MSF + MFG + MAPU + MWBEF + MWBCF + MFIF)$$

(F.161)

Case 3 Empty internal or external fuel tanks, plus external stores, plus ammunition

The total aircraft pitching moment about the nose, in case 3 (ATEW) is,

$$ATEW = MCP * XCPCG + MGA * XGACG + MXT * XB2CG + MB1 * XB1CG + MB2 * XB2CG + MB3 * XB3CG + MB4 * XB4CG + MMUF1 * XM1CG + MMUF2 * XM2CG + MMUF3 * XM3CG + MMUF4 * XM4CG + MCI * XCICG + MGC * XGCG + MAR * XARCG + MAX * XAXCG + MXP1 * XB1CG + MXP2 * XB2CG + MXP3 * XB3CG + MXP4 * XB4CG + MTOUF * XSFCG +MLMUF * XLMCG + MPB * XPBCG + MPR * XPRCG + MPT * XPTCG + MPI * XPICG + MCG * XCCG + MEFC * XEFCG + MWC * XWCG + MSA * XSACG + MSE * XSECG + MSC * XSCCG + MUMG * XUMCG + MUNG * XUNCG + MSF * XSFCG + MFG * XFCG + MAPU * XAPUCG$$

(kg.m)

(F.162)

The aircraft longitudinal c.g. position in case 3 (XTEWCG) is,

```
XTEWCG = ATEW/(MCP + MGA + MXT + MB1 + MB2 + MB3 + MB4 +
               MMUF1 + MMUF2 + MMUF3 + MMUF4 + MCI + MGC +
               MAR + MAX + MXP1 + MXP2 + MXP3 + MXP4 +
               MTOUF + MLMUF + MPB + MPR + MPT + MPI + MCG +
               MEFC + MWC + MSA + MSE + MSC + MUMG + MUNG +
               MSF + MFG + MAPU)
```

(F.163)

Case 4 Full internal or external fuel tanks, plus external stores, plus ammunition

The total aircraft pitching moment about the nose in case 4 (ATTW) is,

```
ATTW = ATEW + MXTF * XB2CG + MWBEF * XWBECG + MWBCF *
       XWBCCG + MFIFDE * XFIFDE + MFIFEF * XFIFEF + MFIFFG *
       XFIFFG
```

(kg.m)

(F.164)

The aircraft longitudinal c.g. position in case 4 (XTTWCG) is,

```
XTTWCG = ATTW/(MCP + MGA + MXT + MB1 + MB2 + MB3 + MB4 +
               MMUF1 + MMUF2 + MMUF3 + MMUF4 + MCI + MGC +
               MAR + MAX + MXP1 + MXP2 + MXP3 + MXP4 +
               MTOUF + MLMUF + MPB + MPR + MPT + MPI +
               MCG + MEFC + MWC + MSA + MSE + MSC + MUMG +
               MUNG + MSF + MFG + MAPU + MXTF + MWBEF +
               MWBCF + MFIF)
```

(F.165)

The most forward (XTFCG) and aft (XTACG) longitudinal c.g. positions are defined from the above results as shown below:

$$XTFCG = \left[\begin{array}{l} XTECG \\ XTTCG \\ XTEWCG \\ XTTWCG \end{array}\right] \quad \text{(the least)} \qquad \text{(F.166)}$$

$$XTACG = \left[\begin{array}{l} XTECG \\ XTTCG \\ XTEWCG \\ XTTWCG \end{array}\right] \quad \text{(the greatest)} \qquad \text{(F.167)}$$

APPENDIX G

AERODYNAMIC LIFT

G.1 INTRODUCTION

The aircraft lift coefficient for a given aircraft incidence within the linear range, is obtained from the estimated lift-curve-slope of the aircraft for the given flight Mach number. A detailed lift-curve-slope estimation method is therefore presented in this appendix, together with methods for determining the lift coefficient increment due to flaps and the positions of the aerodynamic centre. The maximum trimmed lift coefficient and also the critical lift coefficient, are not calculated but supplied in tabular form versus Mach number.

G.2 LIFT-CURVE-SLOPE (L-c-s)

G.2.1 General

A complete and detailed l-c-s estimation method is presented in this section. This was developed by the author and is applicable to close-coupled canard-delta aircraft, flying in the subsonic, transonic or supersonic speed regimes, up to a maximum of Mach 2.85. The method consists of a total of eight modules, which are explained in detail in this section.

The l-c-s of the wing, foreplane and body are initially estimated separately for the subsonic, transonic or supersonic case, accordingly. These three estimates are then used to determine the l-c-s of the isolated wing-body and foreplane-body combinations, by considering the nose, body/wing and body/foreplane interference effects. The l-c-s estimates for the isolated combinations are then individually corrected for the effects of canard-delta interference and added together to give an accurate estimate of the total aircraft l-c-s.

In the following l-c-s modules, the speed regimes are defined as follows:

a) Subsonic (Below Mach 0.6)
b) Transonic (Mach 0.6 - 1.4)
c) Supersonic (Above Mach 1.4)

G.2.2 Wing of Foreplane Subsonic L-c-s (Module WLSUB)

The theoretical incompressible l-c-s of the aerofoil section (GCLWS) is firstly estimated by the following equation which is based on the Kutta Joukowski hypothesis of finite velocity at the trailing edge.

$$GCLWS = 6.28 + 4.70 * RTW1 * (1.0 + 0.00375 * QWST1) \quad (G.1)$$

where, RTW1 = RTW or RTC
QWST1 = QWST or QCST = Total trailing edge angle of the wing or foreplane aerofoil, expressed in degrees.
QWST and QCST are both external variables.

The above low-speed value of the section is then corrected for compressibility effects by applying the Prandtl-Glauert compressibility correction (BETA1)

$$BETA1 = (1.0 - MGCL^{2.0})^{0.5} \quad (G.2)$$

where, MGCL = General Mach number used in l-c-s calculations

The 3-D subsonic l-c-s (GCLWSB) is estimated using the following equation which is the result of a modified lifting line theory.

$$GCLWSB = \frac{2.0 * PI * AWN1}{2.0+\left\{\left(\frac{AWN1*BETA1}{GCLWK}\right)^{2.0} * \left[1.0+\left(\frac{\tan(QW21)}{BETA1}\right)^{2.0}\right]+4.0\right\}^{0.5}} \qquad (G.3)$$

$$\text{where, } GCLWK = \frac{GCLWS}{2.0 * PI} \qquad (G.4)$$

AWN1 = AWN or ACN

QW21 = QW2 or QC2

G.2.3 Wing or Foreplane Transonic l-c-s (Module WLTRAN)

The transonic l-c-s of the wing or foreplane is estimated by a DATCOM method (ref.15) which is largely based on experimental data obtained from wind-tunnel tests.

In the transonic speed regime the l-c-s gradually increases from the subsonic value at Mach 0.6 to a maximum at the force-break Mach number (MFB). Above MFB, the l-c-s gradually decreases through MA and MB down to the supersonic value at Mach 1.4. Therefore in order to fully define the transonic l-c-s variation with Mach number, it is necessary to determine the l-c-s at Mach 0.6, MFB, MA, MB and 1.4.

The l-c-s at Mach 0.6 (GCLW06) is obtained from module WLSUB, while the l-c-s at Mach 1.4 (GCLW14) obtained from module WLSUP for the supersonic case, which is presented in the next section.

The next step is to calculate the force-break Mach number for zero wing sweep(MFBØ). This is obtained from fig.G.1 for the given AWN1 and RTW1. The force-break Mach number, corrected for sweep effects (MFB) is then obtained from fig.G.2 for the calculated MFBØ and QW21. The

theoretical l-c-s value at MFB (GCLW10) is computed by module WLSUB. The actual l-c-s value at MFB (GCLFB) is obtained from the value of ratio (GCLFB/GCLW10) given in fig.G.3 for AWN1 and RTW1.

The next step is to estimate the l-c-s at MA (GCLA)

$$MA = MFB + 0.07 \qquad (G.5)$$

$$GCLA = (1.0 - RAC) * GCLFB \qquad (G.6)$$

The value of RAC for the given AWN1 and RTW1 is obtained from fig.G.4.

Similarly,

$$MB = MFB + 0.14 \qquad (G.7)$$

and the l-c-s at MB (GCLB) is,

$$GCLB = (1.0 - RBC) * GCLFB \qquad (G.8)$$

The value of RBC for RTW1 is obtained from fig.G.5.

G.2.4 Wing or Foreplane Supersonic L-c-s (Module WLSUP)

The supersonic l-c-s of the wing or foreplane (GCLWSP) is estimated by a DATCOM method which is based on theory.

The theoretical value of GCLWSP is determined from the charts in fig.G.6, for the given values of the following parameters:

UWCN1

AWN1 * tan (QWL1)

BETA2/tan (QWL1) or tan (QWL1)/BETA2

where,

$$BETA2 = (MGCL^{2.0} - 1.0)^{0.5} \qquad (G.9)$$

G.2.5 Empirical Thickness Correction (Module TCOR)

When a wing or foreplane is approaching the sonic leading-edge condition, its theoretical value of GCLWSP obtained from module WLSUP, is corrected for thickness effects by multiplying it by an empirical thickness correction factor (RGCL), hence,

$$GCLWSP = GCLWSP * RGCL \qquad (G.10)$$

The factor RGCL is obtained from fig.G.7 for the following parameters:

[BETA2/tan (QWL1)]
RSLE1/cos (QWL1)]

where, RSLE1 = RSLEW or RSLEC = Leading-edge sharpness parameter of the wing or foreplane aerofoil respectively.
Both RSLEW and RSLEC are external variables.

The leading-edge sharpness parameter of an aerofoil is defined as the difference between the upper-surface coordinates expressed in percent chord at the 6-percent and 15-percent chord stations.

G.2.6 Supersonic L-c-s of the Body (Module BLSUP)

A DATCOM mthod is used for the estimation of the supersonic l-c-s of the fuselage (GCLBSP). The value of GCLBSP for RFBCN and RBFN is obtained from fig.G.8, where,

$$RFBCN = \frac{RFBC}{RFBN} \text{ and } RBFN = \frac{BETA2}{RFBN} \text{ or } RBFN = \frac{RFBN}{BETA2} \qquad (G.11)$$

where, RFBN = Fineness-ratio of the nose of the body

RFBC = Fineness-ratio of the forebody excluding the nose

The fineness-ratios RFBN and RFBC are calculated as shown below:

$$RFBN = \frac{LBN1}{DFH1} \text{ and } RFBC = \frac{LBCF1}{DFH1} \qquad (G.12)$$

where, LBN1 = LBN or LBNC = Nose length as defined in wing-body or foreplane-body l-c-s calculations, respectively.

LBCF1 = LBCF or LBCFC = Length of the forebody excluding the nose, as defined in wing-body or foreplane-body l-c-s calculations respectively.

DFH1 = DFH or DFHC = Average fuselage width at the wing-body or foreplane-body junction respectively.

The above variables are mathematically defined below, by assuming from the fuselage geometry, that the nose section extends up to station B.

Hence if, XWLB > XB then,

LBN = XB and LBCF = XWLB - XB (G.13)

Otherwise,

LBN = XWLB and LBCF = 0.0 (G.14)

Similarly, if XCLB > XB then,

LBNC = XB and LBCFC = XCLB - XB (G.15)

Otherwise,

LBNC = XCLB and LBCFC = 0.0 (G.16)

The approximate values of DFH and DFHC are:

DFH = 0.5 * (BFE + BFH) (G.17)

DFHC = 0.5 * (BFD + BFE) (G.18)

G.2.7 Isolated Wing-Body or Foreplane-Body Combination L-c-s (Module WBLCS)

G.2.7.1 General

This module is based on DATCOM. It estimates the l-c-s of the isolated wing-body or foreplane-body combination for the subsonic, transonic and supersonic speed regimes from the results of the previous l-c-s modules by considering the existing interference effects.

The body contribution to the l-c-s of the isolated combination in the subsonic speed regime is determined using slender body theory (2.0/rad). The transonic body contribution is obtained by interpolation between the body

l-c-s values at Mach 0.6 and Mach 1.4. The supersonic body l-c-s contribution is obtained from module BLSUP.

The subsonic, transonic and supersonic wing or foreplane contributions to the l-c-s of the isolated combination are obtained from modules WLSUB, WLTRAN and WLSUP respectively.

The calculations of the interference factors and hence the estimation of the l-c-s of the isolated wing-body or foreplane-body combination (GCLWBR) in the three speed regimes are presented below.

G.2.7.2 Subsonic

The nose interference factor (KN) is,

$$KN = \frac{0.5 * PI * DFH1^{2.0}}{GCLWR * SWN1} \qquad (G.19)$$

where, GCLWR = L-c-s of the wing or foreplane.

The body-on-wing or foreplane (KWB) and wing or foreplane-on-body (KBW) interference factors are jointly defined in this case by,

$$KWB + KBW = \left(\frac{DFH1}{BW1} + 1.0\right)^{2.0} \qquad (G.20)$$

The l-c-s of the isolated combination is therefore,

$$GCLWBR = \left[KN + \left(\frac{DFH1}{BW1} + 1.0\right)^{2.0}\right] * GCLWR * \left(\frac{SWN1}{SW1}\right) \qquad (G.21)$$

G.2.7.3 Transonic

As mentioned earlier the transonic l-c-s of the body (GCLBTR) at a given Mach number M, is obtained by interpolation, hence,

$$GCLBTR = 2.0 - \left(\frac{2.0 - GCLBSP}{0.8}\right) * (M - 0.6) \qquad (G.22)$$

The nose interference factor is,

$$KN = \frac{0.25 * GCLBTR * PI * DFH1^{2.0}}{GCLWR * SWN1} \qquad (G.23)$$

The interference factors KWB and KBW are again jointly defined as,

$$KWB + KBW = \left(\frac{DFH1}{BW1} + 1.0\right)^{2.0} \qquad (G.24)$$

Hence, the l-c-s of the isolated combination is,

$$GCLWBR = \left[KN + \left(\frac{DFH1}{BW1} + 1.0\right)^{2.0}\right] * GCLWR * \left(\frac{SWN1}{SW1}\right) \qquad (G.25)$$

G.2.7.4 Supersonic

In the supersonic case, the nose interference factor is,

$$KN = \frac{0.25 * GCLBSP * PI * DFH1^{2.0}}{GCLWR * SWN1} \qquad (G.26)$$

The values of interference factors KBW and KWB depend on the parameter WB1, where,

$$WB1 = BETA2 * AWN1 * (1.0 + UWCN1) * \left[\frac{\tan(QWL1)}{BETA2} + 1.0\right] \quad (G.27)$$

If, WB1 ≤ 4.0 then,

$$KWB + KBW = \left(\frac{DFH1}{BW1} + 1.0\right) 2.0 \quad (G.28)$$

and hence,

$$GCLWBR = \left[KN + \left(\frac{DFH1}{BW1} + 1.0\right) 2.0\right] * GCLWR * \left(\frac{SWN1}{SW1}\right) \quad (G.29)$$

Otherwise, if WB > 4.0 then,

KWB is obtained from fig.G.9 for the given ratio (DFH1/BW1) and KBW is,

$$KBW = \frac{KBWF}{BETA2 * GCLWR * (UWCN1 + 1.0) * \left(\frac{BW1}{DFH1} - 1.0\right)} \quad (G.30)$$

The product KBWF is determined from fig.G.10 for the calculated parameters WB2 and WB3, where,

$$WB2 = \frac{BETA2 * DFH1}{CWCB1} \text{ and } WB3 = BETA2 * \cot(QWL1) \quad (G.31)$$

Substituting the values of KN, KWB and KBW, in the following expression, the l-c-s of the isolated combination is,

$$GCLWBR = (KN + KWB + KBW) * GCLWR * \left(\frac{SWN1}{SW1}\right) \quad (G.32)$$

G.2.8 Canard-Delta L-c-s Interference (Module LCSINT)

This module is based on a method developed by the author after a long and detailed investigation into the effects of close-coupled canard-delta interference on the l-c-s of the aircraft.

Wind-tunnel data for closed-coupled canard-delta configurations were analysed and the interference effects quantified in the form of factors which are used to individually correct the l-c-s estimates of the isolated wing-body and foreplane-body combinations. The development of this method is presented in more detail in chapter 5.

The foreplane-on-wing (WLCSIF) and the wing-on-foreplane (CLCSIF) l-c-s interference factors are obtained from figs.G.11 for the given values of M. QWL, RSCNW and RZCC,

where, RSCNW = Ratio of the net foreplane area to gross-wing area.

RZCC = Ratio of the foreplane height above the wing-chord plane to the mean geometric chord of the wing

G.2.9 Total Aircraft L-c-s (Module LIFTSL)

Module LIFTSL controls the order of excution of modules WLSUB, WLTRAN, WLSUP, BLSUP, WBLCS and LCSINT and hence determines the total aircraft l-c-s (GCL) at any Mach number M, as shown below.

If $0.0 \leq M \leq 0.6$ then GCLWR is obtained from module WLSUB, therefore,

$$GCLWR = GCLWSB \tag{G.33}$$

If $0.6 < M < 1.4$ then, MFB, MA, MB, GCLFB, GCLA and GCLB are determined from module WLTRAN and GCLW06 and GCLW14 from modules WLSUB and WLSUP respectively.

The value of GCLWR at any Mach number M in the transonic regime is obtained by linear interpolation, hence,

for $0.6 < M \leq MFB$,

$$GCLWR = GCLW06 + \left(\frac{GCLFB - GCLW06}{MFB - 0.6}\right) * (M - 0.6) \tag{G.34}$$

for $MFB < M \leq MA$.

$$GCLWR = GCLFB - \left(\frac{GCLFB - GCLA}{MA - MFB}\right) * (M - MFB) \tag{G.35}$$

for $MA < M \leq MB$,

$$GCLWR = GCLA - \left(\frac{GCLA - GCLB}{MB - MA}\right) * (M - MA) \tag{G.36}$$

for $MB < M \leq 1.4$

$$GCLWR = GCLW14 - \left(\frac{GCLW14 - GCLB}{1.4 - MB}\right) * (1.4 - M) \tag{G.37}$$

If M ≥ 1.4 then GCLWR is obtained from module WLSUP,

$$GCLWR = GCLWSP \qquad (G.38)$$

and GCLBSP from module BLSUP.

The l-c-s of the isolated wing-body (GCLWB) and foreplane-body (GCLCB) combinations at any Mach number M, are obtained from module WBLCS, therefore,

$$GCLWB = GCLWBR \text{ (Wing-body solution)} \qquad (G.39)$$

$$GCLCB = GCLWBR \text{ (Foreplane-body solution)} \qquad (G.40)$$

The corresponding canard-delta interference factors WLCSIF and CLCSIF are obtained from module LCSINT.

The total aircraft l-c-s is finally estimated by the following expression:

$$GCL = GCLWB * WLCSIF + GCLCB * \left(\frac{SC}{SW}\right) * CLCSIF \qquad \text{(per rad)} \quad (G.41)$$

G3 LIFT INCREMENT DUE TO FLAPS (Module DLFLAP)

According to the initial baseline assumptions, plain trailing-edge flaps, is the only form of high lift devices used on the synthesized aircraft. This module determines the lift coefficient increment (DCLF) and the corresponding maximum lift coefficient increment (DCLFH) due to a flap deflection (EQWF).

The increment DCLF is first estimated by the following expression which was obtained from ref.57.

$$DCLF = \left(\frac{GCLWB}{57.296}\right) * \left(\frac{BWF}{BW}\right) * \left(\frac{CWFM}{CWMG}\right) * FQWF \qquad (G.42)$$

where, FQWF = Factor depending on EQWF

EQWF is an external variable expressed in degrees.

The variation of FQWF with EQWF is described in ref.57 by a curve which in this synthesis is expressed in a mathematical form by the following set of equations.

For

$0.0 \leq EQWF < 10.0, \quad FQWF = 2.45 * EQWF \qquad (G.43)$

$10.0 \leq EQWF < 14.0, \quad FQWF = 24.5 + 1.375 * (EQWF - 10.0) \qquad (G.44)$

$14.0 \leq EQWF < 20.0, \quad FQWF = 30.0 + 0.75 * (EQWF - 14.0) \qquad (G.45)$

$20.0 \leq EQWF < 30.0, \quad FQWF = 34.5 + 0.45 * (EQWF - 20.0) \qquad (G.46)$

$30.0 \leq EQWF < 40.0, \quad FQWF = 39.0 + 0.10 * (EQWF - 30.0) \qquad (G.47)$

and for $EQWF \geq 40.0, \quad FQWF = 40.0 \qquad (G.48)$

The above equation for DCLF gives an accurate estimate in the subsonic speed regime. At higher speeds, however, a correction becomes necessary, due to the variations in flap lift effectiveness with Mach number. For this purpose the author analyzed relevant data from ref.11 and hence determined a set of correction factors which are incorporated in the following expressions:

For

$0.0 \leq M \leq 0.6$, $DCLF = DCLF$ (G.49)

$0.6 < M \leq 0.9$, $DCLF = DCLF * [1.0 + 1.333 * (M - 0.6)]$ (G.50)

$0.9 < M \leq 1.2$, $DCLF = DCLF * [1.4 - 2.666 * (M - 0.9)]$ (G.51)

$1.2 < M \leq 1.6$, $DCLF = DCLF * [0.6 - 0.675 * (M - 1.2)]$ (G.52)

and for $M > 1.6$, $DCLF = 0.33 * DCLF$ (G.53)

Finally, from several wind tunnel observations and in agreement with ref.57 the increment in maximum lift coefficient due to flap deflection is,

$$DCLFH = 0.5 * DCLF$$

G.4 AERODYNAMIC CENTRE (Module AEROC)

G.4.1 General

The longitudinal position of the aerodynamic centre of the aircraft is estimated for Mach 0.6 and Mach 1.4 only. These two cases represent the forward and aft positions, due to the transonic shift, which may be compared to the forward

and aft longitudinal c.g. positions in order to determine the degree of stability or instability of the aircraft.

The aerodynamic centre position in each of the above cases is estimated in two parts. The first part considers the wing alone while the second part considers the whole wing-body combination.

G.4.2 Wing

The aerodynamic centre of the wing alone, is estimated using a DATCOM method. The value of the ratio RXAC is determined in each case from the charts in fig.G.12 for the following parameters:

UW
AW * tan (QWL)
BETA1/tan (QWL) (for M = 0.6)
or BETA2/tan (QWL) (for M = 1.4)

where, BETA1 = 0.80 for M = 0.6
BETA2 = 0.98 for M = 1.4

The aerodynamic centre of the wing is located at a distance (RXAC * CWCC) aft of the wing apex.

G.4.3 Wing-body Combination

The aerodynamic centre of the wing-body combination is estimated by considering the fuselage contributions DXAC1 and DXAC2.

where, DXAC1 = Aerodynamic centre shift due to the front and rear fuselage.
DXAC2 = Aerodynamic centre shift due to the fuselage carry-over lift.

DXAC1 and DXAC2 are calculated by the following expressions which were obtained from ref. 3.

For M = 0.6,

$$DXAC1 = - \frac{1.8 * BFE * HFE * XWLB}{GCLWB1 * SW} \qquad (G.55)$$

For M = 1.4,

$$DXAC1 = - \frac{1.8 * BFE * HFE * XWLB}{GCLWB2 * SW} \qquad (G.56)$$

where, GCLWB1 and GCLWB2 are the l-c-s values of the wing-body combination at M = 0.6 and M = 1.4 respectively.

$$DXAC2 = \left(\frac{0.273}{1.0 + UW} \right) * \left[\frac{BFE * CWMG * (BW - BFE)}{CWMA * (BW + 2.15 * BFE)} \right] * \tan(QW4) \qquad (G.57)$$

The total shift of the aerodynamic centre due to the fuselage (DXAC) is therefore,

$$DXAC = DXAC1 + DXAC2 \qquad (G.58)$$

The expression for DXAC2 is valid for (BFE/BW) < 0.2. Above that limit, the DXAC2 contribution will make DXAC > 0.0, therefore in order to allow for this, when DXAC ≥ 0.0 then DXAC is taken as zero.

The axial distance of the aerodynamic centre of the aircraft from the nose at Mach 0.6 (XAC06) and at Mach 1.4 (XAC14) is,

$$XAC06 = XWAPEX + RXAC * CWCC + DXAC$$

with RXAC and DXAC for Mach 0.6. (G.59)

$$XAC14 = XWAPEX + RXAC * CWCC + DXAC$$

with RXAC and DXAC for Mach 1.4. (G.60)

G.4.4 Longitudinal static stability

The maximum longitudinal static stability margins of the aircraft in subsonic and supersonic flight are determined as fractions of the mean aerodynamic chord of the gross wing, by comparing the longitudinal positions of the aerodynamic centre at Mach 0.6 and Mach 1.4 to the forward and aft centre of gravity positions of the aircraft, as shown below. A negative margin indicates instability.

The longitudinal static stability margin, with the aerodynamic centre and centre of gravity in their most forward positions (SMSUBF) is,

$$SMSUBF = \frac{XAC06 - XTFCG}{CWMA} \quad (G.61)$$

The longitudinal static stability margin, with the aerodynamic centre in its most forward position and the centre of gravity in its aft position (SMSUBA) is,

$$SMSUBA = \frac{XAC06 - XTACG}{CWMA} \quad (G.62)$$

The maximum longitudinal static stability margin in subsonic flight (SMSUB) is,

$$SMSUB = \left| \begin{matrix} |SMSUBF| \\ |SMSUBA| \end{matrix} \right| \quad \text{(the maximum)} \quad (G.63)$$

Similarly, the longitudinal static stability margin, with the aerodynamic centre in its most aft position and the centre of gravity in its forward position (SMSUPF) is,

$$SMSUPF = \frac{XAC14 - XTFCG}{CWMA} \qquad (G.64)$$

The longitudinal static stability margin, with the aerodynamic centre and centre of gravity in their most aft positions (SMSUPA) is,

$$SMSUPA = \frac{XAC14 - XTACG}{CWMA} \qquad (G.65)$$

Finally, the maximum longitudinal static stability margin in supersonic flight (SMSUP) is,

$$SMSUP = \left[\begin{matrix} |SMSUPF| \\ |SMSUPA| \end{matrix} \right] \quad \text{(the maximum)} \qquad (G.66)$$

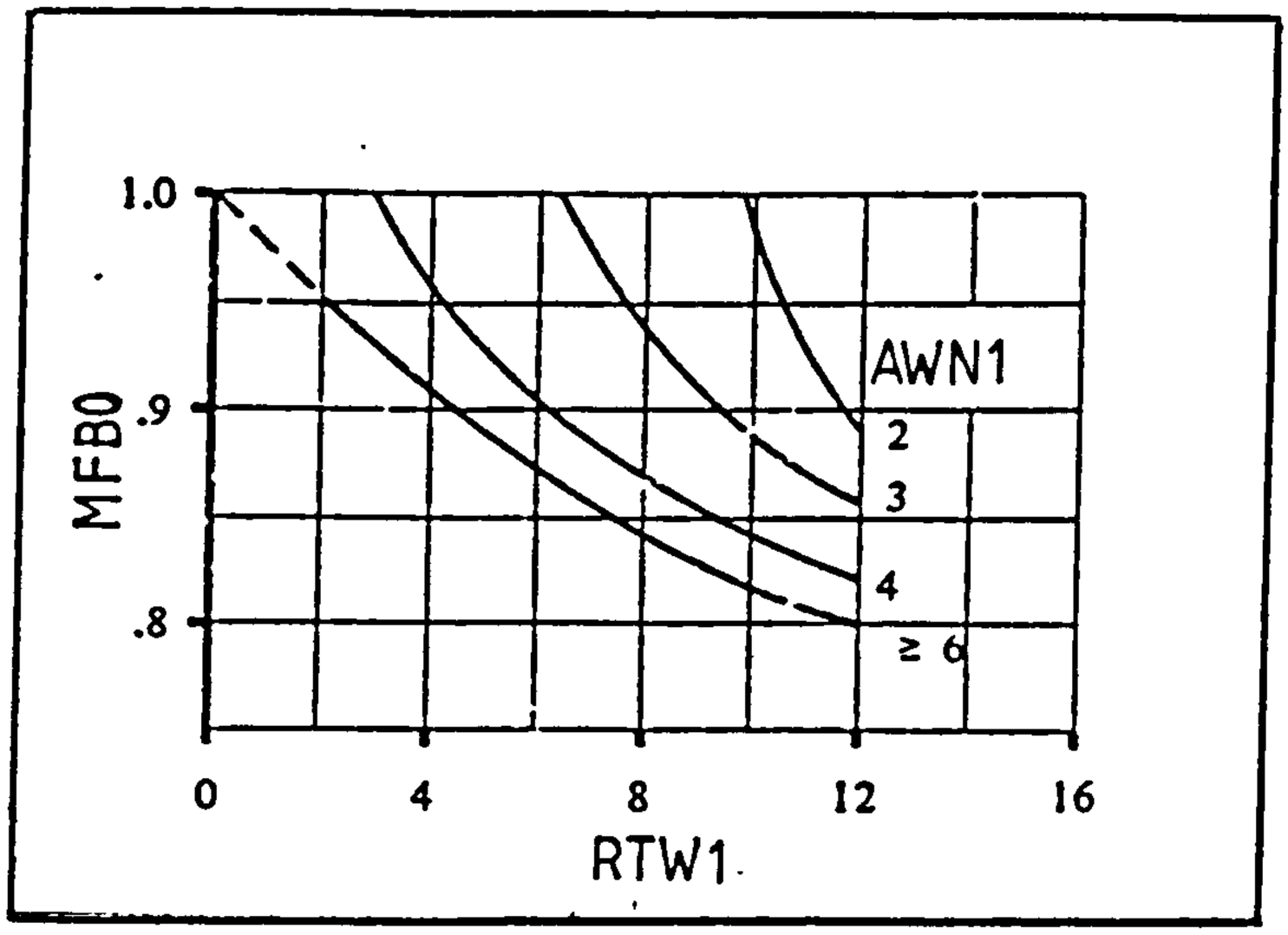

FIG. G1 TRANSONIC FORCE-BREAK MACH NUMBER FOR ZERO SWEEP

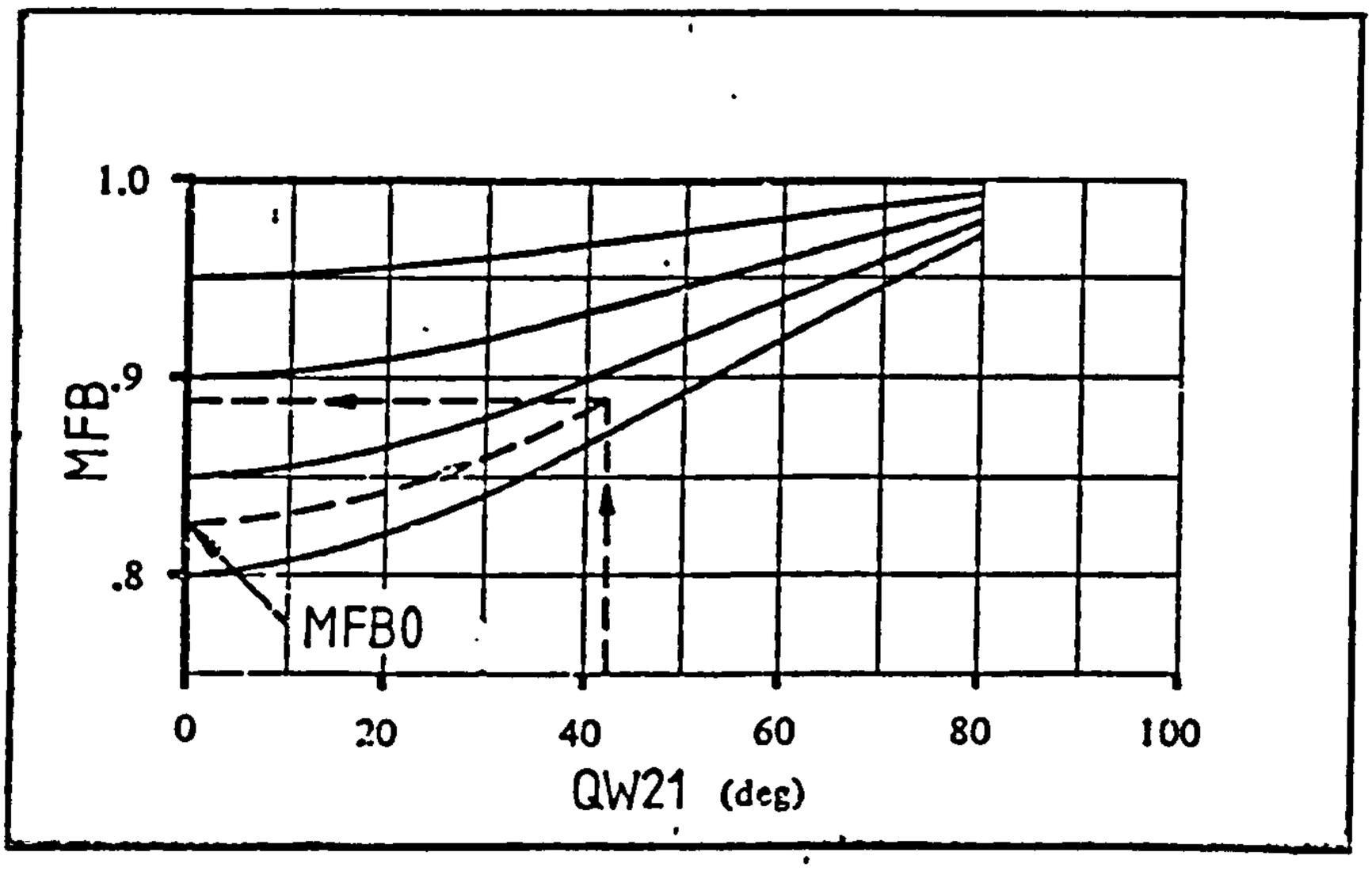

FIG. G2 TRANSONIC SWEEP CORRECTIONS FOR FORCE-BREAK MACH NUMBER

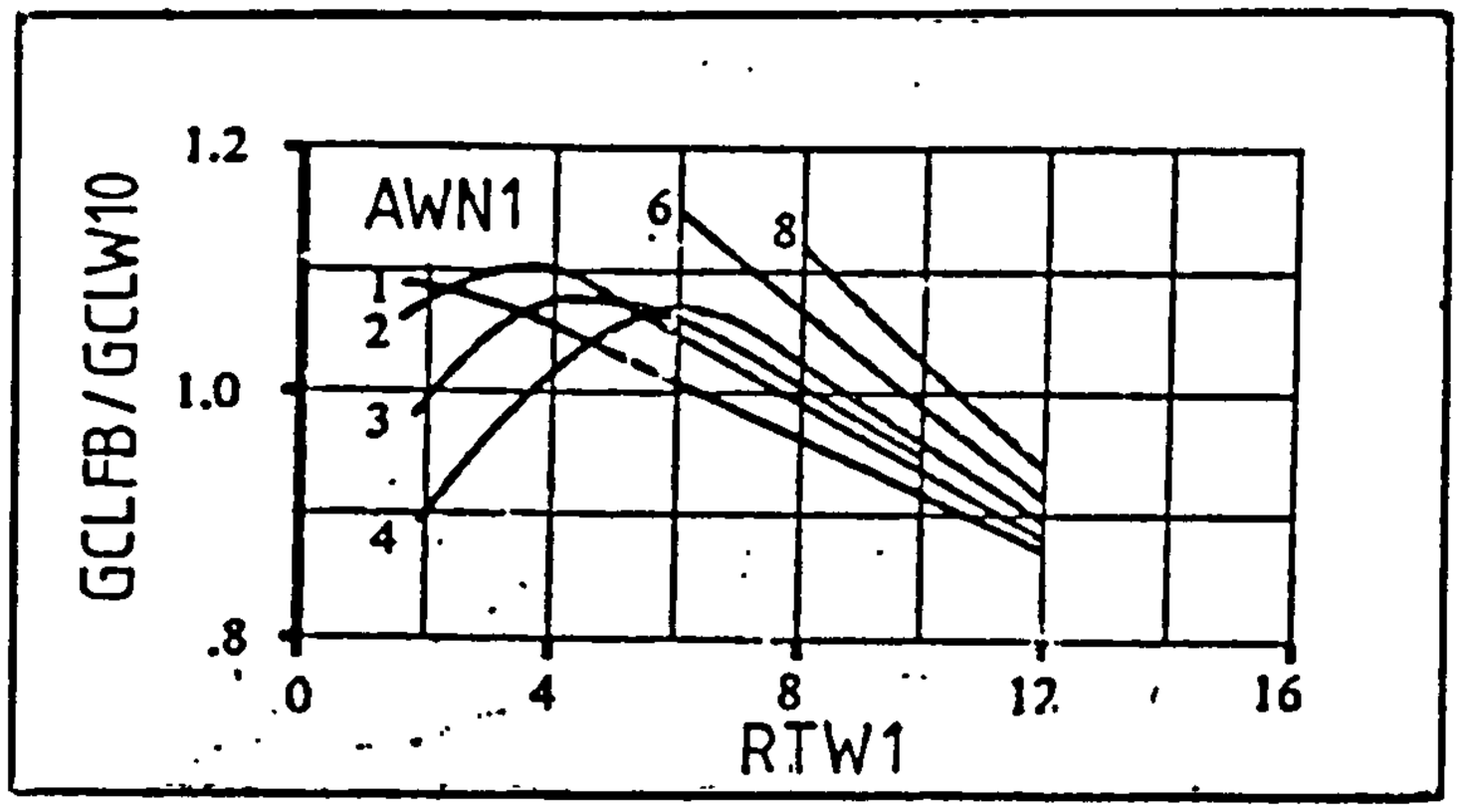

FIG. G3 CORRECTION TO WING L-C-S AT FORCE-BREAK MACH NUMBER

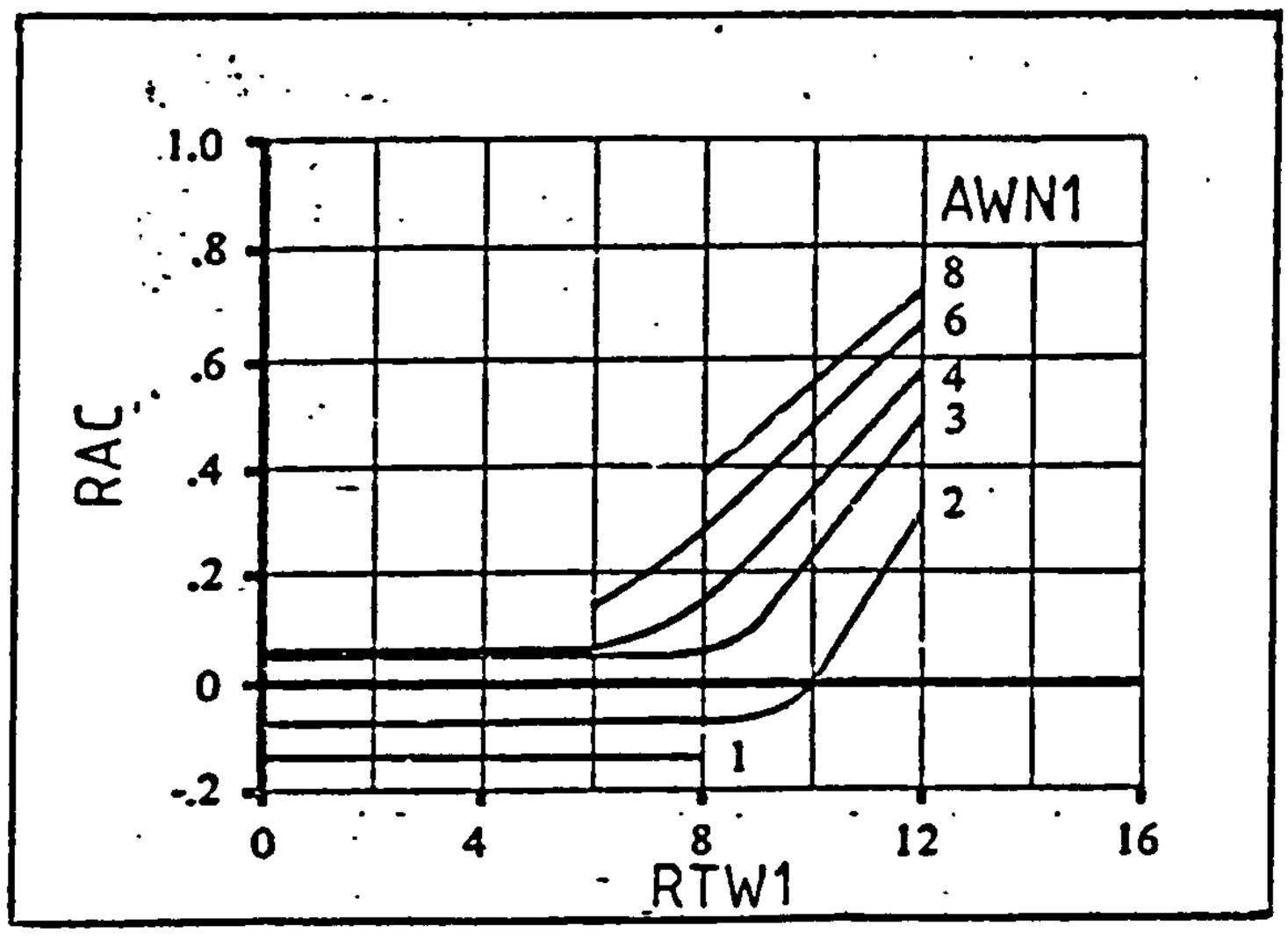

FIG. G4 WING TRANSONIC L-C-S AT MA

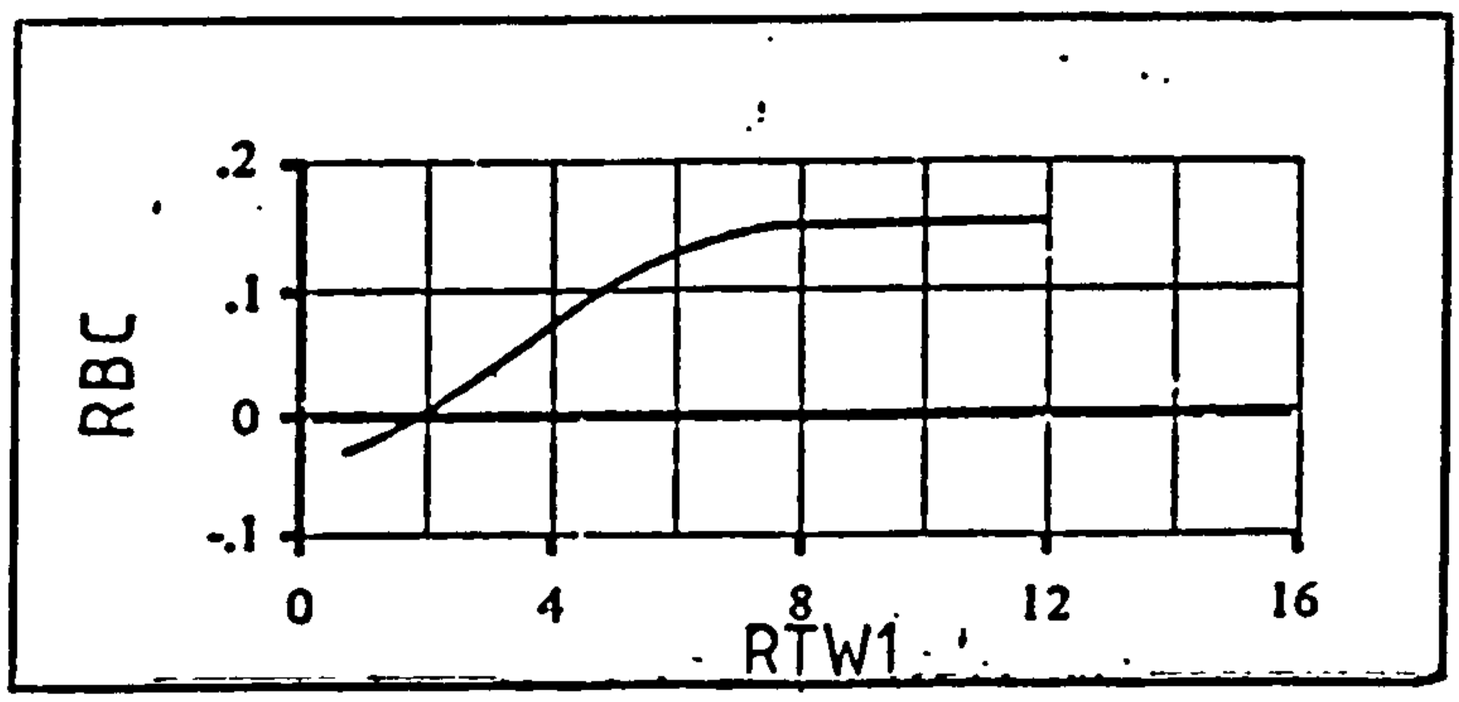

FIG. G5 WING TRANSONIC L-C-S AT MB

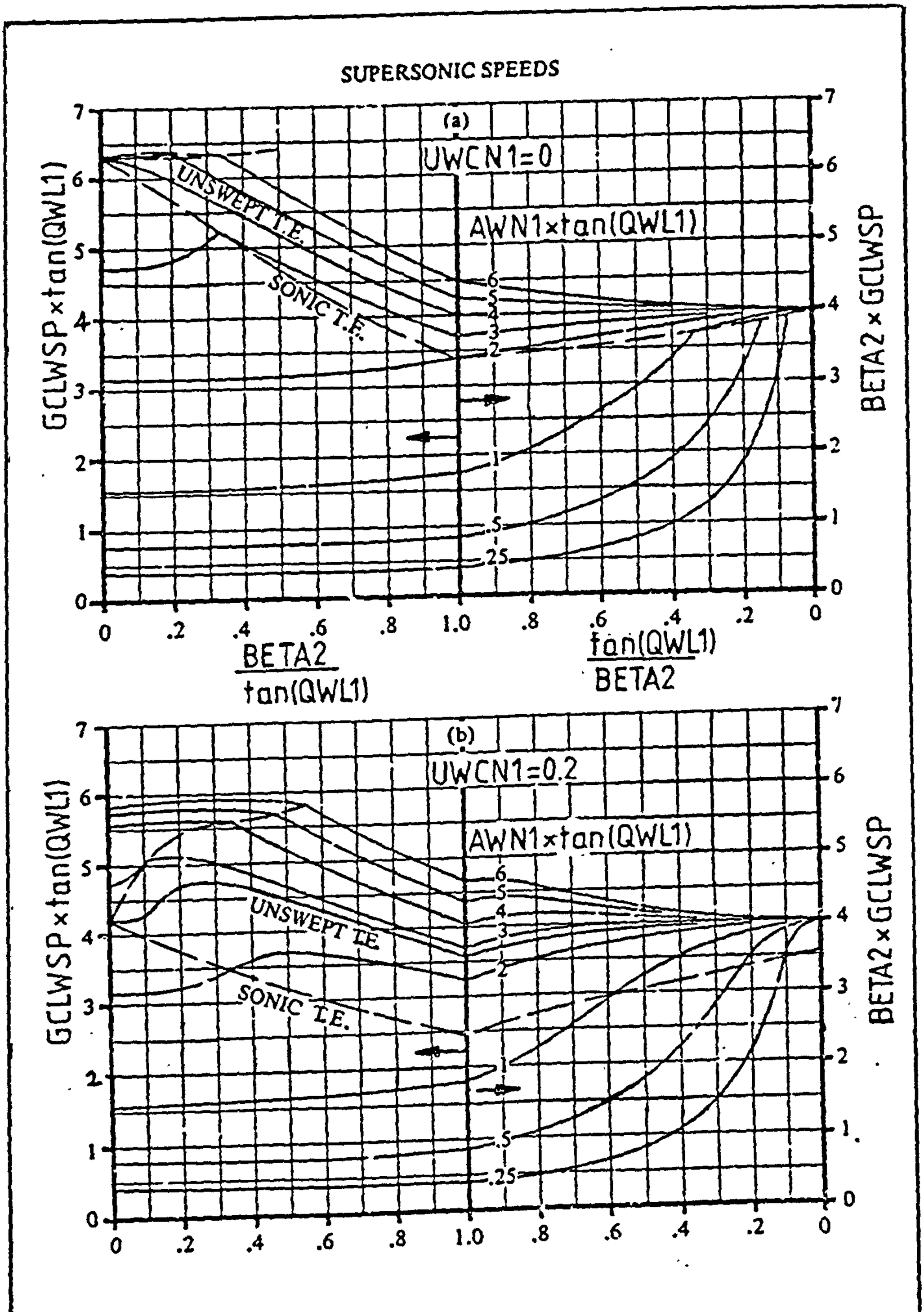

FIG. G6 WING SUPERSONIC L-C-S

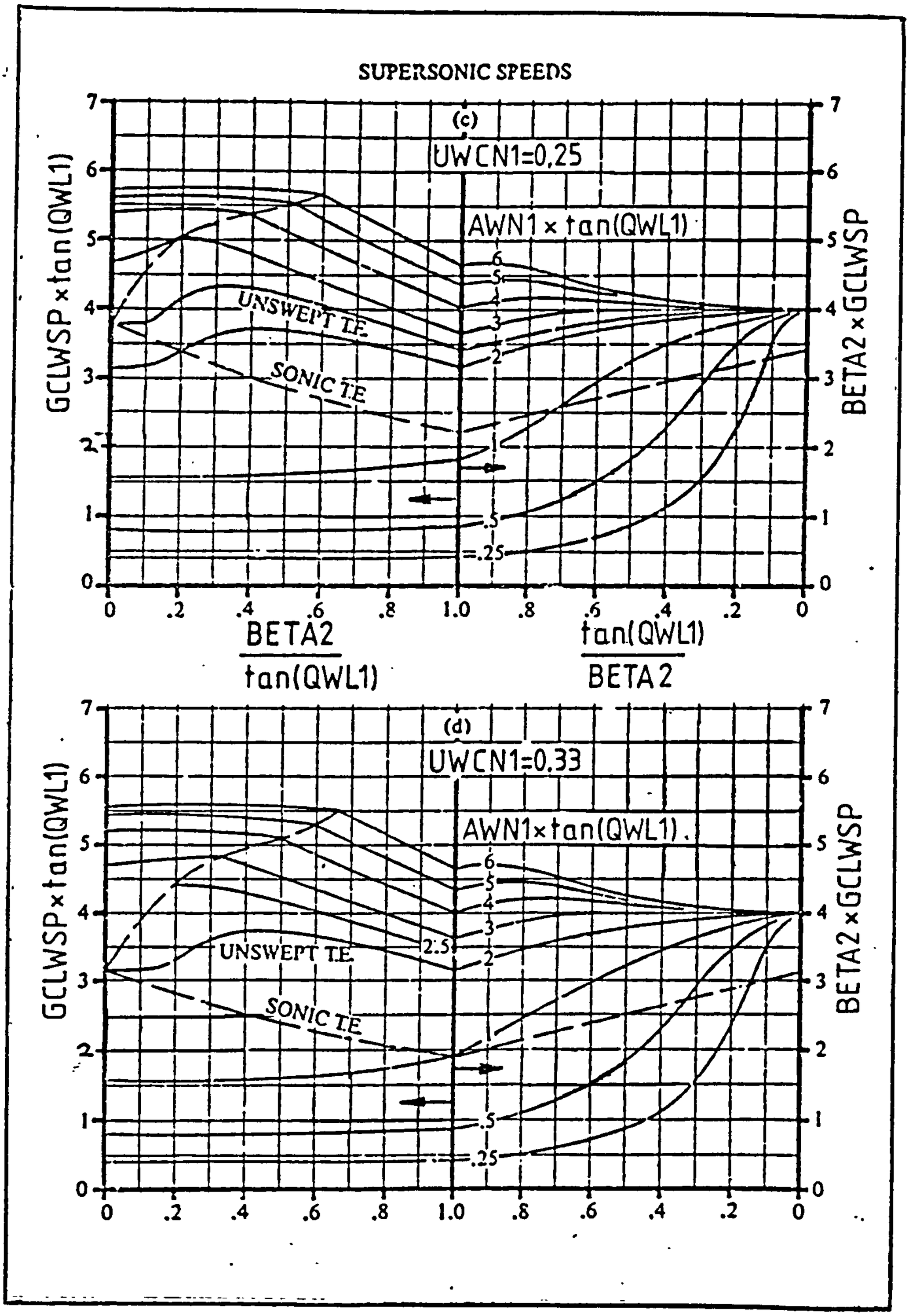

FIG. G6 (CONTINUED ...)

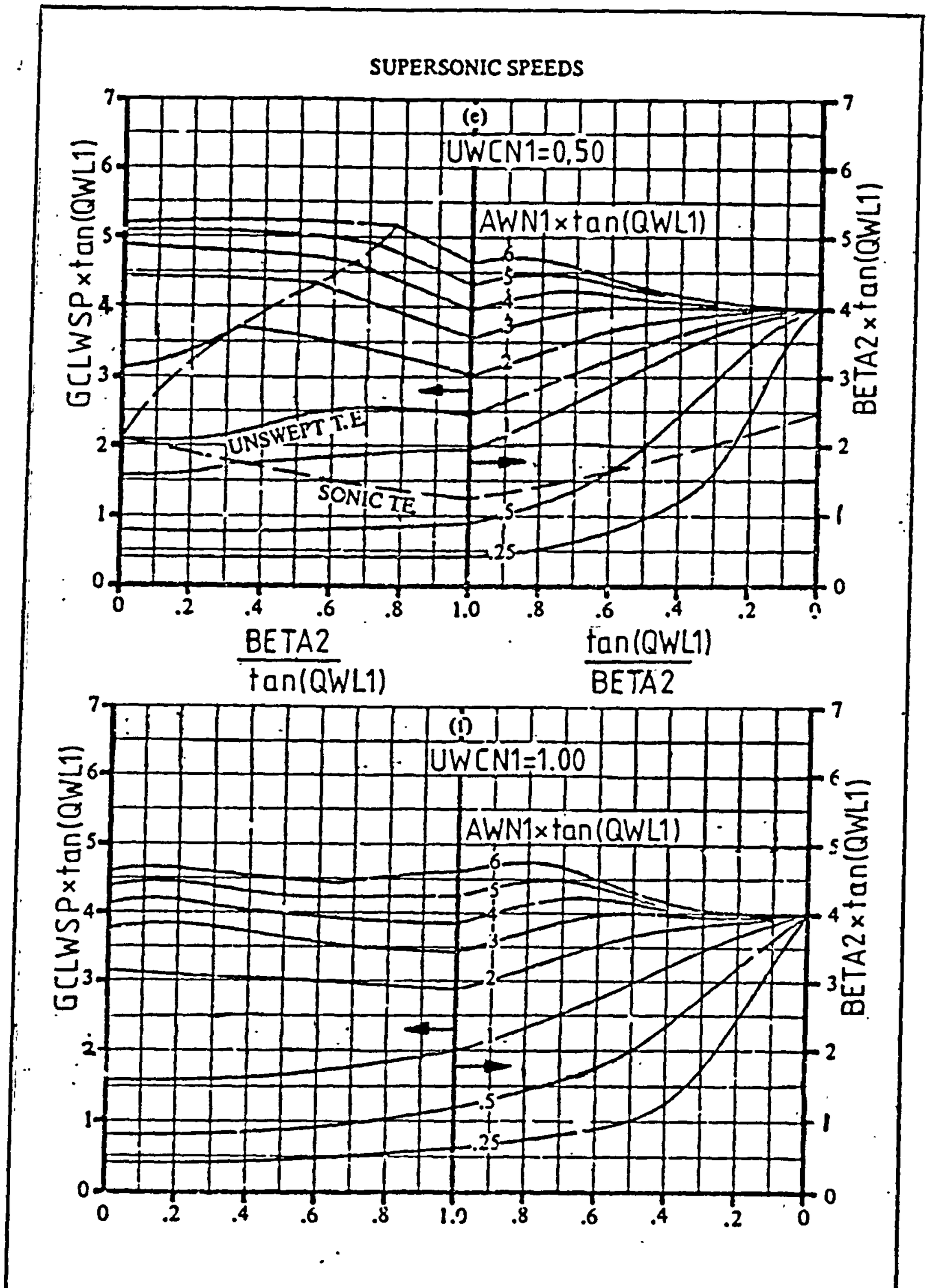

FIG. G6 (CONTINUED)

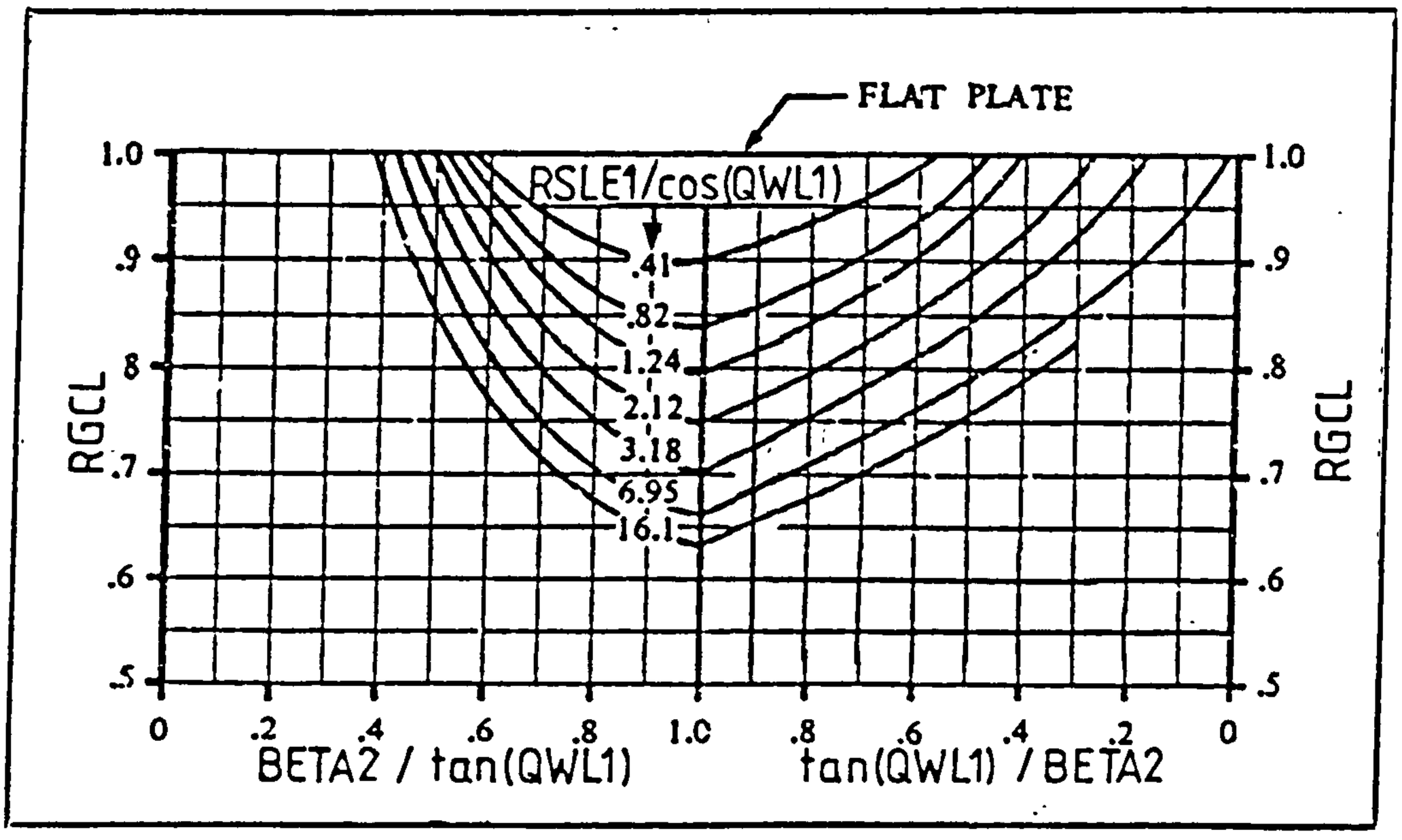

FIG. G7 WING SUPERSONIC L-C-S CORRECTION FACTOR FOR SONIC LEADING-EDGE REGION

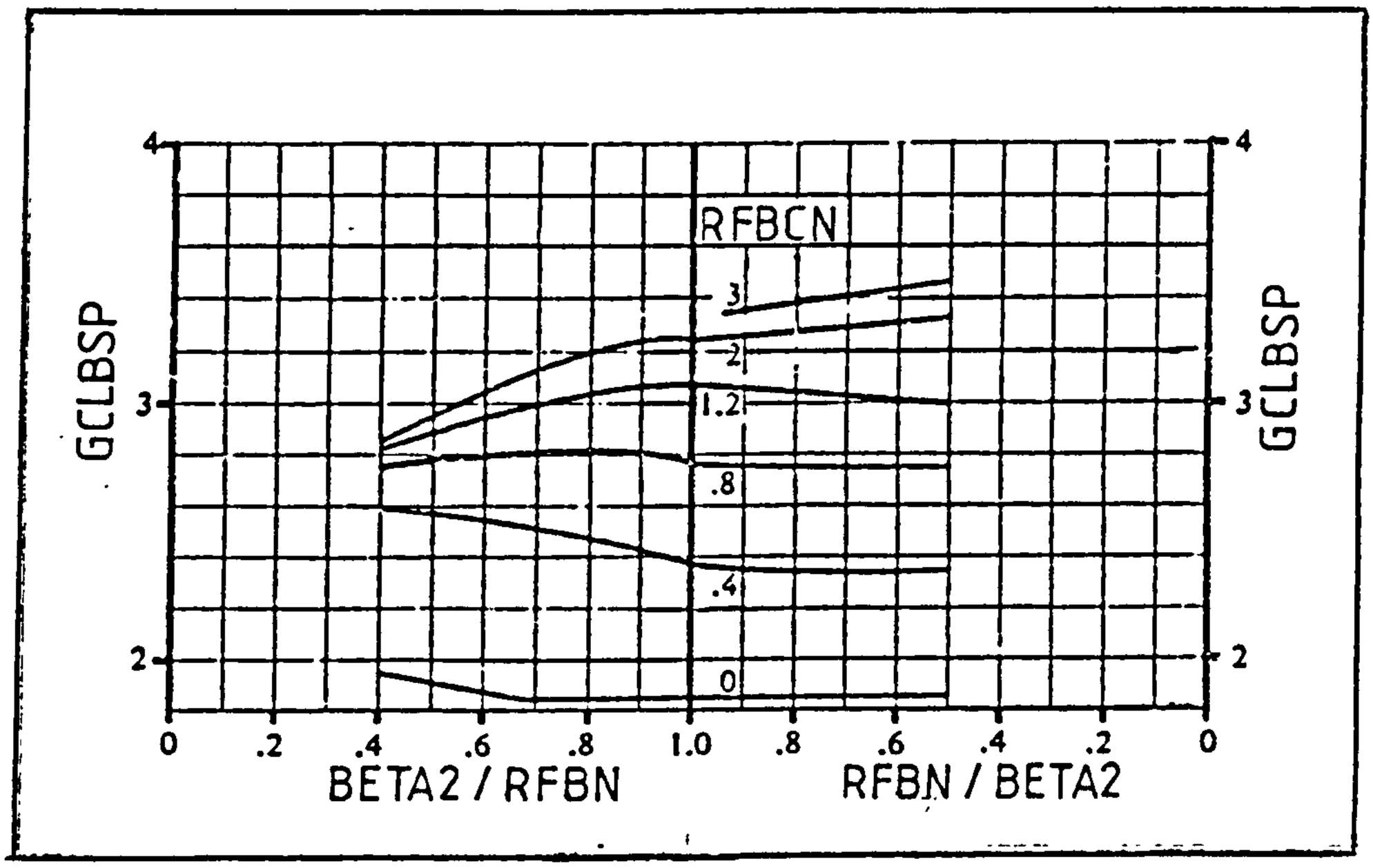

FIG. G8 SUPERSONIC L-C-S FOR BODY

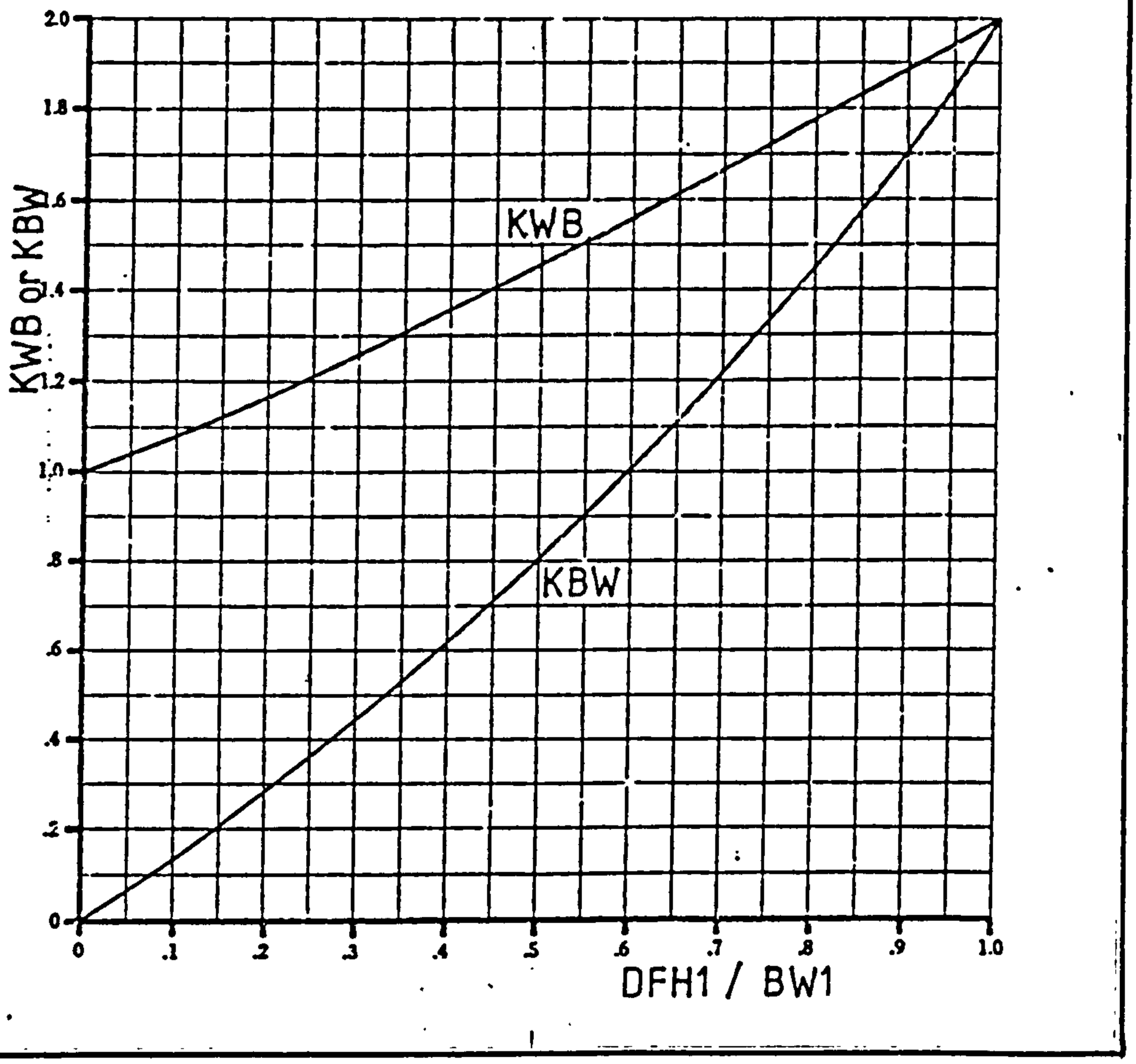

FIG. G9 WING-BODY INTERFERENCE FACTORS KWB AND KBW

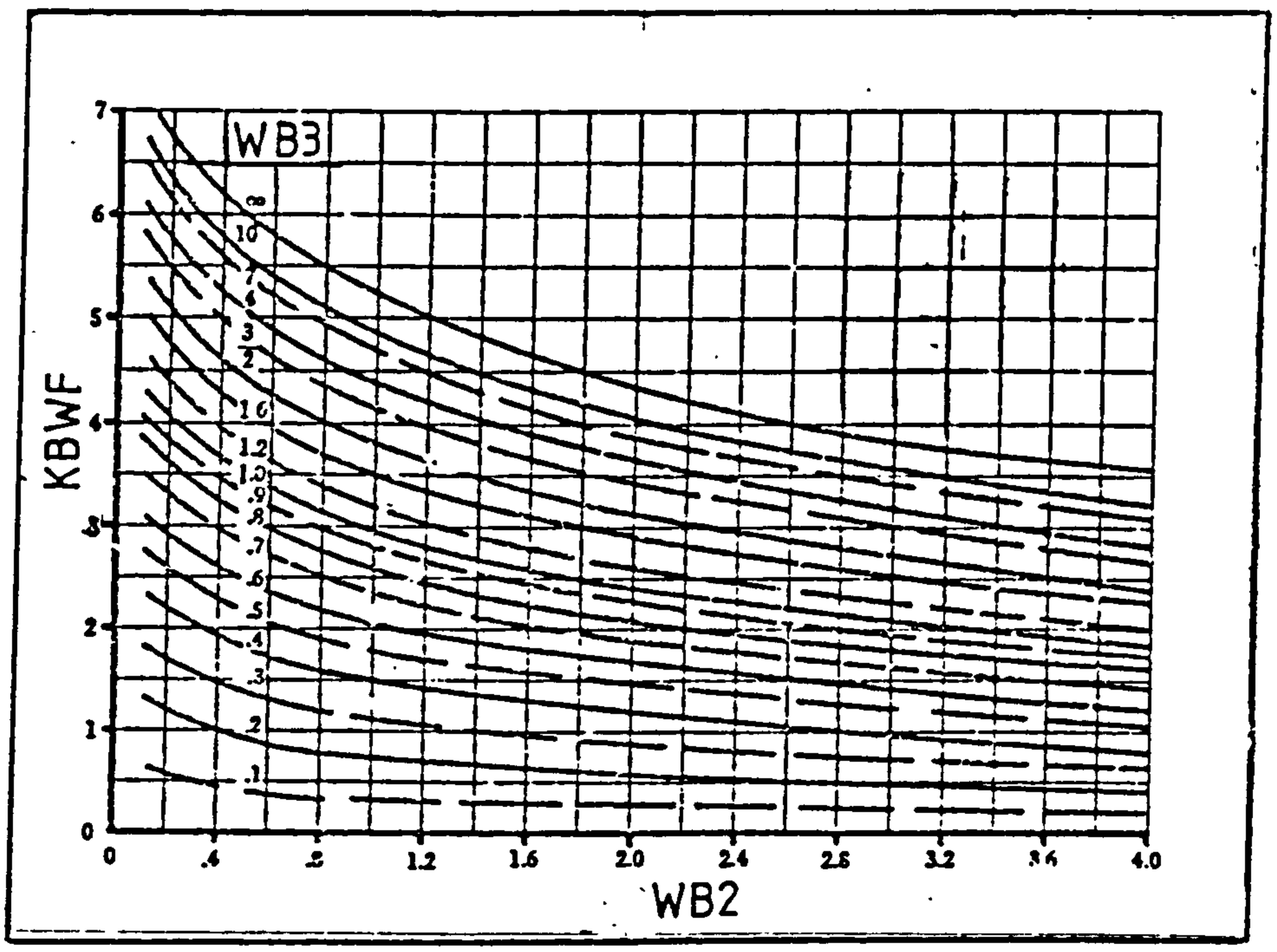

FIG. G10 LIFT ON BODY IN PRESENCE OF WING

CANARD-DELTA INTERFERENCE EFFECTS (LIFT-CURVE-SLOPE)

NOTE : The factors CLCSIF and WLCSIF also include the body interference effects.The supersonic values of CLCSIF are solely due to body interference.

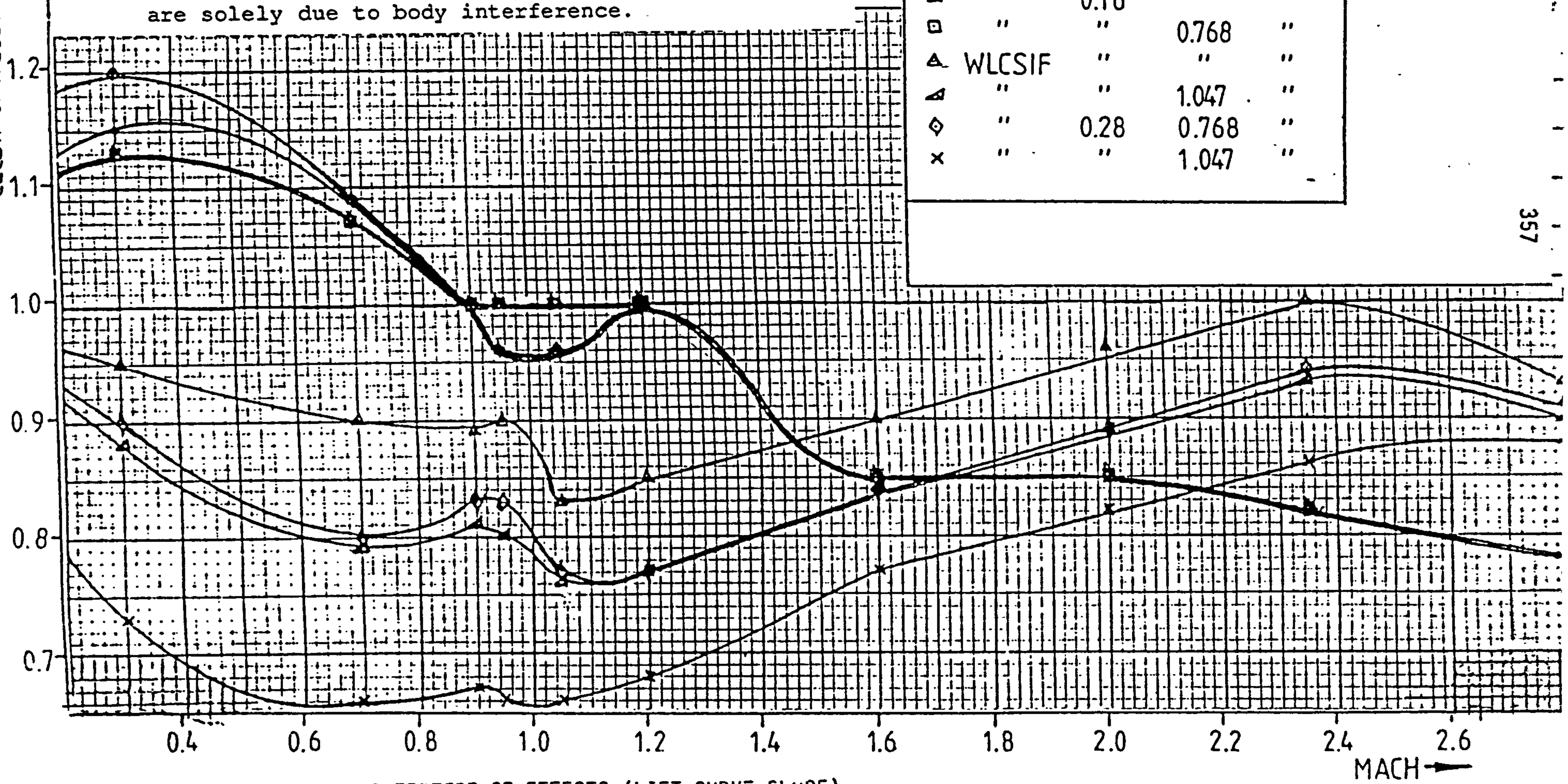

		RSCNW	QWL	RZCC
◇	CLCSIF	0.28	0.768	0.000
+	"	"	1.047	"
△	"	0.16	"	"
□	"	"	0.768	"
△	WLCSIF	"	"	"
◁	"	"	1.047	"
◇	"	0.28	0.768	"
×	"	"	1.047	"

FIG. G11 CANARD-DELTA INTERFERENCE EFFECTS (LIFT-CURVE-SLOPE)

CANARD-DELTA INTERFERENCE EFFECTS (LIFT-CURVE-SLOPE)

NOTE : The factors CLCSIF and WLCSIF also include the body interference effects.The supersonic values of CLCSIF are solely due to body interference.

		RSCNW	QWL	RZCC
○	CLCSIF	0.28	0.768	0.185
+	"	"	1.047	"
△	"	0.16	"	"
□	"	"	0.768	"
▲	WLCSIF	"	"	"
◀	"	"	1.047	"
◇	"	0.28	0.768	"
×	"	"	1.047	"

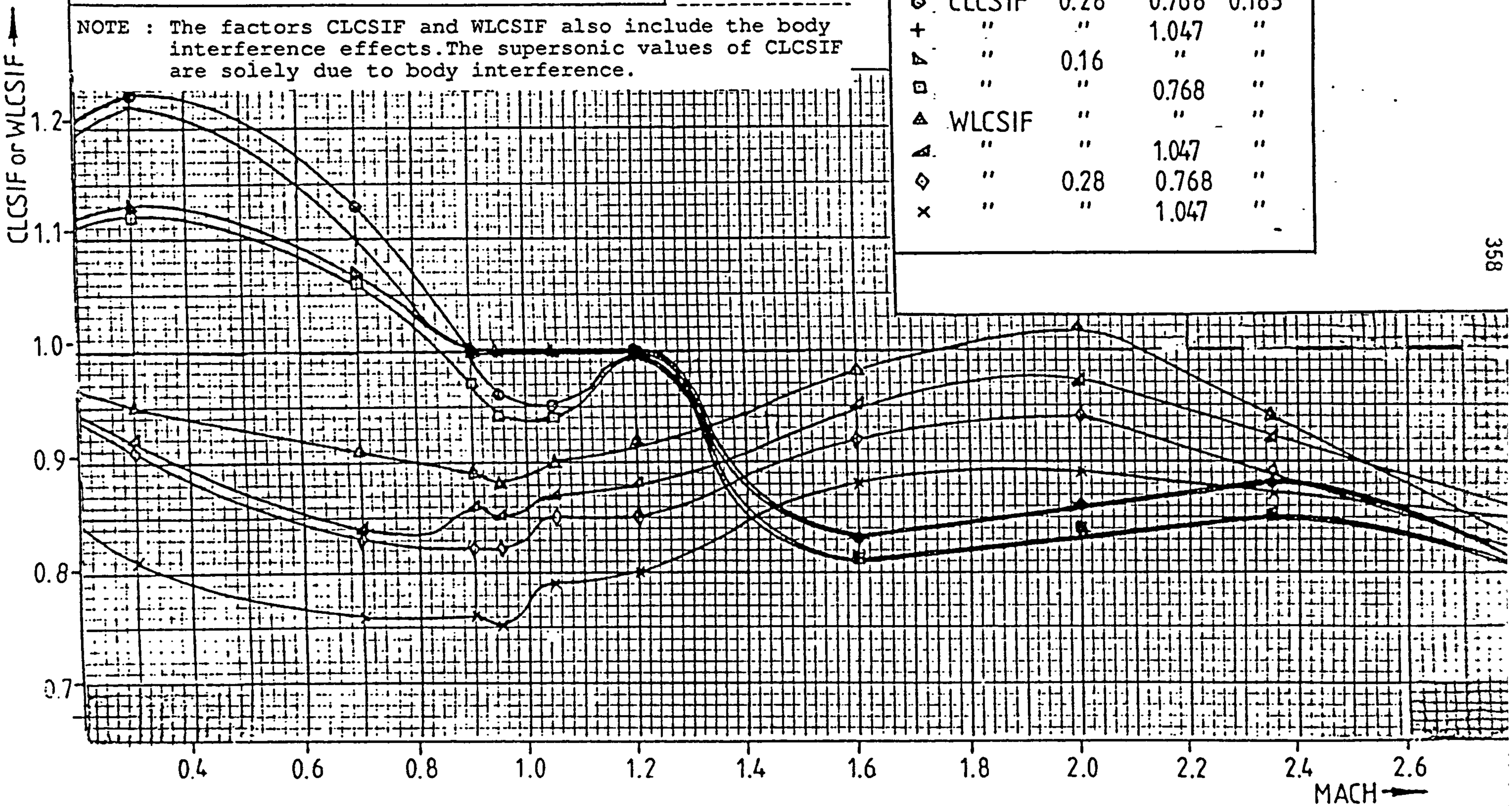

FIG. G.11 (CONTINUED)

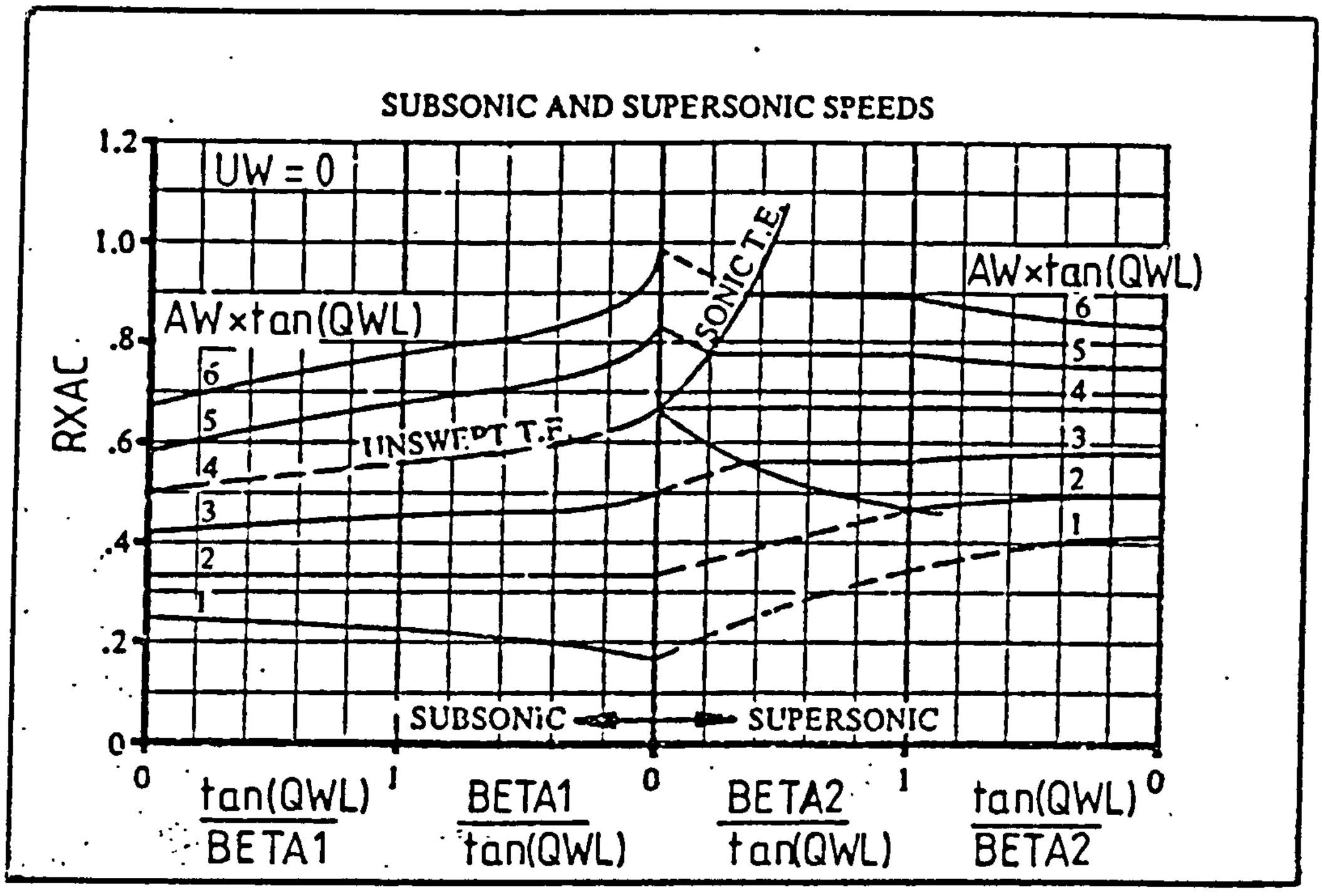

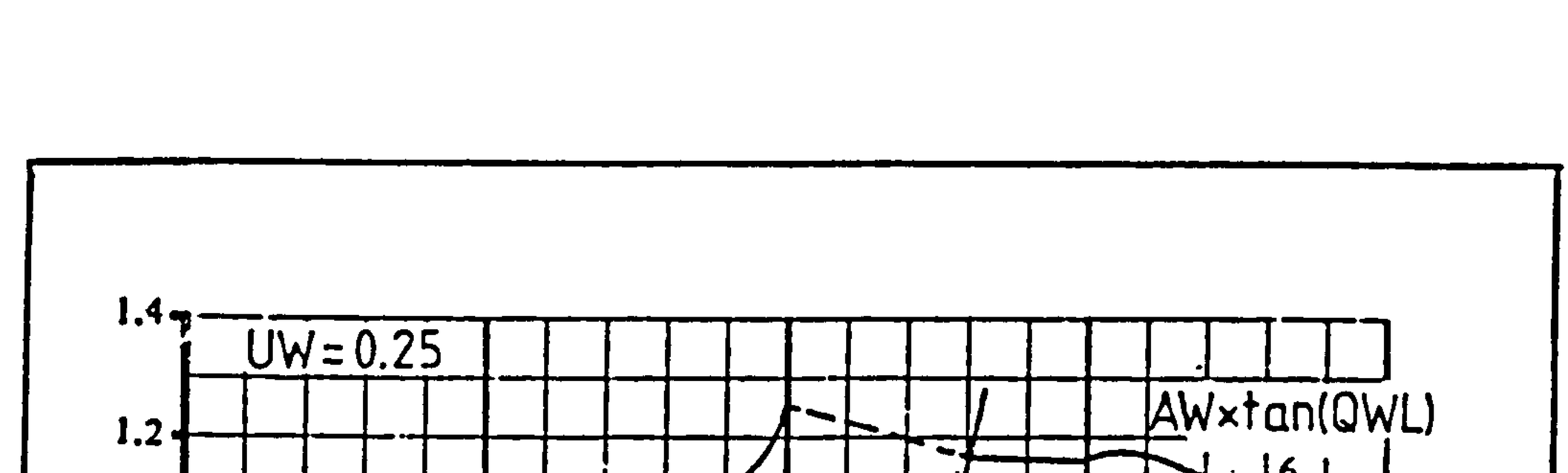

FIG. G.12 WING AERODYNAMIC CENTRE POSITION

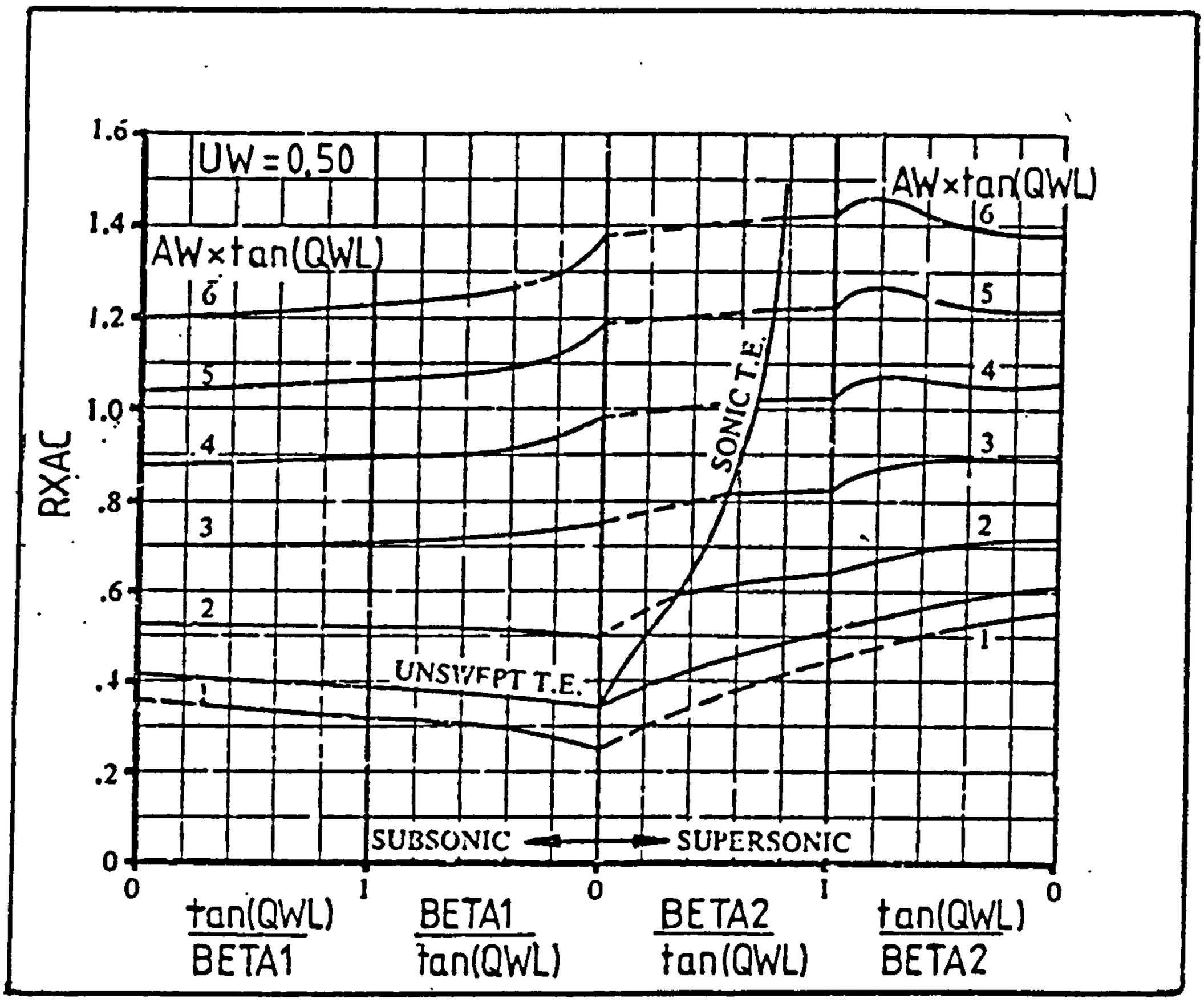

FIG. G.12 (CONTINUED)

APPENDIX H

AERODYNAMIC DRAG

H.1 INTRODUCTION

The overall aircraft aerodynamic drag is made up by five separately estimated components. These are the basic zero lift drag, wave drag, spillage drag, store drag and lift-dependent drag. The estimation of the first three components is based on methods used in ref.1 The store and lift-dependent drag methods were developed by the author. The trim drag contribution to the overall aircraft drag is neglected in this synthesis, for the reasons explained in chapter 5.

Pages 362 - 382

RESTRICTED FROM PUBLICATION (Ref.1)

H.2 Basic Zero Lift drag
H.3 Wave Drag
H.4 Spillage Drag

Actual installed drag coefficient data, for different types of stores are tabulated versus Mach number in file 'STDRAG.DAT'. These are obtained from wind-tunnel tests. Each column in this file represents a different type of store. The type of store selected at each store station is specified by an integer number, known as the drag code which denotes the corresponding column number. The drag codes for the fuselage-mounted stores no. 1 - 4 are, DCMUF1, DCMUF2, DCMUF3 and DCMUF4 respectively. The drag codes for the stores mounted on wing-pylons no. 1-4 are DCB1, DCB2, DCB3 and DCB4 while the drag codes for the wing-pylons alone are, DCXP1, DCXP2, DCXP3 and DCXP4 respectively. All drag codes are external variables.

The drag coefficients of the fuselage-mounted stores, CDMUF1, CDMUF2,CDMUF3 and CDMUF4 are obtained from the appropriate data columns by interpolating with respect to the given flight Mach number. The drag coefficients of the wing-mounted stores, CDB1, CDB2, CDB3 and CDB4 and wing-pylons, CDXP1, CDXP2, CDXP3 and CDXP4 are also obtained in the same way.

It is assumed that each wing-pylon may carry more than one store of the same type, the number of which is specified by external variables NB1, NB2, NB3 and NB4 respectively. Therefore, multiple-carriage factors FMCB1, FMCB2, FMCB3 and FMCB4 are defined in the input data which account for the drag effects due to side-by-side or tandem carriage.

The store release status is a further feature incorporated in this module. This is defined by eight external variables, SRMUF1, SRMUF2, SRMUF3, SRMUF4, SRB1,SRB2, SRB3 and SRB4. Each of these variables refers to one of the eight fuselage or wing store stations, respectively, and indicates the proportion of the initially

selected number of stores that remains at each station, following a release.

The total installed drag coefficient for the stores (CDSTOR) is therefore given by the following expression:

$$CDSTOR = CDMUF1 * SRMUF1 + CDMUF2 * SRMUF2 + CDMUF3 * SRMUF3 + CDMUF4 * SRMUF4 + CDB1 * SRB1 * NB1 * FMCB1 + CDB2* SRB2 * NB2 * FMCB2 + CDB3 * SRB3 * NB3 * FMCB3 + CDB4 * SRB4 * NB4 * FMCB4 + CDXP1 + CDXP2 + CDXP3 + CDXP4 \quad (H.88)$$

H.6 CANARD-DELTA INTERFERENCE EFFECTS ON LIFT-DEPENDENT DRAG (Module LDDINT)

The lift-dependent drag coefficient shows a parabolic variation with lift which is divided into two regions. The lower region below the critical lift coefficient and the upper region above it, which are defined by parameters K1 and K2 respectively. A preliminary investigation by the author into the canard-delta interference effects on lift-depedent drag, indicated that the addition of a close-coupled foreplane to a delta wing-body combination reduces significantly its values of K1 and K2. Therefore a detailed analysis of wind-tunnel data was then carried out and suitable canard-delta interference factors were determined, which individually correct the predicted values of K1 and K2 for the wing-body combination and hence produce accurate lift-dependent drag estimates for the complete aircraft.

The above method is compatible with the previously developed canard-delta l-c-s interference technique and is based on wind-tunnel data from the same models. The

development of the method is presented in more detail in chapter 5.

The canard-delta interference factors for K1(LDDK1F) and K2 (LDDK2F), are obtained from fig.H.1 for the given values of M, QWL, RSCNW and RZCC.

Pages 385 - 388

RESTRICTED FROM PUBLICATION (Ref.1)

H.7 Lift-Dependent Drag (Part)

The value of parameter K2 for any Mach number is,

$$K2 = K1 + DK2 \qquad \text{(H.111)}$$

The increment DK2, together with the critical lift coefficient (CLC) which is the transition point between the lower and upper regions of a drag polar, and also the maximum lift coefficient (CLMAX), depend on the technology used in the design of the wing and high-lift system and they are therefore not estimated but supplied in tabular form versus Mach number, in file 'LDD2.DAT' as data applicable only to each specific case. The required values of DK2, CLC and CLMAX for a given Mach number are obtained by interpolation.

The above estimated values of K1 and K2 are corrected for the effects of canard-delta interference hence,

$$K1 = K1 * LDDK1F \qquad \text{(H.112)}$$

$$K2 = K2 * LDDK2F \qquad \text{(H.113)}$$

The lift-dependent drag coefficient (CDV) is determined from the known values of K1, K2, CLC and CL as shown below:

For CL < (CLC - 0.01) then,

$$CDV = \frac{K1 * CL^{2.0}}{PI * AW} \qquad \text{(H.114)}$$

For (CLC - 0.01) < CL < (CLC + 0.01) then,

$$CDV = \left(\frac{1.0}{PI * AW}\right) * (FCDVK\emptyset + FCDVK1 * CL^{2.0} + FCDVK2 * CL^{4.0} + FCDVK3 * CL^{6.0}) \qquad \text{(H.115)}$$

For CL > (CLC + 0.01) then,

$$CDV = \left(\frac{1.0}{PI * AW}\right) * [K2 * CL^{2.0} + (K1 - K2) * (CLC - 0.01)^{2.0}] \quad (H.116)$$

H.8 TOTAL AIRCRAFT DRAG (Module DRAG)

Module DRAG controls the order of execution of modules ZLDRAG, WDRAG, SPDRAG, STDRAG, LDDINT and LDDRAG and determines the total aircraft drag coefficient (CDTOT) by considering also the low-speed afterbody, extended undercarriage and flap contributions.

According to ref.1 , for M < 0.8, the afterbody drag coefficient (CDB) is,

$$CDB = \left[\frac{0.05 * (OFK - OPJ)}{OFG - OPJ} + 0.014\right] * \left(\frac{OFG}{SW}\right) \quad (H.117)$$

and the extended undercarriage drag coefficient (CDUT) is,

$$CDUT = 0.02 * SUC \quad (H.118)$$

where, SUC = Retractable undercarriage status (SUC = 0 for u/c up and SUC = 1 for u/c down).

SUC is an external variable.

According to ref.57, the drag increment due to trailing - edge flap deflection (DCDF) at any Mach number is,

$$DCDF = 0.0015 * EQWF * \left(\frac{BWF}{BW}\right) \quad (H.119)$$

The total aircraft drag coefficient (CDTOT) is therefore,

$$CDTOT = CD\emptyset V + CDTW + CDS + CDSTOR + CDV + CDB + CDUT + DCDF \quad (H.120)$$

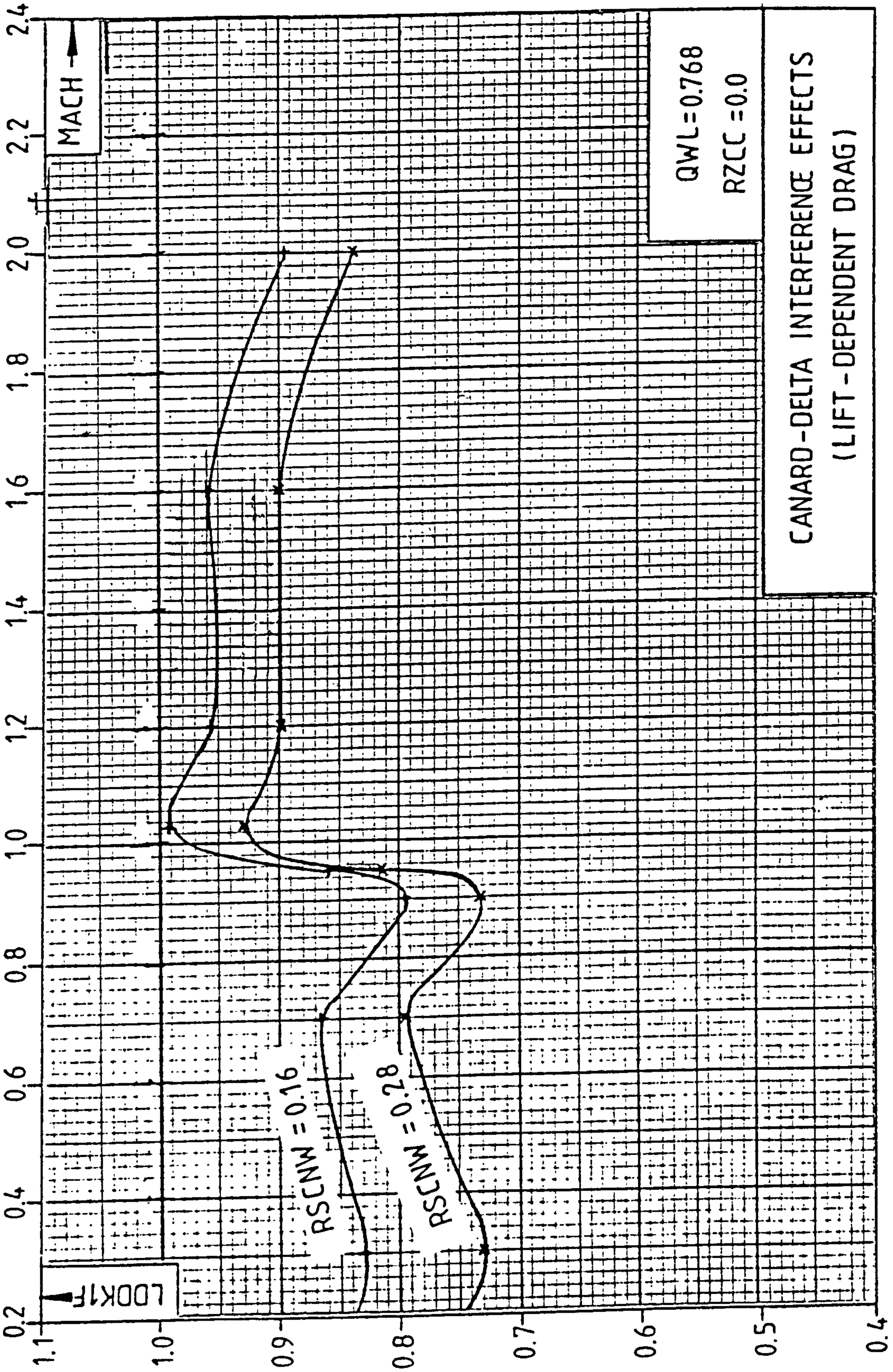

FIG. H.1 CANARD-DELTA INTERFERENCE EFFECTS (LIFT-DEPENDENT-DRAG)

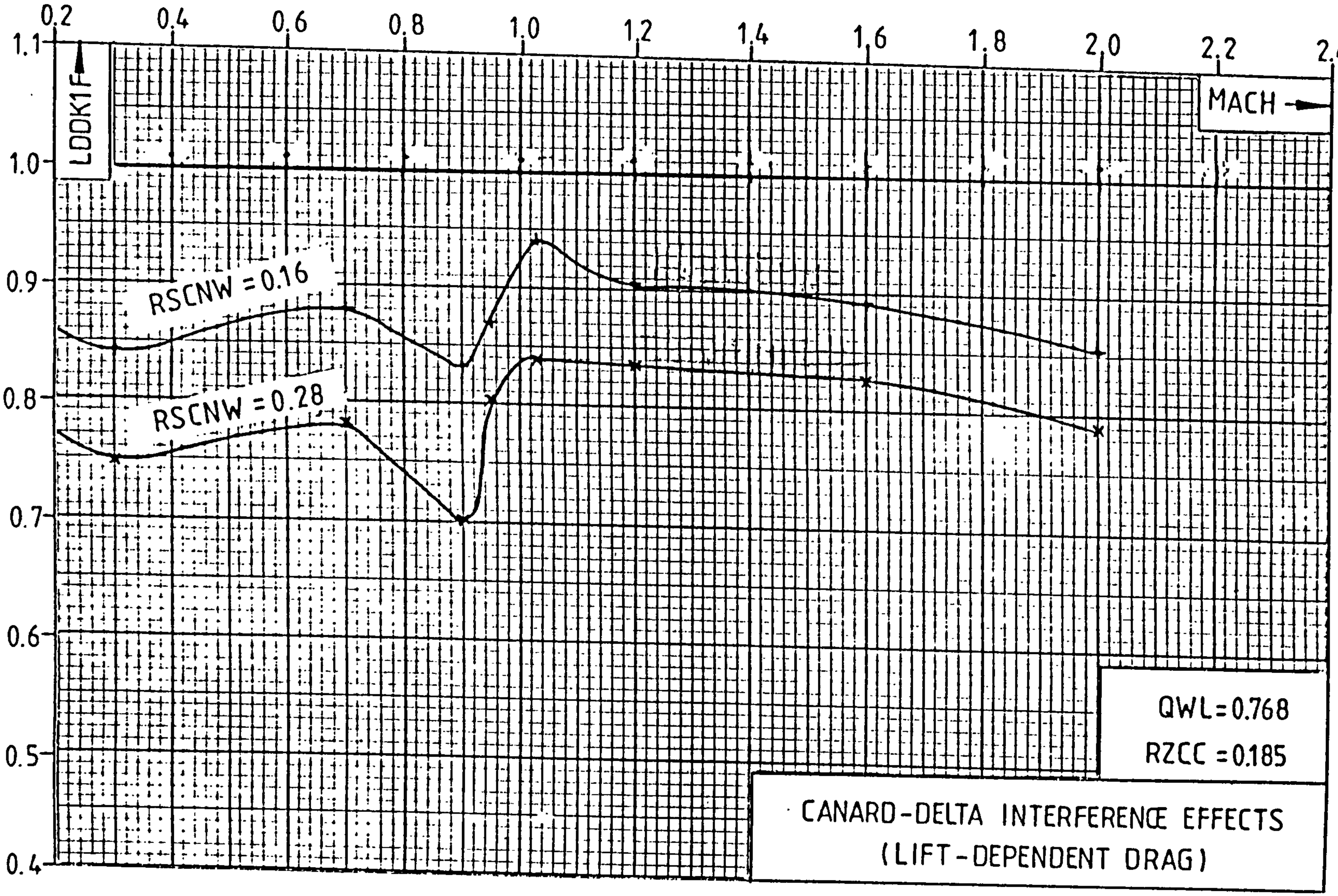

FIG. H.1 (CONTINUED ...)

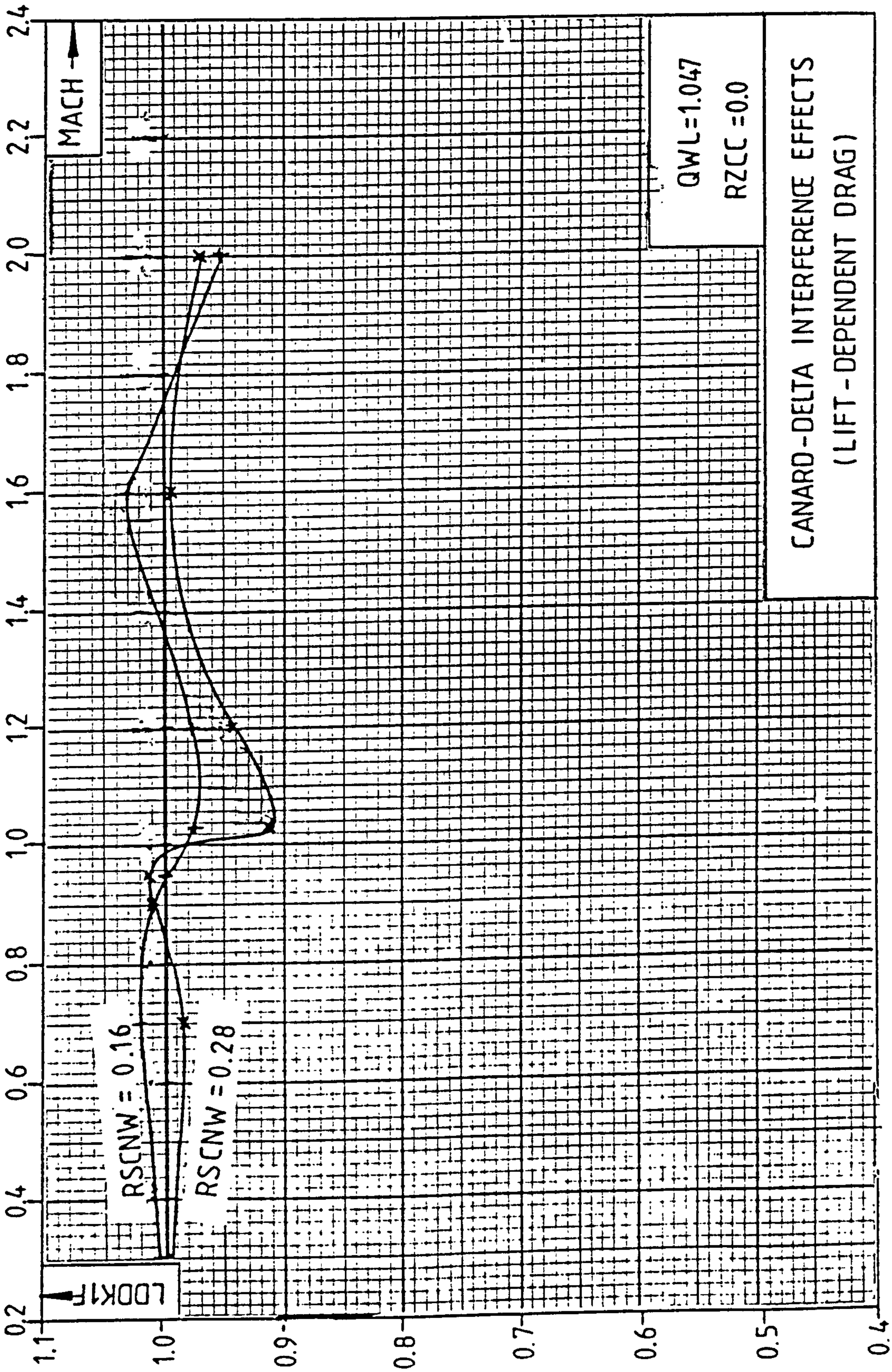

FIG. H.1 (CONTINUED ...)

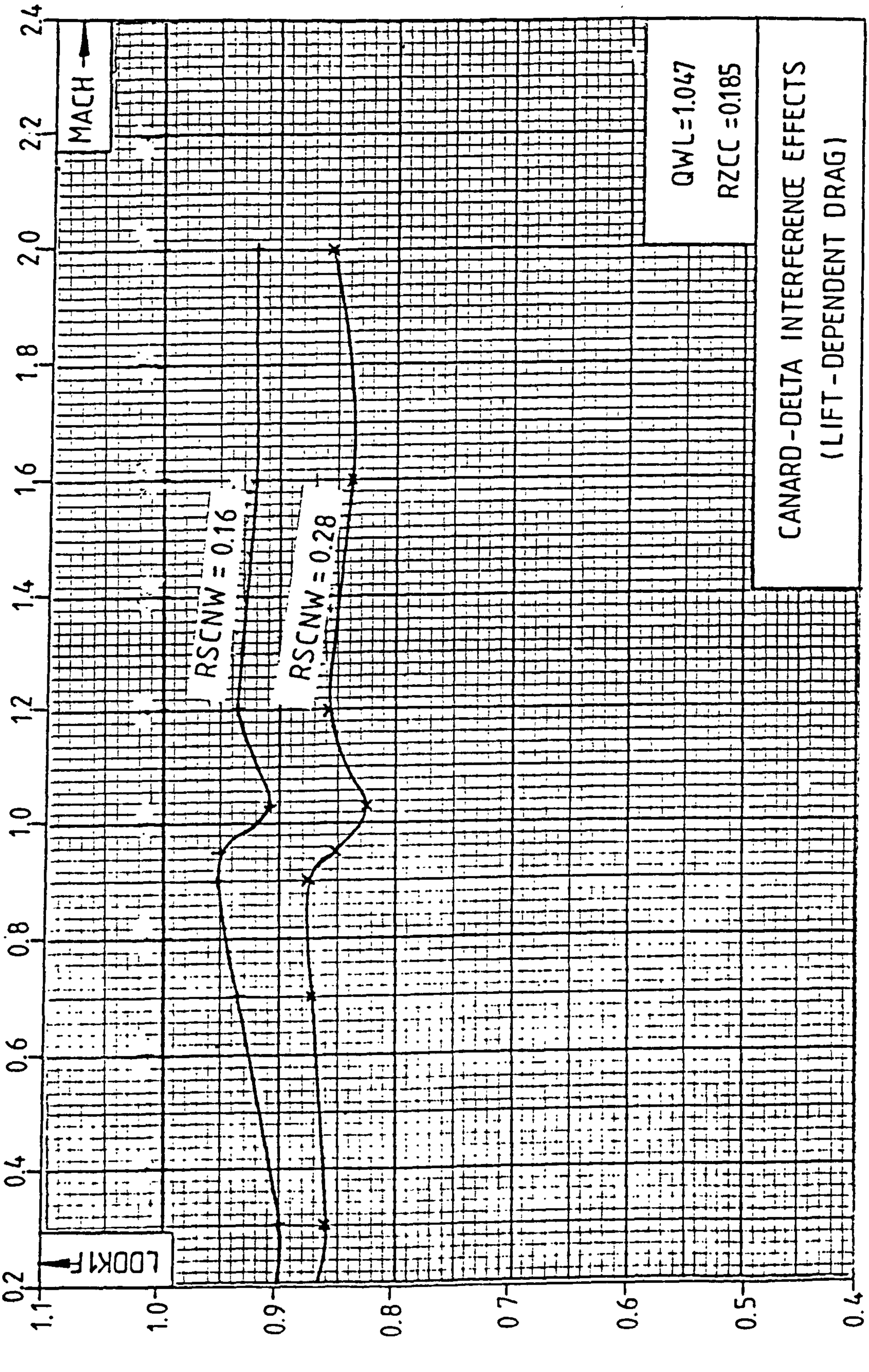

FIG. H.1 (CONTINUED ...)

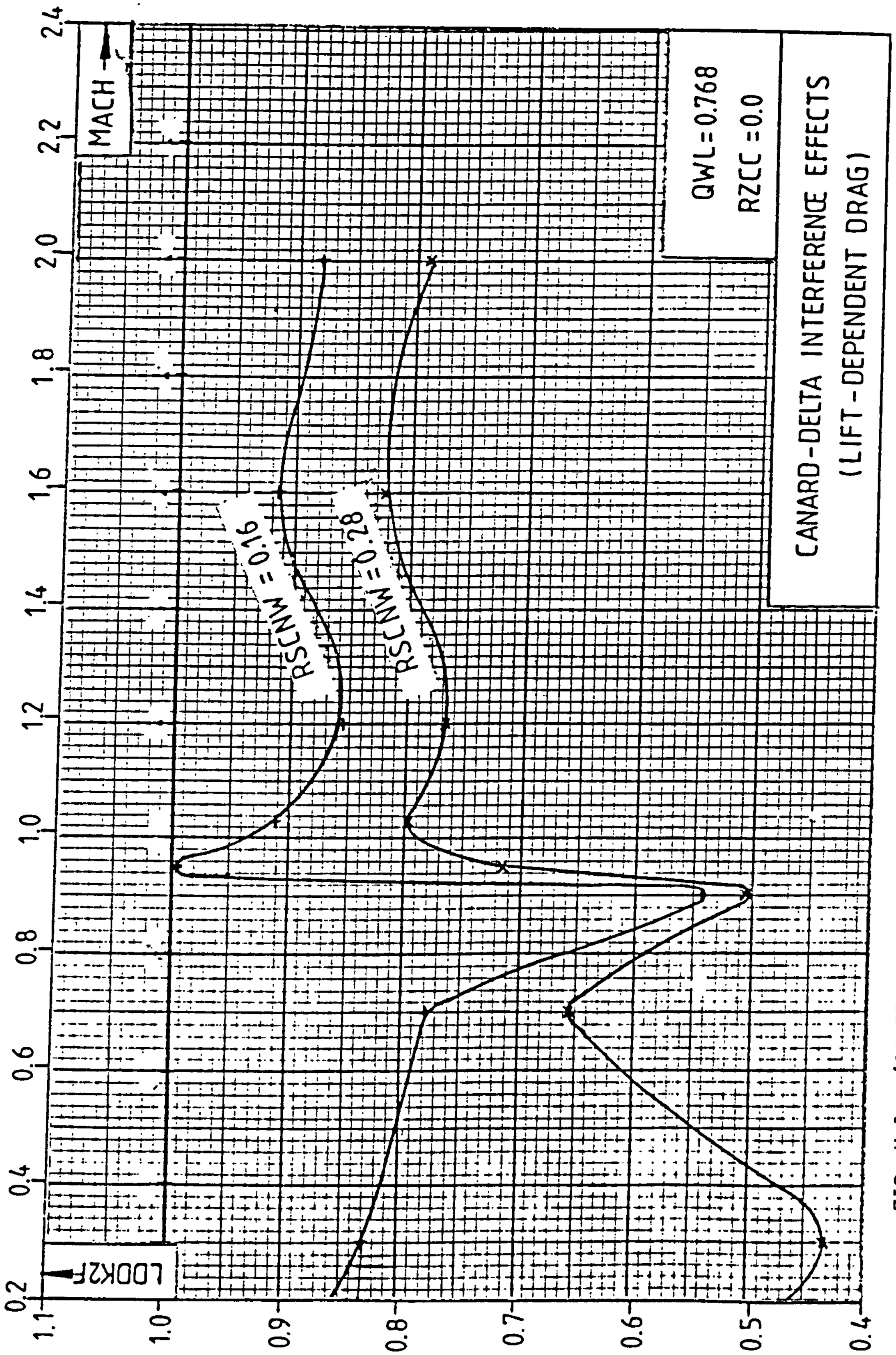

(CONTINUED ...)

FIG. H.1 (C

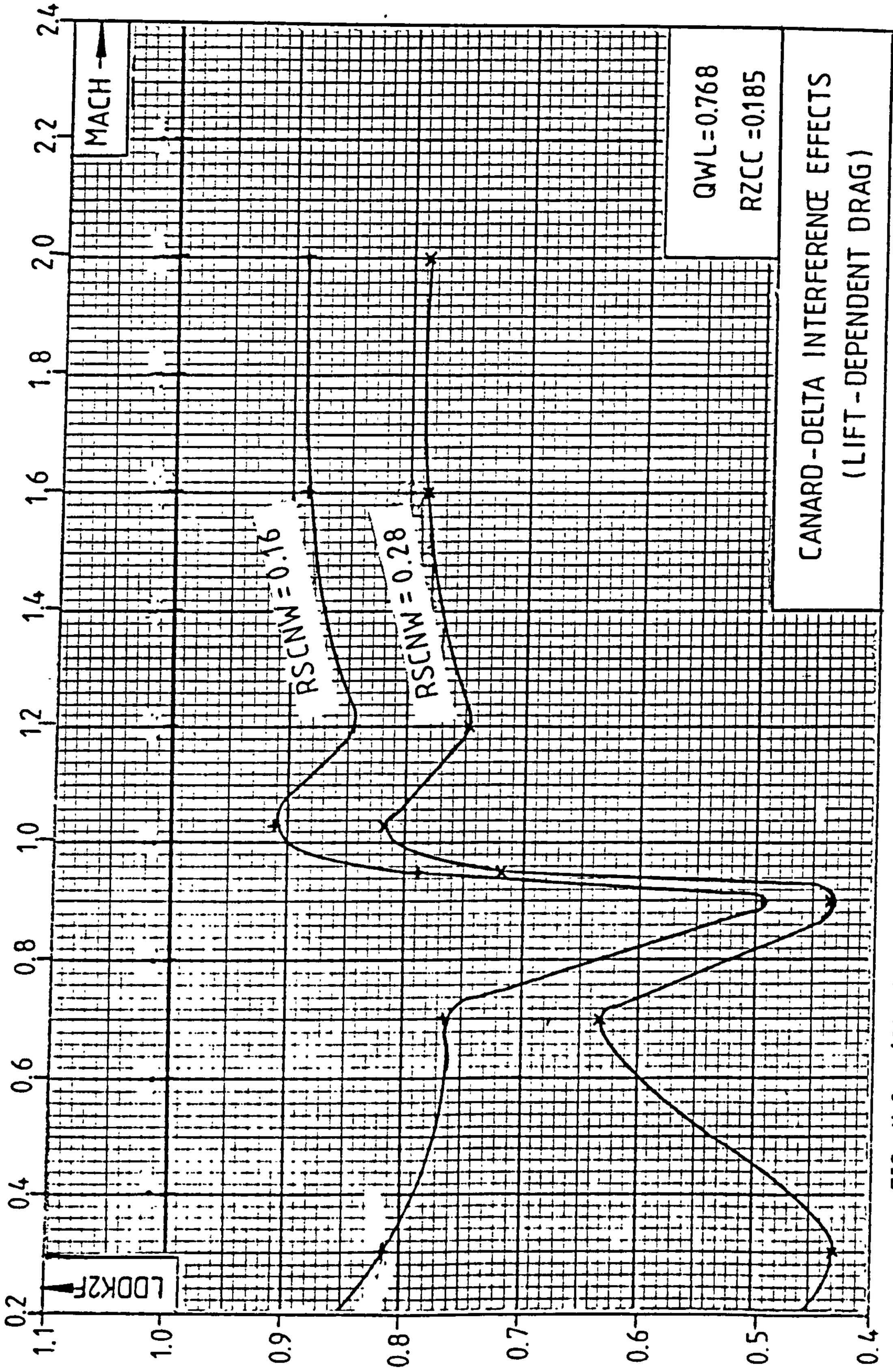

(CONTINUED ...)

FIG. H.1

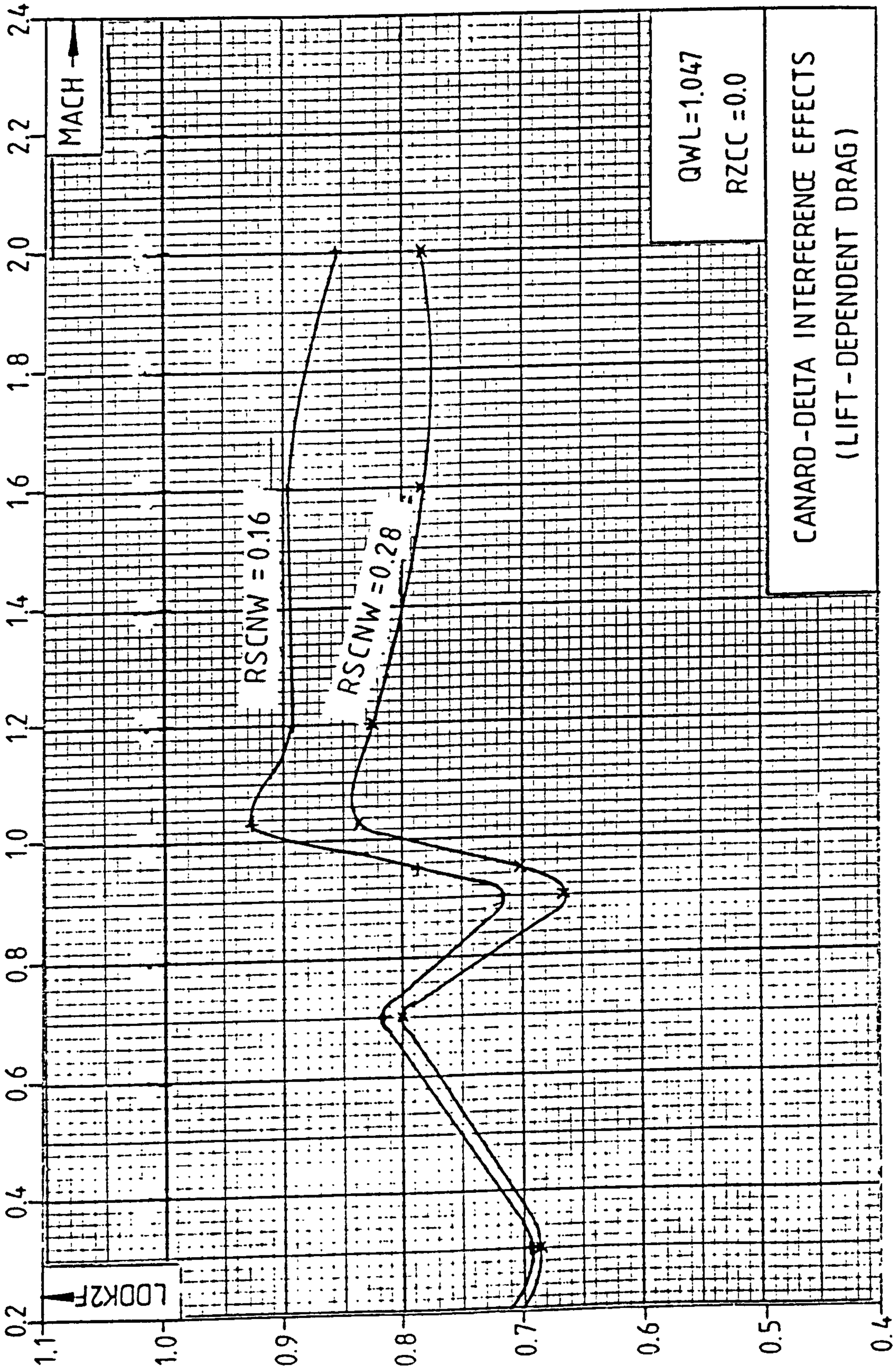

FIG. H.1 (CONTINUED ...)

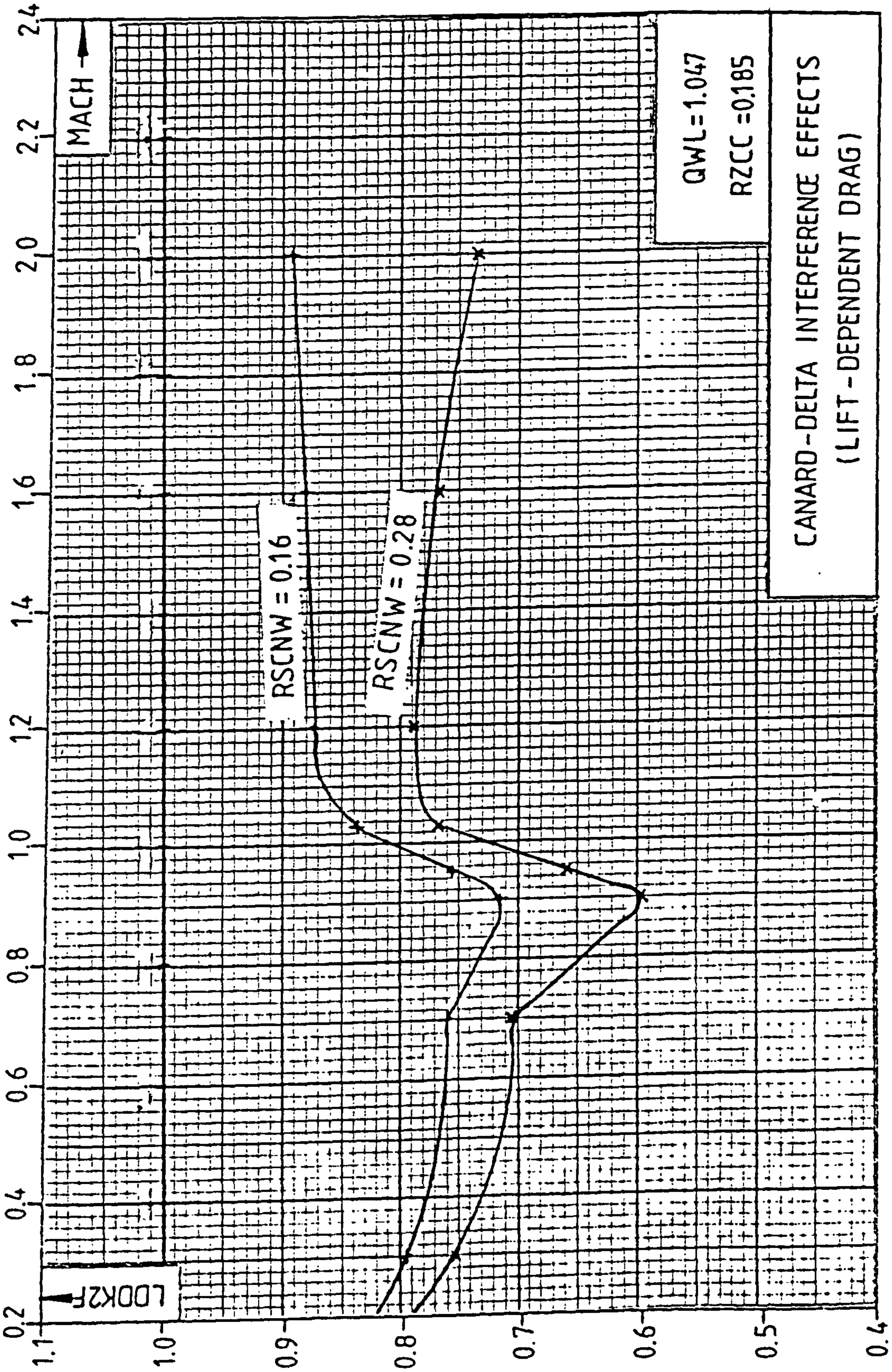

(CONTINUED)

FIG. H.1

APPENDIX I

AIRCRAFT PERFORMANCE ESTIMATION

I.1 INTRODUCTION

The methods used in the synthesis for the estimation of the aircraft's performance are presented and explained in this appendix. These are divided into four groups:

a) Engine Performance
b) Sortie Performance
c) Take-off and Landing Performance
d) Point Performance

I.2 ENGINE PERFORMANCE (Module ENGPER)

This module was developed by RAE(F) and consists of a set of empirical relationships which are based on a modern military turbofan engine. These are scaled using the thrust scale factor RTP, as in the engine sizing calculations.

Module ENGPER may be executed in five different modes as shown below:

MODE = 1: Given TPG, calculates MPA, OPJ, MPF and FPS
MODE = 2: Given TPG, calculates MPA, OPJ, MPF
MODE = 3: Given FPS, calculates TPG, MPA, OPJ, MPF
MODE = 4: Given FPS. calculates TPG, MPA, OPJ
MODE = 5: Given FPS, calculates TPG, MPF

where, TPG = Total gross thrust of the engines for given Mach number, height and throttle setting
FPS = Engine throttle setting
MPA = Air mass flow rate
MPF = Fuel mass flow rate
OPJ = Jet exit area

Some of the expressions in module ENGPER make use of function BLEND (Y1,Y2,E, S). This was developed by RAE(F) (ref.1) and provides a method of fairing the intersection of two functions Y1 and Y2 with a maximum allowable deviation E. If S = 1, it uses the greater of Y1 and Y2. If S = -1, it uses the lesser.

Function BLEND is defined by the following expressions:

$$Z1 = 0.5 * (Y2 - Y1) \qquad (I.1)$$

$$Z2 = 0.375 * Z1 * S \qquad (I.2)$$

$$Z3 = 0.140625 * \left(\frac{Z1}{E}\right)^{2.0} \qquad (I.3)$$

$$\text{If } Z2 < -E, \quad BLEND = Y1 \qquad (I.4)$$

$$\text{If } Z2 > E, \quad BLEND = Y2 \qquad (I.5)$$

$$\text{If } -E < Z2 < E, \quad BLEND = S * E * \left[1 + Z3 * \left(2 - \frac{Z3}{3}\right)\right] + Z1 + Y1 \qquad (I.6)$$

The engine performance estimation starts with the calculation of the datum conditions for maximum dry and reheat thrust.

The maximum combat dry gross thrust (RTPG1H) at any height is,

$$RTPG1H = \frac{TPGD1 * (1.0 + 0.07 * M + 1.4 * M^{2.0})}{TPGD2} \qquad (I.7)$$

The datum values of gross thrust, TPGD1 and TPGD2 are external variables specified in the input data.

The combat dry gross thrust (RTPG1) is,

$$RTPG1 = RTPG1H * BLEND\ (1.573 - 0.414 * M - 0.3338 * RP,\ 1.0,\ 0.005,\ -1.0) \qquad (I.8)$$

RP is obtained from module ATMOS for the given height.

The gross thrust at the combat reheat rating (RTPG2) is,

$$RTPG2 = \frac{(1.0 + 0.07 * M + 1.4 * M^{2.0}) * (1.0 - 0.1 * RP)}{0.9 * (1.0 + 0.048 * RP * M^{4.0})} \quad (I.9)$$

The fuel mass flow rate at the combat dry thrust rating at a height of 11000 m (RMPF1H) is,

$$RMPF1H = 0.164 + 0.01 * M + 0.17 * M^{2.0} \quad (I.10)$$

The fuel mass flow rate at the combat dry thrust rating at any height (RMPF1) is,

$$RMPF1 = 0.0425 + (RMPF1H - 0.0425) * \left(\frac{1.32 * RTPG1}{RTPG1H} - 0.32\right) \quad (I.11)$$

The fuel mass flow rate at the combat reheat thrust rating (RMPF2) is,

$$RMPF2 = RTPG2 * [0.0000145 * HT + 0.035 * (M * RP)^{2.0} + 1.0 - 0.18 * M] \quad (I.12)$$

The maximum air mass flow rate (RMPA1H) is,

$$RMPA1H = 1.0 + 0.375 * M + 0.375 * M^{2.0} \quad (I.13)$$

The jet-exit area at the combat dry thrust rating (ROPJ1) is,

$$ROPJ1 = 0.526 * [1.0 - (RTPG1 + 1.1046)^{-6.704}] + 0.0004 * (RTPG1 + 0.2)^{-4.0} \quad (I.14)$$

The jet-exit area at the combat reheat thrust rating (ROPJ2) is,

$$ROPJ2 = 1.1395 - 0.25375 * RP + 0.13125 * RP^{2.0} \qquad (I.15)$$

The next step following the calculation of the datum conditions above, is to determine the gross thrust for a given throttle setting. It should be noted however, that the external variable XV and the dependent variable R1 have double meaning in the following expressions, depending on the MODE.

Therefore,

for MODE = 1 or 2 , XV = TPG, R1 = FPS
for MODE = 3, 4 or 5 , XV = FPS, R1 = TPG

For MODE = 3, 4 or 5, the non-dimensional gross thrust (RTPG) is as follows:

$$\text{If } XV < 50.0 \text{ then, } RTPG = 0.02 * RTPG1 * XV \qquad (I.16)$$

$$\text{If } XV > 50.0 \text{ then, } RTPG = 0.02 * (RTPG2 - RTPG1) * (XV - 50.0) + RTPG1 \qquad (I.17)$$

The gross thrust is therefore,

$$R1 = RTPG * TPGD * RP \qquad (I.18)$$

$$\text{For MODE = 1 or 2, } RTPG = \frac{XV}{TPGD * RP} \qquad (I.19)$$

The fuel mass flow rate (MPF) for MODE = 1,2,3 or 5 is,

$$MPF = MPFD * RP * RRT * BLEND\ (R21,\ R22,\ 0.005.\ -1.0)\ \ (kg/s) \qquad (I.20)$$

The functions R21 and R22 are:

$$R21 = (RMPF1H - 0.0425) * \left(\frac{1.32 * RTPG}{RTPG1H} - 0.32\right) + 0.0425 \qquad (I.21)$$

and

$$R22 = (RTPG - RTPG1) * \left(\frac{RMPF2 - RMPF1}{RTPG2 - RTPG1}\right) + RMPF1 \qquad (I.22)$$

$$RRT = RT^{0.5} \qquad (I.23)$$

RT and RP are obtained from module ATMOS for the given height.

The air mass flow rate (MPA) for MODE = 1, 2, 3 or 4, is,

$$MPA = MPAD * RP * RMPA1H * BLEND(0.05947 + 0.4676 * RRTPG - 0.21007 * RRTPG^{2.0} + 0.683 * RRTPG^{0.4673},\ 1.0,\ 0.005,\ -1.0)\ \ (Kg/s) \qquad (I.24)$$

where,

$$RRTPG = \frac{RTPG}{RTPG1} \qquad (I.25)$$

The jet-exit area (OPJ) for MODE = 1, 2, 3 or 4, is,

$$OPJ = OPJD * BLEND (R41, R42, 0.005, -1.0) \quad (m^2) \quad (I.26)$$

The functions R41 and R42 are:

$$R41 = 0.526 * [1.0 - (RTPG + 1.1046)^{-6.704}] + 0.0004 * (RTPG + 0.2)^{-4.0} \quad (I.27)$$

and

$$R42 = (RTPG - RTPG1) * \left(\frac{ROPJ2 - ROPJ1}{RTPG2 - RTPG1}\right) + ROPJ1 \quad (I.28)$$

Finally, the throttle setting for MODE = 1 is determined as follows:

$$\text{If } RTPG < RTPG1 \text{ then, } R1 = \frac{50.0 * RTPG}{RTPG1} \quad (I.29)$$

$$\text{If } RTPG > RTPG1 \text{ then, } R1 = \frac{50.0 * (RTPG - RTPG1)}{(RTPG2 - RTPG1)} + 50.0 \quad (I.30)$$

The values of TPGD, MPFD, MPAD and OPJD were determined earlier in module ENGS1Z.

I.3 SORTIE PERFORMANCE (Module SORTIE)

In the sortie performance calculations, the synthesized aircraft is assumed to fly a hypothetical sortie comprising a given number of stages (NSTAG) or legs. Each sortie leg has a specified length (SLEG) expressed in km and is assumed that is flown at a constant height (HT), Mach

number (M) and load factor (GN). This assumption simplifies the sortie performance module and maintains the required computation time within the acceptable synthesis limits. Performance calculations for those sortie legs involving climbing, descending or longitudinal acceleration flight, are therefore approximated by appropriately modifying the leg length or the corresponding load factor. The take-off and landing phases of a flight are not included in the first and last legs of a specified sortie but allowance is made in the calculations for the changing aircraft mass due to fuel consumption by assuming that the fuel mass required for take-off (MTTF) and landing (MTLF) are known.

The sortie performance module offers great flexibility with regard to aircraft configuration changes during the sortie. The release status for each store station is specified in the input data, for every sortie-leg. This allows the release of any combination of stores along any sortie-leg. Similarly specified are also the undercarriage status and the trailing-edge flap deflection. Such configuration changes result in mass, lift and drag changes which are accurately calculated and their effects on the aircraft performance are considered during every step of the sortie analysis.

According to the baseline aircraft assumptions, external fuel tanks may be carried under wing-pylons no.2 and no.3. A special segment is incorporated in module SORTIE which automatically jettisons any externally carried fuel tanks, when the total fuel consumption exceeds the specified external fuel mass. This assumes that the contents of the external tanks are always consumed first during a sortie and that when two tanks are carried, these supply fuel to the engine simultaneously.

The sortie performance calculations start with the estimation of the aircraft mass (MASS) at the beginning of the first leg.

$$MASS = MTT - MTTF \qquad (I.31)$$

MTT was estimated earlier during the mass prediction calculations and MTTF is an external variable.

The aircraft mass at the beginning of a particular sortie-leg is obtained by subtracting the mass of fuel consumed (MPFB2) and the mass of stores released (SRMASS) along the previous leg from the aircraft mass at the beginning of the previous leg, hence,

$$MASS = MASS - MPFB2 - SRMASS \qquad (I.32)$$

where, SRMASS is calculated by the following expression:

$$\begin{aligned} SRMASS = MTS - (&SRB1 * MB1 + SRB2 * MB2 + SRB3 * MB3 + \\ &SRB4 * MB4 + SRMUF1 * MMUF1 + SRMUF2 * MMUF2 + \\ &SRMUF3 * MMUF3 + SRMUF4 * MMUF4) \end{aligned} \qquad (I.33)$$

The initial value of MTS is obtained from the mass prediction results. The value of MTS is revised for each of the subsequent legs, by,

$$MTS = MTS - SRMASS \qquad (I.34)$$

At the beginning of the first leg, MPFB2 is zero. For the subsequent sortie legs, MPFB2 is estimated iteratively as explained later in this section. Preceding to this, however, is another iteration process for the estimation of the maximum sustained aircraft incidence (ALH) and lift coefficient (CL2) as shown below.

The iterations start using a lift coefficient CL1, which is an initial estimate for CL2. This is an external variable specified in the input data for each sortie-leg. The corresponding value of ALH with the flaps up is,

$$ALH = \frac{CL1}{GCL} \quad \text{(rads)} \qquad \text{(I.35)}$$

GCL is obtained from module LIFTSL for the given Mach number.

When the flaps are down, assuming that the wing-fuselage angle is zero, ALH is given by the following expression:

$$ALH = \left(\frac{CL1}{DCLF} - 1.0\right) * \left(\frac{DCLF}{GCL}\right) \quad \text{(rads)} \qquad \text{(I.36)}$$

DCLF is given by module DLFLAP for the given flap deflection angle.

The lift-dependent drag coefficient corresponding to CL2 is,

$$CDV = \frac{TPGC * \cos(ALH) - V * MPAC}{Q * SW} - CDTOT \qquad \text{(I.37)}$$

The value of CDTOT used in the above expression represents the minimum drag of the aircraft for the given Mach number and is obtained from module DRAG for a zero lift coefficient.

The aircraft speed (V) and the corresponding dynamic pressure (Q) are,

$$V = M * SSPD \quad \text{(m/s)} \tag{I.38}$$

$$Q = 0.5 * RO * V^{2.0} \quad \text{(Pa)} \tag{I.39}$$

SSPD and RO are obtained from module ATMOS.

The maximum gross thrust (TPGC) and air mass flow-rate (MPAC) are calculated using module ENGPER in MODE = 3, for FPS = 100.0.

The value of CL2 is calculated as follows:

If CL1 < CLC - 0.01 then,

$$CL2 = \left(\frac{CDV * PI * AW}{K1} \right)^{0.5} \tag{I.40}$$

If CLC - 0.01 < CL1 < CLC + 0.01 then CL2 is calculated iteratively from the following equation, using Newton-Raphson's method.

$$FDVK0 + FCDVK1 * CL2^{2.0} + FCDVK2 * CL2^{4.0} + FCDVK3 * CL2^{6.0} = CDV * PI * AW \tag{I.41}$$

Otherwise if CL1 > CLC + 0.01 then,

$$CL2 = \frac{CDV * PI * AW - (K1 - K2) * (CLC - 0.01)^{2.0}}{K2} \tag{I.42}$$

The values of K1, K2, CLC, FCDVK0, FCDVK1, FCDVK2 and FCDVK3 used in the above expressions are obtained from module DRAG.

The aircraft incidence corresponding to the above calculated value of CL2 is as follows:

With flaps up,

$$ALH1 = \frac{CL2}{GCL} \quad \text{(rads)} \qquad \text{(I.43)}$$

With flaps down,

$$ALH1 = \left(\frac{CL2}{DCLF} - 1.0\right) * \left(\frac{DCLF}{GCL}\right) \quad \text{(rads)} \qquad \text{(I.44)}$$

If CL2 > CLMAX + DCLFH or |ALH - ALH1| < 0.00002 then the iterations stop and CL2 = CL1.

Otherwise the iterations continue with,

$$CL1 = CL1 + 0.93 * (CL2 - CL1) \qquad \text{(I.45)}$$

until any of the above two conditions is satisfied.

A second iteration process then follows, for the estimation of the maximum sustained load factor (GNH) halfway along the sortie leg under consideration.

An estimate (MPFB1) is provided initially for MPFB2, in order to start the iterations. This is also specified as an external variable in the input data for each sortie leg. The corresponding maximum sustained load factor is hence,

$$GNH = \frac{Q * SW * CL2 + TPGC * \sin(ALH)}{G * (MASS - 0.5 * MPFB1)} \qquad \text{(I.46)}$$

The values of CL2 and ALH above, are the results of the previous iteration process.

GNH is automatically constrained not to exceed the maximum human 'g'- tolerance limit (GTCPH), which is an external variable.

The time required to fly a leg (RT1) is,

$$RT1 = \frac{1000.0 * SLEG}{V} \quad \text{(sec)} \qquad \text{(I.47)}$$

The value of MPFB2 corresponding to GNH is,

$$MPFB2 = \frac{MPFC * RT1}{(GNH^{2.0} - 1.0)^{0.5}} \quad \text{(kg)} \qquad \text{(I.48)}$$

If GNH $<$ 1.0 or $|MPFB1 - MPFB2| < 0.01$ then the iterations stop. Otherwise the iterations continue with,

$$MPFB1 = MPFB1 + 0.96 * (MPFB2 - MPFB1) \qquad \text{(I.49)}$$

until any of the above two conditions is satisfied.

The gross-thrust (TPG2), consumed fuel mass (MPFB2), aircraft incidence (AL) and lift coefficient (CL), corresponding to the actual flight conditions, specified for each sortie leg,are estimated by a third iteration process.

This set of iterations start by providing a guess value (TPG1) for TPG2, which is an external variable, specified in the input data for each sortie-leg. Initial estimates for AL and MPFB2 are also similarly provided.

The engine throtle setting, fuel mass flow-rate and air mass flow-rate are calculated by module ENGPER which is executed in MODE = 1 for the given TPG1. The corresponding value of MPFB2 is given by the following expression:

$$MPFB2 = \frac{1000.0 * MPF * SLEG}{V} \quad \text{(Kg)} \quad \text{(I.50)}$$

The aircraft lift coefficient for the given conditions is hence,

$$CL = \frac{GN * G * (MASS - 0.5 * MPFB2) - TPG1 * \sin(AL)}{Q * SW} \quad \text{(I.51)}$$

and the aircraft incidence with flaps up is,

$$AL = \frac{CL}{GCL} \quad \text{(rads)} \quad \text{(I.52)}$$

and with flaps down is,

$$AL = \left(\frac{CL}{DCLF} - 1.0\right) * \left(\frac{DCLF}{GCL}\right) \quad \text{(rads)} \quad \text{(I.53)}$$

The total aircraft drag for the given conditions and estimated lift coefficient, is obtained from module DRAG.

Therefore,

$$TPG2 = \frac{V * MPA + Q * SW * CDTOT}{\cos(AL)} \quad \text{(I.54)}$$

If |MPFB1 - MPFB2| < 0.5 or |TPG1 - TPG2| < 1.0 then, the iterations stop. Otherwise the iterations continue with,

$$MPFB1 = MPFB2 \quad \text{(I.55)}$$

and $$TPG1 = TPG1 + 0.99 * (TPG2 - TPG1) \quad \text{(I.56)}$$

until any of the above two conditions is satisfied.

Finally, the total mass of fuel consumed up to the end of the sortie-leg under consideration (MPFB2T) is calculated by adding up the fuel consumed in the previous legs including MTTF. The value of (MPFB2T + MTLF) at the end of the last leg of the hypothetical sortie, represents the

total fuel mass required for such a mission and it may be compared to the total fuel mass stored in the aircraft tanks. The aircraft landing mass (MTL) is obtained by subtracting MTLF from the mass of the aircraft at the end of the last sortie leg, hence,

$$MTL = MASS - MTLF \qquad (I.57)$$

I.4 TAKE-OFF AND LANDING PERFORMANCE (Module TOLPERF)

This module determines the take-off and landing performance characteristics of the aircraft.

The total take-off distance (TOD) is the sum of the take-off ground roll (TOG) and airborne (TOA) distances which are estimated separately using the following empirical expressions which were obtained from ref.60. These expressions were modified by the author, to account also for the effects of airfield altitude on the take-off performance.

$$TOG = \frac{1.156 * FMTSW * ROSL}{RTPGW * TRATE * CLT * RO} \quad (m) \qquad (I.58)$$

and the airborne distance to clear a 15 m screen height,

$$TOA = \left(\frac{9.79}{RTPGW * TRATE}\right) * \left(\frac{FMTSW * ROSL}{CLT * RO}\right)^{0.5} \quad (m) \qquad (I.59)$$

hence,

$$TOD = TOG + TOA \quad (m) \qquad (I.60)$$

where, FMTSW = Wing mass loading at take-off

$$FMTSW = \frac{MTT}{SW} \quad (kg/m^2) \qquad (I.61)$$

RTPGW = Thrust to weight ratio at take-off.

$$RTPGW = \frac{TPGC}{MTT * G} \qquad (I.62)$$

CLT = Maximum lift coefficient in the take-off configuration

$$CLT = FCLT * CLMAX + DCLFH \qquad (I.63)$$

FCLT = Fraction of CLMAX available for take-off

TRATE = Fraction of TPGC available for take-off

Both FCLT and TRATE are external variables.

MTT is obtained from module MASSPR and TPGC from module ENGPER in MODE = 3, for HT = HTF and FPS = 100.0.

HTF = Airfield altitude (m)

The atmospheric properties used in these calculations are evaluated by a previous execution of module ATMOS for HT = HTF.

The value of DCLFH due to a specified flap deflection in the take-off configuration (EQWFT) is estimated from previous execution of modules LIFTSL and DLFLAP. EQWFT is an external variable specified in the input data in degrees.

The corresponding value of CLMAX is obtained from a table in file 'LDD2.DAT'.

The stall speed of the aircraft in the take-off configuration (VSTTO) is,

$$VSTTO = \left(\frac{MTT * G}{0.5 * RO * SW * CLT} \right)^{0.5} \quad (m/s) \qquad (I.64)$$

The take-off speed (VTO) is,

$$VTO = FVSTTO * VSTTO \quad \text{(m/s)} \qquad \text{(I.65)}$$

where, FVSTTO = Factor defining the take-off speed in terms of the stall speed.

FVSTTO is an exernal variable and its value is given in the appropriate valid MIL-STD.

The landing distance (LD) from an approach height of 15 m to a full stop is calculated by an empirical formula which was obtained from ref.2

$$LD = 7.1 * VAPR + 3.28 * \left[\frac{1.6}{FRK + \left(\frac{TPGREV}{MTL * G}\right)}\right] * \left(\frac{VAPR^{2.0}}{100.0}\right) \quad \text{(m)} \qquad \text{(I.66)}$$

where, VAPR = Approach speed (m/s)

FRK = Ground rolling friction coefficient

TPGREV = Maximum reverse thrust (N)

FRK is an external variable. Its value may be adjusted to include also the retardation effects of the airbrakes.

The approach speed is,

$$VAPR = FVSTAP * VSTAPP \quad \text{(m/s)} \qquad \text{(I.67)}$$

where, FVSTAP = Factor defining the appoach speed in terms of the stall speed

VSTAPP = Stall speed of the aircraft in the landing configuration

$$VSTAPP = \left(\frac{MTL * G}{0.5 * RO * SW * CLMAXL}\right)^{0.5} \quad \text{(m/s)} \qquad \text{(I.68)}$$

MTL is obtained from module SORTIE.

The maximum lift coefficient in the landing configuration is,

$$CLMAXL = FCLL * CLMAX + DCLFH \qquad \text{(I.69)}$$

where, FCLL = Fraction of CLMAX available for landing.

The value of DCLFH due to a specified flap deflection in the landing configuration (EQWFL) is estimated by a previous execution of modules LIFTSL and DLFLAP. Reverse thrust is assumed to be applied at a speed equal to 0.7 * VAPR. Therefore in order to determine the required value of TPGREV for use in the equation for LD, the maximum available forwrd thrust (TPGC) is first estimated by execution of module ENGPER in MODE = 3, for FPS = 100.0 and

$$M = \frac{0.7 * VAPR}{SSPD} \qquad \text{(I.70)}$$

TPGREV is then given by,

$$TPGREV = FTPGC * TPGC \quad \text{(N)} \qquad \text{(I.71)}$$

where, FTPGC = Fraction defining the maximum available reverse thrust in terms of TPGC.

FTPGC, EQWFL, FCLL and FVSTAP, are all external variables specified in the input data.

I.5 POINT PERFORMANCE

I.5.1 General

The point performance of the synthesized aircraft may be estimated for several different flight conditions specified in the input data. A total of six point performance parameters are assessed in separate modules These parameters are:

a) Sustained Turn Rate (STR)
b) Attained Turn Rate (ATR)
c) Specific Excess Power (SEP)
d) Maximum Mach Number (MMAX)
e) Acceleration Time (DT)
f) Ride Quality Factor (RQF)

The modules are presented in detail in the following sections.

I.5.2 Sustained Turn Rate (Module PPSTR)

The STR calculations start by specifying the flight Mach number, altitude, aircraft weight (WT), engine throttle setting and flap deflection angle. These are external variables and their values are given in the input data, for each point of a sortie at which an STR estimate is required.

The maximum sustained aircraft incidence (ALM) for a given throttle setting and the corresponding lift coefficient (CL4) are estimated in this module using again the first iteration process of module SORTIE (sectionI.3). In this case,however, the engine performance is estimated for the specified throttle setting and the variables ALH, ALH1, CL1, CL2 are replaced by ALM, ALM1,CL3 and CL4,

respectively. An initial value for CL3 is also provided in the input data in order to start the iterations.

The corresponding sustained load factor(GNS) is,

$$GNS = \frac{Q * SW * CL4 + TPG * \sin(ALM)}{WT} \qquad (I.72)$$

The above estimated value of GNS is automatically constrained not to exceed its maximum allowable value (GNSH) which is defined below:

$$GNSH = \left[\frac{GTCPH}{\frac{ULTN}{1.5}} \right] \quad \text{(the least)} \qquad (I.73)$$

where, ULTN = Ultimate load factor in structural design

ULTN is also an external variable specified in the input data.

Finally the sustained turn rate is given by the following expression:

$$STR = \left(\frac{180.0 * G}{PI * V} \right) * (GNS^{2.0} - 1.0)^{0.5} \qquad \text{(degrees/sec)} \qquad (I.74)$$

I.5.3 Attained Turn Rate (Module PPATR)

The flight Mach number, altitude, engine throttle setting, aircraft weight and flap deflection angle are specified in the input data for each point of a sortie at which the ATR needs to be evaluated.

The aircraft speed and the corresponding dynamic pressure are calculated first. The engine thrust is then determined for the given throttle setting. The aircraft

lift-curve-slope, maximum lift increment due to flaps and maximum lift coefficient are then estimated in order to calculate the maximum attained load factor (GNA).

With the flaps down,

$$GNA = \frac{Q * SW * (CLMAX + DCLFH) + TPG * \sin\left[\left(\frac{CLMAX + DCLFH}{DCLFH} - 1.0\right) * \left(\frac{DCLFH}{GCL}\right)\right]}{WT} \qquad (I.75)$$

and with the flaps up,

$$GNA = \frac{Q * SW * CLMAX + TPG * \sin\left(\frac{CLMAX}{GCL}\right)}{WT} \qquad (I.76)$$

The above estimated value of GNA is automatically constrained not to exceed $\left(\frac{ULTN}{1.5}\right)$

Having determined GNA, the ATR is given by the following expression:

$$ATR = \left(\frac{180.0 * G}{PI * V}\right) * (GNA^{2.0} - 1.0)^{0.5} \qquad \text{(degrees/sec)} \qquad (I.77)$$

I.5.4 Specific Excess Power (Module PPSEP)

This module calculates the SEP for 1-g flight. The flight Mach number, altitude, engine throttle setting and aircraft weight for the sortie points at which an SEP estimate is required, are specified in the input data.

The aircraft speed and corresponding dynamic pressure and the engine performance characteristics are again

estimated as in the previous modules. Then the aircraft lift coefficient and incidence are estimated for 1-g flight. The total aircraft drag is calculated next, using module DRAG,

The above results are substituted in the following expression for SEP:

$$SEP = \left(\frac{V}{WT}\right) * (TPG - V * MPA - Q * SW * CDTOT) \quad (m/s) \quad (I.78)$$

I.5.5 Maximum Mach Number (Module PPMMAX)

The maximum Mach number (MMAX) the synthesized aircraft can reach in 1-g flight, at a given point in a sortie, is estimated in this module using an iteration process. The altitude, engine throttle setting and aircraft weight are specified in the input data, together with an initial estimate for the maximum Mach number which is used during the first iteration. The aircraft speed (V1) and dynamic pressure (Q1) corresponding to this initial estimate are calculated at the beginning. The engine performance characteristics, aircraft lift coefficient, incidence and total drag coefficient are then determined and used in the following expression to provide a first estimate of the net propulsive force (F1).

$$F1 = TPG * \cos(AL) - Q1 * SW * CDTOT - V1 * MPA \quad (N) \quad (I.79)$$

If $|F1| < 0.01 * TPGD$ then the iterations stop and

$$MMAX = \frac{V1}{SSPD} \quad (I.80)$$

Otherwise, the iterations continue with a new aircraft speed estimate V2 which is obtained from the above equation for F1 using the Newton-Raphson's iteration method, until the above condition is satisfied.

I.5.6 Acceleration Time (Module PPDT)

This module estimates the total acceleration time (SDT) through a specified Mach number increment (DM) for a given altitude, engine throttle setting and aircraft weight, in 1-g flight. DM and the initial Mach number (MSTART) are both external variables, specified in the input data. For the purpose of this synthesis, DM may be specified with an accuracy of one decimal place only, with the minimum DM being equal to 0.1.

The total acceleration time is obtained iteratively. During each iteration, the Mach number is increased by 0.1 and the corresponding acceleration time increment (DT) is estimated by considering the net propulsive force per unit mass. The iterations stop when the Mach number becomes equal to (MSTART + DM). The individual values of DT are added together to give SDT. Therefore, the net propulsive force per unit mass during the first iteration is,

$$F1 = \left(\frac{G}{WT}\right) * [TPG * \cos(AL) - Q1 * SW * CDTOT - V1 * MPA] \quad (m/s^2) \qquad (I.81)$$

The values of V1, Q1, TPG, MPA, AL and CDTOT used in the above expression are obtained as in the previous modules for the given flight conditions and a Mach number M1 = MSTART.

In the second iteration,

$$F2 = \left(\frac{G}{WT}\right) * [TPG * \cos(AL) - Q2 * SW * CDTOT - V2 * MPA] \quad (m/s^2) \quad (I.82)$$

The values of V2, Q2, TPG, MPA, AL and CDTOT used in the expression for F2 are evaluated again for the given flight conditions but for a Mach number M2 = MSTART + 0.1

If F2 = F1 then,

$$DT = \frac{SSPD * (M2 - M1)}{F2} \quad (sec) \quad (I.83)$$

otherwise,

$$DT = SSPD * \left(\frac{M2 - M1}{F1 - F2}\right) * \ln\left(\frac{F1}{F2}\right) \quad (sec) \quad (I.84)$$

The subsequent iterations continue as explained above. If, however, the net propulsive thrust becomes lower or equal than zero, then the iterations stop automatically at that point and the achieved DM and corresponding SDT are calculated and presented. This condition may occur when the selected throttle setting is not sufficient for acceleration to the desired Mach number.

I.5.7 Ride Quality Factor (Module PPRQF)

The aircraft ride quality for a given altitude, flight Mach number and aircraft weight, is directly proportional to a factor (RQF) which is calculated using the following expression:

$$RQF = \frac{RO * V * GCL * SW * G}{WT} \qquad (I.85)$$

RO, G, V and GCL are calculated for the given altitude and Mach number, as in the previous modules.

APPENDIX J

COMPUTER PROGRAM USER'S MANUAL

J.1 INTRODUCTION

Appendix J, is the User's Manual for the Design Synthesis and Graphics computer programs, CANARD.FOR and VIEW.FOR. The architecture of these programs and associated data files, is explained in detail in chapter 7. The guidelines, given in the following sections of this appendix are primarily concerned with the required input variables, the User-created data files and the execution of the programs. The interrelation between the User and the above two computer programs is diagramatically presented in fig. J.1.

J.2 USER-CREATED DATA FILES

Only the files CANARD.DAT, LDD2.DAT and STDRAG.DAT are created or revised by the User. All the remaining data files must not be edited or deleted. The contents of the above three files together with guidelines on the arrangement and range of the data values, are given in subsections J.2.1 - J.2.3, below.

J.2.1 File CANARD.DAT

J.2.1.1 Arrangement of input data

This is the main input data file for the program CANARD.FOR and it is the largest of the three User created files. It contains the data values for 23 Independent (IV's) and 304 External (EV's) Variables. The values of the IV's may, if necessary, be varied accordingly during every loop of the Design Synthesis optimization process, until the desirable aircraft design and performance characteristics are achieved. The EV's are design parameters, the values of which remain fixed during the optimization.

The correct arrangement of the data values of all the required input variables, in file CANARD.DAT, is shown in fig. J.2. All the IV's are specified in four rows at the start of the file, while the EV's are appropriately divided into 18 groups and specified in the subsequent rows. These groups considerably facilitate the evaluation of related EV's because information on their values, may be obtained from common sources of reference. The data must be entered strictly in sequence and in separate rows, as shown in fig. J.2. This arrangement is deliberately designed to minimize any possibility of wrong data entry due to omission of a data value and to allow fast and easy identification of the entered value for each variable.

All the input variables for file CANARD.DAT, are listed in alphabetical order in fig. J.3. This list is designed for quick reference while selecting the values for the IV's and EV's. It also provides information on the corresponding units, the range of typical values for the IV's and specifies any constant EV values.

J.2.1.2 Guidelines on the selection of values for the IV's

At the start of the Design Synthesis, an approximate initial value needs to be assigned to each IV. The range of typical values for each variable is given in the list in fig. J.3. These are reasonable values for the class of aircraft this program is intended, but they do not necessarily constitute the limits of the IV's. Some of the initially assigned values may be obtained from the Air Staff Target for the aircraft, statistics from earlier designs or even a rough sketch of the desired configuration. Good initial IV estimates will lead to a faster optimization and hence lower CPU. It is therefore essential that the User applies engineering judgement at this stage. The IV values

must be approximately analogous to each other and not unreasonable.

J.2.1.3 Guidelines on the selection of values for the EV's

The EV's are considered in this appendix, in groups as they appear in file CANARD.DAT (fig. J.2).

1) Cockpit

The values of the cockpit EV's may be obtained from the appropriate valid MIL-STD and from ejection seat installation information. The value of GTCPH depends on QCSEAT and the pilot's personal equipment. It may be as high as 10.0, for a high-'g' cockpit where QCSEAT may be in excess of 0.5 rads.

2) Undercarriage and bays

The approximate values of PUMW1 and PUNW1 are initially specified in this file. These depend on the type of runway surface from where the aircraft is to operate. Appropriate low tyre pressures should be specified for operations from semi-prepared runways or roads. The values of RPUMLV, FPUNLV, FDUNL, VTLV, EUML and EUMW, may be obtained from u/c design manuals. For fighter aircraft, RPUMLV is 3 - 5 and VTLV is 3 - 5 m/s depending on the landing procedures. The value of EUML when oleo-pneumatic shock absorbers are used, is 0.65 - 0.80. The values of RLUPCW and DHUP depend on the assumed general arrangement of the aircraft. DHUP is negative if the nose u/c pintle is located at a lower height relative to that of the main u/c.

The minimum u/c bay working clearances depend on the u/c size and should be based on previous design experience.

3) Datum Propulsion System

The values of al. EV's within this group remain always constant for this Design Synthesis (see fig. J.3). The User must not alter these constant values.

4) Engine Bays

The engine bay clearances used in the Synthesis are the total height or width clearances at a given engine station, in a twin engine bay. Their minimum values should not be less than the engine envelope specified by the engine manufacturer. This envelope includes the accessories mounted around the engine. The maximum clearances, should be within reasonable limits, known from past engine installation design experience. Unnecessarily excessive limits may reduce the rear fuselage slenderness. The actual clearances, depend on the engine bay clearance factors, the values of which should always be less than unity. The values of these factors are determined by considering maintainability criteria.

5) Inlet and B.L.Diverter

MHH and HTH depend on the proposed maximum Mach number and corresponding altitude for the synthesized aircraft. The value of FLVK is usually between 0.5 and 2.0. RIDX1 usually has a low value which depends on the size of the inlet. The value of AII depends on inlet design experience and on the forward fuselage geometry. The ratio ROIEI is usually between 1.1 and 1.5 and depends on the maximum flight Mach number. The parameter RCDK is assigned values between 0.2 and 0.6 depending on the sharpness of the intake lips.

6) Fuselage

RXFR is usually given values between 1.0 and 2.0, while RXB and RXE are always less than unity. For minimum diffuser losses, RIDL should be between 6.0 and 14.0, if possible, while RIDLS is assigned a constant value equal to 6.0. The lengths LAR ad LAX depend on the size and installation of the relevant equipment. The value of LCCAN must be analogous to the aircraft length and the length of a modern high-'g' cockpit. The clearance EXUNBF depends on the intake fairing aerodynamics and also on the wheel-base. The longitudinal separation ELMUFA must be such as to prevent an overlap betwen the flying surfaces of missiles no.3 and no.4 when installed close to each other. The variables HRA, BRA, EHRA and EBRA are evaluated by considering the dimensions and scanning movements of the radar antenna. The clearances EYFC, EBFD and EYPCH should not be excessive but close to the necessary minimum values. EBFD for example must provide adequate space for the installation of the missile launchers. The size of HFA1 depends on the local packaging requirements. The Y- coordinate YCCANC should always be larger than the half-width of the pilot's shoulders. The variable HFDCU may be adjusted to increase or decrease the squareness of the fuselage cross-sections, accordingly. The angles QCWSC and QCCAN should allow adequate pilot vision. The angles QFPR and QFPRU may be adjusted to improve the rear fuselage slenderness. The powers FZCAN1 and FZCAN2 control the longitudinal curvature of the forward and rear canopy sections. A good typical value for both variables, is 0.75. The volume factor FVCKPT usually takes values between 1.1 and 1.4, depending on the User's judgement.

7) Flying Surfaces

In the present Design Synthesis where it is assumed that no leading-edge devices are used on the wing, the

variables FCWLFT and FCWLHT may be taken as equal to FCWD. The variables FCWTFT and FCWTHL are always equal and their value controls the size of the trailing-edge flaps, which decreases as this value increases. This value however, must not exceed (1.0 - FCWR). The values of RSLEW and QWST, depend on the wing aerofoil section and RTW. Typical values for these two variables may be obtained from DATCOM, section 2. The variables AWA and FBWA depend on the desired roll control characteristics of the aircraft. The value of FBWA should always be lower or equal to (1.0 - FBWF). The factor RCDVK allows for the use of advanced technology, like programmed variable camber devices, used to improve the aerodynamic performance of the aircraft. If no such technology is used then RCDVK is equal to 1.0, otherwise, it is increased slightly according to the degree of aerodynamic improvement. The factors FMD1 and FMD2 adjust the value of the drag rise Mach number. FMD1 is normally equal to 0.15, while FMD2 depends on improvements in aerodynamic technology with regard to drag rise. FMD2 is equal to zero when there are no improvements. The lift-coefficient CLDES refers to the manoeuvring case. A typical value for HTR is, 0.000015.

The foreplane volume coefficient RCSW may be obtained from statistics for close-coupled canard-delta combat aircraft. The foreplane geometric characteristics ACN, UCN, RTC and QCL, depend on the aircraft aerodynamics. Their values may vary within approximately the same typical ranges as those specified for the corresponding wing variables. The parameters RSLEC and QCST, depend on the foreplane aerofoil section and RTC. The values for these two parameters may be obtained from section 2 of DATCOM.

The fin volume coefficient REFFC may be obtained from combat aircraft design statistics. The fin geometric characteristics AEFN, UEFN, RTEF and QEFL should be within the usual range of values for combat aircraft. The variable

NFIN is assigned integer values. When the proposed aircraft has a single fin, then NFIN is equal to 1. When twin fins are used, NFIN is equal to 2.

8) Fuel

The fraction RMTLFI may be assigned values between 0.0 and 1.0, accordingly. If it is assumed that the u/c is designed for landings with full internal fuel tanks, then RMTLFI is taken equal to 1.0. The volume utilization factor UWBEF may be assigned values between 0.0 and 0.9, accordingly. If no fuel is carried in external tanks, then MXTF1 and MXTF2 are equal to zero. Otherwise, MXTF1 or MXTF2, must be specified according to the capacity of standard-size external fuel tanks, only.

9) Design Loads and Speeds

The reference mass MTTR is a rough estimate for the maximum take-off mass of the aircraft. This estimate may be obtained from the Air Staff Target or from statistics for combat aircraft with a similar role. Information on MTPR, ULTN, VD and AMMX may be obtained from AVP-970.

10) Mass

Several EV's in this group have empirical constant values which must remain fixed. These values are given in the list of fig. J.3. The fraction FMSA takes values which are less than unity. The variables FMSC, FMFIR, FMUM and FMUN, are system state-of-the-art mass factors. These factors are set equal to 1.0, if the relevant systems use conventional technology with no mass changes. If, however, the introduction of the state-of-the-art in the design of a particular system results in mass savings, then the corresponding factor should be assigned a value less than

1.0 or vice-versa. The variables FMF1, FMF2, FMC, FMEF, FMWB, FMWT and FMWL are factors allowing for changes in the structural materials used for the relevant components. When conventional aluminium alloys are used, these factors are equal to 1.0. For any other structural materials, the factors should be adjusted accordingly, to reflect the resulting mass changes. The factor FMEF2, allows for the increase in mass due to the extra fuselage structure needed to support the two separate fins when NFIN = 2. FMEF2 should therefore normally be slightly greater than 1.0.

The equipment masses, specified in this group of EV's, may be obtained from manufacturer's specifications for the selected equipment.

The values of variables EQWFH, NWFK and LWFK may be determined from previous experience with other combat aircraft, using plain trailing-edge flaps. The variable SFAIB is assigned a zero value, if the aircraft is not equipped with an airbrake.

11) Densities

The density figures assigned to this group of EV's are installed densities. They include allowances for maintainability, safety, equipment cooling etc. Typical density figures may be obtained from statistical analyses of the systems of existing combat aircraft. The assigned density figures must always be greater than zero.

12) Underfuselage Missiles

The fractions RXMUF1, RXMUF2, RXMUF3 and RXMUF4 are assigned values less than unity, to define the distances of missiles no.1 - 4, respectively, from the aircraft nose. The missile lengths, nose length fractions, diameters and

masses, may be obtained directly from the specifications of the selected missiles. The variables DCMUF1, DCMUF2, DCMUF3 and DCMUF4 are the drag codes of the four missiles. These are assigned integer values, corresponding to the column numbers in file STDRAG.DAT, in which their installed drag coefficients are tabulated versus Mach number.

13) Gun

The fraction RXGF defines the distance of the gun from the aircraft nose and it is assigned values less than unity, accordingly. The values of LGC, MGC and MGA may be obtained directly from the selected gun specifications. The variables BGFA, OGFA and PGFA are evaluated approximately, by considering the dimensions of the protruding gun barrel and thus allowing for a smooth gun fairing.

14) Wing-Stores

The fractions FYB1, FYB2, FYB3 and FYB4 are assigned values less than unity, which define directly the lateral and indirectly the longitudinal c.g. position of the wing-stores and pylons at stations no. 1 - 4. The fraction RXWPCG is also given a value which is less than unity, to define the position of the imaginary wing-store c.g. line, aft of the front wing-spar. This fraction has a direct effect on the longitudinal c.g. positions of the wing-stores and can be adjusted to minimize the aircraft c.g. travel following the release of stores.

The variables NB1, NB2, NB3 and NB4 define the number of stores mounted at wing-pylons no.1 - 4, respectively. They may be assigned integer values 0, 1 or 2, accordingly. Only stores of the same type may be mounted in pairs. The variables MB1, MB2, MB3 and MB4 specify the total mass of stores at each wing-pylon. The multiple carriage factors

specified in this group, for each wing-store station, become automatically active only when pairs of stores are mounted at the corresponding pylons. A value of 1.25 is typically assigned when the pair are side-by-side and 0.90 when in tandem. These factors are specified as equal to 1.0, if no multiple carriage is assumed. The drag codes are specified by the appropriate integers for each type of store.

The User should remember that if any quantity of external fuel was specified earlier, then either or both wing-store stations no.2 and no.3, will be occupied by external tanks. If, for example, a quantity MXTF1 of externally carried fuel was specified in the fuel group, then NB2 = 1, MB2 = 0.0, FMCB2 = 1.0 and DCB2 is set to the column number in STDRAG.DAT, corresponding to the external tank drag coefficients.

When the specified number of stores mounted at a given wing pylon, is equal to zero, then the corresponding mass should be specified as zero and the drag code as 8.

15) Wing-Pylons

The mass of each wing-pylon is specified here from the manufacturer's specification for the selected pylons. The drag codes are assigned appropriate integer values, as in the previous groups. Provided no stores are mounted at a given wing-pylon, it is possible to remove it completely from the aircraft, by specifying the pylon mass as zero and the corresponding drag code as 8.

16) Sortie Performance

The starting point in the evaluation of the sortie performance EV's is the definition of a hypothetical sortie, typical for the proposed role of the synthesized aircraft.

The variable NSTAG is then assigned an integer value equal to the number of legs of this sortie. It must be noted, that as NSTAG increases the required CPU for program execution increases too. Therefore, unnecessary large values for NSTAG. should be avoided. The take-off and landing phases, are excluded from the sortie performance calculations. It is assumed that the first sortie-leg starts immediately after the end of the take-off phase and that the last leg ends just before the start of the landing phase. Therefore in order to have a complete picture of the aircraft mass changes for the performance calculations, from lift-off to touch-down, the fuel mass required for the take-off and landing phases is approximately estimated from experience and specified in this file by variables MTTF and MTLF respectively.

It is assumed that each sortie-leg is flown at a constant height, Mach number and load factor. The legs involving climbing, descending or longitudinal acceleration flight, are approximated by appropriately modifying the leg length or the corresponding load factor.

The values of SLEG, HT, M, GN and EQWF are specified in this file for each leg together with the guess values of TPG1, CL1, AL and MPFB1. The release status of the underfuselage missiles and wing-stores and the u/c status, are also specified for each sortie-leg. A release is indicated by assigning a value equal to 0.0, to the appropriate release status variable. A value of 1.0, indicates no release. For multiple wing-stores however, a value of 0.5 may be used to indicate the release of only one of the two stores on the same pylon. It should be emphasized that the value of release status variable is determined by considering whether the particular store is on the aircraft at the start of the sortie-leg under consideration. This means that whenever a release is

specified in the EV's for a given leg, the actual release takes place along the previous leg. The u/c status SUC, however, is specified for the leg under consideration. When SUC = 0 the retractable u/c is up and when SUC = 1, it is down. EQWF may be specified for combat manoeuvres.

17) Take-off and Landing Performance

The take-off and landing performance of the aircraft at different airfields may be estimated in this program by specifying in this group of EV's, the appropriate values for HTF and FRK. The effects of thrust variations may be considered by appropriate adjustment of fractions TRATE and FTPGC. Flap settings from 0.0 to 50.0 degrees may be specified for EQWFT and EQWFL. The take-off and approach speeds are defined in terms of the corresponding stall speed by factors FVSTTO and FVSTAP, the values of which may be obtained from the appropriate valid MIL-STD. The fractions FCLT and FCLL are assigned values based on previous experience to specify how much of CLMAX is available for take-off and landing, respectively.

18) Point Performance

Six point performance parameters may be estimated for the synthesized aircraft. Each parameter may be estimated several times for various pre-defined flight conditions. The number of times each parameter is calculated is specified in this file by the variables NPP1, NPP2, NPP3, NPP4, NPP5 and NPP6. Although there is no limit for these variables, the User should remember that the CPU for program execution, increases as the number of point performance calculations increases. The store release and u/c status variables are specified here only once for all flight conditions and parameters. The data for each point performance parameter, are repeated for the previously

specified number of times, as shown in fig. J.2. The specified flight altitude and Mach number in all point performance calculations should always be reasonable and within the expected aircraft capabilities. The aircraft weight should be within the expected empty and take-off weight of the aircraft, expressed in Newtons. The selected throttle setting should be reasonable and not greater thah 100.0. The variable EQWF is only specified for the sustained and attained turn rate calculations in which the use of combat flaps is assumed. In the calculation of the maximum Mach number a good estimate M, results in CPU reduction during the execution of the program. A similar reduction may be achieved by avoiding if possible, to specify a large Mach number increment DM, in acceleration calculations.

J.2.2 File LDD2.DAT

This is the smallest of the three User-created files. It contains in tabulated form versus Mach number the values of CLC, DK2 and CLMAX which are defined as EV's in this Design Synthesis. The required values of these variables may be obtained from wind-tunnel data for similar configurations or by appropriate extrapolation of actual data from existing modern combat aircraft.

The data in file LDD2.DAT, must be strictly arranged as shown in fig. J.4, i.e. in four columns and twenty-five rows. The Mach number values from 0.0 to 2.4, in 0.1 intervals, are entered in the first column. The values of CLC, DK2 and CLMAX corresponding to the Mach numbers in the first column, are entered in the second, third and fourth columns respectively. The data in this file become active in calculations involving high-incidence flight. The values of the three variables at intermediate values of Mach number

to those in the first column, are determined by interpolation.

J.2.3 File STDRAG.DAT.

This is the third User-created file and contains in tabulated form versus Mach number the installed drag coefficient data for up to seven different types of stores. This file is designed to offer maximum flexibility in the program with regard to the selection of store-types that may be carried on the aircraft for a particular mission. Installed drag coefficient data for semi-submerged or wing-mounted missiles, external pylons, bombs, fuel tanks etc., may be obtained from wind-tunnel tests carried out by the store manufacturers or other organizations.

The file consists of nine columns and twenty five rows of data as shown in fig. J.5. This arrangement of data must be strictly maintained by the User at all times, during data entry. The Mach number values from 0.0 to 2.4, in 0.1 intervals, are entered in the first column. The last column must be filled always with zero values. The drag coefficient values for a selected type of store may be entered in any one of the other seven intermediate columns. The remaining columns may be similarly filled with drag coefficient data for other types of stores. The accuracy of the data in the intermediate columns should not exceed five decimal places. Whenever less than seven types of stores are used, the remaining intermediate columns for which data are not available must be filled with zero values. The data for a particular type of store are identified in module STDRAG of the Design Synthesis program, by means of drag codes specified in file CANARD.DAT. The drag codes are integer numbers corresponding to the store drag coefficient columns in file STDRAG.DAT, which are numbered from 1 to 8, starting from the second column as shown in fig. J.5. The

first column of the file which contains the Mach number values is excluded from numbering. The drag coefficients at intermediate values of Mach number to those in the first column, are determined by interpolation.

J.3 COMPUTER PROGRAM COMPILATION AND EXECUTION

Guidelines are given in this section for running the computer programs CANARD.FOR and VIEW.FOR on DEC VAX-11/750/780/8650 mainframe computer systems.

Step 1: Enter the necessary input data in files CANARD.DAT, LDD2.DAT and STDRAG.DAT, following the guidelines given in section J.2.

Step 2: Confirm that the following files are all included in the User's directory:
CANARD.FOR, CANARD.DAT, LCS1.DAT, LCS2.DAT, LCS3.DAT, LCS4.DAT, LCS5.DAT, LCS6.DAT, LCS7.DAT, LCS8.DAT, LCS9.DAT, LDD1.DAT, LDD2.DAT, STDRAG.DAT, AEROC.DAT, TYREM.DAT and VIEW.FOR.

Step 3: Compile and link program CANARD.FOR using the following commands:

```
$ FOR CANARD
$ LINK CANARD
```

These will create the files CANARD.OBJ and CANARD.EXE in the User's directory.

Step 4: Compile program VIEW.FOR and link to the GINO-F library by the following commands:

```
$ FOR VIEW
$ LINK VIEW, 'GINLIB
```

These will create the files VIEW.OBJ AND VIEW.EXE in the User's directory.

Step 5: Run program CANARD.FOR, by the command,

$ RUN CANARD

This will produce the main results file CANARD.RES which contains the numerical output of program CANARD and the file VIEW.DAT which is the input data file for the graphics program VIEW. The contents of file CANARD.RES may be read directly from the User's terminal or listed on paper by an on-line printer, using the comands:

$ TYPE CANARD.RES

or $ PRINT CANARD.RES

Step 6: Run program VIEW.FOR, by the command,

$ RUN VIEW

This will produce in the User's directory, the graphical output file FOR007.DAT, which contains three detailed images of the synthesized configuration. These may be displayed only on a suitable graphics terminal (eg. WESTWARD) or plotted on paper by an on-line plotter (eg. BENSON), using the following commands:

$ DISPLAY

Device: WESTWARD or BENSON

File: FOR007.DAT

J.4 COMPUTER PROGRAM IMPLEMENTATION PROCEDURE

The recommended procedure for the implementation of programs CANARD.FOR and VIEW.FOR is presented diagrammatically in fig. J.1 and it is outlined in this section.

The Design Synthesis implementation procedure starts by a study of the design requirements for the proposed aircraft and hence the selection of suitable values for the required input variables and data for files CANARD.DAT, LDD2.DAT and STDRAG.DAT. The data are then entered by the User, in the above files, in accordance with the guidelines given in section J.2. The program CANARD is then run following the procedure in section J.3. The graphics program VIEW is also run following the execution of program CANARD. The numerical output and the computer generated images of the synthesized configuration are both checked by the User, to determine how close this first design is, to the desired specification and to decide at this early stage whether there is a need to change any of the initially specified EV values in file CANARD.DAT. This check also helps to identify any incorrect data entries in the above data files. If any such changes or corrections need to be carried out the User should run both programs as before and repeat the check. Otherwise, the next step, is an optimization process, during which the User runs the program CANARD.FOR alone for several loops and during each loop examines the numerical output, assesses how some selected results compare to the desired specification and hence reassigns appropriate values to some IV's in file CANARD.DAT. The final design should have a take-off mass roughly equal to that in the initial specification, adequate internal fuselage volume to fully accomodate all the systems, components and fuel tanks installed inside the fuselage, sufficient fuel capacity for successful completion of a hypothetical sortie, longitudinal static stability within the desired limits and a performance that compares favourably to the mission requirements. This manual optimization process stops when the User decides that the results are within acceptable limits from those in the initial specification. The computer generated images of the

final aircraft configuration may be then produced by running the program VIEW.FOR.

At present the optimization process is manual and the number of loops required to produce results within acceptable limits from those in the initial specification, depends on the User's experience. Ten loops are typically required. In the future, however, the optimization process will be fully automated using existing Multivariate Optimization Algorithms, developed by RAE(F). This automated process will require much more loops to be completed but the final results will be much more closer to the specified requirements.

J.5 COMPUTER PROGRAM STATISTICS

The minimum total filespace size occupied by programs CANARD.FOR, VIEW.FOR and all their associated files, is about 2000 blocks. The sizes of files CANARD.DAT and CANARD.RES are variable, however, and depend on the specified number of performance calculations.

The CPU and elapsed time required for the execution of program CANARD.FOR also depend on the number of performance calculations. Typically, a single loop of program CANARD.FOR on the VAX-11/750 computer system requires a CPU of about four minutes and an elapsed time of eleven minutes. The same job on the VAX-11/8650 system requires only thirty seconds of CPU and an elapsed time of about one minute. Similarly, a single execution of program VIEW.FOR, on the 750 system requires about thirty seconds of CPU and an elapsed time of about one minute. The above quoted elapsed times are applicable only to single-user system operation.

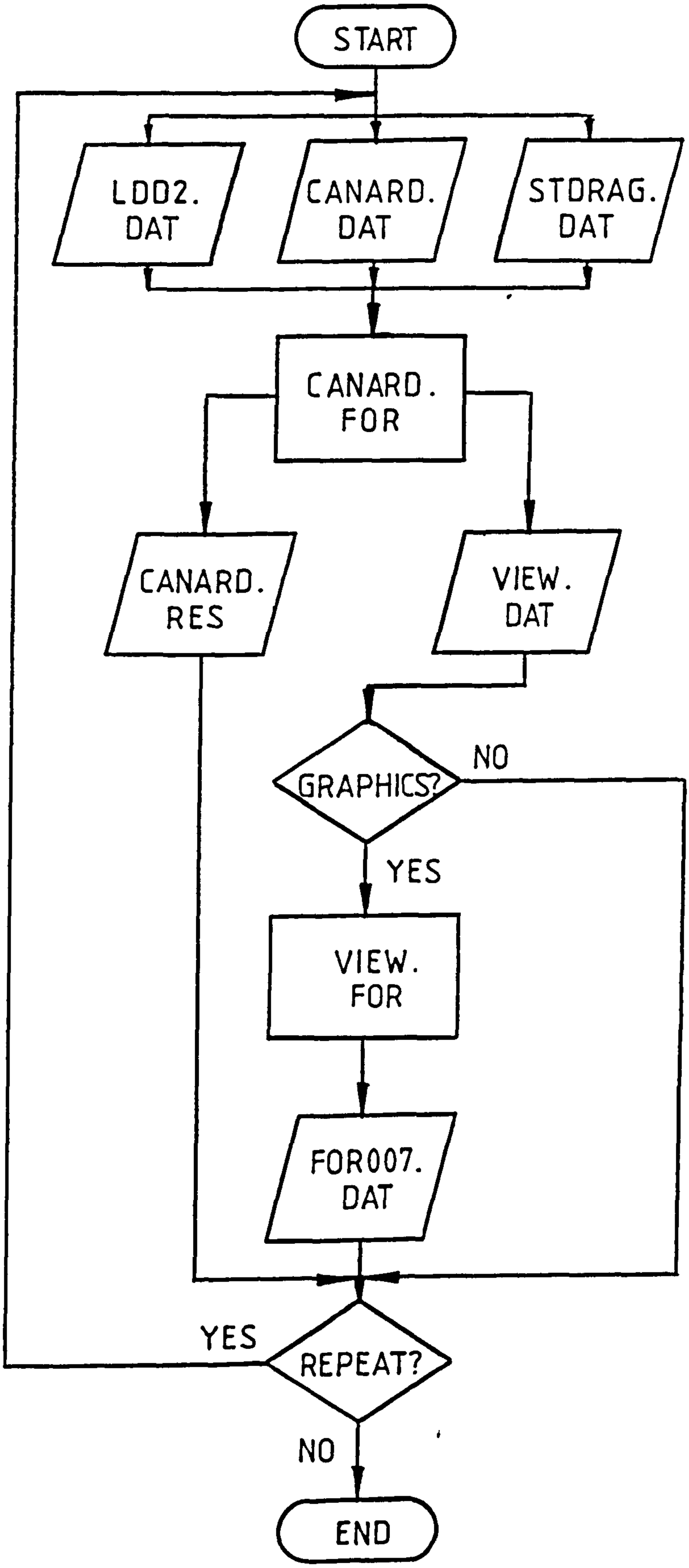

FIG. J.1 COMPUTER PROGRAM IMPLEMENTATION PROCEDURE - FLOW CHART

ARRANGEMENT OF INPUT VARIABLES (FILE : CANARD.DAT)

SW,AW,UW,QW4,RTW,FCWR,FCWD,FBWF
RXWCQM,RXCCQM,RZCC,RTP
XFN,RLTMFN,RLTFFN,RLTCFN,RLTAFN,FOT6N
F8WNF,UWBCF,UFIFDE,UFIFEF,UFIFFG

Independent Variables.

Cockpit.
HC1,HC2,HC3,HC4,EHC5,HCSEAT
QCSEAT,QCEYE,LCFOOT,LCNSPR,GTCPH

Undercarriage and Bays.
PUMW1,PUNW1,RPUMLV,FPUNLV,FDUNL,VTLV,RLUPCW,DHUP
EUML,EUMW,ELUMBF,ELUMBA,EHUMBL,ELUNBF,ELUNBA,EHUNBL

Datum Propulsion System.
LP12R,LP22AR,LP2A4R,LP34R,FLP1K,FLP2K,FLP3K
DP1R,DP2R,DP3R,DP4R,MPBR,MPRR,MPTR,FMPBK,FMPRK,FMPIK
TPGD1,TPGD2,MPFD1,MPAD1,OPJD1

Engine Bays.
FHP1K,FBP1K,FHP2K,FBP2K,FHP3K,FBP3K,FHP4K,FBP4K
EHP1S,EHP1H,EBP1S,EBP1H,EHP2S,EHP2H,EBP2S,EBP2H
EHP3S,EHP3H,EBP3S,EBP3H,EHP4S,EHP4H,EBP4S,EBP4H

Inlet and B.l.diverter.
MHH,HTH,FLVK,RIDX1,AII,ROIEI,RCDK

Fuselage.
RXFR,RXB,RXE,RIDL,RIDLS,LAR,LAX,LCCAN,EXUNBF,ELMUFA
HRA,BRA,EHRA,EBRA,EYFC,EBFD,EYPCH,HFA1,YCCANC,HFDCU
QCWSC,QCCAN,QFPR,QFPRU,FZCAN1,FZCAN2,FVCKPT

Flying Surfaces.
FCWLFT,FCWLHT,FCWTFT,FCWTHL,RSLEW,QWST,AWA,FBWA
RCDVK,FMD1,FMD2,CLDES,HTR
RCSW,ACN,UCN,RTC,QCL,RSLEC,QCST
REFFC,AEFN,UEFN,RTEF,QEFL,NFIN

Fuel.
RMTLFI,UWBEF,MXTF1,MXTF2

Design Loads and Speeds.
MTTR,MTPR,ULTN,VD,AMMX

Mass.
FMUMK,FMUNK,FMUHK,FMSAK,FMSEK,FMSCK,FMSFK
FMSA,FMSC,FMFIR,FMUM,FMUN,FMF1,FMF2,FMC
FMEF,FMEF2,FMWB,FMWT,FMWL
MUMK,MUNK,MUHK,MSAK,MSEK,MSCK
MC1K,MC2K,MC3K,MEF1K,MEF2K,MEF3K,MEF4K

Extern al Variables

MAR,MAX,MCSEAT,MCP,MCFI,MCPI,MCMI,MLMUF,MAPU
EQWFH,NWFK,LWFK,SFAIB

Densities.
RFUL,RGC,RGA,RLMUF,RAPU,RAR,RAX
RSC,RSE,RSA,RSF,RFW,RFIR,RFAIB

Underfuselage Missiles.
RXMUF1,RXMUF2,RXMUF3,RXMUF4
LMUF1,LMUF2,LMUF3,LMUF4
FLMUF1,FLMUF2,FLMUF3,FLMUF4
DMUF1,DMUF2,DMUF3,DMUF4
MMUF1,MMUF2,MMUF3,MMUF4
DCMUF1,DCMUF2,DCMUF3,DCMUF4

Gun.
RXGF,LGC,BGFA,OGFA,PGFA,MGC,MGA

Wing-Stores.
FYB1,FYB2,FYB3,FYB4,FXWPCG
NB1,NB2,NB3,NB4
MB1,MB2,MB3,MB4
FMCB1,FMCB2,FMCB3,FMCB4
DCB1,DCB2,DCB3,DCB4

Wing-Pylons.
MXP1,MXP2,MXP3,MXP4
DCXP1,DCXP2,DCXP3,DCXP4

AIRCRAFT PERFORMANCE

Sortie Performance.

NSTAG,MTTF,MTLF

The following data are specified for each sortie-leg:
(x NSTAG)

SLEG,HT,M,GN,EQWF,TPG1,CL1,AL,MPFB1
SRMUF1,SRMUF2,SRMUF3,SRMUF4,SRB1,SRB2,SRB3,SRB4,SUC
.....
.....

Take-off and Landing Performance.

HTF,TRATE,EQWFT,FVSTTO,FCLT,FRK,FTPGC,EQWFL,FVSTAP,FCLL

Point performance.

NPP1,NPP2,NPP3,NPP4,NPP5,NPP6
SRMUF1,SRMUF2,SRMUF3,SRMUF4,SRB1,SRB2,SRB3,SRB4,SUC

The following data are specified for each point:

Sustained Turn Rate.
HT,M,WT,XV,EQWF,CL3
.....
(x NPP1)

b l e s	E x t e r n a l	V a r i a b l e s	E x t e r n a l	V a r i a b l e s

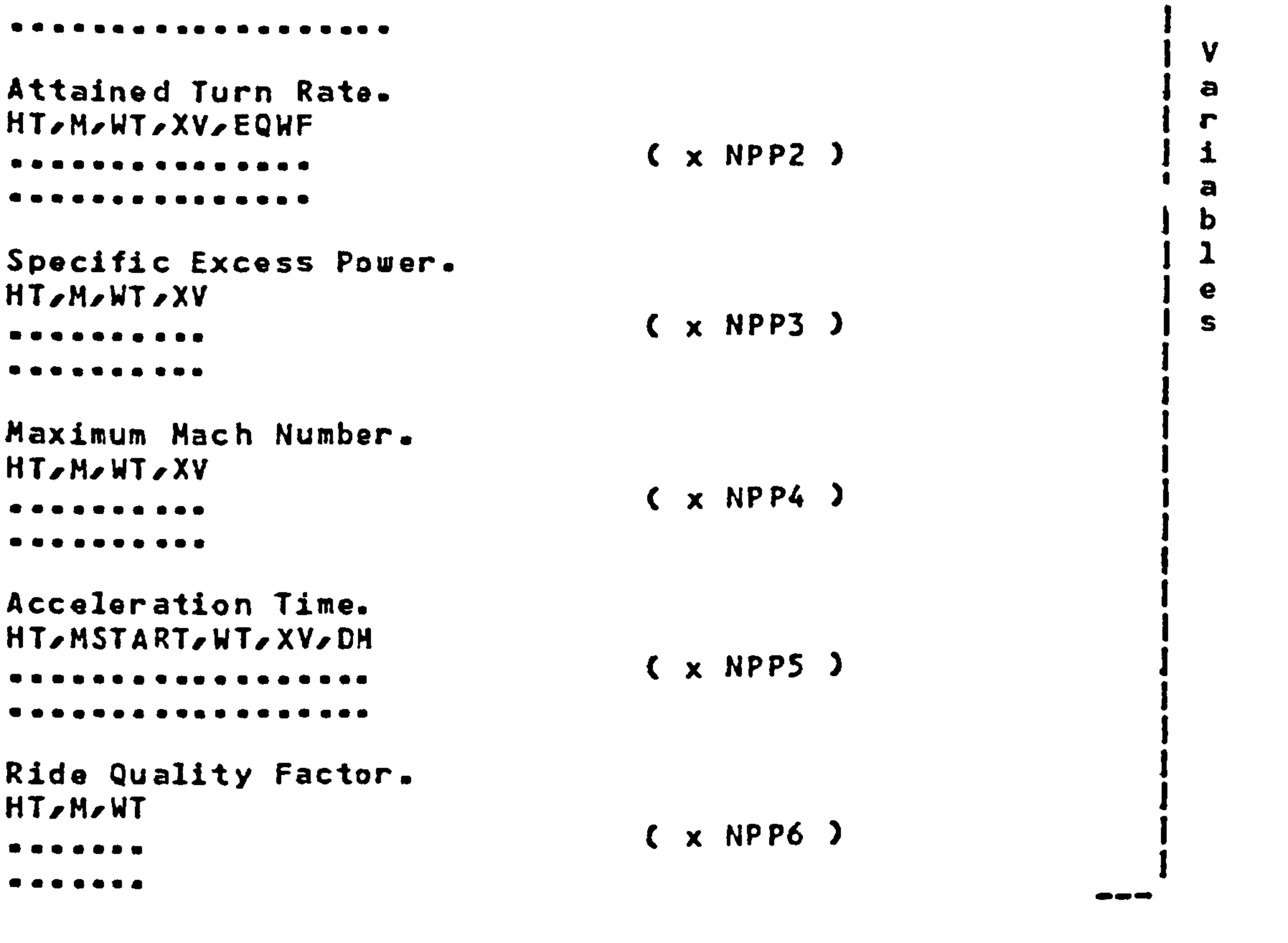

FIG. J.2 ARRANGEMENT OF INPUT VARIABLES IN FILE CANARD.DAT

********** LIST OF INPUT VARIABLES **********
******* DESIGN SYNTHESIS FOR CANARD-DELTA COMBAT AIRCRAFT *******
********** BY V.C.SERGHIDES **********

INDEPENDENT VARIABLES

Symbol	Definition	Units	Typical Values
AW	Gross wing aspect ratio.		1.00-4.00
FBWF	Fractional gross span of T.E. flaps.		0.30-0.70
FBWNF	Fractional span of the net wing-box containing fuel tanks.		0.00-1.00
FCWD	Front spar position as a fraction of the local wing chord.		0.05-0.30
FCWR	Rear spar position as a fraction of the local wing chord.		0.50-0.80
FOT6N	Increment in cross-sectional area at the nozzle exit above datum value (OII+OVI).	m2	0.00-2.00
QW4	Quarter-chord sweep of the wing.	rads	0.55-0.95
RLTAFN	Ratio of the axial distance from the end of the center-section to the point at which the decrease in cross-sectional area is half the maximum increment to the length of the aft fairing.		0.50-1.00
RLTCFN	Ratio of the length of the center-section to length of the fuselage aft of the fwd fairing.		0.00-1.00
RLTFFN	Ratio of the axial distance from the end of the radome to the point at which the increase in cross-sectional area is half of the maximum increment to the length of the fwd fairing.		0.00-0.50
RLTMFN	Ratio of the length of the fwd fairing to the overall fuselage length minus the length of the radome.		0.00-1.00
RTP	Engine scale factor.		0.50-2.00
RTW	Thickness to chord ratio of the wing.		0.02-0.08
RXCCQM	Fraction of the fuselage length defining the distance of the mean 0.25-chord point of the foreplane from the aircraft nose.		0.25-0.55
RXWCQM	Fraction of fuselage length defining the distance of the mean 0.25-chord point of the wing from the a/c nose.		0.45-0.75
RZCC	Ratio of the foreplane height above the wing-chord plane to the mean		0.00-0.19
SW	Gross wing area.	m2	30.0-60.0
UFIFDE	Volume utilization factor for the fuel stored inside section D-E.		0.00-0.40
UFIFEF	Volume utilization factor for the fuel stored inside section E-F.		0.00-0.40

UFIFFG	Volume utilization factor for the fuel stored inside section F-G.		0.00-0.40
UW	Gross wing taper ratio.		0.05-0.50
UWBCF	Volume utilization factor of the center-section of the wing-box for fuel storage.		0.00-0.90
XFN	Axial distance of the nozzle exit from the a/c nose.	m	14.0-19.0

EXTERNAL VARIABLES

Symbol	Definition	Units	Constant Values
ACN	Net foreplane aspect ratio.		
AEFN	Net fin aspect ratio.		
AII	Aspect ratio of an intake diffuser at the intake plane.		
AL	Guess value for aircraft incidence.	rads	
AMMX	Maximum design Mach number for the structure.		
AWA	Aspect ratio of each aileron.		
BGFA	Average width of the gun fairing.	m	
BRA	Radar antenna width.	m	
CL1	Initial estimate of maximum sustained lift coefficient used in sortie performance calcs.		
CL3	Initial estimate of maximum sustained lift coefficient for a selected throttle setting, used in STR calcs.		
CLC	Critical lift coefficient.		
CLDES	Manoeuvring design lift coefficient.		
CLMAX	Maximum lift coefficient (trimmed) at a given Mach number.		
DCB1	Drag code for wing-store no.1.		
DCB2	Drag code for wing-store no.2.		
DCB3	Drag code for wing-store no.3.		
DCB4	Drag code for wing-store no.4.		
DCMUF1	Drag code for fuselage-mounted missile no.1.		
DCMUF2	Drag code for fuselage-mounted missile no.2.		
DCMUF3	Drag code for fuselage-mounted missile no.3.		
DCMUF4	Drag code for fuselage-mounted missile no.4.		
DCXP1	Drag code for external wing-pylon no.1.		
DCXP2	Drag code for external wing-pylon no.2.		
DCXP3	Drag code for external wing-pylon no.3.		
DCXP4	Drag code for external wing-pylon no.4.		
DHUP	Height difference between the nose and main u/c pintles.	m	
DK2	Increment in K1 to define the lift-dependent drag parameter K2.		
DM	Mach number increment.		

DMUF1	Diameter of fuselage-mounted missile no.1.	m	
DMUF2	Diameter of fuselage-mounted missile no.2.	m	
DMUF3	Diameter of fuselage-mounted missile no.3.	m	
DMUF4	Diameter of fuselage-mounted missile no.4.	m	
DP1R	Compressor inlet diameter of datum engine.	m	0.690
DP2R	Turbine section exit diameter of datum engine.	m	0.760
DP3R	Afterburner section exit diameter of datum engine.	m	0.890
DP4R	Nozzle exit diameter of datum engine.	m	0.770
EBFD	Total width clearance between diffusers and fuselage at stn D.	m	
EBP1H	Maximum value of clearance EBP1.	m	
EBP1S	Minimum value of clearance EBP1.	m	
EBP2H	Maximum value of clearance EBP2.	m	
EBP2S	Minimum value of clearance EBP2.	m	
EBP3H	Maximum value of clearance EBP3.	m	
EBP3S	Minimum value of clearance EBP3.	m	
EBP4H	Maximum value of clearance EBP4.	m	
EBP4S	Minimum value of clearance EBP4.	m	
EBRA	Radar antenna width clearance.	m	
EHC5	Perpendicular distance between the seat-back and rear cockpit bulkhead.	m	
EHP1H	Maximum value of clearance EHP1.	m	
EHP1S	Minimum value of clearance EHP1.	m	
EHP2H	Maximum value of clearance EHP2.	m	
EHP2S	Minimum value of clearance EHP2.	m	
EHP3H	Maximum value of clearance EHP3.	m	
EHP3S	Minimum value of clearance EHP3.	m	
EHP4H	Maximum value of clearance EHP4.	m	
EHP4S	Minimum value of clearance EHP4.	m	
EHRA	Radar antenna height clearance.	m	
EHUMBL	Lower height clearance for a main u/c bay.	m	
EHUNBL	Lower height clearance for the nose u/c bay.	m	
ELMUFA	Longitudinal separation between the rear ends of fuselage mounted missiles no.3 and no.4.	m	
ELUMBA	Aft length clearance for a main u/c bay.	m	
ELUMBF	Forward length clearance for a main u/c bay.	m	
ELUNBA	Aft length clearance for the nose u/c bay.	m	
ELUNBF	Forward length clearance for the nose u/c bay.	m	
EQWF	T.E. flap deflection.	degrees	
EQWFH	Maximum T.E. flap deflection.	rads	
EQWFL	T.E. flap deflection in the landing configuration.	degrees	
EQWFT	T.E. flap deflection in the take-off configuration.	degrees	
EUML	Main u/c leg efficiency.		
EUMW	Main u/c tyre efficiency.		

EXUNBF	Clearance between the intake lips and the forward end of the nose u/c bay.	m	
EYFC	Lateral clearance at stn C which accounts for the width of the fuselage structure on each side of the cockpit.	m	
EYPCH	Lateral clearance between the engines for protection purposes.	m	
FBP1K	Constant factor for engine bay width clearance, EBP1.		
FBP2K	Constant factor for engine bay width clearance, EBP2.		
FBP3K	Constant factor for engine bay width clearance, EBP3.		
FBP4K	Constant factor for engine bay width clearance, EBP4.		
FBWA	Total fractional span of all ailerons		
FCLL	Fraction of CLMAX available for landing.		
FCLT	Fraction of CLMAX available for take-off.		
FCWLFT	Chord of fixed L.E. forward of front spar as a fraction of local wing chord.		
FCWLHT	Distance of the T.E. of the L.E. high lift device, forward of the front spar as a fraction of the local wing chord.		
FCWTFT	Distance of the T.E. of the fixed section of the wing T.E. aft of the rear spar as fraction of the local wing chord.		
FCWTHL	Distance of the L.E. of the T.E. flaps aft of the rear spar as a fraction of the local wing chord.		
FDUNL	Fraction of DUNL related to the thickness of the lower end of the nose u/c leg.		
FHP1K	Constant factor for engine bay height clearance, EHP1.		
FHP2K	Constant factor for engine bay height clearance, EHP2.		
FHP3K	Constant factor for engine bay height clearance, EHP3.		
FHP4K	Constant factor for engine bay height clearance, EHP4.		
FLMUF1	Nose length fraction of fuselage-mounted missile no.1.		
FLMUF2	Nose length fraction of fuselage-mounted missile no.2.		
FLMUF3	Nose length fraction of fuselage-mounted missile no.3.		
FLMUF4	Nose length fraction of fuselage-mounted missile no.4.		
FLP1K	Exponent in correlation for length of engine gas generator.		0.870
FLP2K	Exponent in correlation for length of engine reheat fuelling section.		0.500
FLP3K	Exponent in correlation for length		0.500

	of engine nozzle.	
FLVK	Constant factor related to LVG.	
FMC	Foreplane materials mass factor.	
FMCB1	Multiple carriage factor for wing-store stn no.1.	
FMCB2	Multiple carriage factor for wing-store stn no.2.	
FMCB3	Multiple carriage factor for wing-store stn no.3.	
FMCB4	Multiple carriage factor for wing-store stn no.4.	
FMD1	First constant factor for the estimation of MD.	
FMD2	Second constant factor for the estimation of MD, which allows for improvements in aerodynamic tech.	
FMEF	Fin materials mass factor.	
FMEF2	Twin-fin mass factor.	
FMF1	Materials mass factor for fuselage miscellania.	
FMF2	Materials mass factor for fuselage.	
FMFIR	State-of-the-art mass factor for the intake ramps.	
FMPBK	Factor in estimation of the mass of engine gas generator.	0.940
FMPIK	Factor in estimation of the engine installation mass.	0.130
FMPRK	Exponent in estimation of mass of the engine reheat system.	0.650
FMSC	State-of-the-art mass factor for the flying controls.	
FMSCK	Constant factor for the prediction of the flying control mass.	0.0293
FMSA	Mass fraction of air systems parts other than ducts.	
FMSAK	Constant factor for the prediction of the air systems mass.	0.011
FMSEK	Constant factor for the prediction of the electrics mass.	0.0267
FMSFK	Constant factor for the prediction of fuel system mass.	0.0759
FMUHK	Constant factor for the prediction of the u/c hydraulics mass.	0.0068
FMUM	State-of-the-art mass factor for the main u/c.	
FMUN	State-of-the-art mass factor for the nose u/c.	
FMUMK	Constant factor for the prediction of the main u/c mass.	0.0468
FMUNK	Constant factor for the prediction of the nose u/c mass.	0.0064
FMWB	Materials mass factor for the wing-box.	
FMWL	Materials mass factor for the wing L.E.	
FMWT	Materials mass factor for the wing T.E.	
FPUNLV	Constant factor which allows for the additional load on the nose u/c leg due to steady braking.	

FRK	Ground rolling friction coefficient.	
FTPGC	Fraction defining the maximum available reverse thrust in terms of TPGC.	
FVCKPT	Cockpit volume factor.	
FVSTAP	Factor defining the approach speed in terms of the stall speed.	
FVSTTO	Factor defining the take-off speed in terms of the stall speed.	
FXWPCG	Fraction of the local wing-chord between the front and rear spars defining the position of the imaginary wing-store c.g. line.	
FYB1	Net wing span fraction defining the lateral c.g.posn of wing-store stn 1.	
FYB2	Net wing span fraction defining the lateral c.g.posn of wing-store stn 2.	
FYB3	Net wing span fraction defining the lateral c.g.posn of wing-store stn 3.	
FYB4	Net wing span fraction defining the lateral c.g.posn of wing-store stn 4.	
FZCAN1	Power of the Z-coordinate of the front canopy section.	
FZCAN2	Power of the Z-coordinate of the rear canopy section.	
GN	Load factor.	
GTCPH	Maximum human G-tolerance limit.	
HC1	Distance between thigh point and eye point.	m
HC2	Distance between thigh point and heel point.	m
HC3	Distance between thigh point and NSRP.	m
HC4	Vertical gap between eye-point and canopy.	m
HCSEAT	Height of the NSRP above the cockpit floor measured along the seat-back line.	m
HFA1	Cockpit underfloor height at stn A.	m
HFDCU	Height of an upper corner of fuselage stn D.	m
HRA	Height of radar antenna.	m
HT	Flight altitude.	m
HTF	Airfield altitude.	m
HTH	Altitude at which MHH is reached.	m
HTR	Equivalent surface roughness height.	m
LAR	Length of the radar avionics bay.	m
LAX	Length of the extra avionics bay, aft of the radar bay in section R-A.	m
LCCAN	Total length of canopy and windscreen.	m
LCFOOT	Horizontal distance between fwd cockpit bulkhead and heel-point.	m
LCNSPR	Distance between the NSRP and the fwd bulkhead of the cockpit.	m
LGC	Gun length.	m
LMUF1	Length of fuselage-mounted missile no.1.	m
LMUF2	Length of fuselage-mounted missile no.2.	m

LMUF3	Length of fuselage-mounted missile no.3.	m	
LMUF4	Length of fuselage-mounted missile no.4.	m	
LP12R	Length of the gas generator of datum engine.	m	1.600
LP22AR	Reference length of the reheat fuelling section of datum engine.	m	0.400
LP2A4R	Length of the reheat burning section of datum engine.	m	1.400
LP34R	Nozzle length of datum engine.	m	0.900
LWFK	Length of flap tracks as a fraction of the wing chord.	m	
M	Mach numbar.		
MAPU	Mass of APU.	kg	
MAR	Mass of radar avionics.	kg	
MAX	Mass of general avionics.	kg	
MB1	Mass of stores mounted at wing-pylon no.1.	kg	
MB2	Mass of stores mounted at wing-pylon no.2.	kg	
MB3	Mass of stores mounted at wing-pylon no.3.	kg	
MB4	Mass of stores mounted at wing-pylon no.4.	kg	
MC1K	First constant for foreplane mass prediction.		0.004356
MC2K	Second constant for foreplane mass prediction.		1.549
MC3K	Third constant for foreplane mass prediction.		0.3433
MCFI	Mass of cockpit flight instrumentation.	kg	
MCMI	Mass of cockpit miscellaneous instrumentation.	kg	
MCPI	Mass of cockpit powerplant instrumentation.	kg	
MCP	Mass of crew, including personal equipment.	kg	
MCSEAT	Mass of ejection seat.	kg	
MEF1K	First constant for the estimation of MEF.		0.11156
MEF2K	Second constant for the estimation of MEF.		1.300
MEF3K	Third constant for the estimation of MEF.		0.7812
MEF4K	Fourth constant for the estimation of MEF.		0.2422
MGA	Mass of ammunition.	kg	
MGC	Mass of gun.	kg	
MHH	Maximum design Mach number for b.l.diverter sizing.		
MLMUF	Total mass of missile launchers.	kg	
MMUF1	Mass of fuselage-mounted missile no.1	kg	
MMUF2	Mass of fuselage-mounted missile no.2	kg	
MMUF3	Mass of fuselage-mounted missile no.3	kg	
MMUF4	Mass of fuselage-mounted missile no.4	kg	
MPAD1	Value of MPAD for the datum engine.	kg/s	70.0
MPBR	Gas generator reference mass.	kg	600.0
MPFB1	Initial estimate for MPFB2.	kg	

MPFD1	Value of MPFD for the datum engine.	kg/s	5.0
MPRR	Reference reheat system mass.	kg	200.0
MPTR	Thrust reverser reference mass.	kg	100.0
MSAK	Constant related to MSA.		-15.9
MSCK	Constant related to the flying controls mass.		22.2
MSEK	Constant related to MSE.		29.9
MSTART	Initial Mach number value used in acceleration calculations.		
MTLF	Fuel mass required for landing.	kg	
MTPR	Reference load for the definition of MTCR.	kg	
MTTF	Fuel mass required for take-off.	kg	
MTTR	Take-off reference mass.	kg	
MUHK	Constant used in the calculation of MUH.		4.0
MUMK	Constant used in the calculation of MUM.		-42.0
MUNK	Constant used in the calculation of MUN.		6.0
MXP1	Mass of external wing-pylon no.1.	kg	
MXP2	Mass of external wing-pylon no.2.	kg	
MXP3	Mass of external wing-pylon no.3.	kg	
MXP4	Mass of external wing-pylon no.4.	kg	
MXTF1	Mass of fuel in external tank no.1.	kg	
MXTF2	Mass of fuel in external tank no.2.	kg	
NB1	Number of stores mounted at wing-pylon no.1.		
NB2	Number of stores mounted at wing-pylon no.2.		
NB3	Number of stores mounted at wing-pylon no.3.		
NB4	Number of stores mounted at wing-pylon no.4.		
NFIN	Number of fins.		
NPP1	Number of points for STR estimates.		
NPP2	Number of points for ATR estimates.		
NPP3	Number of points for SEP estimates.		
NPP4	Number of points for MMAX estimates.		
NPP5	Number of points for SDT estimates.		
NPP6	Number of points for RQF estimates.		
NSTAG	Number of sortie legs.		
NWFK	Number of flap tracks.		
OGFA	Average cross-sectional area of the gun fairing.	m2	
OPJD1	Value of OPJD for the datum engine.	m2	
PGFA	Average perimeter of gun fairing.	m	
PUMW1	Specified maximum pressure for a main u/c tyre.	Pa	
PUNW1	Specified maximum pressure for a nose u/c tyre.	Pa	
QCCAN	Canopy centerline inclination above the horizontal.	rads	
QCEYE	Pilot's forward and downward view angle measured from the eye-point.	rads	
QCL	Foreplane L.E. sweep.	rads	
QCSEAT	Seat-back angle.	rads	
QCST	Total T.E. angle of the foreplane aerofoil.	degrees	
QCWSC	Windscreen inclination to the	rads	

	horizontal.		
QEFL	Fin L.E. sweep.	rads	
QFPR	Angle between the inner line of the underfuselage recess and the horizontal.	rads	
QFPRU	Angle between the inner line of the upper fuselage recess and the horizontal.	rads	
QWST	Total trailing edge angle of the wing aerofoil.	degrees	
RAPU	APU density.	kg/m3	
RAR	Radar avionics density.	kg/m3	
RAX	General avionics density.	kg/m3	
RCDK	Sharpness parameter for intake lips in spillage drag estimation.		
RCDVK	Factor on K1 to allow for the effects of advanced technology.		
RCSW	Foreplane volume coefficient.		
REFFC	Fin volume coefficient.		
RFAIB	Air-brake density.	kg/m3	
RFIR	Intake ramp density.	kg/m3	
RFUL	Fuel density.	kg/m3	800.0
RFW	Fuselage structure density.	kg/m3	
RGA	Ammunition density.	kg/m3	
RGC	Gun density.	kg/m3	
RIDL	Length to inlet depth ratio of the intake diffuser.		
RIDLS	Minimum allowable value for RIDL.		6.0
RIDX1	Initial corner radius of an intake diffuser.	m	
RLMUF	Density of the fuselage-mounted missile launchers.	kg/m3	
RLUPCW	U/c c.g. position aft of mean 0.25-chord point as fraction MAC.		
RMTLFI	Mass proportion of internal fuel remaining in tanks on landing.		
ROIEI	Fixed area ratio for the intake diffusers.		
RPUMLV	Main u/c leg load factor.		
RSA	Air systems density.	kg/m3	
RSC	Flying control system density.	kg/m3	
RSE	Electrics density.	kg/m3	
RSF	Fuel system density.	kg/m3	
RSLEW	Wing leading edge sharpness parameter.		
RSLEC	Foreplane leading edge sharpness parameter.		
RTC	Thickness to chord ratio of the foreplane.		
RTEF	Thickness to chord ratio of the fin.		
RXB	Fraction of LCEYE defining the distance of stn B from the a/c nose.		
RXE	Fraction of (XH-XD) defining the distance of stn E from the a/c nose.		
RXFR	Fraction of LAR defining the distance of stn R from the a/c nose.		
RXGF	Fraction of (XH-XD) defining the distance of the gun from the a/c nose		
RXMUF1	Fraction of (XH-XD) defining the distance of fuselage-mounted missile		

	no.1 from the a/c nose.		
RXMUF2	Fraction of (XH-XD) defining the distance of fuselage-mounted missile no.2 from the a/c nose.		
RXMUF3	Fraction of (XH-XD) defining the distance of fuselage-mounted missile no.3 from the a/c nose.		
RXMUF4	Fraction of (XH-XD) defining the distance of fuselage-mounted missile no.4 from the a/c nose.		
SFAIB	Total planform area of airbrakes.	m2	
SLEG	Length of a sortie leg in km.	km	
SRB1	Release status for stores mounted at wing-pylon no.1.		
SRB2	Release status for stores mounted at wing-pylon no.2.		
SRB3	Release status for stores mounted at wing-pylon no.3.		
SRB4	Release status for stores mounted at wing-pylon no.4.		
SRMUF1	Release status for fuselage-mounted missile no.1.		
SRMUF2	Release status for fuselage-mounted missile no.2.		
SRMUF3	Release status for fuselage-mounted missile no.3.		
SRMUF4	Release status for fuselage-mounted missile no.4.		
SUC	Retractable u/c status.		
TPG1	Guess value of the gross thrust required along a sortie leg.	N	
TPGD1	Datum value of TPGD.(Dry)	N	45000.0
TPGD2	Datum value of TPGD.(Reheat)	N	80000.0
TRATE	Fraction of TPGC available for take-off.		
UCN	Net foreplane taper ratio.		
UEFN	Net fin taper ratio.		
ULTN	Ultimate load factor for structural design (1.5 x proof factor).		
UWBEF	Exposed wing-box volume utilization factor for fuel storage.		
VD	Maximum design diving speed.	m/s	
VTLV	Maximum vertical landing velocity.	m/s	
WT	Aircraft weight as used in performance estimation methods.	N	
XV	Engine throttle setting/or/gross thrust.	% or N	
YCCANC	Y-coordinate of the canopy at stn C.	m	

FIG. J.3 LIST OF INPUT VARIABLES

MACH	CLC	DK2	CLMAX
0.0	0.79	0.5	1.75
0.1	0.79	0.5	1.75
0.2	0.79	0.5	1.75
0.3	0.79	0.5	1.75
0.4	0.79	0.5	1.75
0.5	0.73	0.5	1.75
0.6	0.67	0.5	1.75
0.7	0.63	0.6	1.80
0.8	0.69	0.7	1.90
0.9	0.75	0.8	1:80
1.0	0.84	0.8	1.60
1.1	0.82	0.8	1.45
1.2	0.80	0.8	1.30
1.3	0.70	0.8	1.20
1.4	0.60	0.7	1.05
1.5	0.50	0.6	0.95
1.6	0.40	0.6	0.80
1.7	0.40	0.6	0.75
1.8	0.40	0.5	0.65
1.9	0.40	0.5	0.55
2.0	0.40	0.5	0.50
2.1	0.40	0.5	0.40
2.2	0.40	0.4	0.35
2.3	0.40	0.4	0.30
2.4	0.40	0.4	0.20

FIG. J.4 FILE LDD2.DAT (EXAMPLE)

MACH	INSTALLED STORE DRAG COEFFICIENT DATA							
	1	2	3	4	5	6	7	8
0.0	0.00030	0.00088	0.00061	0.00067	0.00146	0.00000	0.00000	0.0
0.1	0.00030	0.00088	0.00061	0.00067	0.00146	0.00000	0.00000	0.0
0.2	0.00030	0.00088	0.00061	0.00067	0.00146	0.00000	0.00000	0.0
0.3	0.00030	0.00088	0.00061	0.00067	0.00146	0.00000	0.00000	0.0
0.4	0.00030	0.00088	0.00061	0.00067	0.00146	0.00000	0.00000	0.0
0.5	0.00030	0.00088	0.00061	0.00067	0.00146	0.00000	0.00000	0.0
0.6	0.00030	0.00088	0.00061	0.00067	0.00146	0.00000	0.00000	0.0
0.7	0.00030	0.00088	0.00061	0.00067	0.00146	0.00000	0.00000	0.0
0.8	0.00030	0.00088	0.00061	0.00067	0.00146	0.00000	0.00000	0.0
0.9	0.00040	0.00097	0.00067	0.00079	0.00170	0.00000	0.00000	0.0
1.0	0.00052	0.00134	0.00161	0.00109	0.00368	0.00000	0.00000	0.0
1.1	0.00058	0.00140	0.00000	0.00134	0.00432	0.00000	0.00000	0.0
1.2	0.00058	0.00140	0.00000	0.00140	0.00429	0.00000	0.00000	0.0
1.3	0.00055	0.00134	0.00000	0.00140	0.00423	0.00000	0.00000	0.0
1.4	0.00052	0.00122	0.00000	0.00137	0.00417	0.00000	0.00000	0.0
1.5	0.00052	0.00112	0.00000	0.00134	0.00401	0.00000	0.00000	0.0
1.6	0.00049	0.00106	0.00000	0.00131	0.00392	0.00000	0.00000	0.0
1.7	0.00046	0.00100	0.00000	0.00131	0.00380	0.00000	0.00000	0.0
1.8	0.00046	0.00097	0.00000	0.00128	0.00374	0.00000	0.00000	0.0
1.9	0.00043	0.00097	0.00000	0.00128	0.00362	0.00000	0.00000	0.0
2.0	0.00040	0.00097	0.00000	0.00128	0.00353	0.00000	0.00000	0.0
2.1	0.00036	0.00097	0.00000	0.00128	0.00347	0.00000	0.00000	0.0
2.2	0.00033	0.00097	0.00000	0.00128	0.00341	0.00000	0.00000	0.0
2.3	0.00033	0.00094	0.00000	0.00128	0.00337	0.00000	0.00000	0.0
2.4	0.00033	0.00094	0.00000	0.00128	0.00337	0.00000	0.00000	0.0

FIG. J.5 FILE STDRAG.DAT (EXAMPLE)

APPENDIX K

DESIGN EXAMPLE

CANARD.DAT

```
51.000 2.100 0.150 0.765 0.060 0.850 0.150 0.650
0.605  0.210  0.160 1.05
15.475 0.325  0.345  0.650  0.500  0.500
0.500 0.500 0.150  0.150  0.150
0.762 0.700 0.400 0.254 0.250 0.190
0.524  0.262 0.850  1.700  9.000
950000.0  950000.0  3.000  1.500  0.500 4.000 0.200  0.150
0.700 0.470 0.050  0.050  0.030  0.050  0.050  0.030
1.600 0.400  1.400  0.900 0.870 0.500 0.500
0.690 0.760 0.890 0.770 600.0 200.0 100.0 0.940 0.650 0.130
45000.0 80000.0 5.000 70.000 0.400
0.100 1.000 0.303 0.400 0.129 0.397 0.100 0.100
0.160 0.714 0.278 0.927 0.128 0.332 0.085 0.439
0.043 0.110 0.172 0.304 0.000 0.110 0.000 0.300
2.000 12000.0 0.800 0.040 0.700 1.100 0.200
1.668 0.700 0.230 15.000 6.000 0.835 0.000 3.500 0.124  0.500
0.600 0.800 0.0375 0.0375 0.250 0.150 0.350 0.400 0.42 0.325
0.442 0.175 0.185 0.282 0.750  0.750  1.100
0.050  0.050  0.030  0.030  0.600 6.000 4.570 0.435
1.000 0.150 0.000 0.700 0.000015
0.038 2.500 0.300 0.030 0.923 0.600 6.000
0.033 1.600 0.250 0.040 0.800 1
0.800  0.250 800.0  0.000
17000.0 670.0  15.000 400.0 2.200
0.0468 0.0064 0.0068 0.011 0.0267 0.0293 0.0759
0.750 1.000 0.950 1.000 1.000 1.070 1.000 0.800
0.800 1.000 0.950 0.900 0.900
-42.000 6.000 4.000 -15.900 29.900 22.200
```

```
0.004356 1.549 0.3433 0.11156 1.300 0.7812 0.2422
150.0 300.0 100.0  100.0 30.0 20.0 10.0 160.0 50.0
0.873  6     0.200 1.000
800.0 801.0 801.0 801.0 480.6 640.8 640.8
160.2 480.6 480.6 480.6 101.0 101.0 101.0
0.412  0.412  0.637  0.669
3.550 3.550 3.550 3.550
0.106  0.106  0.106  0.106
0.175 0.175 0.175 0.175
150.0 150.0 150.0 150.0
1       1       1       1
0.428 2.350 0.090 0.010 0.300 160.0 80.0
0.800 0.400 0.400 0.800 0.250
1   2   1   1
90.0  0.0   0.0   90.0
1.000 1.250 1.000 1.000
2    3    5    2
60.0  65.0  65.0  60.0
4     4     4     4


8     300.0  150.0

  7.0  4000.0  0.5  1.5  0.0  60000.0  0.30  0.08  400.0
1.0    1.0    1.0    1.0    1.0  0.0  0.0  1.0  0.0
150.0  8000.0  0.9  1.0  0.0  30000.0  0.20  0.10 1000.0
1.0    1.0    1.0    1.0    1.0  0.0  0.0  1.0  0.0
  6.0  6000.0  1.0  0.7  0.0  50000.0  0.30  0.06  100.0
1.0    1.0    1.0    1.0    1.0  0.0  0.0  1.0  0.0
 50.0  2000.0  1.1  1.0  0.0  60000.0  0.10  0.05  500.0
1.0    1.0    1.0    1.0    1.0  0.0  0.0  1.0  0.0
  2.0  5000.0  1.1  5.0 10.0  90000.0  0.20  0.05  800.0
1.0    1.0    1.0    1.0    1.0  0.0  0.0  1.0  0.0
 10.0 11000.0  1.6  1.3  0.0  80000.0  0.20  0.07  600.0
1.0    1.0    1.0    1.0    0.0  0.0  0.0  0.0  0.0
200.0 14000.0  2.0  1.0  0.0  50000.0  0.30  0.08 1500.0
1.0    1.0    1.0    1.0    0.0  0.0  0.0  0.0  0.0
 13.0  7000.0  0.6  0.6  0.0  40000.0  0.30  0.08  150.0
1.0    1.0    1.0    1.0    0.0  0.0  0.0  0.0  0.0
```

```
0.0     0.95  15.0  1.10    1.00 0.35 0.25  35.0  1.20    1.00

1     1     1     2     1     1
1.0     1.0     1.0     1.0     0.0  0.0  0.0  0.0  0.0

1000.0   0.60 140000.0 100.0 10.0 1.00

9000.0   1.60 140000.0 100.0 10.0

6000.0 0.70 130000.0 100.0

10000.0 2.10 140000.0 100.0
1000.0   1.00 140000.0 100.0

12000.0 0.80    145000.0 100.0 0.30

1000.0 0.50 150000.0
```

LDD2.DAT

```
0.0 0.79 0.5 1.75
0.1 0.79 0.5 1.75
0.2 0.79 0.5 1.75
0.3 0.79 0.5 1.75
0.4 0.79 0.5 1.75
0.5 0.73 0.5 1.75
0.6 0.67 0.5 1.75
0.7 0.63 0.6 1.80
0.8 0.69 0.7 1.90
0.9 0.75 0.8 1.80
1.0 0.84 0.8 1.60
1.1 0.82 0.8 1.45
1.2 0.80 0.8 1.30
1.3 0.70 0.8 1.20
1.4 0.60 0.7 1.05
1.5 0.50 0.6 0.95
1.6 0.40 0.6 0.80
1.7 0.40 0.6 0.75
1.8 0.40 0.5 0.65
1.9 0.40 0.5 0.55
2.0 0.40 0.5 0.50
2.1 0.40 0.5 0.40
2.2 0.40 0.4 0.35
2.3 0.40 0.4 0.30
2.4 0.40 0.4 0.20
```

STDRAG.DAT

0.0	0.00030	0.00088	0.00061	0.00067	0.00146	0.00000	0.00000 0.0
0.1	0.00030	0.00088	0.00061	0.00067	0.00146	0.00000	0.00000 0.0
0.2	0.00030	0.00088	0.00061	0.00067	0.00146	0.00000	0.00000 0.0
0.3	0.00030	0.00088	0.00061	0.00067	0.00146	0.00000	0.00000 0.0
0.4	0.00030	0.00088	0.00061	0.00067	0.00146	0.00000	0.00000 0.0
0.5	0.00030	0.00088	0.00061	0.00067	0.00146	0.00000	0.00000 0.0
0.6	0.00030	0.00088	0.00061	0.00067	0.00146	0.00000	0.00000 0.0
0.7	0.00030	0.00088	0.00061	0.00067	0.00146	0.00000	0.00000 0.0
0.8	0.00030	0.00088	0.00061	0.00067	0.00146	0.00000	0.00000 0.0
0.9	0.00040	0.00097	0.00067	0.00079	0.00170	0.00000	0.00000 0.0
1.0	0.00052	0.00134	0.00161	0.00109	0.00368	0.00000	0.00000 0.0
1.1	0.00058	0.00140	0.00000	0.00134	0.00432	0.00000	0.00000 0.0
1.2	0.00058	0.00140	0.00000	0.00140	0.00429	0.00000	0.00000 0.0
1.3	0.00055	0.00134	0.00000	0.00140	0.00423	0.00000	0.00000 0.0
1.4	0.00052	0.00122	0.00000	0.00137	0.00417	0.00000	0.00000 0.0
1.5	0.00052	0.00112	0.00000	0.00134	0.00401	0.00000	0.00000 0.0
1.6	0.00049	0.00106	0.00000	0.00131	0.00392	0.00000	0.00000 0.0
1.7	0.00046	0.00100	0.00000	0.00131	0.00380	0.00000	0.00000 0.0
1.8	0.00046	0.00097	0.00000	0.00128	0.00374	0.00000	0.00000 0.0
1.9	0.00043	0.00097	0.00000	0.00128	0.00362	0.00000	0.00000 0.0
2.0	0.00040	0.00097	0.00000	0.00128	0.00353	0.00000	0.00000 0.0
2.1	0.00036	0.00097	0.00000	0.00128	0.00347	0.00000	0.00000 0.0
2.2	0.00033	0.00097	0.00000	0.00128	0.00341	0.00000	0.00000 0.0
2.3	0.00033	0.00094	0.00000	0.00128	0.00337	0.00000	0.00000 0.0
2.4	0.00033	0.00094	0.00000	0.00128	0.00337	0.00000	0.00000 0.0

CANARD.RES

COCKPIT

QCFOOT=0.768 HC6=0.000 HCEYE=1.024

LCEYE=1.735 LCFL=1.894 HC5=0.559

MAIN UNDERCARRIAGE(STANDARD TYRE CHARACTERISTICS)

DUMWN= 1.219 BUMWN= 0.381 DUMWH= 1.237 DUMWS= 1.201

BUMWH= 0.387 BUMWS= 0.370 DUMWG= 1.265 BUMWG= 0.399

PUMW= 617310.0 PUMLV= 10886.4

MAIN UNDERCARRIAGE

DHUMW=0.039 DHUML=0.421 DUML=0.110 LUML=1.054

NOSE UNDERCARRIAGE(STANDARD TYRE CHARACTERISTICS)

DUNWN= 0.584 BUNWN= 0.178 DUNWH= 0.589 DUNWS= 0.574

BUNWH= 0.183 BUNWS= 0.173 DUNWG= 0.603 BUNWG= 0.190

PUNW= 754490.0 PUNLV= 2653.6

NOSE UNDERCARRIAGE

DHUNL=0.411 DUNL=0.063 LUNL=1.528

MAIN UNDERCARRIAGE BAY

EDUMW=0.029 EBUMW=0.013

LUMB=1.815 HUMB=0.566 BUMB=1.322

OUMB=0.749 VUMB=1.359

NOSE UNDERCARRIAGE BAY

EDUNW=0.019 EBUNW=0.009

LUNB=1.948 HUNBA=0.270 HUNBF=0.136

BUNB=0.641 LUNWB=0.722 LUNLB=1.226

OUNLBS=0.087 OUNLBH=0.173 OUNWB=0.173

VUNWB=0.125 VUNLB=0.159 VUNB=0.284

GROSS WING

BW=10.349 CWCC=8.571 CWCT=1.286 CWMG=4.928 CWMA=5.825

QWL=0.920 QW2=0.546 QWT=-.096

ENGINE SIZING

LP12=1.462 LP22A=0.410 LP2A4=1.400

LP34=0.922 LP23=0.888 LPG=3.271

DP1=0.707 DP2=0.779 DP3=0.912

DP4=0.789 OPN=0.978 TPGD=168000.00

MPFD=10.500 MPAD=147.000 OPJD= 0.840

ENGINE BAY CLEARANCES

EHP1=0.160 EBP1=0.354 EHP2=0.236 EBP2=0.156

EHP3=0.110 EBP3=0.181 EHP4=0.079 EBP4=0.039

AIR INLET GEOMETRY

OIE= 0.785 OII= 0.714 BIIH= 0.670

BII= 0.670 HII= 0.535

DISTANCE OF FUSELAGE STATIONS FROM THE A/C NOSE

XFR= 1.393 XA= 2.228 XB= 3.442

XC= 3.963 XD= 5.728 XE= 7.553

XF= 9.615 XG=11.496 XH=13.665

XJ=14.553 XK=15.475 XFN=15.475

XII= 4.182 XUNBF= 4.502 XWCQM= 9.362

XP1=12.204 XP2=13.665 XP3=14.553

XP4=15.475 XWAPEX= 5.348 XCCQM= 5.728

XMUF1= 6.065 XMUF2= 6.065 XMUF3=10.115

XMUF4= 9.615 XGF= 7.265

LVG= 1.072 RIDL=15.000 LCCAN= 3.500

B.L.DIVERTER DATA

RNI=.54E+08 HVI=0.080 LVG=1.072

XVE=5.254 BVI=1.340 OVI=0.1066

FUSELAGE STATION R

XFR=1.393 YFR=0.438 ZFR=0.338

OFR=0.464 PFR=2.455

FAIRING CURVE DATA

X1= 1.393 X2= 2.972

X3= 5.970 X4=12.148

X5=13.812 X6=15.475

OTF1K= 2.497 OTF2K= 0.000

OTF3K=-0.218 OTF4K= 0.027

OTA1K= 2.497 OTA2K= 0.000

OTA3K=-0.722 OTA4K= 0.163

FUSELAGE STATION A

[STN= 2.228]

CROSS-SECTIONAL AREA OF F.C. AT STN X

OTXN=0.828

QFRA=0.131 HFA=0.959 BFA=1.099

OFA=0.828 PFA=3.241

RADOME

[STN= 0.000]

FZFRAK=0.748 FYFRAK=0.486

ZFRX=0.000 YFRX=0.000

OFRX=0.000 PFRX=0.000

[STN= 0.696]

FZFRAK=0.748 FYFRAK=0.486

ZFRX=0.201 YFRX=0.312

OFRX=0.197 PFRX=1.650

[STN= 1.393]

FZFRAK=0.748 FYFRAK=0.486

ZFRX=0.338 YFRX=0.438

OFRX=0.464 PFRX=2.455

FUSELAGE SECTION R-A

[STN= 1.393]

FZFRAK=0.748 FYFRAK=0.486

ZFRAX=0.338 YFRAX=0.438

OFRAX=0.464 PFRAX=2.455

[STN= 1.810]

FZFRAK=0.748 FYFRAK=0.486

ZFRAX=0.411 YFRAX=0.497

OFRAX=0.641 PFRAX=2.864

[STN= 2.228]

FZFRAK=0.748 FYFRAK=0.486

ZFRAX=0.480 YFRAX=0.550

OFRAX=0.828 PFRAX=3.241

FUSELAGE STATION D

[STN= 5.728]

INTAKE DIFFUSER GEOMETRY AT STN X

ZIDLX=0.000 ZIDCX=0.267 ZIDUX=0.535

YIDIX=0.000 YIDCX=0.335 YIDOX=0.670

HIDX=0.535 BIDX=0.670 ZPC=1.000

RIDX=0.040 OIDX=0.357

CROSS-SECTIONAL AREA OF F.C. AT STN X

OTXN=2.485

YCWSCB=0.449 YCCAND=0.322 HFDH=1.844

HFD=1.844 HFD2=0.404 HFDCU=0.325

BFD=1.663 BFDCU=0.510

OFD=3.198 PFD=7.190

FUSELAGE STATION B

[STN= 3.442]

CROSS-SECTIONAL AREA OF F.C. AT STN X

OTXN=1.530

ZCWSCB=0.575 YCWSCB=0.449

HFB=0.959 HFBCU=0.426 HFBCL=0.303

BFB=1.252 BFBCU=0.177 BFBCL=0.338

OFB=1.530 PFB=4.690

FUSELAGE SECTION A-B

[STN= 2.228]

CROSS-SECTIONAL AREA OF F.C. AT STN X

OTXN=0.828

ZCWSCX=0.000 YCWSCX=0.000

HFABX=0.959 HFBCUX=0.480 HFBCLX=0.480

YFABX=0.550 BFBCUX=0.550 BFBCLX=0.550

OFABX=0.828 PFABX=3.241 PFTABX=0.000

[STN= 2.835]

CROSS-SECTIONAL AREA OF F.C. AT STN X

OTXN=1.168

ZCWSCX=0.287 YCWSCX=0.389

HFABX=0.959 HFBCUX=0.453 HFBCLX=0.391

YFABX=0.573 BFBCUX=0.185 BFBCLX=0.429

OFABX=1.168 PFABX=3.969 PFTABX=1.074

[STN= 3.442]

CROSS-SECTIONAL AREA OF F.C. AT STN X

OTXN=1.530

ZCWSCX=0.575 YCWSCX=0.449

HFABX=0.959 HFBCUX=0.426 HFBCLX=0.303

YFABX=0.626 BFBCUX=0.177 BFBCLX=0.338

OFABX=1.530 PFABX=4.690 PFTABX=1.620

FUSELAGE STATION C

[STN= 3.963]

CROSS-SECTIONAL AREA OF F.C. AT STN X

OTXN=1.832

HFC=0.959 HFC1=0.400

HFC2=0.092 ZCCANC=0.627 HFCCU=0.403

BFCCU=0.335 HFCCL=0.227 BFCCL=0.343

BFC=1.510 OFC=1.832 PFC=5.411

FUSELAGE SECTION B-C

[STN= 3.442]

CROSS-SECTIONAL AREA OF F.C. AT STN X

OTXN=1.530

HFBCX=0.959 HFC2X=0.000 YCCANX=0.449

ZCCANX=0.575 HFCCUX=0.426 HFCCLX=0.303

YFBCX=0.626 BFCCUX=0.177 BFCCLX=0.338

OFBCX=1.530 PFBCX=4.690 PFTBCX=1.620

[STN= 3.702]

CROSS-SECTIONAL AREA OF F.C. AT STN X

OTXN=1.683

HFBCX=0.959 HFC2X=0.046 YCCANX=0.435

ZCCANX=0.615 HFCCUX=0.414 HFCCLX=0.265

YFBCX=0.686 BFCCUX=0.251 BFCCLX=0.335

OFBCX=1.683 PFBCX=5.043 PFTBCX=1.672

[STN= 3.963]

CROSS-SECTIONAL AREA OF F.C. AT STN X

OTXN=1.832

HFBCX=0.959 HFC2X=0.092 YCCANX=0.420

ZCCANX=0.627 HFCCUX=0.403 HFCCLX=0.227

YFBCX=0.755 BFCCUX=0.335 BFCCLX=0.343

OFBCX=1.832 PFBCX=5.411 PFTBCX=1.677

FUSELAGE SECTION C-D

[STN= 3.963]

CROSS-SECTIONAL AREA OF F.C. AT STN X

OTXN=1.832

INTAKE DIFFUSER GEOMETRY AT STN X

ZIDLX=0.000 ZIDCX=0.000 ZIDUX=0.000

YIDIX=0.000 YIDCX=0.000 YIDOX=0.000

HIDX=0.000 BIDX=0.000 ZPC=1.000

RIDX=0.000 OIDX=0.000

B.L.DIVERTER GEOMETRY AT STN X

BIX=0.000 BVIX=0.000 BVIX1=0.000

OVIX=0.000 OVIX1=0.000

LFCD=1.765 HFD2X=0.092 HFCDX=0.959

ZCCANX=0.627 YCCANX=0.420 HFDCUX=0.403

HFDCLX=0.227 YFCDX=0.755 BFDCUX=0.335

BFDCLX=0.343 OIX=0.000 OIXL1=0.000

OIXL2=0.000 OFCDXU=1.832 OFCDX=1.832

PFCDXU=5.411 PFCDXL=0.000 PFCDX= 5.411

PFTCDX=1.677

[STN= 4.845]

CROSS-SECTIONAL AREA OF F.C. AT STN X

OTXN=2.259

INTAKE DIFFUSER GEOMETRY AT STN X

ZIDLX=0.000 ZIDCX=0.267 ZIDUX=0.535

YIDIX=0.000 YIDCX=0.335 YIDOX=0.670

HIDX=0.535 BIDX=0.670 ZPC=1.000

RIDX=0.040 OIDX=0.357

B.L.DIVERTER GEOMETRY AT STN X

BIX=0.739 BVIX=1.478 BVIX1=0.000

OVIX=0.118 OVIX1=0.000

LFCD=1.765 HFD2X=0.248 HFCDX=1.747

ZCCANX=0.284 YCCANX=0.371 HFDCUX=0.364

HFDCLX=0.098 YFCDX=0.890 BFDCUX=0.520

BFDCLX=0.269 OIX=0.791 OIXL1=0.000

OIXL2=0.256 OFCDXU=1.925 OFCDX=3.090

PFCDXU=5.722 PFCDXL=4.373 PFCDX=10.096

PFTCDX=1.037

[STN= 5.728]

CROSS-SECTIONAL AREA OF F.C. AT STN X

OTXN=2.485

INTAKE DIFFUSER GEOMETRY AT STN X

ZIDLX=0.000 ZIDCX=0.267 ZIDUX=0.535

YIDIX=0.000 YIDCX=0.335 YIDOX=0.670

HIDX=0.535 BIDX=0.670 ZPC=1.000

RIDX=0.040 OIDX=0.357

B.L.DIVERTER GEOMETRY AT STN X

BIX=0.831 BVIX=0.000 BVIX1=1.663

OVIX=0.000 OVIX1=0.132

LFCD=1.765 HFD2X=0.404 HFCDX=1.844

ZCCANX=0.000 YCCANX=0.322 HFDCUX=0.325

HFDCLX=0.000 YFCDX=0.831 BFDCUX=0.510

BFDCLX=0.000 OIX=0.889 OIXL1=0.000

OIXL2=0.449 OFCDXU=1.728 OFCDX=3.198

PFCDXU=3.758 PFCDXL=3.432 PFCDX= 7.190

PFTCDX=0.714

FUSELAGE STATION E

[STN= 7.553]

CROSS-SECTIONAL AREA OF F.C. AT STN X

OTXN=2.497

WEAPON GEOMETRY AT STN X

DMUF1X=0.175 OMUF1X=0.024 PMUF1X=0.550

DMUF2X=0.175 OMUF2X=0.024 PMUF2X=0.550

DMUF3X=0.000 OMUF3X=0.000 PMUF3X=0.000

DMUF4X=0.000 OMUF4X=0.000 PMUF4X=0.000

BGFX=0.090 OGFX=0.010 PGFX=0.300

INTAKE DIFFUSER GEOMETRY AT STN X

ZIDLX=0.085 ZIDCX=0.372 ZIDUX=0.659

YIDIX=0.000 YIDCX=0.335 YIDOX=0.670

HIDX=0.574 BIDX=0.670 ZPC=1.000

RIDX=0.139 OIDX=0.368

HFECU=0.325 YFE2=0.220 HFE2=0.276

HFE=1.775 BFE=1.830 BFECU=0.695

OFE=3.233 PFE= 7.629

FUSELAGE SECTION D-E

[STN= 5.728]

WEAPON GEOMETRY AT STN X

DMUF1X=0.000 OMUF1X=0.000 PMUF1X=0.000

DMUF2X=0.000 OMUF2X=0.000 PMUF2X=0.000

DMUF3X=0.000 OMUF3X=0.000 PMUF3X=0.000

DMUF4X=0.000 OMUF4X=0.000 PMUF4X=0.000

BGFX=0.000 OGFX=0.000 PGFX=0.000

HFDEX=1.844 YFDEX=0.831

HFE2X=0.404 YFE2X=0.322

HFECUX=0.325 BFECUX=0.510

OFDEX=3.198 PFDEX=7.190

[STN= 6.641]

WEAPON GEOMETRY AT STN X

DMUF1X=0.175 OMUF1X=0.024 PMUF1X=0.550

DMUF2X=0.175 OMUF2X=0.024 PMUF2X=0.550

DMUF3X=0.000 OMUF3X=0.000 PMUF3X=0.000

DMUF4X=0.000 OMUF4X=0.000 PMUF4X=0.000

BGFX=0.000 OGFX=0.000 PGFX=0.000

HFDEX=1.809 YFDEX=0.873

HFE2X=0.340 YFE2X=0.271

HFECUX=0.325 BFECUX=0.603

OFDEX=3.196 PFDEX=7.401

[STN= 7.553]

WEAPON GEOMETRY AT STN X

DMUF1X=0.175 OMUF1X=0.024 PMUF1X=0.550

DMUF2X=0.175 OMUF2X=0.024 PMUF2X=0.550

DMUF3X=0.000 OMUF3X=0.000 PMUF3X=0.000

DMUF4X=0.000 OMUF4X=0.000 PMUF4X=0.000

BGFX=0.090 OGFX=0.010 PGFX=0.300

HFDEX=1.775 YFDEX=0.915

HFE2X=0.276 YFE2X=0.220

HFECUX=0.325 BFECUX=0.695

OFDEX=3.233 PFDEX=7.629

FUSELAGE SECTION E-F

[STN= 7.553]

INTAKE DIFFUSER GEOMETRY AT STN X

ZIDLX=0.085 ZIDCX=0.372 ZIDUX=0.659

YIDIX=0.000 YIDCX=0.335 YIDOX=0.670

HIDX=0.574 BIDX=0.670 ZPC=1.000

RIDX=0.139 OIDX=0.368

CROSS-SECTIONAL AREA OF F.C. AT STN X

OTXN=2.497

WEAPON GEOMETRY AT STN X

DMUF1X=0.175 OMUF1X=0.024 PMUF1X=0.550

DMUF2X=0.175 OMUF2X=0.024 PMUF2X=0.550

DMUF3X=0.000 OMUF3X=0.000 PMUF3X=0.000

DMUF4X=0.000 OMUF4X=0.000 PMUF4X=0.000

BGFX=0.090 OGFX=0.010 PGFX=0.300

HFF2X=0.276 YFF2X=0.220

HFEFX=1.775 YFEFX=0.915

HFFCUX=0.325 BFFCUX=0.695 EYFEF=0.075

OFEFX=3.233 PFEFX=7.629

[STN= 8.584]

INTAKE DIFFUSER GEOMETRY AT STN X

ZIDLX=0.185 ZIDCX=0.495 ZIDUX=0.805

YIDIX=0.051 YIDCX=0.389 YIDOX=0.727

HIDX=0.620 BIDX=0.676 ZPC=1.000

RIDX=0.195 OIDX=0.386

CROSS-SECTIONAL AREA OF F.C. AT STN X

OTXN=2.497

WEAPON GEOMETRY AT STN X

DMUF1X=0.175 OMUF1X=0.024 PMUF1X=0.550

DMUF2X=0.175 OMUF2X=0.024 PMUF2X=0.550

DMUF3X=0.000 OMUF3X=0.000 PMUF3X=0.000

DMUF4X=0.000 OMUF4X=0.000 PMUF4X=0.000

BGFX=0.090 OGFX=0.010 PGFX=0.300

HFF2X=0.204 YFF2X=0.162

HFEFX=1.736 YFEFX=0.971

HFFCUX=0.404 BFFCUX=0.809 EYFEF=0.075

OFEFX=3.269 PFEFX=7.603

[STN= 9.615]

INTAKE DIFFUSER GEOMETRY AT STN X

ZIDLX=0.286 ZIDCX=0.618 ZIDUX=0.951

YIDIX=0.173 YIDCX=0.518 YIDOX=0.863

HIDX=0.666 BIDX=0.690 ZPC=1.000

RIDX=0.251 OIDX=0.405

CROSS-SECTIONAL AREA OF F.C. AT STN X

OTXN=2.497

WEAPON GEOMETRY AT STN X

DMUF1X=0.175 OMUF1X=0.024 PMUF1X=0.550

DMUF2X=0.175 OMUF2X=0.024 PMUF2X=0.550

DMUF3X=0.000 OMUF3X=0.000 PMUF3X=0.000

DMUF4X=0.000 OMUF4X=0.000 PMUF4X=0.000

BGFX=0.090 OGFX=0.010 PGFX=0.300

HFF2X=0.132 YFF2X=0.105

HFEFX=1.697 YFEFX=1.028

HFFCUX=0.483 BFFCUX=0.924 EYFEF=0.075

OFEFX=3.307 PFEFX=7.585

FUSELAGE STATION F

[STN= 9.615]

INTAKE DIFFUSER GEOMETRY AT STN X

ZIDLX=0.286 ZIDCX=0.618 ZIDUX=0.951

YIDIX=0.173 YIDCX=0.518 YIDOX=0.863

HIDX=0.666 BIDX=0.690 ZPC=1.000

RIDX=0.251 OIDX=0.405

CROSS-SECTIONAL AREA OF F.C. AT STN X

OTXN=2.497

WEAPON GEOMETRY AT STN X

DMUF1X=0.175 OMUF1X=0.024 PMUF1X=0.550

DMUF2X=0.175 OMUF2X=0.024 PMUF2X=0.550

DMUF3X=0.000 OMUF3X=0.000 PMUF3X=0.000

DMUF4X=0.000 OMUF4X=0.000 PMUF4X=0.000

BGFX=0.090 OGFX=0.010 PGFX=0.300

HFF2=0.132 YFF2=0.105

HFFCU=0.483 BFFCU=0.924

HFF=1.697 BFF=2.057

OFF=3.307 PFF=7.585

FUSELAGE SECTION F-G

[STN= 9.615]

INTAKE DIFFUSER GEOMETRY AT STN X

ZIDLX=0.286 ZIDCX=0.618 ZIDUX=0.951

YIDIX=0.173 YIDCX=0.518 YIDOX=0.863

HIDX=0.666 BIDX=0.690 ZPC=1.000

RIDX=0.251 OIDX=0.405

CROSS-SECTIONAL AREA OF F.C. AT STN X

OTXN=2.497

WEAPON GEOMETRY AT STN X

DMUF1X=0.175 OMUF1X=0.024 PMUF1X=0.550

DMUF2X=0.175 OMUF2X=0.024 PMUF2X=0.550

DMUF3X=0.000 OMUF3X=0.000 PMUF3X=0.000

DMUF4X=0.000 OMUF4X=0.000 PMUF4X=0.000

BGFX=0.090 OGFX=0.010 PGFX=0.300

HFG2X=0.132 YFG2X=0.105

HFFGX=1.697 YFFGX=1.021

HFGCUX=0.483 BFGCUX=0.916 EYFFG=0.075

OFFGX=3.307 PFFGX=7.355

[STN=10.556]

INTAKE DIFFUSER GEOMETRY AT STN X

ZIDLX=0.352 ZIDCX=0.700 ZIDUX=1.048

YIDIX=0.279 YIDCX=0.631 YIDOX=0.982

HIDX=0.696 BIDX=0.702 ZPC=1.000

RIDX=0.302 OIDX=0.410

CROSS-SECTIONAL AREA OF F.C. AT STN X

OTXN=2.497

WEAPON GEOMETRY AT STN X

DMUF1X=0.000 OMUF1X=0.000 PMUF1X=0.000

DMUF2X=0.000 OMUF2X=0.000 PMUF2X=0.000

DMUF3X=0.175 OMUF3X=0.024 PMUF3X=0.550

DMUF4X=0.175 OMUF4X=0.024 PMUF4X=0.550

BGFX=0.000 OGFX=0.000 PGFX=0.000

HFG2X=0.066 YFG2X=0.052

HFFGX=1.662 YFFGX=1.077

HFGCUX=0.554 BFGCUX=1.025 EYFFG=0.075

OFFGX=3.317 PFFGX=7.344

[STN=11.496]

INTAKE DIFFUSER GEOMETRY AT STN X

ZIDLX=0.376 ZIDCX=0.729 ZIDUX=1.083

YIDIX=0.323 YIDCX=0.676 YIDOX=1.030

HIDX=0.707 BIDX=0.707 ZPC=1.000

RIDX=0.354 OIDX=0.393

CROSS-SECTIONAL AREA OF F.C. AT STN X

OTXN=2.497

WEAPON GEOMETRY AT STN X

DMUF1X=0.000 OMUF1X=0.000 PMUF1X=0.000

DMUF2X=0.000 OMUF2X=0.000 PMUF2X=0.000

DMUF3X=0.175 OMUF3X=0.024 PMUF3X=0.550

DMUF4X=0.175 OMUF4X=0.024 PMUF4X=0.550

BGFX=0.000 OGFX=0.000 PGFX=0.000

HFG2X=0.000 YFG2X=0.000

HFFGX=1.626 YFFGX=1.108

HFGCUX=0.626 BFGCUX=1.108 EYFFG=0.075

OFFGX=3.282 PFFGX=7.244

FUSELAGE STATION G

[STN=11.496]

INTAKE DIFFUSER GEOMETRY AT STN X

ZIDLX=0.376 ZIDCX=0.729 ZIDUX=1.083

YIDIX=0.323 YIDCX=0.676 YIDOX=1.030

HIDX=0.707 BIDX=0.707 ZPC=1.000

RIDX=0.354 OIDX=0.393

CROSS-SECTIONAL AREA OF F.C. AT STN X

OTXN=2.497

WEAPON GEOMETRY AT STN X

DMUF1X=0.000 OMUF1X=0.000 PMUF1X=0.000

DMUF2X=0.000 OMUF2X=0.000 PMUF2X=0.000

DMUF3X=0.175 OMUF3X=0.024 PMUF3X=0.550

DMUF4X=0.175 OMUF4X=0.024 PMUF4X=0.550

BGFX=0.000 OGFX=0.000 PGFX=0.000

HFG=1.626 BFG=2.217

HFGCU=0.626 BFGCU=1.108

OFG=3.282 PFG= 7.244

FUSELAGE SECTION G-H

[STN=11.496]

INTAKE DIFFUSER GEOMETRY AT STN X

ZIDLX=0.376 ZIDCX=0.729 ZIDUX=1.083

YIDIX=0.323 YIDCX=0.676 YIDOX=1.030

HIDX=0.707 BIDX=0.707 ZPC=1.000

RIDX=0.354 OIDX=0.393

CROSS-SECTIONAL AREA OF F.C. AT STN X

OTXN=2.497

WEAPON GEOMETRY AT STN X

DMUF1X=0.000 OMUF1X=0.000 PMUF1X=0.000

DMUF2X=0.000 OMUF2X=0.000 PMUF2X=0.000

DMUF3X=0.175 OMUF3X=0.024 PMUF3X=0.550

DMUF4X=0.175 OMUF4X=0.024 PMUF4X=0.550

BGFX=0.000 OGFX=0.000 PGFX=0.000

ENGINE BAY GEOMETRY AT STN X

DP12X=0.000 DP23X=0.000 DP34X=0.000

EHP12X=0.000 EBP12X=0.000 EHP23X=0.000

EBP23X=0.000 EHP34X=0.000 EBP34X=0.000

OP12BX=0.000 OP23BX=0.000 OP34BX=0.000

LFGH=2.169 HFGHX=1.626 HFHCUX=0.626

HFPR1X=0.000 BFPRL=1.352 BFPRUX=0.000

OFHPRX=0.000 YFGHX=1.108 BFHCUX=1.108

OFGHX=3.282 PFGHX=7.393

[STN=12.581]

INTAKE DIFFUSER GEOMETRY AT STN X

ZIDLX=0.000 ZIDCX=0.000 ZIDUX=0.000

YIDIX=0.000 YIDCX=0.000 YIDOX=0.000

HIDX=0.000 BIDX=0.000 ZPC=1.000

RIDX=0.000 OIDX=0.000

CROSS-SECTIONAL AREA OF F.C. AT STN X

OTXN=2.375

WEAPON GEOMETRY AT STN X

DMUF1X=0.000 OMUF1X=0.000 PMUF1X=0.000

DMUF2X=0.000 OMUF2X=0.000 PMUF2X=0.000

DMUF3X=0.175 OMUF3X=0.024 PMUF3X=0.550

DMUF4X=0.175 OMUF4X=0.024 PMUF4X=0.550

BGFX=0.000 OGFX=0.000 PGFX=0.000

ENGINE BAY GEOMETRY AT STN X

DP12X=0.726 DP23X=0.000 DP34X=0.000

EHP12X=0.180 EBP12X=0.302 EHP23X=0.000

EBP23X=0.000 EHP34X=0.000 EBP34X=0.000

OP12BX=0.623 OP23BX=0.000 OP34BX=0.000

LFGH=2.169 HFGHX=1.585 HFHCUX=0.585

HFPR1X=0.203 BFPRL=1.352 BFPRUX=0.124

OFHPRX=0.079 YFGHX=1.115 BFHCUX=0.777

OFGHX=3.236 PFGHX=7.473

[STN=13.665]

INTAKE DIFFUSER GEOMETRY AT STN X

ZIDLX=0.000 ZIDCX=0.000 ZIDUX=0.000

YIDIX=0.000 YIDCX=0.000 YIDOX=0.000

HIDX=0.000 BIDX=0.000 ZPC=1.000

RIDX=0.000 OIDX=0.000

CROSS-SECTIONAL AREA OF F.C. AT STN X

OTXN=1.404

WEAPON GEOMETRY AT STN X

DMUF1X=0.000 OMUF1X=0.000 PMUF1X=0.000

DMUF2X=0.000 OMUF2X=0.000 PMUF2X=0.000

DMUF3X=0.175 OMUF3X=0.024 PMUF3X=0.550

DMUF4X=0.000 OMUF4X=0.000 PMUF4X=0.000

BGFX=0.000 OGFX=0.000 PGFX=0.000

ENGINE BAY GEOMETRY AT STN X

DP12X=0.779 DP23X=0.779 DP34X=0.000

EHP12X=0.236 EBP12X=0.156 EHP23X=0.236

EBP23X=0.156 EHP34X=0.000 EBP34X=0.000

OP12BX=0.683 OP23BX=0.683 OP34BX=0.000

LFGH=2.169 HFGHX=1.544 HFHCUX=0.544

HFPR1X=0.406 BFPRL=1.352 BFPRUX=0.248

OFHPRX=0.197 YFGHX=1.105 BFHCUX=0.428

OFGHX=3.102 PFGHX=7.618

FUSELAGE STATION H

[STN=13.665]

CROSS-SECTIONAL AREA OF F.C. AT STN X

OTXN=1.404

WEAPON GEOMETRY AT STN X

DMUF1X=0.000 OMUF1X=0.000 PMUF1X=0.000

DMUF2X=0.000 OMUF2X=0.000 PMUF2X=0.000

DMUF3X=0.175 OMUF3X=0.024 PMUF3X=0.550

DMUF4X=0.000 OMUF4X=0.000 PMUF4X=0.000

BGFX=0.000 OGFX=0.000 PGFX=0.000

HFH=1.544 BFH=2.209

HFHCU=0.544 BFHCU=0.428

HFPR1H=0.406 BFPRL=1.352 BFPRUH=0.248

OFHPRH=0.197 OFH=3.102 PFH=7.618

FUSELAGE SECTION H-J

[STN=13.665]

CROSS-SECTIONAL AREA OF F.C. AT STN X

OTXN=1.404

ENGINE BAY GEOMETRY AT STN X

DP12X=0.779 DP23X=0.779 DP34X=0.000

EHP12X=0.236 EBP12X=0.156 EHP23X=0.236

EBP23X=0.156 EHP34X=0.000 EBP34X=0.000

OP12BX=0.683 OP23BX=0.683 OP34BX=0.000

LFHJ=0.888

HFHJX=1.544 YFHJX=1.105

HFJCUX=0.544 BFJCUX=0.428

HFJCLX=0.000 BFJCLX=0.428

HFPR2X=0.406 BFPRUX=0.248 BFPRL=1.352

OFJPRX=0.197 OFHJX=3.114 PFHJX=7.613

[STN=14.109]

CROSS-SECTIONAL AREA OF F.C. AT STN X

OTXN=0.948

ENGINE BAY GEOMETRY AT STN X

DP12X=0.000 DP23X=0.845 DP34X=0.000

EHP12X=0.000 EBP12X=0.000 EHP23X=0.173

EBP23X=0.168 EHP34X=0.000 EBP34X=0.000

OP12BX=0.000 OP23BX=0.743 OP34BX=0.000

LFHJ=0.888

HFHJX=1.389 YFHJX=1.141

HFJCUX=0.528 BFJCUX=0.465

HFJCLX=0.106 BFJCLX=0.465

HFPR2X=0.350 BFPRUX=0.299 BFPRL=1.352

OFJPRX=0.184 OFHJX=2.859 PFHJX=7.187

[STN=14.553]

CROSS-SECTIONAL AREA OF F.C. AT STN X

OTXN=0.586

ENGINE BAY GEOMETRY AT STN X

DP12X=0.000 DP23X=0.912 DP34X=0.912

EHP12X=0.000 EBP12X=0.000 EHP23X=0.110

EBP23X=0.181 EHP34X=0.110 EBP34X=0.181

OP12BX=0.000 OP23BX=0.805 OP34BX=0.805

LFHJ=0.888

HFHJX=1.233 YFHJX=1.177

HFJCUX=0.511 BFJCUX=0.501

HFJCLX=0.213 BFJCLX=0.501

HFPR2X=0.295 BFPRUX=0.350 BFPRL=1.352

OFJPRX=0.166 OFHJX=2.582 PFHJX=6.812

FUSELAGE STATION J

[STN=14.553]

CROSS-SECTIONAL AREA OF F.C. AT STN X

OTXN=0.586

HFJ=1.233 BFJ=2.355

HFJCU=0.511 BFJCU=0.501

HFJCL=0.213 BFJCL=0.501

HFPR2J=0.295 BFPRUJ=0.350 BFPRL=1.352

OFJPRJ=0.166 OFJ=2.582 PFJ=6.812

FUSELAGE SECTION J-K

[STN=14.553]

CROSS-SECTIONAL AREA OF F.C. AT STN X

OTXN=0.586

ENGINE BAY GEOMETRY AT STN X

DP12X=0.000 DP23X=0.912 DP34X=0.912

EHP12X=0.000 EBP12X=0.000 EHP23X=0.110

EBP23X=0.181 EHP34X=0.110 EBP34X=0.181

OP12BX=0.000 OP23BX=0.805 OP34BX=0.805

LFJK=0.922

HFJKX=1.233 YFJKX=1.177

HFKCUX=0.511 BFKCUX=0.501

HFKCLX=0.213 BFKCLX=0.501

HFPR2X=0.295 BFPRUX=0.350

HFPR3X=0.000 BFPR3X=0.000

OFPR3X=0.000 OFKPRX=0.166

OFJKX=2.582 PFJKX=6.962

[STN=15.014]

CROSS-SECTIONAL AREA OF F.C. AT STN X

OTXN=0.399

ENGINE BAY GEOMETRY AT STN X

DP12X=0.000 DP23X=0.000 DP34X=0.850

EHP12X=0.000 EBP12X=0.000 EHP23X=0.000

EBP23X=0.000 EHP34X=0.094 EBP34X=0.110

OP12BX=0.000 OP23BX=0.000 OP34BX=0.672

LFJK=0.922

HFJKX=1.072 YFJKX=1.129

HFKCUX=0.494 BFKCUX=0.453

HFKCLX=0.323 BFKCLX=0.453

HFPR2X=0.237 BFPRUX=0.403

HFPR3X=0.116 BFPR3X=0.272

OFPR3X=0.059 OFKPRX=0.144

OFJKX=2.059 PFJKX=6.314

[STN=15.475]

CROSS-SECTIONAL AREA OF F.C. AT STN X

OTXN=0.500

ENGINE BAY GEOMETRY AT STN X

DP12X=0.000 DP23X=0.000 DP34X=0.789

EHP12X=0.000 EBP12X=0.000 EHP23X=0.000

EBP23X=0.000 EHP34X=0.079 EBP34X=0.039

OP12BX=0.000 OP23BX=0.000 OP34BX=0.551

LFJK=0.922

HFJKX=0.910 YFJKX=1.081

HFKCUX=0.476 BFKCUX=0.404

HFKCLX=0.434 BFKCLX=0.404

HFPR2X=0.179 BFPRUX=0.456

HFPR3X=0.232 BFPR3X=0.544

OFPR3X=0.167 OFKPRX=0.116

OFJKX=1.526 PFJKX=5.813

FUSELAGE STATION K

[STN=15.475]

CROSS-SECTIONAL AREA OF F.C. AT STN X

OTXN=0.500

HFK=0.910 BFK=2.161

HFKCU=0.476 BFKCU=0.404

HFKCL=0.434 BFKCL=0.404

HFPR2K=0.179 BFPRUK=0.456

HFPR3K=0.232 BFPR3K=0.544

OFPR3K=0.167 OFKPR=0.116

OFK=1.526 PFK=5.813

VOLUME OF FUSELAGE SECTIONS

VFR= 0.290 VFRA= 0.536 VFAB= 1.422

VFBC= 0.875 VFCD= 5.118 VFDE= 5.848

VFEF= 6.741 VFFG= 6.228 VFGH= 6.984

VFHJ= 2.536 VFJK= 1.897

VFIF1= 4.504 VFIF2= 5.149 VFIF3= 4.699

SURFACE AREA OF FUSELAGE SECTIONS

WFR= 2.101 WFRA= 2.384 WFAB= 4.817

WFBC= 2.624 WFCD= 15.595 WFDE= 13.519

WFEF= 15.680 WFFG= 13.793 WFGH= 16.225

WFHJ= 6.390 WFJK= 5.844

SURFACE AREA OF WINDSCREEN & CANOPY

WCWSC= 1.197 WCCAN= 2.790

GROSS TOTAL FUSELAGE VOLUME AND SURFACE AREA

VFG= 38.476 WFG= 98.972

NET WING GEOMETRY

BWBB= 2.020 BWN= 8.329 CWCB= 7.149

UWCN= 0.180 CWMN= 4.217 SWN=35.126

AWN= 1.975 CWBB= 5.004 CWBT= 0.900

QWB= 0.686 UWB= 0.180 SWB=34.695

AWB= 3.087 HWBB= 0.429 BWA= 4.502

CWA= 0.493 SWA= 2.217 CWCA2= 2.870

QWA= 0.145 SWLF= 0.000 SWLH= 3.513

SWL= 5.269 BWF= 6.727 CWCCT= 3.835

CWFM= 0.645 SWF= 2.819 SWTF= 0.232

SWTG= 5.269 CWBB= 1.759 VWBB= 3.552

VWBCF= 1.776 BWNF= 4.165 UWCNF= 0.590

VWBEF= 1.183 FBWCF= 0.598 SWBF=26.674

VWC= 7.150 XWLB= 6.673

FIN GEOMETRY

SEFN= 4.232 BEFN= 2.602

CEFB= 2.602 AEFN= 1.600

UEFN= 0.250 RTEF= 0.040

REFFC= 0.033 LEFCQM= 4.115

CEFCT= 0.651 CEFMG= 1.626

CEFMA= 1.822 QEFL= 0.800

QEF4= 0.700 QEF2= 0.580

QEFT= 0.273 VEFC= 0.214

NFIN= 1

NET FOREPLANE GEOMETRY

SCN= 3.106 BCN= 2.787 ACN= 2.500

UCN= 0.300 RTC= 0.030 RCSW= 0.038

LCCQM= 3.635 CCB= 1.715 CCCT= 0.514

CCMGN= 1.115 CCMAN= 1.222 QC4= 0.836

QC2= 0.728 QCT= 0.431 VCC= 0.079

GROSS FOREPLANE GEOMETRY

BC= 4.533 CCCC= 3.220 UC= 0.160

SC= 8.463 AC= 2.428 CCMG= 1.867

CCMA= 2.194 XCAPEX= 3.513 XCLB= 5.179

WING STORE STATIONS

QWPCG= 0.71 YB1= 4.34 YB2= 2.68

YB3= 2.68 YB4= 4.34 XB1CG=11.84

XB2CG=10.42 XB3CG=10.42 XB4CG=11.84

FOOTPRINT AND NET FUSELAGE SURFACE AREAS

WFG3= 4.642 WFN= 94.331

INTAKE DIFFUSER & ENGINE BAY VOLUMES

VIDC= 2.900 VPBC= 2.429

MOMENT ARMS OF FUSELAGE STRUCTURE & SKIN

XFXM= 8.584 XFWM= 9.069

AIRCRAFT MASS PREDICTION

MTGFI= 4089.2 MTLR=16182.2 MUM= 715.3

MUN= 109.6 MUH= 114.0 MUNG= 124.7

MUMG= 814.2 MPB= 1256.4 MPR= 412.9

MPT= 210.0 MPI= 244.3 MPG= 2123.6

MSA= 171.1 MSD= 42.8 MSE= 483.8

MSC= 520.3 MSF= 310.4 MFX= 1253.4

MFW= 1132.6 MCW= 47.2 MCC= 82.7

MFAIB= 27.8 MFIR= 86.1 EMFG= 184.1

MFG= 2859.1	MTCR=15383.8	MWB= 1493.1
MWL= 79.3	MWT= 18.9	MWF= 36.6
MWFK= 5.9	MWA= 33.9	MWCX= 57.2
MWBEF= 946.2	MWBCF= 1420.8	MFIF= 1722.2
MFGF= 3143.0		
MWXP= 12.0	MWXF= 17.1	MWC= 1754.0

MC= 74.6	MEF= 86.5	MFXP= 45.2
MCXP= 1.1	MEFXP= 1.4	MCG= 75.6
MEFC= 88.0	MTOUF= 85.0	MXTF= 800.0
MXT= 100.0	MGA= 80.0	MGC= 160.0
MCP= 100.0	MXP1= 60.0	MXP2= 65.0
MXP3= 65.0	MXP4= 60.0	MB1= 90.0
MB2= 100.0	MB3= 0.0	MB4= 90.0
MMUF1= 150.0	MMUF2= 150.0	MMUF3= 150.0
MMUF4= 150.0	MLMUF= 160.0	MCFI= 30.0
MCPI= 20.0	MCMI= 10.0	MCSEAT= 100.0
MCFURN= 90.0	MCARM= 85.0	MCMISC= 27.3
MAPU= 50.0	MCI= 362.3	MTR= 1467.3
MTP= 1060.0	MTT=16791.2	

INTERNAL FUSELAGE VOLUME ACCOUNTING

VCKPT= 1.544	VIDC= 2.900	VPBC= 2.429
VUMB= 1.359	VUNB= 0.284	VFGF= 3.929
VGC= 0.200	VAR= 0.234	VSC= 3.248
VSE= 1.007	VSA= 0.356	VAX= 0.468
VGA= 0.100	VLMUF= 0.200	VAPU= 0.104
VSF= 0.646	VFW= 11.213	VFIR= 0.853
VFAIB= 0.275	VFCR= 38.327	

MOMENT ARMS

XWCG=10.09 XCCG= 5.85 XEFCG=13.66

XFCG= 8.83 XPBCG=12.93 XPRCG=13.67

XPTCG=15.01 XPICG=13.84 XSCCG=12.28

XSECG= 8.84 XCICG= 3.17 XSACG= 5.90

XARCG= 1.81 XAXCG= 4.85 XUNCG= 5.48

XUMCG=10.53 XGCG= 9.03 XGACG= 9.38

XCPCG= 3.93 XLMCG= 9.74 XAPUCG=11.85

XM1CG= 7.84 XM2CG= 7.84 XM3CG=11.89

XM4CG=11.39 XWBECG=10.54 XWBCCG= 9.96

XFIFCG= 0.00 XSFCG=10.54 RLWBC2= 0.46

LWBEF= 3.86 RLWCC= 0.12 RLUPCW= 0.20

XFIFDE= 6.64 XFIFEF= 8.58 XFIFFG=10.56

CG POSITIONS

XTECG= 9.82 XTTCG= 9.74

XTEWCG= 9.88 XTTWCG= 9.82

XTFCG= 9.74 XTACG= 9.88

AIRCRAFT AERODYNAMIC CENTRE AND STATIC STABILITY

XAC06= 9.61 XAC14=10.45

SMSUBF=-0.022 SMSUBA=-0.046

SMSUPF= 0.123 SMSUPA= 0.099

SMSUB=-0.046 SMSUP= 0.123

FUSELAGE STATION I

[STN= 4.172]

CROSS-SECTIONAL AREA OF F.C. AT STN X

OTXN=1.945

INTAKE DIFFUSER GEOMETRY AT STN X

ZIDLX=0.000 ZIDCX=0.000 ZIDUX=0.000

YIDIX=0.000 YIDCX=0.000 YIDOX=0.000

HIDX=0.000 BIDX=0.000 ZPC=1.000

RIDX=0.000 OIDX=0.000

B.L.DIVERTER GEOMETRY AT STN X

BIX=0.000 BVIX=0.000 BVIX1=0.000

OVIX=0.000 OVIX1=0.000

LFCD=1.765 HFD2X=0.129 HFCDX=0.959

ZCCANX=0.527 YCCANX=0.408 HFDCUX=0.394

HFDCLX=0.197 YFCDX=0.851 BFDCUX=0.443

BFDCLX=0.389 OIX=0.000 OIXL1=0.000

OIXL2=0.000 OFCDXU=1.945 OFCDX=1.945

PFCDXU=5.661 PFCDXL=0.000 PFCDX= 5.661

PFTCDX=1.480

[STN= 4.182]

CROSS-SECTIONAL AREA OF F.C. AT STN X

OTXN=1.950

INTAKE DIFFUSER GEOMETRY AT STN X

ZIDLX=0.000 ZIDCX=0.267 ZIDUX=0.535

YIDIX=0.000 YIDCX=0.335 YIDOX=0.670

HIDX=0.535 BIDX=0.670 ZPC=1.000

RIDX=0.040 OIDX=0.357

B.L.DIVERTER GEOMETRY AT STN X

BIX=0.670 BVIX=1.340 BVIX1=0.000

OVIX=0.107 OVIX1=0.000

LFCD=1.765 HFD2X=0.131 HFCDX=1.574

ZCCANX=0.523 YCCANX=0.408 HFDCUX=0.393

HFDCLX=0.195 YFCDX=0.853 BFDCUX=0.446

BFDCLX=0.389 OIX=0.717 OIXL1=0.000

OIXL2=0.000 OFCDXU=1.948 OFCDX=2.771

PFCDXU=5.668 PFCDXL=3.750 PFCDX= 9.418

PFTCDX=1.473

SORTIE PERFORMANCE

Sortie-leg no.1

HT= 4000.0 M=0.50 MASS=16455.8 SLEG= 7.0 RT1= 43.1

GN= 1.50 EQWF= 0.00 GCL= 2.985 CL=0.43 AL=0.143 CDTOT=0.06428

FPS= 32.8 TPG2= 52219.4 GNH= 6.39 CL2=1.73 ALH=0.578

SRMASS= 0.0 MPFB2= 35.4 MPFB2T= 335.4

Sortie-leg no.2

HT= 8000.0 M=0.90 MASS=16030.6 SLEG= 150.0 RT1= 540.9

GN= 1.00 EQWF= 0.00 GCL= 3.355 CL=0.15 AL=0.045 CDTOT=0.03276

FPS= 39.3 TPG2= 57432.0 GNH= 9.00 CL2=1.79 ALH=0.535

SRMASS= 0.0 MPFB2= 425.2 MPFB2T= 760.6

Sortie-leg no.3

HT= 6000.0 M=1.00 MASS=15955.2 SLEG= 6.0 RT1= 19.0

GN= 0.70 EQWF= 0.00 GCL= 3.468 CL=0.06 AL=0.018 CDTOT=0.05461

FPS= 63.3 TPG2=132870.3 GNH= 9.00 CL2=1.60 ALH=0.461

SRMASS= 0.0 MPFB2= 75.4 MPFB2T= 836.0

Sortie-leg no.4

HT= 2000.0 M=1.10 MASS=14143.1 SLEG= 50.0 RT1= 136.7

GN= 1.00 EQWF= 0.00 GCL= 3.196 CL=0.04 AL=0.013 CDTOT=0.06253

FPS= 83.5 TPG2=295339.4 GNH= 9.00 CL2=1.44 ALH=0.452

SRMASS= 0.0 MPFB2= 1812.1 MPFB2T= 2648.1

Sortie-leg no.5

HT= 5000.0 M=1.10 MASS=14069.9 SLEG= 2.0 RT1= 5.7

GN= 5.00 EQWF=10.00 GCL= 3.196 CL=0.29 AL=0.064 CDTOT=0.08304

FPS= 98.9 TPG2=249152.5 GNH= 9.00 CL2=1.49 ALH=0.439

SRMASS= 0.0 MPFB2= 73.2 MPFB2T= 2721.3

Sortie-leg no.6

HT=11000.0 M=1.60 MASS=13869.7 SLEG= 10.0 RT1= 21.2

GN= 1.30 EQWF= 0.00 GCL= 2.739 CL=0.08 AL=0.030 CDTOT=0.04615

FPS= 48.1 TPG2=141036.7 GNH= 9.00 CL2=0.79 ALH=0.288

SRMASS= 180.0 MPFB2= 20.2 MPFB2T= 2741.5

Sortie-leg no.7

HT=14000.0 M=2.00 MASS=12078.1 SLEG= 200.0 RT1= 338.9

GN= 1.00 EQWF= 0.00 GCL= 2.330 CL=0.06 AL=0.026 CDTOT=0.04132

FPS= 85.4 TPG2=129127.1 GNH= 7.58 CL2=0.49 ALH=0.208

SRMASS= 0.0 MPFB2= 1791.6 MPFB2T= 4533.1

Sortie-leg no.8

HT= 7000.0 M=0.60 MASS=12052.6 SLEG= 13.0 RT1= 69.4

GN= 0.60 EQWF= 0.00 GCL= 3.007 CL=0.13 AL=0.044 CDTOT=0.02834

FPS= 22.5 TPG2= 26537.7 GNH= 8.08 CL2=1.69 ALH=0.562

SRMASS= 0.0 MPFB2= 25.5 MPFB2T= 4558.6

TAKE-OFF AND LANDING PERFORMANCE

MTT=16791.2 EQWFT=15.00 CLT=1.81

VSTTO= 54.0 VTO= 59.4 TOG= 217.2 TOA= 136.3 TOD= 353.5

MTL=11902.6 EQWFL=35.00 CLMAXL=1.82

VSTAPP= 45.3 VAPR= 54.3 LD= 600.8

POINT PERFORMANCE

Sustained Turn Rate

HT= 1000.0 M=0.60 WT=140000.0 XV=100.0 EQWF=10.00

GCL=3.007 CDTOT=0.04394 TPG=231993.4

CL4=1.76 ALM=0.555 GNS= 9.00 STR=24.9

Attained Turn Rate

HT= 9000.0 M=1.60 WT=140000.0 XV=100.0 EQWF=10.00

GCL=2.739 TPG=235814.3

CLMAX=0.81 GNA=10.00 ATR=11.5

Specific Excess Power

HT= 6000.0 M=0.70 WT=130000.0 XV=100.0

GCL=3.117 CDTOT=0.03096 TPG=143120.6

CL=0.16 AL=0.050 SEP=160.1

Maximum Mach Number

HT=10000.0 WT=140000.0 XV=100.0

GCL=2.215 CDTOT=0.04442 TPG=281766.8

CL=0.03 AL=0.015 MMAX=2.12

Maximum Mach Number

HT= 1000.0 WT=140000.0 XV=100.0

GCL=3.119 CDTOT=0.06219 TPG=469555.9

CL=0.03 AL=0.008 MMAX=1.31

Acceleration Time

HT=12000.0 MSTART=0.80 WT=145000.0 XV=100.0 DM=0.30

GCL=3.196 CDTOT=0.04682 TPG= 95846.4

CL=0.17 AL=0.054 SDT= 32.8

Ride Quality Factor

HT= 1000.0 M=0.50 WT=150000.0 GCL=2.985 RQF= 1.9

COMPUTER GENERATED IMAGE OF THE SYNTHESIZED CONFIGURATION

(SIDE VIEW)

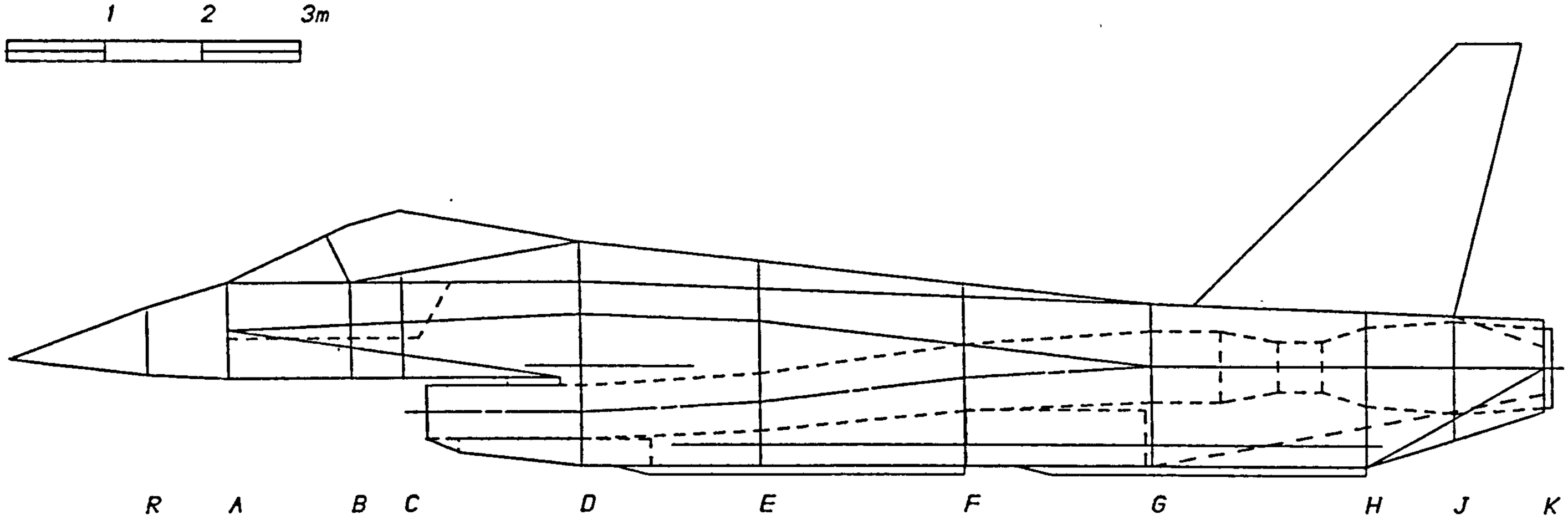

501

DESIGN SYNTHESIS

FOR

CANARD-DELTA COMBAT AIRCRAFT

BY, V.C.SERGHIDES

1985/87

COLLEGE OF AERONAUTICS

CRANFIELD INSTITUTE OF TECHNOLOGY

FOR007.DAT

COMPUTER GENERATED IMAGE OF THE SYNTHESIZED CONFIGURATION

(UPPER PLAN VIEW)

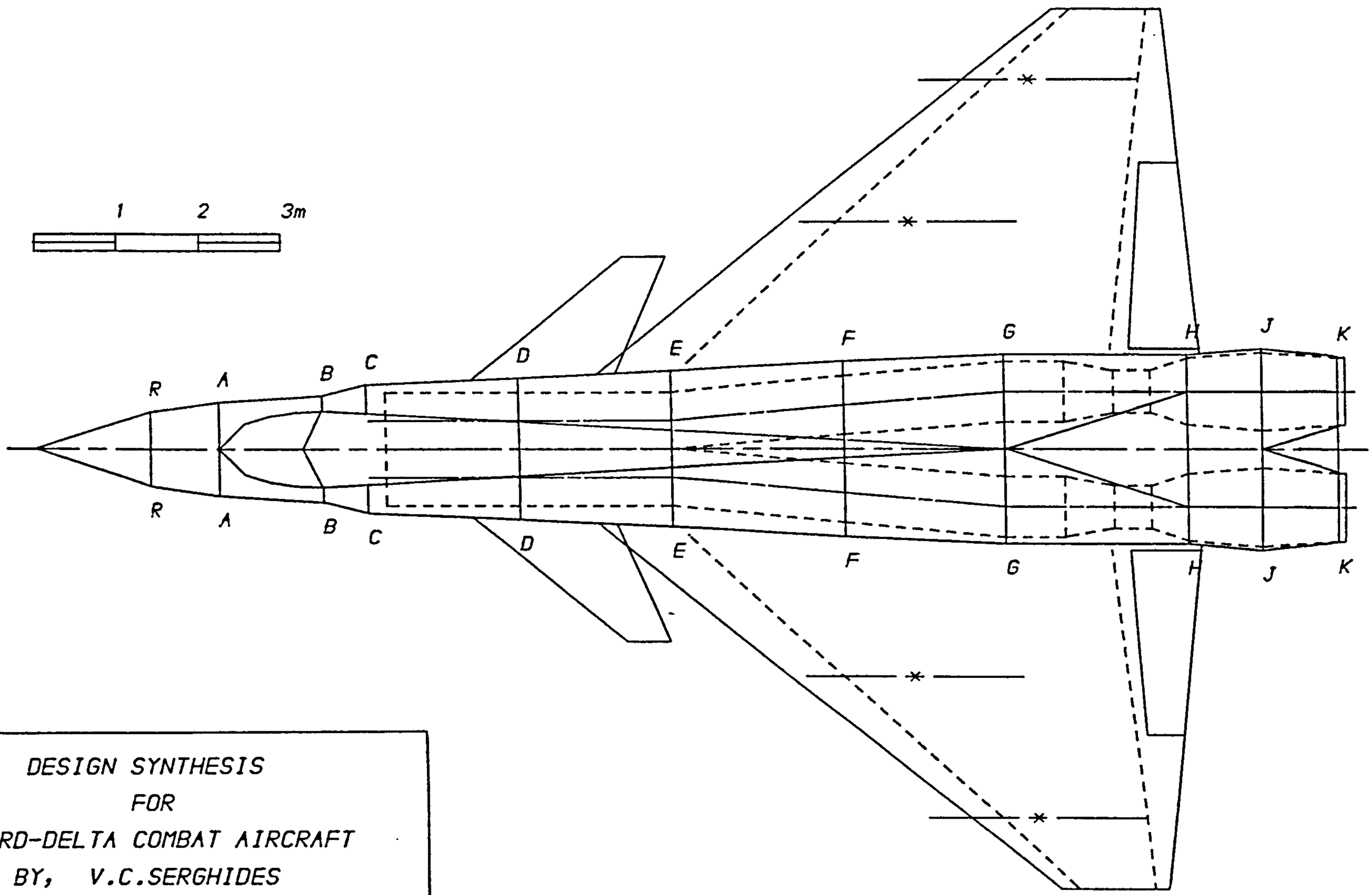

DESIGN SYNTHESIS

FOR

CANARD-DELTA COMBAT AIRCRAFT

BY, V.C.SERGHIDES

1985/87

COLLEGE OF AERONAUTICS

CRANFIELD INSTITUTE OF TECHNOLOGY

COMPUTER GENERATED IMAGE OF THE SYNTHESIZED CONFIGURATION

(LOWER PLAN VIEW)

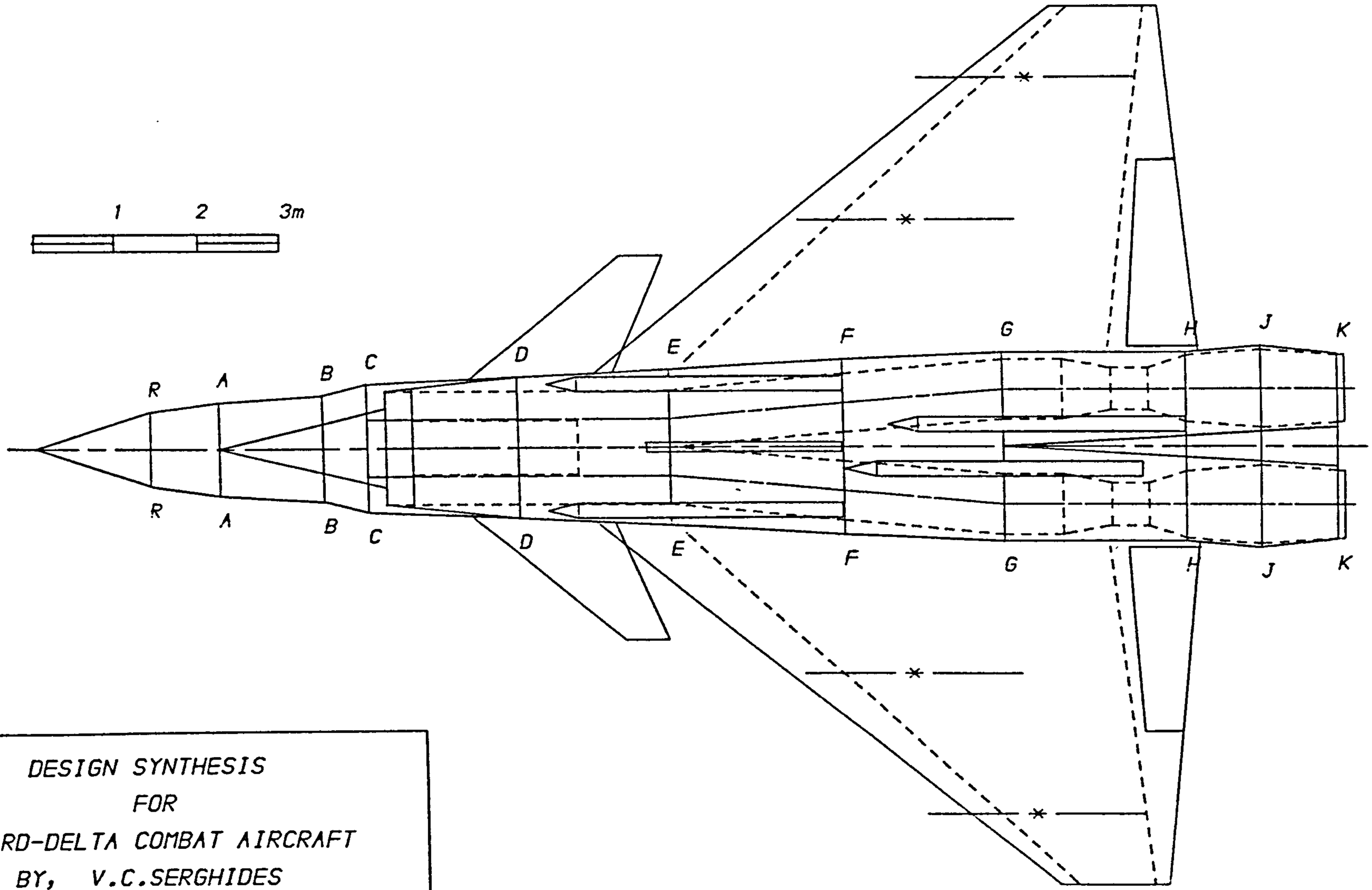

DESIGN SYNTHESIS

FOR

CANARD-DELTA COMBAT AIRCRAFT

BY, V.C.SERGHIDES

1985/87

COLLEGE OF AERONAUTICS

CRANFIELD INSTITUTE OF TECHNOLOGY

TOTAL AIRCRAFT LIFT VS AIRCRAFT INCIDENCE (LINEAR RANGE)

NEUTRAL LONGITUDINAL STABILITY

ZERO PITCHING MOMENT

Fig. K.1

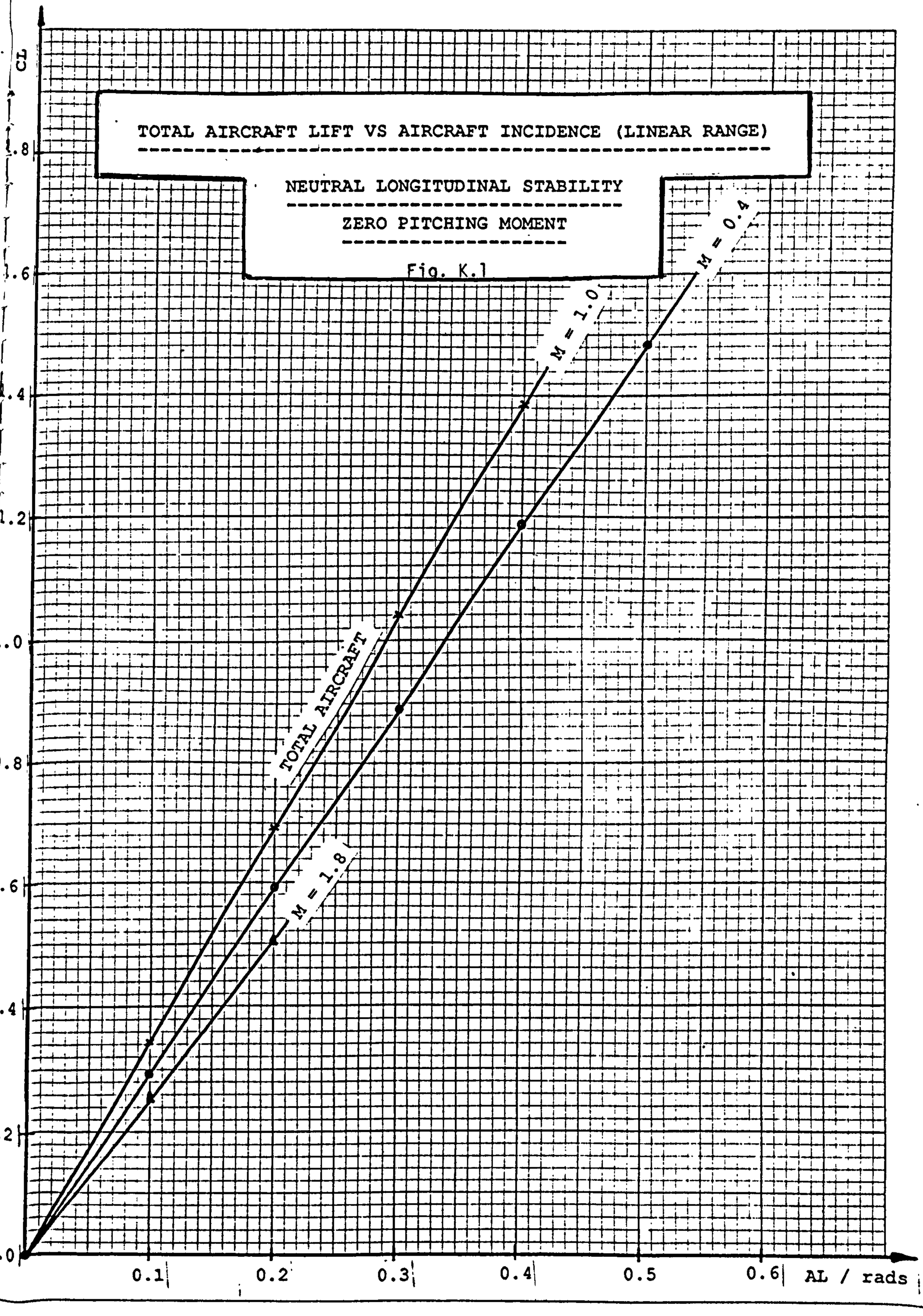

WING-BODY AND FOREPLANE-BODY LIFT CONTRIBUTIONS VS AIRCRAFT INCIDENCE (LINEAR RANGE)

NEUTRAL LONGITUDINAL STABILITY

ZERO PITCHING MOMENT

Fig. K.2

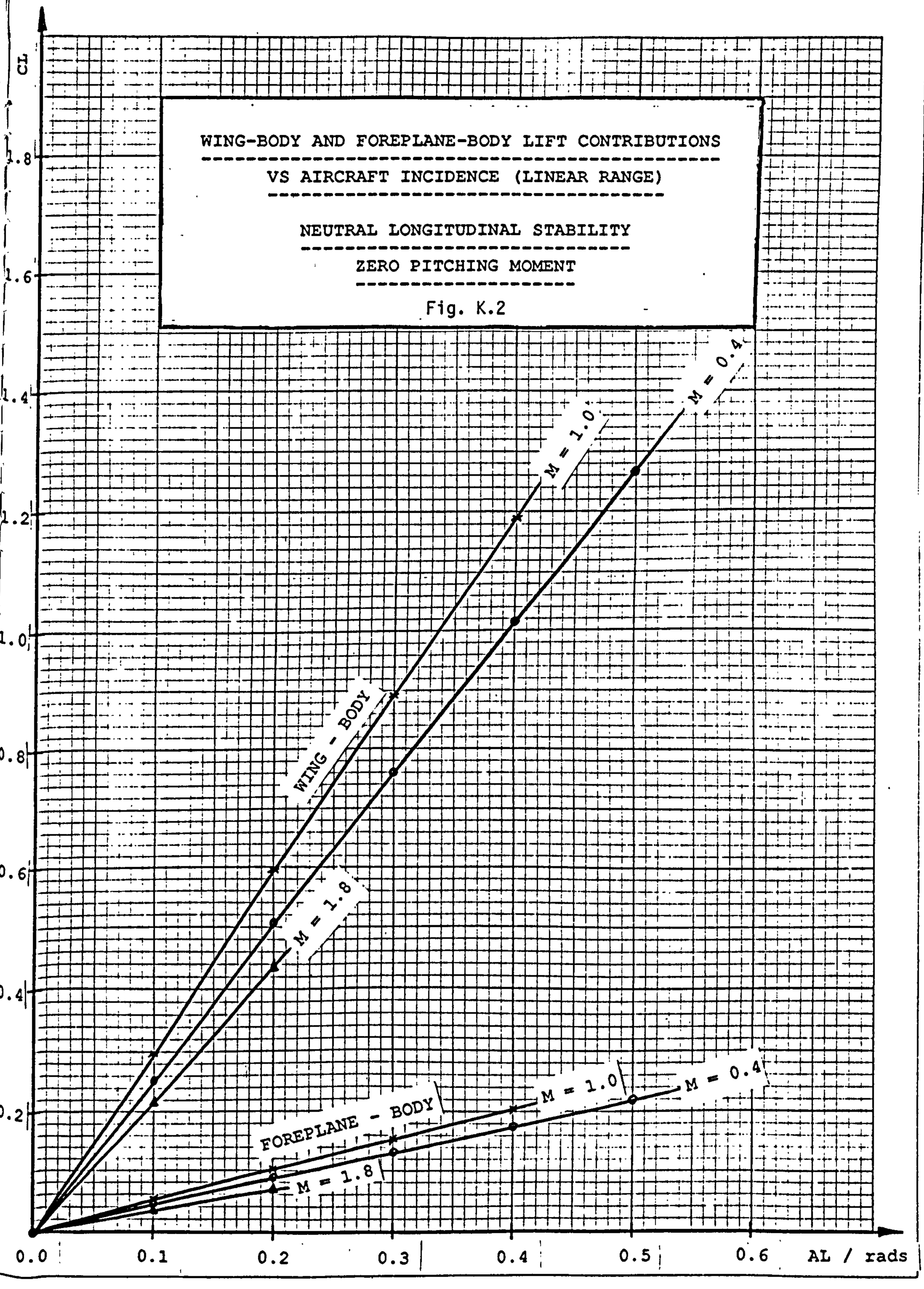

TOTAL AIRCRAFT UNTRIMMED DRAG POLARS (CLEAN)

Fig. K.3

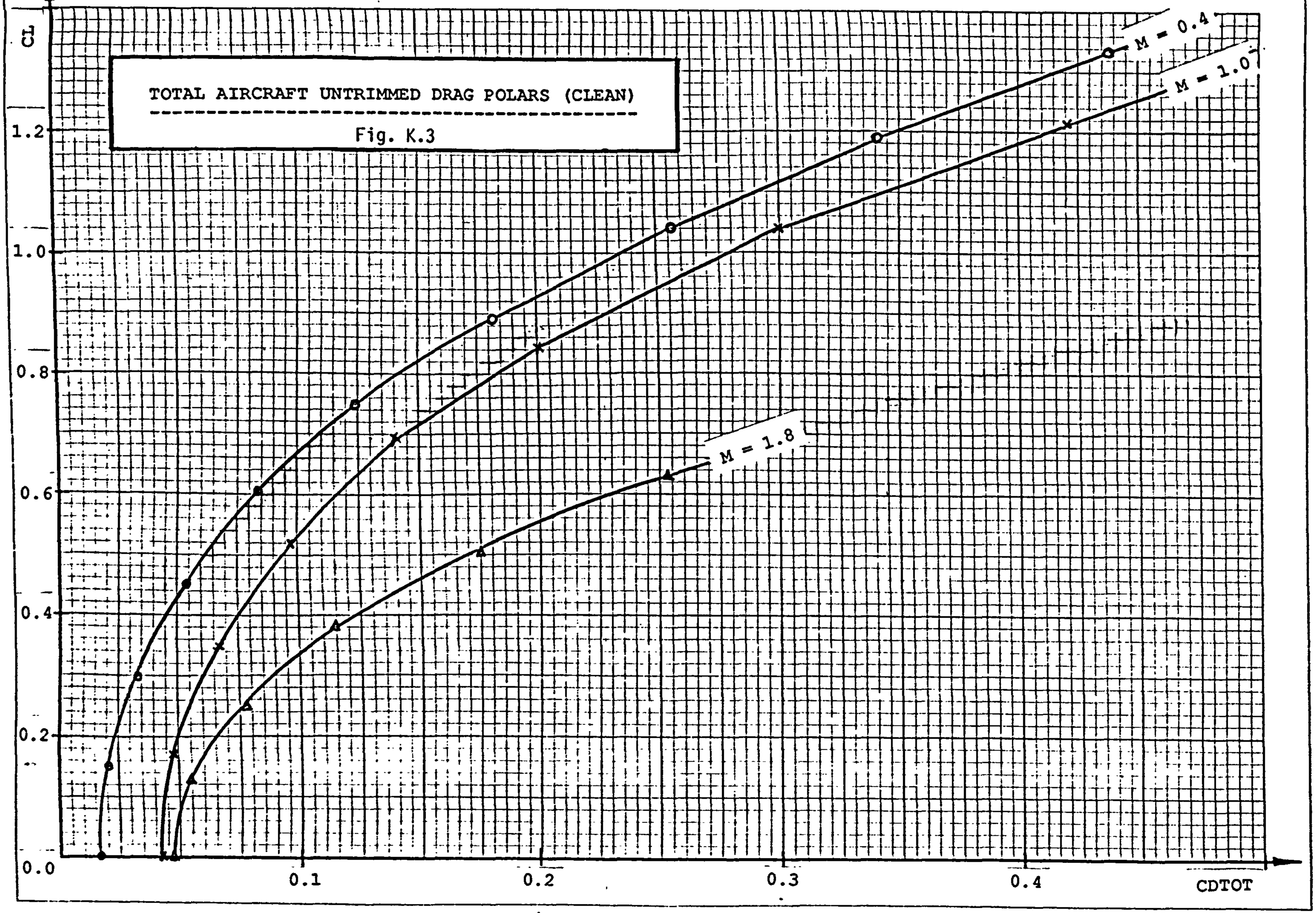

TOTAL AIRCRAFT UNTRIMMED LIFT/DRAG RATIOS (CLEAN)

Fig. K.4